University of Southampton

Faculty of Natural and Environmental Sciences

School of Ocean and Earth Science

Patterns of diversity, connectivity, and evolution in Southern Ocean and deep-sea annelids

By

Regan Drennan

ORCID ID https://orcid.org/0000-0003-0137-5464

Thesis for the degree of Doctor of Philosophy

March 2024

University of Southampton

Abstract

Faculty of Natural and Environmental Sciences

School of Ocean and Earth Science

Doctor of Philosophy

Patterns of diversity, connectivity, and evolution in Southern Ocean and deep-sea annelids

by

Regan Drennan

The Southern Ocean surrounding Antarctica, and the deep oceans of the world more generally, are considered amongst the last remaining marine wildernesses on the planet. However, the remoteness that has protected these marine realms from direct anthropogenic impacts in the past have also made documenting their biodiversity challenging. As both direct and indirect anthropogenic threats increase, there is an urgent need to build an accurate baseline understanding of these ecosystems to evaluate threats, monitor change, and inform conservation efforts. Using benthic annelids as a model group, this thesis investigates biodiversity at various hierarchical levels in Southern Ocean and deep-sea habitats, from species to community level, local to regional, and comparing morphological, genetic, and genomic methods. A new species of deep-sea annelid, *Neanthes goodayi* sp. nov. is described from the abyssal central Pacific using both morphological and molecular data, highlighting polymetallic nodules (mineral resources targeted by potential seabed mining) as a unique microhabitat, in addition to the value of comprehensive integrative taxonomic description. The annelid community of a deep, previously ice-covered channel on the Antarctic Peninsula – the Prince Gustav Channel, is then documented using morphological-level identifications, giving first insights into the biodiversity of this previously unsampled channel, highlighting a functionally and spatially heterogeneous benthic community in a region already affected by climate change. DNA barcoding was then carried out for a subset of representative morphospecies from this dataset to investigate whether a barcode subsample improves morphological species identifications in relation to richness and diversity of the channel community, finding that, while overall biodiversity metrics were relatively unchanged, barcodes improved identification quality, and highlighted potential cryptic diversity. Finally, the first genomic level study of a Southern Ocean annelid using Single Nucleotide Polymorphism (SNP) data was carried out for the nephtyid *Aglaophamus trissophyllus,* using samples spanning much of the species' distributional range across West Antarctica, revealing complex patterns of population structure and connectivity across the Southern Ocean, and finding support for potential cryptic lineages. Results of the thesis are synthesised and discussed in relation to the strengths, weaknesses and synergy of different methods for measuring Southern Ocean and deep-sea benthic biodiversity in the in the context of a global taxonomic impediment.

Table of Contents

Table of Tables

Table of Tables

Table of Figures

Table of Figures

Table of Figures

List of Accompanying Materials

Drennan (2024) Data supporting University of Southampton Doctoral Thesis entitled: Patterns of diversity, connectivity, and evolution in Southern Ocean and deep-sea annelids. University of Southampton doi:10.5258/SOTON/D2958 [Dataset]

Research Thesis: Declaration of Authorship

Print name: REGAN DRENNAN

Title of thesis: Patterns of diversity, connectivity, and evolution in Southern Ocean and deep-sea annelids

I declare that this thesis and the work presented in it are my own and has been generated by me as the result of my own original research.

I confirm that:

1. This work was done wholly or mainly while in candidature for a research degree at this University;
2. Where any part of this thesis has previously been submitted for a degree or any other qualification at this University or any other institution, this has been clearly stated;
3. Where I have consulted the published work of others, this is always clearly attributed;
4. Where I have quoted from the work of others, the source is always given. With the exception of such quotations, this thesis is entirely my own work;
5. I have acknowledged all main sources of help;
6. Where the thesis is based on work done by myself jointly with others, I have made clear exactly what was done by others and what I have contributed myself;
7. Parts of this work have been published as:

    - **Drennan R,** Wiklund H, Rabone M, Georgieva MN, Dahlgren TG and Glover AG (2021a) *Neanthes goodayi* sp. nov. (Annelida, Nereididae), a remarkable new annelid species living inside deep-sea polymetallic nodules. *Eur. J. Taxon.* 760: 160–185. https://doi.org/10.5852/ejt.2021.760.1447
    - **Drennan R,** Dahlgren TG, Linse K and Glover AG (2021b) Annelid Fauna of the Prince Gustav Channel, a Previously Ice–Covered Seaway on the Northeastern Antarctic Peninsula. *Front. Mar. Sci.* 7:595303. https://doi.org/10.3389/fmars.2020.595303

Signature: ..... Date: .....

Acknowledgements

Undertaking a PhD is a challenging enough endeavour without a once in a century global pandemic happening slap bang in the first year, and part of me cannot believe that I've come out the other end, thesis in hand! I truly would not have been able to complete this project without the help and support of a huge number of people, with whom I would like to acknowledge and thank in this space.

First a massive thank you to my supervisory team, Dr. Adrian Glover, Dr. Thomas Dahlgren, Dr. Katrin Linse and Dr. Jon Copley. To Adrian, who first took me on as a Master's student in 2016, a special thank you for all your mentoring and support over the years and for the incredible opportunities to travel, work at sea, and study amazing animals from the ends of the earth. To Thomas, thank you for your guidance and enthusiasm for worms, and for always checking in for those weekly meetings! To Katrin, thank you so much for your support, from setting up meetings just to catch up and chat during those first weeks of lockdown, to helping me push through the writing blocks of my final years. Thank you also to Jon for your advice and support throughout, and for all the help navigating the University ends of things.

A special thank you to Dr. Belen Arias for your added supervision in my final year, teaching me step by step the highs and lows of genomic bioinformatics, and for always being there for me with feedback and friendship! Also, to Dr. Lupita Bribiesca-Contreras – my companion during those long midnight to midday shifts at sea, processing boxcores at record speed – thank you for friendship, support, and guidance over the years, even up until the last minute of thesis panic! To the rest of the NHM Deep Sea lab - Corie, Eva, Georgina, Lenka, Lucas, Muriel - thank you for all the laughs and chats and snack breaks, and of course weekly farmer's market trips!

Thank you to Claire Griffin, and Carla Gustave at the NHM molecular labs for processing my endless sequence data and for putting up with my (despite great effort) terrible handwriting on tube labels. Also at the NHM, thank you to Emma Sherlock for curatorial support, and to Anna Hutson at the NHM graduate centre, who always managed to figure out and help me with my myriad of complicated requests.

Thank you to Dr Sergi Taboada for the incredible opportunity to carry out ddRADseq lab work at the Museo Nacional de Ciencias Naturales Madrid, and for all the help, guidance and support throughout the whole process, from planning to writing up. Thank you also to the molecular lab group at the MNCN for their welcome during my time there, and to Gilberto Bergamo and Carlota Gracia for their great help and assistance during library preparation – especially the never-ending magnetic bead cleaning!

Acknowledgements

Thank you to Sadie Mills and David Bowden at NIWA for help with organising specimen material loans, and to Craig R. Smith for the opportunity to travel to the University of Hawai'i to collect and use material from his incredible Antarctic collections. Thank you also to Arne Nygren at the University of Gothenburg for *Maldane sarsi* material.

A huge thank you to my friends, whether home or away – Alison, Amy, Chloe, Hannah, Juliet, Lauren, Marguerite, Megan, Sarah, Yvonne – for always supporting and believing in me, even when seas apart! A shout out also to the wonderful, the brilliant, bag full of beans pandemic pub quiz team.

My biggest thank you to my family, Mum, Dad, and Olivia, for their unwavering love, faith and eternal support. This one's for you!

Definitions and Abbreviations

ABGD ..... Automatic Barcode Gap Discovery

ABYSSLINE..... Abyssal Baseline Project

ACC ..... Antarctic Circumpolar Current

AGT ..... Agassiz Trawl

AIC ..... Akaike Information Criterion

ASAP ..... Assemble Species by Automatic Partitioning

BAS..... British Antarctic Survey

BIC..... Bayesian Information Criterion

CAML ..... Census of Antarctic Marine Life

CCD ..... Carbonate Compensation Depth

CCZ..... Clarion Clipperton Zone

CFSW ..... Cold filtered Seawater

COI ..... Cytochrome c oxidase subunit I

DAPC..... Discriminant Analysis of Principal Components

ddRADseq ..... Double digest restriction-site associated DNA sequencing

EBS..... Epibenthic Sledge

GYMC..... General Yule Mixed Coalescent Model

LGM ..... Last Glacial Maximum

LIG..... Last Interglacial

MNCN ..... Museo Nacional de Ciencias Naturales Madrid

MOTUs..... Molecular Operational Taxonomic Units

MPA ..... Marine Protected Area

NHM/NHMUK..... Natural History Museum London

NIWA ..... National Institute of Water and Atmospheric research

PCR ..... Polymerase Chain Reaction

PGC ..... Prince Gustav Channel

PTP..... Poisson Tree Process

RAMS ..... Register of Antarctic Marine Species

RRS..... Royal Research Ship

SCAR ..... Scientific Community on Antarctic Research

SCAR-MarBIN..... SCAR-Marine Biodiversity Information Network

SNP ..... Single Nucleotide Polymorphism

SUCS ..... Shallow Underwater Camera System

WAIS ..... West Antarctic Ice Sheet

WAP ..... West Antarctic Peninsula

WoRMS..... World Register of Marine Species

ZMH ..... Zoological Museum Hamburg

Chapter 1 Introduction

1.1 Annelid diversity

1.1.1 The importance of annelids in marine benthic ecosystems

As far as we know, the phylum Annelida has been part of marine benthic ecosystems since the Early Cambrian (Parry et al., 2014). Annelida as a phylum historically included the three classes Polychaeta (mainly marine annelids), Oligochaeta (earthworms) and Hirudinea (leeches), although Polychaeta is now accepted to be paraphyletic, with the Oligochaeta, Hirudinea, and the Phyla Sipuncula and Echiura all nested within the group (Weigert & Bleidorn, 2016). It has become more common to refer to polychaetes as marine annelids. Today, marine annelid worms (or polychaetes) are found globally in virtually all marine ecosystems (Pamungkas et al., 2021), from intertidal habitats to hadal depths at the bottom of marine trenches (Paterson et al., 2009). Marine annelids range in size from microscopic meiofauna inhabiting the interstitial environment between sand grains (Worsaae et al., 2021) to giant megafauna up to three metres in length, such as the giant tube worm *Riftia pachyptila* (Jones, 1981) (McClain et al., 2015), or bobbit worm *Eunice aphroditois* (Pallas, 1788) (Uchida et al., 2009). Marine annelids have huge ecological importance, filling a diverse array of feeding strategies and functional groups, ranging from burrowing deposit feeders, sessile suspension feeders, carnivores, omnivores, herbivores, and parasites, to those with specialised symbiotic bacteria that facilitate chemosynthesis and even the digestion of bone (Jumars et al., 2015).

While annelids are important components of hard-substrate communities, they dominate sedimentary, soft-bottom environments (Hutchings, 1998), which comprise the majority of benthic habitats and is the most widespread habitat-type on the planet (Snelgrove, 1999). Within these habitats, annelids play a key role in bioturbation, i.e. cycling nutrients and aerating sediments (Hutchings, 1998) in addition to the burial of organic carbon (e.g. Levin et al., 1997). In environmental monitoring, annelid species have also been used as bioindicators of marine pollution (e.g. Bellan, 2004; Surugiu, 2005), and proxies for measuring marine biodiversity (e.g. Gladstone et al., 2020; Olsgard et al., 2003). Due to their ubiquity and ecological importance therefore, documenting annelid biodiversity is essential for understanding and characterising benthic ecosystems and monitoring environmental change. In addition, marine annelid biodiversity is also of interest to bioprospecting efforts, i.e. sourcing new bioactive compounds already present in nature (for example from venoms, toxins etc.), with new compounds from annelid sources displaying potential anti-cancer, anaesthetic, anti-microbial, and anti-viral properties, amongst many others (see Rodrigo & Costa, 2019).

1.1.2 A changing picture of annelid diversity

Species are fundamental units of biodiversity (Claridge et al., 1997) and formally naming and identifying species is crucial for linking biological data (e.g. ecological, morphological, physiological, genetic) to the same taxonomic unit across research (Pante et al., 2015). Our understanding of annelid diversity, particularly regarding deeper phylogenetic relationships within the phylum, have changed considerably since the beginning of the 21st century, particularly with the advent of molecular genetic methods (Capa & Hutchings, 2021). Molecular data is also changing perceptions of annelid diversity and distribution at the species level. For example, it was a long-held paradigm that many annelid species held widespread, even global distributions i.e. cosmopolitan species. However, molecular analyses combined with detailed morphological work have consistently found that most cosmopolitan species are in fact composed of multiple sister species or morphologically indistinguishable cryptic species, with previously reported distributions most likely a historic artefact influenced by a European taxonomic bias (see Hutchings & Kupriyanova, 2018).

Cryptic diversity is common across marine annelids (Nygren, 2014), suggesting that morphology alone underestimates true diversity, with morphological descriptions making the bulk of taxonomic descriptions since the late 18th century. Meanwhile some annelid species do genuinely display large distributions (e.g. Ahyong et al., 2017; Meyer et al., 2008), mostly because of recent introductions (e.g. by ship ballast water), while others show remarkable morphological variability within the same genetic species (Nygren et al., 2011). This highlights that resolving true patterns of diversity requires a case-by-case approach. While molecular data has played a key role in the changing picture of annelid diversity, using molecular data alone also has many caveats (see Grant et al., 2021; Zamani et al., 2022a, 2022b). It is increasingly apparent that an integrative taxonomic approach using multiple data sources (i.e. both morphological and molecular) is the most robust method of identifying, discovering, delineating and revising annelid diversity (Pante et al., 2015).

The total number of valid annelid species (mostly marine but including terrestrial and freshwater) is estimated to be around 20,000 (Capa & Hutchings, 2021; Magalhães et al., 2021). The most recent estimate for marine annelids alone is 13,738 valid species (Bouchet et al., 2023). These numbers are in flux with the revision of historic taxonomic groups, with many groups and species still needing thorough taxonomic revision (Capa & Hutchings, 2021) and over 10,000 annelid species potentially left to describe globally (Magalhães et al., 2021 and references therein).

The geographic distribution of current annelid knowledge is uneven. Sampling of marine annelids is greatest around coastal and shallow waters, with hotspots including waters around Europe, North America, South Korea, and Australia while large regions such as the Southern Ocean surrounding Antarctica and deep ocean away from continental margins are relatively poorly sampled (Figure 1.1 a). Both the Southern Ocean and deep-sea environments have been referred to separately as the last great wildernesses on earth (e.g Brooks & Christian, 2023; Ramirez-Llodra et al., 2011). No marine ecosystem is completely unaffected by human impacts (Halpern et al., 2008), and only 13% of the world's oceans remain classified as true marine wildernesses (Jones et al., 2018), i.e. largely intact marine ecosystems mostly free of direct human activity today. Both the Southern Ocean and deepsea environments contribute amongst the largest portions of remaining marine wilderness (Jones et al., 2018) (Figure 1.1 b). These two ecosystems, their habitats, annelid faunas and anthropogenic threats are introduced in the next section.

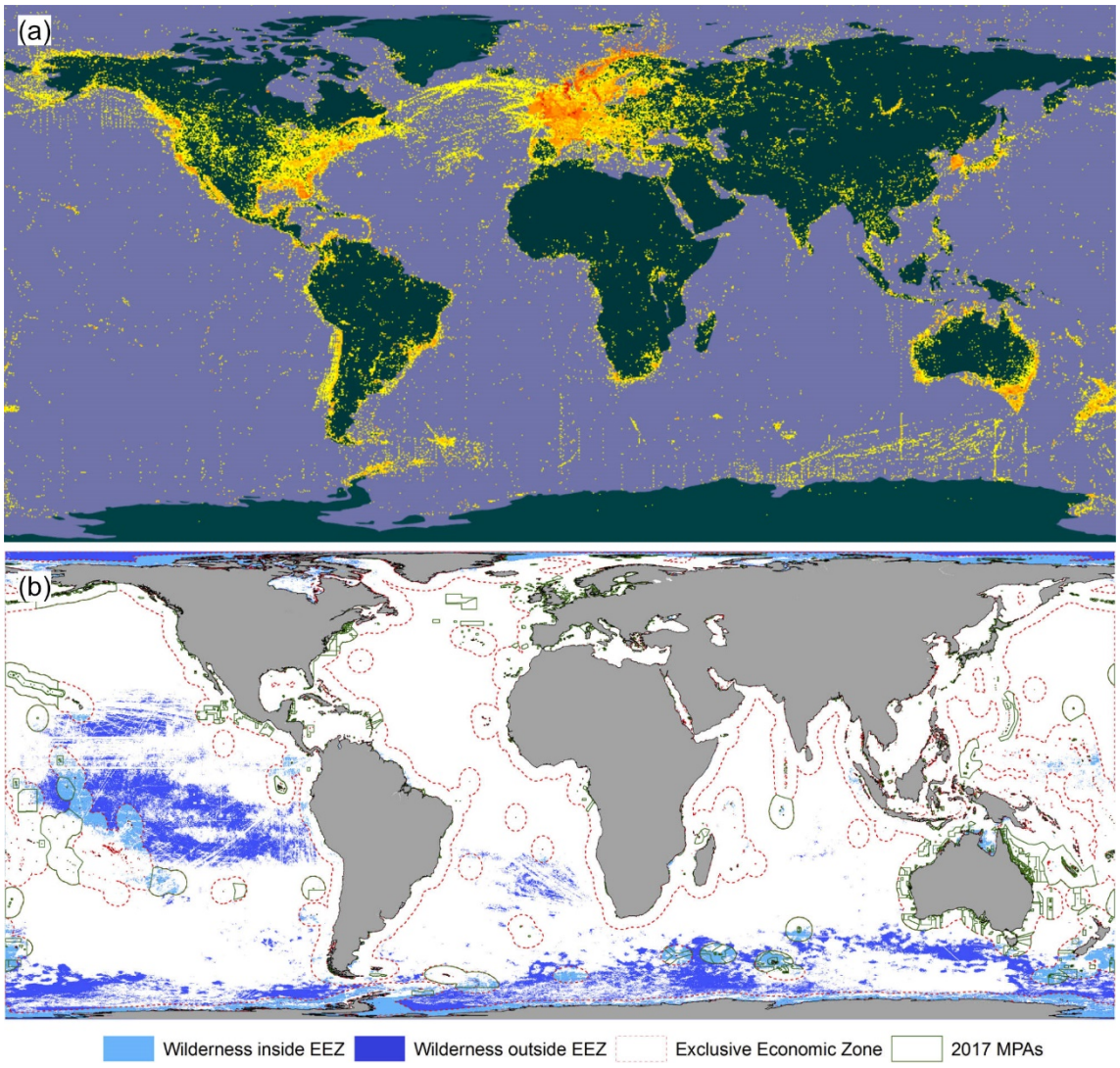

Figure 1.1 (a) Occurrence data from the Global Biodiversity Information Facility (GBIF) with 5,051,456 georeferenced records for Annelida (both marine – pelagic and benthic – freshwater,and terrestrial, accessed 10/11/2023). Yellow markers indicate a single occurrence, while orange and red indicate higher occurence densities. This map is intended as a proxy for sampling effort and density, reflected by number of records uploaded to the GBIF platform. (b) Figure adapted from Jones et al. (2018) showing the extent of remaining global marine wildernesses and their protection. Marine wilderness in exclusive economic zones (EEZ) shown in light blue, areas beyond national jurisdiction in dark blue, and marine protected areas outlined in green.

1.2 Southern Ocean benthic ecosystems

1.2.1 Palaeogeographic context

Completely encircled by deep open ocean, the Antarctic continental shelf is considered to be the most isolated in the world. Full bathymetric isolation of the Antarctic continent occurred following a final separation from South America and the opening of the Drake passage over 40 Mya (Scher & Martin, 2006). This allowed for unrestricted water flow around the continent, facilitating the formation of the Antarctic Circumpolar Current (ACC) (Barker, 2001), which, running clockwise around the continent remains the largest and fastest major water current on the planet today. The ACC is flanked by several oceanic thermal fronts, such as the Antarctic polar front (APF), which are marked by a difference of several degrees in temperature over a small geographic range; these fronts thermally isolate the Southern Ocean and define the boundaries between Antarctic, Sub-Antarctic, and temperate waters (Orsi et al. 1995). In addition to the considerable bathymetric isolation of the Antarctic continental shelf, the strong, eastward flow of the ACC and the thermal and density-driven isolation of water masses, makes the current and its associated fronts act as formidable physical and physiological barriers to the north-south movement of organisms (Moore et al., 2018); the characteristic high endemism of the modern Antarctic biota is largely attributed to this prolonged and continuing isolation (Arntz et al., 1997), though barriers to movement are thought to be less pronounced between abyssal Southern Ocean and other deep-sea basins.

The glacial history of the Antarctic seabed throughout the latter half of the Cenozoic era is also an important consideration. The formation of the ACC and its associated front systems roughly coincided with a significant global cooling event approximately 34 Mya at the Eocene-Oligocene boundary, shifting the climate from greenhouse to icehouse conditions and initiating the onset and formation of permanent Antarctic continental ice sheets (Zachos et al., 2001), followed by progressive cooling and a cyclical waxing and waning of ice-sheet volume that continues to the present day, with alternating cycles of glacial periods (defined by extensive ice sheet coverage and a fall in global sea levels) and warmer interglacial periods (with smaller ice sheet extent and higher sea levels). Sediment core data suggest at least 38 full glacial cycles occurred over the last five million years alone (Naish et al., 2009), and it is estimated that grounded ice shelves may have extended across much of the Antarctic continental shelf during glacial maxima (e.g. Anderson et al., 2002; Huybrechts, 2002). This would have bulldozed shelf systems and destroyed much of the available benthic habitat during the Last Glacial Maximum (approx. 21Ka, Huybrechts, 2002).

Weighed down by the vast continental ice cap and scoured by cycles of intense glacial erosion, the Antarctic seabed is also notably deep, with an average continental shelf depth of around 450 m, which is between two and four times deeper than other shelf systems around the globe (Clarke & Johnston, 2003; Knox, 2006). High polar latitudes cause intense seasonality in shallow waters across many environmental variables including light availability, sea ice cover, and therefore net primary productivity at the surface, with amongst the highest and lowest particulate organic carbon (POC) fluxes on the planet recorded at the same site off the West Antarctic Peninsula during summer and winter respectively (Smith et al., 2008a). Temperature on the other hand, is remarkably stable, more or less remaining at freezing year round, uncoupled from annual variation in primary production (Clarke, 1988), and with little difference in temperature between surface and abyssal waters, i.e. an isothermal water column. The increased depth of the continental shelf reduces the amount of light capable of reaching the benthos, therefore buffering much of the sea floor from the impact of variable surface conditions (Halanych & Mahon, 2018). Furthermore, POC from high summer productivity can be stored in benthic sediments as a persistent, year-round sediment "food-bank", buffering benthic communities from extreme seasonality in trophic input (Smith et al., 2008a). Today, Antarctic sea beds span from some of the most to least naturally disturbed habitats on the planet (Barnes, 2017), from frequently iceberg-scoured shallows to seafloor hundreds of kilometres from open water found beneath permanent ice shelves.

1.2.2 Modern benthic habitats

The traditional view of the Southern Ocean benthos was one of an isolated, homogenous, species-poor fauna, constrained by extreme environmental conditions and destructive glacial cycling (Chown et al., 2015). Today, the benthic diversity of the Southern Ocean both known and undescribed is often referred to as 'high' (De Broyer & Danis, 2011; Gutt et al., 2004; Janosik & Halanych, 2010), with over 8,000 nominal species (De Broyer et al., 2014).(Barnes et al., 2009; Clarke et al., 2004) Once thought to be an evolutionary sink due to its isolation and repeated glacial destruction of benthic habitats, there is growing evidence instead for radiations and *in situ* origination in the Southern Ocean in lineages across many taxonomic groups, such as isopods (Held, 2000), crinoids (Wilson et al., 2007), gastropods (Barco et al., 2012; González-Wevar et al., 2017; Wilson et al., 2009), bivalves (González-Wevar et al., 2019), octopus (Strugnell et al., 2008), octocorals (Dueñas et al., 2016) and ophiuroids (O'Hara et al., 2019). Repeated cycles of habitat destruction and reinvasion have in fact been proposed to act as a "biodiversity pump" (Clarke & Crame, 1992), facilitating allopatric speciation through repeated reproductive isolation of populations (Wilson et al., 2007) and may be the driver of several of the radiations cited above.

This revised picture of biodiversity in the Southern Ocean can be largely attributed to numerous sampling campaigns carried out in recent decades, linked to initiatives such as the Census of Marine Life (reviewed in Kaiser et al., 2013) leading to the discovery of many new taxa, particularly for previously unexplored regions such as the deep Southern Ocean (Brandt et al., 2007a). The ANDEEP (Antarctic Deep-sea biodiversity) campaigns sampling 48 stations in the deep Weddell Sea recovered 647 isopod species alone, with over 80% new to science, and reporting similar patterns of diversity and novelty across several other taxonomic groups (Brandt et al., 2007b). Developments in molecular evolutionary studies have also played a major role in recent decades, revealing greater-than expected diversity and significantly advancing our understanding of the evolutionary origins and current biogeographic patterns of Antarctic biota, so that several long-held assumptions and paradigms are beginning to change.

Some molecular phylogeographic investigations are beginning to suggest that the Southern Ocean is not as isolated as previously assumed. Once thought to be an impenetrable barrier, occasional dispersal events across the Antarctic Polar Front (APF) between Sub-Antarctic and Southern Ocean regions long after the formation of the ACC are increasingly being reported (Chown et al., 2015; Galaska et al., 2017b; Sands et al., 2015), though over long evolutionary timescales and with little ongoing gene flow, suggesting that the APF overall remains a relatively effective barrier (see Moon et al., 2017 and references therein). Deep-sea fauna appear to be less affected by such barriers, with colonisation of temperate and tropical ocean basins by Southern Ocean taxa via deep sea routes reported in brittle stars (O'Hara et al., 2019) and several lineages of octopus (Strugnell et al., 2008). Indeed, analyses of extensive regional databases suggest that endemism is somewhat lower than previously thought, with values of 50% endemism now posited for many Antarctic marine groups, versus previous estimations of 70–90% (Griffiths et al., 2009), perhaps reflecting human error or undersampling.

A high prevalence of widespread, 'circum-Antarctic' distributions is another distinct biogeographic pattern long-associated with the Antarctic benthos (Clarke & Johnston, 2003). The ACC and a complex network of other Southern Ocean currents (Figure 1.2) are thought to have a homogenising effect on populations by transporting larvae and adults around the Southern Ocean (Arntz et al., 1994), contributing to the broad circumpolar distributions reported for much of the Antarctic benthos.

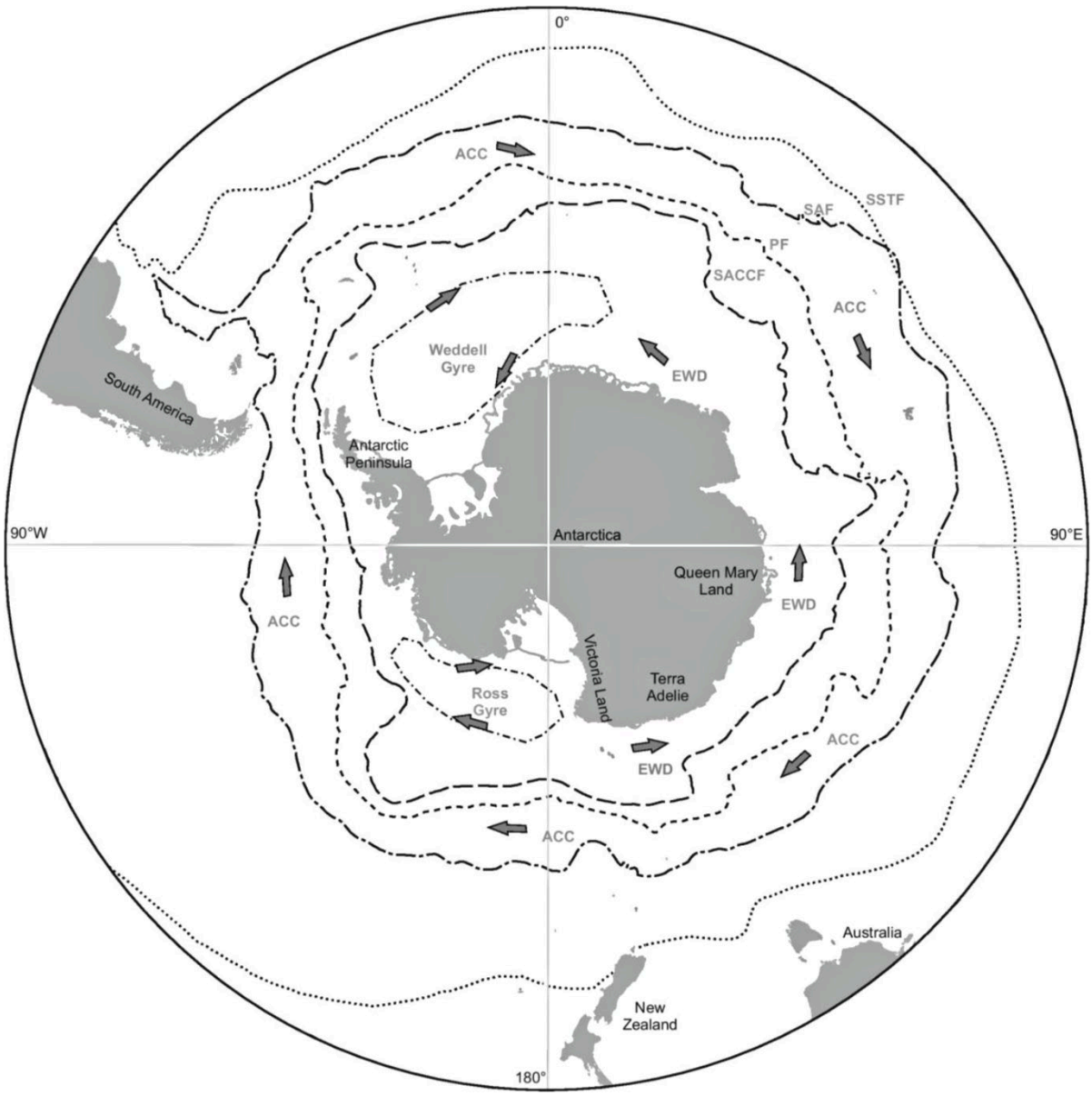

Figure 1.2 Map of major Southern Ocean currents and fronts showing position and direction of Antarctic Circumpolar Current (ACC), East Wind Drift (counter current), Weddell Gyre, Ross Gyre, and the position of the Southern Subtropical Front (SSTF), Subantarctic Front (SAF), Polar Front (PF) and Southern Antarctic Circumpolar Current Front (SACCF). Figure from (Brasier et al., 2017).

However, numerous molecular studies have found evidence of cryptic diversity in previously assumed widespread or circumpolar species, that is, several morphologically similar yet genetically discrete lineages or species, often with much smaller and genetically isolated geographic ranges. This phenomenon has been recorded across a range of taxonomic groups including annelids (Bogantes et al., 2020; Brasier et al., 2016; Neal et al., 2014; Schüller, 2011), amphipods (Baird et al., 2011; Havermans et al., 2011), isopods (Held, 2003; Held & Wägele, 2005; Leese & Held, 2008; Raupach & Wägele, 2006) ostracods (Brandão et al., 2010), pycnogonids (Dietz et al., 2014; Krabbe et al., 2010), crinoids (Hemery et al., 2012; Wilson et al., 2007), ophiuroids (Galaska et al., 2017a; Hunter & Halanych, 2010), bivalves (Linse et al., 2007), cephalopods (Allcock et al., 2011) gastropods (Wilson et al., 2009) and nemerteans (Thornhill et al., 2008).

Similarly, widespread eurybathy (the ability to survive both in shallow and deep waters) is another long held paradigm of the Southern Ocean benthos, posited as an adaptation allowing for survival through glacial cycles via migration to deeper waters during times of glacial maxima (Clarke & Crame, 1989), where grounded ice shelves are estimated to have extended across much of the Antarctic continental shelf (Anderson et al., 2002; Huybrechts, 2002). Movement to and from deeper waters is also facilitated by an isothermal water column. However, cryptic species complexes with restricted depth ranges have been found in many taxa with previously assumed wide bathymetric distributions (see Allcock & Strugnell, 2012) and numerous population genetic analyses have identified molecular signatures more indicative of survival in small ice free refugia on the continental shelf (Allcock & Strugnell, 2012)

The emerging phylogeographic picture is complex; molecular investigations have found that some Antarctic species genuinely do possess widespread distributions, both geographically and bathymetrically (Baird et al., 2012; Brasier et al., 2017; González-Wevar et al., 2010; Hemery et al., 2012; Lau et al., 2021; Mahon et al., 2008; Raupach et al., 2010). Moreover, there does not appear to be a predictable relationship between larval dispersal ability and whether a species displays a widespread or restricted distribution. – within the octopus genus *Pareledone,* species can display patterns either of cryptic or circumpolar distributions, despite sharing a low dispersal reproductive strategy of brooding young and no planktonic larval stage (Allcock et al., 2011; Strugnell et al., 2012). Differences in Southern Ocean species distributions are more likely a result of a complex of factors such as life history, habitat preference, biological responses to environmental factors and both inter and intraspecific ecological reactions, rather than transport capability by oceanographic currents alone (Brasier et al., 2017).

One issue is that the majority of molecular studies of Antarctic benthos to date have used mitochondrial and/or nuclear loci, which lack resolution and precision, often limiting the interpretation of results (Halanych & Mahon, 2018). Additionally, many common marine invertebrate groups such as sponges, cnidarians, and annelids, are poorly represented in molecular studies altogether, reflecting broader sampling gaps and biases (Riesgo et al., 2015). Advances in next generation sequencing methods are facilitating the use of genomic methods in recent studies of population structure, connectivity, and phylogenomic relationships in a small number of Antarctic benthic species at high resolutions (e.g. Galaska et al., 2017a,b; Lau et al., 2023a,b; Leiva et al., 2019, 2022; Moles et al., 2021).

Certain areas of the Southern Ocean, such as parts of the West Antarctic Peninsula or the eastern Weddell Sea, have been heavily sampled to the point that they are considered some of the most well-studied marine areas globally (Clarke, 2008). However, most benthic sampling has been limited to shallow (< 700 m) waters within 150 km of research stations so that much of the Southern Ocean remains completely unexplored, particularly non-shelf areas such as slope and abyssal habitats (Brandt et al., 2014; Griffiths, 2010; Griffiths et al., 2011; Griffiths, et al., 2014). Large regions such as eastern Antarctica and the western Weddell Sea remain poorly sampled, largely due to logistical challenges such as remoteness, a narrow continental shelf, and harsh weather and ice conditions (Halanych & Mahon, 2018).

The seabed beneath floating ice shelves in particular is considered to be one of the last major unexplored habitats on the planet (Kim, 2019). This habitat constitutes over 1.5 million km^2 of Antarctic seafloor yet remains largely inaccessible due to its remoteness and ice-cover up to 1500 m thick (Ingels et al., 2018). While borehole studies have provided glimpses of sub-ice shelf communities, the combined total area observed *in situ* is approximately that of a tennis court (Griffiths et al., 2021). Furthermore, while advances in underwater imagery have provided the greatest insights into our understanding of this habitat, physical samples, which are necessary for species-level identifications, remain extremely challenging to collect.

1.2.3 Southern Ocean annelids

Annelids are amongst the most species rich groups in the Southern Ocean (Clarke and Johnston, 2003), and can represent a dominant component of Antarctic benthic assemblages in terms of both abundance and biomass (e.g. Brandt et al., 2007a; Gambi et al. 1997; Hilbig et al. 2006; Piepenburg et al. 2002; Sañé et al. 2012). According to the Register of Antarctic Marine Species (RAMS), which includes all occurrences south of the Polar Front, there are currently 603 accepted annelid species listed from Antarctic waters (Polychaeta: 549; Oligochaeta: 28; Sipuncula: 15; Echiura 11, De Broyer et al., 2023). Found across the Southern Ocean from intertidal to abyssal depths (Brandt et al. 2009), hydrothermal vent sites (Linse et al., 2019; Rogers et al., 2012) and beneath floating ice shelves, hundreds of kilometres from open ocean (Post et al., 2014; Riddle et al., 2007), annelids fill a diverse array of trophic guilds and functional groups on both hard and soft substrates (e.g. Gambi et al. 1997), and are key group to consider when documenting the biology of Antarctic benthic ecosystems.

As with much of the Antarctic benthos, most Southern Ocean benthic annelid records are limited to a handful of well-sampled regions, such as the western Antarctic Peninsula, and eastern Weddell Sea (Schüller & Ebbe, 2014), with poor sample coverage in other regions such as the western Weddell Sea and East Antarctica. Antarctic annelids are poorly represented in molecular studies and databases relative to other groups such as arthropods or echinoderms (Riesgo et al., 2015). Interestingly , most molecular studies on Antarctic annelids to date have recovered evidence of cryptic genetic diversity in these annelid lineages, independent of morphology (e.g. Bogantes et al., 2020; Brasier et al., 2016; Neal et al., 2014; Schüller, 2011), suggesting that true diversity of Antarctic annelid fauna as we know it today could be greatly underestimated based on morphology alone. However, these results are based on DNA barcodes only, and no genomic level studies have yet been carried out for the phylum in this region.

Southern Ocean annelids appear to display lower endemism and better connectivity to other ocean basins than in other phyla (e.g. Brandt et al., 2007a), with many annelids with non-Southern Ocean type localities reported e.g. (Schüller et al., 2009). Additionally, many Antarctic identification guides are considered out of date (Neal et al. 2018a), and false cosmopolitanism is common in annelids in general (see section 1.1.2). The presence of non-Antarctic species in the Southern Ocean have rarely been tested using either morphological or molecular methods. Another past assumption of Southern Ocean annelids is high eurybathy (e.g. Hilbig, 2004). Molecular investigation found genetic structure by depth in a previously assumed eurybathic annelid (Schüller, 2011), while a large scale comparative morphological study found depth to be a major factor structuring annelid communities, further challenging the prevalent notion of large depth ranges (Neal et al., 2018a).

1.2.4 Anthropogenic threats

Historically, the Antarctic seabed has experienced amongst the least direct anthropogenic impact relative to other marine environments due to its sheer remoteness and isolation (Halpern et al., 2008). However, in the coming decades it is projected that Antarctic biota will be impacted considerably by environmental change and a range of stressors. This includes climate-driven physical changes such as ocean warming, freshening, and acidification, ice loss and changes in perennial sea ice cover, increased disturbance from iceberg scour and sedimentation, alteration of biogeochemical cycles and food webs, and more direct anthropogenic threats such as pollution, fishing, and the introduction of non-native species (reviewed in Gutt et al., 2021 and Rogers et al., 2020).

Anthropogenic climate change is the driver of many of these stressors. In recent decades the Antarctic Peninsula has experienced amongst some of the fastest regional warming on the planet (Vaughan et al. 2003), with substantial increases in both atmospheric and ocean temperatures (e.g. Meredith & King, 2005; Turner et al., 2005; Naughten et al. 2023) These increases are thought to have contributed to the significant thinning, retreat and collapse of ice shelves along the Antarctic Peninsula over the past 60 years (Cook & Vaughan, 2010; Etourneau et al., 2019; Rignot et al., 2013), with significant losses including the collapse of the Larsen A and Prince Gustav Ice Shelves in 1995 (Rott et al., 1996), the Larsen B ice shelf in 2002 (Rack & Rott, 2004) and the calving of a massive 5,800km^2 iceberg from the Larsen C Ice Shelf in 2017 (Marchant, 2017). Considerable warming and ice loss has been projected for parts of Antarctica such as the Amundsen Sea in all future climate scenarios (Naughten et al., 2023). Perennial sea ice has also been impacted, with net overall sea ice extent at record lows in 2016, persisting below long-term averages in years since (Reid et al., 2020). The relationship between sea ice cover, primary production, and resulting downstream effects on pelagic and benthic food webs is very close, and changes in sea ice extent, volume, seasonality, and thickness are expected to have significant impacts across Antarctic marine biotas (Gutt et al., 2021). With the collapse of floating ice shelves, large areas of seabed that existed for thousands of years in oligotrophic conditions without direct primary productivity will be suddenly exposed to massive influxes of phytodetrital input, becoming a more eutrophic benthic system, followed by colonization from non-ice shelf faunas and significant changes in biodiversity at the community level (Gutt et al., 2011). Warming further contributes to accelerated melting of glaciers and grounded ice sheets into the oceans, contributing to ocean freshening, and disturbance in the form of increased sedimentation and iceberg scour (Smale & Barnes, 2008).

Warming poses a further direct threat to the Antarctic benthos as, adapted to temperatures near 0°C, polar marine species display high thermal sensitivity and slow recovery rates, and are amongst the most vulnerable taxa on the planet in terms of responding to changes in environmental temperature (Peck, 2016). Furthermore, lower temperatures facilitate higher solubility of CO_2, which, in combination with regular upwelling of CO_2-eniched waters means that Southern Ocean ecosystems are more at risk from severe ocean acidification than at other latitudes (Fabry et al., 2009). Additionally, warming, combined with a projected increase in tourist activity could facilitate future pole-ward expansion of non-native, potentially invasive species (Chown et al., 2012).

Many Antarctic species have long generation times, slow growth rates, and produce larger but smaller numbers of eggs relative to tropical and temperate taxa, altogether reducing the likelihood that beneficial genetic mutations will arise within the timeframe of current environmental change, and therefore reduces the ability of Southern Ocean biotas to adapt to changing conditions and competition (Peck, 2018).

The high endemism inherent to the Southern Ocean biota means that the loss of a species here often represents a loss on a global scale. Furthermore, the discovery of cryptic species complexes within previously assumed widespread taxa means that we could be significantly underestimating Antarctic biodiversity and could be facing the loss of multiple species before they are even identified (Riesgo et al., 2015).

1.3 Deep-sea benthic ecosystems

1.3.1 Deep-sea floor habitats

The deep-sea floor has been defined as any benthic ecosystem below 1000m depth, comprising most of the world ocean floors and 60% of the entire planetary surface (Glover & Smith, 2003), with 50% of the planet below 3000m and a mean depth of 3800m (Ramirez-Llodra et al., 2010) (Figure 1.3). The deep-sea benthic realm is therefore one of the largest biomes on earth, and includes many habitat types, from rocky sea mounts and volcanic ridges to canyons and trenches, sedimented continental slopes and abyssal plains, cold-water reefs, and unique transient ecosystems such as hydrothermal vents, cold seeps and whale falls (Ramirez-Llodra et al., 2010). Abyssal depths occur between 3000-6000m (Vinogradova, 1997) and abyssal plains (sedimented regions in the centre of oceanic plates) comprise the much of the deep-sea floor. These vast homogenous expanses of sedimented flats and rolling hills dotted with varying densities of seamounts and rocky outcrops (Riehl et al., 2020) or fields of polymetallic nodules (Dutkiewicz et al., 2020) - small mineral accretions that form at the surface of abyssal sediments in some regions.

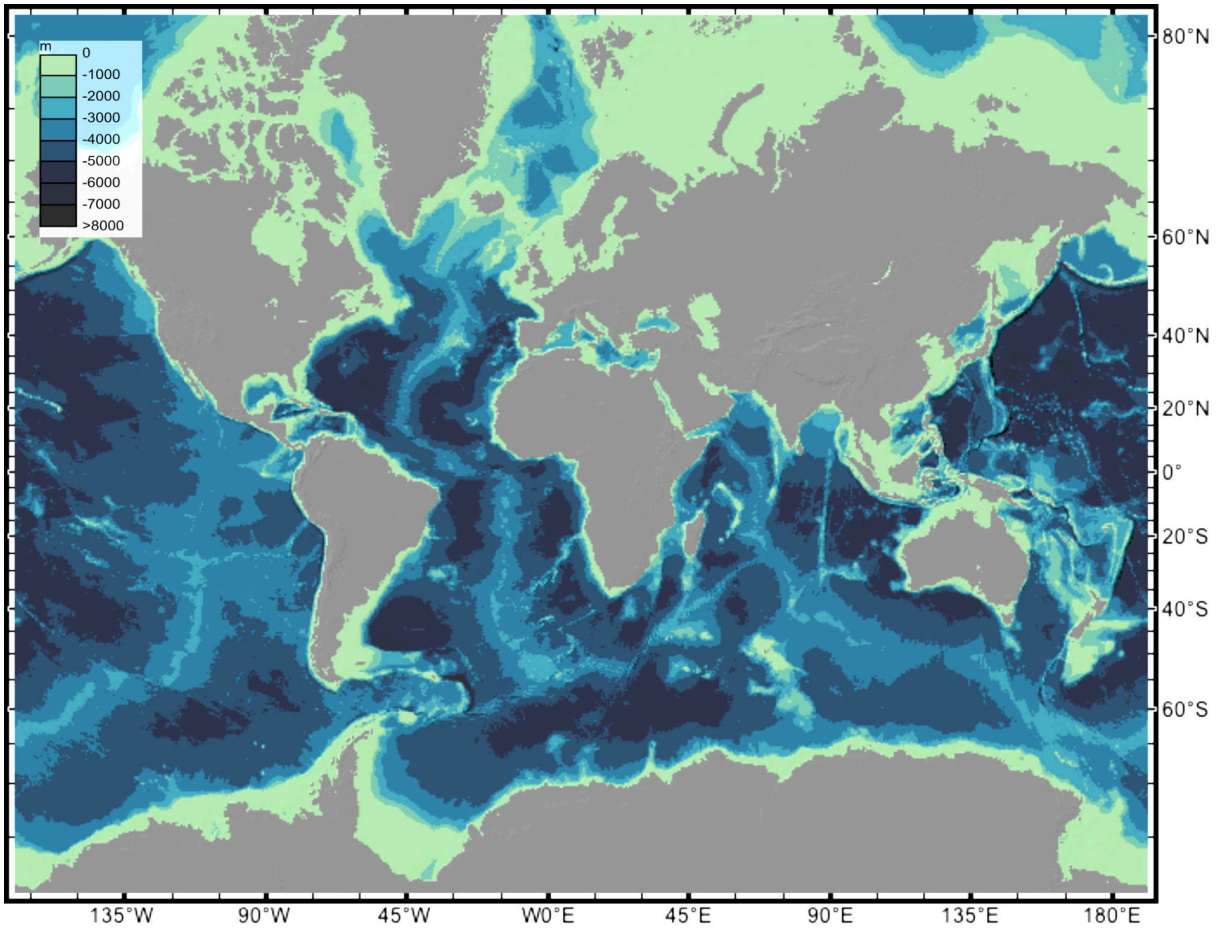

Figure 1.3 Map of the world oceans marked by 1000m depth bins, highlighting the extent of deep sea floor habitat below 1000m. Map made in GeoMapApp v3.7.0.

With the exception of chemosynthesis-based hydrothermal vent and cold seep food chains, most of the energy input depends on a sparse rain of organic detritus from surface waters, typically comprising only a fraction (0.5-2%) of surface net primary production. Input of organic material decreases in quantity with depth (Buesseler et al., 2007) and varies by region (Yool et al., 2007), often ranging from 1-10 grams of organic carbon per m^2 of deep-sea floor per year (Glover & Smith, 2003). This means that most deep-sea ecosystems are extremely food limited, which, in combination with cold temperatures (-1 to 4˚C), result in relatively low rates of growth, reproduction, recruitment and bioturbation (Gage & Tyler, 1991; Smith & Demopoulos, 2003). Deep benthic communities thus often exhibit low population densities and low biomass (Rex et al., 2006) often 0.001-1% of that of shallow water equivalents (Smith & Demopoulos, 2003). Despite this, species richness in deep benthic ecosystems can be remarkably high relative to shallow water equivalents, particularly in soft sediments (e.g. Glover et al., 2002; Grassle & Maciolek, 1992; Hessler & Sanders, 1967; Snelgrove & Smith, 2002) and are considered reservoirs of biodiversity (Bouchet, 2006).

Yet, they are also characterised by low abundances and high rarity, with most taxa often represented by only one or two individuals across deep sea samples, which may partially be a function of incomplete sampling on a regional scale combined with low density (Carney, 1997).

In contrast, hydrothermal vent and cold seep environments display metazoan communities of extremely high biomass and abundances (yet lower diversity) relative to surrounding deep sea habitats, supported by high rates of chemosynthetic primary production from chemicals such as hydrogen sulphide by chemoautotrophic microbes (Van Dover, 2000). Other exceptions to the low biomass rule are found where organic inputs are more abundant, such as the base of marine canyons where organic detritus collects (Vetter & Dayton, 1998), or the sunken carcasses of whales and other large vertebrates that host unique specialised scavenging communities at relatively high densities (Smith & Baco, 2003). However, the exceptions listed above comprise a small fraction of total deep sea marine habitat.

In addition to food limitation, another general factor that characterises many deep-sea environments is low physical energy, such as very slow current speeds (<0.25 knots) and extremely low rates of sedimentation accumulation (0.1–10 cm per thousand years) (Glover & Smith, 2003). Though pulses of organic carbon fluxes, temperature changes, and disturbances such as fast currents and increased rates of sedimentation do occur at local and regional levels over varying temporal scales, deep-sea environments are considered relatively stable over space and time (Smith, 1994). The combination of stability and low energy input has been hypothesised as a possible cause of the high species richness observed in abyssal sediments as a result of extreme niche partitioning in stable environmental conditions over large temporal scales (Sanders, 1968). Polymetallic nodule provinces, where dissolved metals at the sediment water interface of abyssal plains precipitate into potato-sized polymetallic nodules (ferromanganese nodules) at an extremely slow rate of 1-2mm per million years, are possibly the most stable habitats on the planet over geologic time (Glover & Smith, 2003).

Due to sheer size, remoteness and the logistical challenges of sampling at depth, deep-sea ecosystems remain amongst the least explored on the planet with approximately 0.0001% physically sampled or visually observed (Ramirez-Llodra et al., 2010). Though advances in technology such as remotely operated vehicles (ROVs) and autonomous underwater vehicles (AUVs) have contributed to huge progress in recent decades regarding discovering new habitat types (Ramirez-Llodra et al., 2010) and *in situ* observations and collection of epifaunal megafauna (e.g. Amon et al., 2016; Bribiesca-Contreras et al., 2022), these technologies do not capture sediment infauna, a dominant component of deep-sea biotas. Collecting infauna requires sampling equipment such as box, mega, and multi-cores which give quantitative point samples, or trawls that give qualitative samples over a larger range in upper sediment layers.

Of the new eukaryotic marine species described from 2013-2017, only 7% were from depths below 1000m (Bouchet et al., 2023). This reflects the dearth of sampling relative to the size of this biome, with 80-90% of collected benthic deep-sea species often new to science (Glover et al., 2002; Rabone et al., 2023; Snelgrove & Smith, 2002). Though efforts to establish integrative taxonomy using both DNA and morphology for deep sea samples has increased in recent years, most deep-sea species descriptions are based on morphology only (Rabone et al., 2023). Cryptic species appear to be common in the deep sea (e.g. Bonifácio & Menot, 2019; Christodoulou et al., 2019; Knowlton, 1993) suggesting that diversity may be further underestimated where based on morphology alone. The rate of species description for parts of the deep sea are rapidly increasing in certain regions however, particularly the Clarion-Clipperton Zone (CCZ) in the abyssal central Pacific.

The CCZ is a vast region spanning 6 million km^2 that contains high densities of polymetallic nodules (Dutkiewicz et al., 2020) and is a major target for potential seabed mining for its mineral resources. The International Seabed Authority (ISA) regulates the management of this region and mining exploration licences, requiring that biodiversity baseline studies, environmental impact assessments and the establishment of preservation areas are carried out before decisions on whether mining takes place are made (Lodge et al., 2014; Washburn et al., 2021).

The CCZ is an example of how little we know about the diversity of deep-sea habitats. With only seven species described from the CCZ prior to 2000, the new interest in exploration has fuelled biodiversity studies and taxonomic outputs from the CCZ over the past decade, including the description of three new families and 31 new genera and many new species, with 127 of the 185 named species descriptions from the CCZ published in the last five years alone (Rabone et al., 2023). However, this represents only a fraction of the discovered diversity of the CCZ, with 5,142 unnamed species (delineated species without formal names, e.g. morphospecies, molecular taxonomic units etc.) estimated across various studies, and with species accumulation curves from these data not yet reaching asymptote (Rabone et al., 2023). The large proportion of unnamed species is a result of several factors, including sheer taxonomic backlog, with 88-92% of species sampled from the CCZ new to science (Rabone et al., 2023), and small, damaged specimens, often singletons, insufficient for formal description (e.g. Wiklund et al., 2019). Despite the sampling efforts in recent years, most has been concentrated in a small number of mining exploration contracts, with much of the CCZ poorly sampled, including potential no-mining areas (Washburn et al., 2021) making it challenging to carry out regional syntheses, assessments of mining impact, and evaluation of conservation efforts. For example, it is important to understand whether species are truly rare or poorly sampled, as rarity is associated with small species ranges (Pimm et al., 2014) and therefore higher extinction risk where impact occurs.

Furthermore, a lack of formal names makes comparability across studies where samples do exist difficult (i.e. two studies might have different informal names for the same taxon) (Glover et al., 2018). Where named species are established and recorded, the natural history, connectivity and function of a species can be expanded on in further research. For example, based on microsatellite DNA data from the sponge *Plenaster cragi* Lim & Wiklund, 2017 described from the CCZ in 2017 (Lim et al., 2017), authors Taboada et al. (2018a) could examine patterns of genetic connectivity across the CCZ where it has been collected and assess the effectiveness of a potential no-mining zones as genetic reservoirs.

Advances in genomic methods are allowing for high resolution examinations of biodiversity across the deep sea, for example patterns of population structure, dispersal and connectivity in deep sea sponges (Taboada et al., 2022, 2023), crustaceans (Timm et al., 2018; van der Reis et al., 2022; Weston et al., 2022), corals (Bracco et al., 2019), and cephalopods (Timm et al., 2020), in addition to studies of genomic signatures of deep sea adaptations and phyla across a range of groups (Cheng et al., 2019; He et al., 2023; Li et al., 2019; Mu et al., 2018; Thomas-Bulle et al., 2022; Zhang et al., 2021; Zhang et al., 2017).

1.3.2 Deep-sea annelids

With the discovery of unique deep-sea ecosystems such as vents and whale-falls in the late 1970s, specialised deep-sea annelids associated with these habitats such as *Riftia pachyptila* (giant tube worms) and extreme heat tolerating *Alvinella* spp. (Pompeii worms) at vents, or bone eating *Osedax* spp. (zombie worms) on whale falls, have become well known. Where deep-sea annelids truly dominate however are abyssal sedimented habitats, often comprising the bulk of macrofaunal abundance and richness (Brandt et al., 2007a; Glover et al., 2001, 2002; Paterson et al., 1998; Washburn et al., 2021). As with many deep-sea samples, most deep-sea annelids are new to science where collected (Glover et al., 2002; Rabone et al., 2023). Particular taxonomic efforts are being made in the Clarion-Clipperton Zone (CCZ) (see section 1.3.1), with annelids the second-most speciose phylum after Crustacea, and 52 new species and four new genera described from the region in the past seven years (Blake, 2016, 2017, 2019, 2020; Bonifácio & Menot, 2019; Drennan et al., 2021; Maciolek, 2020; Neal et al., 2022a, 2022b; Paterson et al., 2016; Wiklund et al., 2019). Yet, >80% of CCZ annelids remain undescribed (Rabone et al., 2023), and many CCZ annelid species that have been delimited by molecular and morphological means are unable to be formally described owing to specimen damage and often small number of individuals, with 215 species published as informal species (Neal et al., 2022a,2022,b,2023; Wiklund et al., 2019, 2023) that contain preliminary descriptions and corresponding imagery and DNA vouchers to facilitate future research.

Of the 52 formally described CCZ annelids, only 35 are described using an integrative approach (i.e. using morphology and DNA, rather than just morphology) (Bonifácio & Menot, 2019; Drennan et al., 2021; Neal et al., 2022a, 2022b; Wiklund et al., 2019). With a recent molecular study finding high diversity in CCZ annelids based on molecular delimitation methods (Stewart et al., 2023), this suggests that diversity based on morphology alone may be underestimated.

With most deep-sea annelids remaining undescribed, it is difficult to assess factors such as ecology, life history and distribution at the species level. Abyssal annelid abundance and familial composition appears to vary at regional scales based on particulate organic carbon (POC) flux (e.g. Glover et al., 2002; Stewart et al., 2023; Washburn et al., 2021). Inferences on ecological functional group can be extrapolated from known feeding guilds at the family level (Jumars et al., 2015) to give insight into ecosystem dynamics across abyssal environments (e.g. detrivore dominated annelid fauna at one site vs predator scavenger dominated at another, e.g. Stewart et al., 2023).

Species range appears to vary considerably in deep-sea annelids from thousands of kilometres to many taxa only being found at a single site (e.g. Stewart et al., 2023). Differences in species ranges are likely to be based on reproductive mode, though apparent small ranges may also be a function of incomplete sampling (Washburn et al., 2021). Reproductive mode is variable in deep-sea annelids, ranging from free swimming, long lived planktonic larvae, hypothesised to explain genuine pan-oceanic distributions in some deep-sea taxa (e.g. Guggolz et al., 2020), to those that brood eggs on their body (e.g. Fukuda & Barroso, 2019) and have in theory a more limited distribution ability. However, reproductive mode remains unknown for most deep-sea annelids at the species level.

1.3.3 Anthropogenic threats

Though the depth, size and remoteness of the deep ocean floor has protected it from direct human impacts in the past relative to other marine ecosystems (Glover & Smith, 2003; Halpern et al., 2008), the number of threats both direct and indirect that the deep seas are facing is increasing. Though the cold, stable waters of the deep sea have traditionally been seen as decoupled from the dynamism of surface waters (Smith et al., 2008b), contemporary anthropogenic climate change is already impacting this biome, with increases in temperature (Purkey & Johnson, 2010), deoxygenation (Helm et al., 2011; Keeling et al., 2009; Stramma et al., 2010), acidification (Byrne et al., 2010), and alterations to particulate organic carbon (POC) input (Ruhl & Smith, 2004; Smith et al., 2013) recorded for deep waters. Abyssal ocean temperatures are projected to increase by 1°C by 2100 (Sweetman et al., 2017). As well as increasing thermal stress on cold-adapted deep-sea fauna, warming has a number of knock-on effects as briefly listed above.

Warmer temperatures reduce the solubility of O_2 in water and are also likely to amplify thermal stratification and density gradients in the ocean. These combined factors are likely to create widespread reduction in dissolved O_2 for large parts of the ocean, a phenomenon already being observed, with the majority of oxygen loss projected to occur in the deep ocean below 2000m (Oschlies, 2021). The global oceans also act as a natural sink for increasing levels of atmospheric CO_2, which decreases water pH and therefore facilitates ocean acidification. Decreasing pH lowers the calcium carbonate saturation point of colder waters, threatening shell-building organisms such as molluscs, echinoderms, deep-water corals, and some tube building annelids (Ramirez-Llodra et al., 2011 and references therein). Acidification has also been found to reduce the number of viable eggs, and slow embryo growth and development in *Ophryotrocha* sp. annelids (Verkaik et al., 2017). The carbonate compensation depth (CCD) is a deep-water layer below which calcium carbonate is undersaturated, placing constraints on fauna dependent on calcareous structures. This layer is also predicted to shallow with climate change (Sulpis et al., 2018) - this has implications for abyssal plain biodiversity as the depth of the CCD is known to be a major driver of biogeographical patterns of megafaunal assemblages in the CCZ (Simon-Lledó et al., 2023).

Climate change is further predicted to substantially change biogeochemistry and primary production at the surface, altering the quantity and quality of organic carbon to the deep-sea floor. Temperature increases and ocean stratification will reduce nutrient upwelling, therefore reducing primary production capacity, while also facilitating a shift from diatoms and large zooplankton communities at the surface with high POC export efficiencies, to picoplankton and microzooplankton assemblages, which have a poorer POC export capacity to the deep sea (see Smith et al., 2008). The overall result will be reduced food input to an already food limited ecosystem and likely a corresponding loss in deep sea biomass (Smith et al., 2008b).

More direct human impacts such as historical and present-day pollution and contamination are becoming more apparent (e.g. radioactive, pharmaceutical, chemical, organic, industrial – see Ramirez-Llodra et al., 2011). Deep sea sediments are also a major sink for microplastic debris (Woodall et al., 2014), while large debris (metal, glass, and plastic litter etc.) have been observed across deep-sea benthic habitats (Amon et al., 2020; Chiba et al., 2018). This includes the deepest reaches of the ocean with a plastic bag found at the bottom of the Mariana Trench 10,898m deep (Chiba et al., 2018). The effects of litter pollution in the deep sea are not well understood, but range from the entanglement of fauna to the leaching of toxic chemicals, and disturbance of soft sediment benthos (Amon et al., 2020; Jamieson & Onda, 2022).

Human exploitation of deep marine resources includes deep water trawling and long line fishing, and oil and gas drilling (see Ramirez-Llodra et al., 2011); one of the most overt potential impacts, commercial seabed mining, though not currently permitted, may take place in the near future if regulations are enacted (Blanchard et al., 2023). Three types of deep-sea mineral resources are targeted for potential mining, cobalt-rich crusts on seamounts, polymetallic sulphide deposits formed at hydrothermal vent sites, and polymetallic nodules on abyssal plains (Weaver & Billett, 2019). Environmental impacts of deep-sea mining are likely to be variable. For example, nodules are often the only hard substrate for kilometres in sedimented abyssal plain environments, increasing habitat heterogeneity and supporting encrusting fauna such as sponges and corals, as well providing microhabitats within nodule crevices (Mullineaux, 1987; Thiel et al., 1993). Mining of nodules would remove a habitat type within the mined area and therefore hard-substrate dependent species and functional groups, while sediment plumes from mining activity could clog the feeding apparatus of suspension feeders outside the direct path of mining, and bury and dilute organic carbon relied on by detrivores (Glover & Smith, 2003; Jumars, 1981; Thiel, 1992). Though significant efforts have been made to establish and understand ecological baselines for regions potentially targeted by seabed mining, such as the Clarion Clipperton Zone abyssal central Pacific, large data gaps and taxonomic backlogs remain (see section 1.3.1), and the extent of impacts and ecosystem recovery remain uncertain (Washburn et al., 2019).

1.4 Rationale and aims

Using benthic annelids as a model group, this thesis aims to investigate biodiversity at various hierarchical levels in Southern Ocean and deep-sea habitats, from species to community level, local to regional, and comparing morphological, genetic, and genomic methods. The Southern Ocean and the Deep Sea can be seen as two end members in terms of marine ecosystems, with the Southern Ocean defined by its dynamic tectonic and glacial history, extreme seasonality, high productivity, disturbance, and isolation, while the deep oceans of the world are more characterised by (with exceptions) limited food and low energy, connectivity and homogeneity over large spatial scales, and environmental stability over large temporal scales. Deep, dark, cold and diverse, both share ecological similarities too, with both remaining amongst the closest we have to pristine marine ecosystems and thus should be high priorities for conservation. However, the scale and remoteness that have protected these ecosystems from many direct anthropogenic impacts in the past have also made documenting their biodiversity challenging. As both direct and indirect anthropogenic threats increase for both ecosystems, there is an urgent need to build an accurate baseline understanding of these ecosystems and their diversity to evaluate threats, monitor change, and inform conservation efforts.

The thesis is structured into four data chapters, followed by a final chapter comprising a synthesis and conclusion, as follows:

- The first data chapter describes a new species of widespread deep-sea annelid from the abyssal central Pacific using both morphological and molecular data, highlighting polymetallic nodules as a unique microhabitat, and the value of comprehensive integrative taxonomic description.

- The second data chapter documents the annelid community of a deep, previously ice-covered channel on the Antarctic Peninsula – the Prince Gustav Channel. Using morphological-level identifications, this study gives first insights into the biodiversity of this previously unsampled channel, highlighting a functionally and spatially heterogeneous benthic community in a dynamic habitat with continuing glacial influence in a region already affected by climate change.

- The next chapter builds on this Prince Gustav Channel dataset, testing whether sequencing DNA barcodes for subset of representative morphospecies from the previous chapter significantly improves morphological species identifications in relation to species richness and diversity of the channel community. This study found that the resolution from barcode genes was insufficient to significantly change overall biodiversity metrics, instead with strengths as an error check for morphological identifications, improving identification, particularly of damaged specimens, and highlighting potential cryptic diversity for further study.

- The final data chapter returns to the species level and is the first genomic level study of a Southern Ocean annelid using Single Nucleotide Polymorphism (SNP) data. The nephtyid annelid *Aglaophamus trissophyllus*, is a widespread, circumpolar Antarctic species with previous barcode studies finding several potentially cryptic lineages. SNP data generated from *A. trissophyllus* samples spanning much of the species' distributional range are used to resolve genetic lineages, finding support for at least two, recently diverged putative species. Complex patterns of population structure and connectivity across the Southern Ocean are also investigated.

- The synthesis chapter compares results and discusses the strengths, weaknesses and synergy of different methods for measuring Southern Ocean and deep-sea benthic biodiversity in the in the context of a global taxonomic impediment.

Chapter 2 *Neanthes goodayi* sp. nov. (Annelida, Nereididae), a remarkable new annelid species living inside deep-sea polymetallic nodules

REGAN DRENNAN [1,2], HELENA WIKLUND [2,3,4], MURIEL RABONE [3], MAGDALENA N. GEORGIEVA [3], THOMAS G. DAHLGREN [3,4,5] & ADRIAN G. GLOVER [1]

[1] Ocean & Earth Science, University of Southampton, European Way, Southampton SO14 3ZH, UK

[2] Life Sciences Department, Natural History Museum, London SW7 5BD, UK

[3] Department of Marine Sciences, University of Gothenburg, Box 463, 40530 Gothenburg, Sweden

[4] Gothenburg Global Biodiversity Centre, Box 463, 40530 Gothenburg, Sweden.

[5] NORCE Norwegian Research Centre, Bergen, Norway

Abstract A new species of abyssal *Neanthes* Kinberg, 1865, *N. goodayi* sp. nov., is described from the Clarion-Clipperton Zone in the central Pacific Ocean, a region targeted for seabed mineral exploration for polymetallic nodules. It is a relatively large animal found living inside polymetallic nodules and in xenophyophores (giant Foraminifera) growing on nodules, highlighting the importance of the mineral resource itself as a distinct microhabitat. *Neanthes goodayi* sp. nov. can be distinguished from its congeners primarily by its distinctive, enlarged anterior pair of eyes in addition to characters of the head, pharynx and parapodia. Widespread, abundant, and easily recognisable, *N. goodayi* sp. nov. is also considered to be a suitable candidate as a potential indicator taxon for future monitoring of the impacts of seabed mining.

Keywords CCZ, molecular phylogeny, Polychaeta, morphology, abyssal fauna.

Study published as:

Drennan R, Wiklund H, Rabone M, Georgieva MN, Dahlgren TG. & Glover AG (2021) *Neanthes goodayi* sp. nov. (Annelida, Nereididae), a remarkable new annelid species living inside deep-sea polymetallic nodules. *European Journal of Taxonomy* 760: 160–185. https://doi.org/10.5852/ejt.2021.760.1447 [1]

[1] Chapter presented as published in Drennan et al. (2021a). Updates and corrections since publication are presented as footnotes.

2.1 Introduction

Exploration of our deep oceans for potential new industrial activities has increased rapidly in recent decades with the so-called 'blue growth' economy (European Commission, 2020). Critical to a sustainable blue economy is baseline knowledge on the environmental characteristics of these exploration areas, in particular knowledge of the species that live there (Glover et al., 2018). This is especially the case in the central Pacific abyss Clarion-Clipperton Zone (CCZ), a region targeted for seabed mineral exploration for polymetallic nodules, where basic faunistic and taxonomic data are notably lacking and many animals likely undescribed or undocumented (Glover et al., 2018). Here, we describe a new nereidid annelid from the abyss that is not only important for understanding the general baseline biology of the region, but also presents a remarkable natural history – living inside the polymetallic nodules themselves. As the species is relatively large and easy to recognise, it should be added to a list of nodule-dwelling fauna that could be used as indicators in future environmental assessments (Lim et al., 2017). Information on the existence, abundance and distribution of these species could be essential to environmental monitoring and conservation measures in the region.

The CCZ lies in international waters and lacks strictly defined boundaries; however, it is generally accepted to encompass the region between the Clarion and Clipperton Fracture Zones, with multiple polymetallic nodule exploration contracts for seabed minerals issued by the International Seabed Authority (ISA, 2018), extending from 115° W (the easternmost extent of the UK-1 polymetallic nodule exploration area) to approximately 158° W (the westernmost extent of the COMRA polymetallic nodule exploration area). As such, we hereafter use a working definition of the CCZ as comprising the box: 13° N, 158° W; 18° N, 118° W; 10° N, 112° W; 2° N, 155° W – an area spanning almost 6 million km2, approximately 1.4% of the ocean's surface.

Polymetallic nodules are small mineral accretions (usually 5–10 cm in diameter, but occasionally exceeding 20 cm) rich in cobalt, manganese, copper and nickel, among numerous other metals of economic interest (Hein et al., 2013). These nodules sit on the sea floor, often half submerged in sediment, providing the only hard substrate in an otherwise soft sediment environment, contributing to a high habitat heterogeneity compared with regions of the deep sea without nodules or hard substrate. Nodules provide microhabitats for meio- and macrofaunal groups such as annelids and crustaceans (Gooday et al., 2017; Kersken et al., 2019; Thiel et al., 1993), in addition to sites of attachment for sessile megafauna (e.g., *Relicanthus* sp. anemones) (Amon et al., 2016).

Nereididae de Blainville, 1818 is among the most diverse families within Annelida, with over 40 valid genera and up to 750 valid species (Read & Fauchald, 2020b). Members of the family are broadly omnivorous, and most species appear to be facultatively motile, rarely leaving mucus-built tubes and burrows unless disturbed or when conditions become unfavourable (Fauchald & Jumars, 1979; Jumars et al., 2015). Sexually mature individuals may develop into pelagic morphs (epitokes), which are thought to have much greater motility. However, not all nereidids form epitokes during reproduction, and not all epitokes are pelagic, with the degree of modification varying between species and sexes (Bakken & Wilson, 2005).

The genus *Neanthes* Kinberg, 1865 is one of the most diverse genera within the family, with over 80 currently accepted species (Read & Fauchald, 2020a) and can be distinguished from similar genera such as Hediste Malmgren, 1867 and Nereis Linnaeus, 1758 by morphological characters primarily relating to the presence or absence of certain chaetal types, for example in lacking compound falcigers in notopodial fascicles (as in Nereis), but possessing homogomph spinigers in ventral neuropodial fascicles (absent in *Hediste* and *Nereis*) (Bakken & Wilson 2005). However, *Neanthes* is considered to be polyphyletic (Bakken & Wilson, 2005) and a generic revision based on phylogenetic analyses is needed to resolve its taxonomy (Bakken, 2006; Bakken & Wilson, 2005; Glasby et al., 2011; Shimabukuro et al., 2017; Villalobos-Guerrero, 2019). The majority of species of *Neanthes* have been described from shallow or intertidal waters, with only 13 species reported from depths greater than 200 m (Hsueh, 2019; Khlebovich, 1996; Shimabukuro et al., 2017). Notably, Thiel et al. (1993), when examining nodules collected from the South Pacific (outside of the CCZ) as part of the DISCOL project, reported two unidentified species of *Neanthes* when first describing polymetallic nodule crevices as a discrete microhabitat; these were among six annelid taxa that were only found within interstitial mud from nodule crevices, and not from the surrounding soft sediment.

In this study, we describe a new species of abyssal *Neanthes* observed to reside either directly within nodule crevices, within mud balls on nodule surfaces or burrowing within xenophyophores (giant foraminiferans) growing on nodules. This species is notable in that it highlights the potential importance of nodule microhabitats for macrofaunal-sized animals, and is also one of the most abundant and widespread annelid species collected as part of the ABYSSLINE ('ABYSSal baseLINE') UK-1 environmental survey project. Easily recognisable, it is a critical 'target taxon' for further assessments of biogeography and population connectivity patterns, the subject of a separate study (Dahlgren et al., unpublished data)[2].

[2] Study now published as Stewart et al. 2023.

2.2 Materials and Methods

2.2.1 Fieldwork

Specimens were collected across two cruises, the first UK Seabed Resources ABYSSLINE cruise (AB01) sampling the UK-1 exploration contract area aboard the RV Melville, October 2013, and the second cruise (AB02) sampling the UK-1 and OMS (Ocean Mineral Singapore) exploration contract areas as well as an area to the north designated as Area of Particular Environmental Interest 6 (APEI-6) onboard RV Thomas G. Thompson, February–March 2015 (Figure 2.1). A comprehensive description of the DNA taxonomy methodological pipeline used here is provided in Glover et al. (2016). In summary, a range of oceanographic sampling gear, including box corer, epibenthic sledge (EBS), ROV and multiple corer, were used to collect deep-sea benthic specimens from the UK-1, OMS and APEI-6 areas. Geographic data from sampling activities were recorded on a central GIS database. A 'cold-chain' pipeline was used in the live-sorting of specimen samples aboard both vessels, where material was constantly maintained in chilled, filtered seawater held at 2–4 °C. Specimens underwent preliminary identification at sea and were live-imaged using digital cameras attached to stereo microscopes (Glover et al., 2016). All specimens were then stored in individual microtube vials containing an aqueous solution of 80% non- denatured pre-chilled ethanol, which were numbered, barcoded into a database and stored chilled until return to the Natural History Museum, London, UK.

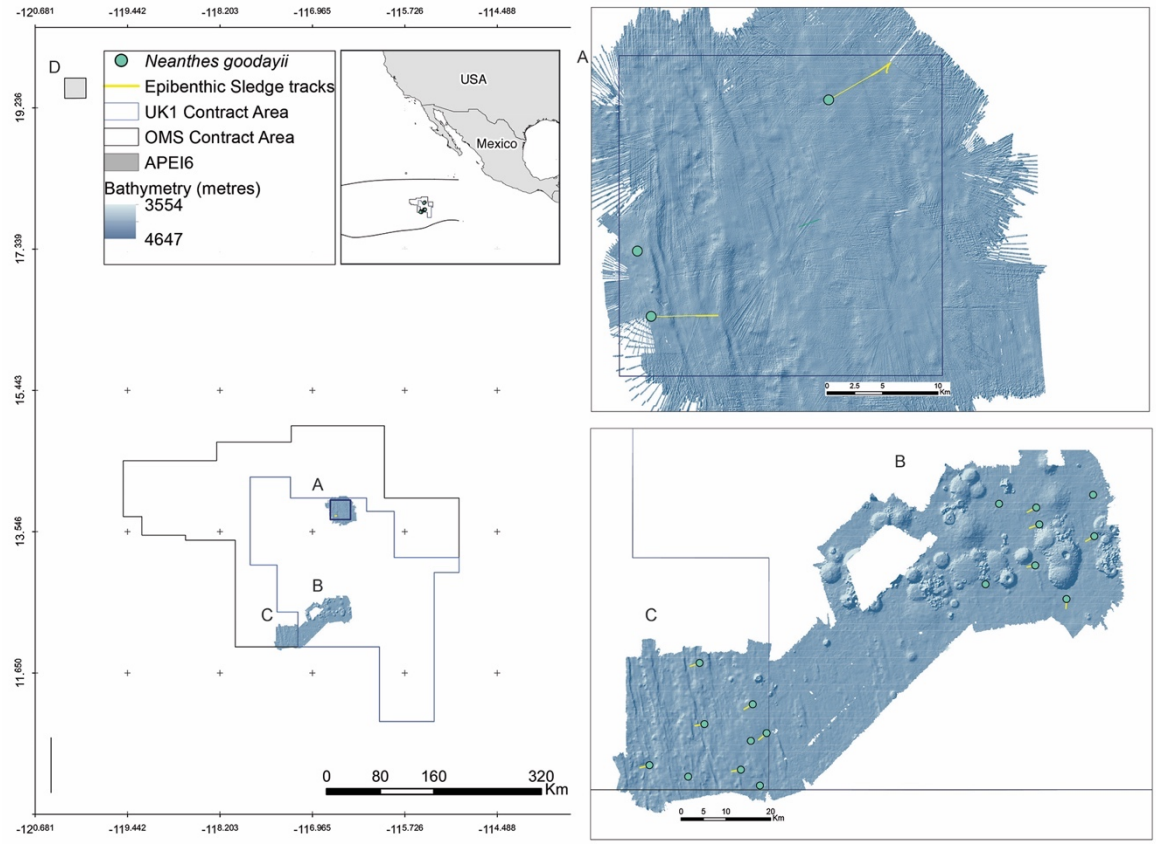

Figure 2.1 Sampling sites, showing occurrences of *Neanthes goodayi* sp. nov. A. UK-1 Stratum-A study area within the UK Seabed Resources UK-1 exploration contract area. B. UK-1 Stratum-B study area within the UK Seabed Resources UK-1 exploration contract area. C. OMS Stratum-A study area, in the Ocean Mineral Singapore (OMS) polymetallic nodule exploration contract area. D. Area of Particular Environmental Interest APEI-6. Inset map showing location of Clarion-Clipperton Fracture Zone in the Central Eastern Pacific. Bathymetric survey data and sampling localities from the AB01 2013 RV Melville survey cruise (MV1313) and AB02 2015 RV Thomas G. Thompson survey cruise (TN319); data courtesy of Craig R. Smith (University of Hawaii), UK Seabed Resources Ltd. and Seafloor Investigations, LLC.

2.2.2 Laboratory work

A total of 43 specimens were identified as conspecific using genetic data (see below) and considered in morphological analyses, with a portion of representative specimens selected as type material for more detailed analyses.

Specimen measurements taken included total length (TL), length to chaetiger 15 (L15), width of chaetiger 15 excluding parapodia (W15), and the total number of chaetigers for complete specimens. Paragnaths for each pharangeal area were counted, with paired areas that differed in numbers distinguished using a and b for the left and right side of the specimen respectively. The number of teeth on the jaws were also counted. For specimens where the pharynx was not everted, a longitudinal dissection was made in the mid-ventral region.

For examination of parapodial features and modifications along the body, several parapodia were removed (from chaetigers 1, 3, 6, 10, every tenth chaetiger thereafter, and a posterior- most chaetiger, where possible) and mounted on glass slides. Parapodia were dissected from either the left or right side of the specimen based on intactness of features such as cirri.

Specimens were examined using compound and light microscopes, and photographed using attached digital cameras on both microscopes. Figures were assembled using Adobe Photoshop CS6 software. A fine white or black line was used to outline and highlight particular morphological features where they were unclear from the images alone. Standardised terminology of nereidid parapodial features follows Villalobos-Guerrero & Bakken (2018); the shape of pharangeal areas and ridge patterns follows Villalobos-Guerrero (2019).

A small tissue sample was taken from each specimen for DNA extraction. The DNeasy Blood and Tissue Kit (Qiagen) was used to extract DNA using a Hamilton Microlab STAR Robotic Workstation. Approximately 1800 bp of 18S rRNA (18S) were amplified using the primers 18SA 5'-AYCTGGTTGATCCTGCCAGT-3' (Medlin et al., 1988) and 18SB 5'-ACCTTGTTACGACTTTTACTTCCTC-3' (Nygren & Sundberg, 2003). Around 450 bp of 16S rRNA (16S) were amplified using the primers ann16Sf 5'-GCGGTATCCTGACCGTRCWAAGGTA-3' (Sjölin et al., 2005) and 16SbrH 5'-CCGGTCTGAACTCAGATCACGT-3' (Palumbi, 1996), and around 650 bp of cytochrome c oxidase subunit I (COI) were amplified using LCO1490 5'-GGTCAACAAATCATAAAGATATTGG-3' (Folmer et al., 1994) and COI-E 5'-TATACTTCTGGGTGTCCGAAGAATCA-3' (Bely & Wray, 2004). PCR mixtures contained 1 µl of each primer (10 µM), 2 µl template DNA and 21 µl of Red Taq DNA Polymerase 1.1X MasterMix (VWR) in a total mixture of 25 µl. The PCR amplification profile consisted of initial denaturation at 95°C for 5 min, 35 cycles of denaturation at 94°C for 45 s, annealing at 55°C for 45 s, extension at 72°C for 2 min and a final extension at 72°C for 10 min. PCR products were purified using the Millipore Multiscreen 96-well PCR Purification System and sequencing was performed on an ABI 3730XL DNA Analyser (Applied Biosystems) at the Natural History Museum Sequencing Facility, using the same primers as in the PCR reactions plus two internal primers for 18S, 620F 5'-TAAAGYTGYTGCAGTTAAA-3' (Nygren & Sundberg, 2003) and 1324R 5'-CGGCCATGCACCACC-3' (Cohen et al., 1998). Overlapping sequence fragments were merged into consensus sequences using Geneious (Kearse et al., 2012). The sequences obtained in this study were aligned together with sequences from Genbank (Table 2.1) using MAFFT (K. Katoh, 2002) for 18S and 16S, and MUSCLE (Edgar, 2004) for COI, both programs used as plugins in Geneious, with default settings. The 18S alignment consisted of 1819 characters, 16S of 514 characters and the COI alignment of 657 characters.

Table 2.1 List of taxa used in phylogenetic analyses with respective NCBI GenBank accession numbers.

Taxon name	GenBank accession numbers		
	18S	16S	COI
Alitta succinea (Leuckart, 1847)	AY210447	KT959483	KT959389
*Alitta virens (*M. Sars, 1835)	Z83754	---	AF221572
Ceratocephale abyssorum (Hartman & Fauchald, 1971)	GQ426585	GQ426618	---
Ceratocephale loveni Malmgren, 1867	DQ442616	DQ442614	---
Ceratonereis longiceratophora Hartmann-Schröder, 1985	AB106251	---	AY583701
Dendronereis aestuarina Southern, 1921	KT900288	---	---
Dendronereis sp. CUGD1	KF586536	---	---
Dendronereis sp. CUGD2	KF586537	---	---
Hediste atoka Sato & Nakashima, 2003	LC323073	AB703090	AB603842
Hediste diadroma Sato & Nakashima, 2003	LC323646	LC323062	---
Hediste diversicolor (O.F. Müller, 1776)	LC381864	LC323090	KR916844
Hediste japonica (Izuka, 1908)	LC323647	LC323064	AB603758
Hediste limnicola (Johnson, 1903)	LC381865	LC323068	---
Namalycastis abiuma group sp. MM-2010	HQ157237	HM138705	JQ081269
Namalycastis hawaiiensis (Johnson, 1903)	LC213729	LC213728	---
Namalycastis jaya Magesh, Kvist & Glasby, 2012	HQ157238	HM138706	HQ456363
***Neanthes goodayi* sp. n. (NHM_171)**	**this study**	**this study**	**this study**
***Neanthes goodayi* sp. n. (NHM_173)**	**this study**	**this study**	**this study**
Neanthes acuminata isolate ABF1	---	KJ538978	KJ539071
Neanthes acuminata isolate LAF1	---	KJ538984	KJ539083
Neanthes acuminata isolate NPF5	---	KJ538994	KJ539092
Neanthes acuminata isolate POF6	---	KJ538966	KJ539101
Neanthes acuminata isolate VLF1	---	KJ538969	KJ539128
Neanthes cf. *glandicincta* (Southern, 1921)	---	LC323071	LC323035
Neanthes fucata (Savigny, 1822)	---	---	KR916874
Neanthes meggitti (Monro, 1931)	---	MF959006	MF958994
Neanthes shinkai Shimabukuro, Santos, Alfaro-Lucas, Fujiwara & Sumida, 2017	---	---	LC331618
Neanthes sp. LH-2011	---	---	JF293305
Neanthes wilsonchani Lee & Glasby, 2015	---	MF850380	MG251655
Nectoneanthes oxypoda (Marenzeller, 1879)	KX290701	---	---
Neogyptis carriebowcayi Pleijel, Rouse, Sundkvist & Nygren, 2012	JN631338	JN631325	JN631315
Neogyptis fauchaldi Pleijel, Rouse, Sundkvist & Nygren, 2012	JN631339	JN631326	JN631316
Neogyptis hinehina Pleijel, Rouse, Sundkvist & Nygren, 2012	JN631340	JN631328	JN631317
Nereididae sp. MB-2010	GQ426586	---	---
Nereis heterocirrata Treadwell, 1931	KC840697	KC833487	GU362684
Nereis pelagica Linnaeus, 1758	AF474279	AY340470	HM473499
Nereis sandersi Blake, 1985	AM159579	---	---
Nereis vexillosa Grube, 1851	DQ790083	GU362677	HM473511
Perinereis aibuhitensis (Grube, 1878)	KC840692	KC833485	JX503021
Perinereis cultrifera (Grube, 1840)	KJ182978	KC833495	KR916911
Perinereis mictodonta (Marenzeller, 1879)	---	KC833496	KC800632
Perinereis nuntia (Lamarck, 1818)	---	LC482156	MH337359
Perinereis wilsoni Glasby & Hsieh, 2006	KC840691	KC833494	KC800623
Platynereis australis (Schmarda, 1861)	KT900290	---	---
Platynereis dumerilii (Audouin & Milne Edwards, 1833)	AY894303	KP640622	KC591838
Pseudonereis sp. pse179	KT900283	---	---
Pseudonereis variegate (Grube, 1857)	KC840693	KC833493	HQ705183

In total 47 terminal taxa were used in the phylogenetic analyses, with 44 from Nereididae, and three taxa from Hesionidae Grube, 1850, another family within Nereidiformia, as the outgroup. While some earlier studies suggest that Chrysopetalidae Ehlers, 1864 is sister taxon to Nereididae (Dahlgren et al., 2000), later analyses have indicated that the Nereidiformia relationships are unresolved (Weigert & Bleidorn, 2016), which justify the use of Hesionidae as the outgroup here. The program jModelTest (Posada, 2008) was used to assess the best model for each partition (18S, 16S and COI) with BIC, which suggested GTR + I + G as the best model for all genes. The data was partitioned into the three parts (18S, 16S and COI) and this evolutionary model was applied to each partition. The parameters used for the partitions were unlinked. Bayesian phylogenetic analyses (BAs) were conducted with MrBayes ver. 3.2.6 (Ronquist et al., 2012) (Ronquist et al. 2012). Analyses were run three times for 10 000 000 generations. Of these, the first 2 500 000 generations were discarded as burn-in. Tree files were interpreted with FigTree ver. 1.4.2 (available from http://tree.bio.ed.ac.uk/software/figtree/).

2.2.3 Data management

The management and transfer of specimen data between a central museum database, a molecular collections database, and external data repositories and aggregators (e.g., GenBank, World Register of Marine Species (WoRMS), Ocean Biodiversity Information System (OBIS), Global Biodiversity Information Facility (GBIF), Global Genome Biodiversity Network (GGBN), and ZooBank) was carried out through the usage of DarwinCore data standards (Wieczorek et al., 2012) including the GGBN DarwinCore extensions (Droege et al., 2016). See Glover et al. (2016) for further elaboration of this data pipeline. All specimens and DNA vouchers are archived in the Natural History Museum London collections. All specimen occurrence (and associated preparation) data are provided in a DarwinCore Archive (DWcA) at the following DOI: https://doi.org/10.5852/ejt.2021.760.1447.4755 [3].

All mapping was carried out using ArcGIS ver. 10.2.2.

2.2.4 Institutional abbreviations

NHMUK = Natural History Museum, London

ZMH = Zoological Museum Hamburg

[3] Online electronic supplementary file DOI from Drennan et al. 2021a

2.3 Results

2.3.1 *Neanthes goodayi* sp. nov.

Phylum Annelida Lamarck, 1809

Class Polychaeta Grube, 1850

Order Phyllodocida Dales, 1962

Family Nereididae Blainville, 1818

Neanthes Kinberg, 1865

Neanthes Kinberg, 1865: 171.

Neanthes – Fauchald 1977: 89. —Wilson 1984: 210; 1988: 5). — Wu et al. 1985: 143–144. — Bakken & Wilson 2005: 527. — Glasby et al. 2011: 363. —Sato 2013: 35. — Ibrahim et al. 2019: 85.

Type species

Neanthes vaalii Kinberg, 1865 by subsequent designation (Hartman 1954:27). Southern Australia.

Neanthes goodayi sp. nov.

urn:lsid:zoobank.org:act:C5CDA152-0C73-46BB-955F-9BD5F02BE0F6

Figures 2.2–2.6, 2.8

2.3.2 Diagnosis

Anterior eye pair very large, distinct, posterior eyes minute. Posterio-dorsal tentacular cirri reaching chaetigers 8–12. Two pigmented spots on dorsum of apodous segment. Palpostyles and palpophores rounded, spherical to ovoid. Paragnaths in pharangeal areas: I = 1–2 , II = 9–12, III = 6, IV = 12–16, V = 0, VI = 1–4, VII-VIII = 12–19; area VI–I–VI pattern λ-shaped on oral ring. Chaetigers 1–2 uni- ramous, remaining chaetigers biramous. Parapodial lobes conical, becoming narrower in posterior chaetigers. Neuracicular postchaetal lobe longer than or equal to neuraciular ligule on anterior chaetigers, shorter on medial chaetigers, papilliform or absent on posterior chaetigers. Dorsal cirri exceed length of ligules on anterior chaetigers, as long as or slightly shorter than ligules on medial chaetigers, becoming longer and exceeding ligules towards posterior end; on largest specimens, dorsal cirri exceed ligules on all chaetigers. Notochatae with homogomph spinigers throughout, supraciular nerurochaetae with homogomph spinigers and heterogomph falcigers throughout, subacicular neurochaetae with homogomph spinigers, homogomph falcigers and heterogomph falcigers throughout.

2.3.3 Etymology

Named in honour of Andy Gooday, member of the science party of both ABYSSLINE cruises. This etymology is part of the ABYSSLINE naming convention where all new taxon names are based on a randomised list of both crew and scientists of the two research cruises in order to recognise the team effort involved in this extensive sampling program (Wiklund et al., 2019).

2.3.4 Material examined

Specimen data, e.g. collection information and GenBank accession numbers, is included as supplementary materials in Appendix A section A.1

2.3.5 Comparative material examined

2.3.5.1 Holotype of *Neanthes heteroculata* (Hartmann-Schröder, 1981)

ATLANTIC OCEAN • North-eastern Atlantic, Bay of Biscay; 46°35.0’ N, 7°45.5’ W; depth 4700 m; 24 Oct. 1967; ZMH P-16464.

2.3.5.2 Paratypes of *Neanthes heteroculata* (Hartmann-Schröder, 1981)

ATLANTIC OCEAN • 2 specs; same collection data as for preceding; ZMH P-16465.

2.3.6 Description

Holotype (NHM_739) complete, TL = 12 mm, L15 = 4.7 mm, W15 = 0.9 mm, for 47 chaetigers. Body somewhat 'baseball bat-shaped', wide, swollen anteriorly but tapering gradually posteriorly (Figure 2.2 A–B). Live specimen pale, iridescent and semi-translucent, with yellow gut and red blood vessels visible through body wall (Figure 2.2 A, C); specimen in ethanol opaque, pale beige, with some red vasculature still visible (Figure 2.2 B, D). Two pigmented spots on either side of dorsum of apodous segment visible in both live specimens and in ethanol, with some pigmentation also visible on dorsum of antero- dorsal tentacular cirrophores (Figure 2.2 C–D).

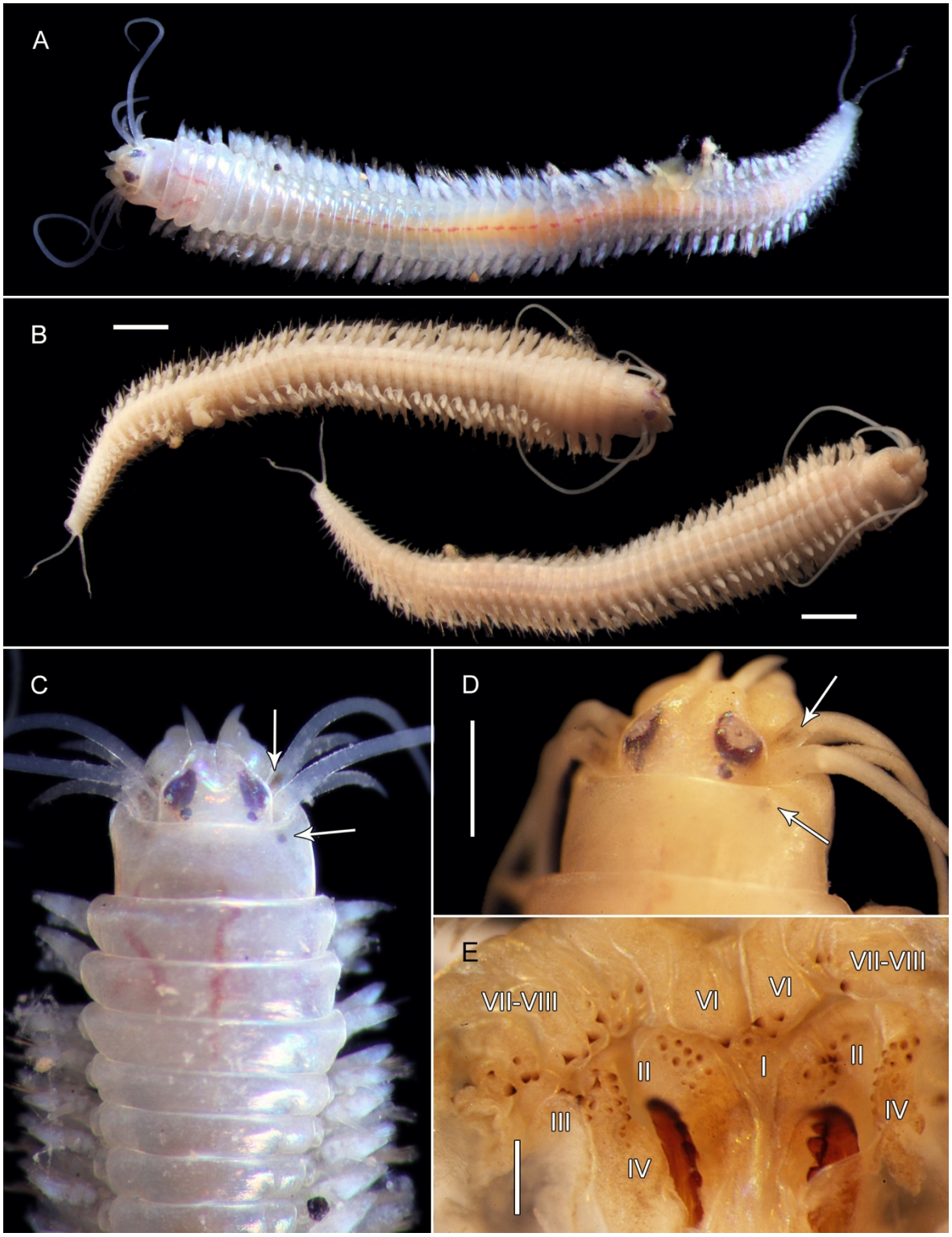

Figure 2.2 *Neanthes goodayi* sp. nov., holotype (NHM_739). **A**. Live image, entire specimen. **B**. Preserved entire specimen, dorsal view (left), ventral view (right). **C**. Live image, anterior view, arrows mark pigmentation. **D**. Preserved specimen, anterior view, arrows mark pigmentation. **E**. Dissected pharynx, with pharyngeal areas I, II, III, IV, VI, VII–VIII highlighted. Scale bars: B = 1 mm; D = 500 µm; E = 250 µm.

Prostomium short, rounded trapezoid with shallow dorsal depression extending anteriorly from midpoint to distal margin (Figure 2.2 C–D); antennae cirriform, medium-sized, barely extending beyond palps. Palps nearly as long as prostomium, with both palpophores and palpostyles short, spherical, with palpostyles half as long as palpophores. Tentacular cirri with short, cylindrical cirrophores; posterior-dorsal pair of tentacular cirri longest, extending to chaetiger 12 (Figure 2.2 A–B). Two pairs of dark red eyes; anterior pair very large, rounded teardrop-shaped, with large, rounded lenses inserted anterolaterally and with an iris- like structure visible in preserved specimen (Figure 2.2 C); posterior pair of eyes minute, rounded, with small anterolateral lenses. Apodous anterior segment collar-like, slightly longer and narrower than chaetiger 1.

Pharynx not everted. Jaws dark red-brown with 6 lateral teeth; All paragnaths brown, conical, arranged as follows (Figure 2.2 E): area I: 2, one large cone, one smaller cone distally; area II: 12 in cluster; area III: approx. 6 (area damaged), four cones in row with two smaller cones laterally; area IV: 13 in teardrop- shaped cluster, with curved line of cones extending from jaws posteriorly, ending in cluster of 7 cones; area V: no paragnaths; area VIa: 1; area VIb: 4, one large and three smaller cones in trapezoid arrangement; areas VII–VIII: 19, eight large cones in a single well-spaced row with 11 smaller cones scattered laterally. Areas VI–V–VI with λ-shaped ridge pattern.

Chaetigers 1 and 2 uniramous, with all subsequent chaetigers biramous.

Dorsal cirri inserted at base of median and dorsal ligule in uniramous and biramous chaetigers, respectively, slightly inflated on uniramous chaetigers (Figure 2.3 A), more slender from chaetiger 3 onwards (Figure 2.3 B–H); dorsal cirri extending beyond median ligule on anteriormost chaetigers (Figure 2.3 A–B), as long as or slightly shorter than median ligules from chaetiger 6 onwards (Figure 2.3 C–D) and extending beyond median ligules from around chaetiger 29 (Figure 2.3 E), up to twice as long as median ligules on posterior chaetigers from chaetiger 40 (Figure 2.3 G–H).

Dorsal ligule conical throughout, slightly shorter than median ligules on anterior chaetigers (Fig. 3B–C), approximately two-thirds the length of median ligules from chaetiger 10 onwards. Dorsal and median ligules reduced in size on posterior chaetigers from chaetiger 40, with dorsal ligule vanishing in posteriormost chaetigers (Fig. 3H). Median ligule slightly inflated on uniramous chaetigers (Figure 2.3 A), conical on biramous chaetigers, narrower from chaetiger 29 (Figure 2.3 E), bluntly conical on posteriormost chaetigers (Fig. 3H). Notopodial prechaetal lobe indistinct.

Neuracicular ligule shorter than ventral neuropodial ligule on anterior chaetigers (Figure 2.3 A–C), becoming equal in length or slightly shorter from chaetiger 10, equal or slightly longer from chaetiger 29 (Figure 2.3 E). Superior neuropodial lobe indistinct, truncate throughout; inferior lobe short, rounded on anterior and medial chaetigers, gradually shortening, giving neuracicular ligule pointed appearance on posterior chaetigers (Figure 2.3 G–H). Neuracicular prechaetal lobe indistinct.

Neuracicular postchaetal lobe conical, longer than neuracicular lobe on anteriormost chaetigers (Figure 2.3 A–B), equal in length at chaetiger 6 (Figure 2.3 C), gradually shortening and becoming more digitiform on subsequent chaetigers to papilliform nub around chaetiger 29 (Fig. 3F), absent in posterior chaetigers from around chaetiger 40.

Ventral neuropodial ligule conical throughout, gradually narrowing on medial (Fig. 3E) and posterior chaetigers (Figure 2.3 G–H). Ligule sub-equal in length to median ligule in anterior and early medial chaetigers (Figure 2.3 A–D), becoming shorter in remaining chaetigers from chaetiger 29 (Figure 2.3 E), to two-thirds as long as ligule from chaetiger 40 (Fig. 3G) and half as long on posteriormost chaetigers (Figure 2.3 H).

Ventral cirri cirriform (Figure 2.3 C–F), inserted basally to ventral neuropodial ligule throughout, slightly shorter than ligule on anterior and medial chaetigers, subequal in length on posteriormost chaetigers (Figure 2.3 F).

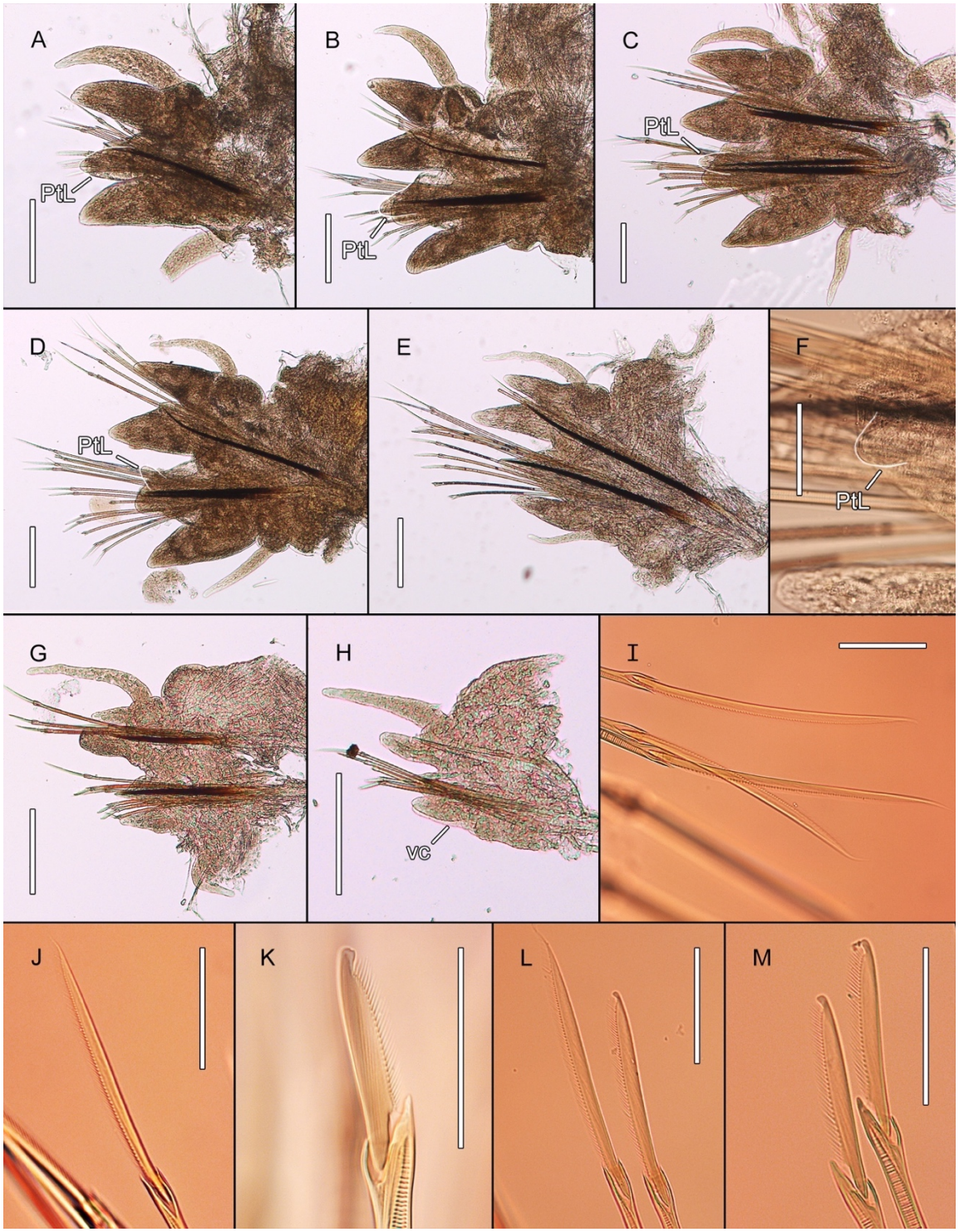

Figure 2.3 *Neanthes goodayi* sp. nov., holotype (NHM_739). **A**. Chaetiger 1, posterior view. **B**. Chaetiger 3, posterior view. **C**. Chaetiger 6, posterior view. **D**. Chaetiger 20, posterior view. **E**. Chaetiger 29, posterior view. **F**. Chaetiger 29, posterior view, detail of neuracicular postchaetal lobe. **G**. Chaetiger 40, posterior view. **H**. Chaetiger 46, posterior view. **I**. Notochaetae, detail of homogomph spinigers, chaetiger 20. **J**. Supraciular neurochaetae, detail of homogomph spiniger, chaetiger 3. **K**. Supracicular neurochaetae, detail of heterogomph falciger, chaetiger 10. **L**. Subacicular neurochaetae, detail of homogomph spiniger (left) and homogomph falciger (right), chaetiger 20. **M**. Subacicular neurochaetae, detail of heterogomph falcigers, chaetiger 20. Abbreviations: PtL = postchaetal lobe; VC = ventral cirrus. Postchaetal lobe in A–D, F outlined with a fine white line. Parapodia in C, E–H dissected from left side of specimen; parapodia in A–B, D dissected from right side of specimen, with images laterally inverted follow direction of other plates. Scale bars: A–E, G–H = 200 µm; F, I–M = 50 µm.

Pygidium somewhat pyriform, truncate distally, with two filamentous anal cirri attached ventro-laterally, extending 8 chaetigers in length (Figure 2.3 A–B). Caecal glands present, small, white, slightly thickened. Multiple aciculae per parapodial lobe observed on some chaetigers in holotype: double neuraciculae in chaetigers 2, 3, 6 and 20 (Figure 2.3 B–D), and triple notoaciculae on chaetiger 6 (Figure 2.3 C). This feature was not observed in parapodial dissections from paratypes.

Notochaetae all homogomph spinigers with long blades, of similar width towards toothed edge but drastically slendering to an aristate distal end (Figure 2.3 I); 4 present in anterior chaetigers, 5 in medial chaetigers, 3 in posterior chaetigers and absent from chaetiger 46.

Supracicular neurochaetae with homogomph spinigers and heterogomph falcigers, both types present in all falcigers except final two chaetigers, where supracicular falcigers are absent. Homogomph spinigers similar in appearance to those of notopodia (Figure 2.3 J), though with blades reducing in length moving ventrally (shortest blades two-thirds as long as longest blade), numbering 4 on first two chaetigers, 3–5 on anterior and medial chaetigers and 2 on posterior chaetigers where fascicles remain. Heterogomph falcigers with knob-like tips (Figure 2.3 K) and blades roughly half the length of shortest spinigers, numbering 1 on anterior chaetigers, 2 on medial chaetigers and 1 on posterior chaetigers where fascicles remain.

Subacicular neurochaetae with homogomph spinigers and both homogomph and heterogomph falcigers. Homogomph spinigers also similar in appearance to those of notopodia (Fig. 3L) but with blades two- thirds as long and numbering 1–2 on all chaetigers. Homogomph falcigers with knob-like tips (Fig. 3L), blades three-quarters the length of spinigers (Figure 2.3 L), numbering 1–3 on all chaetigers. Heterogomph falcigers similar in appearance to those of supracicular fascicles (Figure 2.3 M), numbering 3 on first two chaetigers, 4–6 on anterior, 2–4 on medial and 2–3 on posterior chaetigers.

2.3.7 Variations

Largest specimen (paratype NHM_2069) damaged, in two parts, TL = 17 mm, L15 = 6.7 mm, W15 = 1 mm for 55 chaetigers. Smallest specimen (paratype NHM_127) with TL = 1 mm for 10 chaetigers (see Juveniles section below). Pigment spots on dorsum as in holotype, consistent across most specimens both live and preserved (Figure 2.4 A–D), pigmentation on tentacular cirrophores more variable. Palpophores spherical to ovoid in shape (e.g., Figure 2.4 B). Posterior-dorsal pair of tentacular cirri extending to chaetiger 8–12 in most specimens (max. chaetiger 6 in juveniles). Eyes dark red to purple, anterior pair ranging from circular/ovoid (Figure 2.4 B–D) to teardrop-shaped concave discs or deeper cups (Figure 2.4 A, Figure 2.5 A), becoming more crescent-shaped with decreasing size (Figure 2.5 B–D); posterior pair mostly circular (Figure 2.4 A–B), but occasionally oblong (Fig. 4A) or seeming to fuse with anterior pair (Figure 2.6 A–B), or with one missing (Figure 2.4 D).

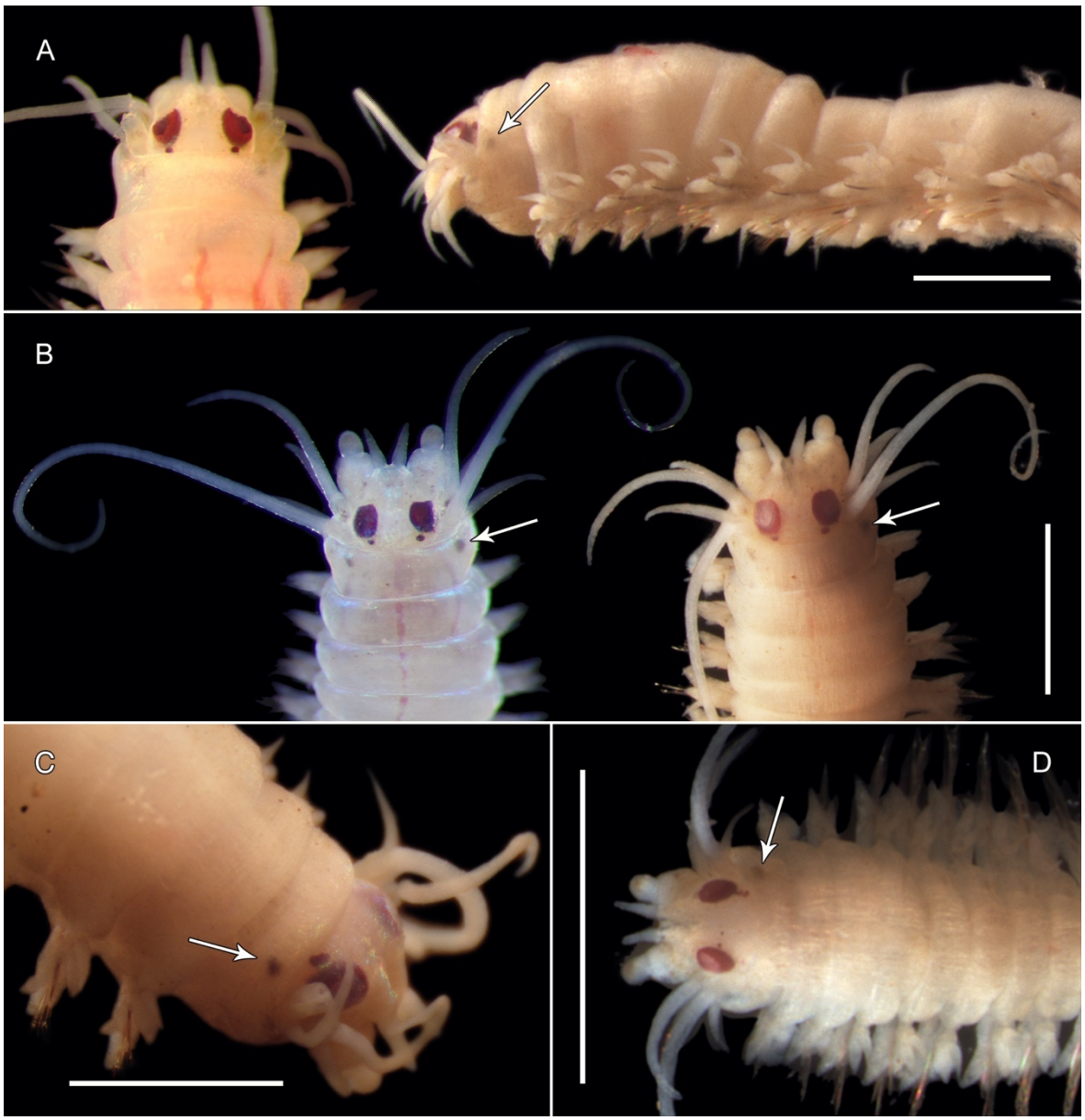

Figure 2.4 *Neanthes goodayi* sp. nov., paratypes. **A**. Paratype (NHM_1624), preserved specimen; dorsal anterior view, live image (left); lateral anterior view, preserved specimen (right). **B**. Paratype (NHM_755); dorsal anterior view, live image (left), preserved specimen (right); arrows marking pigmentation. **C**. Paratype (NHM_238), dorsal anterior view, arrows mark pigmentation. **D**. Paratype (NHM_512), dorsal anterior view, arrows mark pigmentation. Scale bars = 1 mm.

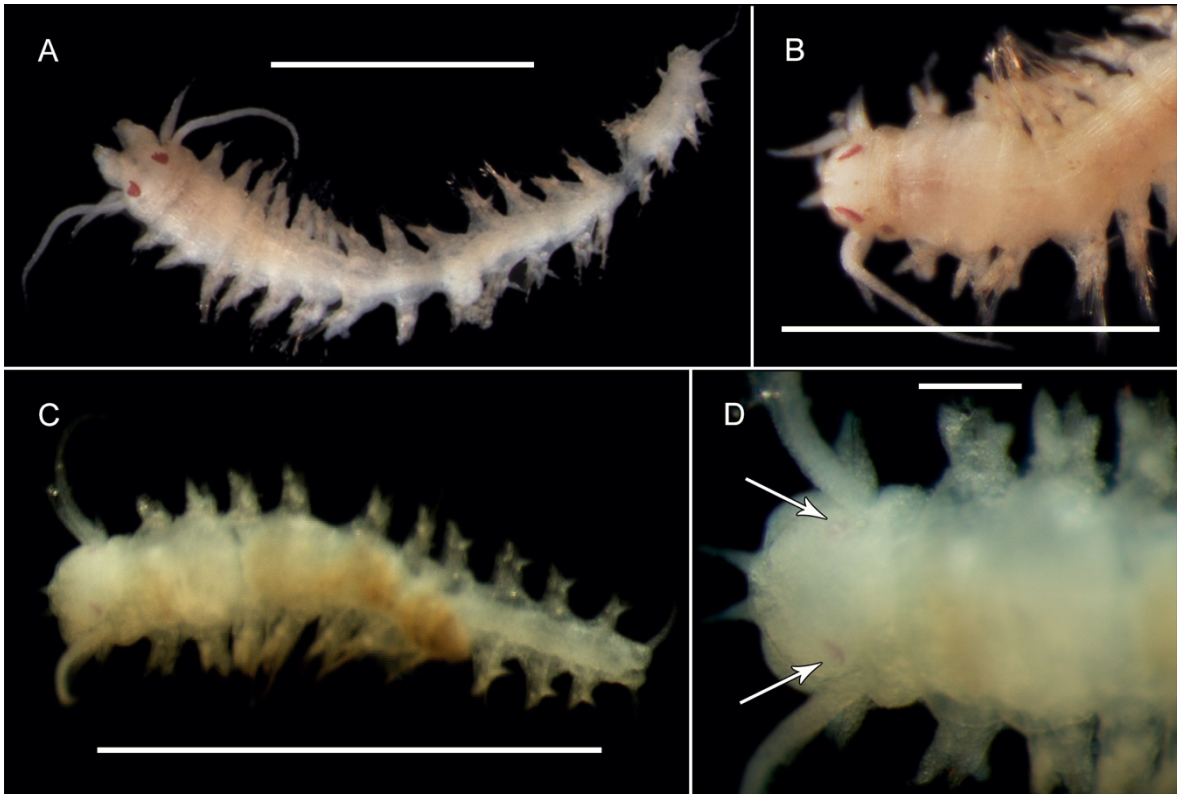

Figure 2.5 *Neanthes goodayi* sp. nov., juvenile specimens. **A**. Paratype (1254), entire specimen, dorsal view. **B**. Paratype (NHM_171) dorsal anterior view. **C**. Paratype (NHM_127) entire specimen, dorsal view. **D**. Paratype (NHM_127), close up of dorsal anterior, arrows mark position of anterior eye pair. Scale bars: A, C = 1 mm; B = 500 µm; D = 100 µm.

Posterior eye pair often less distinct in smaller specimens (Figure 2.5 A–B), becoming tiny spots (Figure 2.5 A) or patchy and irregularly shaped (Fig. 5B), completely absent in smallest specimens (Figure 2.5 C–D), with trace of lens not obvious. Apodous anterior segment longer and narrower than chaetiger 1, as in holotype, to similar in length and width as chaetiger 1 (Figure 2.4 A–D). J

Jaws with 6–7 lateral teeth; paragnaths in pharangeal areas in non-holotype specimens: I = 1–2, II = 9–12, III = 6, IV = 12–16, V = 0, VI = 2–3, VII–VIII = 12–17 (8 large cones in a row as in holotype, varying number of smaller cones scattered laterally). Only one specimen (epitoke male, paratype NHM_1783) with pharynx everted (Figure 2.6 B).

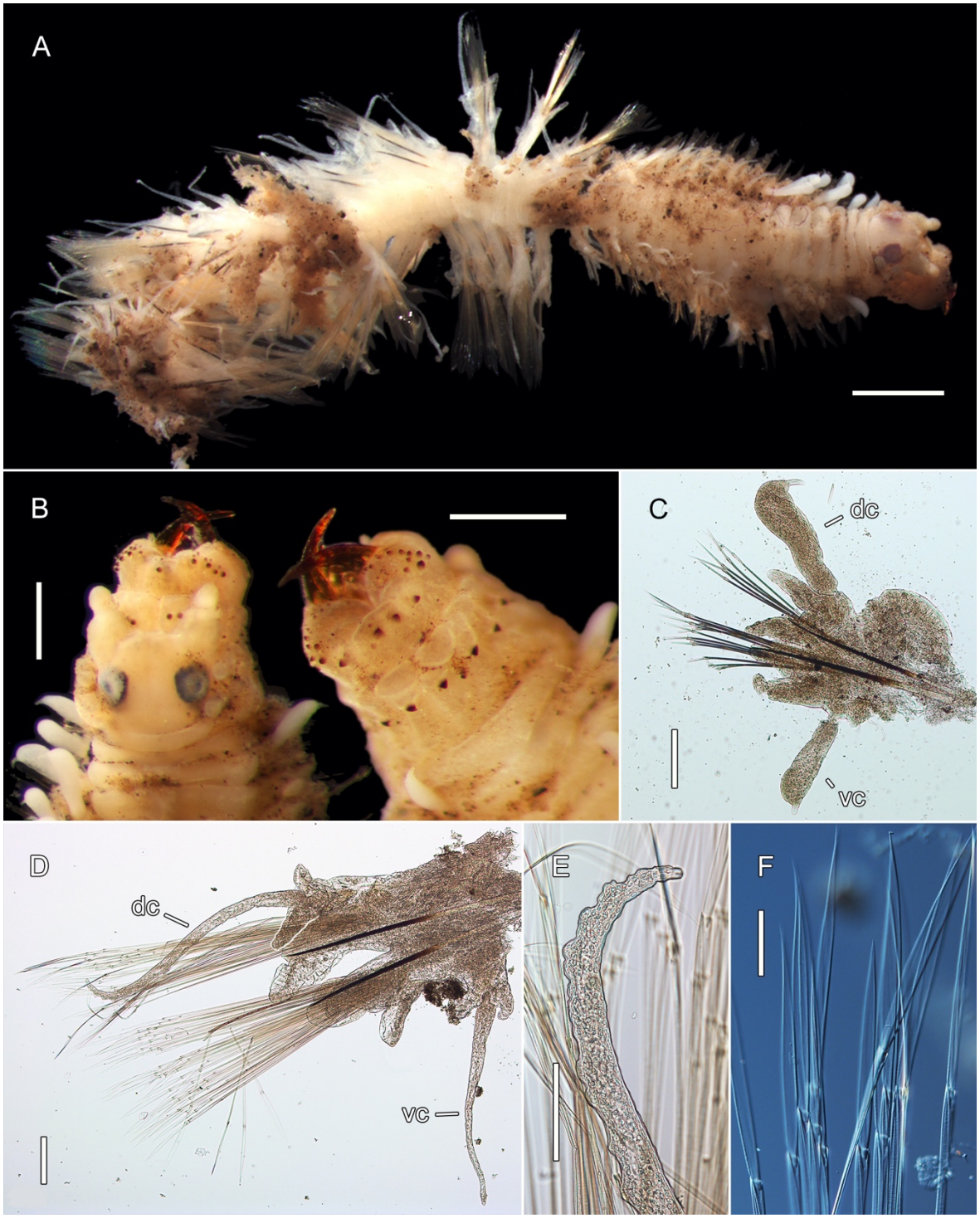

Figure 2.6 *Neanthes goodayi* sp. nov., epitoke paratype (NHM_1783), preserved specimen. **A**. Entire specimen, dorsal view. **B**. Extruded pharynx, dorsal view (left), ventral view (right). **C**. Detail of pre- natatory parapodium 4, with modified dorsal and ventral cirri, posterior view. **D**. Detail of modified natatory swimming parapodium, chaetiger 31, posterior view. **E**. Detail of papillated dorsal cirrus, chaetiger 31, posterior view. **F**. Modified swimming spinigers, subacicular neurocheatal fascicle, chaetiger 32. Abbreviations: DC = dorsal cirrus; VC = ventral cirrus. Lobe at base of dorsal cirrus in D and E outlined with a fine white or black line. Parapodium in C dissected from left side of specimen; parapodium in D dissected from right side of specimen, with images D and E laterally inverted to follow direction of other plates. Scale bars: A = 1 mm; B = 500 µm; C–D = 200 µm; E = 100 µm; F = 50 µm.

In largest specimen, dorsal cirrus exceeds median ligule on all chaetigers, neuracicular ligule remains slightly longer than ventral ligule on median and posterior chaetigers, prechaetal lobe remains as visible papilliform process on posterior chaetigers, ventral ligule subequal to ventral ligule from medial chaetigers onwards and ventral cirri longer than ventral ligule on posteriormost chaetigers.

Numbers of chaetae greater for most fascicles in largest specimen: notochaetae 6 homogomph spinigers on anterior and medial chaetigers, 4 in posterior chaetigers, 1 in posteriormost chaetigers; supracicular neurochaetae with 5–7 homogomph spinigers on first two chaetigers, 2–4 on anterior and medial chaetigers, 1 on posterior chaetigers, heterogomph falcigers 3 on first two chaetigers, 4–6 on anterior chaetigers, 0–3 on medial chaetigers and 1 on posterior chaetigers; subacicular neurochaetae with 2–4 homogomph spinigers most chaetigers, 1 on posteriormost chaetigers, homogmph falcigers 3–5 on anterior chaetigers, 1–2 on medial chaetigers, 1 on posterior chaetigers, heterogomph falcigers 6–9 on anterior chaetigers, 1–3 on medial and posterior chaetigers.

2.3.8 Description of epitoke paratype

One epitokous specimen observed (paratype NHM_1783) (Figure 2.6 A). Specimen moderately damaged, posteriorly incomplete, TL= 10 mm, L15 = 4 mm, for 37 chaetigers (chaetiger 15 damaged, width at chaetiger 14 excluding parapodia 0.8 mm). Body divided into two regions: pre-natatory with 14 chaetigers and natatory with at least 23 chaetigers; post-natatory region unknown. Eyes not notably modified (Figure 2.6 A–B); anterior pair with iris-like structure as in holotype, posterior pair somewhat fused to anterior pair.

Pre-natatory chaetigers with modified dorsal and ventral cirri on chaeigers 1–7; notably thickened, but with distalmost tip remaining fine and cirriform (Figure 2.6 C). Chaetal types in pre-natatory chaetigers as in holotype.

Natatory chaetigers with distinctly enlarged, elongate modified parapodia (Fig. 6D). Noto- and neuropodia elongated basally, with ligules and lobes not significantly larger than on non-modified parapodia. Neuracicular ligule with lamellar structure distally. Both dorsal and ventral cirri notably elongate, with a pair of conical lobes emerging from the upper and lower base of each cirrus, not present on anterior chaetigers; dorsal cirri slightly papillated (Figure 2.6 D–E). Both notopodial and neuropodial fascicles dense, up to 40 chaetae per fascicle, and with only a single chaetal type: long, simple sesquigomph spinigers with ensiform (knife-shaped) blades (Fig. 6F). No gametes observed, though the presence of slightly papillated dorsal cirri on natatory chaetigers suggests that this specimen is a male (Read, 2007).

2.3.9 Juveniles

Several small, possibly juvenile specimens were observed; paratypes NHM_127, NHM_171, NHM_1254, TL = 1.0–2.5 mm, L15 = max. 2.2 mm, W15 = max. 0.2 mm, 10–18 chaetigers (Fig. 5A–D). Posterio-dorsal tentacular cirri extending to chaetiger 6. Eyes poorly developed in these specimens, with anterior eye pair observed only as faintly pigmented crescents (Figure 2.5 B–D), lenses not obvious; posterior eye pair not visible in smallest specimens (Figure 2.5 C–D). The identity of these specimens was confirmed with genetic data. Due to their size and the delicate nature of specimens, pharyngeal and parapodial dissections were not conducted to preserve specimen integrity.

2.3.10 Genetic data

All 43 individuals were sequenced for 16S and COI. The gene 16S was successfully sequenced in all but six specimens. COI sequencing was less successful; however, each specimen had coverage of at least one of the two genes. All specimens formed a single clade with low intraspecific divergence. Several specimens were also sequenced for 18S in order to assess deeper taxonomic relationships. This species was genetically distinct from all other species included in our phylogenetic analyses, and forms the basal branch of a clade including *Neanthes fucata* (Savigny, 1822) and five species of *Perinereis* Kinberg, 1865 (Figure 2.7).

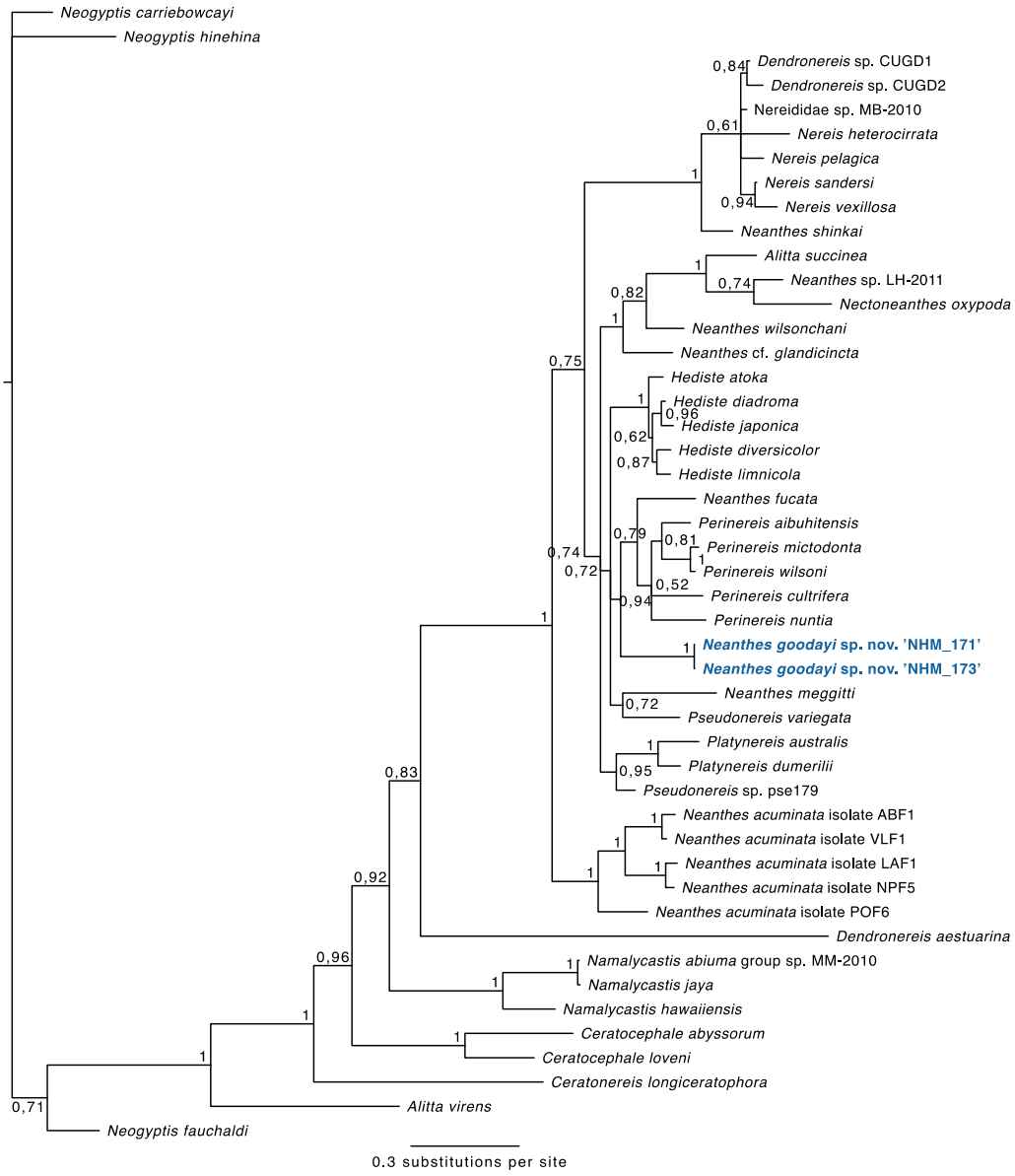

Figure 2.7 Phylogenetic analysis of Nereididae Blainville, 1818. 50% majority rule tree from the Bayesian analyses using 18S, 16S and COI, with posterior probability values on nodes. Forty-five taxa from GenBank were included, using three taxa from another family within Nereidiformia, Hesionidae Grube, 1850, as outgroup.

2.3.11 Remarks

This species is most consistent with the genus *Neanthes* Kinberg, 1865, most recently defined by Ibrahim et al. (2019). Previous analyses based on morphological parsimony suggested that neither of the three most species-rich nereidid genera, *Neanthes*, *Nereis* and *Perinereis*, can be considered monophyletic, with many generic characters displaying high homoplasy (Bakken & Wilson, 2005). Molecular phylogenetic analyses carried out in this study supported the polyphyly of *Neanthes*, as sequences of species currently regarded as *Neanthes*, both from the ABYSSLINE material and from GenBank, rarely grouped together and were evenly distributed throughout a tree that included 11 other nereidid genera.

Neanthes goodayi sp. nov. can be differentiated from the majority of its congeners by the notably large anterior pair of eyes. Only *N. heteroculata* (Hartmann-Schröder, 1981), described from abyssal (4700 m) waters off the Bay of Biscay in the northeastern Atlantic, appears to possess comparably large anterior and minute posterior pairs of eyes. *Neanthes heteroculata* and *N. goodayi* sp. nov. also display similarities with regard to several other characters, such as the appearance of the prostomium, antennae and tentacular cirri, in addition to the types of chaetae present and their appearance and arrangement. Based on an examination of the type material of *N. heteroculata*, *N. goodayi* sp. nov. differs in having distinctly rounded, spherical to ovoid palpophores (e.g., Figure 2.4 B), with palpophores in *N. heteroculata* found to be narrower, bluntly conical in shape. Furthermore, the dorsal cirri are relatively short in *N. heteroculata*, not exceeding the length of the notopodial ligules, whereas they exceed the length of the notopodial ligules in at least anterior and posterior chaetigers in *N. goodayi* sp. nov.

Notably, *N. heteroculata* is one of a handful of species of *Neanthes* reported from the deep sea. Of the 84 currently valid species of *Neanthes* (Read & Fauchald, 2020a) only 13 have been reported from depths greater than 200 m (Hsueh, 2019; Khlebovich, 1996; Shimabukuro et al., 2017). Of these, *N. goodayi* sp. nov. also resembles *N. papillosa* (Day, 1963), described from deep (2745 m) waters off Cape Town, South Africa. *Neanthes papillosa* similarly possesses an enlarged anterior pair of eyes relative to the posterior pair, in addition to long tentacular cirri, relatively elongate, conical parapodial ligules, and dorsal cirri that exceed the length of the notopodial ligules, becoming longer on posterior chaetigers. The holotype of *N. papillosa* is noted to have pale, poorly chitinised paragnaths, thus making them difficult to observe(Day, 1963). However, despite having fewer paragnaths in number across all areas, they appear to be organised in similar arrangements as in *N. goodayi* sp. nov., such as a single row of paragnaths on areas VII–VIII (single row of large cones in *N. goodayi* sp. nov. with varying numbers of smaller cones laterally). However, *N. papillosa* can primarily be differentiated from *N. goodayi* sp. nov. in that the anterior pair of eyes does not appear to be as strikingly large as in *N. goodayi* sp. nov. or *N. heteroculata*; thus, there is less disparity between the anterior and posterior eye pairs in size. Additionally, *N. papillosa* can be further distinguished in that it does not bear homogomph falcigers and that parapodial lobes of midbody and posterior chaetigers bear numerous club-shaped papillae; however, it is worth considering that some characters of *N. papillosa* may be reproductive modifications, as the holotype is described from a single epikotous female specimen.

Neanthes goodayi sp. nov. also bears similarities to *N. vitiazi* Khlebovich, 1996 from abyssal waters (3342–4160 m) of southern Japan, primarily in terms of broadly similar paragnath distributions, bearing homogomph falcigers and in having a large anterior pair of eyes, which are illustrated as rings without strong pigment. *Neanthes vitiazi* differs in that it has long, digitate median ligules positioned at right angles to the notoacicula on midbody and posterior chaetigers. *Neanthes vitiazi* is also described as having brown pigmentation on parapodial appendages and dense spot-like pigmentation on the apodous anterior segment; *N. goodayi* sp. nov. similarly bears two pigmented spots on the dorso-lateral anterior margin of this segment; however, these are relatively small, whereas the spots in *Neanthes vitiazi* span much of the length of the segment and are placed dorsally, behind the eyes.

The geographically most proximal deep-water species, *N. mexicana* Fauchald, 1972, described from abyssal waters off Baja California, and *N. sandiegensis* Fauchald, 1977 from the San Diego Trough (728–855 m), can also be differentiated from *N. goodayi* sp. nov. *Neanthes mexicana* was originally described from a single damaged specimen, re-examined and revised by(de León-González & Solís-Weiss, 2000) with the addition of several nereidids collected from abyssal waters off California USA agreeing with the type specimen. *Neanthes mexicana* is described as bearing a single pair of very large red eyes, with diffuse pigment spots posterior to the eyes noted to perhaps represent the posterior eye pair (Fauchald, 1972). In ABYSSLINE specimens, the appearance of the posterior eye pair was variable, ranging from discrete dark spots to more faint, irregular shapes, occasionally with one or both eyes absent all together, particularly in smaller specimens. The eye morphology of *N. mexicana* therefore falls within the variation observed in the ABYSSLINE samples. *Neanthes mexicana* and *N. goodayi* sp. nov. also share similarities in terms of parapodial morphology, with all parapodial ligules broadly conical to somewhat triangular in shape (see de León-González & Solís-Weiss, 2000: fig. 3). However, *N. mexicana* differs from *N. goodayi* sp. nov. in terms of palp morphology (long, digitate palpostyles), the arrangement and number of paragnaths (4 cones in areas II and IV versus 12 cones in both areas in N. goodayi sp. nov.,) and in lacking homogomph falcigers.

Neanthes sandiegensis is only known from a single damaged specimen. However, it differs from N. goodayi sp. nov. primarily in terms of parapodial morphology, bearing large, foliose dorsal notopodial ligules with medially inserted, long, flattened digitate dorsal cirri, long digitate prechaetal notopodial lobes and notably elongate ventral neuropodial ligules. *Neanthes sandiegensis* also differs in terms of the distribution and number of paragnaths on most pharyngeal areas (I = 0, II =2, VI= 6–8, VII–VIII = 35 in *N. sandiegensis*, I = 2, II = 12, VI = 1–4, VIII–VIII = 19 in the holotype of *N. goodayi* sp. nov.).

While none of the morphologically most similar or geographically proximal congeners had genetic data available for comparison, morphological differences existed in each case. *Neanthes goodayi* sp. nov. can be differentiated from other deep-water *Neanthes* spp. primarily in terms of eye morphology: *N. articulata* Knox, 1960, *N. donggungensis* Hsueh, 2019, *N. kerguelensis* (McIntosh, 1885) and *N. suluensis* Kirkegaard, 1995 bear two relatively small, subequal eye pairs, whereas *N. bioculata* (Hartmann-Schröder, 1975) bears a single pair of small eyes*; N. abyssorum* Hartman 1967*, N. kermadeca* (Kirkegaard, 1995), *N. shinkai* Shimabukuro et al., 2017 and *N. typhla* (Monro, 1930) are recorded as lacking eyes altogether and can be further differentiated from *N. goodayi* sp. nov. in terms of paragnath distribution, among other characters (see Shimabukuro et al. 2017 for comparative morphological table of most deep water *Neanthes* spp.).

2.3.12 Ecology

Neanthes goodayi sp. nov. was found at depths ranging from 4000 to 4400 m living in crevices of polymetallic nodules (Figure 2.8 A–B), burrowing in xenophyophore foraminifera growing on nodules (Figure 2.8 C–E) or in mud balls on nodule surfaces (Figure 2.8 F–H). As in other nereidids, the strong eversible jaws, together with large eyes, indicate an active and predatory behaviour. While we were able to observe live, moving specimens kept at cold temperatures even after recovery from 4000 m water depth, behaviours such as predation were not observed. Polymetallic nodules are thought to contain a diverse meiofaunal community of nematodes, copepods and other small crustaceans; thus, it is possible that *N. goodayi* sp. nov. is a 'sit and wait' predator that is able to remain inside the nodules and detect prey passing overhead through extremely small variations in light (from local bioluminescence, detected by the large eyes) or other physio-chemical cues.

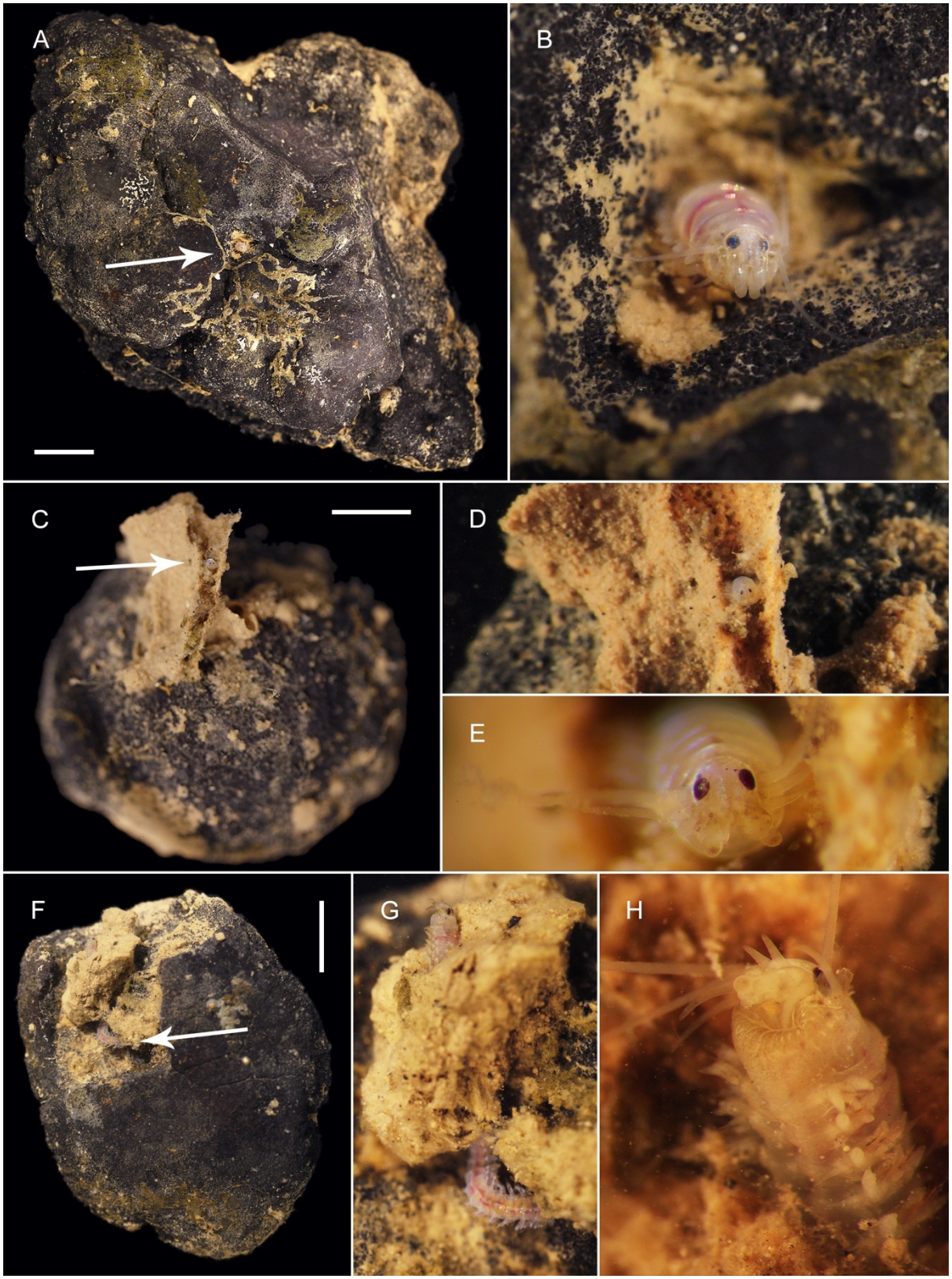

Figure 2.8 *Neanthes goodayi* sp. nov., live specimens, in situ images. **A**. Paratype (NHM_2026), burrowing within nodule crevice. **B**. Detail of paratype (NHM_2026), in burrow. **C**. Paratype (NHM_512), burrowing within a foraminiferan growing on nodule. **D–E**. Detail of paratype (NHM_512), in burrow. **F**. Detail of paratype (NHM_1624), burrowing within a mudball encrusting the nodule surface. **G–H**. Details of paratype (NHM_1624), in burrow. Scale bars: 1 cm.

2.3.13 Distribution

Eastern Clarion Clipperton Fracture Zone, Central Eastern Pacific.

2.4 Discussion

It is perhaps remarkable that one of the more obvious and charismatic animals living on and inside the most investigated mineral resource on the deep seafloor has not been described until now. However, the CCZ region, despite a large number of expeditions and considerable sampling effort, has clearly never received appropriate taxonomic attention (Glover et al., 2018). Only in recent years has any effort been made to describe polychaete species, with 29[4] new species described in two recent papers (Bonifácio & Menot, 2018; Wiklund et al., 2019). Such descriptions are essential to future investigations of population connectivity and resilience, extinction risk modelling, ecosystem function, natural history, ecology and life history (Glover et al., 2018).

The more obvious macrofauna that live on polymetallic nodules are likely to be useful in the future for monitoring the impacts of seabed mining, if it were to start. In this regard, *Neanthes goodayi* can be added to this list of potential 'indicator taxa' alongside the recently described nodule-dwelling sponge, *Plenaster craigi* Lim & Wiklund, 2017. Like *P. craigi*, *N. goodayi* sp. nov. is relatively easy to recognise during routine examination of nodules, and is sufficiently abundant to be counted in replicated samples. The smaller macrofauna dwelling in the sediments around the nodules is still extremely difficult to identify without using genetic methods and as such can only really be identified by specialists. The presence or absence of nodule-dwelling taxa such as *P. craigi* or *N. goodayi* sp. nov. may prove to be a useful measure of ecosystem health.

2.5 Acknowledgements

For detailed acknowledgements as published in Drennan et al. 2021a, see Appendix A section A.2

[4] Now 52 new species, including description presented in this chapter – see introduction section 1.3.2

Chapter 3 Annelid Fauna of the Prince Gustav Channel, a Previously Ice–Covered Seaway on the Northeastern Antarctic Peninsula

REGAN DRENNAN [1,2], THOMAS G. DAHLGREN [3,4]; KATRIN LINSE [5]; ADRIAN G. GLOVER [2]

[1] Ocean & Earth Science, University of Southampton, European Way, Southampton SO14 3ZH, UK

[2] Life Sciences Department, Natural History Museum, London SW7 5BD, UK

[3] NORCE Norwegian Research Centre, Bergen, Norway

[4] Department of Marine Sciences, University of Gothenburg, Box 463, 40530 Gothenburg, Sweden

[5] British Antarctic Survey, High Cross, Madingley Road, Cambridge CB3 0ET, UK

Abstract The Prince Gustav Channel is a narrow seaway located in the western Weddell Sea on the northeastern–most tip of the Antarctic Peninsula. The channel is notable for both its deep (>1200 m) basins, and a dynamic glacial history that most recently includes the break–up of the Prince Gustav Ice Shelf, which covered the southern portion of the channel until its collapse in 1995. However, the channel remains mostly unsampled, with very little known about its benthic biology. We present a preliminary account of the benthic annelid fauna of the Prince Gustav Channel in addition to samples from Duse Bay, a sheltered, glacier–influenced embayment in the northwestern portion of the channel. Samples were collected using an Agassiz Trawl, targeting megafaunal and large macrofaunal sized animals at depths ranging between 200–1200 m; the seafloor and associated fauna were also documented *in situ* using a Shallow Underwater Camera System (SUCS). Sample sites varied in terms of depth, substrate type, and current regime, and communities were locally variable across sites in terms of richness, abundance, and both taxonomic and functional composition. The most diverse family included the motile predator/scavenger Polynoidae, with 105 individuals in at least 12 morphospecies, primarily from a single site. This study provides first insights into diverse and spatially heterogeneous benthic communities in a dynamic habitat with continuing glacial influence, filling sampling gaps in a poorly studied region of the Southern Ocean at direct risk from climate change. These specimens will also be utilized in future molecular investigations, both in terms of describing the genetic biodiversity of this site and as part of wider phylogeographic and population genetic analyses assessing the connectivity, evolutionary origins, and demographic history of annelid fauna in the region.

Keywords polychaeta, Weddell Sea, species checklist, Southern Ocean, benthic, morphology, taxonomy

Study published as:

Drennan R, Dahlgren TG, Linse K and Glover AG (2021) Annelid Fauna of the Prince Gustav Channel, a Previously Ice–Covered Seaway on the Northeastern Antarctic Peninsula. *Front. Mar. Sci.* 7:595303. https://doi.org/10.3389/fmars.2020.595303 [5]

[5] Chapter presented as published in Drennan et al. (2021b). Updates and corrections since publication are presented as footnotes.

3.1 Introduction

Ice shelves are vast, floating platforms of ice that form where continental ice sheets meet the ocean, fringing much of the Antarctic coastline and covering over 30% of the Antarctic continental shelf (Barnes & Peck, 2008). Sub–ice shelf ecosystems thus constitute a significant portion of available benthic habitat in the Southern Ocean, though remain amongst the least known on the planet due to general inaccessibility and are at a direct risk of being lost due to climate change. Ice shelves are extensive along both sides of the Antarctic Peninsula, covering approximately 120,000 km^2 of seafloor today (Cook & Vaughan, 2010). However, in recent decades the Antarctic Peninsula has experienced amongst some of the fastest regional warming on the planet (Vaughan et al., 2003), with substantial increases in both atmospheric and ocean temperatures (e.g. Meredith & King, 2005; Turner et al., 2005). These increases are largely thought to have contributed to the significant thinning, retreat and collapse of ice shelves along the Antarctic Peninsula over the past 60 years (Cook & Vaughan, 2010; Etourneau et al., 2019; Rignot et al., 2013), with significant losses including the collapse of the Larsen A and Prince Gustav Ice Shelves in 1995 (Rott et al., 1996) the Larsen B ice shelf in 2002 (Rack & Rott, 2004), and the calving of a massive 5,800 km^2 iceberg from the Larsen C Ice Shelf in 2017 (Marchant, 2017).

Until its collapse in the early 1990s, the Prince Gustav Ice Shelf (PGIS) was the most northerly ice shelf on the Antarctic Peninsula, spanning the southern portion of the Prince Gustav Channel (PGC) (see Ferrigno et al., 2006), a deep, narrow seaway located on the inner continental shelf of the northwestern Weddell Sea that separates James Ross Island from the northernmost tip of the Antarctic Peninsula (see Figure 3.1). Broadly categorized as a fjord (Camerlenghi et al., 2001), the PGC consists of a discontinuous u–shaped glacial trough with steep sided walls and three over–deepened basins (approximately 900 m, 1000 m, and 1200 m deep moving north to south), separated by two shallower sills (approximately 350 m and 600 m deep respectively) (Camerlenghi et al., 2001). The channel formed before the late Miocene and was progressively deepened by several advances of grounded glaciers during the Neogene and Quaternary periods (Nỳvlt et al., 2011), and with evidence of floating ice shelves from the end of the Pleistocene (Evans et al., 2005; Johnson et al., 2011).

In contemporary terms, the PGIS and other small ice shelves on the northeastern Antarctic Peninsula have been observed for a far longer period than many other Antarctic ice shelves; first visited over 170 years ago and mapped by the Swedish Antarctic Expedition 1901–1903 (Nordenskjöld & Andersson, 1905), these ice shelves are generally thought to have been in retreat since historical observations began, with the PGIS itself once contiguous with the Larsen A ice shelf until the mid 20th century (Cooper, 1997). In contrast to larger ice shelves that can remain stable over tens of

thousands of years, these small northern ice shelves are at the climactic limit of ice shelf viability (Morris & Vaughan, 2003) and may therefore act as more sensitive indicators of recent climatic and oceanographic change (Pudsey et al., 2006), with evidence of periodic advance and retreat of ice shelves in the region throughout the Holocene, as demonstrated by several studies of data from sediment cores (e.g. Brachfeld et al., 2003; Pudsey et al., 2006; Pudsey & Evans, 2001). This includes a period of retreat during the mid–Holocene (~5–2 ka) in which the PGIS was completely absent (Pudsey & Evans, 2001), though with break up and regrowth appearing to occur gradually over centuries as opposed to the decadal scale of changes to contemporary ice shelf extent (Pudsey et al., 2006).

Understanding the biology of previously ice covered habitats is important in the context of unprecedented ice loss along the Antarctic Peninsula. However, despite the dynamic glacial history of the channel, the biology of the PGC, both before and after ice shelf collapse, is virtually unknown. In May 2000, a number of geological and geophysical surveys of the PGC were conducted by the RVIB Nathaniel B. Palmer as part of a larger investigation of the seafloor exposed by the then recent 1995 break–up of the Larsen A ice shelf (Domack et al., 2001). Biological samples were also obtained from collected sediment, however, these sampling sites were restricted to the southern portion of the channel (see Blake, 2015). Furthermore, while a number of polychaete specimens collected from this cruise have been included in several broader taxonomic publications (Blake, 2015, 2017, 2018), a summary of these samples and of the southern PGC benthic community is not currently available. In addition, no further biological investigations have taken place in subsequent years, and the channel remains otherwise unsampled, which is not uncommon for the region, with the western Weddell Sea considered to be one of the most poorly sampled areas of the Southern Ocean (Griffiths et al., 2014).

Annelid worms, or polychaetes, are amongst the most species rich groups in the Southern Ocean (Clarke & Johnston, 2003), and can represent a dominant component of Antarctic benthic assemblages in terms of both abundance and biomass (e.g. Gambi et al., 1997; Hilbig et al., 2006; Piepenburg et al., 2002; Sañé et al., 2012). Found across the Southern Ocean from intertidal to abyssal depths (Brandt et al., 2009), polychaetes fill a diverse array of trophic guilds and functional groups on both hard and soft substrates (e.g. Gambi et al., 1997), and are thus both an important and informative group to consider when assessing the biology of Antarctic benthic ecosystems. The following report documents a preliminary overview of the benthic annelid fauna of the Prince Gustav Channel collected during the expedition JR17003a on board RSS *James Clark Ross* February–March 2018. Samples were collected using an Agassiz trawl from several sites along the northern portion of the channel including the deepest (>1200 m) basin of the PGC. In contrast to the more open channel, samples were additionally collected from Duse Bay, a sheltered, glacier influenced embayment located in the northwestern portion of the PGC.

The aims of this study were to (1) characterize the annelid fauna of the PGC, a previously ice covered channel in the northwestern Weddell Sea and (2) examine spatial variation in annelid assemblages in this habitat by comparing samples from open and sheltered areas of the PGC.

3.2 Materials and methods

3.2.1 Sample sites and sample collection

The annelid specimens examined in this study were collected using an Agassiz Trawl (AGT) during the expedition JR17003a on board the RRS James Clark Ross February–March 2018, which sampled the northern portion of the Prince Gustav Channel (PGC) situated on the northeastern tip of the Antarctic Peninsula. The three main sampling sites were as follows: (1) Duse Bay, a sheltered, glacier influenced bay located in the northwestern portion of the PGC; (2) PGC Mid, located in the main channel, including the second deepest basin of the PGC; (3) PGC South, the southernmost sample site, located in the main channel and including the deepest basin of the PGC (Figure 3.1).

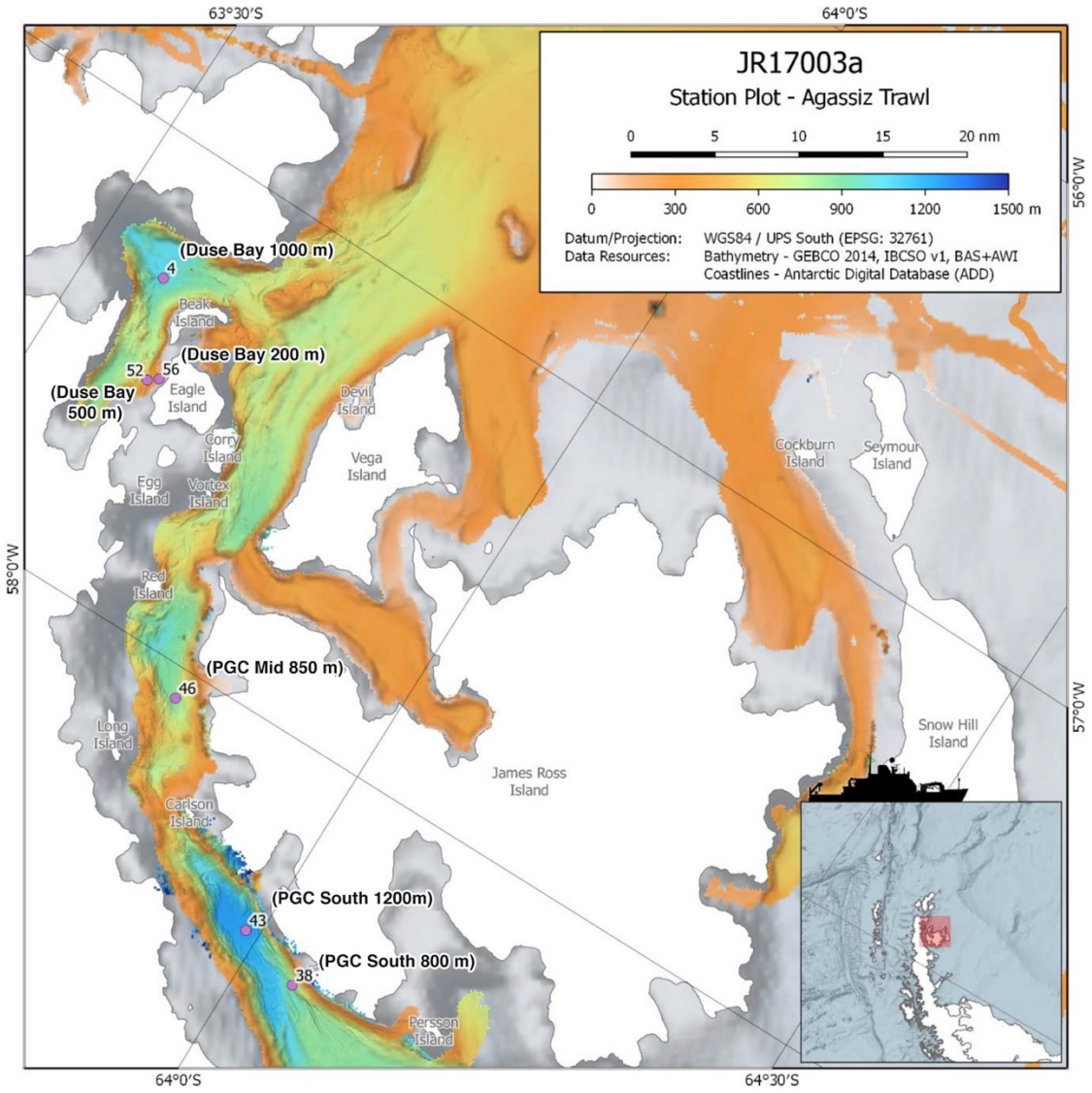

Figure 3.1 Map of study area within the Prince Gustav Channel, showing the six Agassiz trawl sites, marked with event number and sample name. Modified from RRS *James Clark Ross* expedition JR17003a cruise report, accessible via https://www.bodc.ac.uk/resources/inventories/cruise_inventory/report/16954/ See (Dreutter et al., 2020) for archived bathymetry data from the JR17003a expedition.

Three trawling depths (200 m, 500 m, 800/1000 m) were initially planned for each of the main sampling sites, with an additional deep 1200 m trawl of the basin at PGC South. However, only at Duse Bay sites were all three trawling depths achieved, as 200 and 500 m sites in the channel proper were too influenced by boulders to deploy the AGT. In total, six successful AGT deployments between depths of 204 m and 1270 m were carried out across the three sites (Figure 3.1 and Table 3.1) and sorted on board for benthic fauna. The AGT apparatus used comprised of a 1 cm mesh with a mouth width of 2 m, and once on the seabed was trawled at 1 knot for 5–10 min at each site. The AGT targeted macro– and megafaunal sized animals 1 cm and larger, though with some smaller animals additionally captured in the sediment retained in trawls.

Table 3.1 Details of Agassiz Trawl stations within the Prince Gustav Channel sampled during the expedition JR17003a. *H' = Shannon–Weiner diversity index, J' = Pielou's Evenness.*

Event no.	Site	Date	Decimal latitude	Decimal longitude	Max depth (m)	No. of individuals	No. of families	No. of morphospecies	H'	J'
56	Duse Bay 200 m	2018–03–07	–63.62531	–57.48627	203.85	48	10	13	1.99	0.77
52	Duse Bay 500 m	2018–03–07	–63.61614	–57.50349	483.01	99	19	32	2.76	0.80
4	Duse Bay 1000 m	2018–03–01	–63.57554	–57.29537	1080.63	260	8	10	0.95	0.41
46	PGC mid 850 m	2018–03–06	–63.80603	–58.06523	869.95	126	8	21	2.33	0.76
38	PGC south 800 m	2018–03–05	–64.05515	–58.47654	868.42	41	11	19	2.45	0.83
43	PGC south 1200 m	2018–03–06	–63.98811	–58.42253	1271.42	24	3	4	0.84	0.60

A 'cold–chain' live sorting pipeline was followed on board, as outlined in detail in Glover et al. (2016). In summary, AGT sub–samples were carefully washed on 300–micron sieves in cold filtered seawater (CFSW), and annelid specimens were picked from sieve residue, cleaned and maintained in CFSW, and relaxed in Magnesium Chloride solution prior to specimen photography. Specimens were imaged using Canon EOS600D cameras either with 100 mm Macro lens or through a Leica MZ7.5 microscope with SLR camera mount. Specimens were preliminary identified on–board to family level, numbered and recorded into a database, and fixed in 80% non–denatured ethanol. Samples that could not be fully sorted on board due to time restrictions were fixed in bulk for later sorting.

A Shallow Underwater Camera System (SUCS) (Nolan et al., 2017) comprised of a 1000 m fiber optic cable (allowing operation to ~ 900 m) and a tripod–mounted HD camera system was deployed at twelve stations along the PGC, ranging in depth from 200–800 m. SUCS deployments typically involved three consecutive transects spaced 100 m apart, with each transect consisting of 10 photos taken at 10 m intervals. Photos consisted of high resolution stills (2448 × 2050 pixels) covering approximately 0.51 m2 of seafloor (Almond, 2019)[6]. Four SUCS stations corresponded closely with AGT localities, providing a snapshot of the habitat heterogeneity in the vicinity of these samples and *in situ* images of some of the most common species encountered. A dataset of all JR17003a SUCS imagery can be accessed through the following doi: 10.5285/48DCEF16–6719–45E5–A335–3A97F099E451 (Linse et al., 2020).

3.2.2 Laboratory sorting and identification

In the laboratory, remaining bulk–fixed samples were sorted and all specimens were re–examined using a Leica M216 stereomicroscope, and key morphological characters were imaged using a fitted Canon EOS600D camera. Specimens were identified to the best possible taxonomic level using original literature, specimen keys, and comparison with type specimen material from NHM collections. Where named species identifications were not possible, specimens were described as a morphospecies where the voucher number of a representative specimen is used as an informal species name for all specimens deemed to be the same species as the representative individual, e.g., Polynoidae sp. NHM–228. Where named species identifications were uncertain, the open nomenclature 'cf.' was used as a precautionary approach along with a representative voucher number, e.g., *Antarctinoe* cf. *ferox* NHM–232. Where specimens were fragmented, only fragments that clearly bore heads were counted and included in abundance records, as standard practice.

[6] Now published as (Almond et al. 2021)

3.2.3 Data analysis

Specimen data were assembled into a Microsoft Excel database, and data visualization and analyses were carried out using the software R v.3.6.2 (R Core Team, 2023) and the R package 'vegan' v.2.5–6 (Oksanen et al., 2019). Local diversity was assessed for each site using the Shannon–Wiener diversity index (*H'*) and Pielou's evenness (*J')* (Pielou, 1969; Shannon & Weaver, 1949). Figures were assembled and edited using Microsoft PowerPoint and Adobe Photoshop software.

Specimen data can be found online as supplementary data at https://www.frontiersin.org/articles/10.3389/fmars.2020.595303/full#supplementary-material and are also made available through the Global Biodiversity Information Facility (GBIF; http://www.gbif.org/) and Ocean Biogeographic Information Systems (OBIS; http://iobis.org/) databases via the SCAR Antarctic Biodiversity Portal (biodiversity.aq), accessible through the following doi: 10.15468/t223v4 (Drennan et al., 2020).

3.3 Results

3.3.1 Sample sites and SUCS imagery

Four Shallow Underwater Camera System (SUCS) stations corresponded closely with the following AGT sample sites: Duse Bay 200 m, Duse Bay 500 m, PGC Mid 850 m, and PGC South 800 m (see Figure 3.1).

Duse Bay (Figure 3.2 A), a sheltered bay located in the northwestern portion of the PGC, is influenced by several local glacier drainage basins (Ferrigno et al., 2006; Scambos et al., 2014) ; SUCS imagery at both 200 m (Figure 3.2 B,C) and 500 m (Figure 3.2 D,E). Duse Bay sites revealed substrate characterized by mud and soft sediments, though with the presence of coarser sediments and very small dropstones or gravel at the 200 m site. Additional SUCS deployments at 300 m and 400 m (not shown) show similar soft muddy substrates to the 500 m site. While SUCS imagery was not available for the deepest site at this locality, Duse Bay 1000 m, high abundances of burrowing subsurface deposit feeding polychetes in the families Sternaspidae and Maldanidae (see sections 3.3.2 & 3.3.3) suggest that the substrate here similarly includes soft sediments.

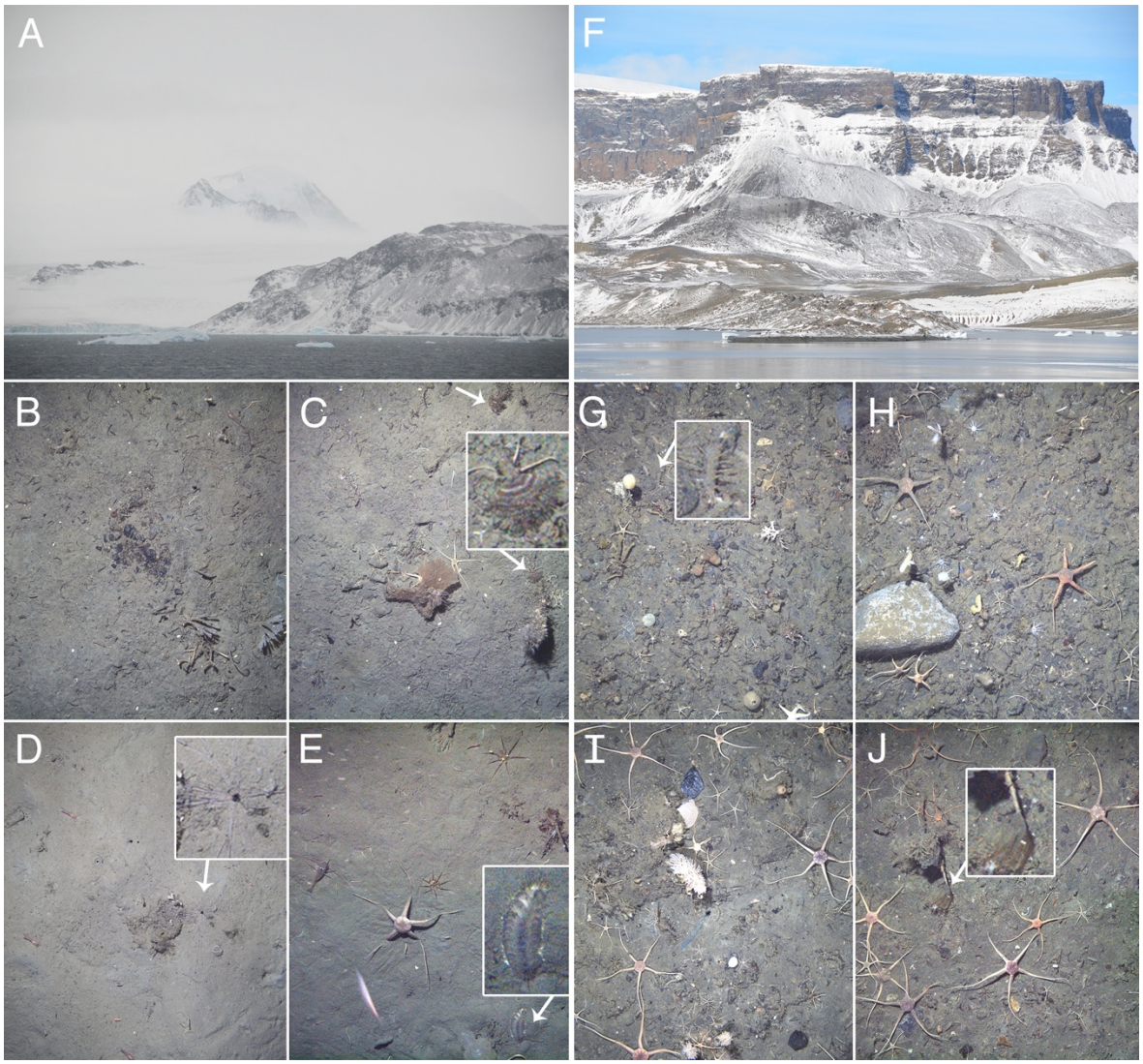

Figure 3.2 Overview of sites within the Prince Gustav Channel (PGC) including Shallow-water camera system (SUCS) imagery of localities corresponding to AGT sampling sites. **(A–**E) Duse bay sites, (F–J) PGC sites. SUCS imagery for deepest sites (Duse Bay 1000 m and PGC South 1200 m) was not available due to depth limitations. (A) Above water image of Duse Bay (image credit Angelika Brandt); (B) SUCS event no. 15, Duse Bay 200 m site; (C) SUCS event no. 15, Duse Bay 200 m site, with detail of sabellidae polychete; (D) SUCS event no. 11, Duse Bay 500 m site, with detail of terebellid polychete; (E) SUCS event no. 11, Duse Bay 500 m site, with detail of polynoid polychete, possibly *Austrolaenilla antarctica* (see Figure 3.4 D); (F) Above water image of the Prince Gustav Channel (image credit Angelika Brandt); (G) SUCS event no. 45, PGC Mid 850 m site, with detail of flabelligerid polychete, possibly *Flabegraviera mundata* (see Figure 3B); (H) SUCS event no. 45, PGC Mid 850 m site; (I) SUCS event no. 22, PGC South 800 m site; (J) SUCS event no. 22, PGC South 800 m site, with detail of sabellid polychete.

Though also fed by a number of small outlet glacier (Ferrigno et al., 2006; Scambos et al., 2014), the Prince Gustav Channel proper (Figure 3.2 F) is more open than Duse Bay sites, with the narrow, steep–sided nature of channel allowing for a more energetic setting with high current speeds and tidal influence (e.g. Camerlenghi et al., 2001). SUCS imagery from the PGC Mid 850 m site (Figure 3.2 G,H) revealed substrate dominated by gravel and small stones covered with a thin sediment, and with a number of small dropstones present. Imagery from PGC South 800 m site (Figure 3.2 I,J) revealed compacted mud and sediment with coarse gravel, and the presence of both small and large dropstones. SUCS imagery from the deepest PGC site, PGC South 1200 m, was similarly unavailable, however an abundance of large surface deposit feeders in the family Flabelligeridae (see section 3.3.3) suggest that some input of food–bearing sediment is occurring here, though with a notable absence of burrowing taxa.

A number of polychetes were visible *in situ* in SUCS imagery (Figure 3.2 C,D,E,G,J) including several taxa that possibly correspond with morphospecies collected in AGT samples, such as the flabelligerid *Flabegraviera mundata* (Figure 3.2 G, 3.3 B) and the polynoid *Austrolaenilla antarctica* (Figure 3.2 E, 3.4 D).

3.3.2 Sample overview

In total, approximately 598 individual annelid specimens in roughly 57 morphospecies and at least 25 families were collected across all six AGT deployments (Tables 3.1, 3.2, 3.3) and Online Supplementary Table 1). The preservation quality of the collected specimens was excellent, with many individuals recovered in full without fragmentation, and delicate features such as cirri and elytra often remaining intact (Figure 3.3, 3.4). Of the morphospecies, 22 were identified to named species, while five were designated as “cf.” and the remaining as morphospecies only (Table 3.3), due to a lack of appropriate taxonomic references and/or poor specimen condition. Morphospecies identified in this study will be subject to future molecular taxonomic and connectivity studies, which may change taxon assignments, for example through the use of genetic data as an error check for morphological assignments (e.g. Neal et al., 2018a), and through the discovery of new taxa and cryptic diversity (e.g. Brasier et al. 2016).

Table 3.2 Number of individuals and morphospecies per polychaete family (or higher taxonomic rank in the case of oligochaeta) sampled during cruise JR17003a. A broad functional category based on shared functional traits such as life habit, motility and feeding behavior is also provided for each family: b (burrowing); msom (motile surface–dwelling omnivorous); msdf (motile surface–dwelling deposit–feeding); pe (pelagic); pa (parasitic); tbsdf (tube–building surface deposit–feeding); tbsf (tube–building suspension–feeding)

Family (or higher)	Functional category	Total Site		Sites											
				Duse Bay 200 m		**Duse Bay 500 m**		**Duse Bay 1000 m**		**PGC Mid 850 m**		**PGC South 800 m**		**PGC South 1200 m**	
		No. ind.	***No. sp.***	***No. ind.***	***No. sp.***	***No. ind.***	***No. sp.***	***No. ind.***	***No. sp.***	***No. ind.***	***No. sp.***	***No. ind.***	***No. sp.***	***No. ind.***	***No. sp.***
Ampharetidae	tbsdf	5	1	2	1	2	1	–	–	–	–	1	1	–	–
Cirratulidae	b	10	4	2	1	7	4	1	1	–	–	–	–	–	–
Dorvilleidae	msom	5	1	–	–	5	1	–	–	–	–	–	–	–	–
Flabelligeridae	msdf	27	2	–	–	–	–	–	–	10	2	–	–	17	1
Hesionidae	msom	1	1	–	–	1	1	–	–	–	–	–	–	–	–
Lumbrineridae	b	12	2	1	1	6	2	4	1	–	–	1	1	–	–
Maldanidae	b	133	4	8	1	36	3	68	2	–	–	21	3	–	–
Myzostomidae	pa	1	1	–	–	–	–	–	–	–	–	1	1	–	–
Nephtyidae	msom[7]	17	2	–	–	4	2	6	1	6	1	–	–	1	1
Oligochaeta	b	3	2	–	–	3	2	–	–	–	–	–	–	–	–
Opheliidae	b	6	2	–	–	6	2	–	–	–	–	–	–	–	–
Orbiniidae	b	4	1	–	–	4	1	–	–	–	–	–	–	–	–
Oweniidae	tbsdf	16	1	–	–	1	1	–	–	15	1	–	–	–	–
Paraonidae	b	1	1	–	–	1	1	–	–	–	–	–	–	–	–
Phyllodocidae	msom	5	3	1	1	–	–	1	1	3	3	–	–	–	–
Polynoidae	msom	105	12	2	2	3	3	6	2	82	10	6	5	6	2
Sabellidae	tbsf	29	2	25	2	2	1	–	–	1	1	1	1	–	–
Scalibregmatidae	b	1	1	–	–	1	1	–	–	–	–	–	–	–	–
Serpulidae	tbsf	1	1	–	–	1	1	–	–	–	–	–	–	–	–
Sternaspidae	b	176	1	2	1	–	–	173	1	–	–	1	1	–	–
Syllidae	msom	19	4	–	–	7	2	–	–	7	2	5	2	–	–
Terebellidae	tbsdf	11	5	4	2	2	2	1	1	2	1	2	2	–	–

[7] Correction to Drennan et al. 2021b – Nephtyids are considered motile carnivores but burrow beneath the sediment water interface (Jumars et al. 1979)

Family (or higher)	Functional category	Total Site		Sites											
				Duse Bay 200 m		**Duse Bay 500 m**		**Duse Bay 1000 m**		**PGC Mid 850 m**		**PGC South 800 m**		**PGC South 1200 m**	
		No. ind.	***No. sp.***	***No. ind.***	***No. sp.***	***No. ind.***	***No. sp.***	***No. ind.***	***No. sp.***	***No. ind.***	***No. sp.***	***No. ind.***	***No. sp.***	***No. ind.***	***No. sp.***
Tomopteridae	pe	1	1	–	–	–	–	–	–	–	–	1	1	–	–
Travisiidae	b	1	1	–	–	–	–	–	–	–	–	1	1	–	–
Trichobranchidae	tbsdf	8	1	1	1	7	1	–	–	–	–	–	–	–	–
Total		598	57	48	13	99	32	260	10	126	21	41	19	24	4

Table 3.3 List of morphospecies identified from Agassiz Trawl samples collected on cruise JR17003a, with individual counts for each site provided. Taxa identified to named species are highlighted in bold. DB Duse Bay; PGC Prince Gustav Channel; M Mid; S South.

Family (or higher)	Morphospecies	Taxon authority	Sites						Total
			DB 200m	DB 500m	DB 1000m	PGCM 850m	PGCS 800m	PGCS 1200m	
Ampharetidae	Ampharetidae sp. NHM_280		2	2	–	–	1	–	**5**
Cirratulidae	*Aphelochaeta* sp. NHM_301		–	3	–	–	–	–	**3**
	Chaetocirratulus andersenensis	**(Augener, 1932)**	2	1	–	–	–	–	**3**
	Cirratulidae sp. NHM_035		–	2	1	–	–	–	**3**
	Cirratulidae sp. NHM_317		–	1	–	–	–	–	**1**
Dorvilleidae	Protodorvillea sp. NHM_290		–	5	–	–	–	–	**5**
Flabelligeridae	***Brada mammillata***	**Grube, 1877**	–	–	–	1	–	17	**18**
	Flabegraviera mundata	**(Gravier, 1906)**	–	–	–	9	–	–	**9**
Hesionidae	Hesionidae sp. NHM_291		–	1	–	–	–	–	**1**
Lumbrineridae	***Augenaria tentaculata***	**Monro, 1930**	1	5	4	–	1	–	**11**
	Lumbrineridae sp. NHM_300		–	1	–	–	–	–	**1**
Maldanidae	***Lumbriclymenella robusta***	**Arwidsson, 1911**	–	1	–	–	5	–	**6**
	Maldane sarsi	**Malmgren, 1865**	8	33	67	–	13	–	**121**
	Maldanidae sp. NHM_125		–	–	1	–	3	–	**4**
	Maldanidae sp. NHM_302		–	2	–	–	–	–	**2**
Myzostomatidae	*Myzostoma* cf. *divisor* NHM_123	Grygier, 1989	–	–	–	–	1	–	**1**
Nephtyidae	***Aglaophamus trissophyllus***	**(Grube, 1877)**	–	3	6	6	–	1	**16**
	Agalophamus sp. NHM_280F		–	1	–	–	–	–	**1**
Oligochaeta	Oligochaeta sp. NHM_287		–	2	–	–	–	–	**2**
	Oligochaeta sp. NHM_289		–	1	–	–	–	–	**1**
Opheliidae	***Ophelina breviata***	**(Ehlers, 1913)**	–	2	–	–	–	–	**2**
	Ophelina cf. *cylindricaudata*	(Hansen, 1878)	–	4	–	–	–	–	**4**
Orbiniiae	***Leitoscoloplos kerguelensis***	**(McIntosh, 1885)**	–	4	–	–	–	–	**4**
Oweniidae	Oweniidae sp. NHM_234C		–	1	–	15	–	–	**16**
Paraonidae	Paraonidae sp. NHM_295		–	1	–	–	–	–	**1**

Family (or higher)	Morphospecies	Taxon authority	Sites						Total
			DB 200m	DB 500m	DB 1000m	PGCM 850m	PGCS 800m	PGCS 1200m	
Phyllodocidae	***Paranaitis bowersi***	**(Benham, 1927)**	1	–	1	1	–	–	**3**
	Phyllodocidae sp. NHM_234D		–	–	–	1	–	–	**1**
	Phyllodocidae sp. NHM_235D		–	–	–	1	–	–	**1**
Polynoidae	***Antarctinoe ferox***	**(Baird, 1865)**	–	1	1	7	1	–	**10**
	Antarctinoe cf. *ferox* NHM_232	(Baird, 1865)	–	–	–	39	–	1	**40**
	Antarctinoe spicoides	**(Hartmann–Schröder, 1986)**	–	–	–	1	–	–	**1**
	Austrolaenilla antarctica	**Bergström, 1916**	–	1	5	1	1	5	**13**
	Barrukia cristata	**(Willey, 1902)**	–	–	–	9	–	–	**9**
	Harmothoe fuligineum	**(Baird, 1865)**	–	–	–	18	1	–	**19**
	Harmothoe cf. *fuligineum* NHM_233	(Baird, 1865)	–	1	–	2	–	–	**3**
	Harmothoe cf. *fullo* NHM_330	(Grube, 1878)	1	–	–	–	–	–	**1**
	Macellicephalinae sp. NHM_234L		–	–	–	1	–	–	**1**
	Polyeunoa laevis	**McIntosh, 1885**	–	–	–	1	1	–	**2**
	Polynoidae sp. NHM_140D		1	–	–	–	2	–	**3**
	Polynoidae sp. NHM_228		–	–	–	3	–	–	**3**
Sabellidae	Sabellidae sp. NHM_272		19	2	–	1	1	–	**23**
	Sabellidae sp. NHM_332		6	–	–	–	–	–	**6**
Scalibregmatidae	Scalibregmatidae sp. NHM_281		–	1	–	–	–	–	**1**
Serpulidae	Serpulidae sp. NHM_280K		–	1	–	–	–	–	**1**
Sternaspidae	***Sternaspis sendalli***	**Salazar–Vallejo, 2014**	2	–	173	–	1	–	**176**
Syllidae	***Pionosyllis kerguelensis***	**(McIntosh, 1885)**	–	–	–	6	1	–	**7**
	Syllidae sp. NHM_140F		–	–	–	–	4	–	**4**
	Syllidae sp. NHM_285		–	1	–	–	–	–	**1**
	Trypanosyllis gigantea	**(McIntosh, 1885)**	–	6	–	1	–	–	**7**
Terebellidae	***Leaena collaris***	**Hessle, 1917**	–	1	–	–	–	–	**1**
	Pista mirabilis	**McIntosh, 1885**	3	1	–	–	–	–	**4**
	Terebellidae sp NHM_142		–	–	1	–	1	–	**2**
	Terebellidae sp NHM_234P		–	–	–	2	1	–	**3**

Family (or higher)	Morphospecies	Taxon authority	Sites						Total
			DB 200m	DB 500m	DB 1000m	PGCM 850m	PGCS 800m	PGCS 1200m	
	Terebellidae sp NHM_337		1	–	–	–	–	–	**1**
Tomopteridae	*Tomopteris* sp NHM_131		–	–	–	–	1	–	**1**
Travisiidae	***Travisia kerguelensis***	**McIntosh, 1885**	–	–	–	–	1	–	**1**
Trichobranchidae	Trichobranchidae sp. NHM_280M		1	7	–	–	–	–	**8**

The two most abundant species (Table 3.3) were the sternaspid *Sternaspis sendalli* (Figure 3.3 H) with 176 individuals, and the maldanid *Maldane sarsi* (Figure 3.3 D) with 121 individuals. If these two species are excluded from the total specimen count, the whole site ratio of individuals to morphospecies is reduced markedly to 301 individuals in 55 morphospecies. Notably, the majority of both of these species were found at a single site, Duse Bay 1000 m (Table 3.3).The most diverse group were scale worms in the family Polynoidae, with 10–12 morphospecies recorded (Table 3.3 and (Figure 3.3 I, 3.4), though with the majority, both in terms of richness and abundance, also found at a single site (Table 3.2). One polynoid individual (Figure 4I) was identified as a representative of the near–exclusively deep–sea subfamily Macellicephalinae (Neal et al., 2012).

Almost all specimens collected were considered benthic with only one individual recovered from a pelagic family, Tomopteridae. One specimen from the parasitic/commensal family Myzostomidae was recovered, though without an obvious host. Several examples of commensalism were also observed, including two individuals of the Polynoid *Polyeunoa laevis*, a known alcyonacean coral associate (Barnich et al., 2012), found living within coral branches (Figure 3.3 I); individuals from the families Syllidae and Polynoidae were also found living within glass sponges (e.g. Figure 3.4 A). The majority of specimens exceeded 1 cm in length, however individual animals ranged in size from several millimeters in families such as Cirratulidae, Dorvilleidae, and Ophelidae to between 15 and 18 cm long in families such as Maldanidae, Nephtyidae, and Terebellidae.

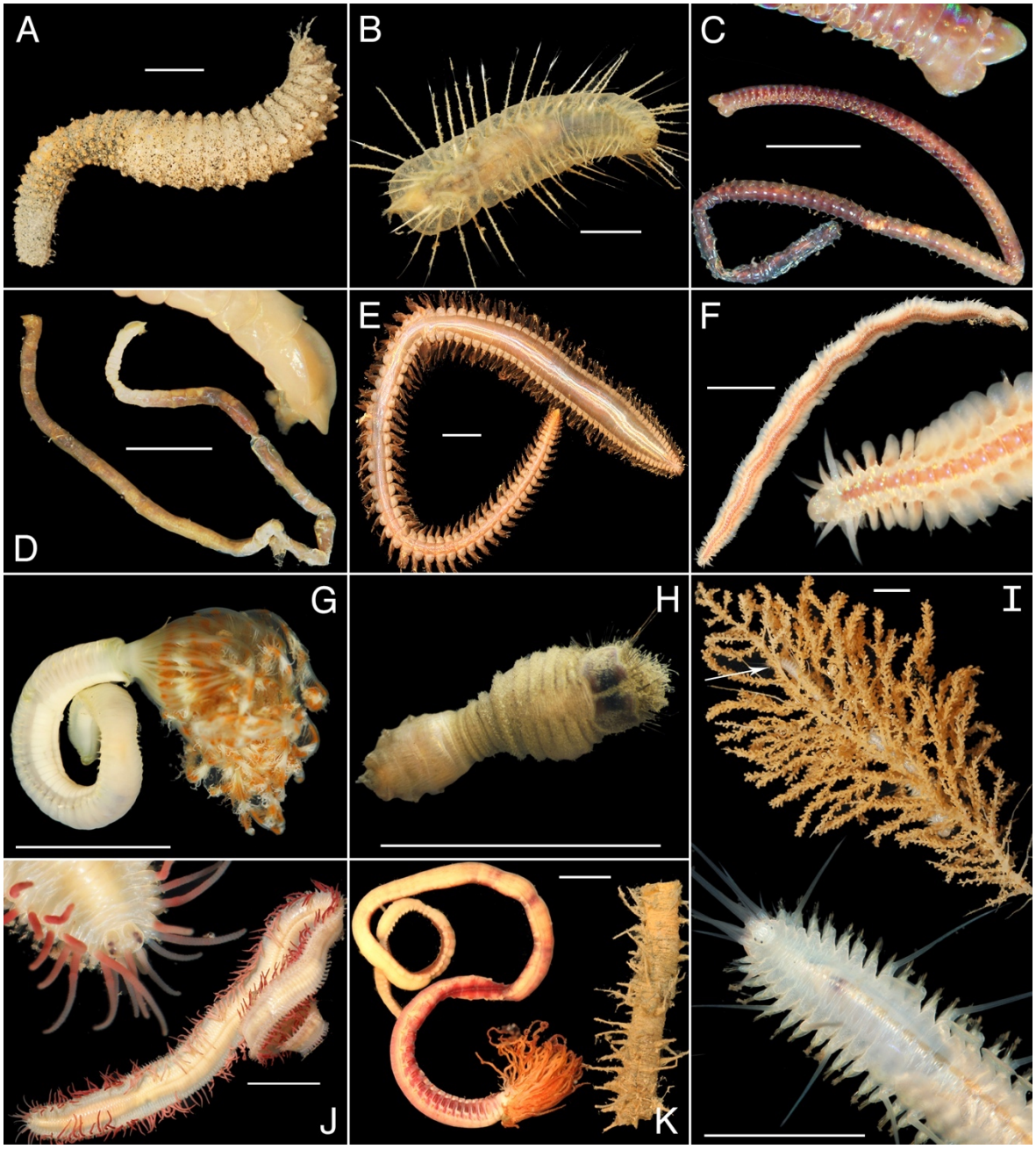

Figure 3.3 Live specimen imagery taken on board the expedition JR17003a of several annelid species or morphospecies across a range of families collected by AGT trawls. (A) *Brada mammillata* (Flabelligeridae); (B) *Flabegraviera mundata* (Flabelligeridae); (C) *Augeneria tentaculata* (Lumbrineridae), whole specimen (bottom), with detail of prostomium (top); (D) *Maldane sarsi* (Maldanidae), whole specimen (bottom) with detail of prostomium (top); (E) *Aglaophamus trissophyllus* (Nephtyidae), (F) *Paranaitis bowersi* (Phyllodocidae), whole specimen (top) with detail of anterior (bottom); (G) Sabellidae sp. NHM_272; (H) *Sternaspis sendalli* (Sternaspidae); (I) *Polyeunoa laevis* (Polynoidae), whole specimen living within branches of coral (top) and detail of specimen anterior (bottom); (J) *Trypanosyllis gigantea* (Syllidae), whole specimen (bottom) with detail of anterior (top); (K) *Pista mirabilis* (Terebellidae) whole specimen (left) alongside portion of tube (right). All scale bars = 1 cm.

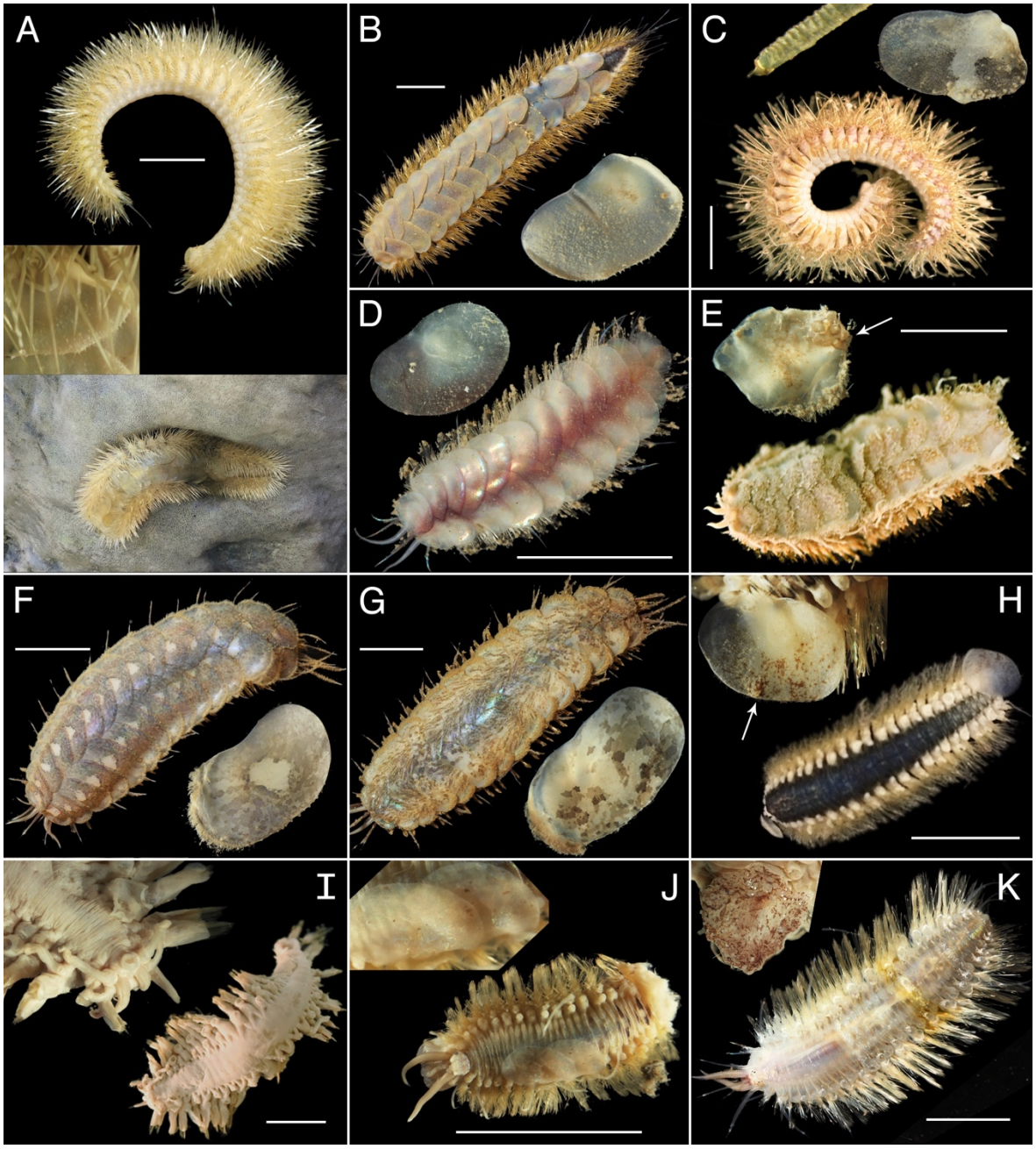

Figure 3.4 Specimen imagery highlighting morphospecies diversity of the family Polynoidae collected from theJR17003a expedition. See also Figure 3.3 I. (A) *Antarctinoe ferox* live image, lateral view (top), detail of elytra on preserved specimen (middle) and live, *in situ* image of specimen sitting in glass sponge; (B) *Antarctinoe* cf. *ferox* NHM_232, live image, with detail of midbody elytron (preserved); (C) *Antarctinoe spicoides*, preserved specimen, lateral view (bottom), detail of long notochaetal spine with pin tip (top left) and detail of midbody elytron (right); (D) *Austrolaenilla antarctica* live image, with detail of midbody elytron (preserved); (E) *Barrukia cristata*, preserved specimen, with detail of elytron with arrow highlighting large macrotubercles; F *Harmothoe* cf. *fuligineum* NHM_233, live image, with detail of elytron (preserved); (G) *Harmothoe fuligineum*, with detail of elytron; (H) *Harmothoe* cf. *fullo* NHM_330, preserved specimen, with detail of elytron, arrow highlighting mound on posterior margin; (I) Macellicephalinae sp. NHM_234L, preserved specimen, with detail of anterior (top left); (J) Polynoidae sp. NHM_140, preserved specimen, with detail of elytra; (K) Polynoidae sp. NHM_228, live image, with detail of elytron (preserved specimen, different individual to one shown in live image). All scale bars = 1 cm.

3.3.3 Comparison of sampling sites

As the size of the sampled area cannot be accurately determined, trawled sampling gear such as the Agassiz trawl are semi– quantitative in nature (Eleftheriou & Holme, 1984), and thus, reliable quantitative assessments and comparisons of abundance and diversity between sites within this study is not possible. However, trawls are efficient at sampling large areas and are useful in preliminary studies in terms of providing a broad qualitative overview of the distribution and structure of communities (Arnaud et al., 1998).

Each of the six sample sites varied in terms of abundance, morphospecies richness, Shannon–Wiener diversity, Pielou's evenness, and familial composition (Tables 3.1, 3.2, 3.3 and Figure 3.5). Sites further varied in terms of the dominant functional group present, and the overall size classes of component specimens (Figure 3.6). Duse Bay sites in general had high proportions of burrowing specimens (Figure 3.6) with representatives of burrowing families such as Cirratulidae, Lumbrineridae (e.g., Figure 3.4 C), and Maldanidae (e.g. Figure 3.4 D) present at each site, though with overall taxonomic composition varying between individual sites (Figure 3.5). Sites in the channel proper varied somewhat more in terms of dominant taxa and functional groups (Figure 3.5 and 3.6).

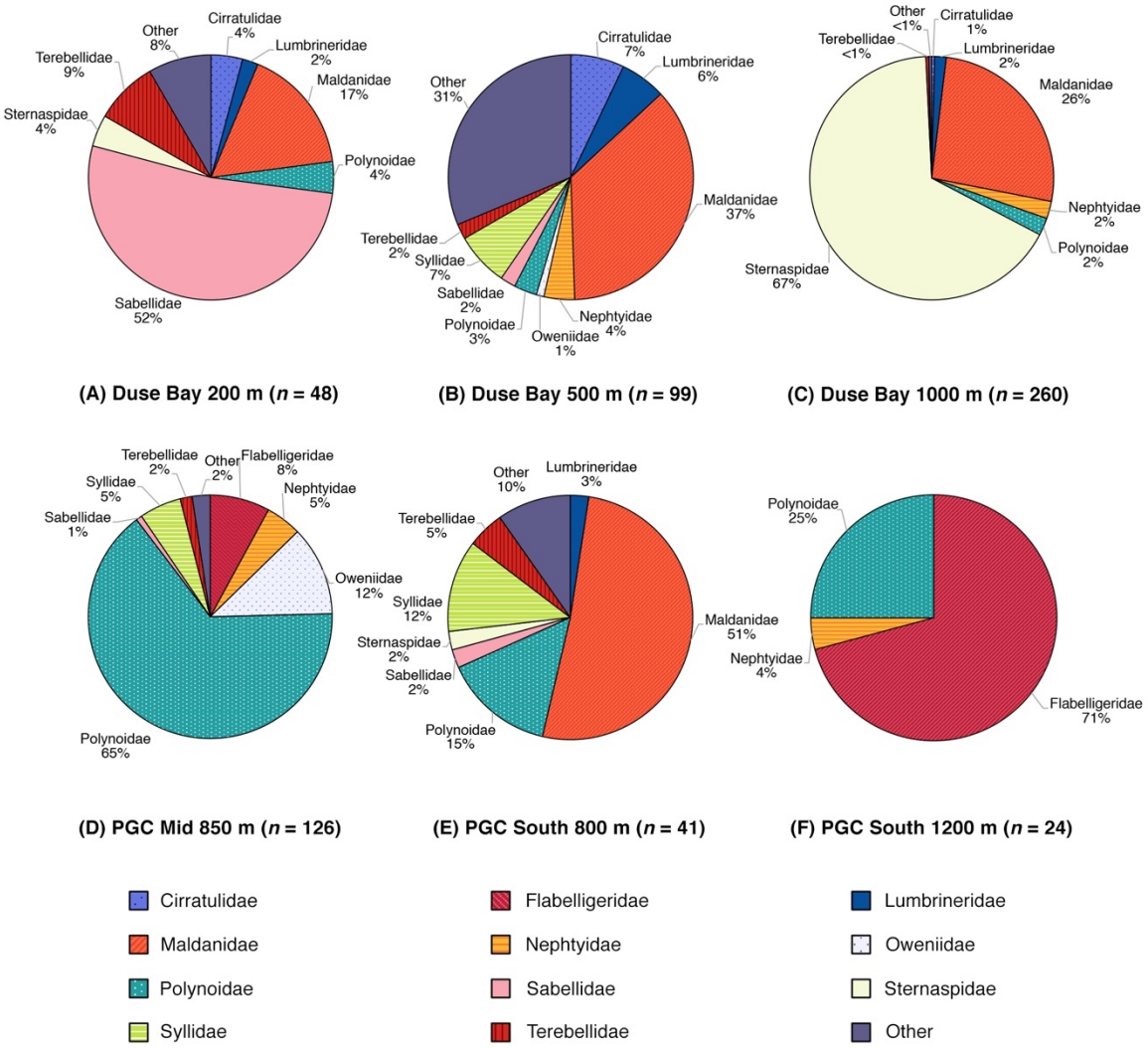

Figure 3.5 Proportions of total specimen abundance by annelid family for each Agassiz Trawl sample site. **(A)** Duse Bay 200 m **(B)** Duse Bay 500 m **(C)** Duse Bay 1000 m **(D)** PGC Mid 850 m **(E)** PGC South 800 m **(F)** PGC South 1200 m. Families that had less than ten individuals across all sites (14 out of a total of 25 families) were combined into a single category, "other."

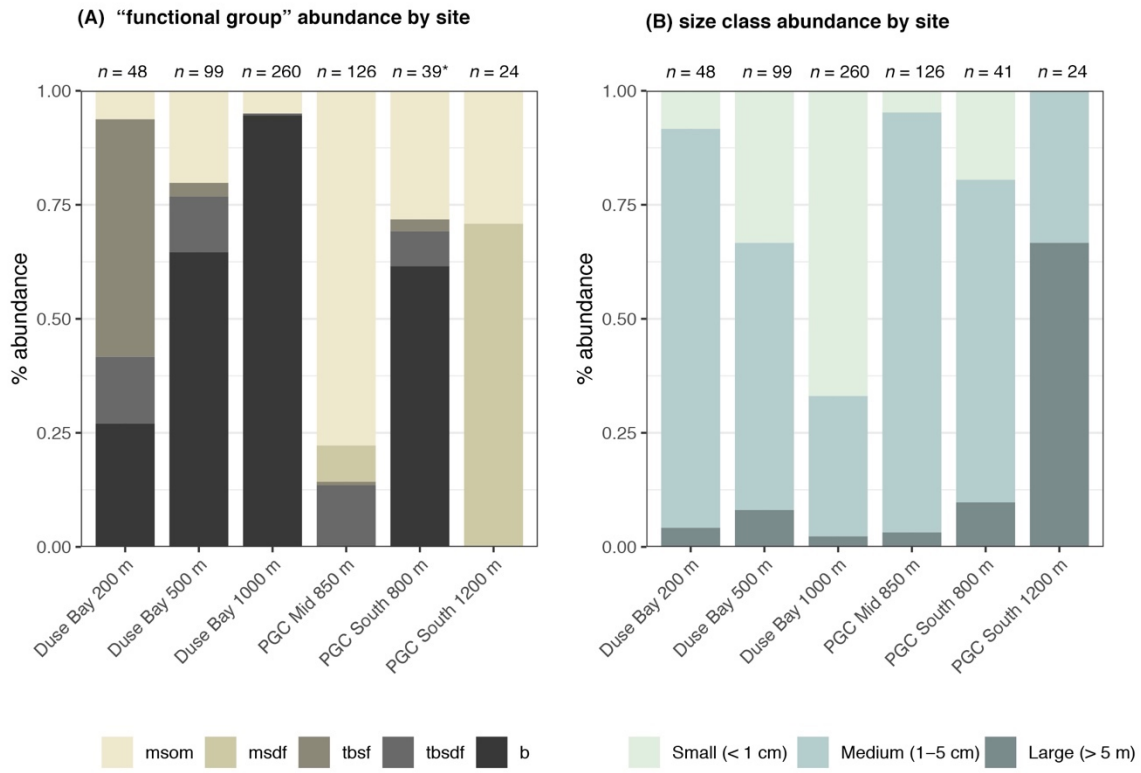

Figure 3.6 Composition of annelid (A) "functional groups" and (B) size classes in terms of percentage abundance of individuals across all sampled AGT stations. (A) Polychete families were separated into broad functional categories based on shared functional traits such as life habit, motility and feeding behavior as follows: msom (motile surface-dwelling omnivorous); msdf (motile surface-dwelling deposit-feeding); tbsdf (tube-building surface deposit-feeding); tbsf (tube-building suspension-feeding); b (burrowing). See Table 3.2 for list of functional groups by family. * Singleton specimens representing parasitic (pa) and pelagic (pe) functional groups (see Table 3.2) were excluded from PGC South 800 m. (B) Specimens were organized into general size classes as follows: small (less than 1 cm in length); medium (between 1–5 cm in length, or for long, slender taxa, less than 0.5 cm in width); large (exceeding 5 cm in length and 0.5 cm in width).

Duse Bay 200 m, the shallowest site sampled, displayed moderate abundance and richness, relative to other sites, and possessed the highest proportion of suspension feeders with 25 individuals from the tube building family Sabellidae in two morphospecies. However, the majority of these consisted of 14 individuals of the morphospecies *Sabellidae* sp. NHM–272 (**Figure 3G**) that formed a single cluster of tubes on the end of a large empty tube, possibly belonging to the terebellid *Pista mirabilis* (**Figure 3K**) of which there were three individuals also present in the sample, up to 15 cm in length.

Duse Bay 500 m displayed relatively high abundances and the highest morphospecies and familial richness by considerable margin, with 32 morphospecies in 19 families across 99 individuals. The sample was dominated by burrowing taxa (Figure 3.6), with Maldanidae representing the most abundant family (36 individuals across three morphospecies), comprising mainly of *Maldane sarsi* (33 individuals) (Figure 3.4 D). In addition to families not well represented at other sites such as Cirratulidae, many families such as Dorvilleidae, Hesionidae, Opheliidae, Orbiniidae, Paraonidae, and Scalibregmatidae were found exclusively at this site (Table 3.2). These families primarily included small, macrofaunal sized individuals approximately 1 cm in length or shorter. In contrast, the sample also included several notably large specimens, including an individual of the terebellid *Pista mirabilis* (Figure 3.3 K) exceeding 18 cm in length, an anterior fragment of the large nephtyid *Aglaophamus trissophyllus* (Figure 3.3 E) exceeding 15 cm in length, and six individuals of the large syllid *Trypanosyllis gigantea* (Figure 3.3 J) (2.5–10 cm long) found living within a glass sponge.

Duse Bay 1000 m presented the highest abundances observed across all sites with 260 individuals, though as discussed in section "Sample Overview," this sample was primarily made up of two species, *Sternaspis sendalli* and *Maldane sarsi,* with richness otherwise relatively low with 10 morphospecies. While *M. sarsi* is moderate in size (~2 mm wide though reaching lengths of up to 12 cm in the largest specimens), *S. sendalli* is small with most specimens not exceeding 1 cm in length – this site therefore displayed the highest proportion of small macrofaunal sized taxa (Figure 3.6). While *M. sarsi* was found at relatively high abundances in all but two sites (PGC Mid 850 m and PGC South 800 m), notably only a handful of *S. sendalli* were found at other sites despite being the most abundant species overall. Both species are burrowing deposit feeders, and Duse Bay 1000 m further presented the highest proportion of burrowing taxa across all sites (Figure 3.6). The remaining sample was primarily composed of medium to large sized motile scavenger/predator taxa including the large nephtyid *Aglaophamus trissophyllus,* the phyllodocid *Paranaitis bowersi* (Figure 3.3 F) and the polynoids *Antarctinoe ferox* and *Austrolaenilla antarctica* (Figure 3.4 A,D).

Sites in the channel proper were more variable. PGC Mid 850 m presented relatively high diversity and both the second highest abundance and richness of any site, with 126 individuals in 21 morphospecies, and is notable in that no burrowing taxa were present (Figure 3.6). While representatives of the family Polynoidae were present in small to moderate numbers across every site, PGC Mid 850 m is further notable in terms of a striking abundance and richness of polynoids with 82 individuals in at least 10 morphospecies (Figure 3.3 I, 3.4 A–I), ranging in size from 2 cm to >6 cm. Other motile scavenger/predator taxa in Nephtyidae, Phyllodocidae, and Syllidae were also moderately abundant. Ten individuals in the motile surface deposit feeding family Flabelligeridae were also present at the site, including nine individuals of the species *Flabegraviera mundata* (Figure 3.3 B), possibly visible *in situ* in SUCS imagery of this site (Figure 3.2 G).

Additionally, 15 individuals of an unidentified oweniid morphospecies, Oweniidae sp. NHM–234C, were present at this site, with the family being rare or absent entirely from other sites.

PGC South 800 m displayed relatively low abundance but moderate richness, with 41 individuals in 19 morphospecies, and was the only non–Duse Bay site with burrowing taxa, primarily comprised of the family Maldanidae (Figure 3.5, 3.6) but also including representatives in families Lumbrineridae, Sternaspis and Travisiidae. The remaining taxa were mainly composed of motile surface scavenger/predators in families Polynoidae and Syllidae.

PGC South 1200 m was the deepest site sampled, with a maximum depth of 1270 m. The site displayed both the lowest abundance and richness of any site, with 24 individuals in four morphospecies, dominated by 17 individuals of the large (4–7 cm) flabelligerid *Brada mammillata* (Figure 3.3 A), in addition to two species of polynoid (*Austrolaenilla antarctica* and *Antarctinoe* cf. *ferox* sp. NHM–232) and the nephtyid *Aglaophamus trissophyllus.* The site therefore was entirely composed of motile surface dwelling taxa, and further displayed the greatest proportion of large, megafaunal sized animals exceeding 5 cm (Figure 3.6).

Shannon–Wiener diversity indexes were lowest in the deepest stations, Duse Bay 1000 m and PGC South 1200 m (H’ = 0.95 and 0.84, respectively) and highest at Duse Bay 500 m (H’ = 2.75). Values for Pielou’s Evenness were also lowest for the two deepest stations (J’ = 0.41 and 0.60, respectively), ranging between J’ = 0.76 and J’ = 0.83 at the remaining sites.

3.4 Discussion

3.4.1 General overview

This study provides a first insight into the benthic annelid fauna of the Prince Gustav Channel, revealing locally variable communities in terms of abundance, richness, and both taxonomic and functional composition.

Fine scale habitat heterogeneity, for example in terms of substrate type and composition and the presence or absence of dropstones, can account for much of the variation observed in faunal composition in several previous studies of Antarctic shelf benthos, including investigations of the East Antarctic Shelf (Post et al., 2017), the Ross Sea (Cummings et al., 2006), King George Island (Quartino et al., 2001), and the South Orkney Islands (Brasier et al., 2018). In the present study, SUCS imagery at Duse Bay sites revealed substrate characterized by mud and soft sediments, reflected in high abundances of burrowing taxa at these sites, primarily subsurface deposit feeding families such as Maldanidae and Sternaspidae.

Though SUCS imagery was not available for the deepest site (Duse Bay 1000 m), high abundances of these taxa suggest substrate also composed of soft sediments. Previous studies of Antarctic shelf annelids have found high abundances of subsurface deposit feeding taxa to correspond with enhanced productivity and food availability in sediments (e.g. Neal et al., 2011). Duse Bay is a sheltered embayment influenced by a number of local outlet glaciers (Ferrigno et al., 2006; Scambos et al., 2014); in addition to the collapse of floating ice shelves, maritime glaciers along the Antarctic Peninsula have also experienced dramatic retreat in recent decades (Cook et al., 2005), with freshening and sedimentation events becoming more frequent due to increased influxes of glacial meltwater and sediment runoff associated with glacial retreat (Smale & Barnes, 2008). These disturbances can affect adjacent benthic communities in a number of ways. For example, the presence of surface meltwater has been associated with nearshore phytoplankton blooms and increased primary productivity (Dierssen et al., 2002), and increased sedimentation with shifts in benthic community structures (Sahade et al., 2015), favoring soft substrate adapted taxa. Glacial input can also locally increase habitat complexity through the deposition of dropstones – land derived rock frozen into glacial ice that enter the sea via icebergs, which deposit the stones as they melt, providing hard substrata where they land (Smale & Barnes, 2008). Both large and small dropstones were visible throughout the channel where SUCS imagery was available, though in Duse Bay these were mainly restricted to the shallowest site (Duse Bay 200 m).

Glaciers that previously fed into the Prince Gustav Ice Shelf experienced accelerated ice loss and discharge into PGC embayments following the collapse of the ice shelf and its buttressing effect in 1995, though with a significant reduction in losses since 2013 (Rott et al., 2014, 2018). In addition to glacial input into the channel, the depth and north-south continuity of the PGC may further facilitate the flow of fine grained sediment and organic matter through the channel from adjacent shelf areas and more productive, seasonally open water, even during periods when the channel was covered by a floating ice shelf, which is possibly indicated by a measurable drape of diatom bearing sediment in the deepest parts of the channel, much thicker than for other glacial troughs in the region (Pudsey et al., 2001). This may have relevance to benthic communities in the channel today, as while the collapse of ice shelves exposed open water leading to massive increases in primary production in the region (Bertolin & Schloss, 2009), the east coast of the Antarctic Peninsula experiences dense pack ice cover for much of the year, with pack ice in the channel occasionally lasting year round (Pudsey et al., 2006). Cut off from surface primary production, benthic communities beneath floating ice shelves are known to rely on the horizontal advection of food particles from open water as a primary food source (Riddle et al., 2007), with distance from the ice shelf edge a major factor in terms of the abundance, diversity and structure of sub-ice benthic communities (e.g. Post et al., 2014; Riddle et al., 2007).

In this study, SUCS imagery corresponding to sampled channel sites revealed higher proportions of hard substrate relative to Duse Bay sites, though with mud and compacted sediment present at PGC South 800 m (possibly reflected in an abundance of maldanids) and only a thin sediment drape at PGC Mid 850 m, the latter displaying remarkable abundance and diversity in the motile predator/scavenger family Polynoidae and the complete absence of sub-surface deposit feeding taxa. While SUCS imagery was not possible for the deepest basin of the channel, PGC South 1200 m, previous acoustic investigations have shown that the deeper parts of the channel are filled by a measurable sediment drape (Pudsey et al., 2001). The benthic fauna of this site was distinct from other samples with the lowest richness, abundance, and diversity, entirely dominated by large motile megafauna, primarily in the surface deposit feeding family Flabelligeridae but also including predator/scavenger families Polynoidae and Nephtyidae. In a comparative study of depth zonation in polychete communities from Scotia and Amundsen seas, deep glacial troughs up to 1500 m deep in the inner shelf of the glacier-influenced Pine Island Bay in the Amundsen Sea were dominated by motile predator/scavengers such as Polynoidae and Nephtyidae and deposit feeding families (both surface and subsurface) at 500 m depth horizons; deeper sites were entirely dominated by the former with a complete absence of deposit feeders (Neal et al., 2018). The basins of the PGC are amongst a number of deep glacial troughs that exceed depths of 800 m in the greater Larsen A area, though are distinct in having a much thicker drape of diatom bearing sediment than other troughs in the region, suggesting that the bathymetry of the channel facilitates the advection of food bearing particles from more productive waters through the channel and to these troughs (Pudsey et al., 2001). This could possibly support deposit feeding communities in the deep basins of the PGC, however comparative samples from other troughs in the region are not available.

In the Amundsen Sea, Antarctic Circumpolar Deep water is known to intrude onto the inner shelf of Pine Island Bay (Thoma et al., 2008), connecting the shelf troughs with deep water and acting as a potential source of the deep-water species found in these troughs (e.g. Kaiser et al., 2009; Linse et al., 2013; Riehl & Kaiser, 2012), including polynoids in the deep sea sub-family Macellicephalinae (Neal et al., 2012; Neal et al., 2018b). An individual of this subfamily was collected in the present study from PGC Mid 850 m site. On the continental shelf of the greater Larsen region, glacial troughs running out to the continental shelf break allow for the inflow of Modified Weddell Deep Water, a derivative of Circumpolar Deep Water, onto the shelf and toward the coast and ice shelf fronts (Nicholls et al., 2004), though it is unknown whether this could similarly act as a source of deep sea taxa on the western Weddell shelf without comparative faunistic studies with deep Weddell communities.

Southern Ocean polychetes are typically reported to have wide depth ranges (Schüller, 2011), however this notion is beginning to be challenged, with recent comparative investigations finding depth to be one of the main factors structuring shelf and slope polychete communities (Neal et al., 2018). As the sample size in this study was small and qualitative, and with three sampling depths only achieved at Duse Bay sites, any effects of depth are difficult to discern. In a separate analysis of the 12 SUCS deployments taken throughout the channel on the JR17003a expedition from depths ranging from 200 m to 850 m, heterogeneity and complexity was found to decrease with depth, with the most complex and heterogeneous sites found at the southern-most sample sites (Almond, 2019).

Without comparable baseline records from the Prince Gustav Channel, either before or directly after ice shelf collapse, any effects of ice loss on the benthos of the channel are similarly difficult to discern. Based on historical records, the maximum northern extent of the Prince Gustav Ice shelf in contemporary terms would have extended to just south of the PGC South 1200 m sampling site (Cooper, 1997; Ferrigno et al., 2006). Sites in this study therefore would have been just proximal to the ice shelf rather than directly covered by it, however the effects of this are similarly unknown.

3.4.2 Sampling biases and comparability

The Agassiz Trawl is best suited for collecting large epifauna or large infauna at or close to the sediment surface interface, and can be hindered by very rocky substrate, hence why 200 m and 500 m trawls in the main channel were not possible due to the influence of boulders. This may explain why the sample site with the largest dropstones, PGC South 800 m, displayed relatively low abundances despite moderately high morphospecies richness. The nature of the trawl further limits the collection of smaller encrusting species, and larger numbers of small infaunal species than otherwise targeted can occasionally be collected when the trawl becomes embedded in soft sediment (Brasier et al., 2018), as likely occurred at Duse Bay 500 m site, which displayed the highest diversity and highest overall familial and morphospecies richness, largely from small infaunal taxa.

Placing these results in wider comparative terms is difficult due to the above sampling biases and general qualitative nature of the AGT, in addition to the range of sampling devices and different spatial and bathymetric scales used by previous benthic sampling projects. The majority of Antarctic macrobenthic abundance and diversity assessments have been carried out using grabs and corers (Linse et al., 2007), including the only previous biological sampling effort of the Prince Gustav Channel in 2000 (see Blake, 2015), and a number of large-scale assessments of Antarctic polychaete diversity (e.g. Hilbig et al., 2006; Neal et al., 2011; Parapar et al., 2011). Coring devices, which are considered more quantitative than dragged gear at the cost of area sampled, may only have a low degree of species overlap with sledged or trawled sampling gear even at the same site (Hilbig, 2004).

Several large Antarctic polychete studies have collected samples using an epibenthic sledge (EBS) (Neal, et al., 2018a; Schüller et al., 2009), however while the EBS is similarly a dragged sampling gear, it targets a smaller size class of fauna than the Agassiz trawl, again limiting comparability. The standardized use of multiple gear types at any one station is an efficient method of getting a comprehensive impression of the benthic fauna of an area, particularly where seafloor is sparsely colonized (Hilbig, 2004). Core and EBS samples were also taken during the JR17003a expedition and will be incorporated in future taxonomic studies using an integrative taxonomy approach (Glover et al., 2016), whereby morphological assessments are streamlined by molecular barcoding, and will provide a more holistic and comparable account of polychete diversity in the Prince Gustav Channel. However, AGT samples provide a good preliminary overview of the megafaunal and larger macrofaunal communities of the channel.

Antarctic AGT-based sampling efforts that are broadly comparable include the second expedition of the Ecology of the Antarctic Sea Ice Zone (EASIZ) program on board the RV Polarstern in 1998, in which 11 AGT trawls from depths ranging from 230 m–2070 m, primarily from the continental shelf and slope of the southeastern Weddell Sea, were sorted to family level (Arntz & Gutt, 1999). If excluding single locally abundant species such as *Sternaspis sendalli* at Duse Bay 1000 m, then the EASIZ AGT samples are broadly similar to the samples of this study in terms of total annelid abundances and familial richness, ranging from 28–101 individuals and 5–17 families per trawl. However, familial composition does differ somewhat, with Syllidae and Terebellidae amongst the most dominant families numerically, and families such as Maldanidae scarce relative to PGC samples. Furthermore, families that are moderately common in the EASIZ samples such as Glyceridae and Nereididae are totally absent from the PGC AGT samples. Maximum abundances also tended to be lower, with 43 syllid individuals the maximum recorded abundance in a single family for a single trawl, in contrast to individual counts of up to 173, 81, and 70 for Sternaspidae, Polynoidae, and Maldanidae respectively in PGC samples.

Closer to the PGC, several AGT trawls were taken from seabed formerly covered by Larsen A and B ice shelves during the expedition ANT-XXIII/8 RV on the Polarstern 2006/2007 (Gutt, 2008) as part of a larger study investigating the biodiversity of the then recently uncovered seabed (Gutt et al., 2011). Macrofaunal presence/absence data published show that several named species identified in the current study were also present in these samples, such as *Antarctinoe ferox, Antarctinoe spicoides, Austrolaeniella antarctica, Flabelligera mundata* (synonym of *Flabegraviera mundata*), *Harmothoe fuligineum, Harmothoe fullo, Maldane sarsi* and *Pista mirabilis* (Gutt et al., 2010), 12 and 5 years after the collapse of the Larsen A and B ice shelves.

The large flabelligerid *Flabegraviera mundata*, found at relatively high abundances at PGC Mid 850 m, is also thought to have been observed under the Amery Ice shelf, East Antarctica, 100 km from open water (as *Flabelligera mundata*) (Riddle et al., 2007), however it is a relatively common species in the Southern Ocean with an assumed circumpolar distribution (though see section 3.4.3)

3.4.3 Morphological limitations and future molecular work

This study provides a good preliminary assessment of polychete communities in the Prince Gustav channel in terms of broad dominant functional groups present and taxonomic composition at the family level. The turnover in community structure and diversity is important to understand in a wider perspective; significantly increased burial of organic carbon caused by loss of ice cover and increased primary production has recently been reported from Antarctic areas (Barnes, 2015; Fogwill et al., 2020; Pineda-Metz et al., 2020; Rogers et al., 2020) but the role of the faunal response to changed nutrient availability and sedimentation rates are not known (Gogarty et al., 2020; Smith & DeMaster, 2008). However, diversity at the species level can be difficult to assess based on morphological identification alone.

Many of the named species identified in this study are considered to have widespread, circum-Antarctic distributions and broad depth ranges – a phenomenon well reported both for Southern Ocean polychaetes and for Antarctic benthos in general (Schüller, 2011). The increasing use of molecular methods such as DNA barcoding in Antarctic sampling however is beginning to challenge this traditional notion (Grant et al., 2011), with numerous studies finding that many previously widespread species across several phyla are instead composed of cryptic species complexes (see Riesgo et al. 2015 and references therein) – morphologically similar yet genetically distinct species. In 2016, DNA barcoding of 16 Antarctic polychaete morphospecies found evidence of cryptic diversity in over half the morphospecies examined, including taxa identified in the present study, such as *Aglaophamus trissophyllus* and *Maldane sarsi* (Brasier et al., 2016), suggesting that assessment based on morphology alone may significantly underestimate true species diversity. More recently, evidence of cryptic diversity has been found in Southern Ocean lineages of the polynoid *Polyeunoa laevis* (Bogantes et al., 2020), a taxon also present in the JR17003a samples.

A further consideration is the fact that traditional faunal lists and taxonomic identification literature available for Southern Ocean polychaetes are considered to be outdated (Nealet al., 2018a), with the presence of several globally widespread taxa with Northern Hemisphere type localities questionable. For example, the supposed cosmopolitan *Maldane sarsi* and its Antarctic subspecies *Maldane sarsi antarctica* Arwidsson, 1911 have both been reported from throughout the Southern Ocean (e.g. Hartman, 1966, 1967) – while the stem and subspecies differ primarily by colour and gland pattern, these are not considered to be robust taxonomic characters (Wang & Li, 2016).

However, Brasier et al. (2016) found that DNA barcode data of morphospecies identified as *M. sarsi* collected from Scotia and Amundsen seas differed from barcodes of *M. sarsi* collected from the stem species' type locality in northwestern Europe[8]. The authors subsequently assigned their Antarctic morphospecies to *M. sarsi antarctica*, questioning whether the subspecies should be investigated as a separate morpho- or cryptic species given the genetic difference and geographic distance from the parent species, and querying the presence of the parent species in the Southern Ocean altogether. *Maldane sarsi* was amongst the most common morphospecies collected in the present study, with all morphotypes assigned to the parent taxon as a conservative approach until further assessment.

Annelids are also prone to fragmentation, and morphology cannot account for missing characters from damaged or incomplete specimens that could otherwise identify or delimit species. Although the preservation quality in the current study was high, the samples still included many posteriorly incomplete or damaged individuals, in addition to fragments without heads that were not included at all, but could be potentially be identified using DNA.

However, morphology can also overestimate species diversity. For example, the only two species of sternaspid polychaetes described from the Southern Ocean, *Sternaspis sendalli* and *Sternaspis monroi,* were recently synonymized (the latter now the junior synonym) based on a molecular investigation that found little genetic structure between the two despite considerable variation in diagnostic morphological characters (Drennan et al., 2019). Furthermore, Polynoidae, the most morphospecies rich family in the current study, can display considerable degrees of intraspecific variation yet remain a single genetic species, as in the case of *Harmothoe imbricata* (Linnaeus, 1767) from waters off Scandinavia and Svalbard, which has at least ten distinct colour morphs yet little genetic variation (Nygren et al., 2011). Additionally, juvenile polychaetes can also show marked morphological differences from adult counterparts, and thus can often be misidentified as separate species when using morphology alone (Neal et al., 2014).

While molecular-based taxonomy can allow for a faster, statistically-rigorous assessment of diversity (though with its own caveats, see Riesgo et al. 2015), morphological assessments are still necessary in terms of providing information on life history, ecology, and ecosystem function, in addition to linking molecular results to described species and traditional pre- molecular taxonomic literature, and are a requisite for useful field identification guides (Glover et al., 2016). Molecular taxonomy should thus complement rather than supplant existing taxonomic methods (Bucklin et al., 2011).

[8] This was a misreading of Brasier et al. 2016 – sequences for *M. sarsi antarctica* were not compared with those from type localities as none were available, though the subspecies was still recommended to be investigated.

The morphospecies identified in the present study will be subject to future molecular taxonomic and connectivity analyses, which will include the DNA barcoding of all specimens; additional annelid specimens collected from the PGC sampling sites on the expedition JR170003a using both Epibenthic Sledge (EBS) and multi-corer sampling gear will also be included in these analyses.

This will allow for a more thorough and comparable assessment of annelid diversity in the channel, for example through assessments of cryptic diversity and as an error check for morphological assignments. Furthermore, while the number of molecular investigations of Southern Ocean fauna have rapidly expanded in recent decades (Grant et al., 2011; Riesgo et al., 2015), major gaps in taxonomic and geographic coverage in terms of genetic data still exist, with annelids poorly represented relative to other groups such as Mollusca and Arthropoda (Riesgo et al., 2015), and regions of the Southern Ocean such as the Western Weddell Sea rarely sampled at all (Griffiths et al., 2014). Future molecular investigations of these samples will aid in filling these sampling gaps and will be included as part of wider phylogeographic and population genetic analyses assessing the connectivity, demographic history, and evolutionary origins of annelid fauna in this ice-influenced region. Understanding how the benthos of the Southern Ocean evolved and persisted through past environmental change over multimillion year timescales can provide insight into their resilience against current and future climactic change (Lau et al., 2020) and could inform current glacial and climactic models by providing an independent biological line of evidence for past ice sheet behaviour (Strugnell et al., 2018).

3.5 Conclusions

This study provides a good snapshot of diverse benthic communities in a habitat with a dynamic recent glacial history and continuing glacial influence, which may be relevant to future habitats if present rates of ice loss and retreat along the Antarctic Peninsula continue. In addition, these specimens begin to fill sampling gaps in a poorly sampled region of the Southern Ocean and will be utilized in future molecular investigations, both in terms of assessing the genetic diversity of the channel and as part of wider phylogeographic and population genetic analyses of annelid fauna in this ice-influenced region. Curating accurate taxonomic and distributional data provides a necessary and important baseline for monitoring ecosystems and understanding current and future environmental change, while insights into the evolutionary history of the Southern Ocean benthos can help inform current climatic debate.

The channel is of further interest as its southern portion (south of 64◦N) is currently included within the margins of a proposed Marine Protected Area for the Weddell Sea, presented in 2014 to the Commission for the Conservation of Antarctic Marine Living Resources (CCAMLR), though as of 2018 has not yet been agreed upon (UN Ocean Conference, 2018). Increased knowledge of the fauna of this region may contribute to future decisions in regards to conservation policy implementation for the Weddell Sea area.

3.6 Acknowledgements

For detailed acknowledgements as published in Drennan et al. 2021b, Appendix B section B.1

Chapter 4 Do molecular barcodes enhance morphological species identification in biodiversity assessments? A case study in integrative identification of annelid fauna from the Prince Gustav Channel, Northeastern Antarctic Peninsula

REGAN DRENNAN [1,2,3], KATRIN LINSE [3], THOMAS G. DAHLGREN [4,5], JONATHAN T. COPLEY [1]; ADRIAN G. GLOVER [2]

[1] Ocean & Earth Science, University of Southampton, European Way, Southampton SO14 3ZH, UK

[2] Life Sciences Department, Natural History Museum, London SW7 5BD, UK

[3] British Antarctic Survey, High Cross, Madingley Road, Cambridge CB3 0ET, UK

[4] NORCE Norwegian Research Centre, Bergen, Norway

[5] Department of Marine Sciences, University of Gothenburg, Box 463, 40530 Gothenburg, Sweden

Abstract

In recent decades, the introduction of molecular barcoding into integrative species identification and biodiversity assessments has revolutionised the fields of taxonomy and ecology. Using molecular barcoding, morphologically similar yet genetically cryptic species can be separated, while morphologically variable yet genetically similar specimens, or polymorphic adults and juveniles, can be united as single taxa. Having an accurate picture of biodiversity is necessary for monitoring both current and future environmental change. However, most biodiversity assessments largely still use morphological identifications only, while full integrative molecular surveys face issues of scale, time, and cost. We used specimens from a recent faunal study of marine annelid communities in the Prince Gustav Channel, Antarctica, to test how barcoding a subset of representative morphospecies changes morphological species identifications in relation to the species richness and diversity of a region. Initial morphological identifications recorded in 57 morphospecies or operational taxonomic units (OTUs) belonging to 25 families across 610 annelid specimens, of which a representative subset of 212 individuals were selected for molecular barcoding. Combined molecular and morphological results revealed 58 molecular OTUs and 23 families. While the total overall species richness in the sampling area did not change considerably, detailed results showed considerable turnover within this number, with increases and decreases in taxonomic resolution, new genetic species, and removal of species due to misidentification or variable morphology.

Furthermore, public sequence databases often displayed insufficient sequence coverage to confirm or refute morphospecies identification. Our results show that morphological identifications are still playing a valuable role in biodiversity assessments of geographic areas for biodiversity and conservation purposes, however for more accurate results and to facilitate future developments in metabarcoding, efforts should be made to increase molecular barcodes with high quality identifications for Southern Ocean benthos in sequence databases.

Keywords: Morphospecies, molecular operational taxonomic unit, biodiversity, Southern Ocean, COI

4.1 Introduction

Current rates of global biodiversity loss are unprecedented in recent times, with rates of extinction predicted to accelerate further in coming decades without significant action to mitigate human impacts (IPBES, 2019). Species are a fundamental unit of biology; accurate species identifications and biodiversity estimates are vital for establishing baselines with which to measure change and manage conservation efforts, particularly for habitats and ecosystems that remain relatively unexplored. Marine ecosystems in particular face a growing number of anthropogenic threats (Halpern et al., 2008); despite this, large knowledge gaps remain, with an estimated 1-2 million marine species yet to be described (Bouchet et al., 2023).

Traditionally, biodiversity has been measured based on using morphological characters to delineate taxonomic units and identify species. However, morphological identification can lead to false interpretations, such as not differentiating morphologically cryptic species, or unnecessarily splitting species with variable morphology. Different life history stages, strongly sexually dimorphic forms, and damaged, fragmented specimens can also be impossible to identify accurately based on morphology alone (Bucklin et al., 2011). Sorting and identifying samples in biological assessments is labour intensive and prone to error based on the taxonomic expertise of the sorter (Krell, 2004; Stribling et al., 2008). The use of DNA barcodes has become standard methodology in many biodiversity studies to complement, or as an alternative to, traditional identification methods, with particular strengths in addressing the limitations listed above. DNA barcodes are short, standardised DNA sequences used to (a) delineate species (recognising species boundaries), by *a priori* sequence divergence thresholds and /or (b) identify species (assign taxonomic name to a species) by comparison with curated reference libraries (Hebert 2003a, 2003b).

A strength of DNA barcoding is its potential to standardize and increase the speed and accuracy of species delimitation and identification (Eberle et al., 2020), particularly in the context of global taxonomic impediments. However, barcode data can be prone to error, for example through poor sequence annotation, poor sequence quality, and incorrect consensus sequencing building (Gostel & Kress, 2022). The most-used barcode gene in Metazoa, mitochondrial cytochrome oxidase unit I (COI) also has a number of methodological caveats, for example not being variable enough to delineate species in some animal groups (e.g. sponges, Huang et al., 2008), mitochondrial genes not necessarily representing species gene trees and evolutionary history (Naciri & Linder, 2015), and a lack of a universal barcode gap (a threshold of genetic divergence with which to delineate species) in some animal groups (e.g. annelids, Kvist, 2014), while insufficient sampling both numerically and geographically can exaggerate genetic structure (Lohse, 2009).

Furthermore, specimen identification using barcode data is most effective where sequence coverage on available databases is broad, and where taxa are known and well-studied – i.e. where curated reference libraries exist (DeSalle & Goldstein, 2019). The utility of barcodes for species identification is weaker for lesser-known taxa and in poorly sampled geographic regions, and often are unable to identify taxa beyond molecular operation taxonomic units in these cases (Mugnai et al., 2021) – in 2021, only 14.5% of 207,821 then-known marine animal species were represented by COI barcode data on public repositories (Mugnai et al., 2021). The quality of the reference library must also be considered. Erroneous data on public sequence databases such as GenBank and Barcode of Life Data Systems (BOLD) can manifest in several different ways, for example from contaminated sequences, amplification of non-target genes, incorrect identification of study organisms, and general error during data entry (see Leray et al. 2019 and references therein). Though major taxonomic errors on GenBank, the largest sequence repository, have been found to be only <1% at the genus level (Leray et al., 2019), a recent analyses of sequences from 7,576 marine invertebrate species on BOLD (which mines data from GenBank) found at least 7% of species to be misidentified or contaminated and that 14% contained multiple COI species based on barcode thresholds, with the quality of an additional 17% remaining ambiguous (i.e. regarding misidentification, or number of COI species) (Radulovici et al., 2021).

The gold standard in taxonomy is an integrative approach, which uses multiple lines of complementary evidence such as morphological, molecular, ecological, behavioural, and developmental data etc. to define species boundaries, which greatly increases the rigour and robustness of species delineation with different data types covering the weaknesses of others (Schlick-Steiner et al., 2010). Until however more cost and time effective barcoding technologies become more widespread (e.g. Srivathsan et al., 2021), sequencing all individuals at the scale of community level biodiversity surveys in addition to morphological analyses can remain unfeasible, particularly where resources are limited.

The Southern Ocean, whilst relatively well protected from industrial activity and development (Halpern et al., 2008), represents a threatened marine ecosystem in the context of rapid ocean warming and ice loss (Lee et al., 2017; Naughten et al., 2023). At least half of known Antarctic benthic species are endemic to the Southern Ocean (Griffiths et al., 2009), while large regions such as the western Weddell Sea and East Antarctica are poorly sampled (Griffiths et al., 2014), and seafloor habitats beneath Antarctic ice shelves amongst the least explored on the planet (Kim, 2019).

Facilitated by large scale sampling campaigns in the 2000s such as the Census of Antarctic Marine Life (CAML http://www.coml.org/census-antarctic-marine-life-caml/), the number of molecular investigations into Antarctic benthic biodiversity, primarily using DNA barcodes, has increased rapidly in recent decades (reviewed in Riesgo et al., 2015), revealing diversity in Antarctic benthic fauna previously unrecognised based on morphology alone. For example, numerous molecular studies have found cryptic diversity in species with previously assumed circumpolar (e.g. Baird et al., 2011; Bogantes et al., 2020; Dietz et al., 2014; Raupach & Wägele, 2006; Wilson et al., 2009) or eurybathic (e.g. Brasier et al., 2017; Schüller, 2011) distributions. Meanwhile, other barcode studies of Antarctic benthos have found taxa previously split by morphology to be single polymorphic species (Drennan et al., 2019), linked juveniles with ambiguous morphology to adult species (Neal et al., 2014), or have acted as an error check for initial morphological analyses (Brasier et al., 2016). However, these still face the methodological limitations of using single or small number of genes as discussed above, and are often focused on single or small groups of species, whereas the majority of community level faunistic studies of Antarctic benthos are still based on morphology (e.g. Barnes et al., 2009; Brandt et al., 2016; Drennan et al., 2021; Ellingsen et al., 2007; Mou et al., 2022; Neal et al., 2018a; Piepenburg et al., 2002).

Taxonomic identification literature and traditional species lists for some taxonomic groups such as Annelids are considered outdated for the Southern Ocean (Neal et al., 2018a), which puts the reliability of morphological identifications into question. For example, many Antarctic records of species with Northern Hemisphere type localities are clearly dubious. While a small number of marine annelids may genuinely display global distributions (Meyer et al., 2008), current evidence suggests that restricted distributions are more common, with documented cosmopolitanism largely a historic artefact (Hutchings & Kupriyanova, 2018). Brief original taxonomic descriptions, damaged or missing type material, cryptic morphology, and a lack of genetic data from type localities on public repositories makes the process of revising traditional annelid taxonomic literature and the status of cosmopolitan taxa in the Southern Ocean challenging.

In this study, we test whether molecular data via DNA barcoding a subsample of representative morphospecies significantly improves taxonomic resolution of a morphology-based assessment of Annelid communities in the Prince Gustav Channel, a previously ice-covered channel on the northeast Antarctic Peninsula (Drennan et al., 2020). The aim of this study is to investigate the effectiveness and practicality of an integrative identification approach for biodiversity assessments for Southern Ocean annelids. In addition, the presence of a north-western European annelid (*Maldane sarsi* Malmgren, 1866) in Antarctic waters from Drennan et al. (2021) samples is tested by comparison of morphology and sequence data to new material collected from a type locality of *M. sarsi* (Kosterfjord, Sweden) as an exemplar integrative approach for addressing outdated taxonomic information and issues such as false cosmopolitanism.

4.2 Materials and Methods

4.2.1 Sample collection and identification

Annelid specimens were collected by Agassiz trawl (AGT) from the Prince Gustav Channel (PGC) on the northeastern tip of the Antarctic Peninsula during the expedition JR17003a on the RRS *James Clark Ross,* February-March 2018 (Linse et al., 2018). Six successful Agassiz Trawl (AGT) deployments were carried out at six sites along the channel across three sampling areas, at depths ranging from 204 m to 1270 m (Figure 4.1; Table 4.1). The 2 m-wide AGT, targeting benthic macro- and megafauna, comprised of a 1 cm mesh inner sampling net, and was trawled at 1 knot for 5-10 mins along the seabed during each deployment. Small macrofauna were also collected in sediment retained in trawls. A live sorting pipeline was carried out on-board following the "cold-chain" method as outlined in Glover et al. (2016). In summary, 300-micron sieves were used to wash AGT subsamples carefully using cold filtered seawater (CFSW), with annelid specimens picked from sieve residue, maintained and cleaned in CFSW, and relaxed in a solution of magnesium chloride for specimen photography.

Table 4.1 Table of Agassiz Trawl deployments in the Prince Gustav Channel during expedition JR17003a

Event no.	Site	Date	Decimal latitude	Decimal longitude	Max depth (m)
56	Duse Bay 200 m	2018–03–07	–63.6253	–57.4863	204
52	Duse Bay 500 m	2018–03–07	–63.6161	–57.5035	483
4	Duse Bay 1000 m	2018–03–01	–63.5755	–57.2954	1081
46	PGC mid 850 m	2018–03–06	–63.8060	–58.0652	870
38	PGC south 800 m	2018–03–05	–64.0552	–58.4765	868
43	PGC south 1200 m	2018–03–06	–63.9881	–58.4225	1271

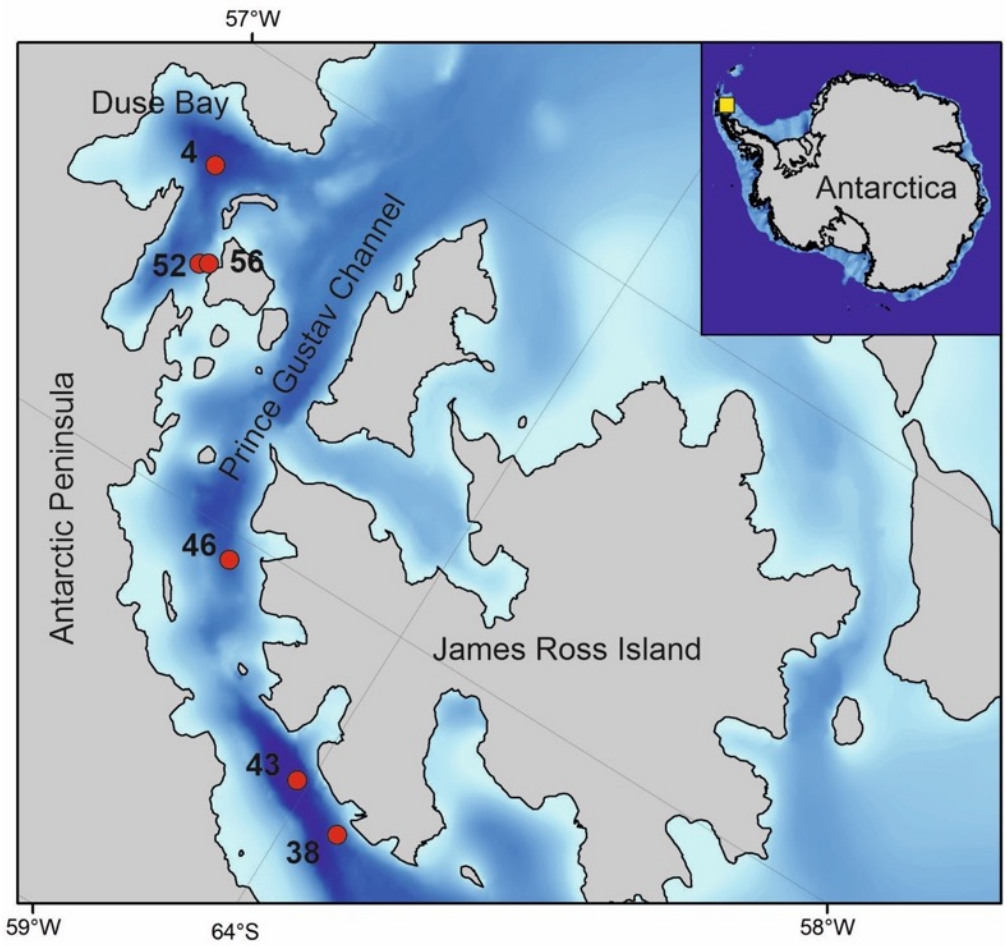

Figure 4.1 Map of Sample site, the Prince Gustav Channel, with Agassiz Trawl deployments highlighted in red and marked with event number. Map credit Huw Griffiths.

Collected specimens were imaged using Canon EOS600D cameras with a 100 mm Macro lens or through a Leica MZ7.5 microscope with SLR camera mount, and identified preliminarily on-board to family level, before being numbered, recorded on a database and fixed in 80% non-denatured ethanol. AGT subsamples that could not be sorted on-board for restricted time were fixed in bulk in 96% ethanol for later sorting.

Specimens were re-examined at the Natural History Museum London and identified morphologically to lowest possible taxonomic rank. Initially, 598 individuals in 57 morphospecies across 25 annelid families were documented across the six PGC AGT sampling sites (Drennan et al., 2020). During specimen selection for DNA extraction, original morphospecies assignments and specimen counts were checked and reviewed, resulting in 612 specimens (Table 4.2). Five headless individuals that were not part of the original specimen count in Drennan et al. 2021 were also included in molecular analyses, with the aim to either match diagnostic characters of a tail fragment to a head fragment to facilitate identification to named species, and to assess the presence of additional families from damaged specimen fragments.

The family Serpulidae (one individual, Serpulidae sp. NHM_280K) was removed, as the specimen originally identified consisted of a serpulid tube containing an animal which upon removal of the animal from the tube revealed to be a nemertean inhabiting an empty serpulid tube and was thus excluded in the updated specimen and morphospecies count. However, the nemertean specimen was still included for barcoding to confirm its identification. Other potential morphospecies with unclear morphological characteristics that could lead to misidentifications were noted for attention upon analysis of the barcoding results. In total for this study, 612 individual polychaetes belonging to 56 morphospecies across 24 families were analysed (Table 4.2). These specimens, identified to morphospecies, served as the basis of the molecular barcoding by extracting DNA from representatives of each morphospecies across all sites in which they occurred.

An additional 15 individuals identified as *Maldane sarsi* were collected from an original type locality: Kosterfjiord, Sweden (Malmgren, 1866) (collected from the same station, lat: 58.6498°, long: 11.0451°, depth 135 m, over 3 years: 2017, 2019, 2021) and included in molecular and morphological analyses in order to assess whether Antarctic records of *M. sarsi* in Drennan et al. (2021) are a distinct and separate species. *Maldane sarsi* was first described in 1886 by Johan Anders Malmgren (Malmgren, 1866), based on no single holotype, but rather several syntypes from several North Atlantic locations from Svalbard, and the west coasts of Norway and Sweden, including Kosterfjord. *Maldane sarsi* has subsequently been reported worldwide, including from the Southern Ocean, though no genetic data from type localities has been publicly available. *Maldane sarsi* includes an Antarctic subspecies *M. sarsi antarctica,* collected in 1902 by the Swedish Antarctic Expedition from South Georgia and the Antarctic Peninsula, and described by Ivar Arwidsson in 1911 (Arwidsson, 1911), differing from the parent species by minor morphological differences. Both subspecies and parent species have been reported from across the Southern Ocean, adding confusion as to whether they are the same taxon, whether they both coexist, and the larger question of whether Antarctic records are a separate and distinct species. *Maldane sarsi antarctica* was described off James Ross Island, which borders the Prince Gustav Channel, so that samples from Drennan et al. (2021) are good representatives of the subspecies type locality. Specimens in Drennan et al. (2021) were identified as the parent taxon rather than the subspecies as a conservative approach.

Table 4.2 Updated table of individual number and morphospecies per polychaete family (or higher taxonomic rank in the case of oligochaeta) sampled during cruise JR17003a following re-examination during specimen extraction. For original table, see Chapter 3 Table 3.2

Family (or higher)	Total Site		Sites											
			Duse Bay 200 m		Duse Bay 500 m		Duse Bay 1000 m		PGC Mid 850 m		PGC South 800 m		PGC South 1200 m	
	No. ind.	*No. sp.*	*No. ind.*	*No. sp.*	*No. ind.*	*No. sp.*	*No. ind.*	*No. sp.*	*No. ind.*	*No. sp.*	*No. ind.*	*No. sp.*	*No. ind.*	*No. sp.*
Ampharetidae	5	1	2	1	2	1	-	-	-	-	1	1	-	-
Cirratulidae	10	4	2	1	7	4	1	1	-	-	-	-	-	-
Dorvilleidae	5	1	-	-	5	1	-	-	-	-	-	-	-	-
Flabelligeridae	27	2	-	-	-	-	-	-	10	2	-	-	17	1
Hesionidae	1	1	-	-	1	1	-	-	-	-	-	-	-	-
Lumbrineridae	12	2	1	1	6	2	4	1	-	-	1	1	-	-
Maldanidae	133	4	7(-1)	1	37(+1)	3	68	2	-	-	21	3	-	-
Myzostomidae	1	1	-	-	-	-	-	-	-	-	1	1	-	-
Nephtyidae	16(-1)	2	-	-	4	2	5(-1)	1	6	1	-	-	1	1
Oligochaeta	6(+3)	2	-	-	6(+3)	2	-	-	-	-	-	-	-	-
Opheliidae	7(+1)	2	-	-	7(+1)	2	-	-	-	-	-	-	-	-
Orbiniidae	3(-1)	1	-	-	3(-1)	1	-	-	-	-	-	-	-	-
Oweniidae	17(+1)	1	-	-	2(+1)	1	-	-	15	1	-	-	-	-
Paraonidae	1	1	-	-	1	1	-	-	-	-	-	-	-	-
Phyllodocidae	5	3	1	1	-	-	1	1	3	3	-	-	-	-
Polynoidae	114(+9)	12	2	2	3	3	10(+4)	3(+1)	86(+4)	10	6	5	7(+1)	2
Sabellidae	29	2	25	2	2	2(+1)	-	-	1	1	1	1	-	-
Scalibregmatidae	1	1	-	-	1	1	-	-	-	-	-	-	-	-
Serpulidae	0(-1)	0(-1)	-	-	0(-1)	0(-1)	-	-	-	-	-	-	-	-
Sternaspidae	176	1	2	1	-	-	173	1	-	-	1	1	-	-
Syllidae	21(+2)	4	-	-	9(+2)	2	-	-	7	2	5	2	-	-
Terebellidae	12(+1)	5	4	2	3(+1)	2	1	1	2	1	2	2	-	-
Tomopteridae	1	1	-	-	-	-	-	-	-	-	1	1	-	-
Travisiidae	1	1	-	-	-	-	-	-	-	-	1	1	-	-
Trichobranchidae	8	1	1	1	7	1	-	-	-	-	-	-	-	-
24(1-)	612(+14)	56(-1)	47(-1)	13	106(+7)	33(+1)	263(+3)	10	130(+4)	21	41	19	25(+1)	4

4.2.2 DNA extraction and sequencing

Tissue samples were taken from representatives of each morphospecies across all sites in which they occurred, as well as 5 unidentified partial specimens. Additional tissues samples to widen extraction coverage were taken from *Maldane sarsi,* and morphospecies with previously reported cryptic diversity (e.g. *Aglaophamus trissophyllus* (Grube, 1877)*, Austrolaenilla antarctica* Bergström, 1916*;* Brasier et al., 2016; Neal et al., 2014), and to members of the family Polynoidae which displayed high diversity at the morphospecies level in the PGC (Drennan et al., 2020).

DNA was initially extracted for 200 selected PGC specimens (including 5 partial specimens) using the BioSprint 96 Extraction Robot and BioSprint 96 DNA Blood Kit (Qiagen Inc., Hilden, Germany) following the supplier's instructions. Plates were set up so that neighbouring wells contained alternating specimens of different families, so that any contamination within the sample would be obvious. For DNA extraction, a small section of tissue was dissected for each specimen, taking care to keep informative morphological characters intact, such as the dissection of a parapodium (or several, depending on animal size) taken from one side of the body, leaving the other side intact. Additional extractions of *Aglaophamus trissophyllus* (*n*=6) and *Maldane sarsi* (PGC *n*=11; Kosterfjord *n*=15) were carried out using DNeasy Blood and Tissue Kit (Qiagen) and QuickExtract DNA Extraction (Epicentre) respectively.

Approximately 650 bp of cytochrome c oxidase subunit I (COI) and 450 bp of 16S rDNA were amplified for each extraction. COI was the primary target gene as it is relatively fast evolving and highly variable (Avise, 2009), often exhibiting greater variation between species than within (Grant & Linse, 2009), and can therefore be used as a tool to aid in defining species boundaries. The COI region is also considered the standard DNA barcode region (Hebert et al. 2003a), and has been widely sequenced across phyla and ecosystems, including the Southern Ocean (Riesgo et al. 2015 and references therein) and can therefore also aid in species identification where curated barcode reference libraries exist. However, as COI can be difficult to obtain for some annelid groups (e.g. Brasier et al., 2016; Radashevsky et al., 2016),a second mitochondrial gene, 16S, despite a slower rate of evolution, can be used as a barcode in place of COI (Vences et al., 2005a,b). Often, 16S displays a higher sequencing success rate across annelids (e.g. Brasier et al., 2016; Wiklund et al., 2019) and has been used previously to detect cryptic diversity in Southern Ocean annelids alongside COI (Brasier et al., 2016). Following initial sequencing, a selection of Antarctic and Swedish *Maldane sarsi* specimens representative of genetic structure found in barcode results were sequenced for ~1800bp of the nuclear 18SrDNA gene to assess deeper phylogenetic relationships. All primers used are listed in Appendix C Table C.1.

PCR mixtures contained 0.5 ul of each primer, 1 ul template DNA and 10.5 ul Red *Taq* DNA Polymerase Master Mix (VWR, UK) for a total volume of 12.5 ul. PCR amplification profiles were as follows: COI – initial denaturation of 5 mins at 95°C followed by 35 cycles of 30s at 95°C, 30s at 49°C, 1 min at 74 °C, with a final extension of 10 min at 74 °C; 16S – initial denaturation of 5 mins at 94°C followed by 35 cycles of 30s at 94°C, 30s at 57°C, 1 min at 68 °C, with a final extension of 7 min at 68 °C; 18S – initial denaturation of 5 mins at 95°C followed by 30 cycles of 30s at 95°C, 1m at 59°C, 2 min at 72 °C, with a final extension of 2 min at 72 °C.

Resulting PCR products were purified and sequenced at the Natural History Museum London Sequencing Facilities using a Millipore Multiscreen 96-well PCR Purification System and ABI 3730XL DNA Analyser (Applied Biosystems). Resulting DNA sequences were processed and aligned in Geneious 10.09.01 (https://www.geneious.com), with contigs assembled from overlapping forward and reverse sequence fragments, and of ambiguous base calls manually corrected.

Sequences were compared against all COI, 16S, and 18S sequence data available on the public database GenBank (NCBI), using the blastn algorithm (M. Johnson et al., 2008) via the Geneious plugin with default settings. The blastn results were used to check for sequence contamination, misidentification errors, improve original taxonomic identification and highlight potential cryptic diversity for downstream phylogenetic analyses. To avoid erroneous or misidentified sequences on GenBank, a conservative approach was taken when using blastn to update morphospecies IDs, with positive matches ideally across multiple sequences from different sources, close to type locality of taxon, and included in taxonomic publications. High percent identity matches at generic level or above were not used.

4.2.3 Phylogenetic analyses and species delimitation

Separate 16S and COI Bayesian phylogenetic analyses were performed for the entire Prince Gustav Channel morphospecies genetic dataset, i.e. including all families, with the aim to compare morphospecies identifications with monophyletic topological clusters and to further highlight misidentification and potential cryptic diversity. Two molluscan taxa were used as outgroups in both analyses (*Solemya velum* Say, 1822: KC984745 COI, KC984675 16S; *Charonia tritonis* (Linnaeus, 1758): MH581312 COI, MH571329 16S).

A combined phylogenetic analysis of three genes 16S, COI, and 18S, was also performed for newly sequenced Antarctic and Swedish *Maldane sarsi* sequences, all *Maldane* spp. sequences available on GenBank, and representatives of *Maldane* subfamilies following (Kobayashi et al., 2018). See Appendix C Table C.2 for list of GenBank accession numbers for maldanids and outgroups used in this analysis.

16S and 18S sequences were aligned using MAFFT *v7.450* (Kazutaka Katoh & Standley, 2013), and COI using MUSCLE (Edgar, 2004), both programs implemented via Geneious plug-ins using default settings. COI alignments were translated into amino acids to check for stop codons to avoid the inclusion of pseudogenes.

Bayesian analyses were run in triplicate for both single gene and combined datasets using MrBayes 3.2.7 (Ronquist et al., 2012) for 10,000,000 generations under default settings, with 2,500,000 discarded as burnin. The most suitable substitution model for each gene was chosen using Modeltest-NG (Darriba et al., 2020) and the Bayesian information criterion. For COI datasets, the most suitable model for each of the three codon positions was chosen.

Phylogenies were reconstructed using Bayesian Inference (BI), assessing branch support by posterior probability (PP) with values ≥ 0.95 considered as highly supported (Felsenstein 1985, Huelsenbeck et al. 2001). Trees were visualised and edited using FigTree 1.4.4 (Rambaut 2009) and Affinity Designer v1.10.5.

For the Maldanidae dataset, haplotype networks were generated separately for 16S and COI alignments of all GenBank and newly generated sequences identified as *Maldane sarsi* in the software PopART (http://popart.otago.ac.nz) using the TCS algorithm.

A phylogenetic species concept was used to define molecular operational taxonomic units (MOTUs), whereby the between species divergence (interspecific) is expected to be on an order of magnitude larger than the within species divergence (intraspecific) – the barcode gap. Following phylogenetic analyses, inter and intraspecific pairwise genetic distances for both genes were calculated for morphospecies and MOTUs using the p-distance model and pairwise deletion of gaps in MEGA v11 (Tamura et al., 2021). Genetic distances were presented as the smallest and largest inter- and intraspecific distances respectively, as using mean values, e.g. mean interspecific distances, can exaggerate the barcoding gap and mask overlap between values (Meier et al., 2008).

For the Prince Gustav Channel datasets, owing to a small number of individuals often representing each morphospecies, a small number of morphospecies per family, and large branch lengths between specimens in different families, automated methods of molecular species delimitation (e.g barcode gap) were uninformative. However, for the family Polynoidae, the most species rich family in Drennan et al. (2021) with up to 12 morphospecies, and often numerous individuals per species, molecular species delimitation methods were attempted.

Using the COI dataset, species in Polynoidae were delimited using the pairwise distance-based method ASAP (Assemble Species by Automatic Partitioning; Puillandre et al., 2021), and two tree-based methods, GYMC (Generalized Mixed Yule Coalescent; Pons et al., 2006), and PTP (Poisson Tree Processes; Zhang et al., 2013).

ASAP builds on a previous method, Automatic Barcode Gap Discovery (ABGD) (Puillandre et al., 2012), which uses pairwise genetic differences to identify a barcode gap in their distribution, which is used as a threshold with which to partition putative species, providing a range of partition scenarios where uncertainty is present. ASAP improves on ABGD by providing a ranked scoring system with which to evaluate partition scenarios and requires no biological prior information on intraspecific diversity. GMYC and PTP require phylogenetic trees as input and identify transition points between inter and intraspecific branching rates in terms of absolute time (GYMC) and number of substitutions (PTP) in order to partition species.

ASAP was performed via the ASAP web interface (https://bioinfo.mnhn.fr/abi/public/asap/) using the evolutionary model Kimura 80 (K80 ts/tv= 2.0). The GMYC method requires an ultrametric tree as an input. A Bayesian ultrametric tree was generated using the BEAST v 2.71 (Bouckaert et al., 2019) program suite with tree and clock models were linked across partitions using the Yule tree model and relaxed clock log normal model respectively. Site models were unlinked and tested with three partitions (codons 1, 2, and 3) or two partitions (codons 1+2, and 3). Models for each partition combination were chosen using Modeltest-NG (Darriba et al., 2020) and the Bayesian information criterion - three partitions: TIM3ef+I, F81, and TrN +G4; two partitions TIM2+I+G and TrN+G. Initial analyses were run using two independent runs of 50-100 million steps. The most optimal run was two partitions, using a simpler model (HKY+G) for partition 1+2. The final run consisted of two independent runs of 100 million steps, which were checked for convergence and combined after discarding 50% as burnin (20% run 1, 30% run 2), with a median consensus tree estimated from combined, post-burnin runs. GYMC analysis was run in R (R Core Team, 2023) using package splits (Ezard et al., 2021) and using the single threshold criterion (Fujisawa & Barraclough, 2013).

As PTP does not require an ultrametric tree, a Bayesian analysis was performed in MrBayes for the polynoid-only COI alignment, as described for the all-morphospecies analysis, to generate the input tree. Three partitions were used, and best fitting models for each partition were adjusted for MrBayes to GTR+I, F81, and GTR + G. PTP analyses were run in triplicate on the bPTP web server https://species.h-its.org/ptp/ using 250,000 MCMC generations and 25% burnin.

For both ultrametric and non-ultrametric trees, the sigalionids *Pholoides asperus* (Johnson, 1897) (JN82924) and *Pisionidens* sp. (JN85293) were used as outgroups.

For ASAP, GMYC and PTP, the final input alignment only included specimens with unique haplotypes due to the unevenness of some morphospecies (e.g. *Barrukia cristata* containing multiple individuals with identical haplotypes, and others by singletons or small numbers with moderate intraspecific distance), which, following experimentation, had the effect of drastically over-splitting species with low intraspecific distances in ultrametric tree (inflating branch lengths), and lumping species despite intraspecific distances >13% in ASAP.

4.2.4 Data handling

All sequence data and an updated DarwinCore archive formatted specimen table is available from the following supporting dataset:

Drennan (2024) Data supporting University of Southampton Doctoral Thesis entitled: Patterns of diversity, connectivity, and evolution in southern ocean and deep-sea annelids. University of Southampton doi:10.5258/SOTON/D2958 [Dataset]

Results of this chapter are planned for publication, with specimen data updated on GBIF and OBIS via the SCAR Antarctic Biodiversity portal (biodiversity.aq). Barcode sequence data will made publicly available on Genbank following publication of results. All specimens and DNA vouchers will be archived in the Natural History Museum London collections.

4.3 Results

4.3.1 DNA extraction

From the available 612 polychaete specimens comprising 56 morphospecies and the one nemertean, 195 specimens were selected for DNA extraction to represent individuals from each morphospecies across all sites they occurred on. All extractions were successful and yielded DNA for PCR amplifications targeting the COI and 16S gene loci.

4.3.2 Sequencing success

The sequencing success rate of the 212 PGC DNA extracts differed slightly between the two target barcoding regions. A total of 176 sequences were amplified for 16S sequences and 159 sequences were amplified for COI. Headless specimens contributed an additional three 16S and four COI sequences respectively but matched existing specimen IDs, and thus may be broken fragments of specimens already counted, and were excluded from further analyses. However, these aid further morphological analysis posterior morphological characters were missing. One damaged specimen was revealed to be a headless fragment following sequencing (see section 4.3.4.3). Three families (Paraonidae, Scalibregmatidae, Travisiidae), each with a single representatives resulted in no sequencing success for either barcode gene.

Following initial blastn analysis of the 16S and COI sequences, three specimens were found to be contaminated during the DNA extraction or sequencing steps, either to a non-Antarctic annelid, or to specimen in a neighbouring extraction well, confirmed by secondary morphological analysis. Therefore, these sequences were removed from further molecular analyses. A further specimen (Oligochaeta_sp_289) was found to be a misidentified nemertean, which was confirmed by secondary morphological analysis, and aligned with the nemertean from the single serpulid tube, and both sequences were removed from the further analyses.

Excluding the above cases, the final total included 172 sequences of 16S and 153 sequences of COI, resulting in a total of 183 specimens with at least one barcode sequence and coverage of 53 morphospecies and 21 families.

4.3.3 Phylogenetic analyses

Due to the large size of the 16S and COI all-family phylogenies, and low support and lack of resolution at branches between families, both trees have been placed in chapter appendices (Appendix C Figures Figure C.1,Figure C.2), with respective sections of trees for each family presented, with corresponding p-distance table and discussion of updated identification, if any.

4.3.4 Results by polychaete families

4.3.4.1 Ampharetidae

Initial morphospecies results indicated a single taxon, Ampharetidae sp. NHM_280A (Figure 4.2 a). Out of five individuals, three were successful in sequencing at least one gene. All sequenced specimens formed a monophyletic clade with high support in phylogenetic analyses, however with a potentially distinct and cryptic lineage in 16S (Figure 4.2 b-c). Specimen NHM_280A_1 and NHM_324_1 collected from Duse Bay 500m and 200m respectively share identical sequences in 16S, with 0.1% pairwise p-distance in COI (Table 4.3) . These sequences match 99.9-100% identity in blastn analysis in both 16S and COI to Ampharetid specimens identified as *Ampheictis* sp., collected from the Ross Sea (Eilertsen et al., 2017).

Table 4.3 Number of individuals, number of sequences for 16S and COI barcodes and maximum intraspecific p-distances (left 16S/right COI) for morphospecies in the family Ampharetidae.

		n	n 16S	n COI	**a**
a	Ampharetidae sp. NHM_280A	5	3	2	0.07/0.001

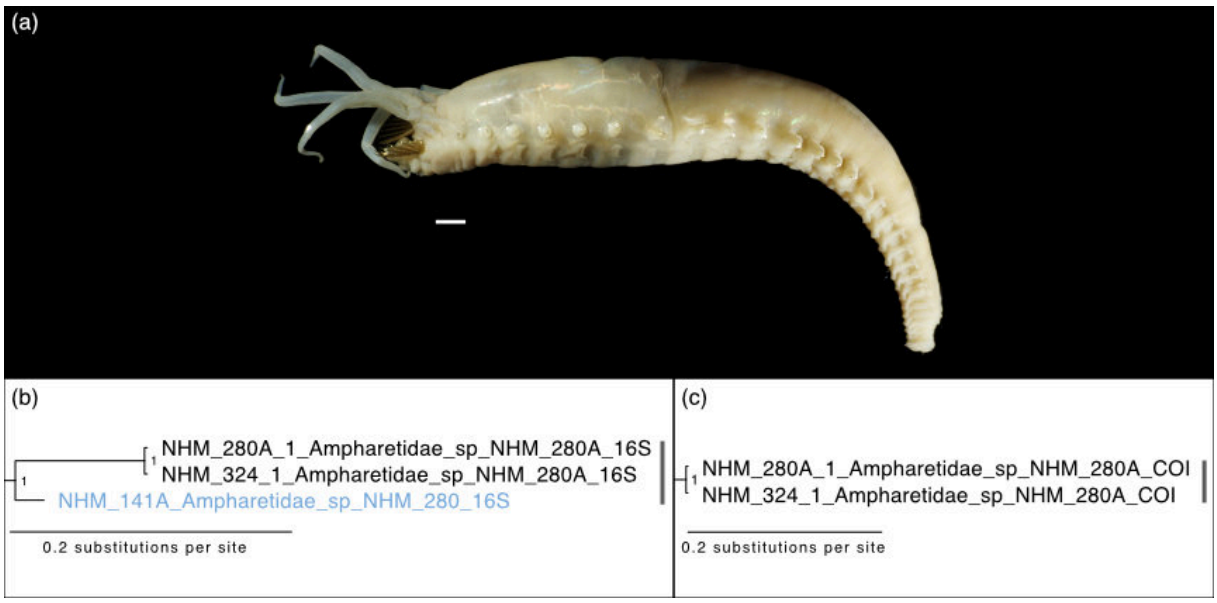

Figure 4.2 (a) Morphospecies Ampharetidae sp. NHM_280A, preserved specimen NHM_324_1. Scale bar 1 mm. (b-c) Sections of Prince Gustav Channel phylogenies generated by Bayesian analysis for family Cirratulidae using (b) 16S and (c) COI. Potentially cryptic lineage (specimen NHM_141A) highlighted in blue. Support values for both phylogenies are given as Bayesian posterior probabilities. Vertical lines indicate final counted taxonomic units.

Specimen NHM_141A collected from PGC South 800m was only successful in 16S sequencing and differed from the other two specimens by 7% p-distance in this gene (Table 4.3). This 16S sequence also matches with lower percent identity to GenBank *Ampheictis* sp. (93.5%). In other studies of Ampharetid taxa using 16S barcodes, intra and interspecific distances range from 0-1.1% and 6.6-20.6% respectively (Alalykina & Polyakova, 2020; Gunton et al., 2020; Kongsrud et al., 2017; Lee, 2021), suggesting that NHM_141A may represent a separate species. However, with only a single specimen and gene, a larger number of samples from each lineage would be needed to assess rates of inter and intraspecific variation.

In summary, barcode data is insufficient to definitively change previous morphospecies identification in terms of taxonomic resolution or number of species. Future work should assess whether specimens morphologically are placed in the *Ampheictis* genus, and investigate whether NHM_141A represents a cryptic or pseudo-cryptic species.

4.3.4.2 Cirratulidae

Initial morphospecies results suggested four taxa (Figure 4.3 a). Barcodes were obtained for all morphospecies, though *Chaetocirratulus andersenensis* (Augener, 1932) was only successful in COI. Morphospecies were supported by Figure 4.3 b-c), forming monophyletic clades with high interspecific distances in COI, ranging from 16-31%, though ranging lower in 16S (2.7-18.7%) with lowest values in both genes found between morphospecies *Aphelochaeta* sp. NHM_301 and Cirratulidae sp. NHM_035. Specimen NHM_294 was originally identified as Cirratulidae sp. NHM_035, but was found to belong to species *Aphelochaeta* sp. NHM_301 in both 16S and COI analyses Table 4.4 b-c), and was moved to this taxon.

Table 4.4 Number of individuals, number of sequences for 16S and COI barcodes and matrix of inter- and intraspecific p-distances for morphospecies in the family Cirratulidae. For matrix, left: minimum 16S interspecific distances; right: minimum COI interspecific distances, diagonal: maximum intraspecific distances 16S/COI

		n	n 16S	n COI	**a**	**b**	**c**	**d**
a	*Aphelochaeta* sp. NHM_301	4	3	3	-/0.002	0.283	0.159	0.224
b	*Chaetocirratulus andersenensis*	3	0	2	-	-/0.003	0.312	0.296
c	Cirratulidae sp. NHM_035	2	1	1	**0.027**	-	-	0.239
d	Cirratulidae sp. NHM_317	1	1	1	0.18	-	0.187	-

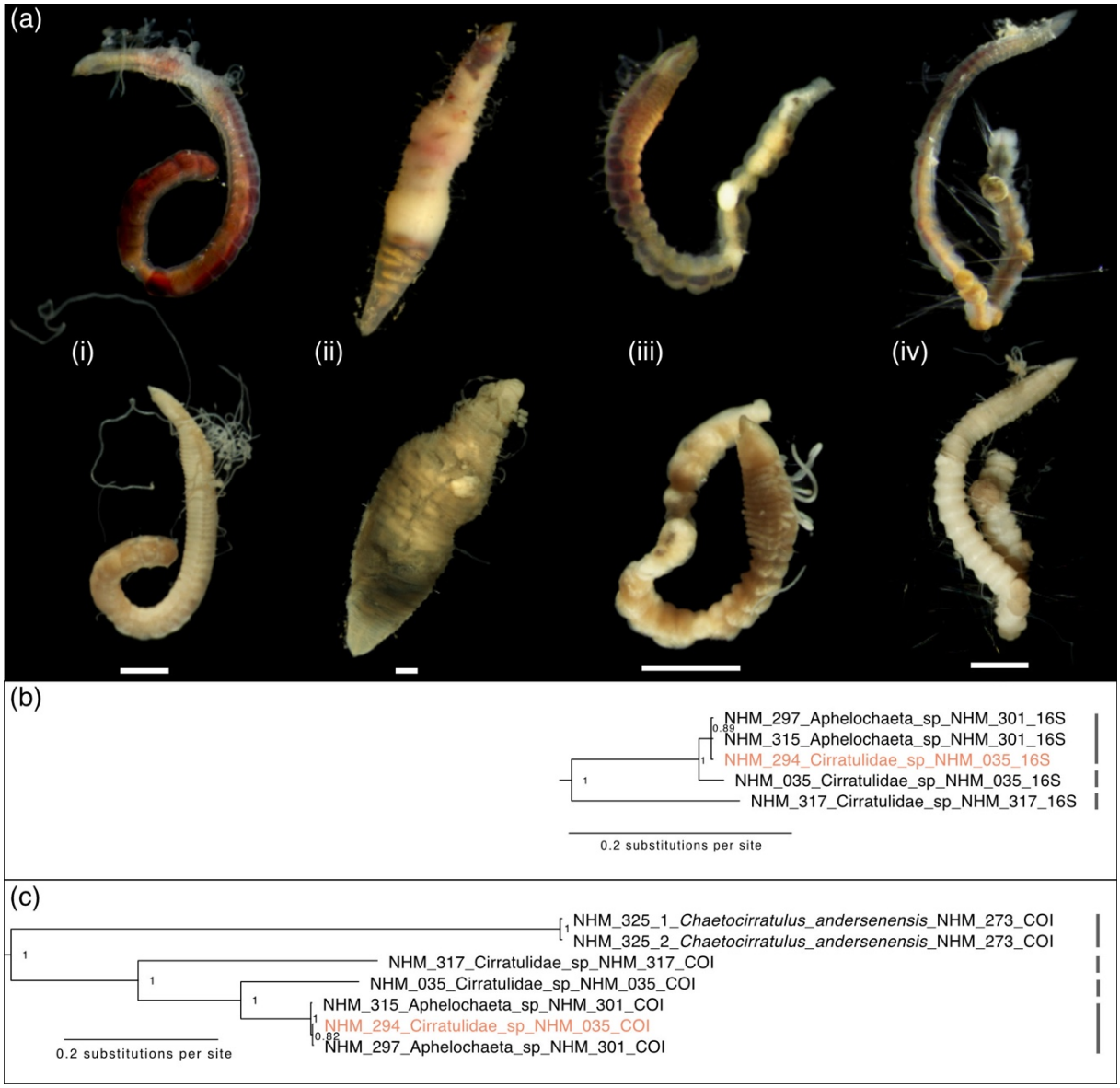

Figure 4.3 (a) The four morphospecies identified in family Cirratulidae with images of live specimens on top row, and respective preserved specimens below (i) *Aphelochaeta* sp. NHM_301, specimen NHM_297 (ii) *Chaetocirratulus andersenensis,* specimen NHM_273 (iii) Cirratulidae sp. NHM_035, specimen NHM_035 (iv) Cirratulidae sp. NHM_317, specimen NHM_317. All scale bars 1 mm. (b-c) Sections of Prince Gustav Channel phylogenies generated by Bayesian analysis for family Cirratulidae using (b) 16S and (c) COI. Specimen marked in orange (NHM_294) originally misidentified as Cirratulidae sp. NHM_035, now in *Aphelochaeta* sp. NHM_301 clade. Support values for both phylogenies are given as Bayesian posterior probabilities. Vertical lines indicate final counted taxonomic units.

GenBank data was insufficient to either confirm the named identification of *Chaetocirratulus andersenensis,* or improve taxonomic resolution in the other species. In summary, barcode data supported the delineation of the four morphospecies, with the only change being the movement of one misidentified individual between similar morphospecies.

4.3.4.3 Dorvilleidae

Initial investigation found five individuals of one dorvilleid morphospecies *Protodorvillea* sp. NHM_290 all from a single site at Duse Bay 500m. Both 16S and COI sequences were obtained (Table 4.5), though GenBank data was insufficient to inform a species-level identification, and top blastn hits were of species in genera other than *Protodorvillea,* with no hits above 95% identity. The taxonomic resolution of this taxon it reduced to Dorvilleidae sp. NHM 290 due to this uncertainty. Both 16S and COI phylogenetic analyses revealed two clades within the Dorvilleidae sp. NHM 290 morphospecies (Figure 4.4) with moderately high maximum intraspecific distances of 3.4% in 16S and 12% COI (Table 4.5). Intra- and interspecific COI distances in literature for the Family Dorvilleidae range 0–3.52% and 17.2-34.7% respectively (e.g. Cossu et al., 2015; Paxton et al., 2017; Taboada et al., 2017) suggesting that these clades may represent two closely related species, however more individuals and a nuclear gene would be needed to resolve this.

Table 4.5 Number of individuals, number of sequences for 16S and COI barcodes and maximum intraspecific p-distances (left 16S/right COI) for morphospecies in the family Dorvilleidae.

		n	n 16S	n COI	a
a	Dorvilleidae sp. NHM_290	5	5	2	**0.034/0.122**

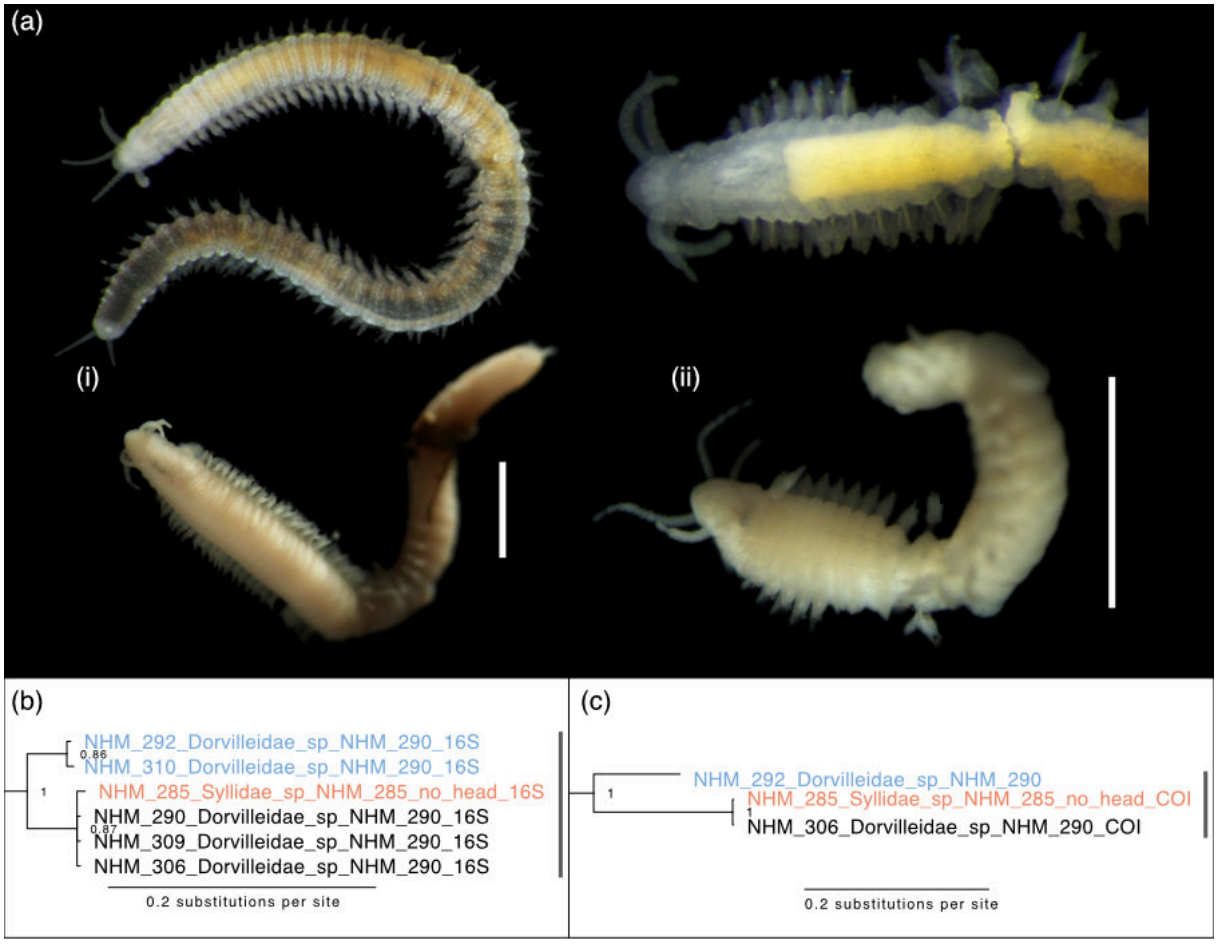

Figure 4.4 (a) (i) Morphospecies Dorvilleidae sp. NHM_290 (specimen NHM_290) and (ii) potentially cryptic lineage (specimen NHM_292) identified in family Dorvilleidae with images of live specimens on top row, and respective preserved specimens below. All scale bars 1 mm. (b-c) Sections of Prince Gustav Channel phylogenies generated by Bayesian analysis for family Dorvilleidae using (b) 16S and (c) COI. Specimens marked in blue represent potentially cryptic lineage. Specimen marked in orange (NHM_285) damaged specimen originally misidentified as syllid. Support values for both phylogenies are given as Bayesian posterior probabilities. Vertical lines indicate final counted taxonomic units.

Barcode data also revealed that a damaged specimen originally identified as the syllid morphospecies Syllidae sp. NHM_285 was a misidentified dorvilleid without a head and, was excluded from final specimen counts (Figure 4.4 b-c)

In summary, barcode data introduced uncertainty to the generic-level morphospecies identification, reducing taxonomic resolution of the taxon family only. Future work should aim to reassess, and also to investigate whether two genetic lineages found in this sample represent cryptic or psuedocryptic species.

4.3.4.4 Flabelligeridae

Two distinct morphospecies, identified as *Brada mammilata* Grube, 1877 and *Flabegraviera mundata* (Gravier, 1906) were recorded in initial studies (Figure 4.5 a). 16S barcoding was successful in *F. mundata* (Table 4.6). 16S phylogenetic analyses split both morphospecies into separate, well supported clades (Figure 4.5), with large minimum interspecific difference between the two species at 15.8% (Table 4.6).

Table 4.6 Number of individuals, number of sequences for 16S and COI barcodes and matrix of inter- and intraspecific p-distances for morphospecies in the family Flabelligeridae. For matrix, left: minimum 16S interspecific distances; right: minimum COI interspecific distances, diagonal: maximum intraspecific distances 16S/COI

		n	n 16S	n COI	a	b
a	*Brada mammilata*	18	3	0	0/-	-
b	*Flabegraviera mundata*	9	1	1	0.158	-

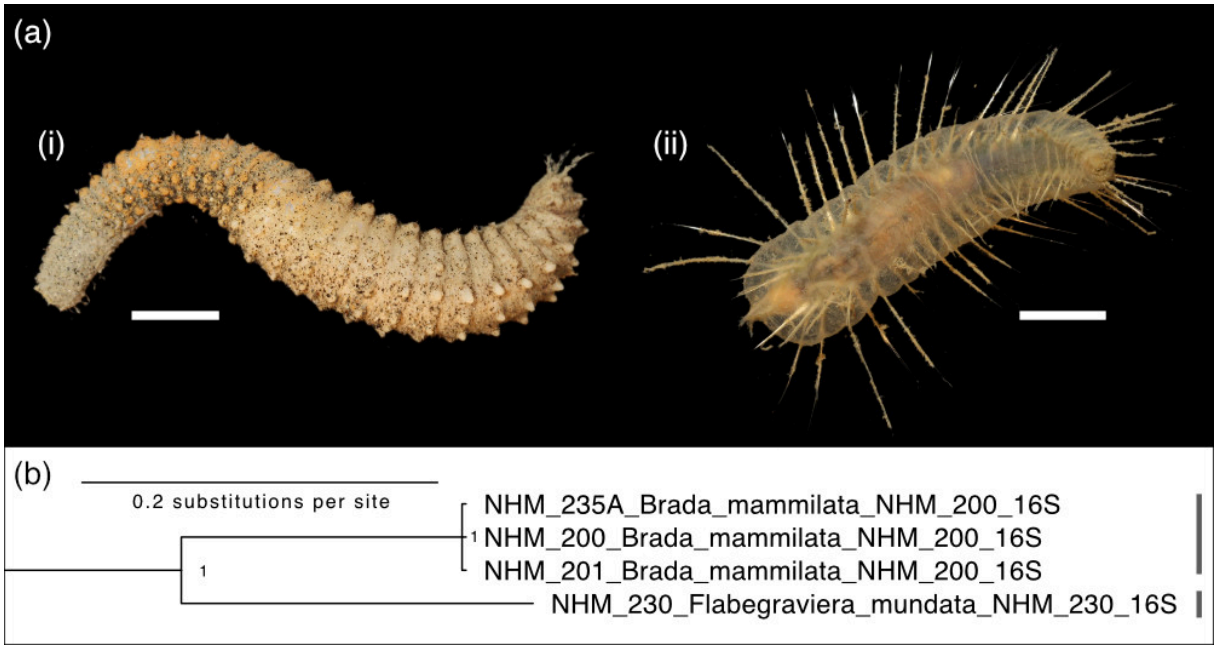

Figure 4.5 (a) The two morphospecies identified in family Flabelligeridae with images of live specimens (i) *Brada mammilata*, specimen NHM_200 (ii) *Flabegraviera mundata,* specimen NHM_231. All scale bars 1 cm (b) Sections of Prince Gustav Channel phylogenies generated by Bayesian analysis for family Flabelligeridae using 16S Support values for both phylogenies are given as Bayesian posterior probabilities. Vertical lines indicate final counted taxonomic units.

Brada mammilata sequences are not available on GenBank, though the top blastn hits were to other *Brada* species (88-90% identity). The identity of *Flabegraviera mundata* was supported 98-4-99.5% matches in COI (HQ326969) and 16S (HQ326958) respectively to sequences identified as *Flabelligera mundata* collected off the South Orkney Islands, and sequenced as part of a phylogenetic analysis of families Acrocirridae and Flabelligeridae (Osborn & Rouse, 2011). This study was published prior to taxonomic revision of the genus *Flabelligera* (Salazar-Vallejo, 2012) in which the Antarctic species *Flabelligera mundata* was moved to a new genus, *Flabegraviera,* so that the positive blastn match still supports the original morphospecies identification. In summary, barcode data supports original species delimitation and identification for this family.

4.3.4.5 Hesionidae

A single, incomplete specimen in the family Hesionidae was identified (

Figure 4.6). Both barcode genes were successful (Table 4.7), with blastn hits of 99.1-100% in 16S and 99.3-99.7% COI to Antarctic sequences collected from South Georgia, Bransfield Strait, and Amundsen sea identified as morphospecies Hesionidae sp. MB2 (Brasier et al., 2016) and to a planktonic larval sequence identified as cf. Hesionidae D7.G5polych02 collected from the Ross Sea (Heimeier et al., 2010). Identification in this study remains at family level without more detailed morphological assessment, however barcode results do show broad Southern Ocean connectivity in mitochondrial genes across a large geographic range.

Table 4.7 Number of individuals, number of sequences for 16S and COI barcodes and maximum intraspecific p-distances (left 16S/right COI) for morphospecies in the family Hesionidae.

		n	n 16S	n COI	a
a	Hesionidae sp. NHM_291	1	1	1	-

Figure 4.6 Images of live (left) and preserved (right) morphospecies Hesionidae sp. NHM_290, specimen NHM_290 (incomplete fragment). Scale bar 1 mm. **Lumbrineridae**

Two morphospecies were identified in initial analyses, *Augeneria tentaculata* Monro, 1930 and Lumbrineridae sp. NHM_300 (Figure 4.7 a). 16S and COI barcodes were obtained for each taxon, with phylogenetic analyses of both genes clearly splitting the taxa (Figure 4.7 b), with minimum interspecific p-distances of 20% and 26.6% in 16S and COI respectively (Table 4.8).

In *Augeneria tentaculata,* intraspecific variation was low, (0% 16S, up to 0.6% COI) even across a large depth range (includes samples from Duse Bay 200m, 500m, and 1000m sites). GenBank data was insufficient to confirm identity, though top hits in both genes (90.2-94% 16S, 82.5-82.6%) were to other *Augeneria* spp.

The single individual of Lumbrineridae sp. NHM_300 matched with 99.3-100% identity to four Antarctic 16S sequences identified as

Lumbrineris sp. MB collected from the Amundsen sea (Brasier et al., 2016). Future morphological work should assess placement in this genus for this taxon. In summary, barcode data supports delimitation of the two species, though is insufficient to confirm or improve species identification.

Table 4.8 Number of individuals, number of sequences for 16S and COI barcodes and matrix of inter- and intraspecific p-distances for morphospecies in the family Lumbineridae. For matrix, left: minimum 16S interspecific distances; right: minimum COI interspecific distances, diagonal: maximum intraspecific distances 16S/COI.

		n	n 16S	n COI	a	b
a	*Augeneria tentaculata*	11	5	6	0.0/0.006	0.266
b	Lumbrineridae_sp. NHM_300	1	1	1	0.2	-

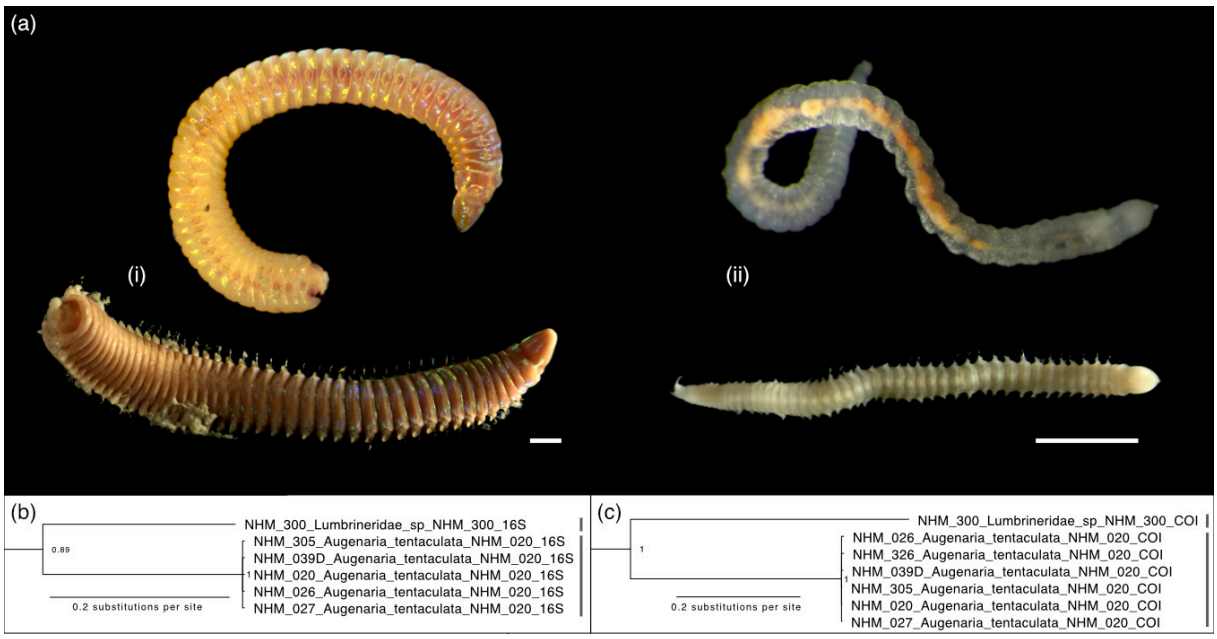

Figure 4.7 (a) The two morphospecies identified in family Lumbrineridae with images of live specimens on top row, and respective preserved specimens below (i) *Augeneria tentaculata,* specimen NHM_020, specimen NHM_020 (ii) Lumbrineridae sp. NHM_200, specimen NHM_300. All scale bars 1 mm. (b-c) Sections of Prince Gustav Channel phylogenies generated by Bayesian analysis for family Lumbrineridae using (b) 16S and (c) COI. Support values for both phylogenies are given as Bayesian posterior probabilities. Vertical lines indicate final counted taxonomic units.

4.3.4.7 Maldanidae

Initial assessments found up to four morphospecies within the Family Maldanidae, two to named species, *Maldane sarsi* Malmgren, 1865 and *Lumbriclymenella robusta* Arwidsson, 1911 and two to morphospecies only, Maldanidae sp. NHM_125, and Maldanidae sp. NHM_313 (Figure 4.8 a).

Both 16S and COI were obtained for representatives of these morphospecies (Table 4.9). In 16S phylogenetic analysis, each morphospecies is well delineated (Figure 4.8 b), with an additional clade comprising of two damaged individuals initially identified as *Maldane sarsi* and *Lumbriclymenella robusta* (Figure 4.8 a v), differing from those clades by minimum interspecific p-distances of 13.5% and 26% respectively. This new clade matched with high percent identity (99.5-99.7%) to four sequences of the Antarctic maldanid species *Asychis amphiglyptus* (Ehlers, 1897), including from the type locality South Georgia, sequenced as part of a molecular barcode study on cryptic species in deep-sea Southern Ocean annelids (Brasier et al., 2016), in which *Asychis amphiglyptus* was also initially misidentified as *Maldane sarsi* until barcode data and secondary morphological analysis by a maldanid specialist. PGC sequences also matched 99.5% identity with a portion of the complete mitochondrial genome of *Asychis amphiglyptus* directly submitted to GenBank (ON360997).

Due to moderately high interspecific distances between the new PGC clade and other maldanid morphospecies, and positive blastn identity with *Asychis amphiglyptus* sequences close to the type locality that underwent thorough morphological examination, this new molecular species in the PGC dataset is identified as cf. *Asychis amphiglyptus* until follow up morphological analysis can take place.

Table 4.9 Number of individuals, number of sequences for 16S and COI barcodes and matrix of inter- and intraspecific p-distances for morphospecies in the family Maldanidae. New molecular species highlighted in bold. For matrix, left: minimum 16S interspecific distances; right: minimum COI interspecific distances, diagonal: maximum intraspecific distances 16S/COI

		n	n 16S	n COI	a	b	c	d	e
a	***Cf. Asychis amphiglyptus* sp. NHM_140A_5**	2	2	0	0.0/-	-	-	-	-
b	*Lumbriclymenella robusta*	4	2	2	0.26	0.002/0.009	0.216	0.228	0.245
c	*Maldane sarsi antarctica*	119	22	22	0.135	0.241	0.009/0.051	0.208	0.248
d	Maldanidae sp. NHM_125	6	3	1	0.297	0.3	0.273	0.002/-	0.287
e	Maldanidae sp. NHM_313	2	1	1	0.295	0.248	0.272	0.301	-

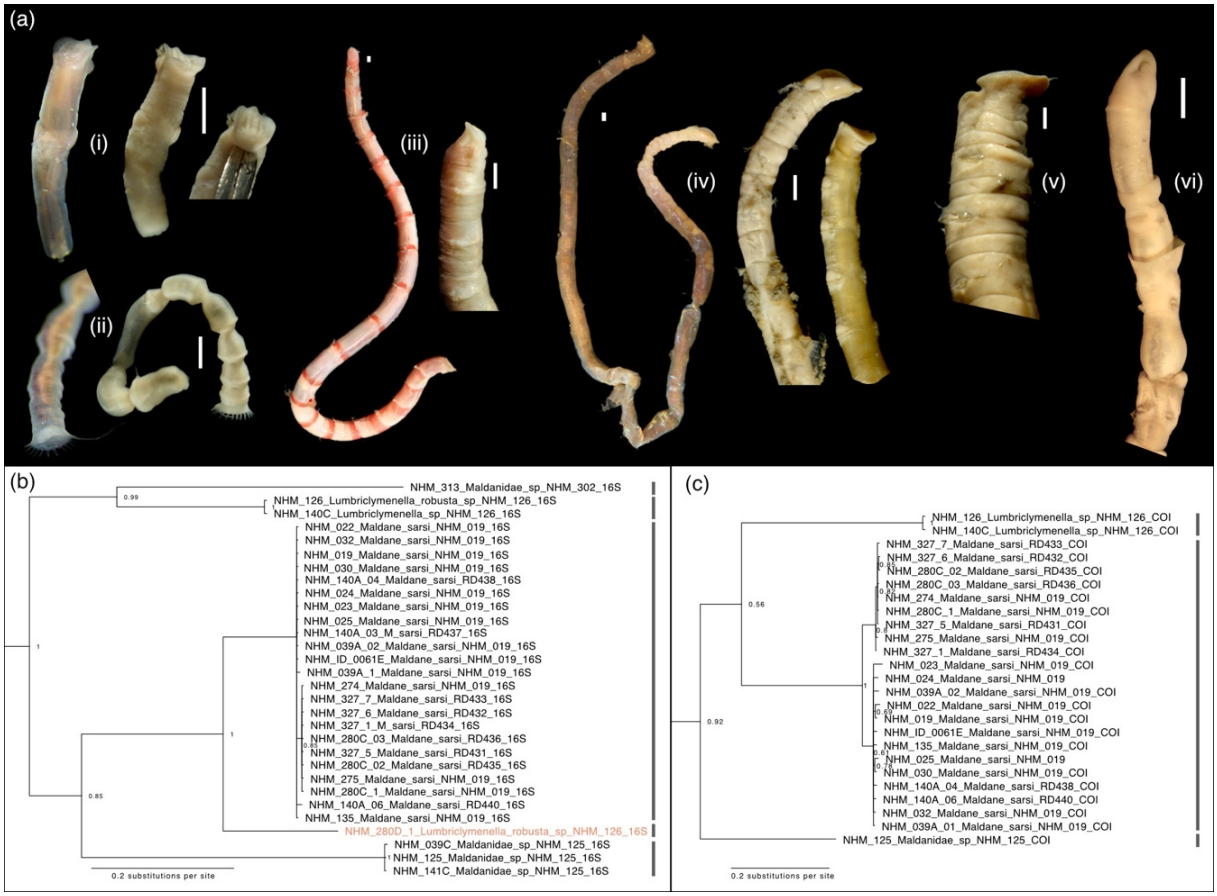

Figure 4.8 (a) Morphospecies and molecular species identified in family Maldanidae (i) Maldanidae sp. NHM_302 specimen NHM_313, live (left), preserved (right); (ii) Maldanidae sp. NHM_302 tail fragment, live (left), preserved (right); (iii) *Lumbriclymenella robusta*, live, specimen NHM_126 (left), preserved, specimen NHM_140C (right); (iv) *Maldane sarsi antarctica*, live, specimen NHM_135 (left), preserved head and tail, specimen NHM_280_C (right); new molecular species cf. *Asychis amphiglyptus* sp. NHM_140A_5, specimen NHM_280D_1, preserved specimen; (vi) Maldanidae sp. NHM_125, specimen NHM_39_C, preserved. All scale bars 1 mm. (b-c) Sections of Prince Gustav Channel phylogenies generated by Bayesian analysis for family Maldanidae using (b) 16S and (c) COI. Specimen highlighted in orange new molecular species cf. *Asychis amphiglyptus,* previously misidentified as *Lumbriclymenella robusta.* Support values for both phylogenies are given as Bayesian posterior probabilities. Vertical lines indicate final counted taxonomic units.

Interspecific distances between remaining morphospecies were high, with minimum p-distance values ranging from 24.1-30% in 16S, and 20.8-28.7% in COI. Maldanidae sp. NHM_313 did not fall within the maldanid clade in the all-family COI phylogeny, falling with non-significant support as sister to a clade including Ampharetidae, Orbiniidae and long-branched singleton taxa (Appendix C Figure C.2). However all top blastn hits in COI are to maldanid genera, suggesting that this is not an issue of contamination or misidentification, but rather low resolution and long branch attraction in a single-gene, multi-family phylogeny.

In 16S Maldanidae sp. NHM_313 does fall within the maldanid clade, and matches with high percent identity (99.4%) to a single, 16S-only Antarctic sequence identified as *Praxillella* sp. MB, also from Brasier et al. (2016), and placement in this genus should be assessed in future morphological work. Two headless maldanid tail fragments (Figure 4.8 a ii) that were barcoded were found to match with Maldanidae sp. NHM_313 (collected from the same sample), making diagnostic characters of the tail available for morphological reassessment.

Genbank data was insufficient to confirm the identification of *Lumbriclymenella robusta*, or to improve the taxonomic resolution of Maldanidae sp. NHM_125.

Maldane sarsi, one of the most abundant morphospecies in the original sample, matched with 99.2-100% identity in blastn analysis to two Antarctic 16S sequences identified as *Maldane sarsi antarctica* Arwidsson, 1911 from Brasier et al. (2016), the Antarctic subspecies of the northern European species *Maldane sarsi.* It is worth noting that the type locality of *M. sarsi antarctica* is just off of James Ross Island, less than 40km away the northern entrance of the Prince Gustav Channel.

The combined phylogenetic analysis of Antarctic *Maldane sarsi* using 16S, COI, and nuclear 18S genes, including Antarctic specimens, all available *Maldane* sequences available on GenBank (Appendix C Table C.2), and new sequence data for specimens identified as *Maldane sarsi* collected from an original type locality (Kosterfjorden Sweden), found that Antarctic sequences formed a monophyletic clade with high support (Figure 4.9). Swedish specimens formed a separate North Atlantic clade with GenBank sequences identified as *M. sarsi* from Russian White Sea and Canadian Newfoundland locations, also with high support.

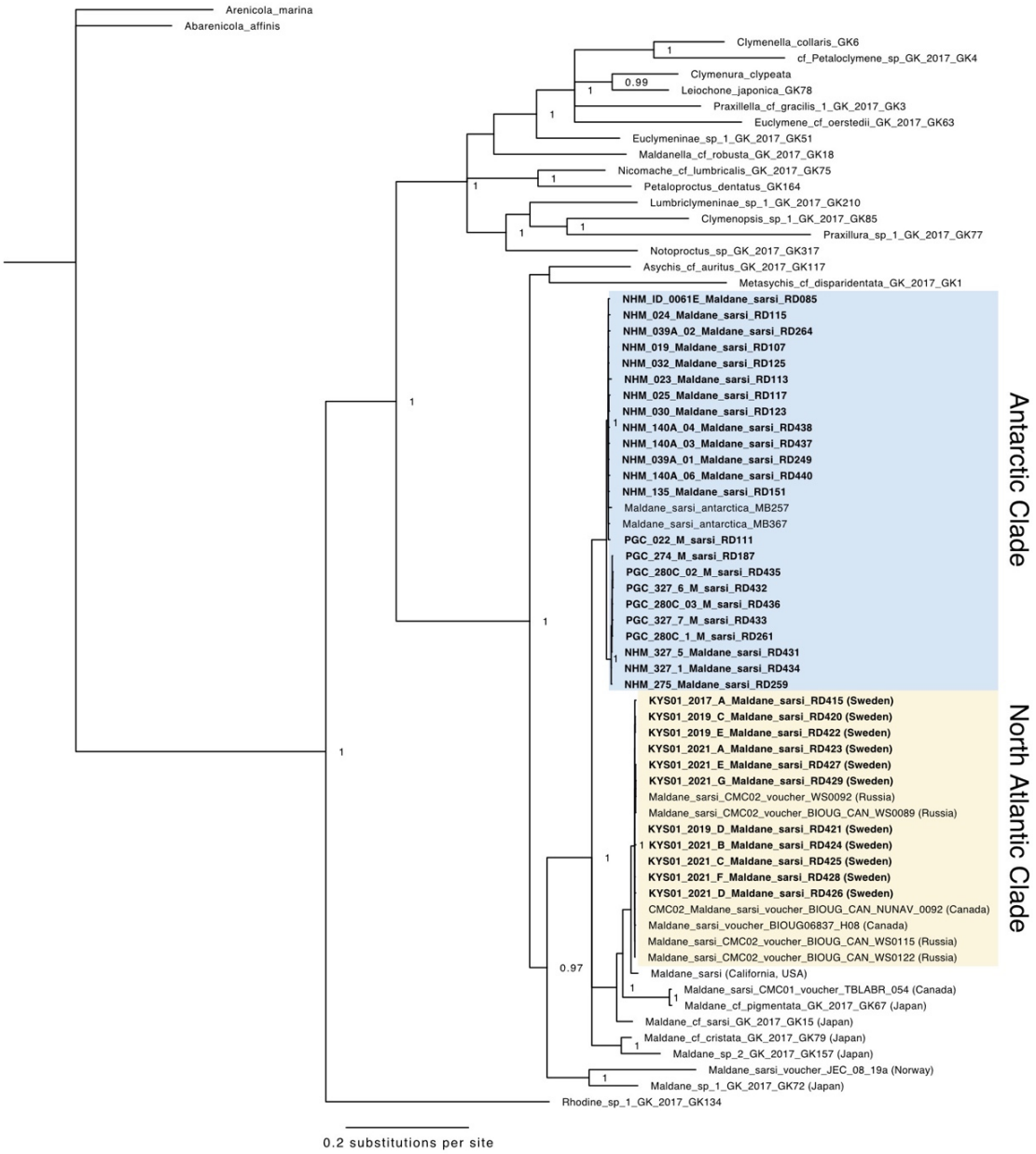

Figure 4.9 Phylogenetic tree of the Annelid family Maldanidae using combined Bayesian analysis of three genes, cytochrome oxidase subunit I (COI), 16S RNA and 18S RNA, with focus on genus *Maldane*. Specimens newly sequenced in this study are marked in bold. The clade of Antarctic *Maldane sarsi* sequences are marked in blue, the North Atlantic clade, including sequences from type locality, Kosterfjord Sweden, is marked in yellow. Support values for both phylogenies are given as Bayesian posterior probabilities.

Single gene analyses also separated Antarctic specimens from the North Atlantic clade and other *Maldane* sequences (e.g. Figure 4.10). Moderate to high genetic distances between Antarctic and Northern Atlantic clades for 16S and COI (minimum interclade uncorrected p-distance 4.2% 16S, 14.2% COI), in addition to one mutation difference in the highly conserved nuclear 18S gene, supports the hypothesis that *Maldane sarsi antarctica* is a separate and distinct species, rather than a subspecies of the North Atlantic *Madane sarsi.*

Intraclade distance within the North Atlantic clade was low (maximum intraclade p-distance 0% for 16S, 1% for COI), despite large geographic distances ranging from the Baltic Sea to Newfoundland and the White Sea. In contrast, sequences from the Prince Gustav Channel displayed high genetic structure in COI (maximum intraclade p-distance 5.1% for COI) and with most individuals forming unique haplotypes despite being collected at the same time from the same geographic location (Prince Gustav Channel), with two genetic subgroups that appear to be structured by depth (Figure 4.11)

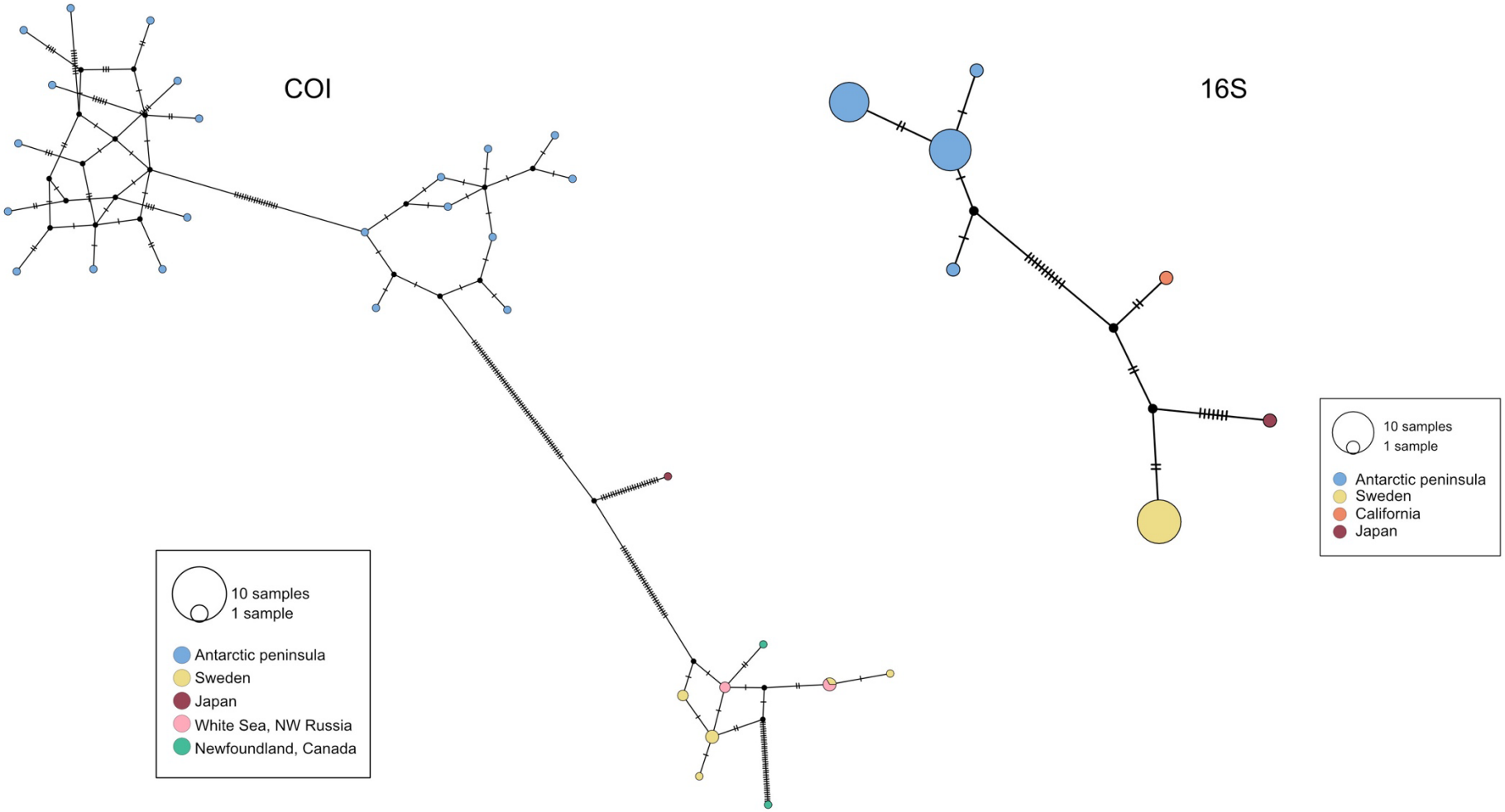

Figure 4.10 Haplotype network analyses for sequences (GenBank and newly generated) identified as *Maldane sarsi* for COI (left) and 16S (right), with colours representing different geographic localities. Each coloured circle represents a sampled haplotype, with circle size proportional to the frequency of that haplotype, as indicated by the key Bars between haplotypes represent one mutation, with missing inferred haplotypes represented by black circles.

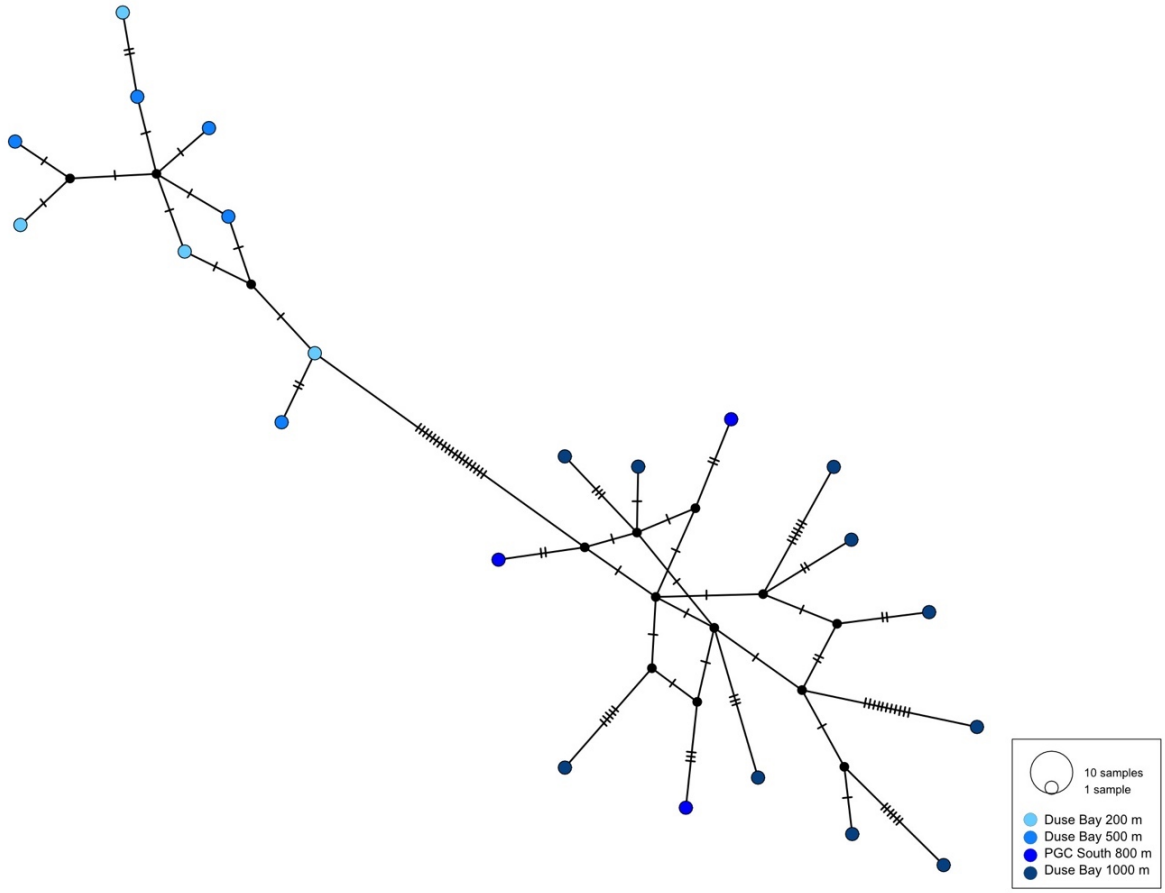

Figure 4.11 COI Haplotype network analysis for Prince Gustav Channel specimens identified as *Maldane sarsi,* coloured by sample sites of different depths ranging 200-1000m. Each coloured circle represents a sampled haplotype, with circle size proportional to the frequency of that haplotype, as indicated by the key Bars between haplotypes represent one mutation, with missing inferred haplotypes represented by black circles.

Initial morphological assessment found that both Swedish and Antarctic species matched primary diagnostic characters of *Maldane sarsi,* including those of the cephalic and anal regions, the number of chaetigers, and the distribution of chaetae. The Swedish specimens were relatively small, with a maximum length of 2 cm, in comparison with up to 15 cm length in Antarctic specimens. However, the original description of *Maldane sarsi* does include specimens of up to 11 cm length (Malmgren, 1866). More detailed morphological work is required to assess whether clear morphological differences are present between the species (e.g. the primary character differentiating both in the original subspecies description is difference in length and width of the largest tooth on uncinate chaetae, Arwidsson, 1911) or whether Antarctic taxon represents a truly cryptic species of *Maldane sarsi*.

Drennan et al 2021 assigned the PGC *Maldane sarsi* morphospecies to the parent taxon rather than subspecies as a conservative approach; in the current study, this identification is updated to *Maldane sarsi antarctica* to distinguish the Antarctic specimens from the European species. However, *Maldane sarsi antarctica* will need to be described as a separate species. This work is planned, along with a neotype description of *Maldane sarsi*.

4.3.4.8 Myzostomatidae

A single specimen in the family Myzostomatidae was collected, host unknown, originally identified as *Myzostoma* cf. *divisor* (Figure 4.12). Both 16S and COI barcodes were successfully obtained for this specimen (Table 4.10), with 100% and 99.7% identity matches respectively to GenBank sequences identified as *Mysoztoma divisor* (16S: KM014271; COI: KM014188) collected from Shag Rocks, Antarctica, and sequenced as part of a phylogenetic study of the order Myzostomatida (Summers & Rouse, 2014). The type locality of *Mysoztoma divisor* Grygier, 1989 is the Ross Sea (Grygier, 1989), however additional material in the original description were also collected from the South Georgia, of which Shag Rocks is proximal to, and is therefore within the known range. The identification of the specimen in this study was changed from *Myzostoma* cf. *divisor* to *Myzostoma divisor* with the addition of barcode support.

Table 4.10 Number of individuals, number of sequences for 16S and COI barcodes and maximum intraspecific p-distances (left 16S/right COI) for morphospecies in the family Myzostomatidae

		n	n 16S	n COI	a
a	*Myzostoma divisor*	1	1	1	-

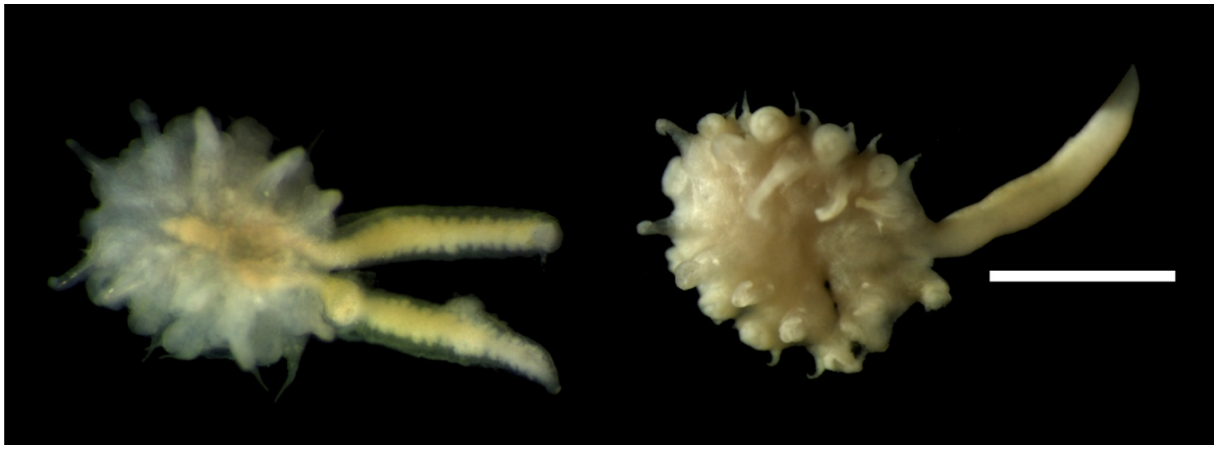

Figure 4.12 Images of live (left) and preserved (right) morphospecies *Myzostoma divisor*, specimen NHM_123. Scale bar 1 mm.

4.3.4.9 Nephtyidae

Initial morphological analyses recorded two nephtyid morphospecies, the majority of which identified as *Aglaophamus trissophyllus* (Grube, 1877), with a single specimen identified to genus only, *Aglaophamus* sp. NHM_280F (Figure 4.13 a).

Though multiple efforts were made, COI was not successfully sequenced for *Aglaophamus* sp. NHM_280F, leaving only 16S for comparison. Interspecific distance was very low between the two morphospecies, with a minimum p-distance of 1.4% (Table 4.11), and phylogenetic analyses placing both in the same clade (Figure 4.13 b). It has previously been recorded that 16S may have insufficient resolution when aiming to delineate closely related or cryptic species lineages in Antarctic annelids relative to COI (Brasier et al., 2016), in which Antarctic specimens initially identified as *Aglaophamus trissophyllus* were recorded in the same clade in 16S, but as separate cryptic lineages with clear barcode gaps in COI (11-14% K2P interspecific distance in COI between lineages *Aglaophamus cf trissophyllus* MBa-c complex*, Aglaophamus* sp. MB2 and *Aglaophamus* sp. MB3). It is noted in that study however that individuals from different COI lineages do differ slightly from one another in 16S (average interspecific K2P distance 2.28%, average intraspecific 0.25%) as is observed in 16S distances in the current study (minimum 1.4% interspecific vs maximum 0.7% intraspecific).

Table 4.11 Number of individuals, number of sequences for 16S and COI barcodes and matrix of inter- and intraspecific p-distances for morphospecies in the family Nephtyidae. For matrix, left: minimum 16S interspecific distances; right: minimum COI interspecific distances, diagonal: maximum intraspecific distances 16S/COI

		n	n 16S	n COI	a	
a	*Aglaophamus trissophyllus*	15	9	15	0.007/0.048	-
b	*Agalophamus* sp. NHM_280F	1	1	0	0.014	-

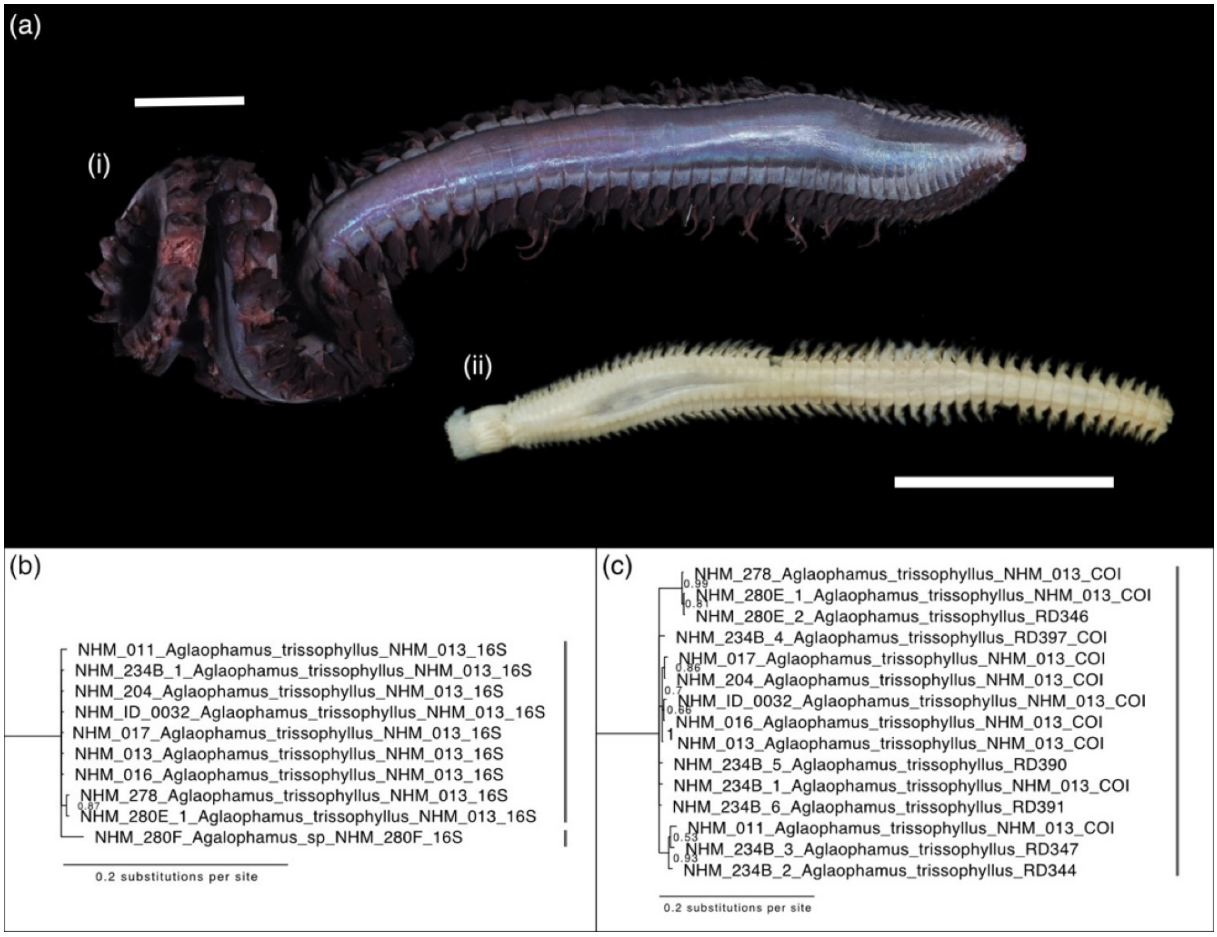

Figure 4.13 (a) The two morphospecies identified in family Nephtyidae (i) *Aglaophamus trissophyllus,* specimen NHM_013*;* (ii) *Aglaophamus* sp. NHM_280F, NHM_280F. All scale bars 1 cm. (b-c) Sections of Prince Gustav Channel phylogenies generated by Bayesian analysis for family Nephtyidae using (b) 16S and (c) COI. Support values for both phylogenies are given as Bayesian posterior probabilities. Vertical lines indicate final counted taxonomic units.

Blastn results find *Aglaophamus* sp. NHM_280F matching with high percent identity (99.5-100%) in 16S to *Aglaophamus* MB spp. from Brasier et al. (2016), and only slightly lower (96.9-97.9%) to *Aglaophamus* cf. *trissophyllus* MBa-c from that same study; *Aglaophamus trissophyllus* from this study likewise has slightly higher percent identity match to *Aglaophamus* cf. *trissophyllus* MBa-c (99.7-98.6) than to *Aglaophamus* MB spp. (98.4-97.1). However in COI blastn analyses the difference was more clear, with ~94-100% identity to *Aglaophamus* cf. *trissophyllus* MBa-c and ~87-89% to *Aglaophamus* MB spp. The difference in variation between 16s and COI in this genus is also observed when comparing intraspecific variation within the PGC samples – maximum 0.7% in 16S vs 4.8% in COI (Table 4.11). High intraspecific variation in *Aglaophamus trissophyllus* is also visualised in COI phylogenetic analysis (Figure 4.13 c); Brasier et al. 2016 described this variation as species complex rather than further cryptic lineages.

Antarctic *Aglaophamus* spp., including all specimens from the Prince Gustav Channel, are the focus of Chapter 5 as part of a broader phylogeographic and population genomic study of the taxon from across the Southern Ocean. This study adds the nuclear gene 18S to 16S and COI barcodes, in addition to ddRADseq single nucleotide polymorphism (SNP) data, with both phylogenetic and genomic data separating *Aglaophamus trissophyllus* and *Aglaophamus* sp. NHM_280F and their conspecifics. This highlights the insight that more specimen coverage and types of genetic data can add, and that caution is needed when making taxonomic decisions based on small numbers of specimens and single genes.

In summary, despite low interspecific variation in 16S barcodes, identification of two nephtyid morphospecies within the PGC samples remains unchanged, due to 16S previously being known to mask genetic diversity between closely related species in Antarctic *Aglaophamus*.

4.3.4.10 Oligochaeta

Originally, two morphospecies in the class Oligochaeta were recorded, Oligochaeta sp. NHM_287 and Oligochaeta sp. NHM_ 289, however the latter was found to be a nemertean following barcoding and a recheck of specimen images, and this morphospecies was excluded from further analyses. In Oligochaeta sp. 287, only two individuals were successful for barcoding, forming a clade in phylogenetic analyses with low intraspecific variation (0.5 % 16S, 0.3% COI) (Figure 4.14; Table 4.12). Genbank data was insufficient to improve the taxonomic resolution of this taxon, and thus the identification remains the same.

Table 4.12 Number of individuals, number of sequences for 16S and COI barcodes and maximum intraspecific p-distances (left 16S/right COI) for morphospecies in the subclass Oligochaeta.

		n	n 16S	n COI	a
a	Oligochaeta sp. NHM_287	5	2	2	0.005/0.003

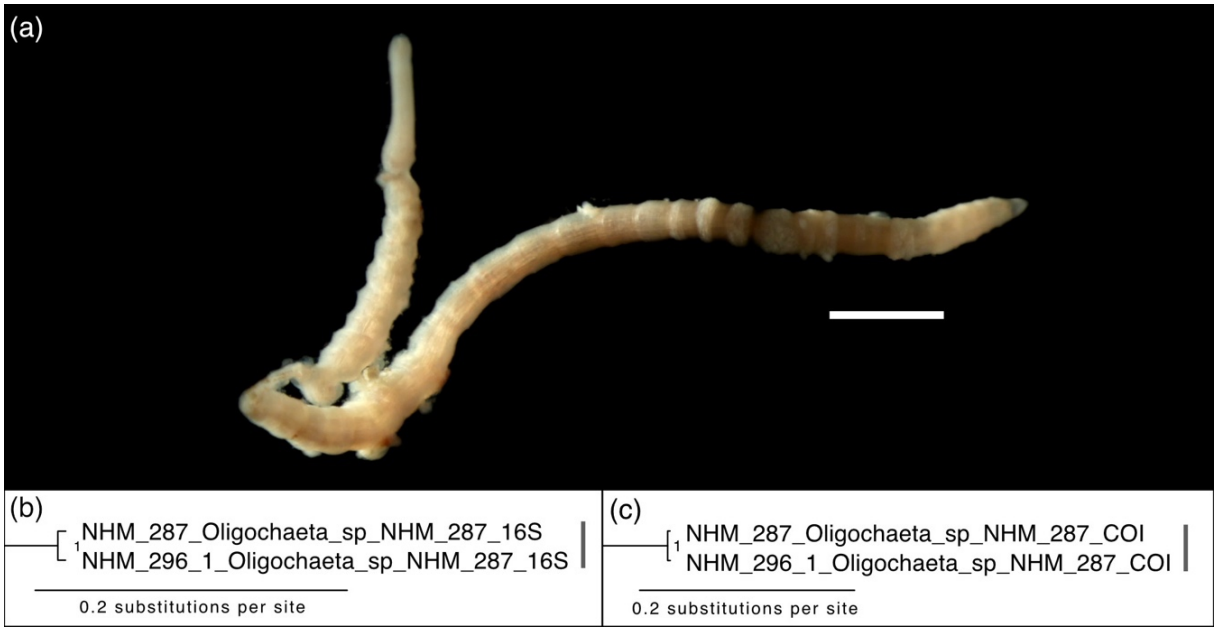

Figure 4.14 Morphospecies Oligochaeta sp. NHM_287, preserved specimen NHM_287_1. Scale bar 1 mm. (b) Section of Prince Gustav Channel 16S phylogeny generated by Bayesian analysis for family Ampharetidae. Potentially cryptic lineage (specimen NHM_141A) highlighted in blue. (c) Section of Prince Gustav Channel COI phylogeny generated by Bayesian analysis for subclass Oligochaeta. Support values for both phylogenies are given as Bayesian posterior probabilities.

4.3.4.11 Opheliidae

Two morphospecies were originally identified, *Ophelina breviata* (Ehlers, 1913) and *Ophelina* cf. *cylindricaudata* sp. NHM_284 (Figure 4.15 a). While *Ophelina breviata* is an Antarctic species, *Ophelina cylindricaudata* (Hansen, 1879) is originally described from Norwegian waters – though it has past records in the Southern Ocean new records should be designated as *Ophelina* cf. *cylindricaudata* as a precaution until a thorough comparison of Arctic and Antarctic specimens can be made (Maciolek & Blake, 2006). 16S phylogenetic analyses split *Ophelina* cf. *cylindricaudata* NHM_284 into two polyphyletic clades (Figure 4.15 a), with very high intraspecific distance (minimum 25.7%), larger than the distance between both clades and *Ophelina breviata* (minimum 24%) (Table 4.13). Pairwise differences in 16S greater than 20%, and polyphyly with *Ophelina breviata,* a species with clear morphological differences from *Ophelina cylindricaudata* led to the assignment of a tentatively cryptic lineage and MOTU, *Ophelina* cf. *cylindricaudata* NHM_286. However, additional data from morphology, and more individuals and genes is warranted.

Table 4.13 Number of individuals, number of sequences for 16S and COI barcodes and matrix of inter- and intraspecific p-distances for morphospecies in the family Opheliidae. New molecular species highlighted in bold. For matrix, left: minimum 16S interspecific distances; right: minimum COI interspecific distances, diagonal: maximum intraspecific distances 16S/COI

		n	n 16S	n COI	a	b	c
a	*Ophelina breviata*	2	1	0	-	-	-
b	*Ophelina* cf. *cylindricaudata* NHM_284	3	2	0	0.24	0.0/-	-
c	***Ophelina* cf. *cylindricaudata* NHM_286**	2	2	1	0.24	0.257	0.003/0

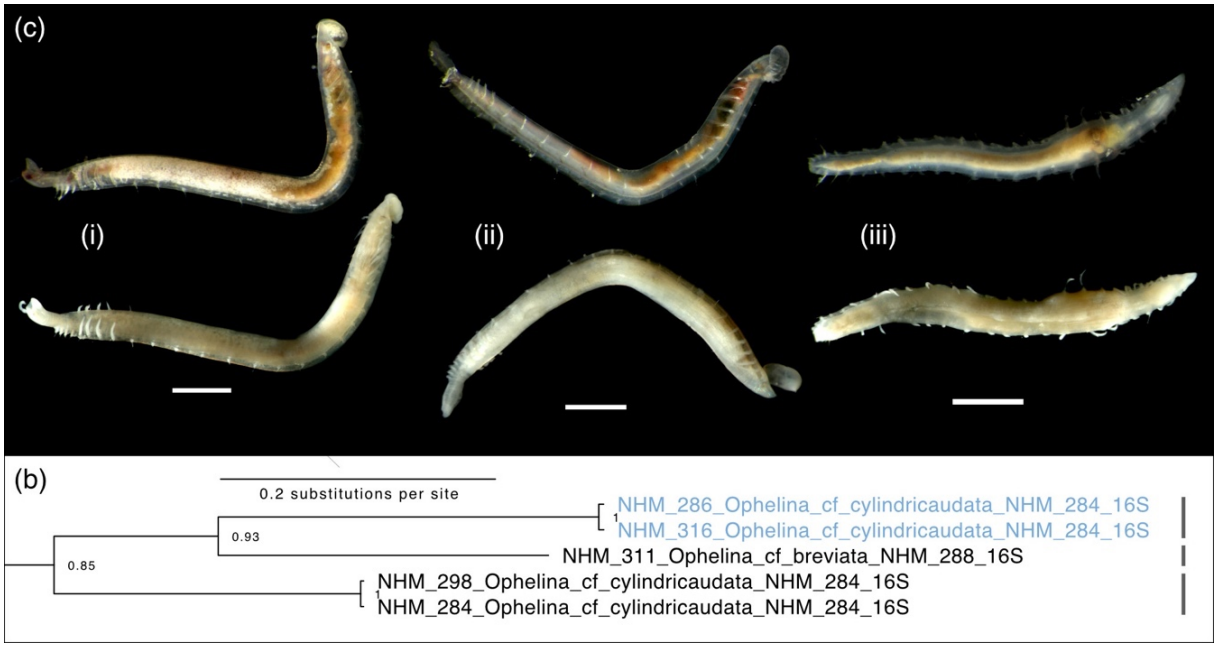

Figure 4.15 (a) Morphospecies (i) *Ophelina* cf. *cylindricaudata sp*. NHM_284, specimen NHM_264; (ii) cryptic lineage *Ophelina* cf. *cylindricaudata* sp. NHM_286, specimen NHM_286; and (iii) *Ophelina breviata,* specimen NHM_288. Images of live specimens on top row, and respective preserved specimens below. All scale bars 1 mm. (b) Section of Prince Gustav Channel phylogenies generated by Bayesian analysis for family Dorvilleidae using 16S. Specimens marked in blue potentially cryptic lineage in specimens originally identified as *Ophelina* cf. *cylindricaudata* sp. NHM_284.. Support values for both phylogenies are given as Bayesian posterior probabilities. Vertical lines indicate final counted taxonomic units

The species *Ophelina breviata* is not represented by sequence data on GenBank, and therefore the ID of this taxon in this study remains unchanged. Though not from the original type locality, a north Atlantic sequence of *Ophelina cylindricaudata* collected off New England, USA is available on Genbank, however *O.* cf. *cylindricaudata* spp. NHM284 and NHM 286 did not share close blastn matches with this sequence (79.2% and 81.9% identity respectively), highlighting the need for a revision of the presence of *Ophelina cylindricaudata* in the Southern Ocean.

In summary, the number of OTUs in the family Opheliidae is tentatively increased by one due to very high pairwise differences and polyphyly in 16S gene analyses within the morphospecies *Ophelina* cf. *cylindricaudata*. Specimens should be revisited to assess morphologically whether this new lineage represents a psuedocryptic or true cryptic species, and to source additional individuals where possible and increase gene coverage and sequencing success in order to better assess inter and intraspecific variation both morphologically and molecularly.

4.3.4.12 Orbiniidae

Three individuals identified as *Leitoscoloplos kerguelensis* (McIntosh, 1885

Figure 4.6 a) were identified from a single site, Duse Bay 500. DNA sequencing was successful for each individual in both 16S and COI, forming a monophyletic clade

Figure 4.6 b), with small intraspecific distances (0.2% and 0.1% respectively, Table 4.14). Sequence data on GenBank was insufficient to confirm species identification. Identification remains unchanged.

Table 4.14 Number of individuals, number of sequences for 16S and COI barcodes and maximum intraspecific p-distances (left 16S/right COI) for morphospecies in the family Orbiniidae

		n 16S	n COI	a
a	*Leitoscoloplos kerguelensis*	3	3	0.002/0.001

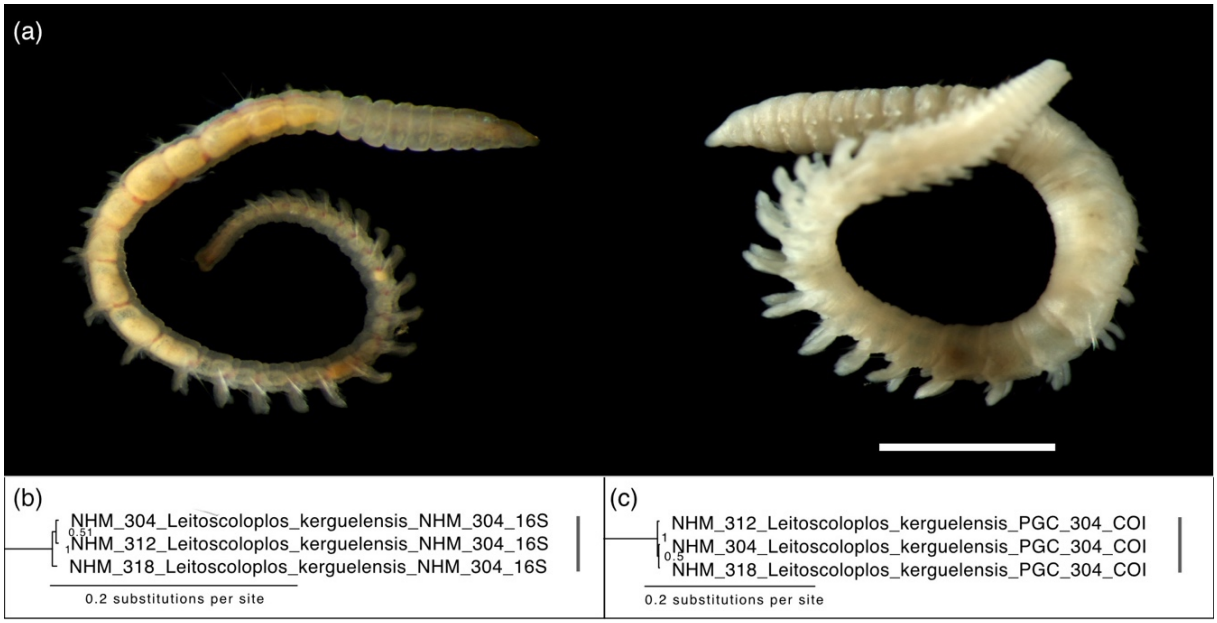

Figure 4.16 (a) Morphospecies *Leitoscoloplos kerguelensis*, live (left) and preserved (right) specimen NHM_312Scale bar 1 mm. (b-c) Sections of Prince Gustav Channel phylogenies generated by Bayesian analysis for family Cirratulidae using (b) 16S and (c) COI. Potentially cryptic lineage (specimen NHM_141A) highlighted in blue. Support values for

both phylogenies are given as Bayesian posterior probabilities. Vertical lines indicate final counted taxonomic units.

4.3.4.13 Paraonidae

Only a single specimen in the Family Paraonidae was identified in initial work (Figure 4.17), and sequencing was unsuccessful in either gene for this specimen (Table 4.15). The initial morphological Identification of Paraonidae sp. NHM_295 remains unchanged.

Table 4.15 Number of individuals, number of sequences for 16S and COI barcodes for morphospecies in the family Paraonidae – sequencing was not successful in this family

		n	n 16S	n COI	a
a	Paraonidae sp. NHM_295	1	0	0	-

Figure 4.17 Image of preserved morphospecies Paraonidae sp. NHM_295, specimen NHM_295. Scale bar 1 mm.

4.3.4.14 Phyllodocidae

Initial analyses identified three morphospecies within the family Phyllodocidae, one to named species *Paranaitis bowersi* (Benham, 1927), and two other unspecified morphospecies (Figure 4.18 a). 16S and COI were sequenced for all morphospecies, and phylogenetic analyses in both genes delineating each taxon (Figure 4.18 b) with minimum interspecific distances ranging from 15.7-19% in 16S and 11.8-16.8 in COI (Table 4.16).

Table 4.16 Number of individuals, number of sequences for 16S and COI barcodes and matrix of inter- and intraspecific p-distances for morphospecies in the family Phyllodocidae. For matrix, left: minimum 16S interspecific distances; right: minimum COI interspecific distances, diagonal: maximum intraspecific distances 16S/COI

		n	n 16S	n COI	a	b	c
a	*Paranaitis bowersi*	3	2	2	0.0/0.025	0.118	0.172
b	Phyllodocidae sp. NHM_234D	1	1	1	0.157	-	0.168
c	Phyllodocidae sp. NHM_235D	1	1	1	0.19	0.161	-

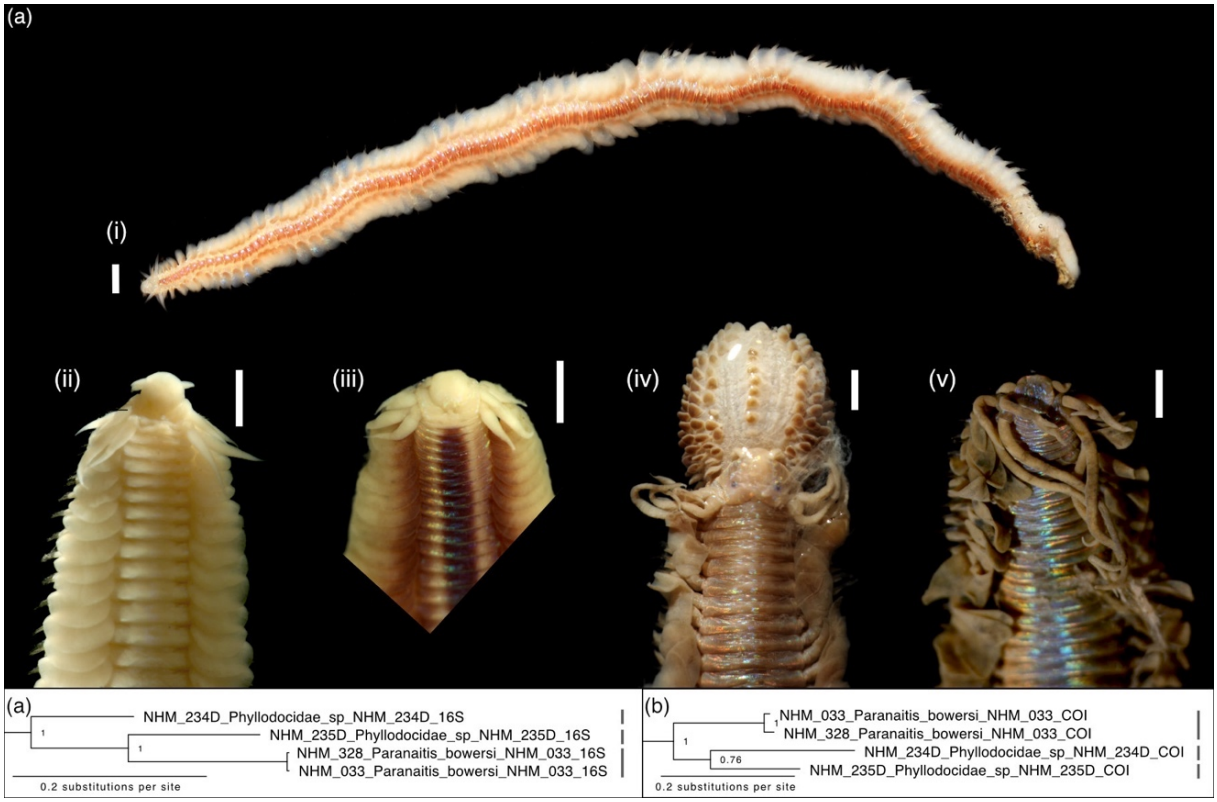

Figure 4.18 (a) Morphospecies identified in family Phyllodocidae (i) *Paranaitis bowersi,* specimen NHM_033 live; (ii) *Paranaitis bowersi,* specimen NHM_033 preserved, detail of head; (iii) *Paranaitis bowersi,* specimen NHM_328, preserved, detail of head, darker colour morph; (iv) Phyllodocidae sp. NHM_234D, specimen NHM_234D, preserved, detail of head (pharynx everted); (v) Phyllodocidae sp. NHM_235D, specimen 235D, preserved, detail of head. All scale bars 1 mm. (b-c) Sections of Prince Gustav Channel phylogenies generated by Bayesian analysis for family Phyllodocidae using (b) 16S and (c) COI. Support values for both phylogenies are given as Bayesian posterior probabilities. Vertical lines indicate final counted taxonomic units.

Paranaitis bowersi displayed a moderately large depth range, with the two specimens successful for sequencing collected from Duse Bay 200m and Duse Bay 1000m sites, with intraspecific distance between these two individuals of 0% in 16S and 2.5% in COI. A third specimen was collected from PGC_mid_850 unsuccessful in sequencing.

Genbank data was insufficient to confirm the identity of *Paranaitis bowersi,* or to improve taxonomic resolution in Phyllodocidae spp. NHM_324D and NHM_325D, and therefore original identifications in this family remain unchanged.

4.3.4.15 Polynoidae

Polynoidae displayed the highest morphospecies richness of any family in initial analyses, with up to 12 recorded morphospecies in 114 individuals. Three molecular species delimitation methods, ASAP, GMYC and PTP were used on a polynoid-only COI dataset to more thoroughly test species limits within this family. ASAP and PTP delineated 16 species, while GYMC estimated 17 (Figure 4.19, Figure 4.20), the additional species a further split within the *Austrolaenilla antarctica* complex, a species previously recognised as a complex with potentially cryptic lineages (Neal et al., 2014). In contrast, the polynoid section of the 16S barcode all-family phylogeny, structure between putative species is less clear, with morphospecies clustering together with low interspecific distances, even identical in some cases, particularly in a complex of species in *Antarctinoe* and *Harmothoe* genera (Figure 4.21; Table 4.17).

A large-scale barcoding analyses of 629 individuals across 24 Antarctic polynoid species (Cowart et al., 2022) found that 16S performed poorly in terms of differentiating closely related polynoid species identified by morphology and COI, including between species in the *Antarctinoe*/*Harmothoe* complex found in the current study. *Antarctinoe* is relatively new genus, described in 2006 as part of a revision of the species *Harmothoe spinosa* Kinberg, 1856, and nine morphologically similar Sub-Antarctic and Antarctic species in *Harmothoe* and *Antarctinoe* genera, which are often mistaken for *Harmothoe spinosa* or each other. Many of these nine species were identified in original morphological analyses in this study, such as *Antarctinoe ferox* (Baird, 1865)*, Antarctinoe spicoides* (Hartmann-Schröder, 1986)*, Harmothoe fuligineium* (Baird, 1865)*,* and *Harmothoe fullo* (Grube, 1878)*,* and an additional three were identified in blastn analyses, *Harmothoe acuminata* Willey, 1902, *Harmothoe antarctica* (McIntosh, 1885), and *Harmothoe crosetensis* (McIntosh, 1885). In the polynoid section of the all-family COI tree, the distinction between MOTUs identified as these taxa is small, with interspecific distances as low as 3.2 and 3.7% (Figure 4.21; Table 4.17). Both 16S and COI results suggest that the historical confusion amongst these species is also reflected in mitochondrial genes. However, in the highest ranked ASAP partition (16 species) the threshold distance (inter/intraspecific cut-off) was 2.6%, and COI interspecific distances as low as 3.7%, 4.8% and 5.3% (Kim et al., 2022; Lindgren et al., 2019) have been reported for new polynoid species described using integrative methods (morphology, non-mitochondrial genes in addition to barcodes).

Furthermore, morphological differences between closely related MOTUs in the *Antarctinoe/Harmothoe* complex were often present, each consistently matching with different morphological species in COI blastn analyses.

New MOTUs or cases of misidentification were often of damaged specimens missing diagnostic characters such as elytra (scales), to which conclusive morphospecies assignment was difficult. A case of merging two polymorphic species as a single MOTU (*Harmothoe fuligineum and Harmothoe* cf. *fuligineum* sp. NHM_233) is also recorded. Due to the case-by-case nature, each MOTU is discussed in turn below, along with the decision whether to include in the final updated species list.

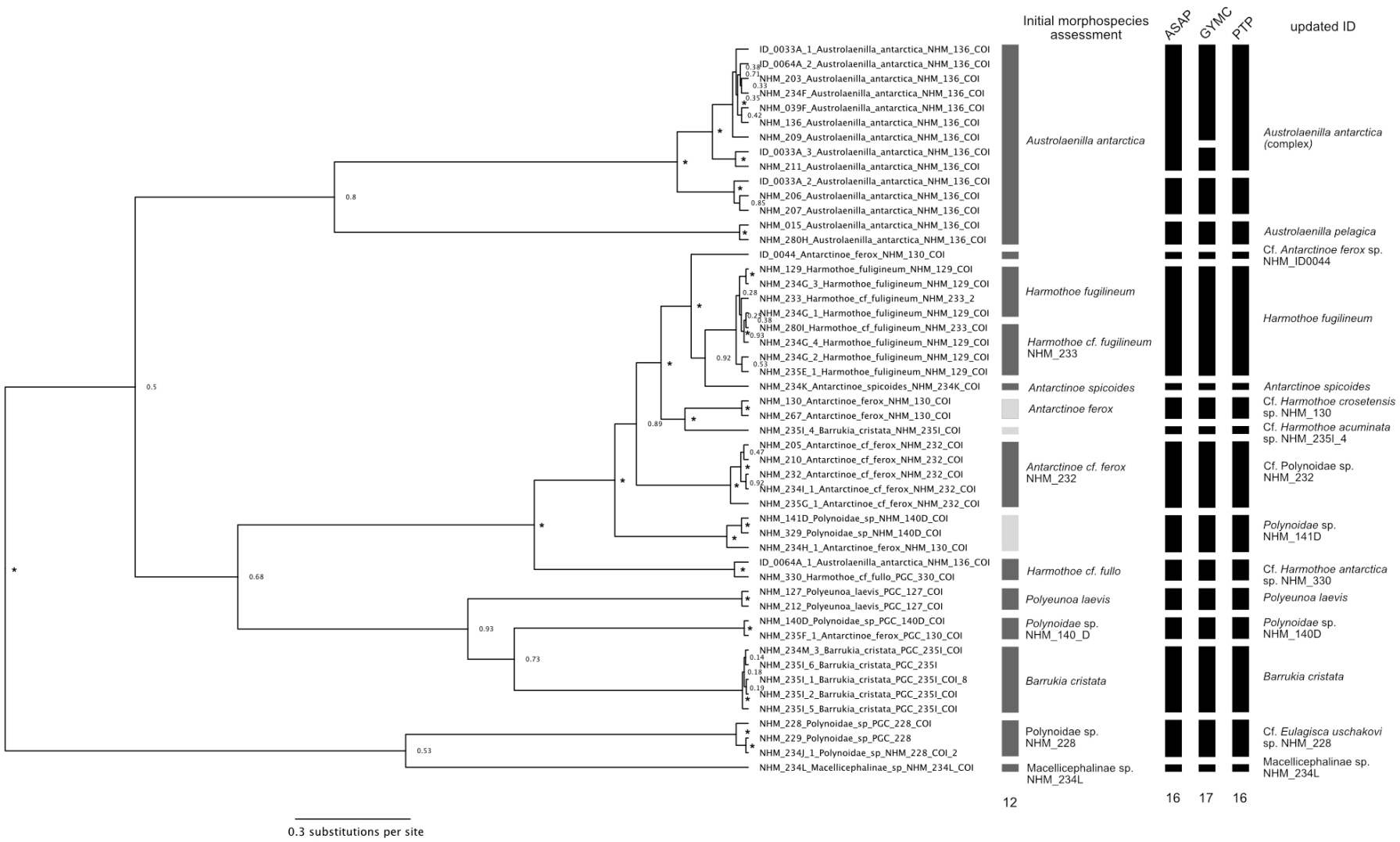

Figure 4.19 Bayesian COI ultrametric gene tree of family Polynoidae. Thick dark grey lines indicate initial morphospecies assignment. Thick black lines indicate putative species delineated by Assemble Species by Automatic Partitioning (ASAP), General Yule Mixed Coalescent model (GYMC) and Poission Tree Process (PTP) methods. Fiinal updated identifications are given on the right. Support values are given as posterior probabilities (values >0.95 denoted by asterisk).

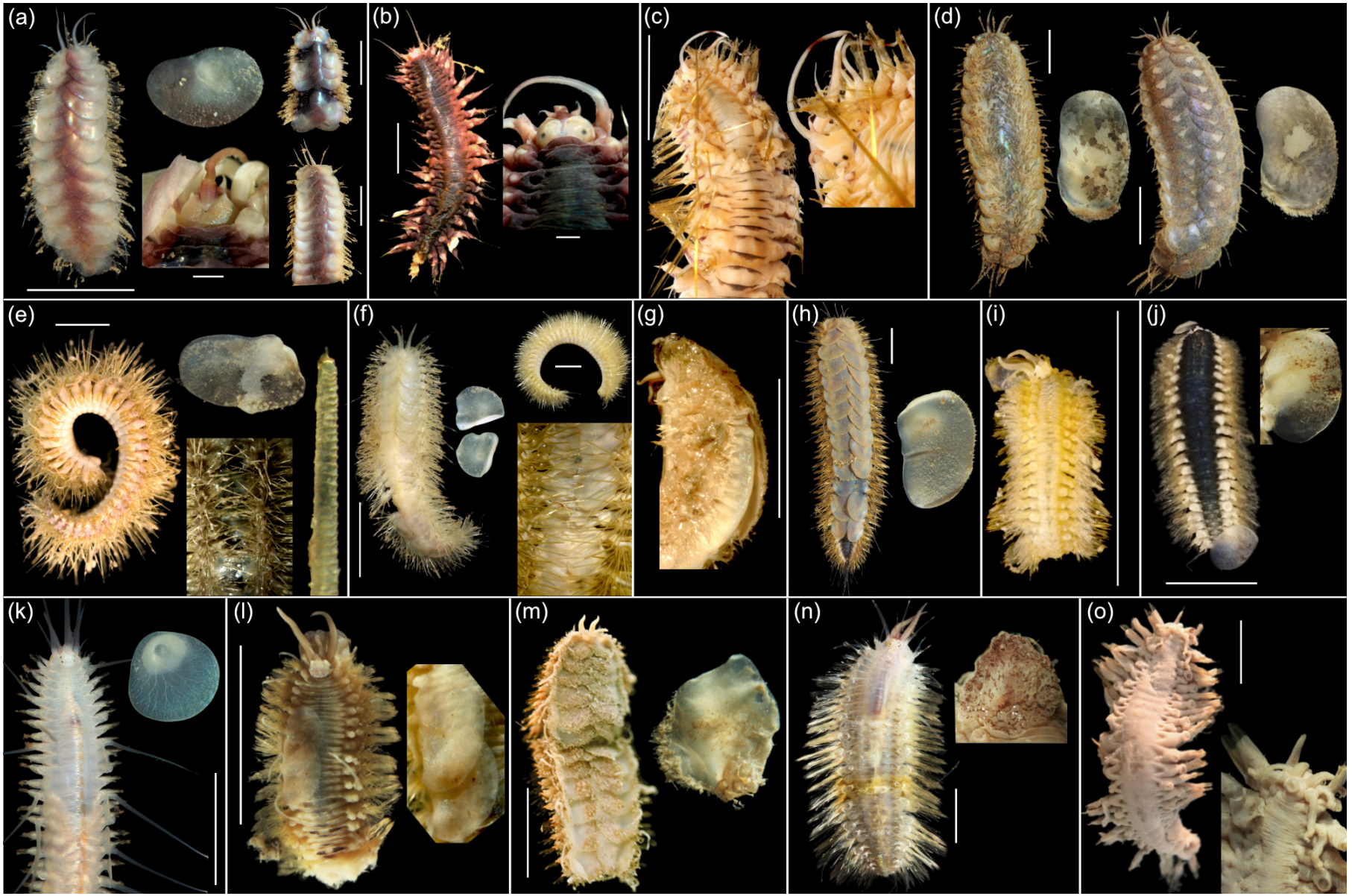
(a)
(b)
(c)
(d)
(e)
(f)
(g)
(h)
(i)
(j)
(k)
(l)
(m)
(n)
(o)

Figure 4.20 Molecular Operational Taxonomic Units identified in the family Polynoidae (a) *Austrolaenilla antarctica,* clockwise from left – specimen NHM_136, live; specimen NHM_136, elytron; specimen NHM_211, preserved; specimen NHM_206, preserved; specimen NHM_203, detail of prostomium, preserved (b) *Austrolaenilla pelagica*, specimen NHM_015 (left) whole specimen, live; (right) detail of prostomium, preserved (c) Cf. *Antarctinoe ferox* sp. NHM_ID044, preserved specimen NHM_ID044 (left) whole specimen, (right) detail of prostomium (d) *Harmothoe fuligineum* (left) specimen NHM_129, live, typical morphotype, with elytron (right) specimen NHM_233, live whites-spot morphotype, with detail of elytron (e) *Antarctinoe spicoides,* preserved specimen NHM_234K, clockwise from left – whole specimen, lateral view; elytron; pin-head tip of stout notochaeta; detail of dorsum (f) Cf. *Harmothoe crosetensis* sp. NHM_130, clockwise from left – specimen NHM_130, whole preserved specimen with detail of elytra; specimen NHM_167, live, whole specimen, lateral view; specimen NHM_167, preserved, detail of dorsum (g) Cf. *Harmothoe acuminata* sp. NHM_235I_4, specimen NHM_235I_4, anterior (h) Polynoidae sp. NHM_233, specimen NHM_233, live, with detail of elytron (i) Polynoidae sp. NHM_141D, specimen NHM_141D, preserved (j) Cf. *Harmothoe antarctica* sp. NHM_330, specimen NHM_330, with detail of elytron (k) *Polyeunoa laevis* specimen NHM_212, anterior, live, with detail of elytron (l) Polynoidae sp. NHM_140D, preserved, with detail of elytra (m) *Barrukia cristata,* specimen NHM_235I_1, with detail of elytron (n) Cf. *Eulagisca uschakovi* sp. NHM_288 (left) specimen NHM_229, live (right) specimen NHM_234_J, detail of elytron (o) Macellicephalinae sp. NHM_234_L, specimen NHM_235L, preserved, with detail of prostomium. All scale bars 1cm.

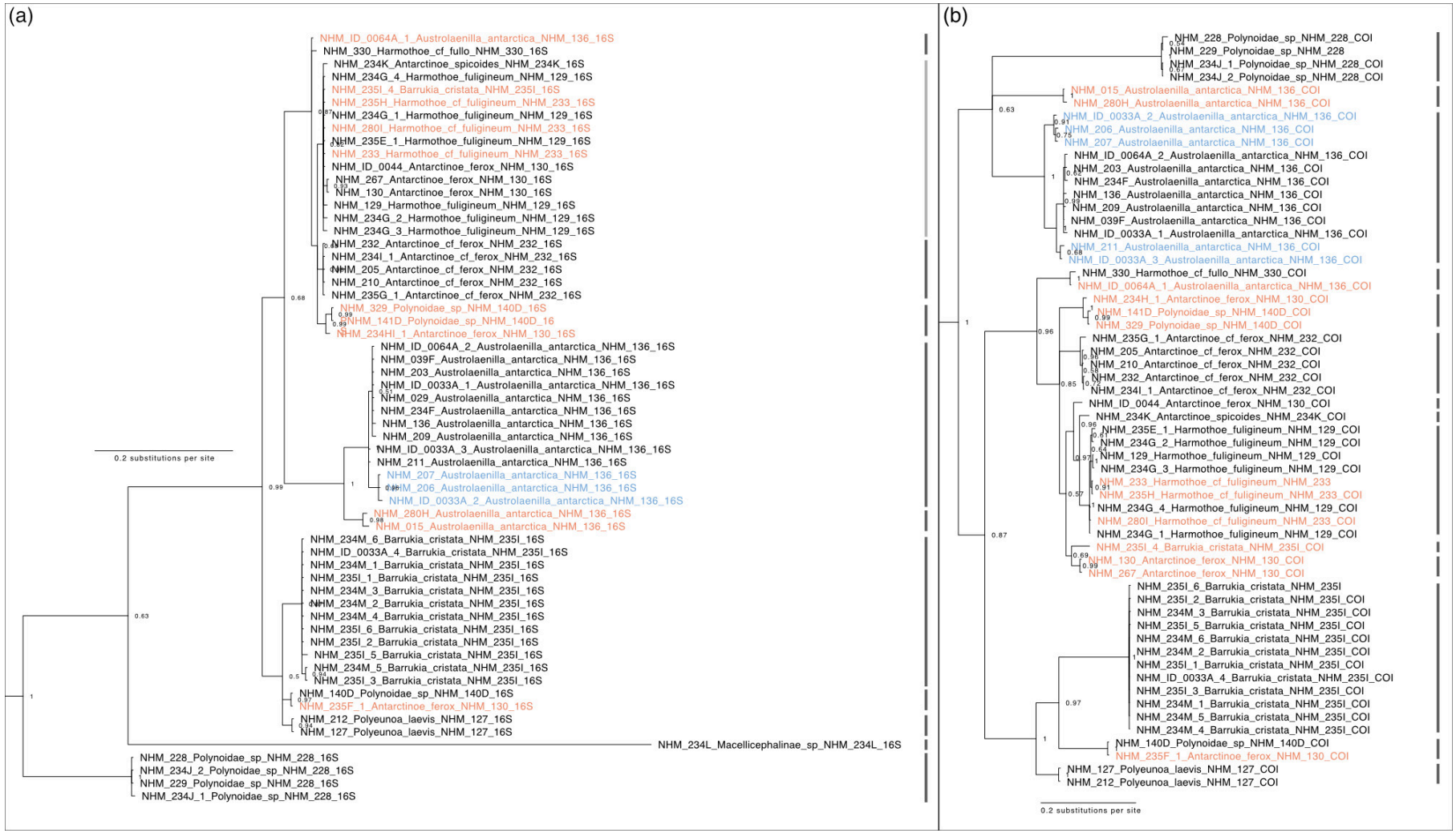

Figure 4.21 Sections of Prince Gustav Channel phylogenies generated by Bayesian analysis for family Polynoidae using (a) 16S and (b) COI. Specimens marked in blue represent potentially cryptic lineage. Specimens marked in orange indicate specimens moved from initial morphospecies identification, for example due to misidentification. Original morphospecies names are given. Support values for both phylogenies are given as Bayesian posterior probabilities. Dark vertical lines indicate final counted taxonomic units. Paler lines indicate where distinction between taxonomic units unclear.

Table 4.17 Number of individuals, number of sequences for 16S and COI barcodes and matrix of inter- and intraspecific p-distances for morphospecies in the family Polynoidae. For matrix, left: minimum 16S interspecific distances; right: minimum COI interspecific distances, diagonal: maximum intraspecific distances 16S/COI. New molecular taxonomic units are highlighted in bold. Interspecific distances below 1% in 16S and below 5% in COI are underlined. High intraspecific distances are presented in italics.

		n	n 16s	n COI	a	b	c	d	e	f	g	h	i	j	k	l	m	n	o
a	*Austrolaenilla antarctica*	13	13	12	*0.014/0.048*	0.146	0.164	0.156	0.164	0.155	0.168	0.164	0.164	0.153	0.162	0.17	0.171	0.191	0.28
b	***Austrolaenilla pelagica***	2	2	2	0.041	0.007/0.007	0.19	0.185	0.2	0.19	0.199	0.19	0.184	0.172	0.167	0.188	0.179	0.21	0.294
c	*Cf. Antarctinoe ferox* NHM_ID044	6	1	1	0.075	0.077	-	0.037	0.041	0.048	0.058	0.058	0.067	0.094	0.151	0.156	0.183	0.2	0.276
d	*Harmothoe fuligineum*	22	9	9	0.075	0.077	0	0.005/0.01	0.032	0.051	0.057	0.063	0.077	0.94	0.151	0.148	0.176	0.192	0.268
e	*Antarctinoe spicoides*	1	1	1	0.077	0.08	0.002	0.002	-	0.05	0.058	0.076	0.076	0.106	0.166	0.164	0.188	0.193	0.278
f	***Cf. Harmothoe crosetensis* NHM_130**	2	2	2	0.077	0.08	0.002	0.002	0.005	0.0/0.004	0.046	0.061	0.07	0.095	0.143	0.155	0.165	0.192	0.273
g	***Cf. Harmothoe acuminata* NHM_235I**	1	1	1	0.077	0.077	0	0	0.002	0.002	-	0.07	0.077	0.098	0.158	0.164	0.185	0.198	0.28
h	Cf. *Eunoe* sp. NHM_232	44	5	5	0.085	0.087	0.01	0.01	0.012	0.012	0.01	0.0/0.015	0.072	0.095	0.156	0.161	0.188	0.203	0.274
i	**Polynoidae sp. NHM_141D**	3	3	3	0.082	0.082	0.014	0.014	0.017	0.017	0.014	0.014	0.007/0.019	0.106	0.161	0.164	0.186	0.195	0.289
j	Cf. *Harmothoe antarctica* NHM_330	2	2	2	0.085	0.085	0.01	0.01	0.012	0.012	0.01	0.01	0.014	0.005/0.011	0.152	0.164	0.178	0.197	0.277
k	*Polyeunoa laevis*	2	2	2	0.094	0.08	0.06	0.06	0.063	0.063	0.06	0.06	0.056	0.053	0.0/0.004	0.115	0.124	0.224	0.291
l	Polynoidae sp. NHM_140D	2	2	2	0.094	0.08	0.017	0.056	0.058	0.058	0.056	0.053	0.053	0.046	0.022	0.0/0.003	0.143	0.224	0.271
m	*Barrukia cristata*	12	12	12	0.099	0.092	0.07	0.075	0.077	0.075	0.075	0.07	0.065	0.063	0.029	0.031	0.007/0.003	0.235	0.301
n	*Eulagisca uschakovi* sp. NHM_228	4	4	4	0.206	0.218	0.199	0.199	0.201	0.199	0.199	0.209	0.199	0.204	0.199	0.197	0.204	0.002/0.012	0.303
o	Macellicephalinae sp. NHM_234L	1	1	1	0.307	0.305	0.29	0.285	0.288	0.288	0.285	0.295	0.288	0.29	0.285	0.285	0.295	0.3	-

4.3.4.15.1 *Austrolaenilla antarctica* (Figure 4.20 a)

Specimens identified as the morphospecies *Austrolaenilla antarctica* Bergström, 1916 displayed notable genetic structure, in addition to a case of misidentification of damaged specimens, with two specimens matching sequences of the congener and new MOTU *Austrolaenilla pelagica* (Monro, 1930) (section 4.3.4.15.2) In remaining *Austrolaenilla antarctica* sequences, genetic structure was high, with two to three MOTUS identified in molecular delimitation analyses (Figure 4.19), and a maximum intraspecific distance across all specimens of 1.4% in 16S and 4.8% in COI (Table 4.17). *Austrolaenilla antarctica* has previously been recognised as potentially including cryptic species, (Neal et al., 2014). This study found three lineages within *Austrolaenilla antarctica,* with a maximum intraspecific COI distance of up to 5.1% in specimens collected from the Amundsen Sea, Weddell Sea, and Bransfield Strait, and a further 7.3% between those specimens and a sequence from South Georgia. After haplotype network analyses, the authors concluded that the South Georgia specimen is likely a different species due to genetic and geographic distance, however a greater sampling effort including additional locations and a larger number of specimens would be to determine whether *Austrolaenilla antarctica* contains distinct cryptic species. Excluding the South Georgia sequence, PGC specimens matched with sequences from(Neal et al., 2014) and additional Antarctic sequences identified as *Austrolaenilla antarctica* from (Cowart et al., 2022), with high to moderate percent identity in blastn analyses (99-99.8% 16S, 95.2-100% COI).

4.3.4.15.2 **Austrolaenilla pelagica** (Figure 4.20 b)

Two specimens originally identified as *Austrolaenilla antarctica* formed a separate MOTU in molecular delimitation analyses (Figure 4.19), differing from *Austrolaenilla antarctica* by 4.1% in 16S and 14.6% in COI in terms of minimum interspecific distances (Table 4.17). These specimens matched with Antarctic GenBank sequences of *Austrolaenilla pelagica* (Cowart et al., 2022; Neal et al., 2014) by 99.43-99.7% in 16S and 99.1-99.4% in COI, and also 99.5% (COI) identity to an unspecified planktonic larval sequence from the Ross Sea (GU227139, Heimeier et al., 2010).

Both specimens were relatively damaged, and missing all elytra (scales) and most chaetae. It was noted however that these specimens had distinct and visible eyes (Figure 4.20 b) whereas PGC specimens of *Austrolaenilla antarctica* had barely visible, or tiny eyes (Figure 4.20 a). While *Austrolaenilla pelagica* is described with eyes (Monro, 1930), Antarctic taxonomic literature has conflicting reports of whether *Austrolaenilla antarctica* has distinct eyes or not (see Fauvel, 1936) with identification literature either reporting one or both morphotypes (Fauvel, 1936; Hartman, 1967; Knox & Cameron, 1998; Monro, 1930) so it is not clear whether this is a relevant character, or possibly an artefact of preservation of the integument over the eye. The damage of these specimens makes further conclusive morphological work challenging without additional specimens.

However, the high percent identity matches to *Austrolaenilla pelagica* specimens from two polynoid-focused studies, including a publication on *Austrolaenilla antarctica* in which *Austrolaenilla pelagica* is described as distinct congeneric species both molecularly and morphologically, we identify PGC specimens in this new MOTU as *Austrolaenilla pelagica.*

4.3.4.15.3 cf. *Antarctinoe ferox* NHM_ID044 (Figure 4.20 c)

Though five individuals from this morphospecies were sequenced for both genes, only one remains within the original taxon due to morphological misidentification and genetic reassignment to new MOTUs or to existing morphospecies.

The genus *Antarctinoe* is endemic to Antarctic waters, and is defined from the similar genus *Harmothoe* by unidentate neurochaetae, and very long, stout notochaetae, distinctly longer than neurochaetae and oriented dorsally (Barnich et al., 2006). *Antarctinoe ferox* is one of two species in the genus, differentiated from its congener *Antarctinoe spicoides* primarily by its long notochaeta having smooth shafts and tips, while *A. spicoides* has ridged shafts with a pin-head tip. The single sequenced specimen remaining in the *A. ferox* morphospecies, specimen NHM_ID044 (Figure 4.20 c), is damaged, without elytra, however does retain notably long, smooth notochaetae.

On Genbank, this specimen matches with relatively high percent identity to specimens identified as *Antarctinoe ferox* (99.5-100% 16S, 96.2-96.4% COI) from the Antarctic Peninsula and Ross Sea (Cowart et al., 2022), Amundsen Sea (Neal et al., 2014; Neal et al., 2018b), and a larval 16S sequence from the Ross Sea (Gallego et al., 2014). However it also matches with similarly high percentage identities in both genes (99.5-100% 16S, 96.2-96.4% COI) to sequences of both *Harmothoe fuligineum* and *Harmothoe crosetensis* in 16S, and *Harmothoe fuligineum* in COI (all Cowart et al., 2022). Interspecific distances between MOTUs identified as these taxa in PGC samples are also low (3.7-4.8% COI, 0-0.2% 16S) (Table 4.17). Due to this uncertainty, and blastn matches for *Antarctinoe ferox* sequences also not exceeding 98%, the name of the PGC morphospecies and MOTU is changed to the open nomenclature cf. *Antarctinoe ferox.* The remarkably long notochaetae in this specimen still confers it to *Antarctinoe* and a distinct morphospecies. With only two valid species in the genus, it is possible there are more to describe – however, this taxon and a PGC specimen identified as *Antarctinoe spicoides* were paraphyletic in phylogenetic analyses, and a complete revision of both this genus and *Harmothoe* remains outstanding (Barnich et al., 2006).

In terms of other PGC specimens originally identified as *Antarctinoe ferox,* NHM_234H_1 and NHM_235F_1 are small moderately damaged specimens, that upon DNA extraction were noted to be more similar to Polynoidae sp. NHM_140 type.

Molecular data confirmed this observation, with NHM_235F_1 forming a clade with specimen NHM_140D, and NHM_234H_1 forming clade and with specimens originally identified as NHM_140D as a new MOTU, Polynoidae sp. NHM_141D (section 4.3.4.15.9). A further two specimens, NHM_130 and NHM_167, formed a new MOTU identified as cf. *Harmothoe crosetensis* following blastn results (see section 4.3.4.15.6). The remaining five specimens originally included in *A. ferox,* but not sequenced are kept within this morphospecies as a conservative approach until further morphological or molecular work can be carried out.

*4.3.4.15.4 **Harmothoe fuligineum*** (Figure 4.20 d)

Initial analyses found specimens identified as *Harmothoe fuligineum* sensu (Barnich et al., 2006) in addition to a second *H. fuligineum*-like morphotype, the former with typical elytra with densely fringed margins and mottled pattern, the latter with elytra with a shorter fringe, and white spot pattern (Figure 4.20 d), along with other minor characters such as pigmentation of cirri and tentacles. These two morphotypes were counted as separate morphospecies, the first as *Harmothoe fuligineum,* the second as *Harmothoe* cf. *fuligineum* sp. NHM_233. However, polynoids are known to include highly polymorphic species in terms of colour (Nygren et al., 2011).

Both 16S and COI were sequenced for each morphotype. COI molecular delimitation analyses and all-family barcode analyses found these morphotypes to be the same MOTU (Figure 4.19), with relatively low intraspecific variation (1%) (Table 4.17), and different morphotypes (mottled and white-spot) often more closely related than with the same morphotype. Intraspecific variation in 16S was also low (0.5%), however 16S phylogenetic analyses found both *Harmothoe fuligineum* morphotypes to be part of the *Antarctinoe/Harmothoe* species complex with cf. *Antarctinoe ferox, Antarctinoe spicoides,* and cf. *Harmothoe crosetensis* (Figure 4.21),with minimum 16S interspecific distances ranging from 0-0.2%. between these taxa (COI 3.2-5.1%) (Table 4.17). Blastn analyses found both morphotypes to match with high percent identity (99.2-100%) in COI to over 60 sequences identified as *Harmothoe fuligineum* from Cowart et al. (2022). 16S also matched closely (99.8-100%) to these specimens, but also with 99-100% identity to sequences of *Antarctinoe ferox* and *Harmothoe crosetensis* from the same study.

In the current study, both morphotypes of *Harmothoe fuligineum* were clearly distinguished from other polynoid morphospecies and COI MOTUs in terms of morphology. PGC specimens did not match with 16S or COI sequences identified as *Harmothoe fuligineum* from two other studies (Brasier et al., 2016; Neal et al., 2014). Specimens in these studies were collected by Epi-benthic sledge (EBS) which targets smaller, macrofaunal (<1cm) sized specimens (ref), compared with megafaunal (<1cm) sized specimens targeted by Agassiz Trawl.

PGC specimens in this study were highly concurrent morphologically with the new. comb. description and live specimen images of *Harmothoe fuligineum* in Barnich et al. (2006), were similar in size to type material (2-3cm long), and distinct from example specimen image in (Brasier et al., 2016) .

In personal communication with the lead author of Neal et al. 2014, *Harmothoe fuligineum* specimens in Neal et al. (2014) and Brasier et al. (2016) were smaller, often juvenile, or missing characters such as elytra, and it is possible that these were misidentified as a result, and future work should re-examine and compare these specimens.

In summary, the white-spot morphotype *Harmothoe cf. fuligineum* sp. NHM_322 is merged with PGC *Harmothoe fuligineum* specimens as a single MOTU. 16S did not discriminate well between this species and closely related morphospecies, however this has previously been documented for these taxa (Cowart et al., 2022). COI molecular delimitation methods distinguish this MOTU from other closely related PGC species, and positive GenBank matches to COI sequences of conspecifics from Cowart et al. (2022) support the original morphospecies identification of *Harmothoe fuligineum.*

4.3.4.15.5 ***Antarctinoe spicoides*** (Figure 4.20 e)

A single specimen in initial morphological analyses was identified as *Antarctinoe spicoides*, one of two species in the genus *Antarctinoe*, with one primary distinguishing character being very long notochaetae that orient dorsally to meet mid dorsum. *Antarctinoe spicoides* can be distinguished from its congener, *Antarctinoe ferox,* by pin-like tips on the long notochaee (Barnich et al., 2006) which were observed in this specimen (Figure 4.20 e). Both 16S and COI sequences were obtained, and COI molecular delimitation analyses distinguished the specimen as a distinct MOTU (Figure 4.19), though closely related to several taxa (minimum COI interspecific distances: *Antarctinoe ferox - 4.1%; Harmothoe fuligineum 3.2%; Harmothoe crosetensis* 4.8% - Table 4.17). 16S interspecific distances between *Antarctinoe spicoides* and these taxa were close to zero (Table 4.17), but as discussed (see section 4.3.4.15), 16s is known to be unreliable for distinguishing these species. Blastn results found highest percent identity matches (100% 16S, 99-99.7% COI) to sequences of *Antarctinoe ferox* (Cowart et al., 2022; Gallego et al., 2014; Neal et al., 2014) matching closer than PGC specimens identified as cf. *Antarctinoe ferox* (section 4.3.4.15.3). However, no sequences of *Antarctinoe spicoides* are available on GenBank to compare, and the PGC specimen's pin-tipped notochaetae support the original identification of *Antarctinoe spicoides.* The identification of this taxon remains unchanged, until a larger scale revision of the genus *Antarctinoe.*

4.3.4.15.6 cf. *Harmothoe crosetensis* NHM_130 (Figure 4.20 f)

Two individuals originally identified as *Antarctinoe ferox* were found to form a separate MOTU in COI molecular delimitation analyses (Figure 4.19). Blastn analyses found highest percent identity matches in COI (98.2-99.4%) to 65 sequences identified as *Harmothoe crosetensis* in Cowart et al. (2022). Records now recognised as *Antarctinoe ferox* (previously *Hermadion ferox*) and *Antarctinoe spicoides,* (previously *Harmothoe (Eunoe) spica spicoides*) were often confused with *Harmothoe crosetensis* and vice versa throughout the 20th century (see Barnich et al., 2006), and these taxa share morphological similarities. The PGC specimens were identified as *Antarctinoe ferox* due to long stout notochaetae oriented dorsolaterally, that meet mid-dorsally from midbody to posterior chaetigars in the largest specimen (NHM_267, Figure 4.20 f). Elytra also do not completely cover the dorsum in specimen NHM _267 which is noted for large specimens in *Antarctinoe ferox* (Barnich et al., 2006). However, the ratio between the length of long stout notochaetae to neurochaetae is not as large as in *cf. Antarctinoe ferox* and *Antarctinoe spicoides* in the present study, and specimen NHM_267 was preserved in a curled position (Figure 4.20 f), which may exaggerate the overlap of notochaetae and space between midbody elytra. Identification of these specimens is changed to cf. *Harmothoe crosetensis* based on blastn results until more detailed morphological analysis can be carried out, for example comparing neurochaetae under high powered microscope.

As with sequences identified as *Harmothoe fuligineum*, cf. *Antarctinoe ferox,* and *Antarctinoe spicoides* in this study 16S sequences could not discriminate well between these taxa (Table 4.17), with overlapping blastn hits between Genbank sequences identified as these species also.

4.3.4.15.7 cf. *Harmothoe acuminata* NHM_235I_4 (Figure 4.20 g)

A single, damaged, incomplete specimen originally identified as *Barrukia cristata* (specimen 235I_4) formed a separate, singleton MOTU in COI molecular delimitation analyses (Figure 4.19). Blastn analyses found highest COI percent identity matches (98.7-99.4%) with sequences identified as *Harmothoe acuminata* from Cowart et al. (2022). This specimen is sister to two PGC specimens identified as cf. *Harmothoe crosetensis* (minimum COI interspecific distance 5%, Table 4.17), and also had high percent identity matches to sequences identified as this species on Genbank (95-95.6%). *Harmothoe acuminata* and *Harmothoe crosetensis* are morphologically similar taxa, often confused or recorded as each other in taxonomic literature (Barnich et al., 2006). If this identification is correct, it again highlights morphological similarity that is reflected in molecular data.

As with other species in the *Antarctinoe*/*Harmothoe* complex, 16S did not discriminate well between COI MOTUs (Table 4.17), in addition 100% identity matches to GenBank sequences of *Harmothoe fuligineum, Harmothoe crosetensis,* and *Antarctinoe ferox* (Cowart et al., 2022).

No 16S sequences of *Harmothoe acuminata* are available on GenBank. This specimen and new MOTU is recorded as cf. *Harmothoe acuminata* until further morphological examination can confirm or refute.

4.3.4.15.8 Polynoidae sp. NHM_232 (Figure 4.20 h)

A potentially second *Antarctinoe ferox* morphotype was identified in initial analyses, *Antarctinoe* cf. *ferox* sp. NHM_232, based on long, dorso-laterally oriented notochaetae, and similarity to specimens now identified as cf. *Harmothoe crosetensis* (section 4.3.4.15.6), differing from that morphospecies in terms of dark blue body colour, and relatively larger elytra/shorter notochaete.

Sequences of these specimens formed a distinct MOTU in COI molecular delimitation analyses (Figure 4.19), though nested within the broader *Antarctinoe/Harmothoe* complex in 16S analyses (Figure 4.21). Minimum interspecific distances to this complex ranged 1-1.2% 16S 5.8-7.6% COI, with maximum intraspecific distances 0% 16S, 1.5% COI (Table 4.17). The highest blastn match was to a single sequence identified as *Eunoe* sp. (100% 16S, 98.1% COI) collected from the Antarctic peninsula (Cowart et al., 2022).

This taxon is distinct molecularly from specimens identified as *Antarctinoe* spp. both this study and on Genbank - on brief re-examination, placement in *Antarctinoe* was a misidentification, as the ratio in length between stout notochaetae and neurochaetae is not notably large. Identification for this morphospecies and MOTU is changed to Polynoidae sp. NHM_232 until further morphological analyses can be carried out. It is worth noting that the genus *Eunoe* is also considered closely related to *Antarctinoe,* with the *-noe* ending of the *Antarctinoe* referring to *Eunoe*, and *Antarctinoe spicoides* previously identified as *Eunoe spica spicoides* (Barnich et al., 2006).

4.3.4.15.9 Polynoidae sp. NHM_141D (Figure 4.20 i)

Two specimens originally in the morphospecies Polynoidae sp. NHM_140D, and one specimen identified as *Antarctinoe ferox*, formed a new, distinct MOTU in COI molecular delimitation analyses (Figure 4.19), though the clade is also part of the broader *Antarctinoe/Harmothoe* complex in 16S all-family phylogenetic analyses (Figure 4.21) . All specimens were relatively small, damaged and missing most elytra, making morphological determination difficult. Highest percent identity matches in blastn analyses are to sequences identified as *Harmothoe* sp. (99.8-100% 16S; 87.9-99.1% COI) from East Antarctica, the Ross Sea, and Antarctic peninsula localities (Cowart et al., 2022). This new MOTU is identified as Polynoidae sp. NHM_141D until more detailed morphological analyses can be carried out.

4.3.4.15.10 cf. Harmothoe antarctica NHM_330 (Figure 4.20 j)

The single specimen identified as morphospecies *Harmothoe* cf. *fullo* sp. NHM_330 in original analyses formed a distinct MOTU along with a misidentified specimen of *Austrolaenila antarctica* in COI delimitation analyses (Figure 4.19). Definition of this clade is less clear in 16S, and is part of the *Antarctinoe*/*Harmothoe* complex (Figure 4.21), however the MOTU has amongst the highest interspecific distances for this complex in COI (Table 4.17). Both specimens were damaged with most or all elytra lost, and original morphospecies identification was given the open nomenclature cf. due to uncertainty. COI blastn analyses found the highest percent identity (99.5% 16S, 98.8% COI) to a sequence identified as *Harmothoe antarctica* (Cowart et al., 2022) in addition to an unidentified planktonic polynoid sequence from the Ross Sea (98% identity COI, accession no. KF713380, Gallego et al., 2014). *Harmothoe fullo* and *Harmothoe antarctica* are two morphologically similar taxa, differentiated by primarily by minor characters of the elytra (Barnich et al., 2006). Identification of this MOTU is changed to cf. *Harmothoe antarctica* sp. NHM_330 until further morphological analyses can be carried out.

4.3.4.15.11 Polyeunoa laevis (Figure 4.20 j)

Two specimens were identified as the species *Polyeunoa laevis* McIntosh, 1885 in initial analyses. In addition to matching morphological descriptions of this species sensu (Barnich et al., 2012), these specimens were also collected living within the branches of *Thouarella* sp. soft coral, of which *Polyeunoa laevis* is a known commensal. These specimens formed a distinct MOTU in COI molecular delimitation analyses (Figure 4.19), and were also well defined in all-family 16S and COI phylogenetic analyses (Figure 4.21), with the lowest minimum interspecific distances between *Polynoidae* sp. NHM_140D (2.2% 16S, 11.5% COI) and *Barrukia cristata* (2.9% 16S, 12.4% COI, Table 4.17).

A recent wide-scale molecular study of *Polyeunoa laevis* (Bogantes et al., 2020) found remarkably high genetic diversity, recognising it as a species complex with at least three major genetic lineages – two within the Southern Ocean and one from Sub-Antarctic and Indian Ocean localities. While some morphological differences were found between non-Antarctic and Antarctic lineages, the two Antarctic lineages were morphologically cryptic, with some geographic sympatry. Cowart et al. (2022) also analysed this species as a case study, adding over 50 new specimens to existing sequence data and also supporting three lineages. Specimens in the current study fell within the Weddell-Ross *Polyeunoa laevis* clade from Bogantes et al. (2020) and *Polyeunoa* cluster 3 from Cowart et al. (2022) with high percent identity matches (99.5-100% 16S, 98.7-100% COI).

In summary, molecular data supports original morphospecies identification, and further aids in placing PGC specimens in one of two cryptic genetic lineages as part of the broader *Polyeunoa laevis* species complex.

4.3.4.15.12 **Polynoidae sp. NHM_140D** (Figure 4.20 k)

The morphospecies Polynoidae sp. NHM_140D formed a wastebasket taxon to small (~1cm), pale damaged specimens that could not be placed in other morphospecies due to lack of characters. Indeed, following molecular delimitation analyses, two specimens from this group formed a separate MOTU (Polynoidae sp. NHM_141D, see section 4.3.4.15.9). Specimen NHM_140D, along with a specimen previously identified as *Antarctinoe* ferox, formed a distinct, separate MOTU in COI molecular delimitation analyses (Figure 4.19) and clades in both 16S and COI analyses (Figure 4.21; Table 4.17). Genbank results were inconclusive, with the highest COI match (99.5%) to two unspecified specimens identified as Polynoidae sp. collected from the Ross Sea (MT139303-4, Cowart et al., 2022). In summary, identification remains unchanged, and Polynoidae sp. NHM_140D is retained as a morphospecies and MOTU. More intact specimens may be required in order to better identify this taxon.

4.3.4.15.13 ***Barrukia cristata*** (Figure 4.20 l)

Specimens were identified as *Barrukia cristata* (Willey, 1902) in initial analyses due to distinct characters such as crested dorsal segments, tufted notochaetae, and elytra with large crenate tubercles (e.g. Knox & Cameron, 1998). Apart from one misidentified specimen (now cf. *Harmothoe acuminata*), all specimens formed a distinct MOTU in COI molecular delimitation analyses (Figure 4.19), and both 16S and COI phylogenetic analyses (Figure 4.21), with low intraspecific variation across 12 sequences (0.7% 16S, 0.3% COI, Table 4.17).

Blastn analyses supported species identification, with high percentage identity matches (99.5-100% 16S, 99.1-100% COI) to 26 of sequences identified as *Barrukia cristata* collected from the Ross Sea, East Antarctica, and Antarctic Peninsula (Cowart et al., 2022). In summary, molecular data supports the original identification of this species and MOTU.

4.3.4.15.14 **cf. Eulagisca uschakovi NHM_288** (Figure 4.20 m)

Four large specimens with most or all elytra missing were grouped as unspecified morphospecies Polynoidae sp. NHM_288 in initial analyses. These specimens formed a distinct MOTU in COI molecular delimitation analyses (Figure 4.19) addition to well defined clades in all-family COI and 16S barcode analyses (Figure 4.21), with minimum interspecific distances not falling below 19% in either gene with other MOTUs (Table 4.17).

Specimens had highest percent identity (99.5-100% 16S, 97.9-99.5% COI) blastn hits with sequences identified as *Eulagisca uschakovi* Pettibone, 1997 collected from Antarctic Peninsula, East Antarctica and Ross Sea sites.

A brief revisit of images and notes for specimens in the current study show congruence with the original description of *Eulagisca uschakovi* (Pettibone, 1997), such as long palps with six longitudinal rows of papillae, lateral antennae inserted at same level to the median antenna, and elytra with mottled brown pigment, sharply pointed tubercles, and spinous globular vesicles. morphospecies and MOTU is identified as cf. E*ulagisca uschakovi* NHM_288 until further morphological analyses can confirm.

4.3.4.15.15 Macellicephalinae sp. NHM_234L (Figure 4.20 n)

A single, damaged specimen was identified in the Polynoid subfamily Macellicephalinae, Macellicephalinae sp. NHM_234L. Macellicephalinae are mostly restricted to the deep-sea, and are defined by lack of lateral antennae (Bonifácio & Menot, 2018). Both COI molecular delimitation analyses and all-family phylogenetic analyses found specimen NHM_234_L to be a distinct MOTU (Figure 4.19), with the highest interspecific distances observed for Polynoidae in this study, (minimum interspecific p-distances 28.5-30.75% 16S, 27.1-30.3% COI, Table 4.17). The top blastn hits in 16S were to macellicephalinid genera (*Bathypolaria, Branchinotogluma, Perinaleopolynoe, Macellicephala, Branchipolynoe*) but with low percent identity (74.4-77%). The COI sequence seemed possibly contaminated at first, not falling within the COI Polynoid clade in all-family analyses (Figure 4.21 b), and with top hits (75-77% identity) to non-Annelids, such as insects. However a blastx analyses (comparing amino acid translation) returned top hits to *Macellicephala* spp. (71-72.3% identity).

In initial morphological analyses, similarities to the macellicephalinid *Macelloides antarctica* sensu Pettibone (1976) were noted based on characters such as very long, sheathed neuropodia. However, investigating the presence of other diagnostic characters such as chitinised plates in place of jaws and detailed analyses of chaetae were beyond the scope and timeframe of initial analyses, and the damage of the single specimen (only one elytra intact, prostomial appendages missing etc) led to a conservative morphospecies identification at the sub-family level. As no sequences for species *Macelloides antarctica* (montotypic genus) are available on Genbank, the sub-family level identification of this specimen and MOTU remains unchanged. However future morphological work should investigate the possible identification of *Macelloides antarctica* in detail, as it would confirm sequence data for this monotypic deep-sea genus, building on recent molecular phylogenetic revisions of the subfamily Macellicephalinae (Bonifácio & Menot, 2019).

4.3.4.16 Sabellidae

Initial analyses identified two morphospecies within Sabellidae (Figure 4.22 a). Only 16S was successful in either species, with phylogenetic analyses clearly delineating the two (Figure 4.22 b)., with large interspecific distances (minimum 30.6%, Table 4.18). Only one sequence was obtained from Sabellidae sp. NHM_332, however a sequence was obtained from each site from which Sabellidae sp. NHM_272 was collected, PGC_South 800m, PGC Mid 850m, and PGC_Duse_Bay 200m, with maximum intraspecific distance of 1.2% (Table 4.18). Genbank data was insufficient to improve the taxonomic resolution of either morphospecies, so no change to original identifications were made.

Table 4.18 Number of individuals, number of sequences for 16S and COI barcodes and matrix of inter- and intraspecific p-distances for morphospecies in the family Sabellidae. For matrix, left: minimum 16S interspecific distances; right: minimum COI interspecific distances, diagonal: maximum intraspecific distances 16S/COI

		n	n 16S	n COI	a	b
a	Sabellidae sp. NHM_272	22	3	0	0.012/-	-
b	Sabellidae sp. NHM_332	7	1	0	0.306	-

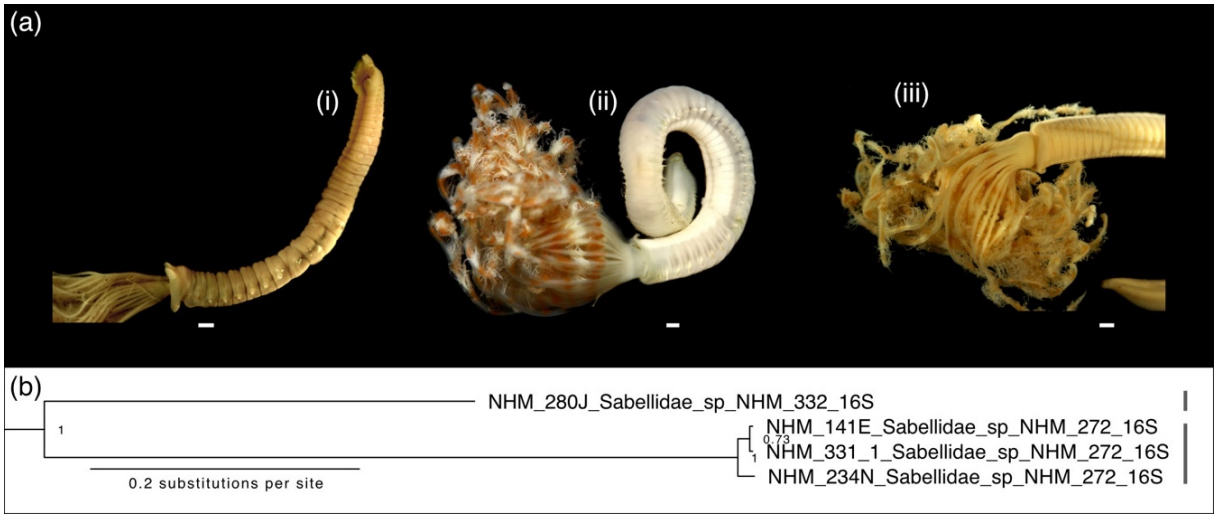

Figure 4.22 (a) Morphospecies identified in family Sabellidae (i) Sabellidae sp. NHM_332, specimen NHM_280J, preserved; (ii) Sabellidae sp. NHM_272, specimen NHM_272, live (iii) Sabellidae sp. NHM_272, specimen NHM_272, live. All scale bars 1 cm. (b) Section of Prince Gustav Channel phylogeny generated by Bayesian analysis for family Sabellidae using 16S. Support values for both phylogenies are given as Bayesian posterior probabilities. Vertical lines indicate final counted taxonomic units.

4.3.4.17 Scalibregmatidae

Only a single specimen in the family Scalibregmatidae was identified in initial work (Figure 4.23), and sequencing was unsuccessful in either gene for this specimen (Table 4.19). The initial morphological Identification of Scalibregmatidae sp. NHM_281 remains unchanged.

Table 4.19 Number of individuals, number of sequences for 16S and COI barcodes for morphospecies in the family Scalibregmatidae – sequencing was not successful in this family

		n	n 16S	n COI	a
a	Scalibregmatidae sp. NHM_281	1	0	0	-

Figure 4.23 Image of live (left) and preserved (right) morphospecies Scalibregmatidae sp. NHM_281, specimen NHM_281. Scale bar 1 mm.

4.3.4.18 Sternaspidae

A single species was identified in the family Sternaspidae, *Sternaspis sendalli* Salazar-Vallejo, 2014 (Figure 4.24 a) which also represented the most abundant taxon across the entire sample set, with 176 individuals, primarily from a single site Duse Bay 1000m, with one individual from PGC South 800m and two from Duse Bay 200m. Both 16S and COI were obtained for 7 individuals, including all sampling sites, with phylogenetic analyses showing that all individuals formed a monophyletic clade (Figure 4.24 b-c) with no intraspecific variation (p-distance 0% in both 16S and COI) (Table 4.20). Genbank data also confirmed identity to *Sternaspis sendalli*, with 100% identity matches in both genes to sequences of Antarctic sternaspids identified as *Sternaspis sendalli* from two studies (Drennan et al., 2019; Ge et al., 2022), including a revision of the species in which specimens close to the original type locality (off South Orkneys) were examined and sequenced (Drennan et al., 2019). In summary, molecular data fully supported the original species designation.

Table 4.20 Number of individuals, number of sequences for 16S and COI barcodes and maximum intraspecific p-distances (left 16S/right COI) for morphospecies in the family Sternaspidae

		n	n 16S	n COI	a
a	*Sternaspis sendalli*	176	7	7	0.0/0.0

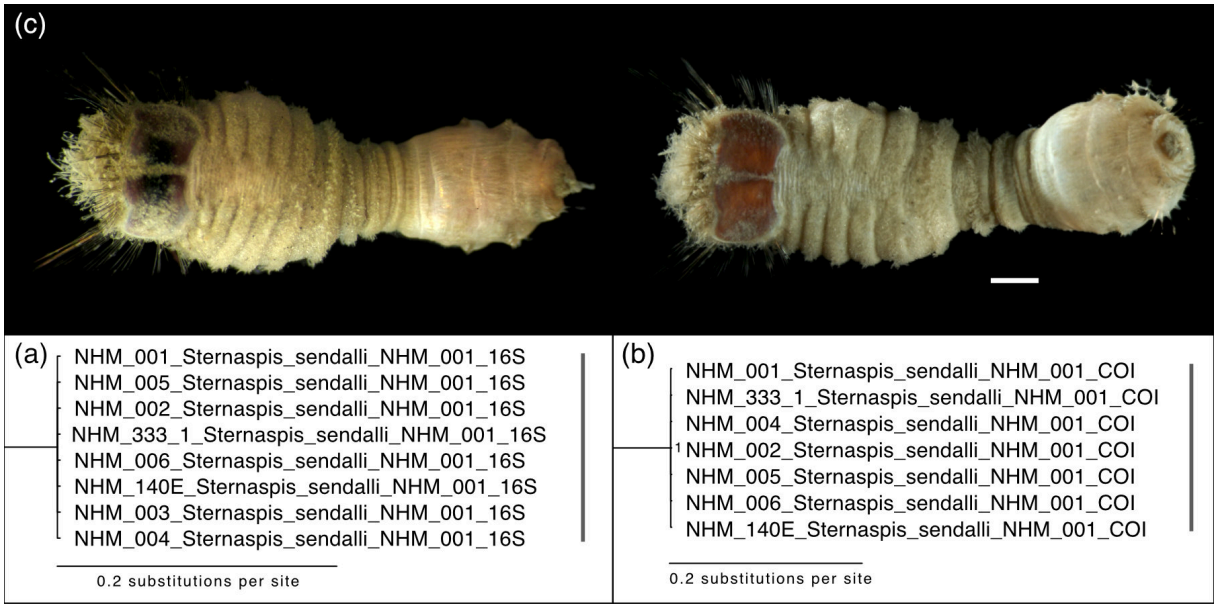

Figure 4.24 (a) Morphospecies *Sternaspis sendalli* live (left) and preserved (right), specimen NHM_001. Scale bar 1 mm. (b-c) Sections of Prince Gustav Channel phylogenies generated by Bayesian analysis for family Sternaspidae using (b) 16S and (c) COI. Potentially cryptic lineage (specimen NHM_141A) highlighted in blue. Support values for both phylogenies are given as Bayesian posterior probabilities. Vertical lines indicate final counted taxonomic units.

4.3.4.19 Syllidae

Originally four syllid morphospecies were identified, but as discussed in section 4.3.4.3, the single damaged specimen in the morphospecies Syllidae sp. NHM_285 was revealed to be a headless dorvilleid following barcode results and re-examination of specimen photos, and the specimen and morphospecies were excluded from further analyses. In addition, an individual in the morphospecies Syllidae sp. NHM_140F (NHM_141), only successful in COI sequencing, matched with high percentage identity (99.1-100% COI) to sequences of the Northern European hesionid species *Nereimyra punctata.*

This included sequences from Norwegian, Swedish and Russian sample sites across a range of studies, including a revision of the taxon. *Nereimyra punctata* (Müller, 1788) superficially somewhat similar to syllids, however on re-examination of specimen images and notes, the specimen NHM_141 matches the morphology of Syllidae NHM_140, and possesses a diagnostic syllid character, the proventricle, not present in Hesionidae. It is therefore likely that this was a contamination with other researchers working on European marine species in the same laboratory rather than connectivity over such large geographic distances, and thus that sequence was excluded from further analyses and considered contamination.

For the remaining syllid morphospecies, Syllidae sp. NHM_140F and two named species, *Pionosyllis kerguelensis* (McIntosh, 1885) and *Trypanosyllis gigantea* (McIntosh, 1885) (Figure 4.25 a) , both 16S and COI sequences were obtained for each with phylogenetic analyses delineating all species (Figure 4.25 b), though relationships between respective clades remains uncertain. Intraspecific p distances also support the delineation of these taxa, with minimum distances ranging from 20.6-32% in 16s and 21.1-26.1% in COI, and low intraspecific variation within species with more than one sequence (Table 4.21).

Table 4.21 Number of individuals, number of sequences for 16S and COI barcodes and matrix of inter- and intraspecific p-distances for morphospecies in the family Syllidae. For matrix, left: minimum 16S interspecific distances; right: minimum COI interspecific distances, diagonal: maximum intraspecific distances 16S/COI

		n	n 16S	n COI	a	b	c
a	*Pionosyllis kerguelensis*	7	2	2	0.004/0.006	0.213	0.251
b	Syllidae sp. NHM_140F	4	1	1	0.206	-	0.261
c	*Trypanodenta gigantea*	9	3	3	0.292	0.324	0.002/0.007

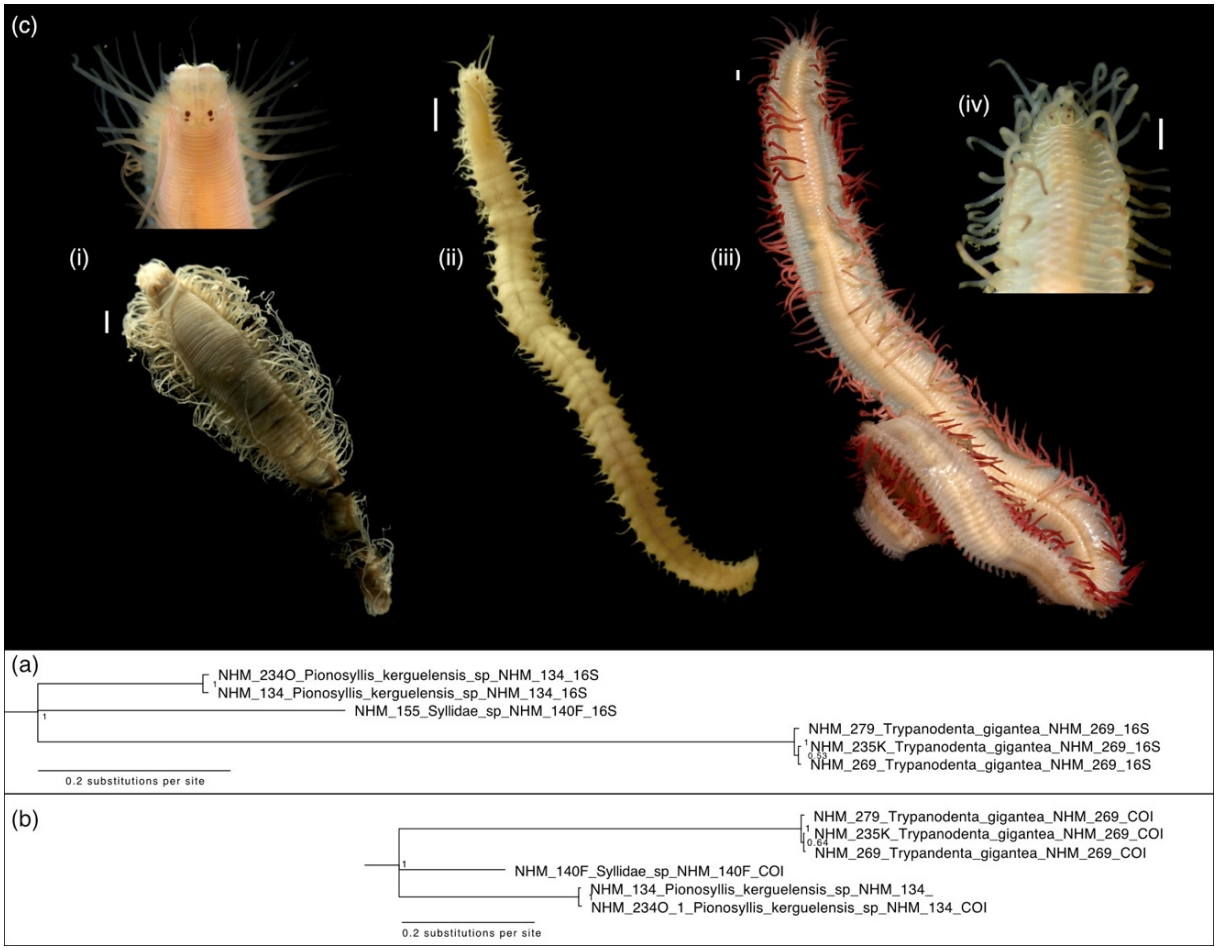

Figure 4.25 (a) Morphospecies identified in family Syllidae (i) *Pionosyllis kerguelensis,* specimen NHM_134 live, detail of head (top), preserved (bottom); (ii) *Syllidae* sp. NHM_140F, specimen NHM_140F, preserved (iii) *Trypanodenta gigantea,* previously identified as *Trypanosyllis gigantea,* specimen NHM_279, live; (v) *Trypanodenta gigantea,* previously identified as *Trypanosyllis gigantea*, specimen NHM_235K, live, detail of head, paler branchiae;, preserved, detail of head. All scale bars 1 mm. (b-c) Sections of Prince Gustav Channel phylogenies generated by Bayesian analysis for family Syllidae using (b) 16S and (c) COI. Support values for both phylogenies are given as Bayesian posterior probabilities. Vertical lines indicate final counted taxonomic units.

Genbank data was insufficient to confirm the identity of *Pionosyllis kerguelensis*, or to improve the taxonomic resolution of Syllidae sp. NHM_140F. However, *Trypanosyllis gigantea* matched with high percent identity (98.9-99% 16S; 96.3-99.7% COI) to Antarctic and sub-Antarctic sequences of *Trypanodenta gigantea.* In 2017, *Trypanosyllis gigantea* was moved to the genus *Trypanodenta* following detailed morphological and molecular phylogenetic analyses in a systematic revision of *Trypanosyllis* (Álvarez-Campos et al., 2017b), with *Trypanodenta gigeantea* (McIntosh, 1885) sequences from that revision matching with PGC sequences following blastn analyses. The species name in this study therefore is updated to *Trypanodenta gigantea,* highlighting the presence of outdated taxonomic data in commonly used Southern Ocean annelid identification guides (e.g. Hartman, 1964, 1967; Knox & Cameron, 1998).

In summary, due to misidentification of a damaged specimen, three of four original syllid morphospecies remain, with *Trypanosyllis gigantea* updated to *Trypanodenta gigantea* to reflect recent developments in the taxonomy of the species.

4.3.4.20 Terebellidae

Original analyses identified up to five terebellid morphospecies (Figure 4.26 a). 16S sequences were obtained for each morphospecies, while COI had a poorer success rate (Table 4.22). In 16S phylogenetic analyses, the family Terebellidae was paraphyletic with Ampharetidae and Trichobranchidae (Figure 4.26 b), however these families are closely related, being in the same suborder Terebelliformia, and short 16S barcodes alone likely lack the resolution to split these families further. Barcode data revealed two cases of misidentification. Both 16S and COI barcodes placed the only morphospecies recorded in the family Oweniidae, Oweniidae sp. NHM_235C, in the clade Terebellidae sp. NHM_234P (Figure 4.26 b-c). This morphospecies was recorded during sorting of bulk fixed samples during limited laboratory access during COVID-19 pandemic, where capacity for detailed morphological assessment was limited due to time constraints relative to samples examined pre-pandemic. The majority of these individuals were in coarse sandy tubes, with head morphology damaged and tentacles missing in specimens where tube was partially removed, leaving branchiae which were mistaken for an oweniid tentacle crown. However, upon revisiting the specimens for DNA extraction and full removal of specimens from tubes, terebellid morphology was noted, with barcodes confirming this. The family Oweniidae is therefore removed, with morphospecies Oweniidae sp. NHM_235C subsumed into Terebellidae sp NHM_234P.

Table 4.22 Number of individuals, number of sequences for 16S and COI barcodes and matrix of inter- and intraspecific p-distances for morphospecies in the family Terebellidae. For matrix, left: minimum 16S interspecific distances; right: minimum COI interspecific distances, diagonal: maximum intraspecific distances 16S/COI

		n	n 16S	n COI	a	b	c	d	e
a	*Leaena collaris*	2	2	0	**0.083/-**	-	-	-	-
b	*Pista mirabilis*	5	4	4	0.205	0.0/0.002	-	0.224	0.228
c	cf. *Thelepus antarcticus* NHM_142	1	1	0	0.226	0.262	-	-	-
d	Terebellidae sp NHM_234P	20	6	2	0.239	0.213	0.232	0.0/0.006	0.192
e	Terebellidae sp NHM_337	1	1	1	0.237	0.211	0.267	0.194	-

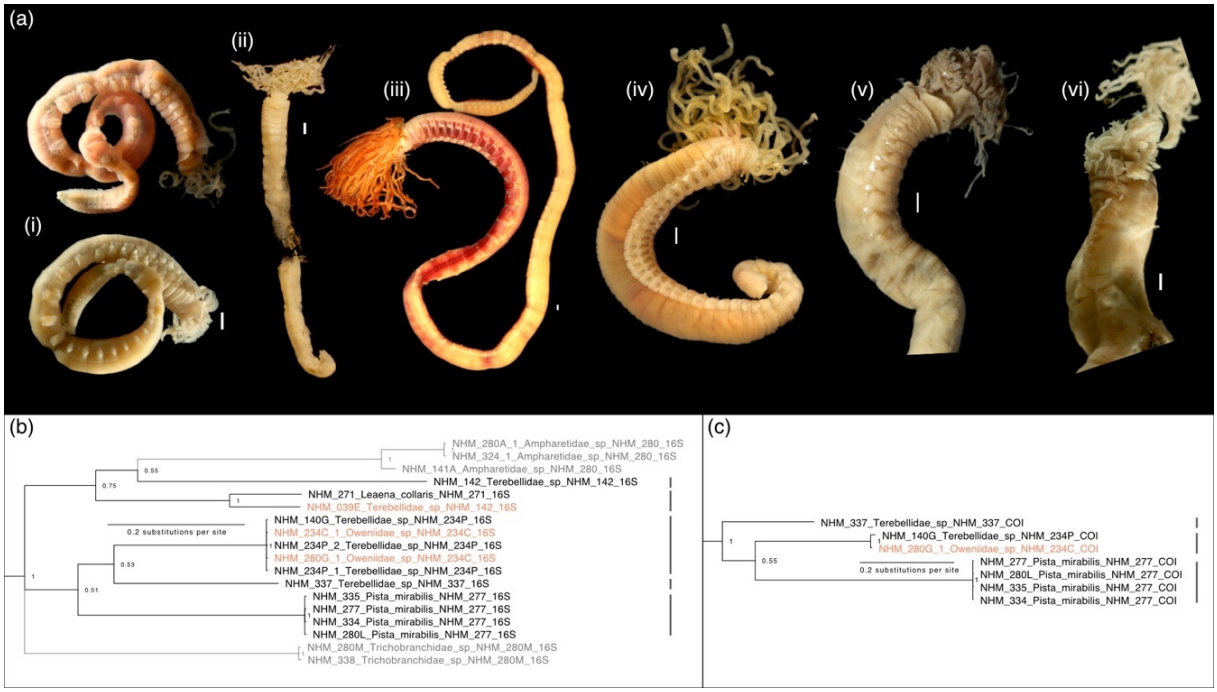

Figure 4.26 (a) Morphospecies identified in family Terebellidae (i) *Laena collaris* sp. NHM_271, specimen NHM_271 live (top) and preserved (bottom); (ii) *Laena collaris* sp. NHM_271, specimen NHM_039E, preserved ,a potentially cryptic/psuedocryptic taxon (iii) *Pista mirabilis*, specimen NHM_277, live (iv) Terebellidae sp. NHM_142, specimen NHM_142, live (v) Terebellidae sp. NHM_234P (iv) Cirratulidae , specimen NHM_234P_1; (vi) Terebellidae sp. NHM_337, specimen NHM_337, preserved. All scale bars 1 mm. (b-c) Sections of Prince Gustav Channel phylogenies generated by Bayesian analysis for family Terebellidae using (b) 16S and (c) COI. Specimen marked in orange originally misidentified as different morphospecies than clade placement (see text). Branches and taxa marked in grey are non-Terebellid families. Support values for both phylogenies are given as Bayesian posterior probabilities. Vertical lines indicate final counted taxonomic units.

Another possible case of misidentification is that one damaged specimen in the morphospecies Terebellidae sp. NHM_142 (specimen NHM_039E, Figure 4.26 a ii) did not form a clade in 16S with Terebellidae sp. NHM_142, but rather formed a clade with *Laena collaris* Hessle, 1917, with high support but moderate intra-clade distance (8.3%) (Table 4.22). Though this would represent relatively high intraspecific variation, particularly in 16S which is generally slower evolving than COI (e.g. in congeneric species in the Terebellid genus *Loima*, COI interspecific p-distances range 16.4-26.3%, intraspecific 0-2.1%, Martin et al. 2022), as this is based on a single damaged specimen and only one gene, a conservative approach is taken to include specimen NHM_039E within *Laena collaris* (as cf. *Laena collaris*) until further morphological and molecular analyses can investigate whether this specimen represents a separate, closely related taxon.

Following these corrections, in 16S phylogenetic analyses the five terebellid morphospecies do form delineated clades (Figure 4.26 b-c), with minimum interspecific p-distances ranging from 19.4-26.7 % (between the three clades for which COI was obtained, this ranges 19.2-22.8%) (Table 4.22). With the exception of *Laena collaris* as previously discussed, the two other clades in which multiple individuals were successfully sequenced (*Pista mirabilis* and Terebellidae sp. NHM_234P) intraspecific variation was zero or near zero in both genes (Table 4.22).

Genbank data was insufficient to confirm the identity of *Laena collaris* or *Pista mirabilis* McIntosh, 1885, or to improve the taxonomic resolution of Terebelllidae sp. NHM_234P. Terebellidae sp. NHM_337 matched with 100% and 99.8% in 16S and COI respectively (GU227018, GU227136) to a planktonic larva sequenced from the Ross Sea identified as cf. Terebellida sp. DH-2009 (Heimeier et al., 2010), however this does not improve the taxonomic resolution of the current ID.

Terebellidae sp. NHM_142 matched with 99.8% identity to an Antarctic sequence from Elephant Island identified as *Thelepus antarcticus* Kinberg, 1866 (MT166847) sequenced as part of a molecular phylogenetic study of Terebelliformia (Stiller et al., 2020). As this is based on a single gene, the ID of this taxon is updated to cf. *Thelepus antarcticus* until a morphological re-evaluation can be taken to confirm the species identification.

In summary, barcoding revealed cases of misidentification within Terebellidae, including the removal of family Oweniidae from final results. However overall, the five original morphospecies taxa remain well delineated, and most identifications remain the same, apart from Terebellidae sp. NHM_142, which is tentatively identified as cf. *Thelepus antarcticus* sp. NHM_142 based on blastn results.

4.3.4.21 Tomopteridae

Only a single specimen in the family Tomopteridae (Figure 4.27), identified as being in the genus *Tomopteris,* was recovered, with sequencing successful for only COI (Table 4.23). Genbank data was insufficient to inform identification to species, however top hits (>90% identity) supported the generic identification. Initial morphological identification remains unchanged.

Table 4.23 Number of individuals, number of sequences for 16S and COI barcodes and maximum intraspecific p-distances (left 16S/right COI) for morphospecies in the family Tomopteridae

		n	n 16S	n COI	a
a	*Tomopteris* sp. NHM_131	1	0	1	-

Figure 4.27 Images of live (left) and preserved, detail of head (right) morphospecies *Tomopteris* sp. NHM_131, specimen NHM_131. Scale bar 1 mm.

4.3.4.22 Travisiidae

Only a single specimen in the family Travisiidae (Figure 4.28) was identified in initial work, and sequencing was unsuccessful in either gene for this specimen (Table 4.24). The initial morphological Identification of *Travisia kerguelensis* McIntosh, 1885 therefore remains unchanged.

Table 4.24 Number of individuals, number of sequences for 16S and COI barcodes for morphospecies in the family Travisiidae – sequencing was not successful in this family

		n	n 16S	n COI	a
a	*Travisia kerguelensis*	1	0	0	-

Figure 4.28 Live image of morphospecies *Travisia kerguelensis*, specimen NHM_281. Scale bar 1 cm.

4.3.4.23 Trichobranchidae

A single morphospecies in the family Trichobranchidae was recorded, Trichobranchidae sp., 280M (Figure 4.29 a) from Duse Bay 200m and 500m sites. Two 16S (both sites) and one COI sequence (Duse Bay 500m) were obtained, forming a single clade in 16S phylogenetic analyses (Figure 4.29 b) with low intraspecific variation (0.2%) (Table 4.25). Genbank sequence data was insufficient to improve taxonomic resolution for this taxon in either 16S or COI, so that the original identification remains the same.

Table 4.25 Number of individuals, number of sequences for 16S and COI barcodes and maximum intraspecific p-distances (left 16S/right COI) for morphospecies in the family Trichobranchidae.

		n	n 16S	n COI	a
a	Trichobranchidae sp. 280M	8	2	1	0.002/-

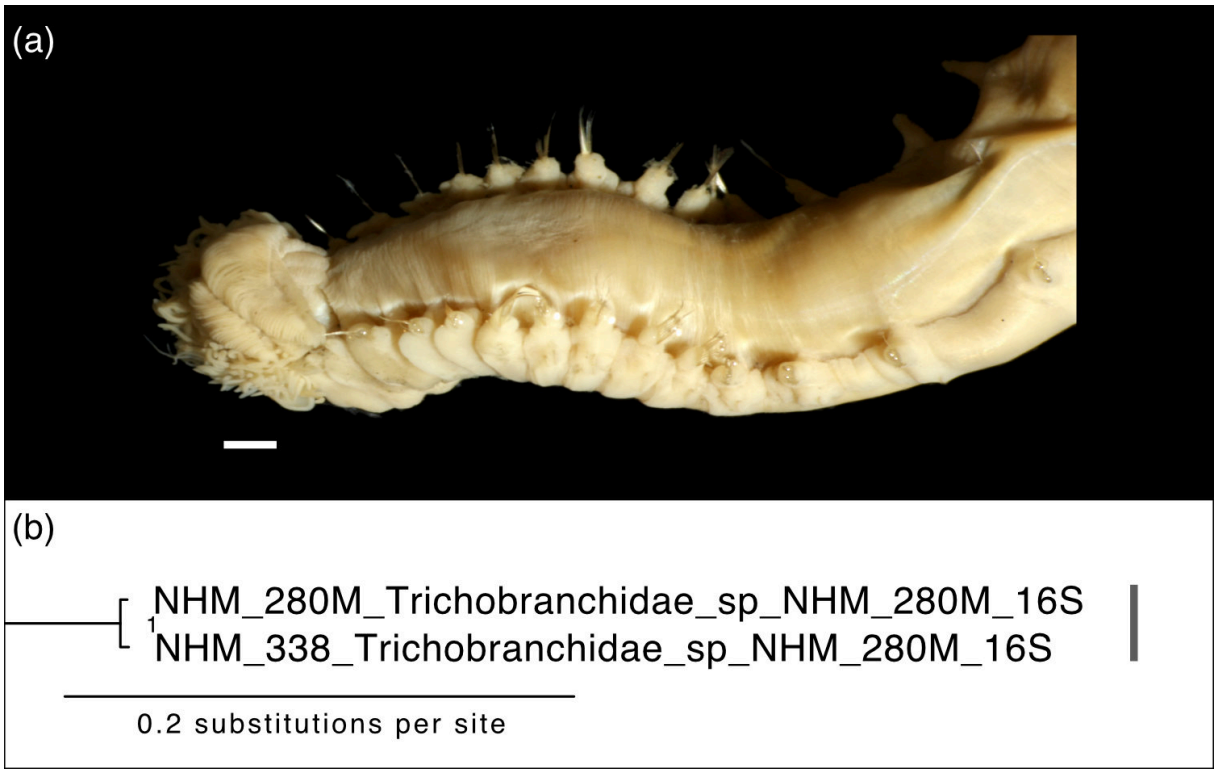

Figure 4.29 (a) Morphospecies Trichobranchidae sp. NHM_280M, specimen NHM_280M live, preserved, anterior portion. Scale bar 1 mm. (b) Section of Prince Gustav Channel phylogeny generated by Bayesian analysis for family Trichobranchidae using 16S Bayesian posterior probabilities. Vertical lines indicate final counted taxonomic units.

4.3.5 Summary of results

Drennan et al. (2021) found 57 species, in 613 individuals and 25 families in the in the Prince Gustav Channel AGT annelid sample set. Following specimen recounting during DNA extraction, and the analyses of DNA barcode data, the final numbers are changed to 58 species in 610 individuals and 23 families. Though the final number has only changed by one this masks turnover within the sample, for example both loss and gain of species, in addition to changes to identification. Different categories of changes, or lack thereof, were as follows, with examples:

1. No change to original identification

    a) no molecular data to confirm or refute ID as sequencing was unsuccessful (e.g. *Travisia kerguelensis*)

    b) Blastn results support the original identification, for example a positive ID to named species (e.g. *Sternaspis sendalli, Barrukia cristata*).

    c) Insufficient sequence coverage on Genbank to confirm or refute morphospecies identification (e.g. *Chaetocirratulus andersenensis* – no sequences of this species are available on public repositories).

2. Change in taxonomic resolution

    a) Increase in taxonomic resolution, such as cf. species to named species, or from family to cf. species (e.g. *Myzostoma cf. divisor*, to *Mysostoma divisor*, Polynoidae NHM_228 to cf. *Eulagisca uschakovi* NHM_288).

    b) Decrease in taxonomic resolution, such as genus to family, (e.g. *Protodorvillea* sp. NHM_290 to Dorvilleidae sp. NHM_290).

    c) Updated outdated taxonomic information (e.g. *Trypanosyllis gigantea* to *Trypanodenta gigantea*).

3. Change in taxonomic ID

    a) Species removed, from misidentification (e.g. Oweniidae sp. NHM_234C to existing morphospecies Terebellidae sp. NHM_234P), or merging of morphologically variable, genetically identical taxa (e.g. *Harmothoe cf. fuligineum*NHM_233 to *Harmothoe fuligineum*).

    b) New molecular species, from misidentification (e.g. two individuals from *Austrolaenilla antarctica* to new genetic species, *Austrolaenilla pelagica*) or splitting of morphologically similar genetically cryptic (e.g. *Ophelina cylindricaudata*).

Results of all changes within these categories are summarised in Table 4.26, with and updated list of species in Table 4.27. (Updated from Chapter 3 Table 3.3)

Table 4.26 Summary of changes to original morphospecies identification using barcode data. *Trypanedenta gigantea* is counted twice (counts with asterisk) as while Blastn results did support the original species identification (*Trypanosyllis gigantea*), it was to sequences named with the updated new. comb. (Álvarez-Campos et al., 2017b).

Category	subcategory	n species
No change	Sequencing unsuccessful – no molecular data	3
	Insufficient sequence coverage on Genbank to confirm or improve morphospecies identification	33
	Blastn results support the original identification (to named species)	8*
Change in taxonomic resolution	Increase in taxonomic resolution	5
	Decrease in taxonomic resolution	3
	Update outdated taxonomic information	1*
Change in taxonomic ID	Species removed (misidentification or to existing molecular species)	5
	New genetic species (misidentification, or splitting morphologically cryptic, genetically distinct morphospecies	6

Table 4.27 Updated list of morphospecies identified in Drennan et al. 2021b (Chapter 3) with individual counts for each site provided, with number of barcodes (16S, COI) in parentheses, and updated species identification following barcode analyses. Specimen counts in green and red represent gains and losses of specimens respectively. Species names in **bold** in updated species list represent an ID change from original identification.

Family	Morphospecies	Sites						Total n	Updated species
		DB 200m	DB 500m	DB 1000m	PGCM 850m	PGCS 800m	PGCS 1200m		
Ampharetidae	Ampharetidae sp. NHM_280	2 (1,1)	2 (1,1)	-	-	1 (1,0)	-	5	Ampharetidae sp. NHM_280
Cirratulidae	*Aphelochaeta* sp. NHM_301	-	4 (3,3)	-	-	-	-	4	*Aphelochaeta* sp. NHM_301
	Chaetocirratulus andersenensis	2 (0,2)	1	-	-	-	-	3	*Chaetocirratulus andersenensis*
	Cirratulidae sp. NHM_035	-	1 (0,0)	1 (1,1)	-	-	-	2	Cirratulidae sp. NHM_035
	Cirratulidae sp. NHM_317	-	1 (1,1)	-	-	-	-	1	Cirratulidae sp. NHM_317
Dorvilleidae	Protodorvillea sp. NHM_290	-	5 (5,2)	-	-	-	-	5	**Dorvilleidae sp. NHM_290**
Flabelligeridae	*Brada mammilata*	-	-	-	1 (1,0)	-	17 (2,0)	18	*Brada mammilata*
	Flabegraviera mundata	-	-	-	9 (1, 1)	-	-	9	*Flabegraviera mundata*
Hesionidae	Hesionidae sp. NHM_291	-	1 (1,1)	-	-	-	-	1	Hesionidae sp. NHM_291
Lumbrineridae	*Augenaria tentaculata*	1 (0,1)	5 (1,1)	4 (4,4)	-	1 (0,0)	-	11	*Augenaria tentaculata*
	Lumbrineridae sp. NHM_300	-	1 (1,1)	-	-	-	-	1	Lumbrineridae sp. NHM_300
Maldanidae		-	1 (1,0)	-	-	1 (1,0)	-	2	***Cf. Asychis amphiglyptus* sp. NHM_140A_5**
	Lumbriclymenella robusta	-	-	-	-	4 (2,2)	-	4	*Lumbriclymenella robusta*
	Maldane sarsi	7 (4,4)	33 (5,5)	67 (9,10)	-	12 (4,3)	-	119	***Maldane sarsi antarctica****
	Maldanidae sp. NHM_125	-	-	1 (1,0)	-	5 (2,1)	-	6	Maldanidae sp. NHM_125
	Maldanidae sp. NHM_302	-	2(1,1)	-	-	-	-	2	Maldanidae sp. NHM_302
Myzostomatidae	*Myzostoma* cf. *divisor* NHM_123	-	-	-	-	1(1,1)	-	1	***Myzostoma divisor***
Nephtyidae	*Aglaophamus trissophyllus*	-	3 (2,3)	5 (5,5)	6(1,6)	-	1(1,1)	15	*Aglaophamus trissophyllus*
	Agalophamus sp. NHM_280F	-	1 (1,0)	-	-	-	-	1	*Agalophamus* sp. NHM_280F
Oligochaeta	Oligochaeta sp. NHM_287	-	5 (2,2)	-	-	-	-	5	Oligochaeta sp. NHM_287
	Oligochaeta sp. NHM_289	-	-	-	-	-	-	0	

Family	Morphospecies	Sites						Total n	Updated species
		DB 200m	DB 500m	DB 1000m	PGCM 850m	PGCS 800m	PGCS 1200m		
Opheliidae	*Ophelina breviata*	-	2 (1,0)	-	-	-	-	2	*Ophelina breviata*
	Ophelina cf. *cylindricaudata*	-	3 (2,0)	-	-	-	-	3	*Ophelina* cf. *cylindricaudata* NHM_284
		-	2 (2,1)	-	-	-	-	2	***Ophelina* cf. *cylindricaudata* NHM_286**
Orbiniiae	*Leitoscoloplos kerguelensis*	-	3(3,3)	-	-	-	-	3	*Leitoscoloplos kerguelensis*
Oweniidae	Oweniidae sp. NHM_234C	-	-	-	-	-	-	0	
Paraonidae	Paraonidae sp. NHM_295	-	1(0,0)	-	-	-	-	1	Paraonidae sp. NHM_295
Phyllodocidae	*Paranaitis bowersi*	1(1,1)	-	1(0,0)	1(1,1)	-	-	3	*Paranaitis bowersi*
	Phyllodocidae sp. NHM_234D	-	-	-	1(1,1)	-	-	1	Phyllodocidae sp. NHM_234D
	Phyllodocidae sp. NHM_235D	-	-	-	1(1,1)	-	-	1	Phyllodocidae sp. NHM_235D
Polynoidae	*Antarctinoe ferox*	-	-	1(1,1)	-	-	-	6	***cf. Antarctinoe ferox* NHM_ID044**
		-	1(1,1)	-	-	1(1,1)	-	2	***cf. Harmothoe crosetensis* NHM_130**
	Antarctinoe cf. *ferox* NHM_232	-	-	-	39 (3,3)	-	2 (2,2)	41	**cf. *Eunoe* sp. NHM_232**
	Antarctinoe spicoides	-	-	-	1 (1,1)	-	-	1	*Antarctinoe spicoides*
	Austrolaenilla antarctica	-	-	6 (6,5)	1 (1,1)	1(1,1)	5 (5,5)	13	*Austrolaenilla antarctica*
		-	1(1,1)	1(1,1)	-	-	-	2	***Austrolaenilla pelagica***
	Barrukia cristata	-	-	1 (1,1)	11 (11,11)	-	-	12	*Barrukia cristata*
		-	-	-	1(1,1)	-	-	1	***cf. Harmothoe acuminata* NHM_235I_4**
	Harmothoe fuligineum	-	1(1,1)	-	20 (7,7)	1(1,1)	-	22	*Harmothoe fuligineum*
	Harmothoe cf. *fuligineum* NHM_233	-	-	-	-	-	-		
	Harmothoe cf. *fullo* NHM_330	1 (1,1)	-	1 (1,1)	-	-	-	2	**cf. *Harmothoe antarctica* NHM_330**
	Macellicephalinae sp. NHM_234L	-	-	-	1(1,1)	-	-	1	Macellicephalinae sp. NHM_234L
	Polyeunoa laevis	-	-	-	1 (1,1)	1(1,1)	-	2	*Polyeunoa laevis*
	Polynoidae sp. NHM_140D	-	-	-	3(1,1)	1(1,1)	-	2	Polynoidae sp. NHM_140D
		1 (1,1)	-	-	4 (1,1)	1(1,1)	-	3	Polynoidae sp. NHM_141D

Family	Morphospecies	Sites						Total n	Updated species
		DB 200m	DB 500m	DB 1000m	PGCM 850m	PGCS 800m	PGCS 1200m		
	Polynoidae sp. NHM_228	-	-	-	4(4,4)	-	-	4	**Cf. *Eulagisca uschakovi* sp. NHM_228**
Sabellidae	Sabellidae sp. NHM_272	19(1,0)	1	-	1(1,0)	1(1,0)	-	22	Sabellidae sp. NHM_272
	Sabellidae sp. NHM_332	6(0,0)	1(1,0)	-	-	-	-	7	Sabellidae sp. NHM_332
Scalibregmatidae	Scalibregmatidae sp. NHM_281	-	1(0,0)	-	-	-	-	1	Scalibregmatidae sp. NHM_281
Serpulidae	Serpulidae sp. NHM_280K	-	-	-	-	-	-		
Sternaspidae	*Sternaspis sendalli*	2(1,1)	-	173 (5,5)	-	1(1,1)	-	176	*Sternaspis sendalli*
Syllidae	*Pionosyllis kerguelensis*	-	-	-	6(1,1)	1(1,1)	-	7	*Pionosyllis kerguelensis*
	Syllidae sp. NHM_140F	-	-	-	-	4(1,1)	-	4	Syllidae sp. NHM_140F
	Syllidae sp. NHM_285	-	-	-	-	-	-	0	
	Trypanosyllis gigantea	-	8(2,2)	-	1(1,1)	-	-	9	***Trypanodenta gigantea***
Terebellidae	*Leaena collaris*	-	1(1,0)	1(1,0)	-	-	-	2	*Leaena collaris*
	Pista mirabilis	3 (2,2)	2 (2,2)	-	-	-	-	5	*Pista mirabilis*
	Terebellidae sp. NHM_142	-	-	-	-	1(1,0)	-	1	***cf. Thelepus antarcticus* NHM_142**
	Terebellidae sp. NHM_234P	-	2(1,1)	-	17(4,0)	1(1,1)	-	20	Terebellidae sp. NHM_234P
	Terebellidae sp. NHM_337	1(1,1)	-	-	-	-	-	1	Terebellidae sp. NHM_337
Tomopteridae	*Tomopteris* sp NHM_131	-	-	-	-	1(0,1)	-	1	*Tomopteris* sp. NHM_131
Travisiidae	*Travisia kerguelensis*	-	-	-	-	1(0,0)	-	1	*Travisia kerguelensis*
Trichobranchidae	Trichobranchidae sp. 280M	1 (1,0)	7 (1,1)	-	-	-	-	8	Trichobranchidae sp. 280M

4.4 Discussion

The aim of this study was to test whether barcoding a subsample of representative morphospecies significantly improves taxonomic resolution of a morphology-based study of a Southern Ocean annelid community. Remarkably, overall species richness for the Prince Gustav Channel annelid dataset changed very little, suggesting that skilled morphological identifications perform well for giving representative measures of biodiversity. Though the number of species increased by one, this masks turnover at the species level, with loss and gain of taxonomic units and changes to identification, as well as cases of misidentification at the specimen level. One of the main benefits to the addition of barcode data was as an error check on initial identifications. This ranges from large family-level misidentifications (e.g. Oweniidae sp. NHM_235C moved to Terebellidae sp. NHM_234P), to smaller misidentifications between conspecific morphospecies (e.g. individuals of *Austrolaenilla antarctica* to *Austrolaenilla pelagica*). As context, much of the specimen identification work took place during periods of limited laboratory access during the 2020 COVID-19 pandemic where time spent on each morphospecies was reduced out of necessity to complete the sample, with identifications continued to be worked on without access to a laboratory and based on notes and images only, and limiting some identifications to family level. However it is also worth noting that barcode data supports many of the morphospecies identifications as distinct taxonomic units, with most morphospecies forming reciprocally monophyletic clades in phylogenetic analyses.

Barcode data was also useful in resolving identification of damaged, fragmented specimens, such as specimens in Polynoidae where characters such as elytra were missing. Barcodes also were able to link tail fragments to Maldanidae sp. NHM_302 of which only head fragments were counted in initial analyses. These posterior fragments include key diagnostic characters that could allow for species-level identification in future morphological analyses. Regarding more typical uses of DNA barcodes – identification and delimitation, the practicality of the subset of barcode data in this study is less clear.

4.4.1 Species identification

In terms of identification of morphospecies by comparison with public reference libraries, over half (*n*=33) of morphospecies had no representatives on Genbank. Only 8 of 22 named species were supported by positive blastn matches to the correct species, while only five morphospecies improved their taxonomic rank, though a conservative approach was still taken for most of these cases, where an open nomenclature was given if based on a single or small number of sequences, e.g. cf. *Thelepus antarcticus* sp. NHM_142.

These results highlight the large data gaps on public repositories that remain for annelids, with a recent review of marine metazoan sequence coverage finding that only 11% of known marine annelid species are represented on GenBank and BOLD databases (Mugnai et al., 2021). Incomplete reference databases linked to museum-vouchered specimens for quality-control are a major bottleneck to the advancement of next generation DNA metabarcoding of bulk or environmental marine samples (van der Loos & Nijland, 2021), which in theory could sequence and document entire communities, yet without curated reference libraries identify little beyond MOTUs.

The value of curated reference sequences was also apparent in the case study of *Maldane sarsi*, where comparison with sequence data from type localities provided a relatively straightforward method of testing the presence of a European taxon in Antarctic waters. A similar approach should be taken to assess the presence of other species identified in this study with non-Antarctic type localities, such as *Pista mirabilis* and *Ophelina cylindricaudata*, in addition to a greater effort to update and revise current taxonomic guides for Southern Ocean annelid fauna.

Though the ability of barcodes to improve identification in the present study was limited, these results highlight that even if morphological identification alone is effective in documenting overall measures of diversity, effort should still be made to sequence taxonomically identified species wherever possible in order to build the curated libraries necessary for streamlining biodiversity assessments (including integrative methods) in the future.

4.4.2 Species delimitation

Most morphospecies were sufficiently distantly related so that large interspecific distances and clear phylogenetic separation were found even between small numbers of sequences. However, barcoding just a representative subsample of recorded morphospecies was insufficient for delimitation in many examples, particularly with more closely related species.

Owing to high variation in terms of inter and intraspecific distances across the phylum, a universal barcoding gap has not been identified for Annelida (Kvist, 2014). While ten times the mean intraspecific variation has been proposed as a base threshold with which to delineate cryptic animal species (Carr et al., 2011; Hebert et al., 2004), this requires comprehensive sampling to accurately assess true rates of intraspecific variation. The methodological limitations of delimitation by mitochondrial genes only must also be a consideration (summarised in Eberle et al., 2020). As a conservative approach therefore, where small number of individuals and sequences were present, many morphospecies/MOTUs were not split into cryptic species despite conventionally high intraspecific variation (intraspecific variation is typically on the order of 1% rather than 10% , Puillandre et al., 2021), such as Dorvilleidae sp. NHM_290 (12% intraspecific distance in COI).

An exception was the splitting of *Ophelina* cf. *cylindricaudata* into putative cryptic species due to intraspecific distances >20%, and a polyphyletic relationship with the congener *Ophelina breviata* which has clear morphological differences.

In this context, a strength of barcoding in this study was not necessarily for delimitation, but rather to guide targeted future morphological work. Several annelid studies upon finding high genetic structure and potentially cryptic lineages in species have found genuine morphological differences upon secondary analyses (psuedocryptic species, e.g. Álvarez-Campos et al., 2017a,b; Brasier et al., 2016).

For the family Polynoidae, the most diverse group in initial analyses, three methods of molecular species delineation analyses were tested, which proposed increasing the 12 morphospecies to 16-17 molecular taxonomic units. Additional species were either new genetic species-based misidentifications, or proposed cryptic lineages, while two species were merged as a single polymorphic species, *Harmothoe fuligineum*. While more individuals in general were sequenced for polynoid morphospecies than in other taxa, numbers were still relatively low which can negatively affect the performance of delimitation methods (Puillandre et al., 2021) and must be taken into consideration for the interpretation of these results

Delimitation analyses found 2-3 cryptic lineages in *Austrolaenilla antarctica*, with overall intraspecific differences of up to 4.8% - a finding that corroborates previous barcode studies of this species (Neal et al., 2014). Antarctic benthic species with previously assumed cryptic lineages based on barcode data have been found to constitute a single well-connected species following greater sampling and geographic coverage, with additional samples filling intermediate haplotypes between lineages (e.g. the ophiuroid *Ophionotus victoriae,* Galaska et al., 2017; Lau et al., 2021). Like Neal et al. (2014), we consider *A. antarctica* to be a single species complex until additional data (increase in sampling, nuclear genes, genomic methods etc.)

In contrast, despite having lower COI interspecific distances than intraspecific distances *in A. antarctica,* the delineation of a number of closely related polynoids (the Antarctinoe/Harmothoe complex -see section 4.3.4.15) by molecular analyses were maintained. Low intraspecific distances have previously been found for these species in a large scale molecular study of Antarctic polynoids that also incorporated morphological identification (Cowart et al. 2022). In addition to matching barcodes of different species identified in Cowart et al. (2022), species in this complex often had clear morphological differences, for example as seen in the species pair with the lowest interspecific distances in this complex (3.2%) *Antarctinoe spicoides* and *Harmothoe fuligineum*.

Barcodes perform poorly when differentiating recently split species (Grant et al., 2021); in contrast, morphological differentiation can be more easily distinguished than genetic structure amongst species in young radiations (Eberle et al., 2020). Recent radiations are common in the Southern Ocean, thought to be a result of frequent isolation of populations during repeated glacial cycles throughout the Pleistocene/Pliocene (Wilson et al., 2009), which may explain some of the patterns observed in Polynoidae.

The complexity of the above samples highlights the case-by-case approach needed when approaching species delimitation questions, and the challenges faced when trying to establish a single rule or universal threshold with which to define species boundaries.

Chapter 5 Population genomics, cryptic diversity and phylogeographic structure in the Southern Ocean circumpolar annelid, *Aglaophamus trissophyllus* (Annelida: Nephtyidae)

REGAN DRENNAN [1,2,3], SERGI TABOADA [4], ADRIAN G. GLOVER [2], THOMAS G. DAHLGREN [5,6], KATRIN LINSE [3], JONATHAN T. COPLEY [1], MARIA BELEN ARIAS [2]

[1] Ocean & Earth Science, University of Southampton, European Way, Southampton SO14 3ZH, UK

[2] Life Sciences Department, Natural History Museum, London SW7 5BD, UK

[3] British Antarctic Survey, High Cross, Madingley Road, Cambridge CB3 0ET, UK

[4] Department of Biodiversity, Ecology, and Evolution, Universidad Complutense de Madrid, Madrid, Spain

[5] NORCE Norwegian Research Centre, Bergen, Norway

[6] Department of Marine Sciences, University of Gothenburg, Box 463, 40530 Gothenburg, Sweden

Abstract

Understanding patterns of genetic diversity and connectivity in species and populations is essential for managing conservation strategies and monitoring future environmental change. The use of single-gene barcodes has revealed previously unrecognised diversity in Antarctic benthic fauna, however interpretations based on single genes alone face several methodological limitations. Using newer genomic methods to generate genome-wide single nucleotide polymorphism (SNP) data can examine diversity at much higher resolutions yet have only been applied to a small number of Antarctic taxa. The nephtyid annelid *Aglaophamus trissophyllus* is a large, widespread, easily recognisable species in the Southern Ocean, with molecular studies using traditional barcode markers finding multiple potentially cryptic lineages in specimens morphologically identified as *A. trissophyllus*. This study performs the first SNP analysis of an Antarctic annelid, *A. trissophyllus,* using SNPs generated by double digest restriction-site associated DNA sequencing (ddRADseq) to resolve genetic lineages and examine population structure and connectivity in samples spanning much of the species' distributional range. Phylogenetic analyses using traditional barcode markers (COI, 16S and 18S) are also compared. SNP data supports at least two major genetic lineages found in phylogenetic analyses, though with some introgression between the two putative species.

At the population level, genetic structure in mitochondrial COI data was reflected in SNP genomic analyses for the putative species Agla 1, where individuals collected from South Georgia formed a distinct isolated genetic cluster. The remaining specimens from different collection sites presented intraspecific genetic clusters across overlapping sampling sites supporting a well-mixed population. When bathymetry is included, specimens of the putative species "Agla 1" collected below 1000m presented only one genetic cluster reflecting a potential structure by depth. In the putative species Agla 2, genetic structure in COI was not reflected in genomic analyses, the latter revealing a single panmictic population, though with poorer sampling coverage. This potential mito-nuclear discordance highlights the limitations of interpretations from single barcodes only. Results of this study give further insight into the diversity of Antarctic *Aglaophamus* species, and demonstrate the complex of factors that may shape distributional patterns in modern Southern Ocean populations.

Keywords: population genomics, ddRAD, biogeography, Single Nucleotide Polymorphisms, Antarctica, cryptic species

5.1 Introduction

The modern benthos of the Southern Ocean shelf ecosystem has survived periods of extreme disturbance *in situ* throughout Pliocene–Pleistocene glacial cycles (5Ma-10Ka) despite the fact that much of the available benthic habitat would have been destroyed by grounded ice during glacial maxima (Convey et al., 2009). It is hypothesised that benthic fauna would have survived these periods either in ice free refugia on the shelf, waters around sub-Antarctic islands, or through migration to the deep sea (Thatje et al., 2005). Repeated cycles of habitat destruction and reproductive isolation of populations in different refugia may have acted as a "biodiversity pump" in the Southern Ocean (Clarke & Crame, 1992) driving vicariant events and allopatric speciation, and has been proposed as a driver of a number of radiations in Antarctic benthic invertebrates (see Wilson et al., 2009).

These processes have also been linked to a high prevalence of cryptic diversity in the Southern Ocean, with numerous molecular investigations into widespread Antarctic species uncovering previously unrecognised genetic structure and potential cryptic species across a range of taxonomic groups in recent decades, including annelids (Bogantes et al., 2020; Brasier et al., 2016; Leiva et al., 2018, 2022; Neal et al., 2014; Schüller, 2011), amphipods (Baird et al., 2011; Havermans et al., 2011), isopods (Held, 2003; Held & Wägele, 2005; Leese & Held, 2008; Raupach & Wägele, 2006) ostracods (Brandão et al., 2010), pycnogonids (Dietz et al., 2014; Krabbe et al., 2010), crinoids (Hemery et al., 2012; Wilson et al., 2007), ophiuroids (Galaska et al., 2017a; Hunter & Halanych, 2010), bivalves (Linse et al., 2007), cephalopods (Allcock et al., 2011), gastropods (Maroni et al., 2022; Wilson et al., 2009), sponges (Leiva et al., 2022), and nemerteans (Leiva et al., 2022; Taboada et al., 2018b; Thornhill et al., 2008). These results suggest that our current understanding of Antarctic marine biodiversity may be considerably underestimated. Signatures in genetic structure have also been used to infer how benthic fauna persisted through past glacial cycles (e.g. shelf vs deep sea refugia) and may give insight into resilience against future environmental change (Allcock & Strugnell, 2012; Lau et al., 2020).

Most population genetic and phylogeographic studies of Southern Ocean taxa to date have used single genetic markers. While these single-gene studies have created significant inroads into our understanding of the Southern Ocean diversity and evolution (Lau et al., 2020; Riesgo et al., 2015) interpretations from single genes are limited to the coalescent history of those specific genes. Importantly, these interpretations may differ from other loci in terms of mutation rates and genetic drift and may not necessarily represent true population and phylogenetic history (Jenkins et al., 2018).

The development of high-throughput techniques, in particular restriction site-associated DNA sequencing (RADseq) methods, are revolutionising the field in non-model organisms due to their ability to rapidly generate hundreds and thousands of Single Nucleotide Polymorphisms (SNPs) – unlinked neutral loci sequenced randomly across the genome (Andrews et al., 2016). This multi-locus method allows for high-resolution population genomic and phylogeographic analyses and can overcome the limitations of using single genes. While the field of RADseq-based population genomics in the Southern Ocean remains nascent, a small but growing number of investigations have been conducted in recent years, with studies of krill (Deagle et al., 2015), pycnogonid (Collins et al., 2018), ophiuroid (Galaska et al., 2017a, 2017b; Lau et al., 2023a) , gastropod (Moles et al., 2021), cephalopod (Lau et al., 2023b), poriferan (Leiva et al., 2019, 2022), and nemertean (Leiva et al., 2022) species. However, studies at genomic resolutions remain lacking for many key taxonomic groups in the Southern Ocean, such as annelids, which comprise a dominant component of Antarctic benthic fauna in terms of species richness (Clarke & Johnston, 2003) and both abundance and biomass (Gambi et al., 1997; Hilbig et al., 2006; Piepenburg et al., 2002; Sañé et al., 2012).

The annelid family Nephtyidae are burrowing worms found in sedimented habitats worldwide across all depths (Ravara et al., 2010, 2017), filling ecological roles as both important intermediate predators of benthic macrofauna and as prey items for larger megafauna such as crustaceans and fish (Schubert & Reise, 1986). *Aglaophamus trissophyllus* (Grube, 1877) is a common, charismatic Antarctic nephtyid species found throughout the Southern Ocean (SCAR Antarctic Biodiversity Portal, 2022), known to have planktotrophic larvae (Heimeier et al., 2010), and frequently collected in benthic biodiversity surveys (Angulo-Preckler et al., 2018; Brasier et al., 2016; Cummings et al., 2018; Drennan et al., 2021; Hilbig et al., 2006; Knox & Cameron, 1998; Parapar et al., 2011). *Aglaophamus trissophyllus* is easily recognizable due to its large size, up to 20 cm long (Knox & Cameron, 1998), and often striking and variable iridescent colours. However, the taxonomic history and status of this species has seen considerable confusion over the past century (Knox & Cameron, 1998), while recent molecular work using 16S and COI barcodes has begun to find evidence of cryptic diversity within the currently recognized species (Brasier et al., 2016), finding up to five potentially cryptic lineages using COI but only two lineages using 16S in specimens morphologically identified as *A. trissophyllus*. A lack of certainty regarding true diversity patterns makes it challenging to understand the phylogeographic history of the species as well as monitor future change, particularly in the context of substantial ice-loss and ocean warming projected for parts of the Southern Ocean in all future climate scenarios (Naughten et al., 2023).

As far as we are aware, this study conducts the first RADseq investigation of an annelid species in the Southern Ocean, the nephtyid *Aglaophamus trissophyllus,* using double-digest restriction-site associated DNA sequencing (ddRADseq). Traditional barcode markers (COI, 16S and 18S) are also

sequenced and compared with ddRADseq derived SNP genomic data. The aims of this study are: (i) to resolve the number of genetic lineages within Antarctic specimens identified as *Aglaophamus trissophyllus*, and (ii) to describe patterns of diversity and connectivity within populations. Collection sites span much of the species' distributional range, and from depths of 65-1580m. Sites include the Ross Sea and South Georgia, regions currently protected by established MPAs in addition to the Weddell Sea, South Orkneys and West Antarctic Peninsula, for which MPAs have been proposed but not yet ratified. Assessments of population connectivity can give insight into population resilience and extinction risk (Taboada et al., 2018a), and will be a key tool in assessing the effectiveness and design of current and future Antarctic MPAs (Leiva et al., 2022).

5.2 Materials and methods

5.2.1 Sample collection

A total of 141 specimens identified as *Aglaophamus trissophyllus* or *Aglaophamus* spp. were sourced from 10 international Antarctic expeditions that took place between 2004-2018 covering a wide range of sampling localities across the Southern Ocean, including off South Georgia, Southern Thule, South Orkney Islands, Weddell Sea (Eastern and Western), South Shetland Islands/Bransfield Strait (King George Island, Elephant Island, Livingston Island), the West Antarctic Peninsula, Amundsen Sea, Ross Sea, and Balleny Islands (Table 5.1; Figure 5.1).

Table 5.1 List of Antarctic expeditions, sampling regions, and collection sites from which collected material was used in this study. Depth range of samples and sample number per expedition collection is also given.

Expedition	Vessel	Year	Region	Collection sites	Depth range	*n*
BioRoss (TAN0402)	R/V Tangaroa	2004	Ross Sea, East Antarctica	Hallett Peninsula (HP), Balleny Islands (BI)	65-1382m	42
BIOPEARL I (JR144)	RRS James Clark Ross	2006	Scotia Arc	South Georgia (SG), Southern Thule (ST), Elephant Island (EI), King George Island (KG), Livingston Island (LI)	111-1473m	28
BIOPEARL II (JR179)	RRS James Clark Ross	2008	Amundsen Sea	Pine Island Bay (PI)	496-508m	7
JR275	RRS James Clark Ross	2012	Eastern Weddell Sea	off Brunt Ice shelf (BR), Filchner Trough (FT)	390-1580m	13
LARISSA (NBP 12-03)	R/V Nathaniel B. Palmer	2012	Western Weddell Sea	Former Larsen A ice shelf (LA)	431-686m	4
JR308	RRS James Clark Ross	2015	West Antarctic Peninsula	Adelaide Island (AI)	399-528m	19
FjordEco I (LMG 15-10)	R/V Laurence M. Gould	2015	West Antarctic Peninsula	NW Peninsula Fjords (WF)	534-557m	2
SoAntEco (JR15005a)	RRS James Clark Ross	2016	Scotia Arc	South Orkney Islands (SO)	617-1003m	6
FjordEco II (NBP-16-03)	R/V Nathaniel B. Palmer	2014	West Antarctic Peninsula	NW Peninsula Fjords (WF)	678m	1
Larsen C Benthos (JR17003a)	RRS James Clark Ross	2018	Western Weddell Sea	Prince Gustav Channel (PG)	483-1271m	19

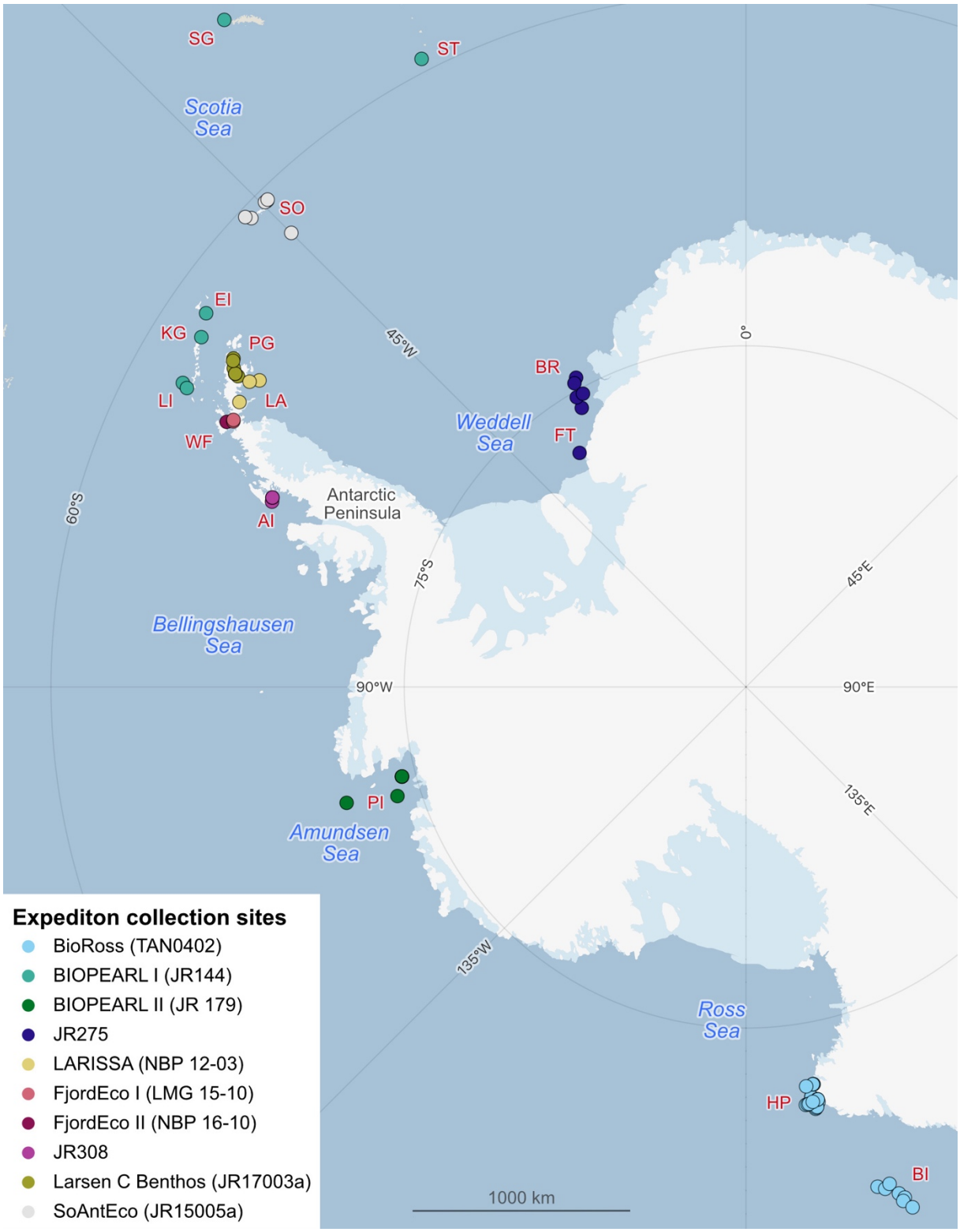

Figure 5.1 Map of Antarctic expeditions and respective collection sites for specimens used in this study. A two letter code is given for collection sites as follows: SG – South Georgia; ST – Southern Thule; SO – South Orkney Islands; EI – Elephant Island; KG – King George Island; LI – Livingston Island; PG – Prince Gustav Channel; LA – Former Larsen A/B Ice Shelf; BR – off Brunt Ice Shelf; FT – Filchner Trough; WF – NW Antarctic Peninsula Fjords; AI – Adelaide Island; PI – Pine Island Bay; HP – Hallett Peninsula; BI – Balleny Islands. Map made in Quantarctica 3.0.

These sites included a depth range of 65-1580m, and a maximum straight-line distance between furthest sampling sites (South Georgia and Balleny Islands) of ~ 6,500km. A range of sampling gears were used in the collection of these specimens, primarily Agassiz Trawl (AGT) and Epibenthic sledge (EBS) (Appendix D Table D.1). In most cases, specimens were preserved in an EtOH solution, either in individual vials or bulk fixed with other specimens; specimens collected on LARISSA and FjordEco expeditions were frozen dry at sea at -80°C in vials or whirl-pak bags and stored at -80°C at the University of Hawaii Oceanography Department. Tissue subsamples of frozen specimens were subsequently taken and preserved in RNA-later and sent to the NHM London for this study. The majority of other expedition material is held at the NHM, except for BioRoss samples, which were sent on loan from the National Institute of Water and Atmospheric Research (NIWA). Specimens from BIOPEARL expeditions include a number of those previously sequenced in Brasier et al., (2016), but that were re-extracted and barcoded for the purposes of ddRADseq (see 'record number' column in Appendix D Table D.1).

5.2.2 DNA extraction and barcoding

All preserved specimens were imaged using a Canon EOS600D camera prior to DNA extraction, and, depending on specimen size, varying numbers of parapodia were dissected for DNA extraction to make up ~0.5cm^3 of tissue. In smaller individuals (< 5 cm), fewer parapodia were used to preserve specimen integrity. DNA was extracted from all samples using DNeasy Blood and Tissue Kit (Qiagen) with two minor modifications to the manufacture's protocol – lysis time was extended to an overnight incubation, and the final elution step was performed twice with a smaller final elution volume to increase DNA concentration (37.5 µl of elution buffer twice for a total of 75µl; for small or deteriorated individuals, 25 µl twice for total of 50µl). DNA quality and quantity was measured using Nanodrop ND-8000 spectrophotometer (Thermo Scientific) and Qubit dsDNA HS assay (Life Technologies).

A fragment of the mitochondrial cytochrome c oxidase subunit I (COI) barcode gene (~650bp) was amplified for each extraction for initial population genetic and phylogenetic analyses. As COI has variable success in annelids (e.g. Brasier et al., 2016; Capa et al., 2011; Radashevsky et al., 2016), a second mitochondrial barcode, a fragment of the 16S rDNA gene (~450bp), was sequenced for specimens for which COI was unsuccessful, and for representative individuals COI clades and haplogroups. 16S has been used successfully as an alternate barcode to COI in Antarctic *Aglaophamus* spp. (Brasier et al., 2016).

Following initial phylogenetic analyses, representatives of distinct clades identified by the two molecular barcodes described above were additionally sequenced for the nuclear 18S rDNA gene (~1800bp) to improve phylogenetic support. 18S is used widely in studies aiming to resolve deeper annelid phylogenetic relationships (e.g. Colgan et al., 2006; Rousset et al., 2007), and is most useful at the level within recognised families (Halanych & Janosik, 2006).

Molecular barcodes were obtained by individual PCR reactions using 0.5 µl of each primer, 1 µl template DNA and 10.5 µl Red *Taq* DNA Polymerase Master Mix (VWR). Primer details are listed in (Appendix D Table D.3). DNA extractions with concentrations >100 ng/µl and >1000ng/µl were diluted 1:10 or 1:100, respectively. PCR amplification profiles were as follows: COI – initial denaturation of 5 mins at 95°C followed by 35 cycles of 30s at 94°C, 30s at 48°C, 1 min at 72 °C, with a final extension of 10 min at 72 °C; 16S – initial denaturation of 5 mins at 94°C followed by 35 cycles of 30s at 94°C, 30s at 57°C, 1 min at 68 °C, with a final extension of 7 min at 68 °C. 18S – initial denaturation of 5 mins at 95°C followed by 30 cycles of 30s at 95°C, 1m at 59°C, 2 min at 72 °C, with a final extension of 2 min at 72 °C. PCR products were purified and sequenced using the primers mentioned above (forward and reverse) at the Natural History Museum London Sequencing Facilities using a Millipore Multiscreen 96-well PCR Purification System and ABI 3730XL DNA Analyser (Applied Biosystems).

5.2.3 Phylogenetic and haplotype network analysis

DNA sequences were processed and aligned in Geneious 10.09.01 (https://www.geneious.com), with contigs assembled from overlapping forward and reverse sequence fragments, with ambiguous base calls manually corrected. All sequences were checked against the NCBI GenBank database using the blastn algorithm (Johnson et al., 2008) via the Geneious plugin with default settings to confirm identity. Genbank sequences of *Aglaophamus* spp., and additional nephtyid genera and non-nephtyid outgroups were also included in phylogenetic analyses (Appendix D Table D.2) following (Ravara et al., 2010).

COI sequences were aligned using MUSCLE (Edgar, 2004) 16S and 18S were aligned using MAFFT *v7.450* (Kazutaka Katoh & Standley, 2013), both programs implemented via Geneious plug-ins using default settings. COI alignments were translated into amino acids to check for stop codons to avoid the inclusion of pseudogenes. Alignments were prepared for single gene phylogenetic analyses, and a combined analysis of all COI, 16S and 18S. Only individuals with at least two genes were included in combined analyses. The most suitable substitution model for each gene was chosen using Modeltest-NG (Darriba et al., 2020) and Aikake and Bayesian information criteria (AIC and BIC, respectively), and adapted for the Bayesian Inference analysis. For the COI dataset, the most suitable model for each

codon position was chosen. Substitution models were as follows: combined, GTR+I+G; 16S, GTR+G; 18S, GTR+I+G, COI, GTR+G, GTR+I, GTR+G per three codon positions. Bayesian phylogenetic analyses were performed in triplicate for each gene dataset and for the concatenated dataset using MrBayes 3.2.7 (Ronquist et al., 2012) for 10,000,000 generations under default settings, with 2,500,000 discarded as burnin. Trees were visualised using FigTree v.1.4.4 (Rambaut, 2018). COI and 16S alignments were further trimmed, excluding shorter sequences or sequences with ambiguous bases to build haplotype networks for putative species using the software PopART v 1.7 (Leigh & Bryant, 2015) with the TCS network algorithm (Clement et al., 2002). Genetic distances within and between putative species was calculated for these alignments using the p-distance model with default settings in MEGA v11 (Tamura et al., 2021).

Additional barcode sequence data Appendix D Table D.2) was downloaded from NCBI GenBank (https://www.ncbi.nlm.nih.gov/genbank/) via the Geneious NCBI module. Sequences included additional Antarctic *Aglaophamus* cf. *trissophyllus* specimens, other *Aglaophamus* species, wider nephtyid genera, and outgroups from families Phyllodocidae, Amphinomidae, Nereididae, Glyceridae and Lacydoniidae following (Ravara et al., 2010). In-house sequences collected as part of the ABYSSLINE project at the NHM Deep-Sea Lab from four unidentified nephtyids from the abyssal Clarion-Clipperton Zone (CCZ), central Pacific, were also included in phylogenetic analyses (unpublished data, Appendix D Table D.2).

5.2.4 ddRADseq library preparation and sequencing

A total of 130 individuals exceeded Qubit DNA concentrations of 5 ng/µl and were included in the ddRAD library preparation. Library preparation was performed following Taboada et al. (2022), based on Peterson et al. (2012) with modifications from Combosch et al. (2017), and was carried out at the National Museum of Natural Sciences of Madrid (MNCN-CSIC). A total of 500 ng of double-stranded genomic DNA per sample was digested for 6h at 37°C using high-fidelity restriction enzymes BfaI and EcoRI (New England Biolabs). Digested fragments were cleaned using Agencourt AMPure beads (1.5X volume ratio; Beckham Coulter) via manual pipetting. Cleaned fragments were quantified using a Qubit dsDNA HS assay, and ligated to custom P1 and P2 adapters with sample-specific primer annealing sites and barcodes. Barcoded samples were pooled into libraries (max 12 individuals per library) and cleaned again using AMPure beads (1.5X volume ratio, manual pipetting), followed by size-selection (200-400bp range) using a BluePippin (Sage Science). Libraries were PCR-amplified with a unique set of Illumina index primers for library multiplexing using Phusion polymerase (Thermo Scientific). The amplification PCR profile was as follows: initial denaturation of 30s at 98°C followed by 12 cycles of 10s at 98°C, 30s at 65°C, 1.5 min at 72 °C, with a final extension of 10 min at 72 °C.

PCR products were cleaned once more using AMPure beads (1.5X volume ratio, manual pipetting), and quantified Qubit dsDNA HS assay, in addition to a quality check step using a Tapestation 2200 (Agilent Technologies). All libraries were pooled, normalising concentration to 25nM in a final volume of 40 µl. Libraries were pair-end sequenced (150bp) at Novogene Europe (Cambridge UK) on an Illumina Novaseq 6000 platform.

5.2.5 ddRADseq filtering and locus assembly

Quality assessment of sequenced libraries was performed using FASTQC v. 0.12.0 (Andrews, 2012). The *Stacks* pipeline v 2.64 (Catchen et al., 2013) was used to process each library for further analysis. Initial processing and quality filtering was carried out using *process-radtags,* where amplified and sequenced DNA fragments with both restriction enzyme cut sites (BfaI and EcoRI), known as RAD-tags, were demultiplexed. Low-quality reads, reads with uncalled bases, and reads without complete barcodes or restriction cut sites were removed using options *-c* and *-q*. Option *-r* was used to recover minimally diverged barcodes and RAD-tags, while the number of mismatches allowed in the adapter sequence was set to 2 using *--adapter_mm 2.* Option *-t* was used to trim the remaining reads to 145 bp based on FASTQC results. Individuals with number of reads below 600,000 following *process-radtags* filtering were excluded from further analyses to increase confidence in SNP calling.

Three putative species (also referred to as clades during the phylogenetic section of this chapter) were established using barcode data (see results 5.3.1). For population genomics analyses, to avoid confusion between phylogenetic clades and genomic clusters, Clade 1 is referred to as Agla 1 (*n*= 83), Clade 2 is referred to Agla 2 (*n*=38), Clade 3 is referred to Agla 3 (*n*=4), while Agla X corresponds to five individuals without successful barcode sequencing, but that exceeded the >5ng/µl genomic DNA threshold and were included in library preparation but not in the bioinformatic analyses.

As a nephtyid reference genome is not currently available, ddRADseq loci were assembled *de novo* using the *denovo_map.pl* implemented in *Stacks* (see Rochette & Catchen, 2017). This pipeline was run successively testing different dataset combinations. Datasets were as follows: all specimens (Agla 1, Agla 2, Agla 3, & Agla X), Agla 1&2 combined, Agla 1 only, and Agla 2 only. For each dataset, the *Stacks populations* module was run using *–write_single_SNP* to retain only the first SNP from each RAD-tag, thus reducing linkage disequilibrium among loci. In order to maximise number of loci retained while reducing missing data, the *populations* option *--min-samples-per-pop* (*-r*) was used to define the minimum percentage of individuals a locus is present in, in order to be retained for further analyses for each dataset: All specimens, loci present in at least 60% of individuals (*r*=0.6); Agla 1&2 combined, 65% (*r*=0.65); Agla 1, 70% (*r*=0.7); Agla 2, 75% (*r*=0.75). Resulting datasets and distribution of missing data were visualised using the *Matrix Condenser* online interface (de Medeiros & Farrell,

2018). Individuals with more than 60% missing data were removed from each dataset for subsequent analyses. Further filtering was performed using *populations*; the option *–min-maf 0.05* was implemented to retain loci with a minimum allele frequency of >0.05, and *–hwe* to calculate heterozygosity (H_o). Loci with an excess of heterozygosity (H_o > 0.05) were removed from further analyses. Under the assumption of putative species, additional filtering steps were taken on Agla 1 only and Agla 2 only datasets. SNPs deviating from Hardy Weinberg equilibrium (*p*-value = 0.05, also identified using *--hwe*) were removed when present in at least two populations (by geographic region). The resulting filtered dataset was further analysed with *ARLEQUIN* v. 3.5.2 (Excoffier & Lischer, 2010) and *BAYESCAN* v2.1 (Foll & Gaggiotti, 2008) to identify SNPs under selection. For *ARLEQUIN*, the settings used were "non-hierarchical island model" with 100,000 simulations, 1000 demes, and "allowed missing level per site" 0.05; obtained *p*-values for each locus were corrected to *q*-values using the R function *p.adjust* with the FDR method (R Core Team, 2023). *BAYESCAN* was run using 10,000 output iterations and 100 prior odds. In both analyses, loci with *q*-value < 0.05 were considered outliers. *BAYESCAN* identified 0 loci under selection in either dataset; *ARLEQUIN* identified 111 SNPs for Agla 1, and 160 SNPs for Agla 2, which were removed from each dataset to generate a neutral set of SNPs.

The final datasets included 2,099 SNPs for all species (Agla 1, Agla 2, Agla 3, & Agla X) (*n*=113); 1,225 SNPs for Agla 1&2 combined (*n*=93); 907 SNPs for Agla 1 (*n*= 73); 1,111 SNPs for Agla 2 (*n*=28).

5.2.6 Population genomic analyses

Overall measures of genetic diversity, including nucleotide diversity, expected and observed heterozygosity, and inbreeding coefficient and private alleles were calculated using the *populations* option *–fstats* implemented in the *Stacks* program.

Genetic differentiation between species and between sample locations within species was broadly measured using pairwise F_{st} values, calculated in *GenoDive* v3.06 (Meirmans, 2020) with 10,000 permutations, and *Post hoc* Bonferroni correction to significance values as recommended by *Genodive* to account for multiple pairwise comparisons. Genetic structure and differentiation between and within species were also assessed via two clustering methods, discriminant analysis of principal components (DAPC) (Jombart et al., 2010) using the package *adegenet* v2.1.10 (Jombart & Ahmed, 2011; Jombart & Bateman, 2008) in *R* v4.2.3 (R Core Team, 2023), and admixture analysis using *ADMIXTURE* v1.3.0 (Alexander et al., 2009; Alexander & Lange, 2011), with results visualised in *R* using *pophelper* v2.3.1 (Francis, 2017).

More specifically these analyses were used to assess the boundaries between all specimens and whether genetically distinct populations existed within Agla 1 and Agla 2. For DAPC, the function *snapclust* with genetic clustering mode *snapclust.choose.k* was used to assess genetic structure via the Aikake Information Criterion (AIC) and using the k-means algorithm, with a maximum *K* (number of genetic clusters) of 10 and number of iterations of 100 (n.start.kmeans=100), with the optimal number of genetic clusters corresponding to the lowest output value of AIC. The optimal number of principal components (PCs) to retain were chosen by grouping the samples by species or area for within species and using the cross-validation function *xvalDapc* with a training set of 0.9 (90% of the data) and 100 replicates, choosing the optimal number of PCs as those achieving the lowest mean square error (MSE). Final DAPC analyses were run implementing optimal clusters and PCs using the functions *snapclust* and *dapc,* respectively, with the function *assignplot* used to plot the probability that an individual would be assigned to different clusters, and *scatter.dapc* to visualise DAPC results as scatterplots. In ADMIXTURE*,* the optimal number of genetic clusters (*K*) was assessed using the software's cross-validation procedure (ten-fold, *--cv=10*) for a maximum of 10 clusters (*for K in echo $(seq 10)*) and 2000 bootstraps (*-B2000*), with the optimal number of genetic clusters chosen as the value of *K* with the lowest cross-validation error. ADMIXTURE analyses were run with the optimal number of *K* values using the function *admixture* with results assessed and visualised in R.

A further analysis to assess recent shared ancestry between species and populations at high resolutions was carried out using the software *fineRADstructure* v 0.3.2r109 (Malinsky et al., 2018). As *fineRADstructure* requires ddRAD haplotype linkage information, *populations* module in Stacks was run for each dataset with the output option *–radpainter,* and without the option *-write-single-SNPS*, which allows for linked SNPs to be included, increasing the number of SNPs for all specimens to 21267; Agla 1&2 to 19439; Agla 1 to 10718; Agla 2 to 176549. Each dataset was run in *fineRADstructure* using default settings as per the tutorial (http://cichlid.gurdon.cam.ac.uk/fineRADstructure.html), with results visualised in R using both the Finestructure R library and *fineRADstructurePlot.R* script included in the *fineRADstructure* package.

5.2.7 Data handling

All sequence and genomic data, in addition to detailed specimen collection and occurrence data, are available from the following supporting dataset:

Drennan (2024) Data supporting University of Southampton Doctoral Thesis entitled: Patterns of diversity, connectivity, and evolution in southern ocean and deep-sea annelids. University of Southampton doi:10.5258/SOTON/D2958 [Dataset]

Results of this chapter are planned for publication. Sequence and genomic data will be made publicly available on Genbank following publication of results. Specimens and DNA vouchers will be archived in the Natural History Museum London and NIWA collections.

5.3 Results

5.3.1 Phylogenetic analysis of Antarctic *Aglaophamus* spp. using barcodes

In total, 94 COI, 73 16S, and 15 18S sequences were successfully retrieved from 141 new DNA extractions, in addition to two COI and four 16S sequences from (Brasier et al., 2016), with 133 individuals having at least one genetic marker (Table 5.2). Of the remaining specimens, two extractions were found to be contaminated and removed from remaining analyses, while six were unsuccessful in barcoding prior to ddRAD library building but were still included in library preparation.

Table 5.2 Table of specimens used in this study, including phylogenetic clade assignment, collection information, barcoding and ddRAD success. Clade, region, collection site, depth, and extraction number are used to create a unique molecular specimen ID, with four and two letter codes for Region and collection site, respectively, and S, M, and D for 0-499m, 500-999m, and >1000m depth bins, respectively. Specimens with contaminated extractions, or no success in either barcode or ddRAD analyses are excluded. For table of additional specimen and collection data, see (Appendix D Table D.1)

Clade	Region	Collection site	latitude	longitude	depth (m)	Extraction number	Molecular specimen ID	COI	16S	18S	ddRAD	ddRAD >600k reads
1	East Antarctica	Balleny Islands	-67.2658	164.5220	212	RD313	Agla1_EAnt_BI_S_RD313		yes		yes	yes
1	East Antarctica	Balleny Islands	-66.9137	163.2247	85	RD314	Agla1_EAnt_BI_S_RD314	yes			yes	yes
1	East Antarctica	Balleny Islands	-66.1802	162.2795	400	RD315	Agla1_EAnt_BI_S_RD315	yes	yes		yes	yes
1	East Antarctica	Balleny Islands	-67.4178	163.9155	230	RD349	Agla1_EAnt_BI_S_RD349	yes			yes	yes
1	East Antarctica	Balleny Islands	-66.9137	163.2247	85	RD410	Agla1_EAnt_BI_S_RD410	yes			yes	yes
1	East Antarctica	Balleny Islands	-66.9137	163.2247	85	RD411	Agla1_EAnt_BI_S_RD411	yes			yes	
1	East Antarctica	Balleny Islands	-66.9137	163.2247	85	RD412	Agla1_EAnt_BI_S_RD412	yes			yes	yes
1	Eastern Weddell Sea	off Brunt Ice Shelf	-74.6741	-29.4246	587	RD316	Agla1_EWed_BR_M_RD316	yes	yes		yes	yes
1	Eastern Weddell Sea	off Brunt Ice Shelf	-74.6741	-29.4246	587	RD317	Agla1_EWed_BR_M_RD317	yes	yes		yes	yes
1	Eastern Weddell Sea	off Brunt Ice Shelf	-74.6741	-29.4246	587	RD318	Agla1_EWed_BR_M_RD318	yes			yes	yes
1	Ross Sea	Hallett Peninsula	-71.4875	171.8623	564	RD309	Agla1_Ross_HP_M_RD309	yes			yes	yes
1	Ross Sea	Hallett Peninsula	-71.7995	170.9487	168	RD295	Agla1_Ross_HP_S_RD295	yes			yes	yes
1	Ross Sea	Hallett Peninsula	-71.8010	170.9413	151	RD296	Agla1_Ross_HP_S_RD296	yes			yes	yes
1	Ross Sea	Hallett Peninsula	-72.3153	170.3610	130	RD298	Agla1_Ross_HP_S_RD298	yes	yes		yes	yes
1	Ross Sea	Hallett Peninsula	-72.3248	170.4277	206	RD299	Agla1_Ross_HP_S_RD299	yes			yes	yes
1	Ross Sea	Hallett Peninsula	-72.3217	170.4787	303	RD300	Agla1_Ross_HP_S_RD300	yes			yes	yes
1	Ross Sea	Hallett Peninsula	-72.2768	171.4490	414	RD301	Agla1_Ross_HP_S_RD301	yes	yes		yes	yes
1	Ross Sea	Hallett Peninsula	-71.5300	170.1110	220	RD302	Agla1_Ross_HP_S_RD302	yes			yes	yes
1	Ross Sea	Hallett Peninsula	-71.2575	170.6347	470	RD303	Agla1_Ross_HP_S_RD303	yes			yes	yes
1	Ross Sea	Hallett Peninsula	-71.6477	170.1802	162	RD304	Agla1_Ross_HP_S_RD304	yes		yes	yes	yes
1	Ross Sea	Hallett Peninsula	-71.6447	170.2188	249	RD305	Agla1_Ross_HP_S_RD305	yes			yes	
1	Ross Sea	Hallett Peninsula	-71.6447	170.2188	249	RD306	Agla1_Ross_HP_S_RD306	yes	yes	yes	yes	yes
1	Ross Sea	Hallett Peninsula	-71.6417	170.1525	65	RD307	Agla1_Ross_HP_S_RD307	yes			yes	yes

Clade	Region	Collection site	latitude	longitude	depth (m)	Extraction number	Molecular specimen ID	COI	16S	18S	ddRAD	ddRAD >600k reads
1	Ross Sea	Hallett Peninsula	-71.6417	170.1525	65	RD308	Agla1_Ross_HP_S_RD308	yes			yes	yes
1	Ross Sea	Hallett Peninsula	-71.5005	171.6070	480	RD310	Agla1_Ross_HP_S_RD310	yes	yes		yes	yes
1	Ross Sea	Hallett Peninsula	-71.5120	171.4252	390	RD311	Agla1_Ross_HP_S_RD311	yes			yes	yes
1	Ross Sea	Hallett Peninsula	-71.5120	171.4252	390	RD312	Agla1_Ross_HP_S_RD312	yes			yes	yes
1	Ross Sea	Hallett Peninsula	-71.7995	170.9487	168	RD399	Agla1_Ross_HP_S_RD399	yes	yes		yes	yes
1	Ross Sea	Hallett Peninsula	-71.8010	170.9413	151	RD400	Agla1_Ross_HP_S_RD400		yes		yes	yes
1	Ross Sea	Hallett Peninsula	-71.8010	170.9413	151	RD401	Agla1_Ross_HP_S_RD401	yes	yes		yes	yes
1	Ross Sea	Hallett Peninsula	-71.2575	170.6347	470	RD405	Agla1_Ross_HP_S_RD405	yes			yes	yes
1	Ross Sea	Hallett Peninsula	-71.6417	170.1525	65	RD406	Agla1_Ross_HP_S_RD406	yes			yes	yes
1	Ross Sea	Hallett Peninsula	-71.5120	171.4252	390	RD407	Agla1_Ross_HP_S_RD407	yes			yes	yes
1	Ross Sea	Hallett Peninsula	-71.5120	171.4252	390	RD408	Agla1_Ross_HP_S_RD408	yes			yes	yes
1	Ross Sea	Hallett Peninsula	-71.5120	171.4252	390	RD409	Agla1_Ross_HP_S_RD409	yes			yes	yes
1	Ross Sea	Hallett Peninsula	-71.2988	170.5405	312	RD413	Agla1_Ross_HP_S_RD413	yes			yes	yes
1	Ross Sea	Hallett Peninsula	-71.5748	170.8707	231	RD414	Agla1_Ross_HP_S_RD414	yes			yes	yes
1	Ross Sea	Hallett Peninsula	-71.3237	170.4090	85	RD441	Agla1_Ross_HP_S_RD441		yes			
1	Scotia Arc (Bransfield Strait)	Elephant Island	-61.5775	-55.2603	988	RD375	Agla1_Scot_EI_M_RD375	yes	KX867147		yes	yes
1	Scotia Arc (Bransfield Strait)	King George Island	-61.9663	-57.2437	111	RD341	Agla1_Scot_KG_S_RD341	yes	yes		yes	yes
1	Scotia Arc (Bransfield Strait)	Livingston Island	-62.5250	-61.8286	193	RD352	Agla1_Scot_LI_S_RD352	yes	yes	yes	yes	yes
1	Scotia Arc (Bransfield Strait)	Livingston Island	-62.5250	-61.8286	193	RD354	Agla1_Scot_LI_S_RD354	yes			yes	yes
1	Scotia Arc (Bransfield Strait)	Livingston Island	-62.5250	-61.8286	193	RD355	Agla1_Scot_LI_S_RD355		yes		yes	yes
1	Scotia Arc (Bransfield Strait)	Livingston Island	-62.5250	-61.8286	193	RD373	Agla1_Scot_LI_S_RD373	yes			yes	yes
1	Scotia Arc (Bransfield Strait)	Livingston Island	-62.5250	-61.8286	193	RD376	Agla1_Scot_LI_S_RD376	KX867391	yes		yes	yes
1	Scotia Arc (Bransfield Strait)	Livingston Island	-62.5250	-61.8286	193	RD378	Agla1_Scot_LI_S_RD378		yes		yes	yes
1	Scotia Arc (Bransfield Strait)	Livingston Island	-62.5250	-61.8286	193	RD379	Agla1_Scot_LI_S_RD379	yes	KX867140		yes	yes
1	Scotia Arc (Bransfield Strait)	Livingston Island	-62.5250	-61.8286	193	RD383	Agla1_Scot_LI_S_RD383	yes			yes	
1	Scotia Arc (Bransfield Strait)	Livingston Island	-62.5250	-61.8286	193	RD384	Agla1_Scot_LI_S_RD384	yes			yes	yes
1	Scotia Arc (Bransfield Strait)	Livingston Island	-62.5250	-61.8286	193	RD385	Agla1_Scot_LI_S_RD385	yes			yes	yes
1	Scotia Arc (Bransfield Strait)	Livingston Island	-62.5250	-61.8286	193	RD386	Agla1_Scot_LI_S_RD386		yes		yes	

Clade	Region	Collection site	latitude	longitude	depth (m)	Extraction number	Molecular specimen ID	COI	16S	18S	ddRAD	ddRAD >600k reads
1	Scotia Arc (Bransfield Strait)	Livingston Island	-62.5250	-61.8286	193	RD387	Agla1_Scot_LI_S_RD387	yes			yes	yes
1	Scotia Arc	South Orkney Islands	-60.4728	-44.7188	1003	RD332	Agla1_Scot_SO_D_RD332	yes		yes	yes	yes
1	Scotia Arc	South Orkney Islands	-60.5348	-46.4846	788	RD331	Agla1_Scot_SO_M_RD331	yes	yes		yes	yes
1	Scotia Arc	South Orkney Islands	-60.4964	-44.5238	617	RD333	Agla1_Scot_SO_M_RD333	yes			yes	yes
1	Scotia Arc	South Orkney Islands	-60.4760	-44.4196	787	RD335	Agla1_Scot_SO_M_RD335	yes	yes		yes	yes
1	Scotia Arc	South Orkney Islands	-62.1536	-44.9898	668	RD336	Agla1_Scot_SO_M_RD336	yes	yes		yes	yes
1	South Georgia	South Georgia	-53.7891	-37.9781	306	RD337	Agla1_SGeo_SG_S_RD337	yes			yes	yes
1	South Georgia	South Georgia	-53.7891	-37.9781	306	RD338	Agla1_SGeo_SG_S_RD338	yes			yes	yes
1	South Georgia	South Georgia	-53.7891	-37.9781	306	RD339	Agla1_SGeo_SG_S_RD339	yes	yes		yes	yes
1	South Georgia	South Georgia	-53.7891	-37.9781	306	RD340	Agla1_SGeo_SG_S_RD340	yes	yes		yes	yes
1	South Sandwich Islands	Southern Thule	-59.4705	-27.2762	266	RD372	Agla1_SSan_ST_S_RD372	yes	KX867143		yes	yes
1	West Antarctic Peninsula	NW Peninsula Fjiords	-64.8762	-62.4375	557	RD294	Agla1_WAPe_WF_M_RD294	yes		yes	yes	yes
1	West Antarctic Peninsula	NW Peninsula Fjiords	-64.8997	-62.5765	534	RD361	Agla1_WAPe_WF_M_RD361	yes	yes		yes	yes
1	West Antarctic Peninsula	NW Peninsula Fjiords	-64.8650	-62.4125	540	RD362	Agla1_WAPe_WF_M_RD362	yes			yes	
1	Western Weddell Sea	former Larsen A ice shelf	-64.6692	-58.3647	537	RD360	Agla1_WWed_LA_M_RD360	yes	yes		yes	yes
1	Western Weddell Sea	Prince Gustav Channel	-63.9798	-58.4314	1200	RD342	Agla1_WWed_PG_D_RD342	yes			yes	yes
1	Western Weddell Sea	Prince Gustav Channel	-63.9798	-58.4314	1200	RD343	Agla1_WWed_PG_D_RD343	yes			yes	yes
1	Western Weddell Sea	Prince Gustav Channel	-63.5755	-57.2954	1081	RD363	Agla1_WWed_PG_D_RD363	yes	yes	yes	yes	yes
1	Western Weddell Sea	Prince Gustav Channel	-63.5755	-57.2954	1081	RD364	Agla1_WWed_PG_D_RD364	yes	yes		yes	yes
1	Western Weddell Sea	Prince Gustav Channel	-63.5755	-57.2954	1081	RD365	Agla1_WWed_PG_D_RD365	yes	yes		yes	yes
1	Western Weddell Sea	Prince Gustav Channel	-63.5755	-57.2954	1081	RD366	Agla1_WWed_PG_D_RD366	yes	yes		yes	yes
1	Western Weddell Sea	Prince Gustav Channel	-63.5755	-57.2954	1081	RD367	Agla1_WWed_PG_D_RD367	yes	yes		yes	yes
1	Western Weddell Sea	Prince Gustav Channel	-63.9833	-58.4279	1271	RD368	Agla1_WWed_PG_D_RD368	yes	yes		yes	yes
1	Western Weddell Sea	Prince Gustav Channel	-64.1284	-58.5051	850	RD282	Agla1_WWed_PG_M_RD282	yes			yes	yes
1	Western Weddell Sea	Prince Gustav Channel	-63.8082	-58.0677	870	RD344	Agla1_WWed_PG_M_RD344	yes			yes	yes
1	Western Weddell Sea	Prince Gustav Channel	-63.6161	-57.50349	483	RD346	Agla1_WWed_PG_M_RD346	yes			yes	yes
1	Western Weddell Sea	Prince Gustav Channel	-63.8082	-58.0677	870	RD347	Agla1_WWed_PG_M_RD347	yes			yes	yes
1	Western Weddell Sea	Prince Gustav Channel	-63.6161	-57.50349	483	RD369	Agla1_WWed_PG_M_RD369	yes	yes		yes	

Clade	Region	Collection site	latitude	longitude	depth (m)	Extraction number	Molecular specimen ID	COI	16S	18S	ddRAD	ddRAD >600k reads
1	Western Weddell Sea	Prince Gustav Channel	-63.8082	-58.0677	870	RD370	Agla1_WWed_PG_M_RD370	yes	yes		yes	yes
1	Western Weddell Sea	Prince Gustav Channel	-63.6161	-57.50349	483	RD371	Agla1_WWed_PG_M_RD371	yes	yes	yes	yes	yes
1	Western Weddell Sea	Prince Gustav Channel	-63.8082	-58.0677	870	RD390	Agla1_WWed_PG_M_RD390	yes			yes	yes
1	Western Weddell Sea	Prince Gustav Channel	-63.8082	-58.0677	870	RD391	Agla1_WWed_PG_M_RD391	yes			yes	yes
1	Western Weddell Sea	Prince Gustav Channel	-63.8082	-58.0677	870	RD397	Agla1_WWed_PG_M_RD397	yes			yes	yes
2	Amundsen Sea	Pine Island Bay	-74.3982	-104.6334	508	RD288	Agla2_Amun_PI_M_RD288	yes	yes		yes	yes
2	Amundsen Sea	Pine Island Bay	-73.9782	-107.4159	547	RD444	Agla2_Amun_PI_M_RD444		yes		yes	yes
2	Amundsen Sea	Pine Island Bay	-71.7915	-106.2139	578	RD445	Agla2_Amun_PI_M_RD445		yes		yes	yes
2	Amundsen Sea	Pine Island Bay	-74.3985	-104.6322	504	RD446	Agla2_Amun_PI_M_RD446		yes		yes	yes
2	Amundsen Sea	Pine Island Bay	-74.3985	-104.6322	504	RD447	Agla2_Amun_PI_M_RD447		yes		yes	
2	Amundsen Sea	Pine Island Bay	-74.4023	-104.6151	496	RD453	Agla2_Amun_PI_S_RD453		yes		yes	
2	East Antarctica	Balleny Islands	-66.5583	163.0180	555	RD350	Agla2_EAnt_BI_M_RD350		yes		yes	yes
2	East Antarctica	Balleny Islands	-66.6752	162.7570	380	RD442	Agla2_EAnt_BI_S_RD442		yes		yes	yes
2	Eastern Weddell Sea	off Brunt Ice Shelf	-75.7612	-30.4372	429	RD319	Agla2_EWed_BR_S_RD319		yes		yes	
2	Eastern Weddell Sea	off Brunt Ice Shelf	-75.2495	-29.0271	390	RD320	Agla2_EWed_BR_S_RD320	yes	yes		yes	
2	Eastern Weddell Sea	off Brunt Ice Shelf	-75.2495	-29.0271	390	RD321	Agla2_EWed_BR_S_RD321	yes	yes	yes	yes	yes
2	Eastern Weddell Sea	off Brunt Ice Shelf	-75.2526	-30.2584	419	RD449	Agla2_EWed_BR_S_RD449		yes		yes	
2	Eastern Weddell Sea	Filchner Trough	-77.3569	-35.3606	650	RD452	Agla2_EWed_FT_M_RD452		yes			
2	Eastern Weddell Sea	X			X	RD450	Agla2_EWed_XX_X_RD450		yes		yes	
2	Eastern Weddell Sea	X			X	RD451	Agla2_EWed_XX_X_RD451		yes		yes	
2	Eastern Weddell Sea	X	-75.7433	-31.2462	583	RD454	Agla2_EWed_XX_X_RD454		yes			
2	Scotia Arc (Bransfield Strait)	Livingston Island	-62.2752	-61.5976	1473	RD351	Agla2_Scot_LI_D_RD351	yes			yes	yes
2	Scotia Arc (Bransfield Strait)	Livingston Island	-62.2752	-61.5976	1473	RD374	Agla2_Scot_LI_D_RD374		yes		yes	
2	Scotia Arc (Bransfield Strait)	Livingston Island	-62.2752	-61.5976	1473	RD377	Agla2_Scot_LI_D_RD377	KX867386	yes		yes	yes
2	Scotia Arc (Bransfield Strait)	Livingston Island	-62.5250	-61.8286	193	RD356	Agla2_Scot_LI_S_RD356		yes		yes	yes
2	Scotia Arc (Bransfield Strait)	Livingston Island	-62.5250	-61.8286	193	RD380	Agla2_Scot_LI_S_RD380	yes	KX867124	yes	yes	yes
2	Scotia Arc (Bransfield Strait)	Livingston Island	-62.5250	-61.8286	193	RD388	Agla2_Scot_LI_S_RD388		yes		yes	yes
2	Scotia Arc	South Orkney Islands	-60.3226	-46.7691	721	RD334	Agla2_Scot_SO_M_RD334	yes	yes	yes	yes	yes

Clade	Region	Collection site	latitude	longitude	depth (m)	Extraction number	Molecular specimen ID	COI	16S	18S	ddRAD	ddRAD >600k reads
2	West Antarctic Peninsula	Adelaide island	-67.7548	-68.1599	528	RD329	Agla2_WAPe_AI_M_RD329		yes		yes	yes
2	West Antarctic Peninsula	Adelaide island	-67.7548	-68.1599	528	RD330	Agla2_WAPe_AI_M_RD330	yes		yes	yes	yes
2	West Antarctic Peninsula	Adelaide island	-67.7537	-68.1736	399	RD322	Agla2_WAPe_AI_S_RD322	yes		yes	yes	
2	West Antarctic Peninsula	Adelaide island	-67.7537	-68.1736	399	RD323	Agla2_WAPe_AI_S_RD323	yes	yes		yes	
2	West Antarctic Peninsula	Adelaide island	-67.7537	-68.1736	399	RD324	Agla2_WAPe_AI_S_RD324		yes		yes	yes
2	West Antarctic Peninsula	Adelaide island	-67.7537	-68.1736	399	RD325	Agla2_WAPe_AI_S_RD325		yes		yes	yes
2	West Antarctic Peninsula	Adelaide island	-67.7537	-68.1736	399	RD326	Agla2_WAPe_AI_S_RD326	yes			yes	yes
2	West Antarctic Peninsula	Adelaide island	-67.8037	-68.6148	425	RD327	Agla2_WAPe_AI_S_RD327		yes			
2	West Antarctic Peninsula	Adelaide island	-67.8037	-68.6148	425	RD328	Agla2_WAPe_AI_S_RD328		yes			
2	West Antarctic Peninsula	Adelaide island	-67.7537	-68.1736	399	RD381	Agla2_WAPe_AI_S_RD381		yes		yes	yes
2	West Antarctic Peninsula	Adelaide island	-67.7537	-68.1736	399	RD382	Agla2_WAPe_AI_S_RD382	yes			yes	yes
2	West Antarctic Peninsula	Adelaide island	-67.7537	-68.1736	399	RD392	Agla2_WAPe_AI_S_RD392	yes			yes	yes
2	West Antarctic Peninsula	Adelaide island	-67.7537	-68.1736	399	RD393	Agla2_WAPe_AI_S_RD393		yes		yes	yes
2	West Antarctic Peninsula	Adelaide island	-67.7537	-68.1736	399	RD394	Agla2_WAPe_AI_S_RD394	yes			yes	yes
2	West Antarctic Peninsula	Adelaide island	-67.7537	-68.1736	399	RD395	Agla2_WAPe_AI_S_RD395	yes			yes	yes
2	West Antarctic Peninsula	Adelaide island	-67.7537	-68.1736	399	RD396	Agla2_WAPe_AI_S_RD396		yes		yes	yes
2	West Antarctic Peninsula	Adelaide island	-67.8037	-68.6148	425	RD398	Agla2_WAPe_AI_S_RD398		yes			
2	West Antarctic Peninsula	Adelaide island	-67.8037	-68.6148	425	RD457	Agla2_WAPe_AI_S_RD457		yes			
2	West Antarctic Peninsula	Adelaide island	-67.8037	-68.6148	425	RD458	Agla2_WAPe_AI_S_RD458		yes			
2	Western Weddell Sea	Former Larsen A ice shelf	-64.7383	-60.6033	686	RD358	Agla2_WWed_LA_M_RD358	yes		yes	yes	yes
2	Western Weddell Sea	Former Larsen A ice shelf	-64.6692	-58.3647	537	RD359	Agla2_WWed_LA_M_RD359	yes	yes		yes	yes
2	Western Weddell Sea	Prince Gustav Channel	-63.6161	-57.50349	483	RD345	Agla2_WWed_PG_M_RD345		yes		yes	yes
3	East Antarctica	Balleny Islands	-67.4362	165.2742	1382	RD348	Agla3_EAnt_BI_D_RD348		yes		yes	yes
3	Eastern Weddell Sea	off Brunt Ice Shelf	-74.4962	-28.7373	1580	RD456	Agla3_EWed_BR_D_RD456		yes		yes	yes
3	Eastern Weddell Sea	Filchner Trough	-77.3590	-35.3703	654	RD455	Agla3_EWed_FT_M_RD455		yes		yes	yes
3	Western Weddell Sea	former Larsen A ice shelf	-64.9939	-57.7412	431	RD357	Agla3_WWed_LA_S_RD357	yes	yes	yes	yes	yes
X	Ross Sea	Hallett Peninsula	-71.7987	170.9328	127	RD297	AglaX_Ross_HP_S_RD297				yes	yes
X	Ross Sea	Hallett Peninsula	-71.7987	170.9328	127	RD402	AglaX_Ross_HP_S_RD402				yes	yes

Clade	Region	Collection site	latitude	longitude	depth (m)	Extraction number	Molecular specimen ID	COI	16S	18S	ddRAD	ddRAD >600k reads
X	Ross Sea	Hallett Peninsula	-71.7987	170.9328	127	RD403	AglaX_Ross_HP_S_RD403				yes	
X	Ross Sea	Hallett Peninsula	-71.7987	170.9328	127	RD404	AglaX_Ross_HP_S_RD404				yes	yes
X	Scotia Arc (Bransfield Strait)	Livingston Island	-62.5250	-61.8286	193	RD353	AglaX_Scot_LI_S_RD353				yes	yes

Combined analysis of COI, 16S and 18S markers found the two major nephtyid genera, *Nephtys* and *Aglaophamus* to be monophyletic, with a high posterior probability support, as in a previous phylogenetic investigation of Nephtyidae (Ravara et al., 2010). Our phylogenetic analysis also recovered three fully supported lineages or clades for all Antarctic *Aglaophamus* specimens examined in this study in (Figure 5.2).

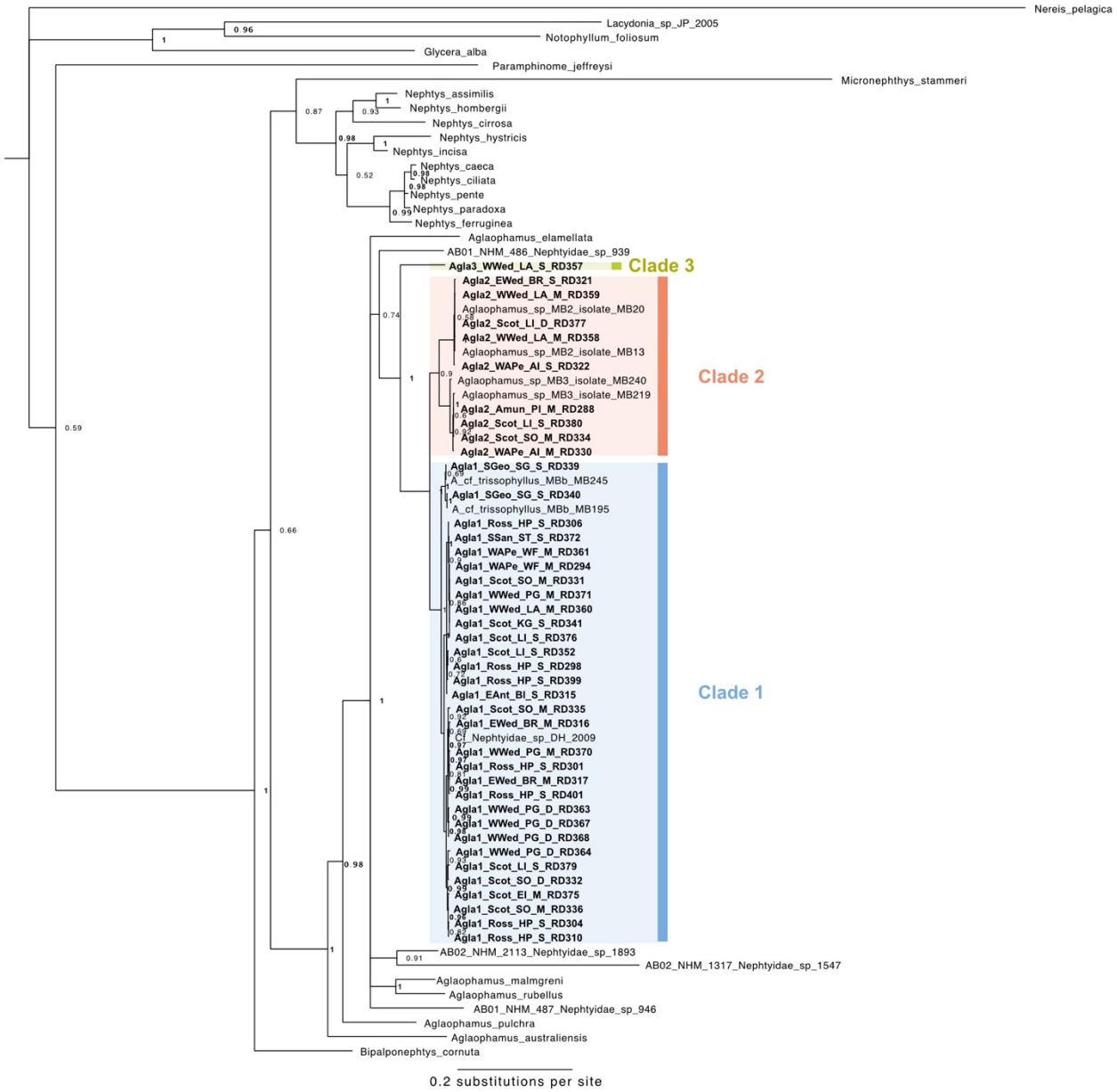

Figure 5.2 Phylogenetic tree of the annelid family Nephtyidae using combined Bayesian analysis of three markers, cytochrome oxidase subunit I (COI), 16S RNA and 18S RNA. Antarctic *Aglaophamus* spp. newly sequenced in this study are marked in bold. Clades within Antarctic *Aglaophamus* spp. are identified with boxes. Bayesian posterior probability values are given as support.

Clade 1 includes all individuals with typical *Aglaophamus trissophyllus* morphology (e.g. Knox & Cameron, 1998), large (up to 15cm long, >1cm wide) with pigmentation in preserved specimens ranging from no pigment to tan, pink, red-brown, purple, and blue-black, in addition to smaller individuals (< 5cm long, <0.5 cm wide) without pigmentation (Figure 5.3 a). Clades 2 and 3 consisted of smaller individuals (Clade 2: 3-8cm long, 0.25-0.5 cm wide; Clade 3: ~3cm long, 0.25 cm wide) and without strong pigmentation (Figure 5.3 b-c).

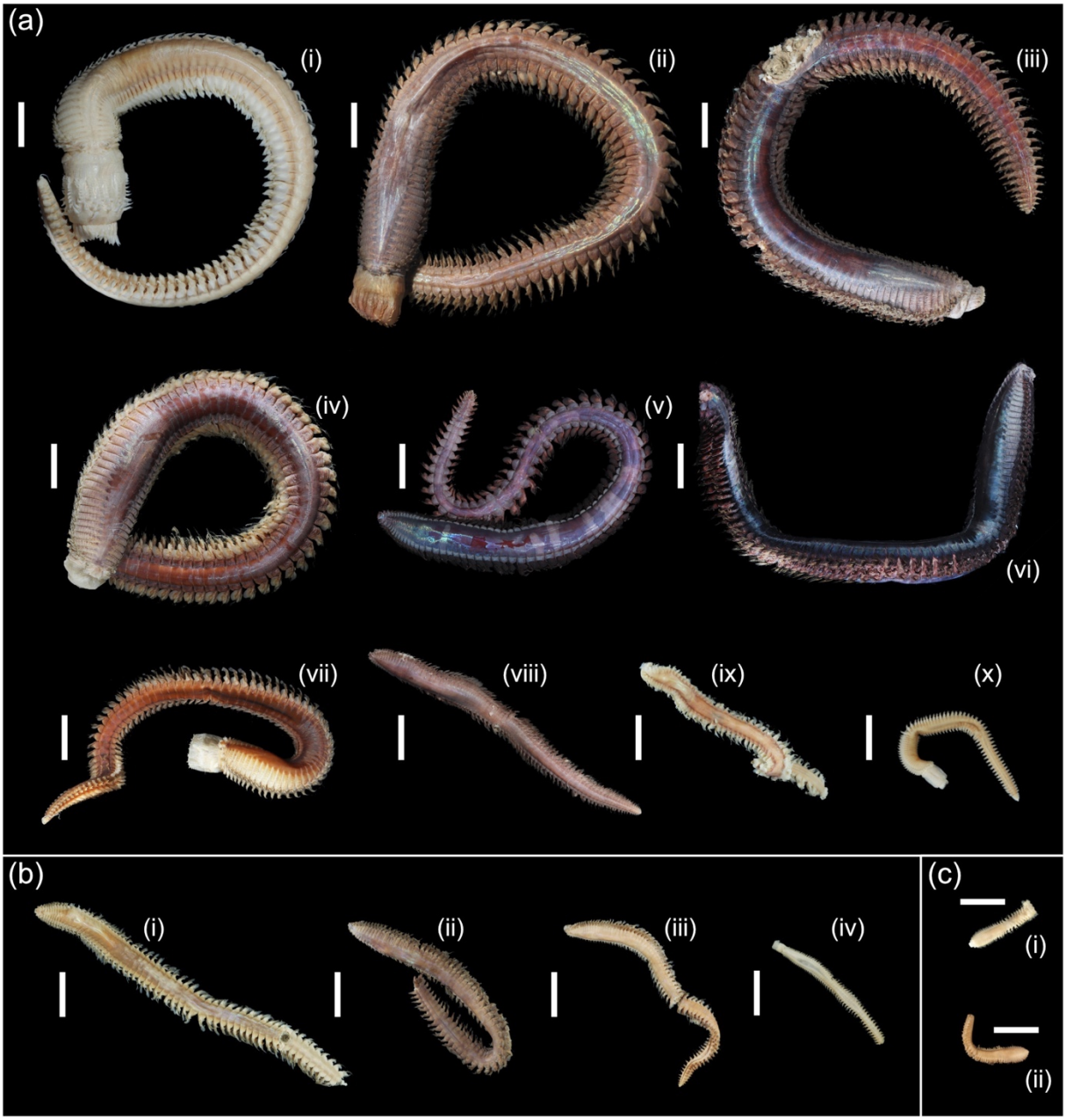

Figure 5.3 Plate showing variation in size and pigmentation amongst and between Antarctic genetic clades of Antarctic *Aglaophamus* spp. identified in the phylogenetic analyses. All scale bars = 1cm. (a) CLADE 1 (i) Agla1_Ross_HP_S_RD298, (ii) Agla1_WWed_PG_M_RD371, (iii) Agla1_Scot_KG_S_RD341, (iv) Agla1_Ross_HP_S_RD307, (v) Agla1_WWed_PG_D_RD363, (vi) Agla1_EAnt_BI_S_RD315, posterior missing, (vii)

Agla1_Ross_HP_S_RD305, (viii) Agla1_WWed_PG_D_RD343, (vx) Agla1_Scot_SO_D_RD332, posterior missing (x) Agla1_Ross_HP_S_RD399; (b) CLADE 2 (i) Agla2_Scot_SO_M_RD334, posterior missing, (ii) Agla2_WAPe_AI_S_RD322, posterior missing; (iii) Agla2_WAPe_AI_M_RD329 , (iv) Agla2_WWed_PG_M_RD345; (c) CLADE 3 (i) Agla3_EAnt_BI_D_RD348, anterior fragment, (ii) Agla3_EWed_FT_M_RD455, anterior fragment.

The highest number of barcode sequences were recovered for COI (*n*=94) however these were primarily obtained from samples associated with Clade 1, with a lower sequencing success rate amongst individuals in Clades 2 and 3. 16S presented better performance and was easily obtained and sequenced as an alternative marker for individuals without COI. A subsample of individuals successful in COI sequencing, representative of genetic structure in COI analyses, were also sequenced for 16S. Therefore, individuals included in separate 16S and COI phylogenetic analyses do not completely overlap, with only individuals with two or more markers included in combined analyses. The 16S analysis (Figure 5.4) returned the same clades as the concatenated analysis, with slightly different interclade configuration (Clade 3 is not sister to Clades 1 and 2 in this analysis, but with low support).

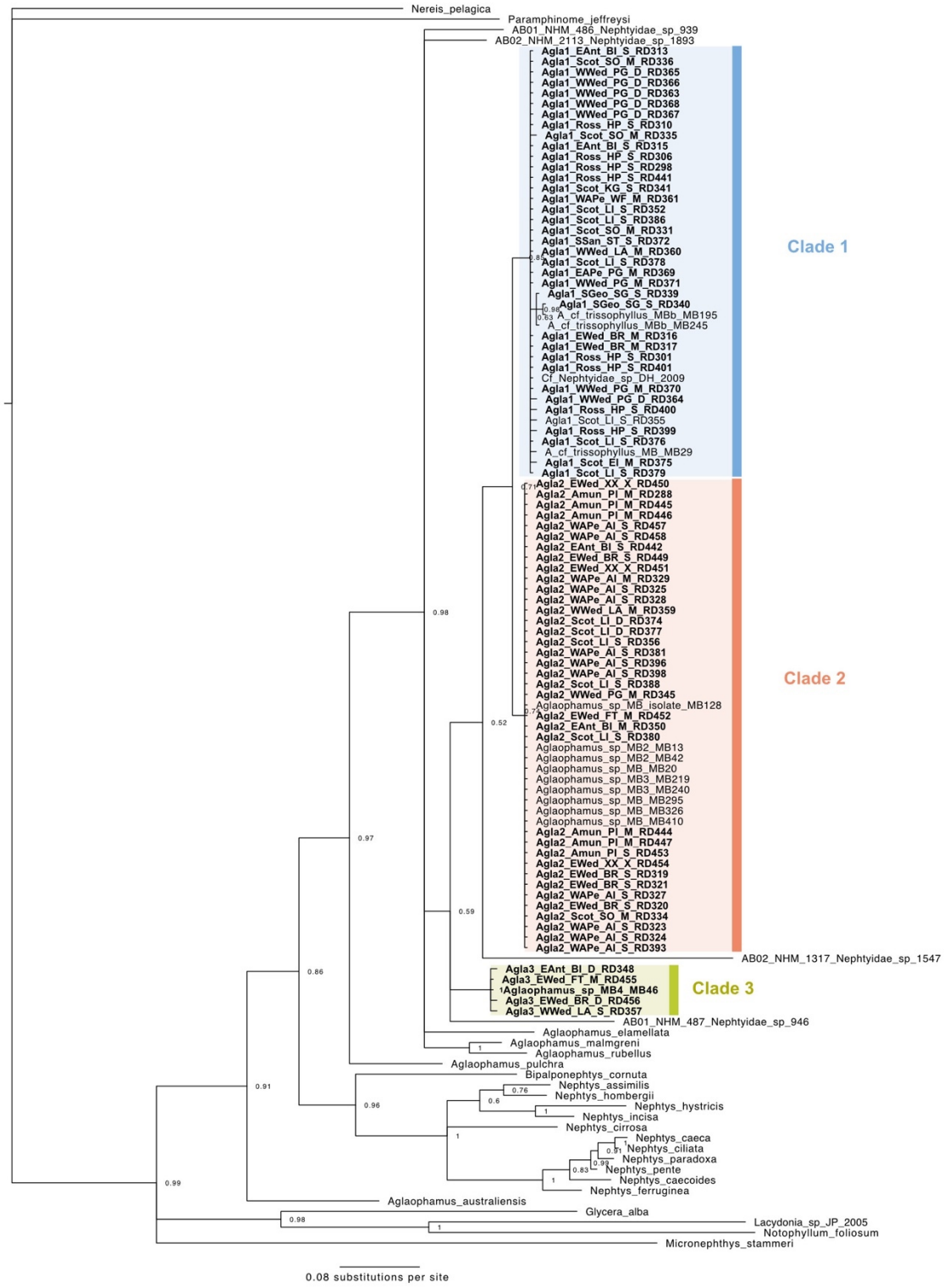

Figure 5.4 Phylogenetic tree of the annelid family Nephtyidae using Bayesian analysis of 16S RNAmarker. Antarctic *Aglaophamus* spp. newly sequenced in this study are marked in bold. Clades within Antarctic *Aglaophamus* spp. are identified with boxes. Bayesian posterior probability values are given as support.

Clades 1 and 2 were closely related in 16S analyses (minimum inter-clade uncorrected p-distance 1.2%) (Table 5.3). However, in the COI analysis (Figure 5.5), Clade 2 is split into two paraphyletic clades (Clade 2a & Clade 2b) with large genetic distances between groups (minimum 11.1% uncorrected p-distance between Clade 2a and Clade 2b; Table 5.3), despite individuals from both having 100% identical sequences in 16S (maximum p-distance of 0% across all individuals in Clade 2; Table 5.3). Clades 2a and 2b correspond to COI clades *Aglaophamus* sp. MB2 and MB3, respectively in Brasier et al., (2016). Clade 1 is also more divergent from Clade 2 groups than in 16S (minimum interclade p-distance 9.3-11% in COI; Table 5.3).

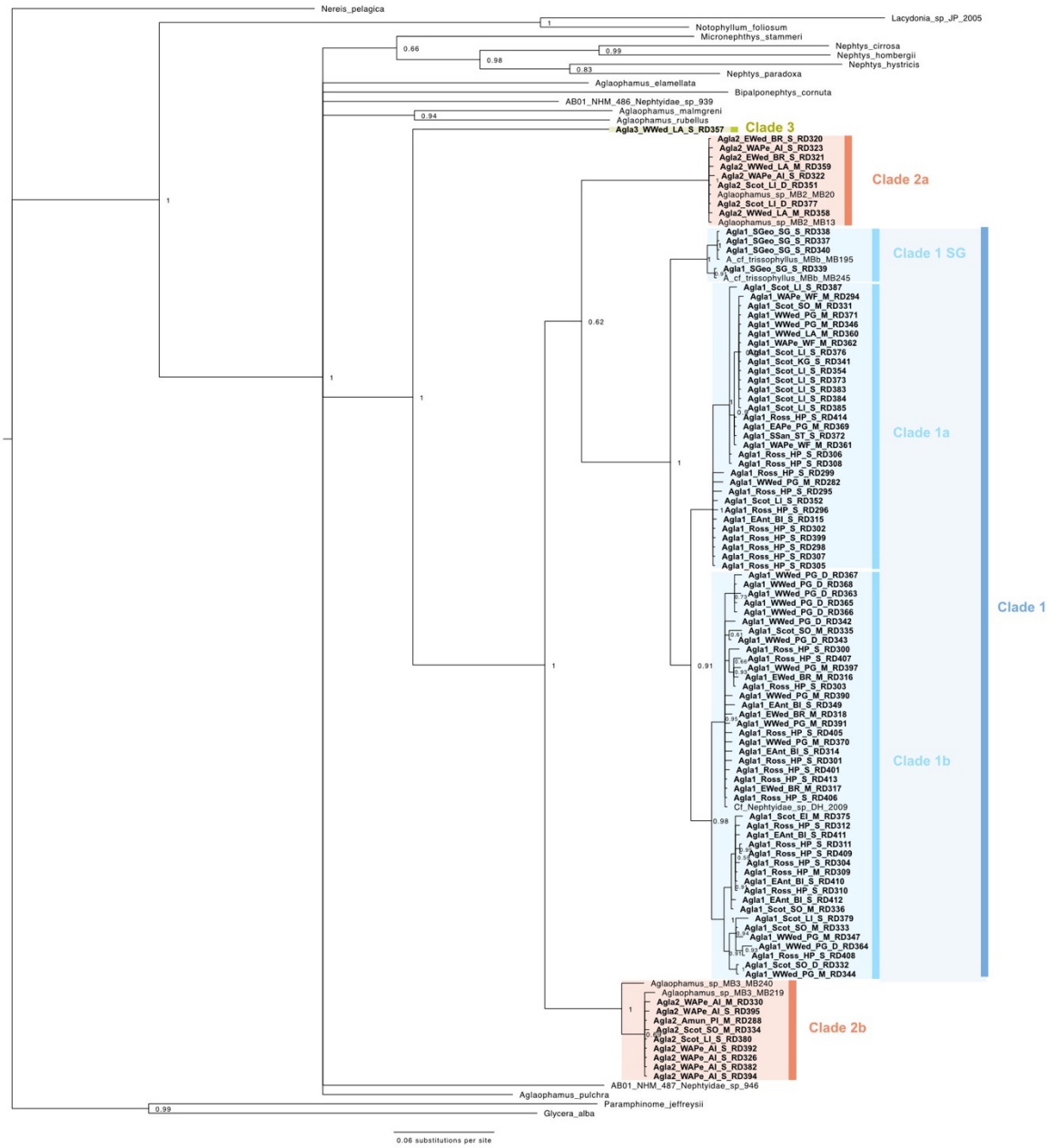

Figure 5.5 Phylogenetic tree of the annelid family Nephtyidae using Bayesian analysis of cytochrome oxidase subunit I (COI) marker. Antarctic *Aglaophamus* spp. newly sequenced in this study are marked in bold. Clades and subclades within Antarctic *Aglaophamus* spp. are identified with boxes. Bayesian posterior probability values are given as support.

The COI analysis further reveals considerable genetic structure within Clade 1 with a maximum intraclade p-distance of 6.2% (1.1% in 16S) (Table 5.3). Individuals from South Georgia (Clade 1 SG) form a subclade sister to all other individuals, and remaining individuals form two additional subclades (Clade 1a, Clade 1b) without clear geographic structure. These three clades (Clade 1a, Clade 1b, Clade 1 SG) correspond to COI clades *Aglaophamus* cf. *trissophyllus* MBc, MBa, and MBb, respectively in Brasier et al. (2016). Maximum p-distance measures within these sub-clades are much lower than for Clade 1, and with minimum interclade p-distances of >4% between the South Georgia Clade and Clades 1a and 1b (Table 5.3).

Table 5.3 Table of p-distance measures for COI and 16S analyses. Minimum inter-clade uncorrected p-distance values for COI (below diagonal) and 16S (above diagonal). Diagonal maximum intra-clade p-distance values for COI (left) and 16S (right). Clades not highlighted in bold are only found in COI analyses.

	Clade 1	Clade 1 no SG	Clade 1 SG	Clade 1a	Clade 1b	**Clade 2**	Clade 2a	Clade 2b	**Clade 3**
Clade 1	0.062/0.011	-	-	-	-	0.017	-	-	0.054
Clade 1 no SG	-	0.053/-	-	-	-	-	-	-	-
Clade 1 SG	-	0.044	0.009/-	-	-	-	-	-	-
Clade 1a	-	-	0.044	0.024/-	-	-	-	-	-
Clade 1b	-	-	0.049	0.027	0.029/-	-	-		-
Clade 2	0.093	0.093	0.102	0.095	0.093	0.12/0	-	-	0.054
Clade 2 a	0.111	0.111	0.119	0.115	0.111	-	0.002/-	-	-
Clade 2 b	0.093	0.093	0.102	0.095	0.093	-	0.093	0.007/-	-
Clade 3	0.161	0.161	0.164	0.162	0.161	0.168	0.172	0.168	/0.006

In both 16S and COI analyses, Clade 3 is distinct from Clades 1 and 2 (minimum uncorrected p-distance from both clades 5.4% in 16S and >16% in COI; Table 5.3), however only one individual was included in COI and combined analyses due to unsuccessful COI sequencing. Clade 3 corresponds with the 16S clade *Aglaophamus* sp. MB4 in Brasier et al. (2016). In 18S analysis, Clades 1 and 2 are identical (Appendix D Figure D.1), with Clade 3 differing by two nucleotide substitutions.

5.3.2 Population structure and connectivity using COI barcodes

COI haplotype networks were constructed for Clade 1 to further investigate genetic structure among sampling sites and bathymetrical ranges (Figure 5.6). Overall, a total of 52 haplotypes (h) were identified in 77 individuals, and they were segregated mainly by major clades found in phylogenetic analyses. Clade 1a displayed more shared haplotypes across the sampling sites (h=12 in 27 individuals, whereas the majority of individuals in Clade 1b were represented by single haplotypes, which is associated with higher genetic diversity (h=38 in 44 individuals) and two potential star-like shaped haplotypes, which require further investigation. Other than the separation of South Georgia specimens, no clear geographic structure was observed. However, there is a possible association with depth, with the majority of shallowest specimens in Clade 1a (65-850m, mean 318m ± 37.3 SE) and all specimens >850m in Clade1b (65-1271m, mean 611m ± 57.2).

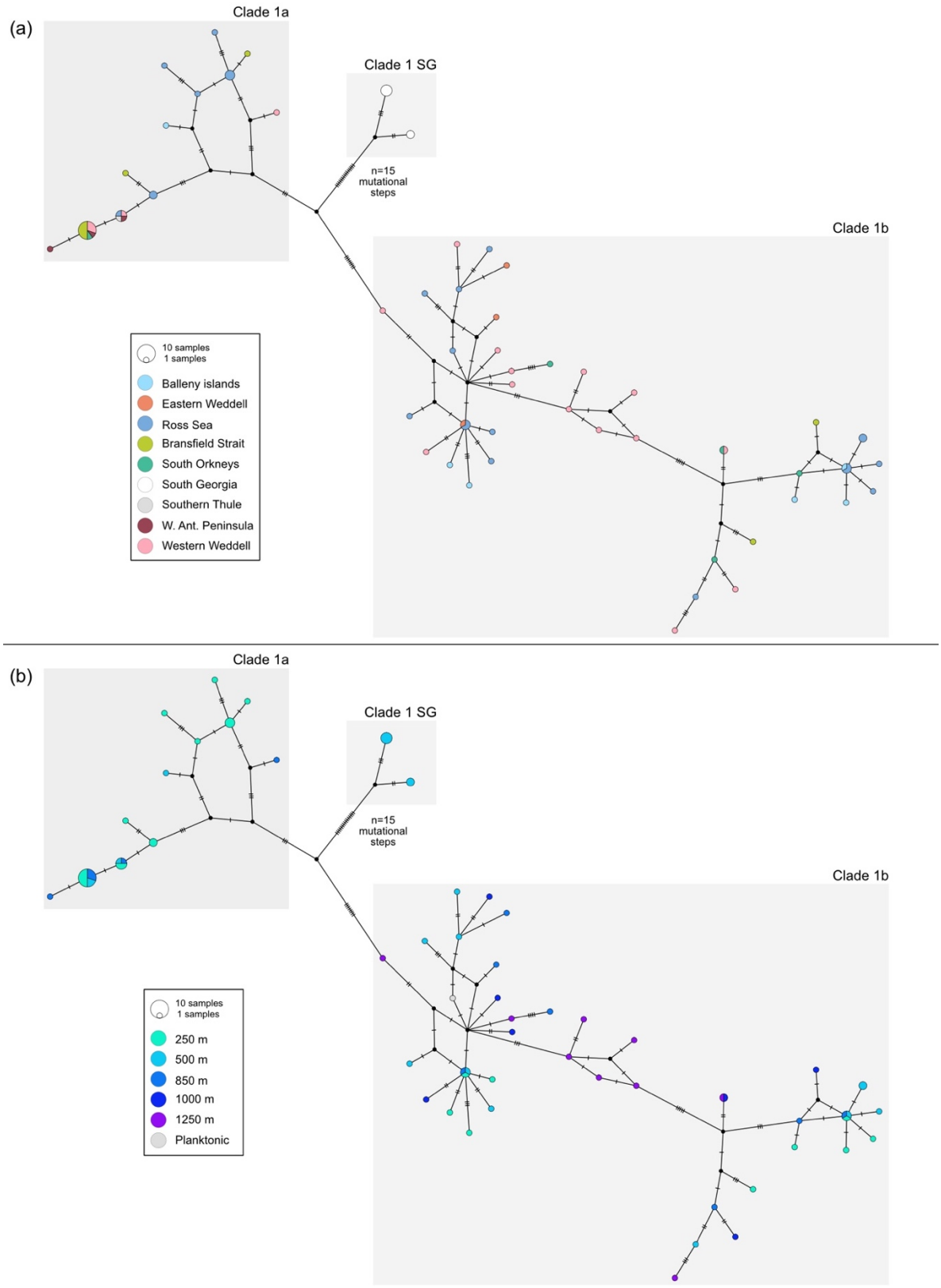

Figure 5.6 COI haplotype network analyses for Clade 1 *Aglaophamus* individuals (n=77, 548bp) by (a) and (b) depth, with colours representing different sampling localities and depths, respectively. Depth bins are >250m,251-500m, 501- 850m, 851-1000m, 1001->1250m, and planktonic for single GenBank sequence collected as plankton (Heimeier et al., 2010). Subclades found in phylogenetic analysed are highlighted using boxes. Each coloured circle represents a sampled haplotype, with circle size proportional to the frequency of that haplotype, as indicated by the key Bars between haplotypes represent one mutation, with missing inferred haplotypes represented by black circles.

5.3.3 ddRAD-seq analysis and filtering quality

A total of 719,387,736 reads were retained following RADtag processing for 130 *Aglaophamus* individuals, with the *denovo* assembly pipeline pre-filtering producing a base catalogue of 7,350,084 loci. Treating Clades 1, 2 and 3 from phylogenetic analyses as putative species, to avoid confusion with genetic clusters in genomic analyses, individuals from phylogenetic Clade 1 are henceforth referred to as Agla 1, Clade 2 as Agla 2, Clade 3 as Agla 3, and undetermined specimens without barcodes Agla X. One library of 12 individuals (library 8), consisting mostly of Agla 2 individuals, failed sequencing with samples not exceeding 17,000 reads. Excluding this library and other low read individuals, 113 samples remained with >600,000 reads (Agla 1 *n*=77, Agla 2 *n*=28, Agla 3 *n*=4, undetermined *n*=4). Of these samples, an average of 6,358,996 ± 4,380,618 SD reads were retained for each sample.

5.3.4 Species boundaries using SNPs

Initial cluster analyses of the all-specimen dataset could not distinguish individuals of Agla 3 from Agla 1 or 2, despite the evident separation detected in previous phylogenetic analyses using mitochondrial and nuclear markers Table 5.3; Figure 5.2Figure 5.4Figure 5.5; Appendix D Figure D.2). Due to the small sample size (*n*=4) and high missing data in some individuals, Agla 3 was excluded from further analyses. Specimens without barcodes (Agla X) were also excluded also due to small sample size (*n*=5), high missing data in some individuals, and the fact that without barcode data, these individuals could not be distinguished from Agla 3 or other putative species.

After the exclusion of low quality or undetermined individuals from the dataset, the population genetic structure and differentiation was assessed only for Agla 1 and Agla 2 together. The optimal number of clusters across both DAPC and ADMIXTURE analyses was three (*K*=3), followed by four (*K*=4) then two (*K*=2) (Appendix D Figure D.3). In the *K*=3 analysis (Figure 5.7)Figure 5.7, two genetic clusters were formed by Agla 1 individuals, with a separate third cluster containing near-exclusively Agla 2 individuals (Figure 5.7; (Appendix D Figure D.4). Notably, Cluster 1 and Cluster 2 (Agla 1 individuals) generally correspond to Clades 1b and 1a in phylogenetic analyses respectively, though South Georgia is not defined. Three individuals also show some degree of admixture between Agla 1 and Agla 2 genetic clusters, corresponding to two specimens from the Ross Sea (Agla1_Ross_HP_S_RD409 and Agla1_Ross_HP_S_RD414), and one from the Balleny Islands (Agla1_EAnt_BI_S_RD349) in *K* = 3 ADMIXTURE analyses (Figure 5.7 c). This is also visible in the *K*=3 DAPC analysis, with Agla1_Ross_HP_S_414 and Agla1_EAnt_BI_S_349 included the Agla 2 cluster (Cluster 3), and Agla1_Ross_HP_S_RD409 more intermediate between Agla 1 and Agla 2 individuals

(Figure 5.7 b; (Appendix D Figure D.4). These individuals are not distinct in previous phylogenetic analyses using barcodes nested within Clade 1 (Agla 1) Figure 5.2Figure 5.4Figure 5.5 .

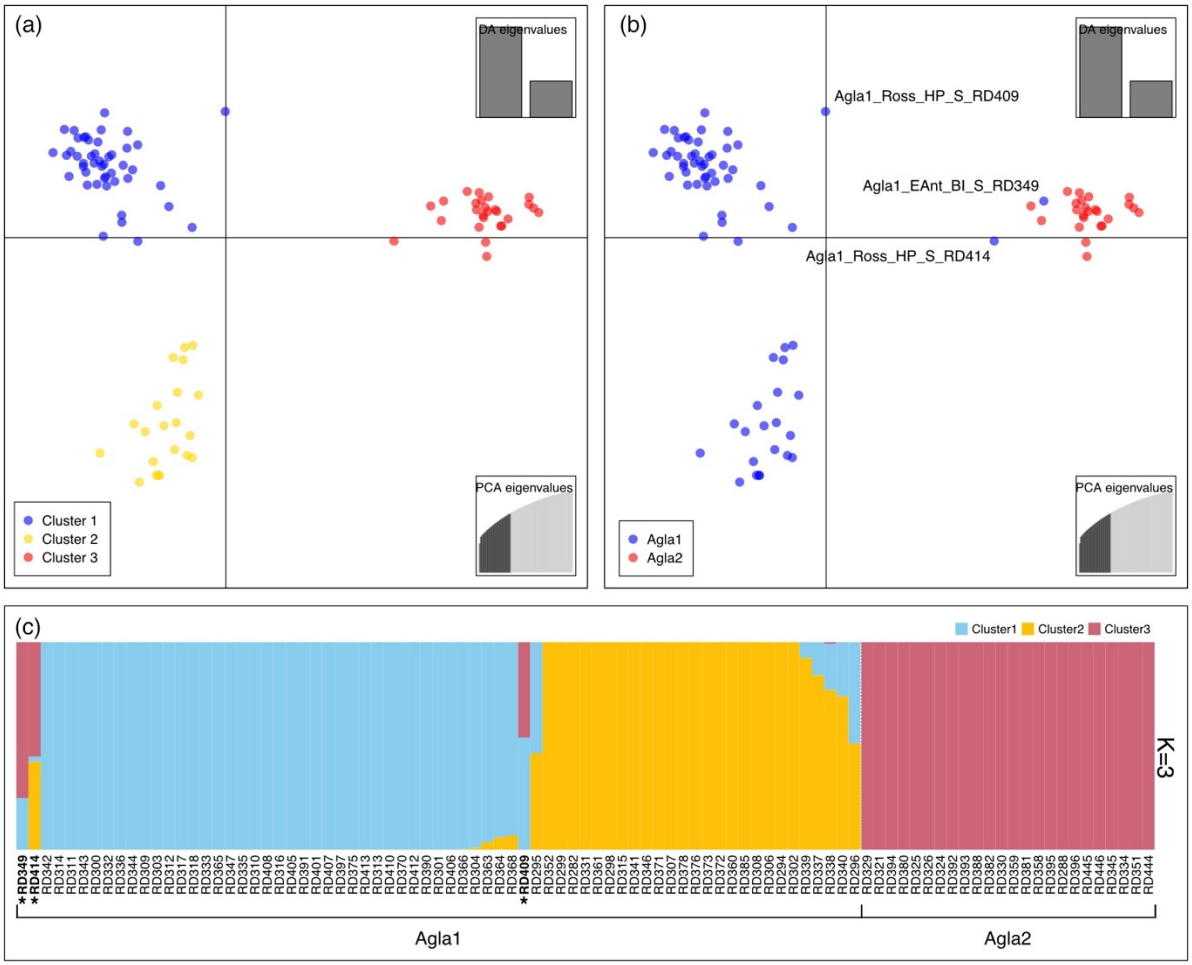

Figure 5.7 Combined analysis and genotype assignment of *Aglaophamus* cf. *trissophyllus* Clades 1 and 2 (Agla 1, Agla 2) identified in phylogenetic analyses (a) DAPC results with *K*=3 as inferred by the function *snapclust*; (b) DAPC *K*=3 results with phylogenetic clade membership indicated by colour: Agla 1 (blue), Agla 2 (red). Agla 1 individuals within or proximal to the Agla 2 cluster are highlighted; (c) ADMIXTURE results with *K*=3, grouped by phylogenetic clade membership. Individuals are given by extraction number. Only three individuals of Agla 1 show a significant degree of introgression with the Agla 2 cluster (Cluster 3 in red) and are highlighted in bold and marked with an asterisk.

The second most optimal clustering configuration *K*=4 differed between analyses, with DAPC splitting Agla 2 individuals into two clusters (Appendix D Figure D.5) while ADMIXTURE refined Agla 1 genetic clusters, separating out South Georgia individuals as a distinct cluster (dark green in Figure 5.8 a; Appendix D Figure D.6).

The two Agla 2 clusters in DAPC *K*=4 (Appendix D Figure D.5) do not correspond to Clade 2a and Clade 2b in COI phylogenetic analyses. Furthermore, the co-ancestry matrix generated by fineRADstructure (Figure 5.8 b) shows Agla 2 individuals as a homogenous cluster with moderate values of co-ancestry. South Georgia specimens form a distinct cluster in this analysis, with the highest values of co-ancestry across all specimens, nested within a broader cluster of Agla 1 individuals. Within the remaining Agla 1 individuals, there were two nested sub-clusters that correspond to clusters 1 and 2 identified in *K*=3 and *K*=4 analyses. Agla 1 clusters 1 and 2 broadly correspond with individuals in Clade 1b and 1a in phylogenetic analyses, respectively. Notable were two individuals, Agla1_Ross_HP_S_RD295 and Agla1_Ross_HP_S_RD296, intermediate between the two Agla 1 clusters, which also showed introgression in ADMIXTURE analyses (Figure 5.8 a, also in Figure 5.7 c). The three Agla 1 individuals that displayed admixture with Agla 2 in DAPC and ADMIXTURE analyses (Figure 5.7,Figure 5.8 a) had similar co-ancestry values between Agla 1 and Agla 2 clusters in fineRADstructure analyses.

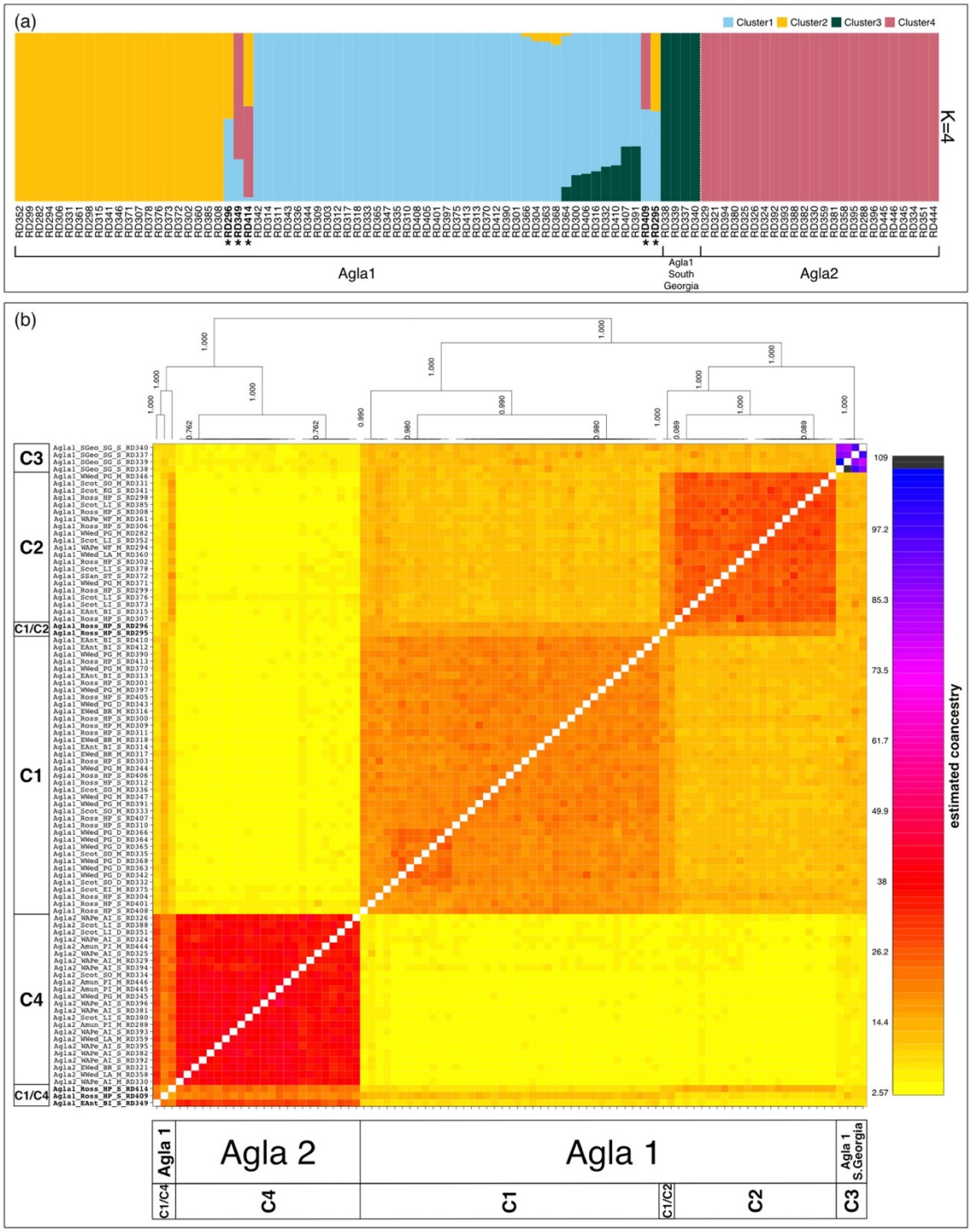

Figure 5.8 Genotype assignment (a) and co-ancestry analysis (b) of combined dataset of *Aglaophamus* cf. *trissophyllus* clades 1 and 2 (Agla 1, Agla 2) identified in phylogenetic analyses. (a) ADMIXTURE results with *K*=4, assigning individuals to one of four genetic clusters, grouped by phylogenetic clade membership. Individuals are given by extraction number. The four individuals assigned completely to Cluster 3 (dark green) include all specimens collected from South Georgia. Individuals with admixture between genetic clusters are highlighted in bold and marked with an asterisk. (b) FineRADstructure simple co-ancestry matrix heatmap – top: simple hierarchical tree from raw data matrix with posterior population assignment probabilities; left: specimen IDs and cluster assignment results from *K*=4 ADMIXTURE. Individuals displaying admixture between clusters are highlighted in bold; bottom: Phylogenetic clade assignment of individuals, and cluster assignments results from *K*=4 ADMIXTURE

The pairwise F_{ST} value between Agla1 and Agla 2 in combined analyses was significant (p=0.05) and moderately high (F_{ST} = 0.582). Genetic clusters in K=2 were near-identical in both DAPC and ADMIXTURE analyses (Appendix D Figures Figure D.7, Figure D.8) broadly split into Agla 1 and Agla 2 individuals, with the same three individuals showing admixture between genetic clusters as discussed above in results of K=3.

5.3.5 Population structure and connectivity using SNPs

5.3.5.1 Genetic Diversity indices

Population genetic statistics for Agla 1 and Agla 2 are shown in Table 5.4. For Agla 1, two individuals from the West Antarctic Peninsula sites were grouped with Bransfield strait group (Elephant Island, King George Island, Livingston Island) due to geographic proximity, however other sites with low number of specimens such as Southern Thule were not combined with other sites due to large distances between collection sites. Hence, results for population genetic statistics for sites with small number of specimens should be taken with caution. Overall expected heterozygosity (normally considered as a measure of genetic diversity) was relatively low (0.08 ± 0.003), ranging from 0.031 to 0.075 (H_E), with average observed heterozygosity (H_O) showing a smaller range of 0.055 to 0.082. As measures of genetic diversity, sites with the highest number of specimens such as the Ross Sea (n=25) and the Western Weddell Sea (n=18) had the largest number of private alleles, however Balleny islands (n=6), South Orkneys (n=5) and South Georgia (n=4) all had higher nucleotide diversity (π), though this metric did not vary widely across samples, ranging from 0.059-0.080. F_{IS} was close to zero and similar across all sample site.

In Agla 2, the number of individuals (n=28) was fewer, with only four out of seven sites having three or more individuals. Overall expected heterozygosity was higher than that for Agla 1 (0.278 ± 0.004), as it also occurred for observed heterozygosity and nucleotide diversity (H_O 0.378 ± 0.009, π 0.284 ± 0.004). F_{IS} remained similarly close to zero across sampling sites although it was -0.155 ± 0.043 for the whole sample.

Table 5.4 Population genetic statistics from Agla 1 (907 SNPS) and Agla 2 (1,111 SNPS) neutral datasets. H_O = Observed heterozygosity; H_E = expected heterozygosity; π = nucleotide diversity; F_{IS} = fixation index

		n	depth range (m)	private alleles	H_O	H_E	π	F_{IS}
Agla 1	Balleny Islands	6	85-400	44	0.067 ± 0.005	0.069 ± 0.004	0.08 ± 0.005	0.033 ± 0.035
	Bransfield Strait & WAP	11	111-988	76	0.071 ± 0.005	0.067 ± 0.004	0.073 ± 0.005	0.012 ± 0.054
	Eastern Weddell Sea	3	587	19	0.055 ± 0.006	0.046 ± 0.004	0.059 ± 0.006	0.006 ± 0.021
	Ross Sea	25	65-564	145	0.064 ± 0.004	0.073 ± 0.004	0.075 ± 0.004	0.046 ± 0.089
	South Georgia	4	306	51	0.082 ± 0.009	0.055 ± 0.006	0.079 ± 0.008	-0.004 ± 0.041
	South Orkneys	5	617-1003	41	0.072 ± 0.005	0.07 ± 0.004	0.08 ± 0.005	0.018 ± 0.029
	Southern Thule	1	266	1	0.063 ± 0.011	0.031 ± 0.006	0.063 ± 0.011	-
	Western Weddell Sea	18	483-1271	135	0.068 ± 0.004	0.075 ± 0.004	0.078 ± 0.004	0.035 ± 0.072
	Total	73	65-1271	-	0.067 ± 0.003	0.08 ± 0.003	0.081 ± 0.004	0.1 ± 0.214
Agla 2	Amundsen Sea	4	504-578	82	0.134 ± 0.007	0.115 ± 0.115	0.14 ± 0.007	0.011 ± 0.027
	Balleny Islands	2	380-555	28	0.134 ± 0.012	0.08 ± 0.08	0.136 ± 0.012	0.002 ± 0.019
	Eastern Weddell Sea	1	390	14	0.115 ± 0.012	0.057 ± 0.057	0.115 ± 0.012	-
	Livingston Island	5	193-1473	92	0.119 ± 0.007	0.105 ± 0.105	0.129 ± 0.007	0.02 ± 0.035
	South Orkneys	1	721	22	0.13 ± 0.012	0.065 ± 0.065	0.13 ± 0.012	-
	West Antarctic Peninsula	12	399-528	184	0.11 ± 0.005	0.112 ± 0.112	0.12 ± 0.005	0.029 ± 0.066
	Western Weddell	3	483-686	63	0.118 ± 0.007	0.1 ± 0.1	0.129 ± 0.007	0.018 ± 0.019
	Total	28	193-1473	-	0.378 ± 0.009	0.278 ± 0.004	0.284 ± 0.004	-0.155 ± 0.043

5.3.5.2 Agla 1 structure

Refined population genomic analyses were performed using only individuals assigned to Agla 1 (Clade 1) in phylogenetic analyses (section 5.3.1), following the same approach described above for the combined dataset. The optimal number of clusters for Agla 1 in DAPC and ADMIXTURE analyses was *K*=2 (Figure 5.9 a-b) followed by *K*=3 and *K*=4 (Appendix D Figure D.9). The two clusters in *K*=2 analyses again identified Clades 1a and 1b as in the COI phylogenetic analysis (Figure 5.5), thus showing no clear geographic structure, with most localities contain both clusters, and no separation of South Georgia individuals (Figure 5.9 b; (Appendix D Figure D.10).

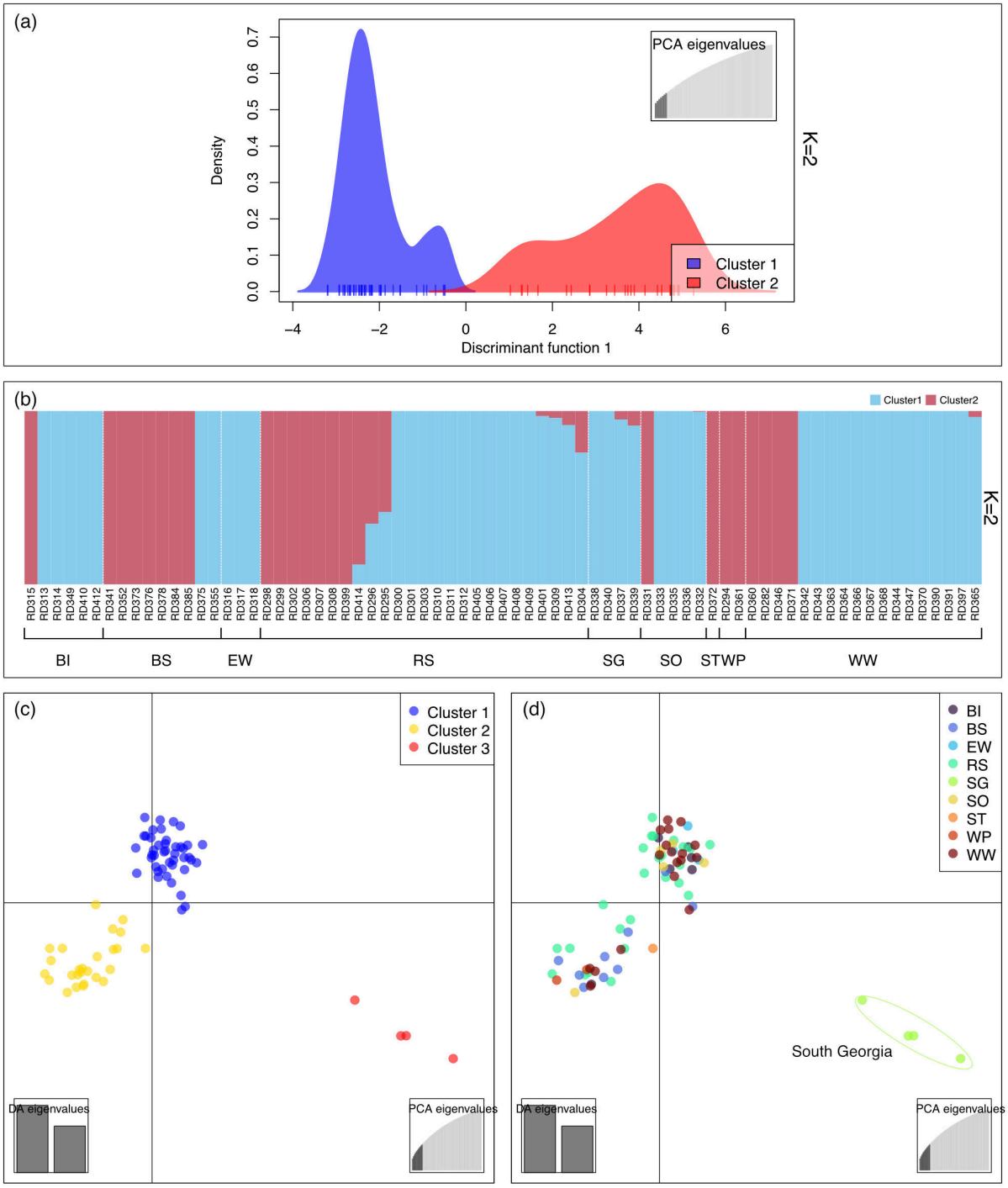

Figure 5.9 Population structure and differentiation analysis for *Aglaophamus cf. trissophyllus* Clade 1 (Agla 1) (a) DAPC results with *K*=2 showing proximity and slight overlap of the two clusters; (b) ADMIXTURE results with *K*=2, with individuals grouped by geographic locality. Individuals are given by extraction number. (c) DAPC results with *K*=3 with no assignation of geographic information to samples; (d) DAPC *K*=3 results with geographic locality of individuals indicated by colour - Cluster 3 is distinct and comprised of individuals collected from South Georgia. BI = Balleny Islands; BS = Bransfield Strait; EW = Eastern Weddell Sea; RS = Ross Sea; SG = South Georgia; SO = South Orkneys; ST = Southern Thule; WP = West Antarctic Peninsula; WW = Western Weddell Sea.

The DAPC results for *K*=3 identified an additional distinct cluster formed by South Georgia individuals (Figure 5.9 c; (Appendix D Figure D.11) Appendix D Figure 11) however this pattern was not detected in ADMIXTURE results using *K*= 3 (Appendix D Figure D.12 a) (Appendix D Figure 12 a). South Georgia is somewhat separate in *K*=4 ADMIXTURE results but admixed with individuals from the Western Weddell Sea, South Orkneys and Bransfield Strait (Appendix D Figure D.12 b) (Appendix D Figure 12 b). Pairwise F_{ST} results showed significant values only between South Georgia and sites with the highest number of specimens (Ross Sea, Bransfield Strait and West Antarctic Peninsula, and the Western Weddell Sea), with moderate values ranging from 0.271-0.289 (Table 5.5).

Table 5.5 Pairwise F_{ST} values by sampling locality for *Aglaophamus* Agla 1. BI = Balleny Islands; BS = Bransfield Strait; EW = Eastern Weddell Sea; RS = Ross Sea; SG = South Georgia; SO = South Orkneys; ST = Southern Thule; WP = West Antarctic Peninsula; WW = Western Weddell Sea. Figures in bold are significant, Bonferroni correction *p*-value = 0.0018. F_{ST} coloured by heat map, red > 0, blue < 0

		BI	BS & WP	EW	RS	SG	SO	ST	WW
Agla 1	Balleny Islands	--							
	Bransfield Strait & WAP	0.12	--						
	Eastern Weddell Sea	-0.014	0.233	--					
	Ross Sea	-0.002	0.085	0.03	--				
	South Georgia	0.229	**0.289**	0.407	**0.271**	--			
	South Orkneys	-0.015	0.129	0.006	0.005	0.256	--		
	Southern Thule	0	0	0	0	0	0	--	
	Western Weddell Sea	-0.003	0.131	0.02	0.014	**0.235**	-0.007	0	--

To refine the resolution of the population assignment comparisons, further analyses were performed for Agla 1 individuals, excluding South Georgia. After filtering the dataset using the Stacks pipeline, a neutral dataset of 1,643 SNPs and 69 individuals was obtained. The optimal number of clusters was again *K*=2 (Figure 5.10 a) followed by *K*=3 and *K*=4 in both, DAPC and ADMIXTURE (Appendix D Figure D.13). As in the previous analysis, both clusters are broadly congruent with Clades 1a and 1b in COI phylogenetic analyses (Figure 5.5), with unclear geographic structure (Figure 5.10 c; (Appendix D Figure D.14). In terms of depth, however, genetic Cluster 2 (corresponding to Clade 1a in phylogenetic analyses) is not found below 850m and includes most specimens above 250m, whereas genetic Cluster 1 (corresponding to Clade 1b) displays a broader depth range from >250m to over 1250m (Figure 5.10 b, d).

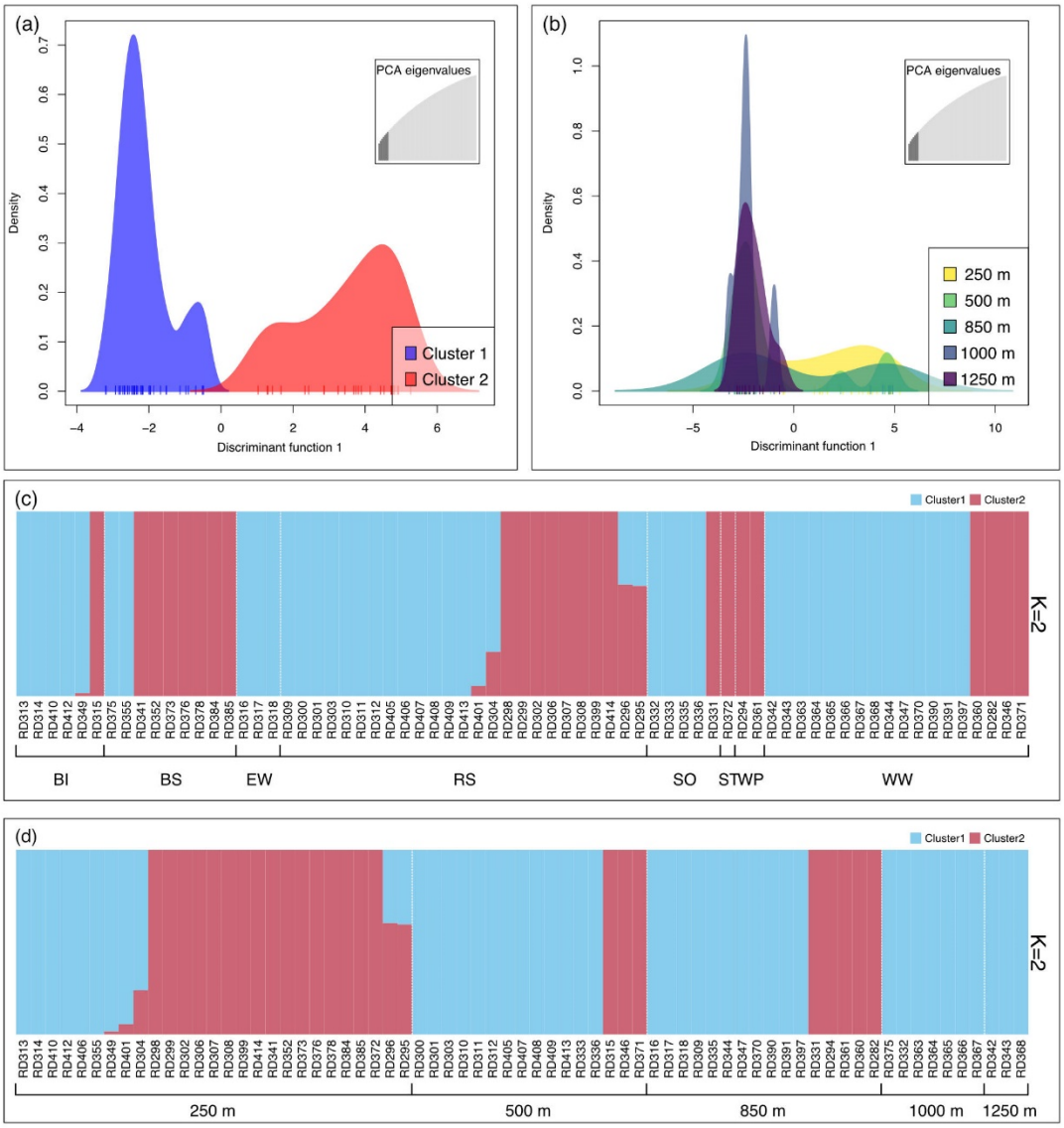

Figure 5.10 Population structure and differentiation analysis for *Aglaophamus* cf. *trissophyllus* Clade 1 (Agla 1), excluding South Georgia (a) DAPC results with *K*=2 as inferred by the function *snapclust* showing proximity and slight overlap of the two clusters; (b) DAPC *K*=2 results with depth groupings (c) ADMIXTURE results with *K*=2, with individuals grouped by geographic locality (d) ADMIXTURE results with *K*=2, assigning individuals to one of two clusters, with individuals grouped by depth. Individuals are given by extraction number. BI = Balleny Islands; BS = Bransfield Strait; EW = Eastern Weddell Sea; RS = Ross Sea; SG = South Georgia; SO = South Orkneys; ST = Southern Thule; WP = West Antarctic Peninsula; WW = Western Weddell Sea. Depth bins = >250m;251-500m;501- 850m; 851-1000m; 1001->1250m.

For *K*=3 DAPC analyses, a third cluster containing most specimens between 1000 and over 1250m depth is observed (Figure 5.11 a-c; (Appendix D Figure D.15). Most of the deepest specimens in this study were collected from the Prince Gustav Channel in the Western Weddell Sea, however, this third cluster also includes the deepest specimen from the South Orkneys (Agla1_Scot_SO_D_RD332, 1003m), with the deepest specimen from the Bransfield Strait, off Elephant Island (Agla1_Scot_EI_M_RD375, 988m) proximal to this cluster (Figure 5.11 c).

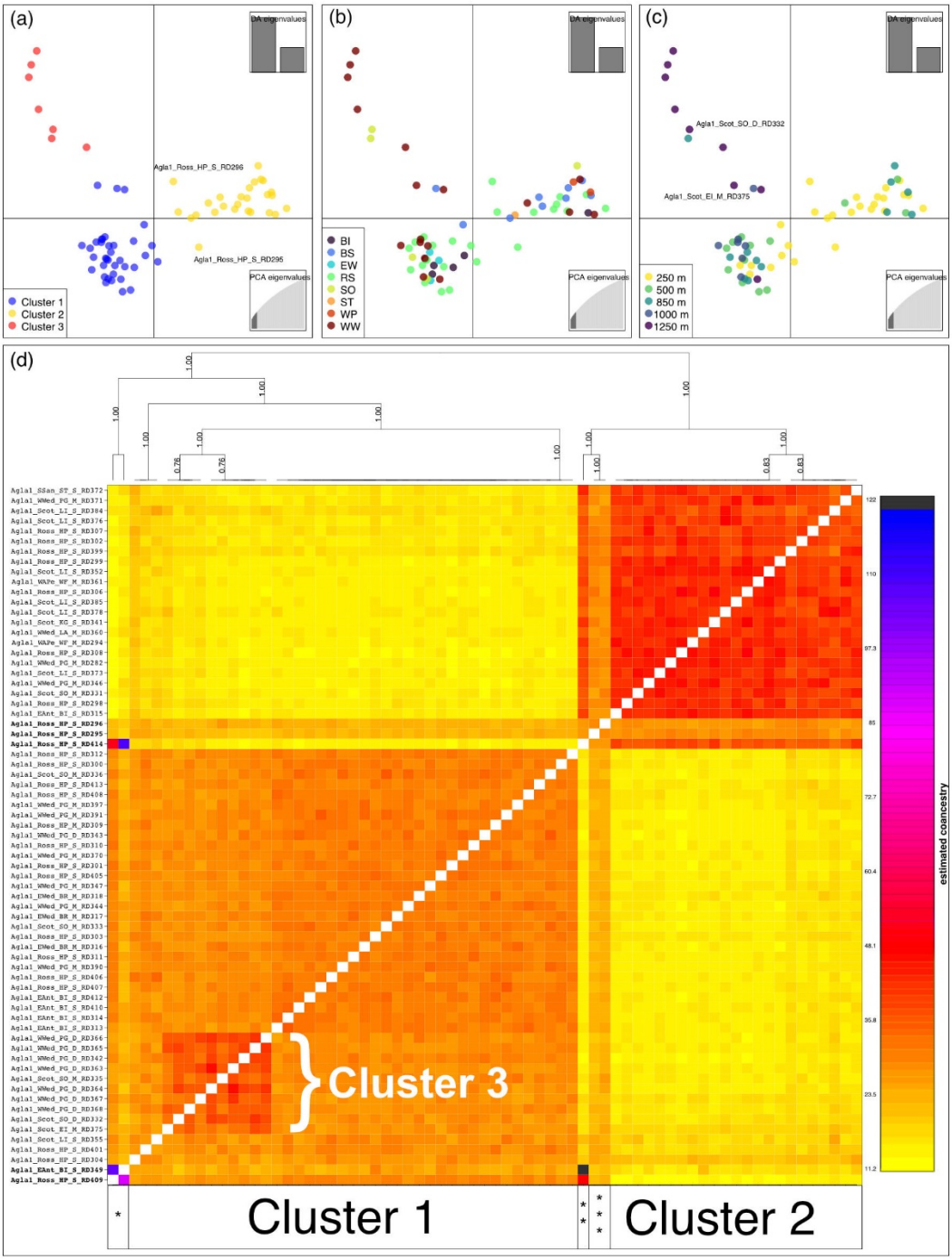

Figure 5.11 Population structure (a) and co-ancestry analysis (b) of *Aglaophamus* cf. *trissophyllus* Clade 1 (Agla 1), excluding South Georgia (a) DAPC results with *K*=3 (b) DAPC *K*=3 results with geographic locality of individuals indicated by colour; (c) DAPC *K*=3 results with depth of individuals indicated by colour. Deepest individuals from non-Western Weddell sampling sites highlighted. (d) FineRADstructure simple co-ancestry matrix heatmap – top: simple hierarchical tree from raw data matrix with posterior population assignment probabilities; left: specimen IDs; bottom: cluster assignments in *K*=3 DAPC analysis (Cluster 3 marked with parentheses on matrix). Individuals displaying admixture between clusters highlighted in bold and with asterisks: * = individuals with admixture between Agla 1 and Agla 2 in previous analyses; ** = individual with admixture between Agla 1 and Agla 2 in previous analyses; *** individuals with admixture between Cluster 1 and Cluster 2 in Agla 1 analyses. BI = Balleny Islands; BS = Bransfield Strait; EW = Eastern Weddell Sea; RS = Ross Sea; SG = South Georgia; SO = South Orkneys; ST = Southern Thule; WP = West Antarctic Peninsula; WW = Western Weddell Sea. Depth bins = >250m;251-500m;501- 850m; 851-1000m; 1001->1250m.

The co-ancestry matrix of this dataset also identifies this third, deep-water cluster nested within the Cluster 1 (Figure 5.11c). Higher co-ancestry values are found amongst individuals in Cluster 2, while other individuals of note include Agla1_Ross_HP_S_RD295 and Agla1_Ross_HP_S_RD296, with intermediate co-ancestry values between the Agla 1 genetic clusters 1 and 2 as in previous analyses (see also Figure 5.11 a), while the highest co-ancestry values are found between the three individuals previously identified as displaying admixture between Agla 1 and Agla 2 (Agla1_Ross_HP_S_RD414, Agla1_EAnt_BI_S_RD349, Agla1_Ross_HP_S_RD409). Neither clear geographic nor bathymetric structure was observed in ADMIXTURE results using *K*=3 clusters (Appendix D Figure D.16).

5.3.5.3 Agla 2 structure

In the Agla 2 dataset, neither DAPC nor ADMIXTURE analyses found distinct genetic clusters, with *K*=1 returned as optimal in both analyses Appendix D Figure D.17). Co-ancestry analysis also found an overall homogenous grouping with moderately high values of co-ancestry (Appendix D Figure D.18) (Appendix D Figure 18). Pairwise F_{ST} analysis only returned one significant value, near zero (0.044), between the Amundsen Sea and West Antarctic Peninsula Table 5.6.

Table 5.6 Pairwise F_{ST} values by sampling locality for *Aglaophamus* Clade 2. AS = Amundsen Sea; BI = Balleny Islands; BS = Bransfield Strait; EW = Eastern Weddell Sea; SO = South Orkneys; WP = West Antarctic Peninsula; WW = Western Weddell Sea. Figures in bold are significant, Bonferroni correction p-value = 0.002. F_{ST} coloured by heat map, red > 0

		AS	BI	BS	EW	SO	WP	WW
Agla 2	Amunsden Sea	--						
	Balleny Islands	0	--					
	Bransfield Strait	0.028	0	--				
	Eastern Weddell Sea	0	0		--			
	South Orkneys	0	0	0	0	--		
	West Antarctic Peninsula	**0.044**	0	0.011	0	0	--	
	Western Weddell Sea	0.041	0	0.042	0	0	0.038	--

5.4 Discussion

5.4.1 Species boundaries

Phylogenetic analyses using traditional barcode markers (e.g. COI, 16S and 18S) found multiple genetic lineages within specimens identified as *Aglaophamus trissophyllus,* corresponding with potentially cryptic lineages as found in a prior barcoding study (Brasier et al., 2016) while greatly increasing the number and sampling range of available sequences (94 COI and 73 16S sequences, building on 11 COI, 30 16S sequences in Brasier et al. 2016). As in Brasier et al. (2016), genetic clades were not consistent across 16S and COI barcode genes. 16S analyses found three major lineages, Agla 1 (Clade 1) including most large and/or pigmented specimens with typical adult *Aglaophamus trissophyllus* morphology *sensu* Knox & Cameron (1998), in addition to Agla 2 (Clade 2) and Agla 3 (Clade 3), composed primarily of smaller, unpigmented individuals. COI analyses revealed more genetic structure, finding three sub-clades within Agla 1, and splitting Agla 2 into two separate, polyphyletic clades, with interclade distances up to 9.3%, despite sequences being identical in 16S analyses. Agla 1 and both Agla 2 clades were similarly 9.3% different from each other in COI analyses, despite small interspecific distance in 16S. While only one individual in Clade 3 was successful for COI sequencing, this also formed a distinct lineage in COI analyses. Depending on whether sub-clades within Agla 1 are counted, this means that COI found 4-6 clades in specimens identified as *Aglaophamus trissophyllus* versus only three in 16S. Although an independent nuclear gene (18S) was also sequenced, this marker is slower evolving, and is used more often for deeper phylogenetic relationships than at the species level. However, 18S supported the close relationship of the three major lineages, finding Agla 1 and Agla 2 to be identical, and Agla 3 differing by two mutations only.

In previous studies examining genetic structure in Antarctic annelids, 16S shows low to very low genetic variability, in contrast to high variability in COI (Brasier et al., 2016; Cowart et al., 2022; Leiva et al., 2018; Neal et al., 2014), something that has also been reported in other marine invertebrates from elsewhere (e.g. Pérez-Portela et al., 2013), which may be expected due to the relatively slower mutation rate of 16S. However, both are mitochondrial genes, which are linked due to maternal inheritance, and thus may be considered to behave as a single marker (Dellicour & Flot, 2018), and interpretations of population and phylogenetic history from single genes may not reflect the evolutionary history of a species as a whole (see Naciri & Linder, 2015).

Mitochondrial introgression can also blur well supported species boundaries (Toews & Brelsford, 2012), whereas a lack of recombination, high mutation rate, and low effective population size relative to nuclear genes means that mitochondrial gene fragments alone can also overestimate species numbers, especially where geographic sampling is incomplete (e.g. Ahrens et al., 2016; Eberle et al., 2020; Gaytán et al., 2020; Ortiz et al., 2021). For example, a recent study of Iberian spiders (Ortiz et al., 2021) found up to 13 lineages based on COI with clear barcode gaps, yet only two lineages supported by SNP genomic data generated by ddRADseq, despite COI intraspecific differences of 7.2 and 10.1% within these two lineages were recovered far exceeding limits cited for most studied animal species (e.g. 2%, Ratnasingham & Hebert, 2013), including spiders (Ortiz et al., 2021 and references therein).

In the current study, higher resolution genomic data using genome-wide SNPs consistently separated Agla 1 and Agla 2 across DAPC, ADMIXTURE and co-ancestry analyses, forming distinct genetic clusters. However, some introgression between three Agla 1 individuals and the Agla 2 cluster was observed, which was not detected in our phylogenetic analyses. Similarly, a recent study (Lau, et al., 2023a) of two species of Antarctic ophiuroid, also using ddRAD generated SNPs, found some introgression between the two species where distributions overlapped, despite clear differences in morphology and lifestyle (*Ophionotis victoriae*: broadcast spawner, five arms; *O. hexactis*: brooder, six arms). These species are considered phylogenetically close, with previous investigations of these species also finding small interspecific distances in COI barcode data (4.2-5.3% p-distance) (Galaska et al., 2017a). The divergent life history and morphological characteristics of *O. hexactis* were hypothesised as recent adaptations to survival in glacial and island refugia during Pleistocene glacial cycles (Lau et al., 2021; Lau et al., 2023a).

Aglaophamus trissophyllus is not the only *Aglaophamus* species recorded in the Southern Ocean, with other Antarctic congeners, mostly described in Hartman (1967), including *Aglaophamus digitatus* Hartman, 1967, *Aglaophamus foliosis* Hartman, 1967, and *Aglaophamus posterobranchus* Hartman, 1967. Only *A. trissophyllus* (described as *A. ornatus* in Hartman ,1967), synonymised with *A. trissophyllus* in Knox & Cameron (1998) is reported with such large sizes up to 20 cm and a range of colours (pale to purple to nearly black), with other diagnostic characters including a sub-rectangular prostomium and interramal cirri beginning on chaetiger 2. While many Agla 1 individuals matched *A. trissophyllus* description, some morphological differences were observed in Agla 2 individuals following barcoding, such as interramal cirri beginning on later chaetigers and more rounded prostomia. However, detailed morphological examination of parapodial series and chaetae, primary diagnostic characters in Antarctic *Aglaophamus* spp., was not possible within the scope and time frame of this study. Furthermore, morphological characters were difficult to discern in small or damaged specimens, even within Agla 1 individuals.

Therefore, definitive assignment to any one of the remaining Antarctic species was challenging for these reasons in addition to general morphological similarity between those species. In the synonymy of *A. ornatus* with *A. trissophyllus*, Knox & Cameron (1998) reported that a review of Antarctic *Aglaophamus* spp. was in preparation, however this was never published. Indeed, the type locality of *A. trissophyllus* itself is the sub-Antarctic Kerguelen islands, however no molecular data is available from type locality specimens. A thorough integrative taxonomic revision of Antarctic *Aglaophamus* spp. is needed going forward.

If Agla 1 and Agla 2 are considered separate putative species, the results of the current study do confirm their phylogenetic closeness, for example in both 16S and 18S barcode genes, COI interspecific distances <10%, and introgression evident in genome-wide SNP data; this may also suggest a recent evolutionary split. To definitively delineate these lineages and establish evolutionary history, future work should not only employ detailed morphological analyses, but phylogenetic methods that can include SNP data, such as RaxML-NG (Kozlov et al., 2019). Agla 3, despite being distinct in barcode analyses, could not be distinguished from Agla 1 or Agla 2 in genomic analyses. This may be due to the small sample size obtained for this lineage.

5.4.2 Population structure and connectivity

5.4.2.1 Putative species Agla 1

Individuals in the phylogenetic Clade 1 (Agla 1) displayed notable genetic structure in COI phylogenetic analyses, which was further explored using haplotype networks. These analyses also split individuals into sub-clades identified in the phylogenetic analyses, revealing large number of unique haplotypes and a diffuse network pattern with little geographic structure. This pattern is likely to be a result of survival in deep-sea refugia during glacial cycles in Antarctic species with a planktonic larval stage (Allcock & Strugnell, 2012), a reproductive trait known for *Aglaophamus trissophyllus* (Heimeier et al., 2010). The only notable geographic structure was the separation of South Georgia individuals, which also formed a distinct clade in the COI phylogenetic analyses (Clade 1 SG). Genetic differentiation between the sub-Antarctic South Georgia and other Antarctic localities has been found for many benthic Antarctic species across a range of animal phyla and reproductive strategies, in barcode, microsatellite, and RADseq data (see Leiva et al., 2022 and references therein). In the current study, separation of South Georgia was strongly supported in the co-ancestry analyses of SNP data, and in a number of clustering scenarios in ADMIXTURE and DAPC analyses. The fact that differentiation of South Georgia was not evident in all *K* scenarios may be due to the small sample size of South Georgia (*n*=4) relative to remaining Antarctic samples. However, pairwise F_{st} analyses in Agla 1 only showed significant values when comparing South Georgia to other sampling sites, supporting the uniqueness of the *A. trissophyllus* collected from this site.

This finding builds on evidence that genetic isolation of the South Georgia and South Sandwich Islands Marine Protected Area (SGSSI-MPA, established in 2012) limits its role to protecting local biodiversity rather than that of the wider Southern Ocean, and questions its ability to export biodiversity to nearby ecosystems (Leiva et al., 2022). Notably, a single sample from Southern Thule, the southernmost island of the South Sandwich Islands, also within the SGSSI-MPA, was nested within the remaining Antarctic clades and genetic clusters in both barcode and ddRAD analyses. Unlike South Georgia, Southern Thule lies beyond the southern boundary of the Antarctic Circumpolar current (ACC) (Allen & Smellie, 2008) and other oceanographic features such as the Southern Antarctic Circumpolar Front (SACCF) (Thorpe et al., 2002), while also lying proximal to the Weddell Gyre, the latter a clockwise current that connects Weddell Sea shelf waters with the South Shetland islands and the South Sandwich Islands (Vernet et al., 2019). The relationship of these oceanographic features to southern areas of the SGSSI-MPA may allow for greater connectivity to the wider Southern Ocean, increasing conservation relevance, and warrants further exploration and sampling, particularly of the South Sandwich Islands and other sub-Antarctic regions to better test the effect of oceanographic features such as the ACC on gene flow.

Two other subclades (Clades 1a and 1b) were found amongst Agla 1 individuals in the phylogenetic and haplotype network analyses. These subclades were also identified in population genomic analyses using SNP data (DAPC, ADMIXTURE, and fineRADstructure) across all datasets (e.g. combined Agla 1 & Agla 2 analyses, and Agla 1 alone). However, no geographic structure was identified, with both genetic clusters present in many of the same sampling regions (e.g., Ross Sea, Western Weddell Sea), and low but non-significant F_{ST} values between most regions, and relatively little introgression between clusters.

A 2017 study of the ophiuroid *Ophionotus victoriae* using COI barcodes from samples collected primarily from West Antarctica found high genetic structuring, similar to haplotype analyses in the current study, with samples containing four distinct lineages and possibly multiple cryptic species in a species complex (Galaska et al., 2017a). However, a subsequent study (Lau et al., 2021) greatly increased the number of sampled individuals from 414 to 862, including poorly represented regions such as East Antarctica, to give a comprehensive circum-Antarctic sampling range. The COI results from Lau et al., (2021) found a single connected network rather than multiple haplotype clusters as found previously, with additional samples filling in intermediate haplotypes between clusters. In contrast, a similar effort to increase geographic sampling in order to assess cryptic diversity was carried out by Maroni et al. (2022), in which over 1000 new individuals of the Antarctic sea slug species complex *Doris kerguelenensis* were sampled from across the Southern Ocean, with COI data not only supporting previous findings of cryptic diversity, but discovering up to 27 new cryptic lineages.

Like Galaska et al. (2017a), our samples were mostly restricted to West Antarctica, with number of individuals between different sample sites relatively uneven, based on specimen availability in collections. For instance, areas such as the Amundsen Sea are not represented in Agla 1 specimens at all, likely due to a bias from sampling gear rather than reflecting a natural distributional pattern . During the BIOPEARL II (JR179) expedition to the region, only specimens collected by Epibenthic Sledge, which targets small (<1cm) macrofauna, were preserved in ethanol, while larger (>1cm) megafauna samples (including large nephtyids) collected by Agassiz Trawl were preserved in formalin, making DNA unavailable. The potential influence of such sampling gaps must be taken into account considering the findings of Lau et al. 2021 etc., and conclusions as to whether Agla 1 contains cryptic lineages is limited until more complete sampling is carried out. However, results of ddRAD analyses are still informative regarding genetic structure within Agla 1, particularly when compared with similar studies.

The *O. victoriae* samples as described above were also included in a subsequent ddRAD-based population genomic study (Lau et al., 2023a), finding a single circumpolar species with multiple intraspecific genetic clusters. South Georgia specimens are similarly distinct, with other Antarctic sites such as the Ross Sea and Western Weddell Sea also containing at least two discrete genetic clusters with little introgression. Though some geographic structuring is present, major genetic clusters have wide ranging and sympatric distributions. Similar to *A. trissophyllus, O. victoriae* has planktonic larvae, with modern gene flow patterns hypothesised to be the product of complex current systems of the of the Southern Ocean. For example, Ross Sea shelf waters are circulated by the Ross Gyre, which is in turn connected to the Antarctic Peninsula, Scotia Arc and Weddell Gyre by the Antarctic Circumpolar Current, potentially explaining genetic similarities between Ross and Weddell sea communities, as was observed in the present study.

Lau et al. (2023) also linked the presence of multiple genetic clusters to glacial history during glacial maxima, where grounded ice would have removed much of the available benthic shelf habitat (Anderson et al., 2002; Huybrechts, 2002). Deep-water samples of *O. victoriae* >1000m, exhibited a distinct demographic history from shallow continental shelf (<1000m) and Antarctic Island localities, hypothesised to be a result of differing survival strategies in deep water refugia versus ice-free shelf and island refugia during the Last Glacial Maximum (Lau et al. 2023a). Similarly, in the current study, DAPC (*K*=3) and co-ancestry analyses in the Agla 1 dataset (excluding South Georgia) found a third genetic cluster containing the majority of specimens below 1000m, forming a distinct genetic cluster from specimens collected at shallower depths from the same sampling region. Most of these specimens were collected from the Prince Gustav Channel (PGC) in the Western Weddell Sea, but also included samples from off Elephant Island and the South Orkneys.

If depth is an important factor, a lack of geographic structure as observed in genomic analyses may be expected, with some sample regions such as those listed above having large bathymetric ranges. Studies using both morphology and genetic means are beginning to find that depth is more of an important driver of Southern Ocean annelid community structure than previously thought (Neal et al., 2018; Schüller, 2011). Greater bathymetric coverage will also be necessary in future work in addition to statistical methods such as Analysis of Molecular Variance (AMOVA) (Excoffier & Lischer, 2010) to examine whether an effect of depth is present and to further explore possible links to survival strategies during glacial maxima.

5.4.2.2 Putative species Agla 2

In contrast to Agla 1 results, the high genetic structure observed in COI phylogenetic analyses for Agla 2 (Clade 2a and 2b) was not observed in ddRAD cluster or co-ancestry analyses. The results revealed a single homogenous genetic cluster, associated with panmixia, across sites for which Agla 2 was sampled, including a depth range spanning 193-1473m. This is despite individuals forming two polyphyletic clades with up to 12% interclade p-distance between individuals in COI analyses. Similar instances of mitonuclear discordance have been hypothesised to have been caused by ancestral isolation in multiple glacial refugia during glacial maxima, followed by range expansion and genomic homogenisation following ice retreat and secondary contact in Southern Ocean sea spiders (Dietz et al., 2014; Dömel et al., 2020) and notothenoid fishes (Ceballos et al., 2019), as well as in Palaearctic terrestrial systems (Ortiz et al., 2021 and references therein). However, the number of individuals for Agla 2 per sampling site was relatively low, with even less included in ddRAD analyses due to the failure of a library during sequencing containing mostly Agla 2 individuals. Sampling was therefore uneven, and interpretations limited without more comprehensive sampling.

5.4.3 Drivers of dispersal, isolation and evolution in Antarctic invertebrates

Drivers of biodiversity, distribution and connectivity are important for predicting impacts of future change and conservation strategies. To summarise, the results of this study present the first SNP level genomic investigation of an Antarctic annelid, giving further insight into the diversity patterns of species identified as *Aglaophamus trissophyllus* and demonstrating some of the complex factors that drive distributional patterns in modern Southern Ocean populations.

In the Southern Ocean, repeated vicariant events and reproductive isolation from repeated glacial cycles is thought to be a driver of speciation (Clarke & Crame, 1992). It is estimated that between 50-60 glacial-interglacial cycles may have occurred over the past 2.4 million years (Imbrie, 1984; Tiedemann et al., 1994) with the potential for massive diversification at multiple taxonomic levels (Wilson et al., 2009).

In this study, morphological similarity, phylogenetic closeness in both mitochondrial and nuclear genes, and evidence of introgression in a small number of individuals between putative species, may suggest a recent split between sister species. In addition, the apparent depth structuring with some introgression between major genetic clusters in Agla 1, and potential mitonuclear discordance in Agla 2 could suggest periods of genetic isolation in refugia and some secondary contact at the population level.

More comprehensive sampling is needed to resolve the true evolutionary and demographic histories of these taxa, however these results build on similar findings in other Antarctic invertebrates, and provide more robust insight in a comparative context where patterns are observed across multiple co-distributed taxa (Hickerson et al., 2010; Leiva et al., 2022). As discussed in above sections, a recent ddRADseq study of two closely related Antarctic ophiuroid species also found some introgression (i.e. gene flow) between *Ophionotus victoriae,* and *O. hexactis* despite clear morphological and reproductive differences (Lau et al., 2023a), with previous studies suggesting that the species diverged 1.64 million years ago during the Pleistocene (O'Hara et al., 2017), and morphological differences in *O. hexactis* linked to adaptation to shelf refugia (Lau et al., 2021), highlighting the dynamism and plasticity of speciation in the Southern Ocean.

Glacial history is only one of many drivers of biodiversity in the Southern Ocean. Invertebrate larvae have great dispersal potential around the continent by a complex network of currents, including the Antarctic Circumpolar Current (ACC), a coastal counter current (East Wind Drift), and Ross and Weddell Sea Gyres (Fahrbach et al., 1994; Linse et al., 2007; Orsi et al., 1993, 1995). Treating Agla 1 as *Aglaophamus trissophyllus* sensu Knox & Cameron (1998), this study confirms a widespread distribution in this species, with shared genetic clusters spanning from the Ross Sea and Balleny Islands to the Weddell Sea. Similar distributions have been recorded in other Antarctic SNP-based studies as in *Ophionotus victoriae* (Lau et al., 2023a), and the pycnogonid *Nymphon australe* Hodgson, 1902 (Collins et al., 2018), attributed to the ACC and regional gyres, even with differences in larval strategy. A SNP study of several Antarctic gastropod species also linked distribution patterns across the Weddell Sea and Scotia arc to the Weddell Gyre and other regional currents (Moles et al., 2021). The ACC further plays a role in isolating waters beyond its southern boundary, which may be reflected in the genetic isolation of South Georgia observed in this study and across both genetic and genomic investigations in other Southern Ocean species (Leiva et al., 2022).

Chapter 6 Synthesis and Conclusions

6.1 Thesis summary and implications

The overall aim of this thesis was to investigate biodiversity in Southern Ocean and deep-sea habitats across hierarchical levels using annelids as a model group. This aim was achieved through:

- Chapter 2: A description of a new species of deep-sea annelid, *Neanthes goodayi* Drennan, Wiklund, Rabone, Georgieva, Dahlgren & Glover, 2021 using morphological and molecular data, in a region of the central abyssal Pacific where seabed mining of polymetallic nodules may occur.
- Chapter 3: A faunistic study documenting the annelid community of a previously ice-covered and unsampled channel on the Antarctic Peninsula using morphological methods.
- Chapter 4: A study testing whether barcoding a subsample of representative morphospecies from the Prince Gustav Channel dataset significantly improves morphological species identifications in relation to species richness and diversity of the channel community.
- Chapter 5: A genomic-level investigation of phylogenetic diversity, population distribution and connectivity in the widespread Antarctic annelid, *Aglaophamus trissophyllus* (Grube, 1877) across much of its distributional range.

The scope of these data chapters ranged from species to the community level, from local to regional geographic scales, and utilised morphological, genetic, and genomic methods of measuring biodiversity. The results of these chapters, their context and broader research implications, in addition to a comparison of effectiveness and synergy across different methodological approaches, are synthesised in the following sections.

6.1.1 Integrative taxonomy and identification

The world is currently facing a taxonomic impediment. Of the estimated 15 million extant eukaryotic species on earth, only around 13% have been discovered and described (Mora et al., 2011; Zamani et al., 2021). Current estimates of the rate of annual species description (~18,000 species a year) are similar to estimates of annual rates of species loss and extinction (Zamani et al., 2021). This backlog and race against time is particularly acute for relatively unexplored regions such as parts of the Southern Ocean and the global deep sea, which face an increasing number of anthropogenic threats as introduced in Chapter 1. A lack of baseline taxonomic knowledge in these regions not only limits our ability to predict and manage environmental change, but also means that large portions of biodiversity could be lost before it is even documented.

Despite the advent of low-cost molecular methods, the majority of new species descriptions are still based on morphology only (Pante et al., 2015). Morphological descriptions take time, and have methodological caveats that include missing cryptic diversity, and unnecessarily splitting polymorphic, juvenile and reproductive forms. A minimalist DNA taxonomy approach, e.g. *sensu* Meierotto et al. (2019), whereby species are delimited and named based on COI barcodes only has been proposed as a method of rapidly speeding up the process of species description to address the taxonomic impediment. However, DNA-only methods also have a number of methodological issues (e.g. as discussed in Löbl et al., 2023; Zamani et al., 2022a, 2022b), with molecular methods also susceptible to lumping and splitting based on the thresholds used, the number of sequences, and geographic coverage. With DNA-only approaches, there is also a disconnection from past morphological taxonomic work and ecological data.

Integrative taxonomic methods that combine multiple lines of evidence (e.g. morphology and molecular, also ecological, behavioural etc.), are widely considered the most robust method of describing new species, but do not accelerate the rate of species description, at least in the short term (Pante et al., 2015). At present, the average description “shelf life” for a single marine species is 13.5 years from collection to publication (Bouchet et al., 2023), linked to increasing institutional and regulatory barriers to taxonomy (see Bouchet et al., 2023; Löbl et al., 2023). However, the results of Chapter 2 show the high value of taking the time to publish detailed integrative taxonomic descriptions, with implications reaching beyond the documentation of a single species.

In the description of *Neanthes goodayi* Drennan, Wiklund, Rabone, Georgieva, Dahlgren & Glover, 2021 from the Clarion-Clipperton Zone (CCZ), detailed morphological information and imagery is given not only for adult specimens, but juvenile and reproductive forms too, linking each to same taxon using DNA barcodes. Future ecological surveys of the CCZ, for example for environmental monitoring purposes, can therefore also link these different forms to the same species rather than falsely splitting as separate morphospecies if using morphology only.

The *in situ* imagery and ecological observations of *N. goodayi* inhabiting polymetallic nodules highlights the nodules as distinct microhabitats for mobile macrofauna within abyssal nodule habitat - an important consideration when evaluating the environmental impact of nodule removal and potential seabed mining in the region. Furthermore, *N. goodayi* is a relatively abundant and widespread annelid taxon in the CCZ, and therefore may be a suitable candidate for population genetics. Sequence data from Chapter 2 has already been utilised in a large-scale barcode study of biodiversity, biogeography and connectivity patterns in the eastern CCZ polychaetes (Stewart et al., 2023). At the time of writing this conclusion, the paper published from this chapter (Drennan et al., 2021) has been cited by 12 peer reviewed publications (including Stewart et al. 2023), one doctoral thesis and one cruise report (via Google Scholar search). Notably, sequence data from Chapter 2 has been used in integrative taxonomic descriptions of several new nereid species (Bergamo et al., 2023; Georgieva et al., 2023; Mahcene et al., 2023), in addition to a phylogenetic revision of the genus *Neanthes* (Villalobos-Guerrero et al., 2022) and the family Nereididae (Alves et al., 2023) highlighting the use of integrative descriptions beyond the documentation of the species itself and inferences on local ecology.

At the level of community, however, an integrative approach becomes more challenging regarding time and resource constraints. A “turbo taxonomy” approach, whereby DNA is used as the primary method of species classification and delimitation, followed by morphological information as proposed by Glover et al. 2016), still requires sequencing of all individuals, and the associated time, resources, and bioinformatic processing. In the case of the Prince Gustav Channel, of which very little of the biology was known beforehand, the morphospecies approach taken in Chapter 3 and tested in Chapter 4 still provided valuable insights into the biodiversity of this channel, presenting a baseline documentation of its benthic annelid fauna, and highlighting a taxonomically and functional variable community driven by fine scale habitat heterogeneity. This implies that for broad-scale estimates of diversity, morphological identification still has value in ecological assessments.

A closer look at the results of Chapter 4 reveals the complex and case-by-case nature of species delimitation and shows that subsample level of barcode data simply does not provide the resolution required for delimiting species with confidence, although it can highlight potential cryptic diversity for future investigation. Regarding identification, a subsample of barcodes did aid in improving some identifications (particularly of damaged specimens) and in general as an error check. Had online repositories been more comprehensive and better curated, the integrative approach tested in Chapter 4 could have been more effective, as only a fraction of named species identified in this study were represented on GenBank. The value of curated reference sequences was apparent in the case study of *Maldane sarsi* Malmgren, 1865 in Chapter 4, where comparison with sequence data from type localities provided a relatively straightforward method of testing whether this European taxon is present in Antarctic waters.

This highlights the need for sequencing wherever quality morphological work is taking place, even if at a subsample level, to improve the coverage of reference libraries, and will streamline integrative methods of identification in the future. In addition, curated reference libraries will facilitate metabarcoding methods capable of identifying taxa beyond molecular taxonomic operational units, which could allow for biodiversity assessments at much greater scales. Technological advances in barcode sequencing in terms of speed, economy, and portability, for example such as the portable MinION (Srivathsan et al., 2021) may be key to reducing the resource bottleneck of barcode sequencing at large scales to build these libraries.

6.1.2 Genetic versus genomic methods

Population genomic methods in general offer much higher resolutions than population genetic analyses based on single mitochondrial or few nuclear genes and can combat methodological caveats such as incomplete lineage sorting and mitonuclear discordance. For example, in the case of the putative species “Agla 2” in Chapter 5, two potentially cryptic lineages were found in COI data (also identified as Aglaophamus MB2 and MB3 in Brasier et al., 2016), yet this genetic structure was not reflected in genomic data. This may also have implications for delimitation decisions in Chapter 4. Yet, interpretations of results from Chapter 5 were still limited, and a key takeaway is that genomic methods such as ddRADseq are not a magic bullet for resolving questions of diversity and population structure in annelids. Furthermore, though genomic sequencing advances have been made in recent years in terms of reducing cost (ddRADseq an example of this), it can still be prohibitively expensive for some projects and is also time-consuming at both the library preparation and bioinformatic stages, in addition to requiring substantial computational and digital storage capacity.

Genomic methods in general are well developed for model organisms, though less so for non-model species, as in this study, and for marine invertebrates in general. For example, no reference genome was available for nephtyid annelids. With a reference genome, enzyme combinations might be tested *in silico* to identify optimal cutting enzymes providing better SNP coverage and resolution across the genome in the ddRAD method. A reference genome also allows for estimations of mutation rate, which could be used to assess when phylogenetic divergences took place in a temporal context (e.g. Kim et al., 2019) and could be linked to known climatic and geological events. Furthermore, a lack of reference genome or transcriptomic data limits the ability to study adaptation, for example what genes are being selected for across populations, which can then be linked to environmental factors and give insight into evolutionary drivers (e.g. Leiva et al. 2019).

In addition to a push for whole genome sequencing of Antarctic and deep-sea invertebrates wherever possible, advances in alternative genomic methods may also be more informative for developing our understanding of mechanisms involved in dynamic environments such as the Southern Ocean. One example is a recent study using different genomics tools (e.g., Oxford Nanopore Technology and transcriptomics) to identify signatures of DNA methylation (epigenetic alteration to DNA sequences) in hydrothermal vent annelids (Perez et al., 2023). While DNA methylation is poorly studied in marine invertebrates, the results of this study suggested that it plays a key role in adaptation of these species to extreme hydrostatic pressure and can provide insights on environmental stressors and drivers.

The results of Chapter 5 are still notable in supporting growing evidence for the genetic isolation of South Georgia across several invertebrate species and confirming that *A. trissophyllus* is a widespread Antarctic taxon. This study also highlights need for taxonomic revision of Antarctic *Aglaophamus* species, demonstrating the need for integrative approach even in the genomic era. Further analyses will be carried out on data generated in this chapter, including parameter optimisation tests for the bioinfomatic pipeline used, implementation of migration models (e.g divMigrate), and phylogenomic analyses for more conclusive delineation of putative species, with the aim to publish results.

Finally, both genetic and genomic methods were limited by sample number and geographic coverage, stressing the importance of collaborative efforts in the future to maximise coverage in this kind of investigation. In Chapter 5, the sample coverage was only possible through collaboration with the National Institute of Water and Atmosphere (NIWA) and the University of Hawaii (UH).

6.1.3 Broader implications for the Southern Ocean

Chapters using samples from the Prince Gustav Channel (PGC) build on a suite of recent published work documenting its benthic biology, including *in situ* image analysis of habitat heterogeneity (Almond et al., 2021), and patterns of abundance and diversity in nematodes (Pantó et al., 2021), molluscs (Anderson et al., 2021) and peracarid crustaceans (Di Franco et al., 2020, 2021). These works give important first insights into the benthic communities established following the retraction of the Prince Gustav Ice sheet. In a study of molluscan diversity patterns in the PGC and broader Weddell Sea, Anderson et al. (2021) found that the PGC is still undergoing colonisation, 20 years since ice shelf collapse. In this thesis, both *Maldane sarsi* and *Aglaophamus trissophyllus* populations displayed depth structuring in the PGC, which could suggest a possible older deep-channel sub-ice population, and a newer, colonising shallow population and is worth further exploration. With sobering recent projections for substantial ice loss and warming for regions of the Southern Ocean in all future climate scenarios (Naughten et al., 2023), present day PGC communities may provide a snapshot into future Antarctic shelf environments following ice shelf collapse. Baseline biodiversity measures, samples and sequences from the PGC therefore, present valuable datasets for future research in this context.

6.2 Conclusions

With a growing urgency to document biodiversity across marine habitats, it is clear that different methods vary in strengths depending on the question asked, taxonomic level required, and resources available. Advances in molecular methods present many new tools for species identification and delimitation and may provide better resolution at population and evolutionary levels, but still face many practical and methodological limitations. An integrative approach using as many data streams as possible remains important, crucial for linking ecological, morphological, physiological, genetic information to the same taxonomic units, and will be vital for building foundations for more streamlined molecular methods in the future.

Appendices

Appendix A Chapter 2 supplementary materials

A.1 Material examined

A.1.1 Holotype

PACIFIC OCEAN • Eastern Central Pacific, Clarion Clipperton Fracture Zone; 12.53717° N, 116.60417° W; depth 4425 m; 20 Feb. 2015; A.G. Glover, H. Wiklund, T. Dahlgren and M. Brasier leg.; Brenke epibenthic sled, collected from epi-net; specimen guid: 21b3d59f-5ec4-40da-9d65-4177e7674f63, field ID: NHM_739, DNA voucher barcode: 0109493268, GenBank COI gene: MZ407918; NHMUK ANEA 2020.260.

A.1.2 Paratypes

PACIFIC OCEAN – **Eastern Central Pacific, Clarion Clipperton Fracture Zone** • 1 spec.; 13.75833° N, 116.69852° W; depth 4080 m; 11 Oct. 2013; A.G. Glover, H. Wiklund, T.G. Dahlgren and M.N. Georgieva leg.; Brenke epibenthic sled, collected from epi-net; specimen guid: 2d448c5f-bf70-4ed1-a541-9b505ec46434, field ID: NHM_127, DNA voucher barcode: 0109492959, GenBank 16S gene: MZ408645; NHMUK ANEA 2020.33 • 1 spec.; 13.93482° N, 116.55018° W; depth 4082 m; 14 Oct. 2013; same collectors and collection method as for preceding; specimen guid: f5f08fc7-49b4-446f-9f04-fbbca84f7886, field ID: NHM_171, DNA voucher barcode: 0109492952, GenBank 18S gene: MZ408643, 16S gene: MZ408646, COI gene: MZ407911; NHMUK ANEA 2020.34 • 1 spec.; 13.81167° N, 116.71° W; depth 4076 m; 16 Oct. 2013; same collectors as for preceding; USNEL box corer, collected from 0–2 cm fraction; specimen guid: fb66da6c-f627-487f-a386-3454541ad33a, field ID: NHM_238, DNA voucher barcode: 0109493276, GenBank 16S gene: MZ408648, COI gene: MZ407913; NHMUK ANEA 2020.36 • 1 spec.; 12.41628° N, 116.71485° W; depth 4127 m; 16 Feb. 2015; A.G. Glover, H. Wiklund, T.G. Dahlgren and M. Brasier leg.; USNEL box corer, collected from nodule; specimen guid: e1461d7d-c6c8-46fc-b951-f5ee88550a5b, field ID: NHM_512, DNA voucher barcode: 0109493273, GenBank 16S gene: MZ408651; NHMUK ANEA 2020.1 • 1 spec.; 12.53717° N, 116.60417° W; depth 4425 m; 20 Feb. 2015; same collectors as for preceding; Brenke epibenthic sled, collected from epi net; specimen guid: 0d2be1b6-4348-46a2-a1a7-b214562c7b18; field ID: NHM_790, DNA voucher barcode: 0109493261, GenBank 16S gene: MZ408660; NHMUK ANEA 2020.7 • 1 spec.; 12.25733° N, 117.30216° W; depth 4302 m; 1 Mar. 2015; same collectors and collection method as for preceding; specimen guid: bb93253e-2d66-4592-b569-cfa5976fed33, field ID: NHM_1254, DNA voucher barcode: 0109493252, GenBank 16S gene: MZ408667; NHMUK ANEA 2020.17 • 1 spec.; 12.59688° N, 116.49357° W; depth 4258 m; 9 Mar. 2015; same collectors as for

preceding; USNEL box corer, collected from nodule; specimen guid: 333370c7-eb36-429c-96ed-fce5658f2ad2, field ID: NHM_1624, DNA voucher barcode: 0109493249, GenBank 16S gene: MZ408670; NHMUK ANEA 2020.20 • 1 spec.; 12.17383° N, 117.19283° W; depth 4045 m; 11 Mar. 2015; same collectors as for preceding; Brenke epibenthic sled, collected from epi-net; specimen guid: 6d7f58fc-a657-47f4-9261-7517228de6a1, field ID: NHM_1783, DNA voucher barcode: 0109493246, GenBank 16S gene: MZ408673, COI gene: MZ407927; NHMUK ANEA 2020.23 • 1 spec.; 12.02738° N, 117.3252° W; depth 4139 m; 17 Mar. 2015; same collectors as for preceding; USNEL box corer, collected from nodule; specimen guid: 8abc43ad-193d-4e35-b548-6d2d0b7777f8, field ID: NHM_2069, DNA voucher barcode: 0109493237, GenBank 16S gene: MZ408681; NHMUK ANEA 2020.31.

A.1.3 Other material

PACIFIC OCEAN – **Eastern Central Pacific, Clarion Clipperton Fracture Zone** • 1 spec.; 13.93482° N, 116.55018° W; depth 4082 m; 14 Oct. 2013; A.G. Glover, H. Wiklund, T.G. Dahlgren and M.N. Georgieva leg.; Brenke epibenthic sled, collected from epi-net; specimen guid: 022c1d2a-8b2a-479f-8ed2-20ff4e9610dd, field ID: NHM_173, DNA voucher barcode: 0109493277, GenBank 18S gene: MZ408644, 16S gene: MZ408647, COI gene: MZ407912; NHMUK ANEA 2020.35 • 1 spec.; 13.81167° N, 116.71° W; depth 4076 m; 16 Oct. 2013; same collectors as for preceding; USNEL box corer, collected from 0–2 cm fraction; specimen guid: 57002bc8-fa3a-4a55-b823-0af978cd2fcd, field ID: NHM_239, DNA voucher barcode: 0109493275, GenBank 16S gene: MZ408649, COI gene: MZ407914; NHMUK ANEA 2020.37 • 1 spec.; same collection data as for preceding; specimen guid: 4a8718c5-d675-4044-9d2b-613f1d8d5fda, field ID: NHM_240, DNA voucher barcode: 0109493274, GenBank 16S gene: MZ408650, COI gene: MZ407915; NHMUK ANEA 2020.38 • 1 spec.; 12.38624° N, 116.54867° W; depth 4202 m; 17 Feb. 2015; A.G. Glover, H. Wiklund, T.G. Dahlgren and M. Brasier leg.; Brenke epibenthic sled, collected from epi-net; specimen guid: f61f9136-a39a-4696-8fdc-68aee0af5101, field ID: NHM_614, DNA voucher barcode: 0109493272, GenBank 16S gene: MZ408652, COI gene: MZ407916; NHMUK ANEA 2020.2 • 1 spec.; same collection data as for preceding; specimen guid: 1033aa6b-4093-41fc-af75-9ad090dd4c56, field ID: NHM_644, DNA voucher barcode: 0109493271, GenBank 16S gene: MZ408653, COI gene: MZ407917; NHMUK ANEA 2020.257 • 1 spec.; 12.53717° N, 116.60417° W; depth 4425 m; 20 Feb. 2015; same collectors and collection method as for preceding; specimen guid: 9a97230a-4b78-4823-88a5-d02d9c874db9; field ID: NHM_678, DNA voucher barcode: 0109493270, GenBank 16S gene: MZ408654; NHMUK ANEA 2020.258 • 1 spec.; same collection data as for preceding; specimen guid: 954c9c61-3e45-45a4-8522-7aadd1c86c60; field ID: NHM_692, DNA voucher barcode: 0109493269, GenBank 16S gene: MZ408655; NHMUK ANEA 2020.259 • 1 spec.; same collection data as for preceding; specimen guid: 76f62614-0cae-4177-8312-e231f5107f8c; field ID: NHM_743, DNA voucher barcode: 0109492976,

GenBank 16S gene: MZ408656; NHMUK ANEA 2020.261 • 1 spec.; same collection data as for preceding; specimen guid: 3951d751-f1ba-44ae-8368-261047c07b12; field ID: NHM_755, DNA voucher barcode: 0109493257, GenBank COI gene: MZ407919; NHMUK ANEA 2020.3 • 1 spec.; same collection data as for preceding; specimen guid: 67a9133b-c57b-49c6-b6e4-124eb1315eac; field ID: NHM_757, DNA voucher barcode: 0109493258, GenBank 16S gene: MZ408657; NHMUK ANEA 2020.4 • 1 spec.; same collection data as for preceding; specimen guid: b13dc262-c631-44dc-927e-6a04c3608bda; field ID: NHM_766, DNA voucher barcode: 0109493259, GenBank 16S gene: MZ408658; NHMUK ANEA 2020.5 • 1 spec.; same collection data as for preceding; specimen guid: d9e557c5-3ffd-4a39-9eed-5ecead5e735f; field ID: NHM_783A, DNA voucher barcode: 0109493260, GenBank 16S gene: MZ408659; NHMUK ANEA 2020.6 • 1 spec.; same collection data as for preceding; specimen guid: 792a4c9a-9653-4ce1-8683-ca2556c1999a8; field ID: NHM_793, DNA voucher barcode: 0109493262, GenBank COI gene: MZ407920; NHMUK ANEA 2020.8 • 1 spec.; 12.57903° N, 116.68697° W; depth 4237 m; 22 Feb. 2015; same collectors as for preceding; USNEL box corer, collected from 0–2 cm fraction; specimen guid: a933dd63-64d1-4e45-95ad-7d68282dd892; field ID: NHM_865, DNA voucher barcode: 0109493263, GenBank COI gene: MZ407921; NHMUK ANEA 2020.9 • 1 spec.; 12.57133° N, 116.6105° W; depth 4198 m; 23 Feb. 2015; same collectors as for preceding; Brenke epibenthic sled, collected from epi-net; specimen guid: 3e7262c7-fd75-4a53-9d6c-9d01955d1bef; field ID: NHM_950, DNA voucher barcode: 0109493264, GenBank 16S gene: MZ408661, COI gene: MZ407922; NHMUK ANEA 2020.10 • 1 spec.; same collection data as for preceding; specimen guid: 06c15319-2b89-4899-b2e5-1fcd8e4a9413; field ID: NHM_971, DNA voucher barcode: 0109493265, GenBank COI gene: MZ407923; NHMUK ANEA 2020.11 • 1 spec.; 12.13367° N, 117.292° W; depth 4122 m; 24 Feb. 2015; same collectors and collection method as for preceding; specimen guid: 165a459f-8b81-4e97-8e82-cdcd013e1ed1; field ID: NHM_1011, DNA voucher barcode: 0109493266, GenBank 16S gene: MZ408662, COI gene: MZ407924; NHMUK ANEA 2020.12 • 1 spec.; 12.1155° N, 117.1645° W; depth 4100 m; 26 Feb. 2015; same collectors and collection method as for preceding; specimen guid: a343e242-410a-4817-98c6-7125db7d03e7; field ID: NHM_1079, DNA voucher barcode: 0109493267, GenBank 16S gene: MZ408663; NHMUK ANEA 2020.13 • 1 spec.; same collection data as for preceding; specimen guid: 7ead0546-d0bd-4381-83af-89f58d8f8f4c; field ID: NHM_1167A, DNA voucher barcode: 0109492975, GenBank 16S gene: MZ408664; NHMUK ANEA 2020.14 • 1 spec.; same collection data as for preceding; specimen guid: 6b51d602-83f1-4bb4-b71a-e85cdbcbe8dc; field ID: NHM_1171, DNA voucher barcode: 0109493254, GenBank 16S gene: MZ408665, COI gene: MZ407925; NHMUK ANEA 2020.15 • 1 spec.; 12.00945° N, 117.17812° W; depth 4144 m; 27 Feb. 2015; same collectors as for preceding; USNEL box corer, collected from nodule; specimen guid: 9e903864-55e8-4a1a-b532-c47af39b95f4; field ID: NHM_1194, DNA voucher barcode: 0109493253, GenBank 16S gene: MZ408666; NHMUK ANEA 2020.16 • 1 spec.; 12.45433° N, 116.61283° W; depth 4137 m; 3 Mar. 2015; same collectors as for preceding; Brenke epibenthic sled, collected from epi-net; specimen

guid: e5797775-7141-4eb5-bb5e-dbcb29f7b42e; field ID: NHM_1480E, DNA voucher barcode: 0109493251, GenBank 16S gene: MZ408668; NHMUK ANEA 2020.18 • 1 spec.; 12.51317° N, 116.49133° W; depth 4252 m; 5 Mar. 2015; same collectors and collection method as for preceding; specimen guid: 35bae0ad-f00e-442b-a8f5-b1b318bf1015; field ID: NHM_1515, DNA voucher barcode: 0109493250, GenBank 16S gene: MZ408669, COI gene: MZ407926; NHMUK ANEA 2020.19 • 1 spec.; 12.59688° N, 116.49357° W; depth 4258 m; 9 Mar. 2015; same collectors as for preceding; USNEL box corer, collected from nodule; specimen guid: 29f1c1bf-5bca-4ed1-a893-edcd45493e04; field ID: NHM_1631A, DNA voucher barcode: 0109493248, GenBank 16S gene: MZ408671; NHMUK ANEA 2020.21 • 1 spec.; 12.17383° N, 117.19283° W; depth 4045 m; 11 Mar. 2015; same collectors as for preceding; Brenke epibenthic sled, collected from epi-net; specimen guid: 83507a57-c168-4b6f-b984-1c69ccbebc27; field ID: NHM_1764, DNA voucher barcode: 0109493247, GenBank 16S gene: MZ408672; NHMUK ANEA 2020.22 • 1 spec.; 12.0999° N, 117.1966° W; depth 4051 m; 12 Mar. 2015; same collectors as for preceding; USNEL box corer, collected from 0–2 cm fraction; specimen guid: f79fb7b6-ed29-4cc3-9f7f-8d4ace75c585; field ID: NHM_1836A, DNA voucher barcode: 0109493245, GenBank 16S gene: MZ408674; NHMUK ANEA 2020.24 • 1 spec.; 12.0415° N, 117.21717° W; depth 4094 m; 13 Mar. 2015; same collectors as for preceding; Brenke epibenthic sled, collected from epi-net; specimen guid: 0508d326-ef73-4f52-bdc6-757b2ab745fe; field ID: NHM_1866, DNA voucher barcode: 0109492983, GenBank 16S gene: MZ408675, COI gene: MZ407928; NHMUK ANEA 2020.25 • 1 spec.; same collection data as for preceding; specimen guid: 922ad1d7-bd75-4588-ba2e-be32cfe432c5; field ID: NHM_1891, DNA voucher barcode: 0109492960, GenBank 16S gene: MZ408676; NHMUK ANEA 2020.26 • 1 spec.; same collection data as for preceding; specimen guid: e991eafe-0593-4e08-8967-d77e017eabac; field ID: NHM_1929A, DNA voucher barcode: 0109493233, GenBank 16S gene: MZ408677, COI gene: MZ407929; NHMUK ANEA 2020.27 • 1 spec.; same collection data as for preceding; specimen guid: 62b28de1-a797-4ec0-99cf-e38625b0e01c; field ID: NHM_1929B, DNA voucher barcode: 0109493234, GenBank 16S gene: MZ408678; NHMUK ANEA 2020.28 • 1 spec.; same collection data as for preceding; specimen guid: 25953aef-8a48-48d1-9fc2-b0a86ec7d052; field ID: NHM_1947D, DNA voucher barcode: 0109493235, GenBank 16S gene: MZ408679; NHMUK ANEA 2020.29 • 1 spec.; 12.0505° N, 117.40467° W; depth 4235 m; 16 Mar. 2015; same collectors and collection method as for preceding; specimen guid: d8edb41d-51d6-4fbd-a547-92fa290209d4; field ID: NHM_2014, DNA voucher barcode: 0109493236, GenBank 16S gene: MZ408680, COI gene: MZ407930; NHMUK ANEA 2020.30 • 1 spec.; 12.57133° N, 116.6105° W; depth 4198 m; 23 Feb. 2015; same collectors as for preceding; Brenke epibenthic sled, collected from supra-net; specimen guid: 1c30624d-19a0-43f0-92dc-9a315a3e43fc; field ID: NHM_3074, DNA voucher barcode: 0109493238, GenBank 16S gene: MZ408682; NHMUK ANEA 2020.32.

A.2 Acknowledgements

The UK Seabed Resources ABYSSLINE (ABYSSal baseLINE) environmental surveys were supported by a collaborative partnership between six non-profit global academic research institutes (University of Hawaii at Manoa, Natural History Museum, NORCE Norwegian Research Centre, National Oceanography Centre, Senckenberg Institute and Heriot-Watt University) and through an arrangement with UKSRL (UK Seabed Resources Ltd.). Additional support was provided by the Swedish research council FORMAS (TGD). We acknowledge Madeleine Brasier from the Natural History Museum team and Swee Cheng Lim from the National University of Singapore for support with sorting and sampling on board ship, and Chief Scientist Craig R. Smith for organizing the project and leading the sampling program. We also acknowledge the expert support from the Senckenberg Institute team in the deployment and recovery of successful Brenke epibenthic sledge samples. This study was made possible only by the dedicated help of the entire scientific party, the masters and crew of the RV Melville during the first cruise of the ABYSSLINE project in October 2013 and the masters and crew of the RV Thomas G. Thompson during the second ABYSSLINE cruise in February and March 2015. We sincerely thank reviewers for their effort in providing detailed comments and suggestions, which helped improve and clarify this manuscript. RD would like to thank and acknowledge support from the NERC INSPIRE DTP for the time needed to complete the manuscript. Thank you also to Emma Sherlock, Senior Curator of Annelida, Jackie Mackenzie-Dodds at the Molecular Collection Facility, and Harry Rousham and Robyn Fryer, Consultancy Group, all at the Natural History Museum.

Appendix B Chapter 3 supplementary materials

B.1 Acknowledgements

This work was supported by the National Environment Research Council grants: RD has support by the NERC INSPIRE DTP (NE/S007210/1). KL is part of the British Antarctic Survey's Polar Science for Planet Earth Programme (NC-Science). TD was funded by the Norwegian Research Centre NORCE and the RSS James Clark Ross expedition JR17003a was funded by the NERC urgency grant NE/R012296/1 and enabled the participation of KL, AG, and TD.

We would like to thank the Master and crew of RRS James Clark Ross and the scientific and technical participants of JR17003a for their support. Special thanks to Simon Dreuter for providing the bathymetric map. A special thank you also to Anton Van de Putte for their great assistance and guidance throughout the process of publishing data through biodiversity.aq. The fieldwork in the western Weddell Sea during JR17003a was undertaken under the permit No. 43/2017 issued by the Foreign and Commonwealth Office, London to section 3 of the Antarctic Act 1994.

Appendix C Chapter 4 supplementary materials

C.1 Tables

Table C.1 Primers used for PCR and sequencing for all material newly sequenced in Chapter 4

Gene	Primer	Sequence 5′–3′	Reference
16S	16SarL	CGCCTGTTTATCAAAAACAT	Palumbi (1996)
	16SbrH	CCGGTCTGAACTCAGATCACGT	Palumbi (1996)
	Ann16SF	GCGGTATCCTGACCGTRCWAAGGTA	Sjölin et al. (2005)
	Ann16SR	TCCTAAGCCAACATCGAGGTGCCAA	Sjölin et al. (2005)
18S	18SA	AYCTGGTTGATCCTGCCAGT	Medlin et al. (1988)
	18SB	ACCTTGTTACGACTTTTACTTCCTC	Nygren and Sundberg (2003)
	620F	TAAAGYTGYTGCAGTTAAA	Nygren and Sundberg (2003)
	1324R	CGGCCATGCACCACC	Cohen et al. 1998
COI	HCO2198	TAAACTTCAGGGTGACCAAAAAATCA	Folmer et al. (1994)
	LCO1490	GGTCAACAAATCATAAAGATATTGG	Folmer et al. (1994)
	polyLCO	GAYTATWTTCAACAAATCATAAAGATATTGG	Carr et al. (2011)
	polyHCO	TAMACTTCWGGGTGACCAAARAATCA	Carr et al. (2011)
	COIE	CCAGAGATTAGAGGGAATCAGTG	Palumbi et al. (1991)

Table C.2 List of GenBank sequence accession numbers for Maldanidae and outgroup specimens included in phylogenetic analyses focusing on *Maldane sarsi*

Taxon	Locality	Reference	16S	COI	18S
Abarenicola affinis (outgroup)	-	Bleidorn et al. 2005	AY569687	-	AY569661
Arenicola marina (outgroup)	-	Pieres & Fieres 2014	KM042095	KM042098	AF508116
Asychis cf. *auritus* GK-2017 GK117	Japan	Kobayashi et al. 2018	LC365928	LC342631	LC366931
Cf. *Petaloclymene* sp. GK-2017 GK4	Japan	Kobayashi et al. 2018	LC365946	LC342658	LC366958
Clymenella collaris GK6	Japan	Kobayashi et al. 2018	LC365948	LC342660	LC366960
Clymenopsis sp. 1 GK-2017 GK85	Japan	Kobayashi et al. 2018	LC365961	LC342673	LC366974
Clymenura clypeata 16S	France	Rousset et al. 2007	AY340449	-	AY340423
Euclymene cf. *oerstedii* GK-2017 GK63	Japan	Kobayashi et al. 2018	LC365949	LC342661	LC366961,
Euclymeninae sp. 1 GK-2017 GK51	Japan	Kobayashi et al. 2018	LC365947	LC342659	LC366959
Leiochone japonica GK78	Japan	Kobayashi et al. 2018	LC365957	LC342669	LC366969
Lumbriclymeninae sp. 1 GK-2017 GK210	Japan	Kobayashi et al. 2018	LC365940	LC342645	LC366945
Maldane cf. cristata GK-2017 GK79	Japan	Kobayashi et al. 2018	LC365958	LC342670	LC366970
Maldane cf. *pigmentata* GK-2017 GK67	Japan	Kobayashi et al. 2018	LC365951	LC342663	LC366963
Maldane cf. *sarsi* GK-2017 GK15	Japan	Kobayashi et al. 2018	LC365935	LC342639	LC366939
Maldane sarsi	Santa Monica Bay, CAL, USA	Bleidorn et al. 2005	AY569681	-	AY569655
Maldane sarsi antarctica isolate MB257	Antarctica	Brasier et al. 2016	KX867345	-	-
Maldane sarsi antarctica isolate MB367	Antarctica	Brasier et al. 2016	KX867346	-	-
Maldane sarsi CMC01 voucher TBLABR-054	Newfoundland & Labrador, Canada	Carr et al. 2011	-	HQ023885	-
Maldane sarsi CMC02 voucher BIOUG:NUNAV-0092	Nunavut, Canada	Carr et al. 2011	-	HQ024362	-
Maldane sarsi CMC02 voucher BIOUG:WS0089	Kandalashka Bay, Russia	Hardy et al. 2011	-	GU672596	-
Maldane sarsi CMC02 voucher BIOUG:WS0115	Kandalashka Bay, Russia	Hardy et al. 2011	-	GU672576	-
Maldane sarsi CMC02 voucher BIOUG:WS0122	Kandalashka Bay, Russia	Hardy et al. 2011	-	GU672571	-
Maldane sarsi CMC02 voucher WS0092	Kandalashka Bay, Russia	Hardy et al. 2011	-	GU672597	-
Maldane sarsi voucher BIOUG06837-H08	Newfoundland & Labrador, Canada	Deeward 2017	-	MG421523	-
Maldane sarsi voucher JEC-08-19a	Norwegian Sea	Hestetun. 2022	-	OQ053050	OQ071256
Maldane sp. 1 GK-2017 GK72	Japan	Kobayashi et al. 2018	LC365952	LC342665	LC366965
Maldane sp. 2 GK157	Japan	Kobayashi et al. 2018	-	LC342640	LC366940
Maldanella cf. *robusta* GK-2017 GK18	Japan	Kobayashi et al. 2018	LC365939	LC342644	LC366944
Metasychis cf. *disparidentata* GK-2017 GK1	Japan	Kobayashi et al. 2018	LC365927	LC342630	LC366930
Nicomache cf. *lumbricalis* GK-2017 GK75	Japan	Kobayashi et al. 2018	LC365954	LC342667	LC366967
Notoproctus sp. GK-2017 GK317	Japan	Kobayashi et al. 2018	LC365969	LC342652	LC366952
Petaloproctus dentatus GK164	Japan	Kobayashi et al. 2018	LC365936	LC342641	LC366941
Praxillella cf. *gracilis* 1 GK-2017 GK3	Japan	Kobayashi et al. 2018	LC365945	LC342650	LC366950
Praxillura sp. 1 GK-2017 GK77	Japan	Kobayashi et al. 2018	LC365955	LC342668	LC366968
Rhodine sp. 1 GK-2017 GK134	Japan	Kobayashi et al. 2018	LC365932	LC342636	LC366936

C.2 Figures

Figure C.1 Phylogenetic tree of Prince Gustav Channel morphospecies using Bayesian analysis of 16S RNA gene. Bayesian posterior probability values are given as support.

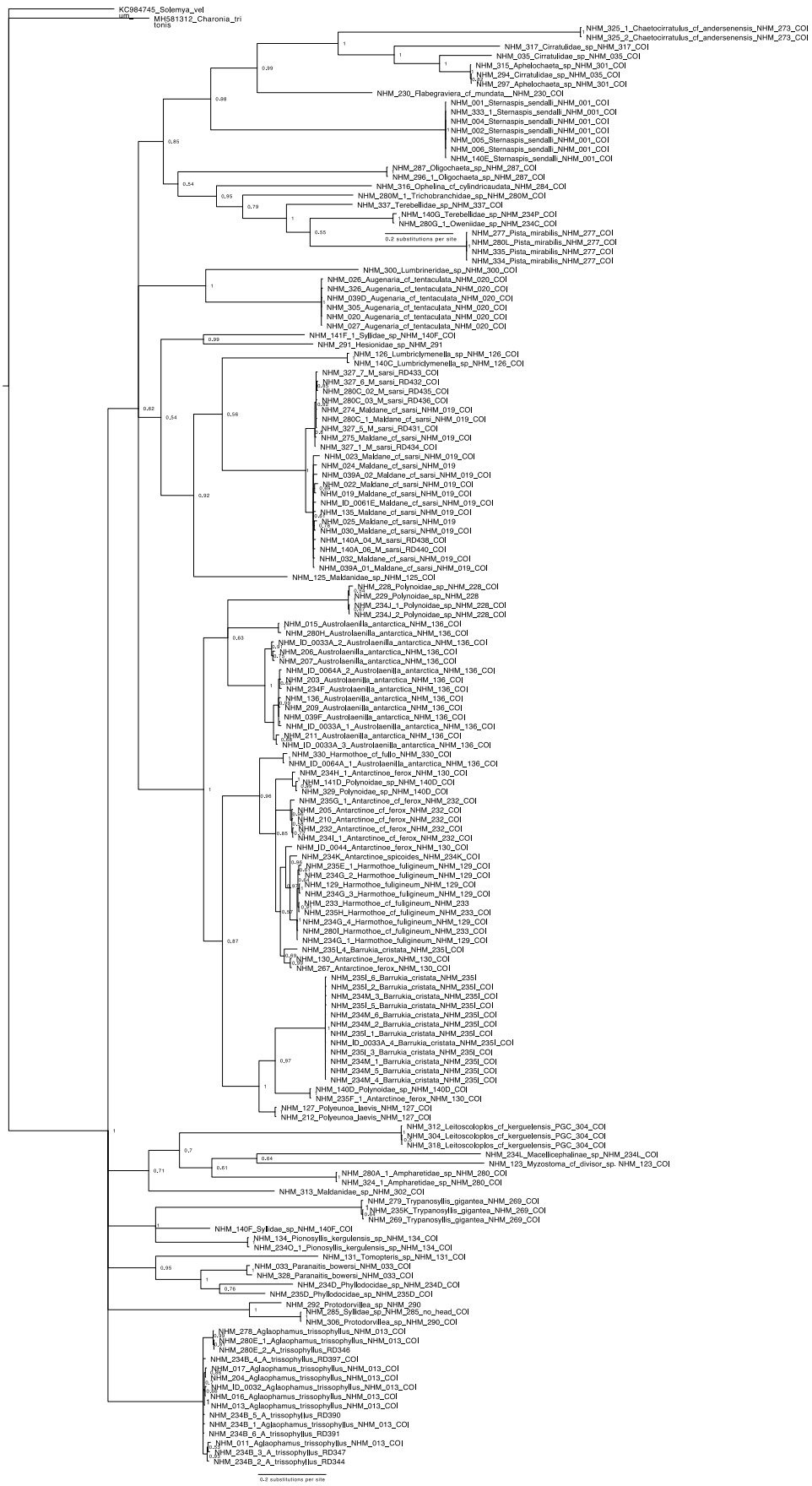

Figure C.2 Phylogenetic tree of Prince Gustav Channel morphospecies using Bayesian analysis of Cytochrome Oxidase Subunit I (COI) gene. Bayesian posterior probability values are given as support

Appendix D Chapter 5 supplementary materials

D.1 Tables

Table D.1 Additional collection data for *Aglaophamus* specimens investigated in Chapter 5

Molecular specimen ID	Record number	Event ID	Event date	Sampling protocol	Expedition	Project	institution
Agla1_Scot_EI_M_RD375	EI-AGT-2_MB274	EI-AGT-2	12/03/2006	Agassiz Trawl	RSS James Clark Ross JR144	BIOPEARL I	NHMUK
Agla1_Scot_KG_S_RD341	KGI_RBOT_1	KGI_RBOT	11/03/2006	Otter Trawl	RSS James Clark Ross JR144	BIOPEARL I	NHMUK
Agla1_Scot_LI_S_RD352	LI_AGT_4_1	LI_AGT_4	04/03/2006	Agassiz Trawl	RSS James Clark Ross JR144	BIOPEARL I	NHMUK
Agla1_Scot_LI_S_RD354	LI_AGT_4b_06	LI_AGT_4b	04/03/2006	Agassiz Trawl	RSS James Clark Ross JR144	BIOPEARL I	NHMUK
Agla1_Scot_LI_S_RD355	LI_AGT_4b_08	LI_AGT_4b	04/03/2006	Agassiz Trawl	RSS James Clark Ross JR144	BIOPEARL I	NHMUK
Agla1_Scot_LI_S_RD373	LI-AGT-4_MB268	LI-AGT-4	04/03/2006	Agassiz Trawl	RSS James Clark Ross JR144	BIOPEARL I	NHMUK
Agla1_Scot_LI_S_RD376	LI-AGT-4b_MB279	LI_AGT_4b	04/03/2006	Agassiz Trawl	RSS James Clark Ross JR144	BIOPEARL I	NHMUK
Agla1_Scot_LI_S_RD378	LI-AGT-4b_MB285	LI_AGT_4b	04/03/2006	Agassiz Trawl	RSS James Clark Ross JR144	BIOPEARL I	NHMUK
Agla1_Scot_LI_S_RD379	LI-AGT-4_MB376	LI-AGT-4	04/03/2006	Agassiz Trawl	RSS James Clark Ross JR144	BIOPEARL I	NHMUK
Agla1_Scot_LI_S_RD383	LI_AGT_4b_01	LI_AGT_4b	04/03/2006	Agassiz Trawl	RSS James Clark Ross JR144	BIOPEARL I	NHMUK
Agla1_Scot_LI_S_RD384	LI_AGT_4b_02	LI_AGT_4b	04/03/2006	Agassiz Trawl	RSS James Clark Ross JR144	BIOPEARL I	NHMUK
Agla1_Scot_LI_S_RD385	LI_AGT_4b_03	LI_AGT_4b	04/03/2006	Agassiz Trawl	RSS James Clark Ross JR144	BIOPEARL I	NHMUK
Agla1_Scot_LI_S_RD386	LI_AGT_4b_04	LI_AGT_4b	04/03/2006	Agassiz Trawl	RSS James Clark Ross JR144	BIOPEARL I	NHMUK
Agla1_Scot_LI_S_RD387	LI_AGT_4b_07	LI_AGT_4b	04/03/2006	Agassiz Trawl	RSS James Clark Ross JR144	BIOPEARL I	NHMUK
Agla1_SGeo_SG_S_RD337	SG_AGT_5_1	SG_AGT_5	09/04/2006	Agassiz Trawl	RSS James Clark Ross JR144	BIOPEARL I	NHMUK
Agla1_SGeo_SG_S_RD338	SG_AGT_5_2	SG_AGT_5	09/04/2006	Agassiz Trawl	RSS James Clark Ross JR144	BIOPEARL I	NHMUK
Agla1_SGeo_SG_S_RD339	SG_AGT_5_3	SG_AGT_5	09/04/2006	Agassiz Trawl	RSS James Clark Ross JR144	BIOPEARL I	NHMUK
Agla1_SGeo_SG_S_RD340	SG_AGT_5_4	SG_AGT_5	09/04/2006	Agassiz Trawl	RSS James Clark Ross JR144	BIOPEARL I	NHMUK
Agla1_SSan_ST_S_RD372	ST-EBS-4-S_MB259	ST-EBS-4-S	27/03/2006	Epibenthic Sledge	RSS James Clark Ross JR144	BIOPEARL I	NHMUK
Agla2_Scot_LI_D_RD351	LI_AGT_1_1	LI_AGT_1	03/03/2006	Agassiz Trawl	RSS James Clark Ross JR144	BIOPEARL I	NHMUK
Agla2_Scot_LI_D_RD374	LI-AGT-1_MB272	LI-AGT-1	03/03/2006	Agassiz Trawl	RSS James Clark Ross JR144	BIOPEARL I	NHMUK
Agla2_Scot_LI_D_RD377	LI-AGT-1_MB282	LI-AGT-1	03/03/2006	Agassiz Trawl	RSS James Clark Ross JR144	BIOPEARL I	NHMUK
Agla2_Scot_LI_S_RD356	LI_AGT_4b_11	LI_AGT_4b	04/03/2006	Agassiz Trawl	RSS James Clark Ross JR144	BIOPEARL I	NHMUK
Agla2_Scot_LI_S_RD380	LI-AGT-4_MB434	LI-AGT-4	04/03/2006	Agassiz Trawl	RSS James Clark Ross JR144	BIOPEARL I	NHMUK
Agla2_Scot_LI_S_RD388	LI_AGT_4b_09	LI_AGT_4b	04/03/2006	Agassiz Trawl	RSS James Clark Ross JR144	BIOPEARL I	NHMUK
AglaX_Scot_LI_S_RD353	LI_AGT_4b_05	LI_AGT_4b	04/03/2006	Agassiz Trawl	RSS James Clark Ross JR144	BIOPEARL I	NHMUK
Agla2_Amun_PI_M_RD288	BIO5_EBS_3A_Epi	BIO5_EBS_3A_Epi	07/03/2008	Epibenthic Sledge	RSS James Clark Ross JR179	BIOPEARL II	NHMUK
Agla2_Amun_PI_M_RD444	BIO5_EBS_3D_MB184	BIO5_EBS_3D	07/03/2008	Epibenthic Sledge	RSS James Clark Ross JR179	BIOPEARL II	NHMUK
Agla2_Amun_PI_M_RD445	BIO3_EBS_1B_MB261	BIO3_EBS_1B	04/03/2008	Epibenthic Sledge	RSS James Clark Ross JR179	BIOPEARL II	NHMUK

Molecular specimen ID	Record number	Event ID	Event date	Sampling protocol	Expedition	Project	institution
Agla2_Amun_PI_M_RD446	BIO4_EBS_3A_MB302	BIO4_EBS_3A	07/03/2008	Epibenthic Sledge	RSS James Clark Ross JR179	BIOPEARL II	NHMUK
Agla2_Amun_PI_M_RD447	BIO4_EBS_3A_MB316	BIO4_EBS_3A	07/03/2008	Epibenthic Sledge	RSS James Clark Ross JR179	BIOPEARL II	NHMUK
Agla2_Amun_PI_S_RD453	BIO4_EBS_3B_MB447	BIO4_EBS_3B	07/03/2008	Epibenthic Sledge	RSS James Clark Ross JR179	BIOPEARL II	NHMUK
Agla1_EAnt_BI_S_RD313	NIWA_21584	TAN0402/222	03/03/2004	Epibenthic Sledge	RV Tangaroa TAN402	BioRoss	NIWA
Agla1_EAnt_BI_S_RD314	NIWA_21586_2	TAN0402/239	04/03/2004	Van Veen Grab	RV Tangaroa TAN402	BioRoss	NIWA
Agla1_EAnt_BI_S_RD315	NIWA_21595	TAN0402/259	05/03/2004	Epibenthic Sledge	RV Tangaroa TAN402	BioRoss	NIWA
Agla1_EAnt_BI_S_RD349	NIWA_21585	TAN0402/233	04/03/2004	Epibenthic Sledge	RV Tangaroa TAN402	BioRoss	NIWA
Agla1_EAnt_BI_S_RD410	NIWA_21586_1	TAN0402/239	04/03/2004	Van Veen Grab	RV Tangaroa TAN402	BioRoss	NIWA
Agla1_EAnt_BI_S_RD411	NIWA_21586_3	TAN0402/239	04/03/2004	Van Veen Grab	RV Tangaroa TAN402	BioRoss	NIWA
Agla1_EAnt_BI_S_RD412	NIWA_21586_4	TAN0402/239	04/03/2004	Van Veen Grab	RV Tangaroa TAN402	BioRoss	NIWA
Agla1_Ross_HP_M_RD309	NIWA_21578	TAN0402/171	26/02/2004	Epibenthic Sledge	RV Tangaroa TAN402	BioRoss	NIWA
Agla1_Ross_HP_S_RD295	NIWA_21555_1	TAN0402/21	09/02/2004	Van Veen Grab	RV Tangaroa TAN402	BioRoss	NIWA
Agla1_Ross_HP_S_RD296	NIWA_21556_1	TAN0402/22	09/02/2004	Epibenthic Sledge	RV Tangaroa TAN402	BioRoss	NIWA
Agla1_Ross_HP_S_RD298	NIWA_21558	TAN0402/47	12/02/2004	Van Veen Grab	RV Tangaroa TAN402	BioRoss	NIWA
Agla1_Ross_HP_S_RD299	NIWA_21559	TAN0402/54	13/02/2004	Epibenthic Sledge	RV Tangaroa TAN402	BioRoss	NIWA
Agla1_Ross_HP_S_RD300	NIWA_21560	TAN0402/63	13/02/2004	Epibenthic Sledge	RV Tangaroa TAN402	BioRoss	NIWA
Agla1_Ross_HP_S_RD301	NIWA_21561	TAN0402/91	14/02/2004	Epibenthic Sledge	RV Tangaroa TAN402	BioRoss	NIWA
Agla1_Ross_HP_S_RD302	NIWA_21562	TAN0402/94	17/02/2004	Beam Trawl	RV Tangaroa TAN402	BioRoss	NIWA
Agla1_Ross_HP_S_RD303	NIWA_21566_1	TAN0402/105	18/02/2004	Epibenthic Sledge	RV Tangaroa TAN402	BioRoss	NIWA
Agla1_Ross_HP_S_RD304	NIWA_21572	TAN0402/132	23/02/2004	Epibenthic Sledge	RV Tangaroa TAN402	BioRoss	NIWA
Agla1_Ross_HP_S_RD305	NIWA_21573_1	TAN0402/133	23/02/2004	Epibenthic Sledge	RV Tangaroa TAN402	BioRoss	NIWA
Agla1_Ross_HP_S_RD306	NIWA_21573_2	TAN0402/133	23/02/2004	Epibenthic Sledge	RV Tangaroa TAN402	BioRoss	NIWA
Agla1_Ross_HP_S_RD307	NIWA_21574_1	TAN0402/134	23/02/2004	Epibenthic Sledge	RV Tangaroa TAN402	BioRoss	NIWA
Agla1_Ross_HP_S_RD308	NIWA_21574_2	TAN0402/134	23/02/2004	Epibenthic Sledge	RV Tangaroa TAN402	BioRoss	NIWA
Agla1_Ross_HP_S_RD310	NIWA_21579	TAN0402/184	27/02/2004	Epibenthic Sledge	RV Tangaroa TAN402	BioRoss	NIWA
Agla1_Ross_HP_S_RD311	NIWA_21580_1	TAN0402/186	27/02/2004	Beam Trawl	RV Tangaroa TAN402	BioRoss	NIWA
Agla1_Ross_HP_S_RD312	NIWA_21580_2	TAN0402/186	27/02/2004	Beam Trawl	RV Tangaroa TAN402	BioRoss	NIWA
Agla1_Ross_HP_S_RD399	NIWA_21555_2	TAN0402/21	09/02/2004	Van Veen Grab	RV Tangaroa TAN402	BioRoss	NIWA
Agla1_Ross_HP_S_RD400	NIWA_21556_2	TAN0402/22	09/02/2004	Epibenthic Sledge	RV Tangaroa TAN402	BioRoss	NIWA
Agla1_Ross_HP_S_RD401	NIWA_21556_3	TAN0402/22	09/02/2004	Epibenthic Sledge	RV Tangaroa TAN402	BioRoss	NIWA
Agla1_Ross_HP_S_RD405	NIWA_21566_2	TAN0402/105	18/02/2004	Epibenthic Sledge	RV Tangaroa TAN402	BioRoss	NIWA

Molecular specimen ID	Record number	Event ID	Event date	Sampling protocol	Expedition	Project	institution
Agla1_Ross_HP_S_RD406	NIWA_21574_3	TAN0402/134	23/02/2004	Epibenthic Sledge	RV Tangaroa TAN402	BioRoss	NIWA
Agla1_Ross_HP_S_RD407	NIWA_21580_3	TAN0402/186	27/02/2004	Beam Trawl	RV Tangaroa TAN402	BioRoss	NIWA
Agla1_Ross_HP_S_RD408	NIWA_21580_4	TAN0402/186	27/02/2004	Beam Trawl	RV Tangaroa TAN402	BioRoss	NIWA
Agla1_Ross_HP_S_RD409	NIWA_21580_5	TAN0402/186	27/02/2004	Beam Trawl	RV Tangaroa TAN402	BioRoss	NIWA
Agla1_Ross_HP_S_RD413	NIWA_21568	TAN0402/116	18/02/2004	Epibenthic Sledge	RV Tangaroa TAN402	BioRoss	NIWA
Agla1_Ross_HP_S_RD414	NIWA_21581	TAN0402/189	27/02/2004	Van Veen Grab	RV Tangaroa TAN402	BioRoss	NIWA
Agla1_Ross_HP_S_RD441	NIWA_21570	TAN0402/127	19/02/2004	Van Veen Grab	RV Tangaroa TAN402	BioRoss	NIWA
Agla2_EAnt_BI_M_RD350	NIWA_21591	TAN0402/249	05/03/2004	Fish Bottom Trawl	RV Tangaroa TAN402	BioRoss	NIWA
Agla2_EAnt_BI_S_RD442	NIWA_21589	TAN0402/245	05/03/2004	Epibenthic Sledge	RV Tangaroa TAN402	BioRoss	NIWA
Agla3_EAnt_BI_D_RD348	NIWA_21582	TAN0402/213	03/03/2004	Epibenthic Sledge	RV Tangaroa TAN402	BioRoss	NIWA
AglaX_Ross_HP_S_RD297	NIWA_21557_1	TAN0402/25	09/02/2004	Epibenthic Sledge	RV Tangaroa TAN402	BioRoss	NIWA
AglaX_Ross_HP_S_RD402	NIWA_21557_2	TAN0402/25	09/02/2004	Epibenthic Sledge	RV Tangaroa TAN402	BioRoss	NIWA
AglaX_Ross_HP_S_RD403	NIWA_21557_3	TAN0402/25	09/02/2004	Epibenthic Sledge	RV Tangaroa TAN402	BioRoss	NIWA
AglaX_Ross_HP_S_RD404	NIWA_21557_4	TAN0402/25	09/02/2004	Epibenthic Sledge	RV Tangaroa TAN402	BioRoss	NIWA
Agla1_WAPe_WF_M_RD294	FjordEco_CRS_1717	LMG1510-142	16/12/2015	Blake Trawl	ARSV Laurence M. Gould LMG1510	FjordEco	NHMUK
Agla1_WAPe_WF_M_RD361	FjordEco_CRS_1744	LMG1510-271	16/12/2015	Blake Trawl	ARSV Laurence M. Gould LMG1510	FjordEco	NHMUK
Agla1_WAPe_WF_M_RD362	FjordEco_CRS_1811	NBP1603-209	16/04/2016	Blake Trawl	RVIB Nathaniel B. Palmer NBP1603	FjordEco	NHMUK
Agla1_EWed_BR_M_RD316	JR275_1244_1	JR275-085	29/02/2012	Agassiz Trawl	RSS James Clark Ross JR275	JR275	NHMUK
Agla1_EWed_BR_M_RD317	JR275_1244_2	JR275-085	29/02/2012	Agassiz Trawl	RSS James Clark Ross JR275	JR275	NHMUK
Agla1_EWed_BR_M_RD318	JR275_1244_3	JR275-085	29/02/2012	Agassiz Trawl	RSS James Clark Ross JR275	JR275	NHMUK
Agla2_EWed_BR_S_RD319	JR275_565	JR275-042	22/02/2012	Agassiz Trawl	RSS James Clark Ross JR275	JR275	NHMUK
Agla2_EWed_BR_S_RD320	JR275_1533_1	JR275-103	04/03/2012	Agassiz Trawl	RSS James Clark Ross JR275	JR275	NHMUK
Agla2_EWed_BR_S_RD321	JR275_1533_2	JR275-103	04/03/2012	Agassiz Trawl	RSS James Clark Ross JR275	JR275	NHMUK
Agla2_EWed_BR_S_RD449	JR275_810	JR275-052	23/02/2012	Agassiz Trawl	RSS James Clark Ross JR275	JR275	NHMUK
Agla2_EWed_FT_M_RD452	JR275_23_EBS	JR275-23-EBS		Epibenthic Sledge	RSS James Clark Ross JR275	JR275	NHMUK
Agla2_EWed_XX_X_RD450	JR275_196				RSS James Clark Ross JR275	JR275	NHMUK
Agla2_EWed_XX_X_RD451	JR275_91				RSS James Clark Ross JR275	JR275	NHMUK
Agla2_EWed_XX_X_RD454	JR275_50_EBS	JR275-50-EBS		Epibenthic Sledge	RSS James Clark Ross JR275	JR275	NHMUK
Agla3_EWed_BR_D_RD456	JR275_1216	JR275-082	28/02/2012	Agassiz Trawl	RSS James Clark Ross JR275	JR275	NHMUK
Agla3_EWed_FT_M_RD455	JR275_107	JR275-020	19/02/2012	Agassiz Trawl	RSS James Clark Ross JR275	JR275	NHMUK
Agla2_WAPe_AI_M_RD329	JR308_278_01	JR308-047	03/01/2015	Agassiz Trawl	RSS James Clark Ross JR308	JR308	NHMUK

Molecular specimen ID	Record number	Event ID	Event date	Sampling protocol	Expedition	Project	institution
Agla2_WAPe_AI_M_RD330	JR308_278_02	JR308-047	03/01/2015	Agassiz Trawl	RSS James Clark Ross JR308	JR308	NHMUK
Agla2_WAPe_AI_S_RD322	JR308_212_01	JR308-045	03/01/2015	Agassiz Trawl	RSS James Clark Ross JR308	JR308	NHMUK
Agla2_WAPe_AI_S_RD323	JR308_212_03	JR308-045	03/01/2015	Agassiz Trawl	RSS James Clark Ross JR308	JR308	NHMUK
Agla2_WAPe_AI_S_RD324	JR308_212_04	JR308-045	03/01/2015	Agassiz Trawl	RSS James Clark Ross JR308	JR308	NHMUK
Agla2_WAPe_AI_S_RD325	JR308_212_05	JR308-045	03/01/2015	Agassiz Trawl	RSS James Clark Ross JR308	JR308	NHMUK
Agla2_WAPe_AI_S_RD326	JR308_212_06	JR308-045	03/01/2015	Agassiz Trawl	RSS James Clark Ross JR308	JR308	NHMUK
Agla2_WAPe_AI_S_RD327	JR308_060_01	JR308-012	01/01/2015	Agassiz Trawl	RSS James Clark Ross JR308	JR308	NHMUK
Agla2_WAPe_AI_S_RD328	JR308_060_02	JR308-012	01/01/2015	Agassiz Trawl	RSS James Clark Ross JR308	JR308	NHMUK
Agla2_WAPe_AI_S_RD381	JR308_212_02	JR308-045	03/01/2015	Agassiz Trawl	RSS James Clark Ross JR308	JR308	NHMUK
Agla2_WAPe_AI_S_RD382	JR308_212_07	JR308-045	03/01/2015	Agassiz Trawl	RSS James Clark Ross JR308	JR308	NHMUK
Agla2_WAPe_AI_S_RD392	JR308_212_08	JR308-045	03/01/2015	Agassiz Trawl	RSS James Clark Ross JR308	JR308	NHMUK
Agla2_WAPe_AI_S_RD393	JR308_212_09	JR308-045	03/01/2015	Agassiz Trawl	RSS James Clark Ross JR308	JR308	NHMUK
Agla2_WAPe_AI_S_RD394	JR308_212_10	JR308-045	03/01/2015	Agassiz Trawl	RSS James Clark Ross JR308	JR308	NHMUK
Agla2_WAPe_AI_S_RD395	JR308_212_11	JR308-045	03/01/2015	Agassiz Trawl	RSS James Clark Ross JR308	JR308	NHMUK
Agla2_WAPe_AI_S_RD396	JR308_212_12	JR308-045	03/01/2015	Agassiz Trawl	RSS James Clark Ross JR308	JR308	NHMUK
Agla2_WAPe_AI_S_RD398	JR308_060_03	JR308-012	01/01/2015	Agassiz Trawl	RSS James Clark Ross JR308	JR308	NHMUK
Agla2_WAPe_AI_S_RD457	JR308_060_04	JR308-012	01/01/2015	Agassiz Trawl	RSS James Clark Ross JR308	JR308	NHMUK
Agla2_WAPe_AI_S_RD458	JR308_060_05	JR308-012	01/01/2015	Agassiz Trawl	RSS James Clark Ross JR308	JR308	NHMUK
Agla3_WWed_LA_S_RD357	Larissa_CRS_1401	NBP1203-08	21/03/2012	Multicore	RVIB Nathaniel B. Palmer NBP1203	LARISSA	NHMUK
Agla2_WWed_LA_M_RD358	Larissa_CRS_1413	NBP1203-17	27/03/2012	Multicore	RVIB Nathaniel B. Palmer NBP1204	LARISSA	NHMUK
Agla2_WWed_LA_M_RD359	Larissa_CRS_1456_1	NBP1203-32	07/04/2012	Blake Trawl	RVIB Nathaniel B. Palmer NBP1205	LARISSA	NHMUK
Agla1_WWed_LA_M_RD360	Larissa_CRS_1456_2	NBP1203-32	07/04/2012	Blake Trawl	RVIB Nathaniel B. Palmer NBP1206	LARISSA	NHMUK
Agla1_WWed_PG_D_RD342	PGC_NHM_195	JR17003a-41	05/03/2018	Epibenthic Sledge	RSS James Clark Ross JR17003a	Larsen C Benthos	NHMUK
Agla1_WWed_PG_D_RD343	PGC_NHM_213	JR17003a-41	05/03/2018	Epibenthic Sledge	RSS James Clark Ross JR17003a	Larsen C Benthos	NHMUK
Agla1_WWed_PG_D_RD363	PGC_NHM_ID0032	JR17003a-04	01/03/2018	Agassiz Trawl	RSS James Clark Ross JR17003a	Larsen C Benthos	NHMUK
Agla1_WWed_PG_D_RD364	PGC_NHM_011	JR17003a-04	01/03/2018	Agassiz Trawl	RSS James Clark Ross JR17003a	Larsen C Benthos	NHMUK
Agla1_WWed_PG_D_RD365	PGC_NHM_013	JR17003a-04	01/03/2018	Agassiz Trawl	RSS James Clark Ross JR17003a	Larsen C Benthos	NHMUK
Agla1_WWed_PG_D_RD366	PGC_NHM_016	JR17003a-04	01/03/2018	Agassiz Trawl	RSS James Clark Ross JR17003a	Larsen C Benthos	NHMUK
Agla1_WWed_PG_D_RD367	PGC_NHM_017	JR17003a-04	01/03/2018	Agassiz Trawl	RSS James Clark Ross JR17003a	Larsen C Benthos	NHMUK
Agla1_WWed_PG_D_RD368	PGC_NHM_204	JR17003a-43	06/03/2018	Agassiz Trawl	RSS James Clark Ross JR17003a	Larsen C Benthos	NHMUK
Agla1_WWed_PG_M_RD282	PGC_NHM_081	JR17003a-34	04/03/2018	Epibenthic Sledge	RSS James Clark Ross JR17003a	Larsen C Benthos	NHMUK

Molecular specimen ID	Record number	Event ID	Event date	Sampling protocol	Expedition	Project	institution
Agla1_WWed_PG_M_RD344	PGC_NHM_234B_2	JR17003a-46	06/03/2018	Agassiz Trawl	RSS James Clark Ross JR17003a	Larsen C Benthos	NHMUK
Agla1_WWed_PG_M_RD346	PGC_NHM_280E_2	JR17003a-52	07/03/2018	Agassiz Trawl	RSS James Clark Ross JR17003a	Larsen C Benthos	NHMUK
Agla1_WWed_PG_M_RD347	PGC_NHM_234B_3	JR17003a-46	06/03/2018	Agassiz Trawl	RSS James Clark Ross JR17003a	Larsen C Benthos	NHMUK
Agla1_WWed_PG_M_RD369	PGC_NHM_278	JR17003a-52	07/03/2018	Agassiz Trawl	RSS James Clark Ross JR17003a	Larsen C Benthos	NHMUK
Agla1_WWed_PG_M_RD370	PGC_NHM_234B_1	JR17003a-46	06/03/2018	Agassiz Trawl	RSS James Clark Ross JR17003a	Larsen C Benthos	NHMUK
Agla1_WWed_PG_M_RD371	PGC_NHM_280E_1	JR17003a-52	07/03/2018	Agassiz Trawl	RSS James Clark Ross JR17003a	Larsen C Benthos	NHMUK
Agla1_WWed_PG_M_RD390	PGC_NHM_234B_5	JR17003a-46	06/03/2018	Agassiz Trawl	RSS James Clark Ross JR17003a	Larsen C Benthos	NHMUK
Agla1_WWed_PG_M_RD391	PGC_NHM_234B_6	JR17003a-46	06/03/2018	Agassiz Trawl	RSS James Clark Ross JR17003a	Larsen C Benthos	NHMUK
Agla1_WWed_PG_M_RD397	PGC_NHM_234B_4	JR17003a-46	06/03/2018	Agassiz Trawl	RSS James Clark Ross JR17003a	Larsen C Benthos	NHMUK
Agla2_WWed_PG_M_RD345	PGC_NHM_280F	JR17003a-52	07/03/2018	Agassiz Trawl	RSS James Clark Ross JR17003a	Larsen C Benthos	NHMUK
Agla1_Scot_SO_D_RD332	JR16_DNA_356	JR15005-094	13/03/2016	Agassiz Trawl	RSS James Clark Ross JR15005	SoAntEco	NHMUK
Agla1_Scot_SO_M_RD331	JR16_DNA_177	JR15005-054	09/03/2016	Agassiz Trawl	RSS James Clark Ross JR15005	SoAntEco	NHMUK
Agla1_Scot_SO_M_RD333	JR16_DNA_330	JR15005-091	13/03/2016	Agassiz Trawl	RSS James Clark Ross JR15005	SoAntEco	NHMUK
Agla1_Scot_SO_M_RD335	JR16_DNA_369	JR15005-101	13/03/2016	Agassiz Trawl	RSS James Clark Ross JR15005	SoAntEco	NHMUK
Agla1_Scot_SO_M_RD336	JR16_DNA_136	JR15005-033	06/03/2016	Agassiz Trawl	RSS James Clark Ross JR15005	SoAntEco	NHMUK
Agla2_Scot_SO_M_RD334	JR16_DNA_232	JR15005-070	10/03/2016	Agassiz Trawl	RSS James Clark Ross JR15005	SoAntEco	NHMUK

Table D.2 List of GenBank sequence accession numbers for Nephtyidae and outgroup specimens included in phylogenetic analyses

	ID	COI	16S	18S	Location	reference
Nephtyidae	*Aglaophamus australiensis*		GU179347	GU179371	Gulf St. Vincent, Australia	Ravara et al. 2010
	Aglaophamus cf. *trissophyllus* MB isolate MB209		KX867142		South Georgia	Brasier et al. 2016
	Aglaophamus cf. *trissophyllus* MBb isolate MB195	KX867381	KX867145		South Georgia	Brasier et al. 2016
	Aglaophamus cf. *trissophyllus* MBb isolate MB245	KX867382	KX867146		South Georgia	Brasier et al. 2016
	Aglaophamus elamellata	GU179404	GU179361	GU179365	Setúbal submarine canyon, Portugal	Ravara et al. 2010
	Aglaophamus malmgreni	GU179405	GU179362	GU179366	Svalbard, Arctic	Ravara et al. 2010
	Aglaophamus pulchra	GU179413	GU179360	GU179384	Nazaré submarine canyon, Portugal	Ravara et al. 2010
	Aglaophamus rubellus	GU179406	GU179363	GU179367	Bohusla¨n, Sweden	Ravara et al. 2010
	Aglaophamus sp. MB isolate MB128		KX867135		Amundsen Sea	Brasier et al. 2016
	Aglaophamus sp. MB isolate MB295		KX867129		Amundsen Sea	Brasier et al. 2016
	Aglaophamus sp. MB isolate MB326		KX867131		Amundsen Sea	Brasier et al. 2016
	Aglaophamus sp. MB isolate MB410		KX867125		Amundsen Sea	Brasier et al. 2016
	Aglaophamus sp. MB2 isolate MB13	KX867384	KX867117		Amundsen Sea	Brasier et al. 2016
	Aglaophamus sp. MB isolate MB20	KX867385	KX867139		Amundsen Sea	Brasier et al. 2016
	Aglaophamus sp. MB2 isolate MB42		KX867118		Amundsen Sea	Brasier et al. 2016
	Aglaophamus sp. MB3 isolate MB219	KX867387	KX867120		South Georgia	Brasier et al. 2016
	Aglaophamus sp. MB3 isolate MB240	KX867388	KX867121		Amundsen Sea	Brasier et al. 2016
	Aglaophamus sp. MB4 isolate MB46		KX867122		Amundsen Sea	Brasier et al. 2016
	Bipalponephtys cornuta	GU179409	GU179352	GU179375	San Francisco Bay, California, USA	Ravara et al. 2010
	Cf. Nephtyidae sp. DH_2009	GU227129	GU227024	GU227081	McMurdo Sound, Ross Sea	Hemerier et al. 2010
	Micronephthys stammeri	GU179407	GU179364	GU179369	Tanabe Bay, Japan	Ravara et al. 2010
	Nephtys assimilis		GU179346	GU179370	Off Cascais, Portugal	Ravara et al. 2010
	Nephtys caeca		GU179348	GU179372	Bohusla¨n, Sweden	Ravara et al. 2010
	Nephtys ciliata		GU179350	GU179373	Svalbard, Arctic	Ravara et al. 2010
	Nephtys cirrosa	GU179408	GU179351	GU179374	Galiza, Spain*	Ravara et al. 2010
	Nephtys ferruginea		GU179353	GU179376	San Francisco Bay, California, USA	Ravara et al. 2010
	Nephtys hombergii	GU179410	GU179354	GU179377	Ria Aveiro, Portugal*	Ravara et al. 2010
	Nephtys hystricis	GU179411	GU179355	GU179378	Bohusla¨n Sweden	Ravara et al. 2010
	Nephtys incisa		GU179356	GU179379	Bohusla¨n, Sweden	Ravara et al. 2010
	Nephtys paradoxa	GU179412	GU179358	GU179382	Trondheimsfjord, Norway	Ravara et al. 2010
	Nephtys pente		GU179359	GU179383	Bohusla¨n, Sweden	Ravara et al. 2010
	AB01_NHM_486_Nephtyidae_sp_939	yes	yes	yes	Clarion Clipperton Zone, central Pacific	NOT PUBLISHED (ABYSSLINE)
	AB01_NHM_487_Nephtyidae_sp_946	yes	yes	yes	Clarion Clipperton Zone, central Pacific	NOT PUBLISHED (ABYSSLINE)

	ID	COI	16S	18S	Location	reference
	AB02_NHM_1317_Nephtyidae_sp_1547		yes	yes	Clarion Clipperton Zone, central Pacific	NOT PUBLISHED (ABYSSLINE)
	AB02_NHM_2113_Nephtyidae_sp_1893		yes	yes	Clarion Clipperton Zone, central Pacific	NOT PUBLISHED (ABYSSLINE)
Outgroups	*Paramphinome jeffreysi*	AY838875	AY838840	AY838856		Struck et al. 2004
	Lacydonia sp	AY996120	AY996061	AY996082		Persson et al. 2007
	Notophyllum foliosum	AY996117	DQ779627	AY996079		Persson et al. 2007, Rousset et al. 2007
	Nereis pelagica	JN852947	AY340470	AY340438		Norlinder et al. 2012; Rousset et al. 2007
	Glycera alba	JN852946	DQ779615	DQ779651		Norlinder et al. 2012; Roussett et al. 2007

Table D.3 Primers used for PCR and sequencing for all new material newly sequenced in this study

Gene	Primer	Sequence 5'–3'	Reference
16S	16SarL	CGCCTGTTTATCAAAAACAT	Palumbi (1996)
	16SbrH	CCGGTCTGAACTCAGATCACGT	Palumbi (1996)
	Ann16SF	GCGGTATCCTGACCGTRCWAAGGTA	Sjölin et al. (2005)
	Ann16SR	TCCTAAGCCAACATCGAGGTGCCAA	Sjölin et al. (2005)
18S	18SA	AYCTGGTTGATCCTGCCAGT	Medlin et al. (1988)
	18SB	ACCTTGTTACGACTTTTACTTCCTC	Nygren and Sundberg (2003)
	620F	TAAAGYTGYTGCAGTTAAA	Nygren and Sundberg (2003)
	1324R	CGGCCATGCACCACC	Cohen et al. 1998
COI	HCO2198	TAAACTTCAGGGTGACCAAAAAATCA	Folmer et al. (1994)
	LCO1490	GGTCAACAAATCATAAAGATATTGG	Folmer et al. (1994)
	polyLCO	GAYTATWTTCAACAAATCATAAAGATATTGG	Carr et al. (2011)
	polyHCO	TAMACTTCWGGGTGACCAAARAATCA	Carr et al. (2011)
	COIE	CCAGAGATTAGAGGGAATCAGTG	Palumbi et al. (1991)

D.2 Figures

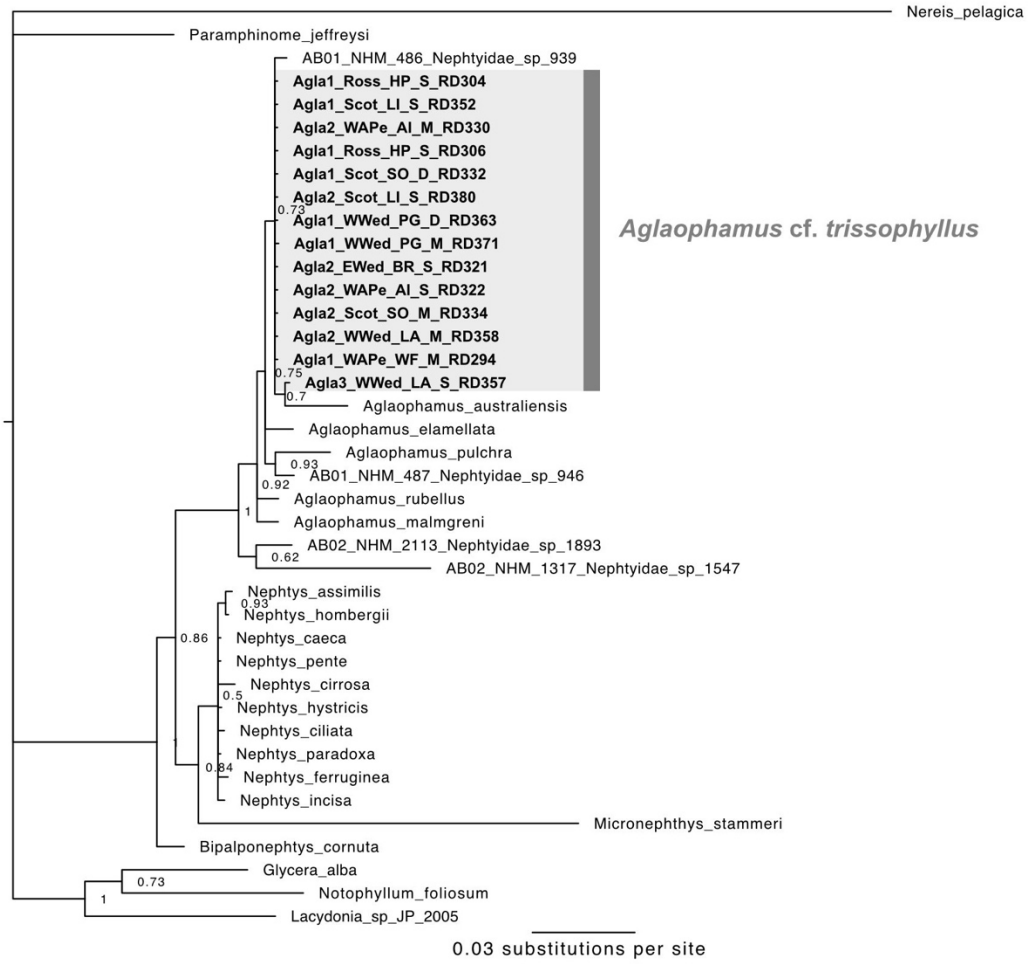

Figure D.1 Phylogenetic tree of the Annelid family Nephtyidae using Bayesian analysis of 18S RNA gene. Antarctic *Aglaophamus* spp. identified as *Aglaophamus* cf. *trissophyllus* newly sequenced in this study are marked in bold. Antarctic *Aglaophamus* spp. are marked with a box. Bayesian posterior probability values are given as support.

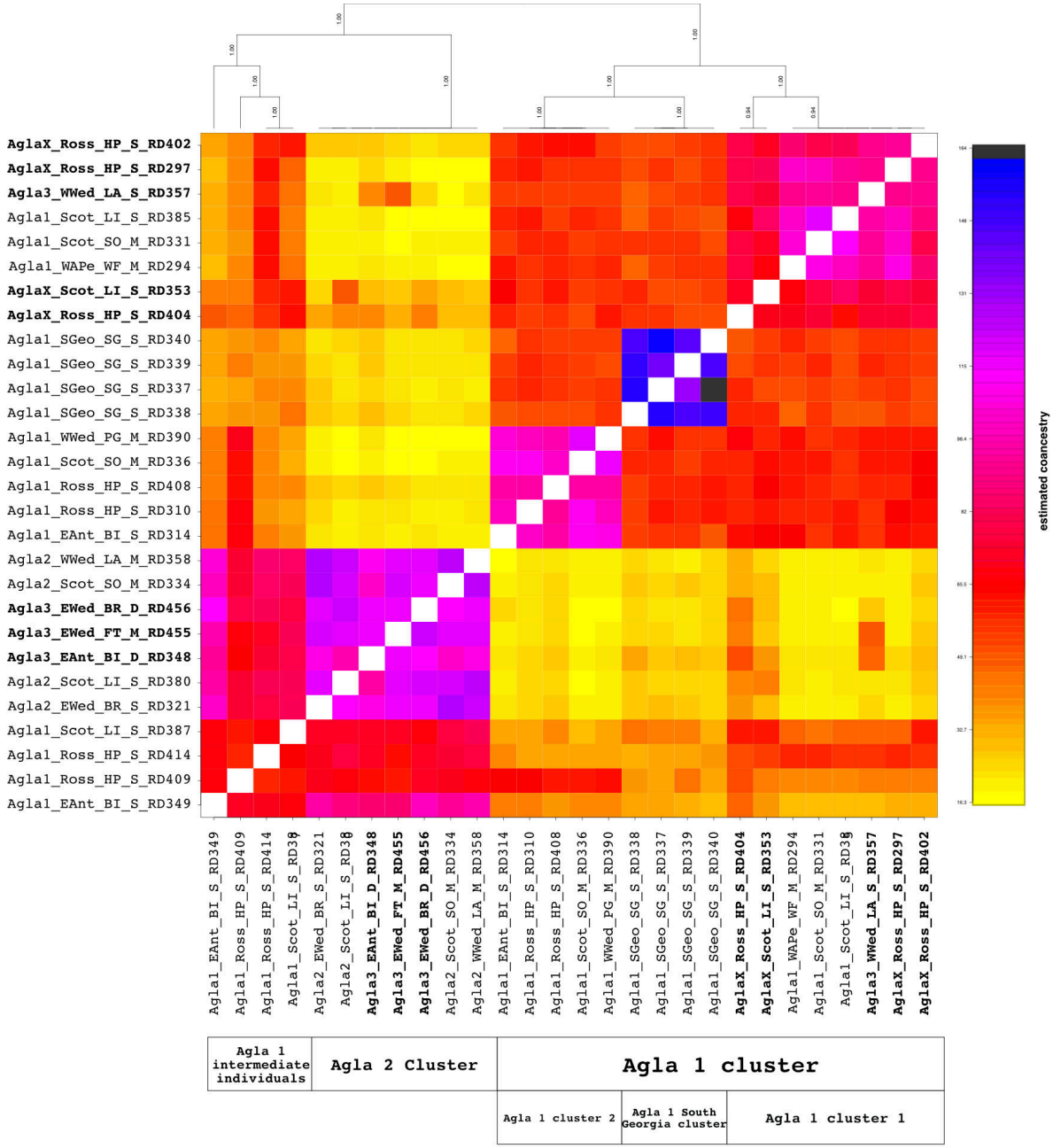

Figure D.2 Co-ancestry analysis of subset of all *Aglaophamus* cf. *trissophyllus* clades identified in phylogenetic analyses (Clades 1, 2 and 3 - Agla 1, Agla 2, and Agla 3), in addition to undetermined individuals without barcode data (Agla X), displayed as a simple co-ancestry matrix heatmap – top: simple hierarchical tree from raw data matrix with posterior population assignment probabilities; left: specimen IDs, Agla 3 and Agla X individuals are highlighted in bold; bottom: specimen IDs, Agla 3 and Agla X individuals are highlighted in bold, and genetic cluster assignment in population genomic analyses.

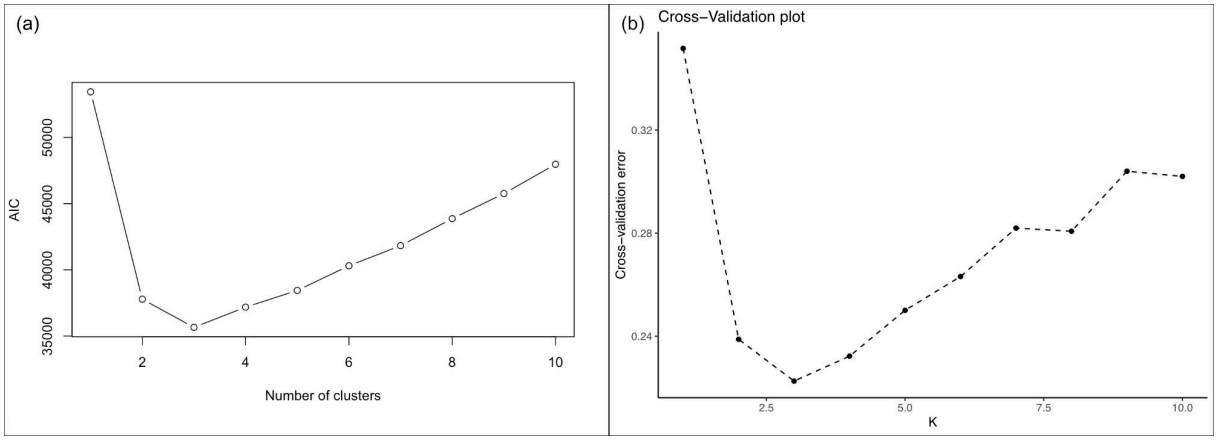

Figure D.3 Cross validation plots for *Aglaophamus* cf. *trissophyllus* Clades 1 and 2 (Agla 1, Agla 2) combined dataset (a) for DAPC using function *snapclust* and Aikaike information Criterion (AIC), optimal number of clusters K corresponding with lowest AIC (b) ADMIXTURE cross validation analysis, optimal number of clusters K corresponding with lowest cross validation error. For both analyses, optimal clustering solutions *K*=3 > *K*=4 > *K*=2

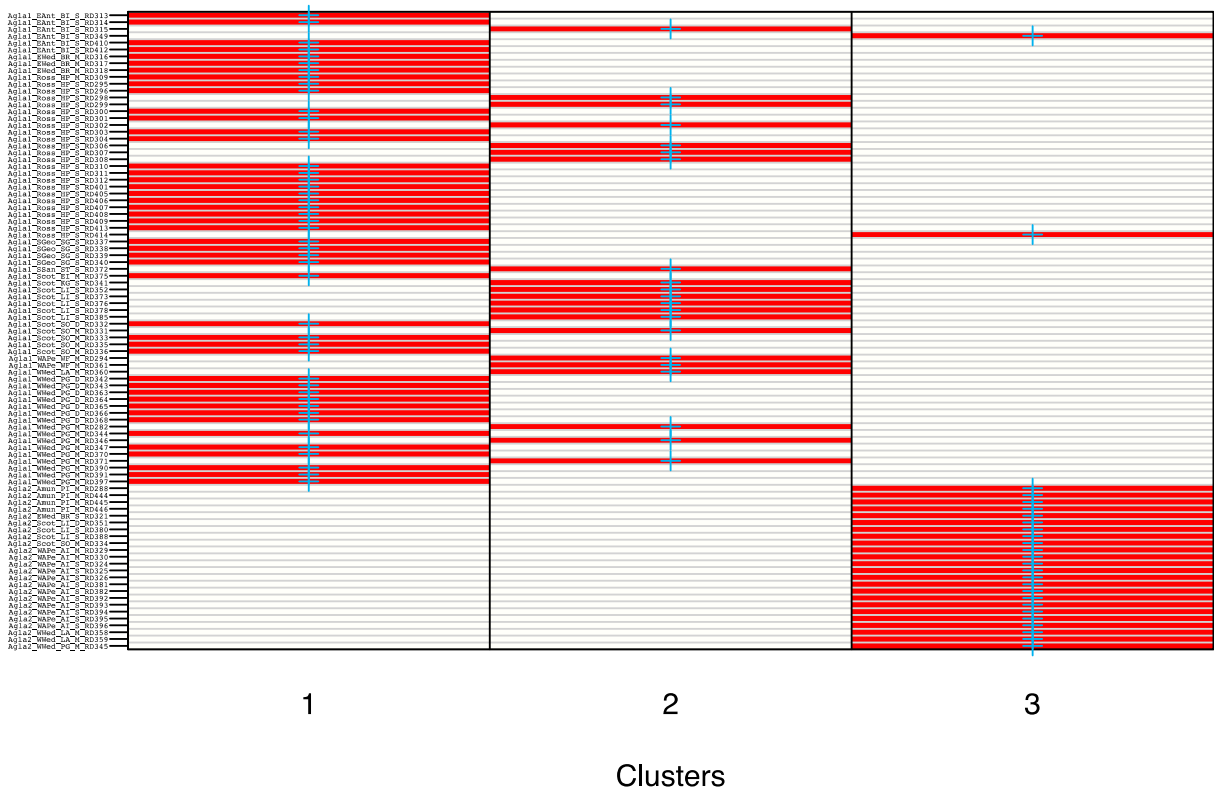

Figure D.4 Assignplot for *K*=3 DAPC analysis of *Aglaophamus* cf. *trissophyllus* Clades 1 and 2 (Agla 1, Agla 2) combined dataset showing the individual specimens assigned to each cluster. Colours represent membership probabilities (red=1, white=0); blue crosses represent the prior cluster assignment provided to DAPC

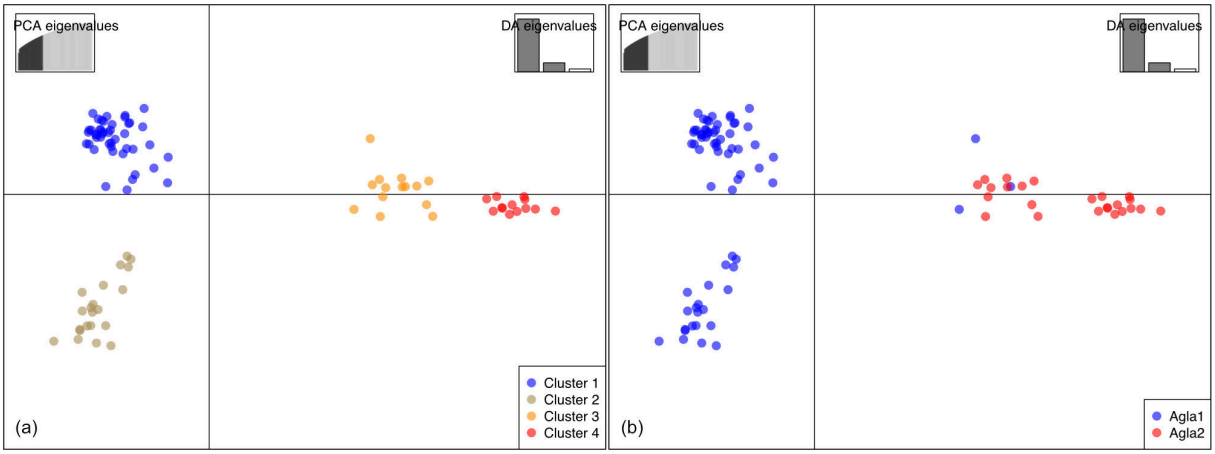

Figure D.5 Combined analysis and genotype assignment of *Aglaophamus* cf. *trissophyllus* Clades 1 and 2 (Agla 1, Agla 2) identified in phylogenetic analyses. (a) DAPC results with *K* =4 as inferred by the function *snapclust*, assigning samples to one of four clusters; (b) DAPC *K* =4 results with phylogenetic clade membership indicated by colour.

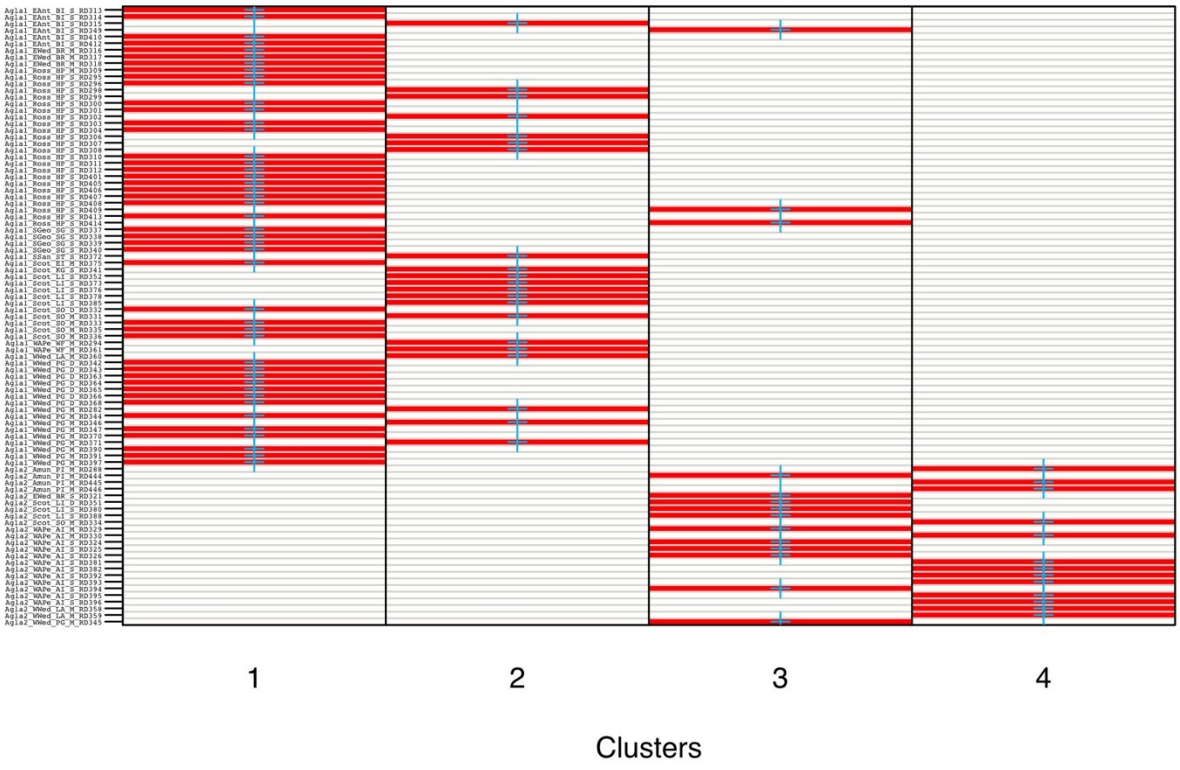

Figure D.6 Assignplot for *K*=4 DAPC analysis of *Aglaophamus* cf. *trissophyllus* Clades 1 and 2 (Agla 1, Agla 2) combined dataset showing the individual specimens assigned to each cluster. Colours represent membership probabilities (red=1, white=0); blue crosses represent the prior cluster assignment provided to DAPC

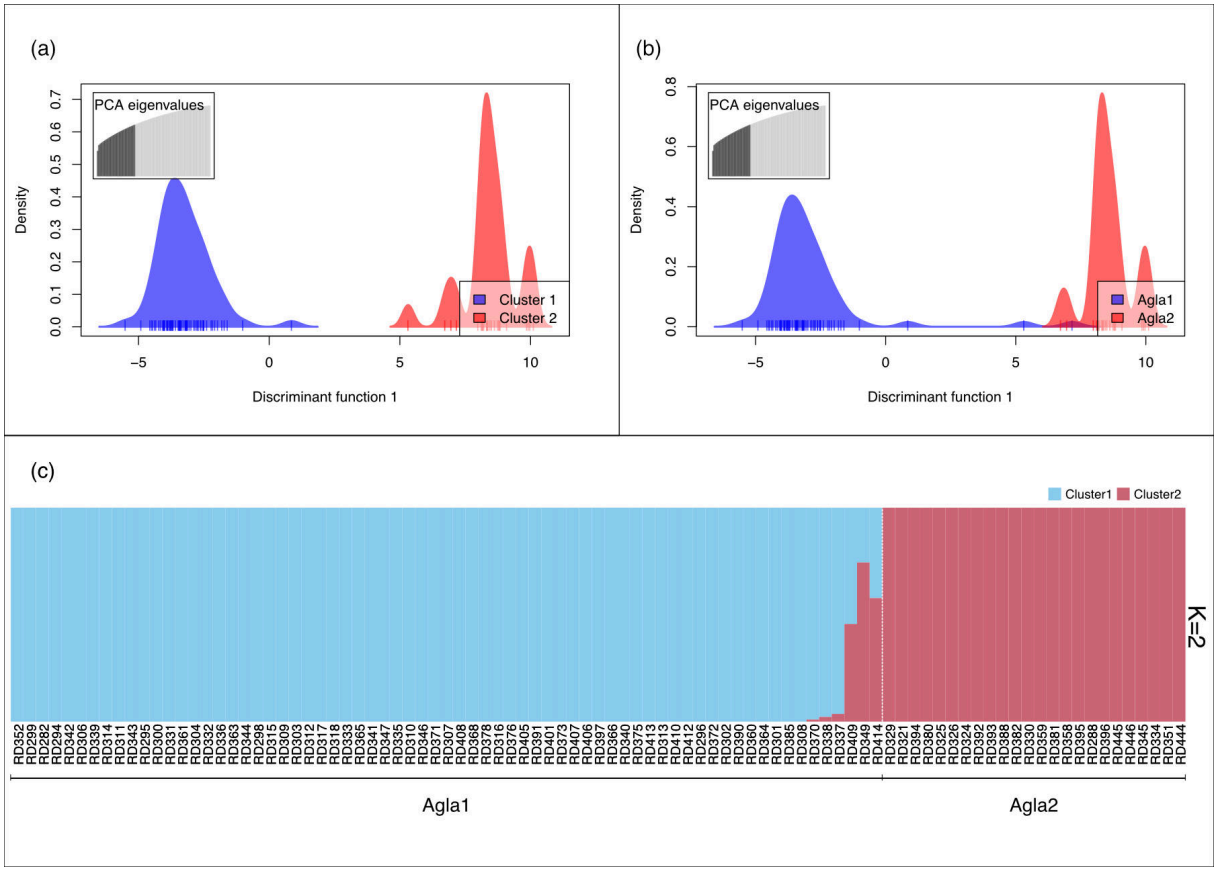

Figure D.7 Combined analysis and genotype assignment of *Aglaophamus* cf. *trissophyllus* Clades 1 and 2 (Agla 1, Agla 2) identified in phylogenetic analyses(a) DAPC results with *K*=2 as inferred by the function *snapclust*, assigning samples to one of three clusters; (b) DAPC *K*=2 results with phylogenetic clade membership indicated by colour. (c) ADMIXTURE results with *K*=2, assigning individuals to one of three clusters, grouped by phylogenetic clade membership. Individuals given by extraction number

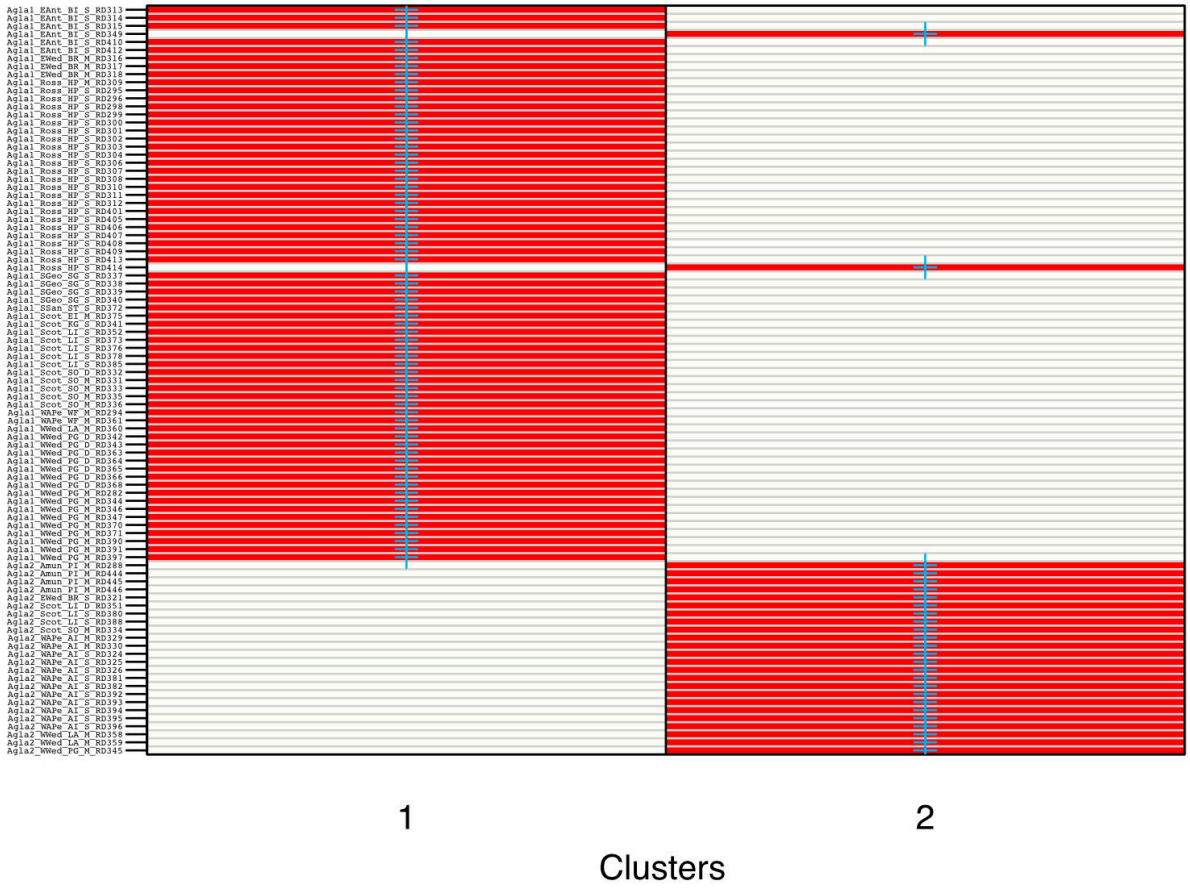

Figure D.8 Assignplot for *K* =2 DAPC analysis of *Aglaophamus* cf. *trissophyllus* Clades 1 and 2 (Agla 1, Agla 2) combined dataset showing the individual specimens assigned to each cluster. Colours represent membership probabilities (red=1, white=0); blue crosses represent the prior cluster assignment provided to DAPC

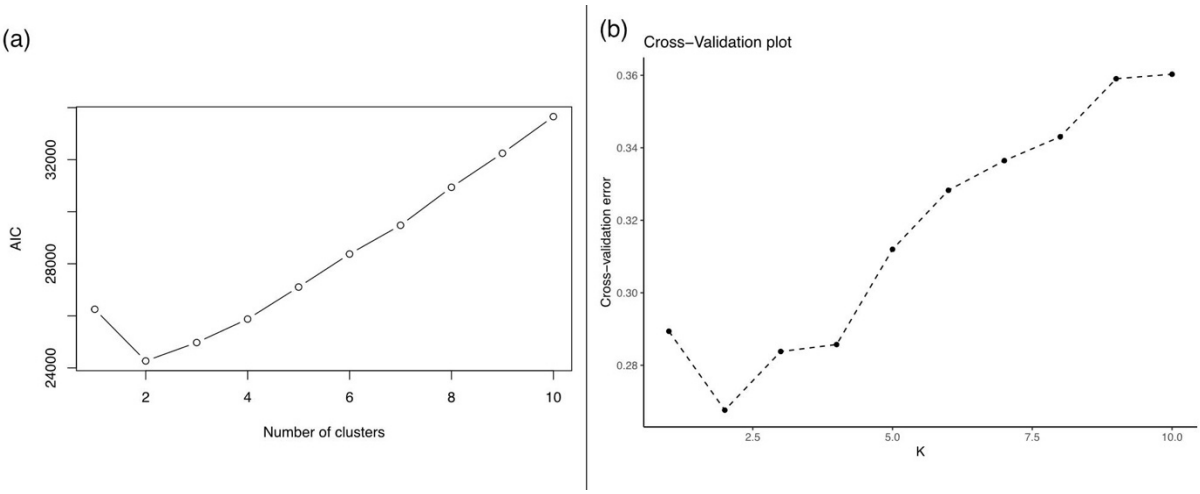

Figure D.9 Cross validation plots for *Aglaophamus* Clade 1 (a) for DAPC using function *snapclust* and Aikaike information Criterion (AIC), optimal number of clusters K corresponding with lowest AIC (b) ADMIXTURE cross validation analysis, optimal number of clusters K

corresponding with lowest cross validation error. For both analyses, optimal clustering solutions K=2 > K=3> K=4

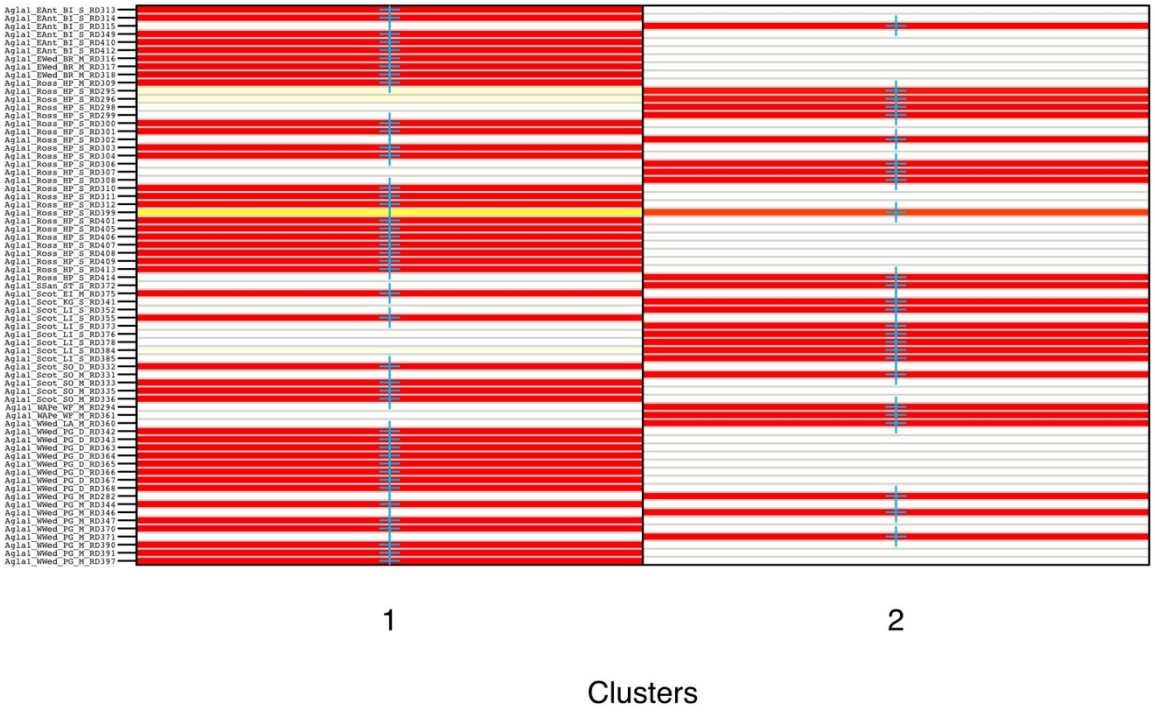

Figure D.10 Assignplot for *K*=2 DAPC analysis of *Aglaophamus* cf. *trissophyllus* Clade 1 showing the individual specimens assigned to each cluster. Colours represent membership probabilities (red=1, white=0); blue crosses represent the prior cluster assignment provided to DAPC

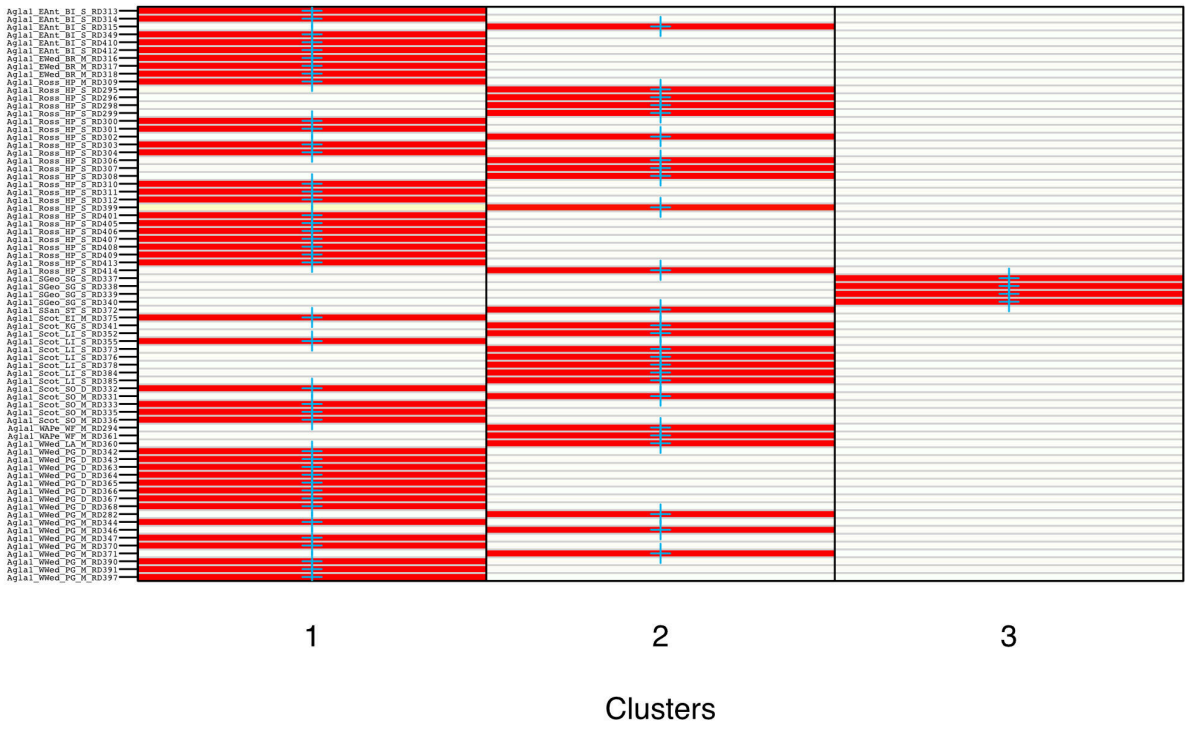

Figure D.11 Assignplot for *K*=3 DAPC analysis of *Aglaophamus* cf. *trissophyllus* Clade 1 showing the individual specimens assigned to each cluster. Colours represent membership probabilities (red=1, white=0); blue crosses represent the prior cluster assignment provided to DAPC

Figure D.12 Population structure and differentiation analysis for *Aglaophamus* cf. *trissophyllus* Clade 1 (a) ADMIXTURE results with *K*=3, assigning individuals to one of three clusters, with individuals grouped by geographic locality (b) ADMIXTURE results with k=4, assigning individuals to one of four clusters, with individuals grouped by geographic locality. Individuals given by extraction number. BI = Balleny Islands; BS = Bransfield Strait; EW = Eastern Weddell Sea; RS = Ross Sea; SG = South Georgia; SO = South Orkneys; ST = Southern Thule; WP = West Antarctic Peninsula; WW = Western Weddell Sea.

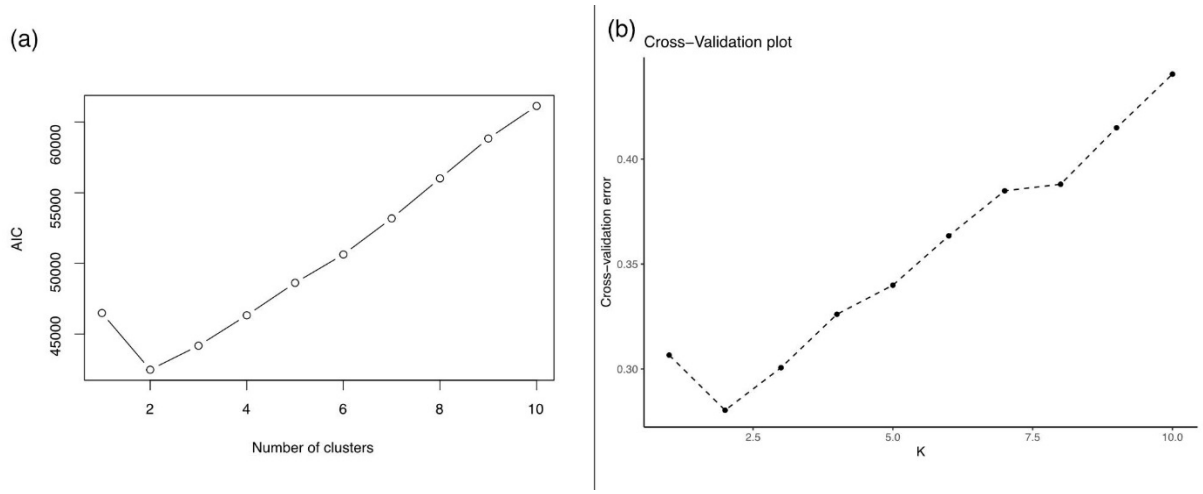

Figure D.13 Cross validation plots for *Aglaophamus* Clade 1 excluding South Georgia individuals (a) for DAPC using function *snapclust* and Aikaike information Criterion (AIC), optimal number of clusters K corresponding with lowest AIC (b) ADMIXTURE cross validation analysis, optimal number of clusters K corresponding with lowest cross validation error. For both analyses, optimal clustering solutions K=2 > K=3> K=4

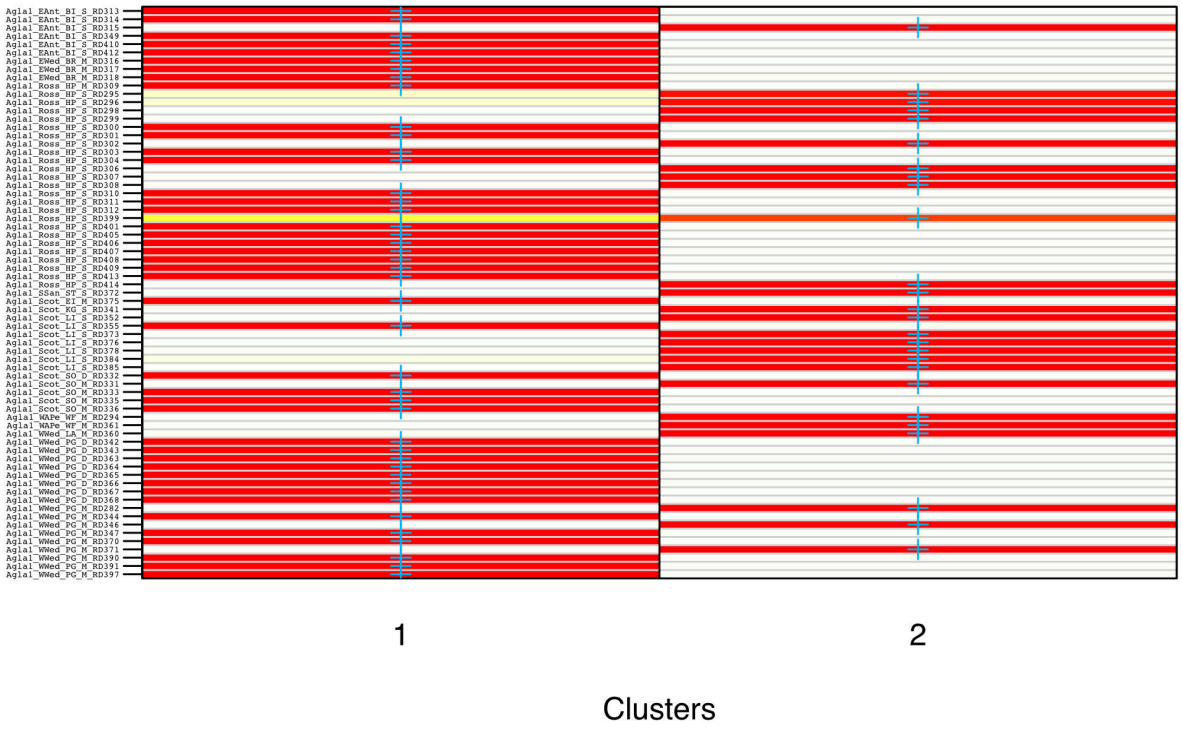

Figure D.14 Assignplot for k=2 DAPC analysis of *Aglaophamus* Clade 1 excluding South Georgia individuals showing the individual specimens assigned to each cluster. Colours represent membership probabilities (red=1, white=0); blue crosses represent the prior cluster assignment provided to DAPC

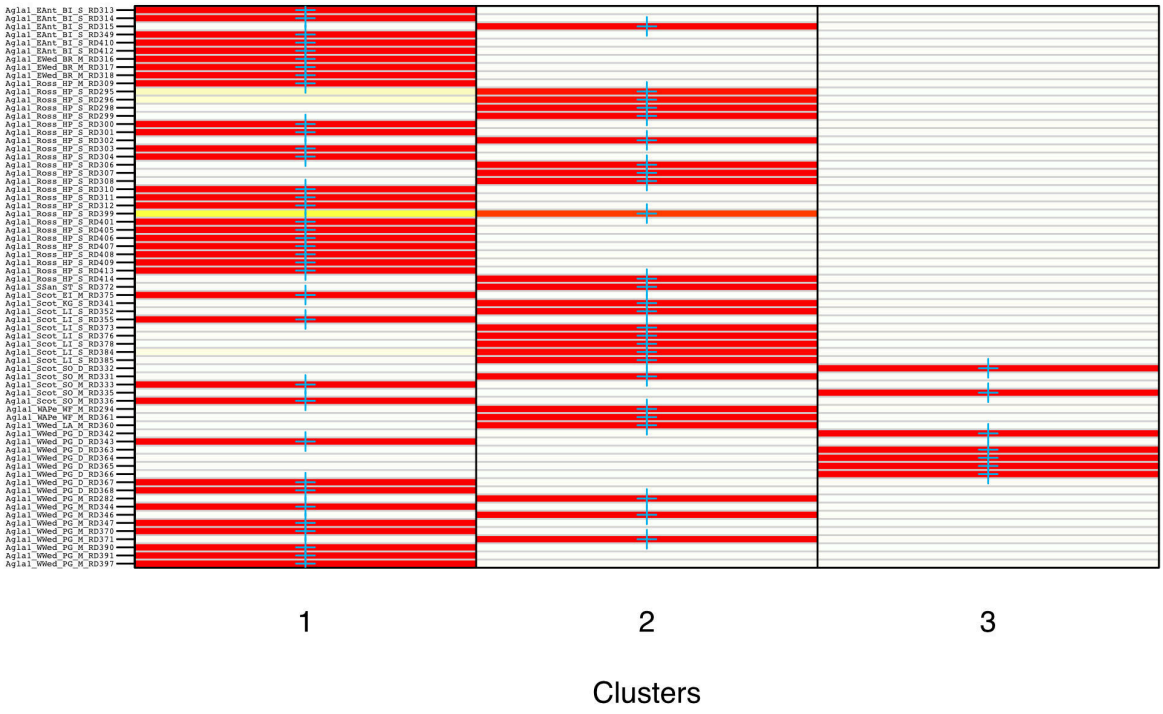

Figure D.15 Assignplot for k=3 DAPC analysis of *Aglaophamus* Clade 1 excluding South Georgia showing the individual specimens assigned to each cluster. Colours represent membership probabilities (red=1, white=0); blue crosses represent the prior cluster assignment provided to DAPC

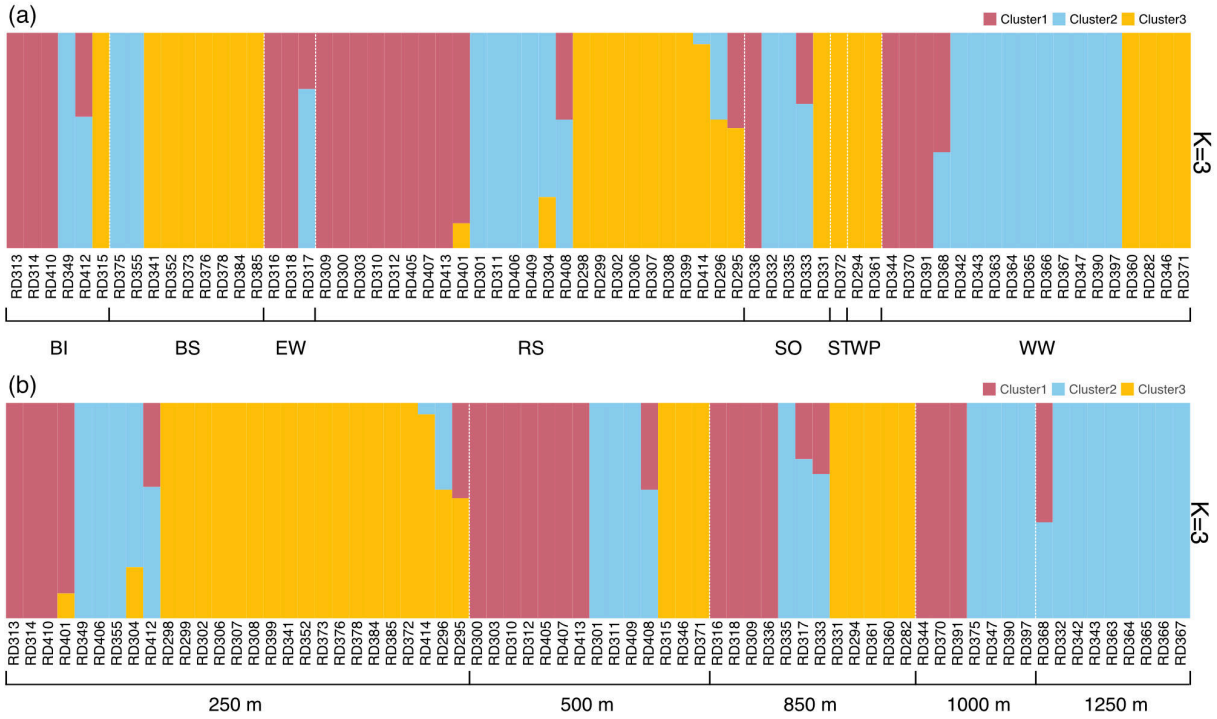

Figure D.16 Population structure and differentiation analysis for *Aglaophamus* cf. *trissophyllus* Clade 1 (Agla 1) excluding South Georgia individuals (a) ADMIXTURE results with *K* =3, assigning individuals to one of three clusters, with individuals grouped by geographic locality(b) ADMIXTURE results with *K* =3, assigning individuals to one of three clusters, with individuals grouped by depth. BI = Balleny Islands; BS = Bransfield Strait; EW = Eastern Weddell Sea; RS = Ross Sea; SG = South Georgia; SO = South Orkneys; ST = Southern Thule; WP = West Antarctic Peninsula; WW = Western Weddell Sea. Depth bins = >250m;251-500m;501- 850m; 851-1000m; 1001->1250m.

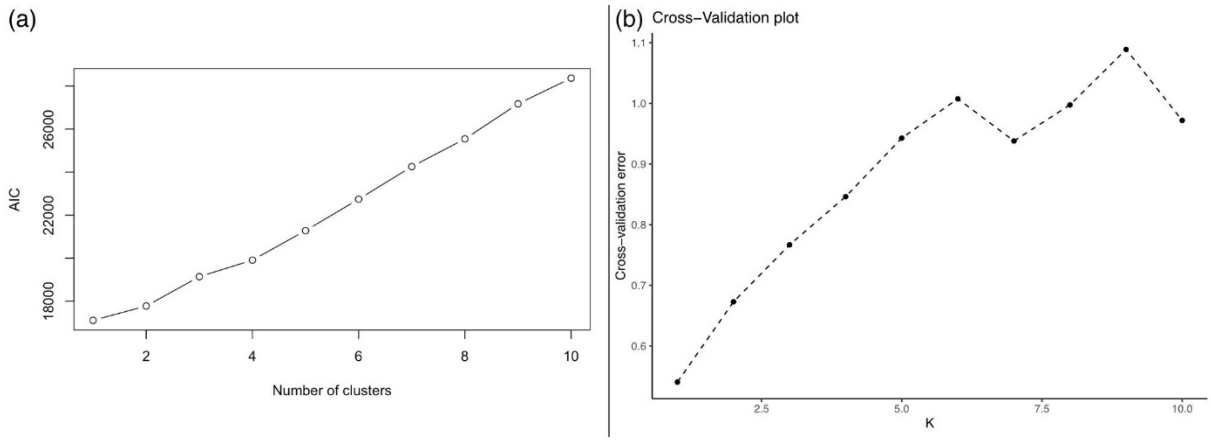

Figure D.17 Cross validation plots for *Aglaophamus* cf. *trissophyllus* Clade 2 (Agla 2) (a) for DAPC using function *snapclust* and Aikaike information Criterion (AIC), optimal number of clusters K corresponding with lowest AIC (b) ADMIXTURE cross validation analysis, optimal number of clusters K corresponding with lowest cross validation error. For both analyses, optimal clustering solutions *K*=1 > *K* =2> *K* =3

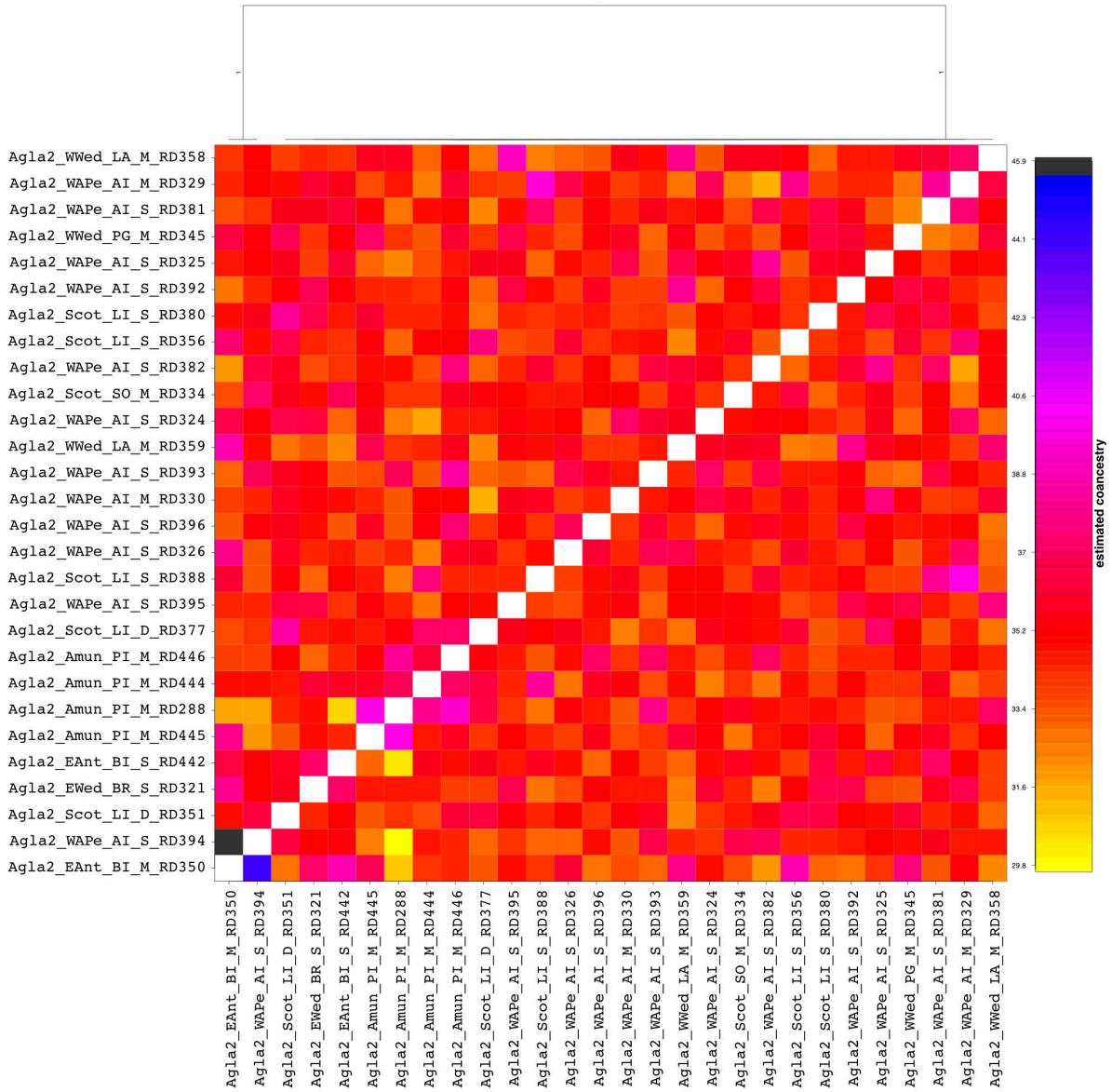

Figure D.18 Coancestry analysis of subset of *Aglaophamus* cf. *trissophyllus* Clade 2 (Agla 2) displayed as a simple co-ancestry matrix heatmap – top: simple hierarchical tree from raw data matrix with posterior population assignment probabilities; left and bottom: specimen IDs

Appendix E Research papers co-authored during course of PhD

Wiklund H, Rabone M, Glover AG, Bribiesca-Contreras G, **Drennan R**, Stewart ECD, Boolukos CM, King LD, Sherlock E, Smith CR, Dahlgren TG, Neal L (2023) Checklist of newly-vouchered annelid taxa from the Clarion-Clipperton Zone, central Pacific Ocean, based on morphology and genetic delimitation. Biodiversity Data Journal 11: e86921. doi:10.3897/BDJ.11.e86921

Bribiesca-Contreras G, Dahlgren TG, Amon DJ, Cairns S, **Drennan R,** Durden JM, Eléaume MP, Hosie AM, Kremenetskaia A, McQuaid K, O'Hara TD, Rabone M, Simon-Lledó E, Smith CR, Watling L, Wiklund H, Glover AG (2022) Benthic megafauna of the western Clarion-Clipperton Zone, Pacific Ocean. Zookeys, 1113:1-110. doi: 10.3897/zookeys.1113.82172

Bribiesca-Contreras G, Dahlgren TG, Horton T, Drazen JC, **Drennan R,** Jones DOB, Leitner AB, McQuaid KA, Smith CR, Taboada S, Wiklund H and Glover AG (2021) Biogeography and Connectivity Across Habitat Types and Geographical Scales in Pacific Abyssal Scavenging Amphipods. Frontiers in Marine Science. 8:705237. doi: 10.3389/fmars.2021.705237

Glossary of Terms

Annelida..... animal phylum, known as segmented worms. Includes earthworms, leeches, and marine polychaete worms.

Benthic..... relating to the seafloor

Brooder..... an organism that protects its larvae on or near its body

Circumpolar distribution ..... a biogeographic term for the range of a taxon that encompasses the entirety of a polar region in relevant habitats

Cosmopolitan distribution... a biogeographic term for the range of a taxon that extends across all, or most of, the world in relevant habitats

Cryptic Species..... Genetically distinct, morphologically indistinguishable species

Eurybathy ..... relating to the ability to live at wide depth ranges

Introgression ..... the transfer of genetic information from one species to another as a result of hybridization between them and repeated backcrossing

Lecithotrophic ..... developmental mode where larva feed on egg yolk during dispersal

Macrofauna ..... benthic fauna typically retained on a 1 mm sieve. Smaller than megafauna

Megafauna ..... large benthic fauna typically retained on a 1 cm sieve or net.

Metabarcoding ..... simultaneous sequencing and identification of multiple taxa within the same sample

Meiofauna ..... benthic fauna retained on a 0.1 mm sieve but that pass through a 1 mm sieve. Smaller than macrofauna

Mitonuclear discordance..... disagreement between mitochondrial and nuclear gene trees

Monophyletic ..... taxonomic group containing a most recent common ancestor and all its descendants

Paraphyly..... taxonomic group containing a most recent common ancestor but not all of its descendants

Pelagic ..... relating to inhabitation of the water column of seas and oceans

Planktotrophic..... developmental mode where larva feed in the water column and can be dispersed on ocean currents

Polyphyly ..... taxonomic group containing individuals that don't share a most recent common ancestor

Population Genetics ..... comparison of DNA sequences of populations at the level of single genes

Population Genomics ..... large scale comparison of DNA sequences of populations at the level of the genome

Psuedocryptic Species ..... species recognised to have morphological differences only after other methods have revealed their existance (e.g. molecular)

Species delimitation ..... recognising the boundaries between species

Species description..... the process of giving a recognised species a formal taxonomic name

Species identification ..... assigning a taxonomic name to a delimited species

Taxonomy ..... the science of naming, describing and classifying organisms

List of References

Ahrens, D., Fujisawa, T., Krammer, H. J., Eberle, J., Fabrizi, S., & Vogler, A. P. (2016). Rarity and Incomplete Sampling in DNA-Based Species Delimitation. *Systematic Biology*, *65*(3), 478–494. https://doi.org/10.1093/SYSBIO/SYW002

Ahyong, S. T., Kupriyanova, E., Burghardt, I., Sun, Y., Hutchings, P. A., Capa, M., & Cox, S. L. (2017). Phylogeography of the invasive Mediterranean fan worm, *Sabella spallanzanii* (Gmelin, 1791), in Australia and New Zealand. *Journal of the Marine Biological Association of the United Kingdom*, *97*(5), 985–991. https://doi.org/10.1017/S0025315417000261

Alalykina, I. L., & Polyakova, N. E. (2020). New deep-sea species of *Anobothrus* (Annelida: Ampharetidae) from the Kuril-Kamchatka Trench and adjacent abyssal regions. *Progress in Oceanography*, *182*, 102237. https://doi.org/10.1016/J.POCEAN.2019.102237

Alexander, D. H., & Lange, K. (2011). Enhancements to the ADMIXTURE algorithm for individual ancestry estimation. *BMC Bioinformatics*, *12*(1), 1–6. https://doi.org/10.1186/1471-2105-12-246/FIGURES/3

Alexander, D. H., Novembre, J., & Lange, K. (2009). Fast model-based estimation of ancestry in unrelated individuals. *Genome Research*, *19*(9), 1655–1664. https://doi.org/10.1101/GR.094052.109

Allcock, A. L., Barratt, I., Eléaume, M., Linse, K., Norman, M. D., Smith, P. J., Steinke, D., Stevens, D. W., & Strugnell, J. M. (2011). Cryptic speciation and the circumpolarity debate: A case study on endemic Southern Ocean octopuses using the COI barcode of life. *Deep Sea Research Part II: Topical Studies in Oceanography*, *58*(1–2), 242–249. https://doi.org/10.1016/J.DSR2.2010.05.016

Allcock, A. L., & Strugnell, J. M. (2012). Southern Ocean diversity: new paradigms from molecular ecology. *Trends in Ecology & Evolution*, *27*(9), 520–528. https://doi.org/10.1016/J.TREE.2012.05.009

Allen, C. S., & Smellie, J. L. (2008). Volcanic features and the hydrological setting of Southern Thule, South Sandwich Islands. *Antarctic Science*, *20*(3), 301–308. https://doi.org/10.1017/S0954102008001156

Almond, P. M. (2019). *Benthic Assemblage and Habitat Heterogeneity in the Prince Gustav Channel of the Antarctic Peninsula*. Newcastle University, Kings Road, Newcastle Upon Tyne, NE1 7RU.

Almond, P. M., Linse, K., Dreutter, S., Grant, S. M., Griffiths, H. J., Whittle, R. J., Mackenzie, M., & Reid, W. D. K. (2021). In-situ Image Analysis of Habitat Heterogeneity and Benthic Biodiversity in the Prince Gustav Channel, Eastern Antarctic Peninsula. *Frontiers in Marine Science*, *8*, 614496. https://doi.org/10.3389/fmars.2021.614496

Álvarez-Campos, P., Giribet, G., & Riesgo, A. (2017a). The *Syllis gracilis* species complex: A molecular approach to a difficult taxonomic problem (Annelida, Syllidae). *Molecular Phylogenetics and Evolution*, *109*, 138–150. https://doi.org/10.1016/J.YMPEV.2016.12.036

Álvarez-Campos, P., Giribet, G., San Martín, G., Rouse, G. W., & Riesgo, A. (2017b). Straightening the striped chaos: systematics and evolution of *Trypanosyllis* and the case of its pseudocryptic type species *Trypanosyllis krohnii (*Annelida, Syllidae). *Zoological Journal of the Linnean Society*, *179*(3), 492–540. https://doi.org/10.1111/ZOJ.12443

Alves, P. R., Halanych, K. M., Silva, E. P., & Santos, C. S. G. (2023). Nereididae (Annelida) phylogeny based on molecular data. *Organisms Diversity and Evolution*, *23*(3), 529–541. https://doi.org/10.1007/S13127-023-00608-9/FIGURES/3

Amon, D. J., Kennedy, B. R. C., Cantwell, K., Suhre, K., Glickson, D., Shank, T. M., & Rotjan, R. D. (2020). Deep-Sea Debris in the Central and Western Pacific Ocean. *Frontiers in Marine Science*, *7*, 507007. https://doi.org/10.3389/FMARS.2020.00369/BIBTEX

Amon, D. J., Ziegler, A. F., Dahlgren, T. G., Glover, A. G., Goineau, A., Gooday, A. J., Wiklund, H., & Smith, C. R. (2016). Insights into the abundance and diversity of abyssal megafauna in a polymetallic-nodule region in the eastern Clarion-Clipperton Zone. *Scientific Reports*, *6*(1), 1–12. https://doi.org/10.1038/srep30492

Anderson, J. B., Shipp, S. S., Lowe, A. L., Wellner, J. S., & Mosola, A. B. (2002). The Antarctic Ice Sheet during the Last Glacial Maximum and its subsequent retreat history: a review. *Quaternary Science Reviews*, *21*(1–3), 49–70. https://doi.org/10.1016/S0277-3791(01)00083-X

Anderson, M. P. B. C., Fenberg, P. B., Griffiths, H. J., & Linse, K. (2021). Macrobenthic Mollusca of the Prince Gustav Channel, Eastern Antarctic Peninsula: An Area Undergoing Colonisation. *Frontiers in Marine Science*, *0*, 1857. https://doi.org/10.3389/FMARS.2021.771369

Andrews, K. R., Good, J. M., Miller, M. R., Luikart, G., & Hohenlohe, P. A. (2016). *Harnessing the power of RADseq for ecological and evolutionary genomics*. *17*(2), 81–92. https://doi.org/10.1038/nrg.2015.28

Andrews, S. (2012). *FastQC: a quality control tool for high throughput sequence data* (0.12.0). Babraham Institute. https://www.bioinformatics.babraham.ac.uk/projects/fastqc/

Angulo-Preckler, C., Figuerola, B., Núñez-Pons, L., Moles, J., Martín-Martín, R., Rull-Lluch, J., Gómez-Garreta, A., & Avila, C. (2018). Macrobenthic patterns at the shallow marine waters in the caldera of the active volcano of Deception Island, Antarctica. *Continental Shelf Research*, *157*, 20–31. https://doi.org/10.1016/J.CSR.2018.02.005

Arnaud, P. M., López, C. M., Olaso, I., Ramil, F., Ramos-Esplá, A. A., & Ramos, A. (1998). Semi-quantitative study of macrobenthic fauna in the region of the South Shetland Islands and the Antarctic Peninsula. *Polar Biology*, *19*(3), 160–166.

Arntz, W. E., Brey, T., & Gallardo, V. A. (1994). Antarctic zoobenthos. *Oceanography and Marine Biology: An Annual Review*, *32*, 241–304.

Arntz, W. E., Gutt, J., & Klages, M. (1997). Antarctic marine biodiversity: an overview. *Antarctic Communities: Species, Structure and Survival. Cambridge University Press, Cambridge*, 3–14.

Arntz, W. E., & Gutt, J. (1999). The expedition ANTARKTIS XV/3 (EASIZ II) of RV" Polarstern" in 1998. *Berichte Zur Polarforschung (Reports on Polar Research)*, *301*.

Arwidsson, I. (1911). *Die Maldaniden. Wissenschaftliche Ergebnisse der Schwedischen Südpolar Expedition 1901-1903 Stockholm Zoologie II, Band 6, Lieferung*. 1–44.

Avise, J. C. (2009). Phylogeography: retrospect and prospect. *Journal of Biogeography*, *36*(1), 3–15. https://doi.org/10.1111/j.1365-2699.2008.02032.x

Baird, H. P., Miller, K. J., & Stark, J. S. (2011). Evidence of hidden biodiversity, ongoing speciation and diverse patterns of genetic structure in giant Antarctic amphipods. *Molecular Ecology*, *20*(16), 3439–3454. https://doi.org/10.1111/j.1365-294X.2011.05173.x

Baird, H. P., Miller, K. J., & Stark, J. S. (2012). Genetic Population Structure in the Antarctic Benthos: Insights from the Widespread Amphipod, Orchomenella franklini. *PLoS ONE*, *7*(3), e34363. https://doi.org/10.1371/journal.pone.0034363

Bakken, T. (2006). Redescription of two species of Neanthes (Polychaeta: Nereididae) possessing a large notopodial prechaetal lobe. *Scientia Marina*, *70*(SUPPL. 3), 27–33. https://doi.org/10.3989/scimar.2006.70s327

Bakken, T., & Wilson, R. S. (2005). Phylogeny of nereidids (Polychaeta, Nereididae) with paragnaths. *Zoologica Scripta*, *34*(5), 507–547. https://doi.org/10.1111/j.1463-6409.2005.00200.x

Barco, A., Schiaparelli, S., Houart, R., & Oliverio, M. (2012). Cenozoic evolution of Muricidae (Mollusca, Neogastropoda) in the Southern Ocean, with the description of a new subfamily. *Zoologica Scripta*, *41*(6), 596–616. https://doi.org/10.1111/j.1463-6409.2012.00554.x

Barker, P. F. (2001). Scotia sea regional tectonic evolution: Implications for mantle flow and palaeocirculation. *Earth-Science Reviews*, *55*(1–2), 1–39. https://doi.org/10.1016/S0012-8252(01)00055-1

Barnes, D. K. A. (2015). Antarctic sea ice losses drive gains in benthic carbon drawdown. *Current Biology 25*(18) PR789–R790. https://doi.org/10.1016/j.cub.2015.07.042

Barnes, D. K. A. (2017). Iceberg killing fields limit huge potential for benthic blue carbon in Antarctic shallows. *Global Change Biology*, *23*(7), 2649–2659. https://doi.org/10.1111/gcb.13523

Barnes, D. K. A., Kaiser, S., Griffiths, H. J., & Linse, K. (2009). Marine, intertidal, freshwater and terrestrial biodiversity of an isolated polar archipelago. *Journal of Biogeography*, *36*(4), 756–769. https://doi.org/10.1111/j.1365-2699.2008.02030.x

Barnes, D. K. A., & Peck, L. (2008). Vulnerability of Antarctic shelf biodiversity to predicted regional warming. *Climate Research*, *37*(2–3), 149–163. https://doi.org/10.3354/cr00760

Barnich, R., Fiege, D., Micaletto, G., & Gambi, M. C. (2006). Redescription of *Harmothoe spinosa* Kinberg, 1856 (Polychaeta: Polynoidae) and related species from Subantarctic and Antarctic waters, with the erection of a new genus. *Journal of Natural History*, *40*(1–2), 33–75. https://doi.org/10.1080/00222930500445044

Barnich, R., Gambi, M. C., & Fiege, D. (2012). Revision of the genus *Polyeunoa* McIntosh, 1885 (Polychaeta, Polynoidae). *Zootaxa*, *3523*(2012), 25–38.

Belan, T. A. (2004). Marine environmental quality assessment using polychaete taxocene characteristics in Vancouver Harbour. *Marine Environmental Research*, *57*(1–2), 89–101. https://doi.org/10.1016/S0141-1136(03)00062-X

Bely, A. E., & Wray, G. A. (2004). Molecular phylogeny of naidid worms (Annelida: Clitellata) based on cytochrome oxidase I. *Molecular Phylogenetics and Evolution*, *30*(1), 50–63. https://doi.org/http://dx.doi.org/10.1016/S1055-7903(03)00180-5

Bergamo, G., Carrerette, O., Shimabukuro, M., Santos, C. S. G., & Sumida, P. Y. G. (2023). Revealing a new eyeless *Nereis* (Nereididae: Annelida) clade from deep-sea organic falls. *Zoological Journal of the Linnean Society*. https://doi.org/10.1093/ZOOLINNEAN/ZLAD122

Bertolin, M. L., & Schloss, I. R. (2009). Phytoplankton production after the collapse of the Larsen A Ice Shelf, Antarctica. *Polar Biology*, *32*(10), 1435–1446. https://doi.org/10.1007/s00300-009-0638-x

Blake, J. A. (2015). New species of Scalibregmatidae (Annelida, Polychaeta) from the East Antarctic Peninsula including a description of the ecology and post-larval development of species of Scalibregma and Oligobregma. *Zootaxa*, *4033*(1), 57–93. https://doi.org/10.11646/zootaxa.4033.1.3

Blake, J. A. (2016). *Kirkegaardia* (Polychaeta, Cirratulidae), new name for *Monticellina* Laubier, preoccupied in the Rhabdocoela, together with new records and descriptions of eight previously known and sixteen new species from the Atlantic, Pacific, and Southern Oceans. *Zootaxa*, *4166*(1), 1–93–1–93. https://doi.org/10.11646/ZOOTAXA.4166.1.1

Blake, J. A. (2017). Polychaeta orbiniidae from antarctica, the southern ocean, the abyssal pacific ocean, and off South America. *Zootaxa*, *4218*(1), 1–145. https://doi.org/10.11646/zootaxa.4218.1.1

Blake, J. A. (2018). Bitentaculate Cirratulidae (Annelida, Polychaeta) collected chiefly during cruises of the R/V Anton Bruun , USNS Eltanin , USCG Glacier , R/V Hero , RVIB Nathaniel B. Palmer , and R/V Polarstern from the Southern Ocean, Antarctica, and off Western South A. *Zootaxa; Vol 4537, No 1*https://www.biotaxa.org/Zootaxa/article/view/zootaxa.4537.1.1/37861

Blake, J. A. (2019). New species of Cirratulidae (Annelida, Polychaeta) from abyssal depths of the Clarion-Clipperton Fracture Zone, North Equatorial Pacific Ocean. *Zootaxa*, *4629*(2), 151–187–151–187. https://doi.org/10.11646/ZOOTAXA.4629.2.1

Blake, J. A. (2020). New species and records of deep-water Orbiniidae (Annelida, Polychaeta) from the Eastern Pacific continental slope, abyssal Pacific Ocean, and the South China Sea. *Zootaxa*, *4730*(1), 1–61–1–61. https://doi.org/10.11646/ZOOTAXA.4730.1.1

Blanchard, C., Harrould-Kolieb, E., Jones, E., & Taylor, M. L. (2023). The current status of deep-sea mining governance at the International Seabed Authority. *Marine Policy*, *147*, 105396. https://doi.org/10.1016/J.MARPOL.2022.105396

Bogantes, V. E., Whelan, N. V., Webster, K., Mahon, A. R., & Halanych, K. M. (2020). Unrecognized diversity of a scale worm, Polyeunoa laevis (Annelida: Polynoidae), that feeds on soft coral. *Zoologica Scripta*, *49*(2), 236–249. https://doi.org/10.1111/zsc.12400

Bonifácio, P., & Menot, L. (2018). New genera and species from the Equatorial Pacific provide phylogenetic insights into deep-sea Polynoidae (Annelida). *Zoological Journal of the Linnean Society*, *185*(3), 555–635. https://doi.org/10.1093/zoolinnean/zly063

Bonifácio, P., & Menot, L. (2019). New genera and species from the Equatorial Pacific provide phylogenetic insights into deep-sea Polynoidae (Annelida). *Zoological Journal of the Linnean Society*, *185*(3), 555–635.

Bouchet, P. (2006). The magnitude of marine biodiversity. *The Exploration of Marine Biodiversity: Scientific and Technological Challenges*, 31–62.

Bouchet, P., Decock, W., Lonneville, B., Vanhoorne, B., & Vandepitte, L. (2023). Marine biodiversity discovery: the metrics of new species descriptions. *Frontiers in Marine Science*, *10*, 929989. https://doi.org/10.3389/FMARS.2023.929989/BIBTEX

Bouckaert, R., Vaughan, T. G., Barido-Sottani, J., Duchêne, S., Fourment, M., Gavryushkina, A., Heled, J., Jones, G., Kühnert, D., De Maio, N., Matschiner, M., Mendes, F. K., Müller, N. F., Ogilvie, H. A., Du Plessis, L., Popinga, A., Rambaut, A., Rasmussen, D., Siveroni, I., … Drummond, A. J. (2019). BEAST 2.5: An advanced software platform for Bayesian evolutionary analysis. *PLOS Computational Biology*, *15*(4), e1006650. https://doi.org/10.1371/JOURNAL.PCBI.1006650

Bracco, A., Liu, G., Galaska, M. P., Quattrini, A. M., & Herrera, S. (2019). Integrating physical circulation models and genetic approaches to investigate population connectivity in deep-sea corals. *Journal of Marine Systems*, *198*, 103189. https://doi.org/10.1016/J.JMARSYS.2019.103189

Brachfeld, S., Domack, E., Kissel, C., Laj, C., Leventer, A., Ishman, S., Gilbert, R., Camerlenghi, A., & Eglinton, L. B. (2003). Holocene history of the Larsen - A Ice Shelf constrained by geomagnetic paleointensity dating. *Geology*, *31*(9), 749–752. https://doi.org/10.1130/G19643.1

Brandão, S. N., Sauer, J., & Schön, I. (2010). Circumantarctic distribution in Southern Ocean benthos? A genetic test using the genus *Macroscapha* (Crustacea, Ostracoda) as a model. *Molecular Phylogenetics and Evolution*, *55*(3), 1055–1069. https://doi.org/10.1016/J.YMPEV.2010.01.014

Brandt, A., De Broyer, C., De Mesel, I., Ellingsen, K. ., Gooday, A. ., Hilbig, B., Linse, K., Thomson, M. R. ., & Tyler, P. (2007a). The biodiversity of the deep Southern Ocean benthos. *Philosophical Transactions of the Royal Society B: Biological Sciences*, *362*(1477), 39–66. https://doi.org/10.1098/rstb.2006.1952

Brandt, A., Gooday, A. J., Brandao, S. N., Brix, S., Brökeland, W., Cedhagen, T., Choudhury, M., Cornelius, N., Danis, B., De Mesel, I., Brandão, S. N., Brix, S., Brökeland, W., Cedhagen, T., Choudhury, M., Cornelius, N., Danis, B., De Mesel, I., Diaz, R. J., … Vanreusel, A. (2007b). First insights into the biodiversity and biogeography of the Southern Ocean deep sea. *Nature*, *447*(7142), 307. https://doi.org/10.1038/nature05827

Brandt, A., Grif Ths, H., Gutt, J., Linse, K., Schiaparelli, S., Ballerini, T., Danis, B., & Pfannkuche, O. (2014). Challenges of deep-sea biodiversity assessments in the Southern Ocean. *Adv Polar Sci*, *25*(3), 204–212. https://doi.org/10.13679/j.advps.2014.3.00204

Brandt, A., Linse, K., Ellingsen, K. E., & Somerfield, P. J. (2016). Depth-related gradients in community structure and relatedness of bivalves and isopods in the Southern Ocean. *Progress in Oceanography*, *144*, 25–38. https://doi.org/10.1016/J.POCEAN.2016.03.003

Brandt, A., Linse, K., & Schüller, M. (2009). Bathymetric distribution patterns of Southern Ocean macrofaunal taxa: Bivalvia, Gastropoda, Isopoda and Polychaeta. *Deep Sea Research Part I: Oceanographic Research Papers*, *56*(11), 2013–2025. https://doi.org/10.1016/J.DSR.2009.06.007

Brasier, M. J., Grant, S. M., Trathan, P. N., Allcock, L., Ashford, O., Blagbrough, H., Brandt, A., Danis, B., Downey, R., Eléaume, M. P., Enderlein, P., Ghiglione, C., Hogg, O., Linse, K., Mackenzie, M., Moreau, C., Robinson, L. F., Rodriguez, E., Spiridonov, V., … Griffiths, H. J. (2018). Benthic biodiversity in the South Orkney Islands Southern Shelf Marine Protected Area. *Biodiversity*, *19*(1–2), 5–19. https://doi.org/10.1080/14888386.2018.1468821

Brasier, M. J., Harle, J., Wiklund, H., Jeffreys, R. M., Linse, K., Ruhl, H. A., & Glover, A. G. (2017). Distributional Patterns of Polychaetes Across the West Antarctic Based on DNA Barcoding and Particle Tracking Analyses. *Frontiers in Marine Science*, *4*, 356. https://doi.org/10.3389/fmars.2017.00356

Brasier, M. J., Wiklund, H., Neal, L., Jeffreys, R., Linse, K., Ruhl, H., & Glover, A. G. (2016). DNA barcoding uncovers cryptic diversity in 50% of deep-sea Antarctic polychaetes. *Royal Society Open Science*, *3*(11), 160432. https://doi.org/10.1098/rsos.160432

Bribiesca-Contreras, G., Dahlgren, T. G., Amon, D. J., Cairns, S., Drennan, R., Durden, J. M., Eléaume, M. P., Hosie, A. M., Kremenetskaia, A., McQuaid, K., O'hara, T. D., Rabone, M., Simon-Lledó, E., Smith, C. R., Watling, L., Wiklund, H., & Glover, A. G. (2022). Benthic megafauna of the western Clarion-Clipperton Zone, Pacific Ocean. *ZooKeys*, *1113*(1113), 1. https://doi.org/10.3897/ZOOKEYS.1113.82172

Brooks, C., & Christian, C. (2023). Antarctica and the Southern Ocean: Our Last Great Wilderness. In *The Ocean and Us* (pp. 185–193). Springer.

Bucklin, A., Steinke, D., & Blanco-Bercial, L. (2011). DNA Barcoding of Marine Metazoa. *Annual Review of Marine Science*, *3*(1), 471–508. https://doi.org/10.1146/annurev-marine-120308-080950

Buesseler, K. O., Lamborg, C. H., Boyd, P. W., Lam, P. J., Trull, T. W., Bidigare, R. R., Bishop, J. K. B., Casciotti, K. L., Dehairs, F., Elskens, M., Honda, M., Karl, D. M., Siegel, D. A., Silver, M. W., Steinberg, D. K., Valdes, J., Van Mooy, B., & Wilson, S. (2007). Revisiting carbon flux through the ocean's twilight zone. *Science*, *316*(5824), 567–570. https://doi.org/10.1126/SCIENCE.1137959/SUPPL_FILE/BUESSELER.SOM.PDF

Byrne, R. H., Mecking, S., Feely, R. A., & Liu, X. (2010). Direct observations of basin-wide acidification of the North Pacific Ocean. *Geophysical Research Letters*, *37*(2). https://doi.org/10.1029/2009GL040999

Camerlenghi, A., Domack, E., Rebesco, M., Gilbert, R., Ishman, S., Leventer, A., Brachfeld, S., & Drake, A. (2001). Glacial morphology and post-glacial contourites in northern Prince Gustav Channel (NW Weddell Sea, Antarctica). *Marine Geophysical Research*, *22*(5–6), 417–443. https://doi.org/10.1023/A:1016399616365

Capa, M., & Hutchings, P. (2021). Annelid Diversity: Historical Overview and Future Perspectives. *Diversity 2021, Vol. 13, Page 129*, *13*(3), 129. https://doi.org/10.3390/D13030129

Capa, M., Hutchings, P., Teresa Aguado, M., & Bott, N. J. (2011). Phylogeny of Sabellidae (Annelida) and relationships with other taxa inferred from morphology and multiple genes. *Cladistics*, *27*(5), 449–469. https://doi.org/10.1111/J.1096-0031.2010.00341.X

Carney, R. S. (1997). Basing conservation policies for the deep-sea floor on current, diversity concepts: A consideration of rarity. *Biodiversity and Conservation*, *6*(11), 1463–1485. https://doi.org/10.1023/A:1018310302215/METRICS

Carr, C. M., Hardy, S. M., Brown, T. M., Macdonald, T. A., & Hebert, P. D. N. (2011). A Tri-Oceanic Perspective: DNA Barcoding Reveals Geographic Structure and Cryptic Diversity in Canadian Polychaetes. *PLOS ONE*, *6*(7), e22232. https://doi.org/10.1371/JOURNAL.PONE.0022232

Catchen, J., Hohenlohe, P. A., Bassham, S., Amores, A., & Cresko, W. A. (2013). Stacks: an analysis tool set for population genomics. *Molecular Ecology*, *22*(11), 3124–3140. https://doi.org/10.1111/MEC.12354

Ceballos, S. G., Roesti, M., Matschiner, M., Fernández, D. A., Damerau, M., Hanel, R., & Salzburger, W. (2019). Phylogenomics of an extra-Antarctic notothenioid radiation reveals a previously unrecognized lineage and diffuse species boundaries. *BMC Evolutionary Biology*, *19*(1), 1–14. https://doi.org/10.1186/S12862-019-1345-Z/FIGURES/6

Cheng, J., Hui, M., & Sha, Z. (2019). Transcriptomic analysis reveals insights into deep-sea adaptations of the dominant species, *Shinkaia crosnieri* (Crustacea: Decapoda: Anomura), inhabiting both hydrothermal vents and cold seeps. *BMC Genomics*, *20*(1), 1–16. https://doi.org/10.1186/S12864-019-5753-7/FIGURES/5

Chiba, S., Saito, H., Fletcher, R., Yogi, T., Kayo, M., Miyagi, S., Ogido, M., & Fujikura, K. (2018). Human footprint in the abyss: 30 year records of deep-sea plastic debris. *Marine Policy*, *96*, 204–212. https://doi.org/10.1016/J.MARPOL.2018.03.022

Chown, S. L., Clarke, A., Fraser, C. I., Cary, S. C., Moon, K. L., & McGeoch, M. A. (2015). The changing form of Antarctic biodiversity. *Nature*, *522*(7557), 431–438. https://doi.org/10.1038/nature14505

Chown, S. L., Lee, J. E., Hughes, K. A., Barnes, J., Barrett, P. J., Bergstrom, D. M., Convey, P., Cowan, D. A., Crosbie, K., Dyer, G., Frenot, Y., Grant, S. M., Herr, D., Kennicutt, M. C., Lamers, M., Murray, A., Possingham, H. P., Reid, K., Riddle, M. J., … Wall, D. H. (2012). Challenges to the future conservation of the antarctic. *Science 337* (6091), 158–159) https://doi.org/10.1126/science.1222821

Christodoulou, M., O'Hara, T. D., Hugall, A. F., & Arbizu, P. M. (2019). Dark Ophiuroid Biodiversity in a Prospective Abyssal Mine Field. *Current Biology*, *29*(22), 3909-3912.e3. https://doi.org/10.1016/J.CUB.2019.09.012

Claridge, M. F., Dawah, H. A., & Wilson, M. R. (Eds.) (1997). *Species : the units of biodiversity*. Springer Dordrecht.

Clarke, A. (1988). Seasonality in the antarctic marine environment. In *Comparative Biochemistry and Physiology -- Part B: Biochemistry and*

90(3) 461–473. https://doi.org/10.1016/0305-0491(88)90285-4

Clarke, A. (2008). Antarctic marine benthic diversity: patterns and processes. *Journal of Experimental Marine Biology and Ecology*, *366*(1–2), 48–55. https://doi.org/10.1016/j.jembe.2008.07.008

Clarke, A., Aronson, R. B., Crame, J. A., Gili, J.-M., & Blake, D. B. (2004). Evolution and diversity of the benthic fauna of the Southern Ocean continental shelf. *Antarctic Science*, *16*(4), 559–568. https://doi.org/10.1017/S0954102004002329

Clarke, A., & Crame, J. A. (1989). The origin of the Southern Ocean marine fauna. *Geological Society, London, Special Publications*, *47*(1), 253–268. https://doi.org/10.1144/GSL.SP.1989.047.01.19

Clarke, A., & Crame, J. A. (1992). The Southern Ocean benthic fauna and climate change: a historical perspective. *Philosophical Transactions of the Royal Society of London. Series B: Biological Sciences*, *338*(1285), 299–309. https://doi.org/10.1098/rstb.1992.0150

Clarke, A., & Johnston, N. M. (2003). Antarctic Marine Benthic Diversity. https://doi.org/10.1201/9780203180570-8

Clement, M., Snell, Q., Walker, P., Posada, D., & Crandall, K. (2002). TCS: estimating gene genealogies. *Ipdps*, 184.

Cohen, B. L., Gawthrop, A., & Cavalier–Smith, T. (1998). Molecular phylogeny of brachiopods and phoronids based on nuclear–encoded small subunit ribosomal RNA gene sequences. *Philosophical Transactions of the Royal Society of London. Series B: Biological Sciences*, *353*(1378), 2039. http://rstb.royalsocietypublishing.org/content/353/1378/2039.abstract

Colgan, D. J., Hutchings, P. A., & Braune, M. (2006). A multigene framework for polychaete phylogenetic studies. *Organ Divers Evol*, *6*. https://doi.org/10.1016/j.ode.2005.11.002

Collins, E. E., Galaska, M. P., Halanych, K. M., & Mahon, A. R. (2018). Population genomics of *Nymphon australe* Hodgson, 1902 (Pycnogonida, Nymphonidae) in the Western Antarctic. *Biological Bulletin*, *234*(3), 180–191. https://doi.org/10.1086/698691/ASSET/IMAGES/LARGE/FGA4.JPEG

Combosch, D. J., Lemer, S., Ward, P. D., Landman, N. H., & Giribet, G. (2017). Genomic signatures of evolution in Nautilus—An endangered living fossil. *Molecular Ecology*, *26*(21), 5923–5938. https://doi.org/10.1111/MEC.14344

Convey, P., Stevens, M. I., Hodgson, D. A., Smellie, J. L., Hillenbrand, C.-D., Barnes, D. K. A. A., Clarke, A., Pugh, P. J. A. A., Linse, K., & Cary, S. C. (2009). Exploring biological constraints on the glacial history of Antarctica. *Quaternary Science Reviews*, *28*(27–28), 3035–3048. https://doi.org/10.1016/J.QUASCIREV.2009.08.015

Cook, A. J., Fox, A. J., Vaughan, D. G., & Ferrigno, J. G. (2005). Retreating glacier fronts on the Antarctic Peninsula over the past half-century. *Science*, *308*(5721), 541–544. https://doi.org/10.1126/science.1104235

Cook, A. J., & Vaughan, D. G. (2010). Overview of areal changes of the ice shelves on the Antarctic Peninsula over the past 50 years. *The Cryosphere.*, *4*(1), 77–98.

Cooper, A. P. R. (1997). Historical observations of Prince Gustav Ice Shelf. *Polar Record*, *33*(187), 285–294. https://doi.org/10.1017/S0032247400025389

Cossu, P., Maltagliati, F., Pannacciulli, F. G., Simonini, R., Massamba-N'Siala, G., Casu, M., Lardicci, C., Prevedelli, D., & Castelli, A. (2015). Phylogeography of Ophryotrocha labronica (Polychaeta, Dorvilleidae) along the Italian coasts. *Marine Ecology*, *36*(4), 1088–1097. https://doi.org/10.1111/MAEC.12203

Cowart, D. A., Schiaparelli, S., Alvaro, M. C., Cecchetto, M., Port, A.-S. Le, Jollivet, D., & Hourdez, S. (2022). Origin, diversity, and biogeography of Antarctic scale worms (Polychaeta: Polynoidae): a wide-scale barcoding approach. *Ecology and Evolution*, *12*(7), e9093. https://doi.org/10.1002/ECE3.9093

Cummings, V. J., Hewitt, J. E., Thrush, S. F., Marriott, P. M., Halliday, N. J., & Norkko, A. (2018). Linking ross sea coastal benthic communities to environmental conditions: Documenting baselines in a spatially variable and changing world. *Frontiers in Marine Science*, *5*. https://doi.org/10.3389/fmars.2018.00232

Cummings, V. J, Thrush, S., Norkko, A., Andrew, N., Hewitt, J., Funnell, G., & Schwarz, A. (2006). Accounting for local scale variability in benthos: implications for future assessments of latitudinal trends in the coastal Ross Sea. *Antarctic Science*, *18*(4), 633.

Dahlgren, T. G., Lundberg, J., Pleijel, F., & Sundberg, P. (2000). Morphological and molecular evidence of the phylogeny of Nereidiform polychaetes (Annelida). *Journal of Zoological Systematics and Evolutionary Research*, *38*(4), 249–253. https://doi.org/10.1046/j.1439-0469.2000.384150.x

Darriba, Di., Posada, D., Kozlov, A. M., Stamatakis, A., Morel, B., & Flouri, T. (2020). ModelTest-NG: A New and Scalable Tool for the Selection of DNA and Protein Evolutionary Models. *Molecular Biology and Evolution*, *37*(1), 291–294. https://doi.org/10.1093/MOLBEV/MSZ189

Day, J. H. (1963). The polychaete fauna of South Africa : Part 8. New species and records from grab samples and dredgings. *Bulletin of the British Museum (Natural History).*, *10*, 381–445. https://doi.org/10.5962/bhl.part.20530

De Broyer, C., Clarke, A., Koubbi, P., Pakhomov, E., Scott, F., Vanden Berghe, E., & Danis, B. (2023). *Register of Antarctic Marine Species*.

De Broyer, C., & Danis, B. (2011). How many species in the Southern Ocean? Towards a dynamic inventory of the Antarctic marine species. *Deep Sea Research Part II: Topical Studies in Oceanography*, *58*(1–2), 5–17. https://doi.org/10.1016/J.DSR2.2010.10.007

De Broyer, C., Koubbi, P., Griffiths, H., & Grant, S. A. (2014). *Biogeographic atlas of the Southern Ocean*. Scientific Committee on Antarctic Research Cambridge.

de León-González, J. A., & Solís-Weiss, V. (2000). A review of the polychaete family Nereididae from western Mexico. *Bulletin of Marine Science*, *67*(1), 549–569.

de Medeiros, B. A. S., & Farrell, B. D. (2018). Whole-genome amplification in doubledigest RADseq results in adequate libraries but fewer sequenced loci. *PeerJ*, *2018*(7), e5089. https://doi.org/10.7717/PEERJ.5089/SUPP-10

Deagle, B. E., Faux, C., Kawaguchi, S., Meyer, B., & Jarman, S. N. (2015). Antarctic krill population genomics: apparent panmixia, but genome complexity and large population size muddy the water. *Molecular Ecology*, *24*(19), 4943–4959. https://doi.org/10.1111/MEC.13370

Dellicour, S., & Flot, J. F. (2018). The hitchhiker's guide to single-locus species delimitation. *Molecular Ecology Resources*, *18*(6), 1234–1246. https://doi.org/10.1111/1755-0998.12908

DeSalle, R., & Goldstein, P. (2019). Review and Interpretation of Trends in DNA Barcoding. *Frontiers in Ecology and Evolution*, *7*, 302. https://doi.org/10.3389/FEVO.2019.00302/BIBTEX

Di Franco, D., Linse, K., Griffiths, H. J., & Brandt, A. (2021). Abundance data of benthic peracarid crustaceans from the South Atlantic and Southern Ocean. *Data in Brief*, *39*, 107468. https://doi.org/10.1016/J.DIB.2021.107468

Di Franco, D., Linse, K., Griffiths, H. J., Haas, C., Saeedi, H., & Brandt, A. (2020). Abundance and Distributional Patterns of Benthic Peracarid Crustaceans From the Atlantic Sector of the Southern Ocean and Weddell Sea. *Frontiers in Marine Science*, *7*. https://doi.org/10.3389/FMARS.2020.554663

Dierssen, H. M., Smith, R. C., & Vernet, M. (2002). Glacial meltwater dynamics in coastal waters west of the Antarctic peninsula. *Proceedings of the National Academy of Sciences of the United States of America*, *99*(4), 1790–1795. https://doi.org/10.1073/pnas.032206999

Dietz, L., Arango, C. P., Dömel, J. S., Halanych, K. M., Harder, A. M., Held, C., Mahon, A. R., Mayer, C., Melzer, R. R., Rouse, G. W., Weis, A., Wilson, N. G., & Leese, F. (2014). Regional differentiation and extensive hybridization between mitochondrial clades of the Southern Ocean giant sea spider Colossendeis megalonyx. *Royal Society Open Science*, *2*(7). https://doi.org/10.1098/RSOS.140424

Domack, E., Leventer, A., Gilbert, R., Brachfeld, S., Ishman, S., Camerlenghi, A., Gavahan, K., Carlson, D., & Barkoukis, A. (2001). Cruise reveals history of Holocene Larsen Ice Shelf. *Eos, Transactions American Geophysical Union*, *82*(2), 13–13. https://doi.org/10.1029/01EO00009

Dömel, J. S., Dietz, L., Macher, T. H., Rozenberg, A., Mayer, C., Spaak, J. M., Melzer, R. R., & Leese, F. (2020). Analyzing drivers of speciation in the Southern Ocean using the sea spider species complex Colossendeis megalonyx as a test case. *Polar Biology*, *43*(4), 319–342. https://doi.org/10.1007/S00300-020-02636-Z/FIGURES/3

Drennan, R., Dahlgren, T. G., Linse, K., & Glover, A. G. (2020). *Annelid Fauna of the Prince Gustav Channel, a previously ice-covered seaway on the northeastern Antarctic Peninsula - Data. v1.5. SCAR - AntOBIS. Dataset/Occurrence.* Frontiers in Marine Science; Frontiers. https://doi.org/10.3389/fmars.2020.595303

Drennan, R., Wiklund, H., Rabone, M., Georgieva, M. N., Dahlgren, T. G., & Glover, A. G. (2021a). *Neanthes goodayi* sp. nov. (Annelida, Nereididae), a remarkable new annelid species living inside deep-sea polymetallic nodules. *European Journal of Taxonomy*, *760*, 160–185. https://doi.org/10.5852/EJT.2021.760.1447

Drennan R., Dahlgren T.G., Linse K. and Glover A.G. (2021b) Annelid Fauna of the Prince Gustav Channel, a Previously Ice–Covered Seaway on the Northeastern Antarctic Peninsula. *Frontiers in Marine Science*. 7:595303. https://doi.org/10.3389/fmars.2020.595303

Drennan, R., Wiklund, H., Rouse, G. W., Georgieva, M. N., Wu, X., Kobayashi, G., Yoshino, K., & Glover, A. G. (2019). Taxonomy and phylogeny of mud owls (Annelida: Sternaspidae), including a new synonymy and new records from the Southern Ocean, North East Atlantic Ocean and Pacific Ocean: challenges in morphological delimitation. *Marine Biodiversity*. https://doi.org/10.1007/s12526-019-00998-0

Dreutter, S., Dorschel, B., & Linse, K. (2020). *Swath sonar bathymetry data of RRS JAMES CLARK ROSS during cruise JR17003a with links to multibeam raw data.* PANAGAEA 2020:EM122. https://doi.org/10.1594/PANGAEA.916177

Droege, G., Barker, K., Seberg, O., Coddington, J., Benson, E., Berendsohn, W. G., Bunk, B., Butler, C., Cawsey, E. M., Deck, J., Döring, M., Flemons, P., Gemeinholzer, B., Güntsch, A., Hollowell, T., Kelbert, P., Kostadinov, I., Kottmann, R., Lawlor, R. T., … Zhou, X. (2016). The Global Genome Biodiversity Network (GGBN) Data Standard specification. *Database*, *2016*, baw125. https://doi.org/10.1093/database/baw125

Dueñas, L. F., Tracey, D. M., Crawford, A. J., Wilke, T., Alderslade, P., & Sánchez, J. A. (2016). The Antarctic Circumpolar Current as a diversification trigger for deep-sea octocorals. *BMC Evolutionary Biology*, *16*(1), 2. https://doi.org/10.1186/s12862-015-0574-z

Dutkiewicz, A., Judge, A., & Müller, R. D. (2020). Environmental predictors of deep-sea polymetallic nodule occurrence in the global ocean. *Geology*, *48*(3), 293–297. https://doi.org/10.1130/G46836.1

Eberle, J., Ahrens, D., Mayer, C., Niehuis, O., & Misof, B. (2020). A Plea for Standardized Nuclear Markers in Metazoan DNA Taxonomy. *Trends in Ecology & Evolution*, *35*(4), 336–345. https://doi.org/10.1016/J.TREE.2019.12.003

Edgar, R. C. (2004). MUSCLE: multiple sequence alignment with high accuracy and high throughput. *Nucleic Acids Research*, *32*(5), 1792–1797. http://dx.doi.org/10.1093/nar/gkh340

Eilertsen, M. H., Kongsrud, J. A., Alvestad, T., Stiller, J., Rouse, G. W., & Rapp, H. T. (2017). Do ampharetids take sedimented steps between vents and seeps? Phylogeny and habitat-use of Ampharetidae (Annelida, Terebelliformia) in chemosynthesis-based ecosystems. *BMC Evolutionary Biology*, *17*(1), 1–15. https://doi.org/10.1186/S12862-017-1065-1/FIGURES/5

Eleftheriou, A., & Holme, N. A. (1984). Macrofauna techniques. *Methods for the Study of Marine Benthos*, 140–216.

Ellingsen, K. E., Brandt, A., Ebbe, B., & Linse, K. (2007). Diversity and species distribution of polychaetes, isopods and bivalves in the Atlantic sector of the deep Southern Ocean. *Polar Biology*, *30*(10), 1265–1273. https://doi.org/10.1007/s00300-007-0287-x

Etourneau, J., Sgubin, G., Crosta, X., Swingedouw, D., Willmott, V., Barbara, L., Houssais, M. N., Schouten, S., Damsté, J. S. S., Goosse, H., Escutia, C., Crespin, J., Massé, G., & Kim, J. H. (2019). Ocean temperature impact on ice shelf extent in the eastern Antarctic Peninsula. *Nature Communications*, *10*(1), 1–8. https://doi.org/10.1038/s41467-018-08195-6

European Commission. (2020). *Blue Growth*. https://ec.europa.eu/maritimeaffairs/policy/blue_growth_en

Evans, J., Pudsey, C. J., ÓCofaigh, C., Morris, P., & Domack, E. (2005). Late Quaternary glacial history, flow dynamics and sedimentation along the eastern margin of the Antarctic Peninsula Ice Sheet. *Quaternary Science Reviews*, *24*(5–6), 741–774. https://doi.org/10.1016/j.quascirev.2004.10.007

Excoffier, L., & Lischer, H. E. L. (2010). Arlequin suite ver 3.5: a new series of programs to perform population genetics analyses under Linux and Windows. *Molecular Ecology Resources*, *10*(3), 564–567. https://doi.org/10.1111/J.1755-0998.2010.02847.X

Ezard, T., Fujisawa, T., & Barraclough, T. (2021). *splits: Species' Limits by Threshold Statistics. R package* (1.0-20/r56). https://r-forge.r-project.org/projects/splits/

Fabry, V. J., McClintock, J. B., Mathis, J. T., & Grebmeier, J. M. (2009). Ocean acidification at high latitudes: the bellwether. *Oceanography*, *22*(4), 160–171.

Fahrbach, E., Rohardt, G., Schröder, M., & Strass, V. (1994). Transport and structure of the Weddell Gyre. *Annales Geophysicae*, *12*(9), 840–855. https://doi.org/10.1007/S00585-994-0840-7/METRICS

Fauchald, K. (1972). Benthic polychaetous annelids from deep water off western Mexico and adjacent areas in the eastern Pacific Ocean. *Allan Hancock Monographs in Marine Biology*.

Fauchald, K. (1977). The polychaete worms. Definitions and keys to the orders, families and genera. *Natural History Museum of Los Angeles County, Science Series*.

Fauchald, K., & Jumars, P. A. (1979). *The diet of worms: a study of polychaete feeding guilds*.

Fauvel, P. (1936). *Polychètes*. J.E. Buschman.

Ferrigno, J. G., Cook, A. J., Foley, K. M., Williams Jr., R. S., Swithinbank, C., Fox, A. J., Thompson, J. W., & Sievers, J. (2006). *Coastal-change and Glaciological Map of the Trinity Peninsula Area and South Shetland Islands, Antarctica, 1843-2001*. US Department of the Interior, US Geological Survey. https://doi.org/10.3133/i2600A

Fogwill, C. J., Turney, C. S. M., Menviel, L., Baker, A., Weber, M. E., Ellis, B., Thomas, Z. A., Golledge, N. R., Etheridge, D., Rubino, M., Thornton, D. P., van Ommen, T. D., Moy, A. D., Curran, M. A. J., Davies, S., Bird, M. I., Munksgaard, N. C., Rootes, C. M., Millman, H., … Cooper, A. (2020). Southern Ocean carbon sink enhanced by sea-ice feedbacks at the Antarctic Cold Reversal. *Nature Geoscience*, *13*(7), 489–497. https://doi.org/10.1038/s41561-020-0587-0

Foll, M., & Gaggiotti, O. (2008). A Genome-Scan Method to Identify Selected Loci Appropriate for Both Dominant and Codominant Markers: A Bayesian Perspective. *Genetics*, *180*(2), 977–993. https://doi.org/10.1534/GENETICS.108.092221

Folmer, O., Black, M., Hoeh, W., Lutz, R., & Vrijenhoek, R. (1994). DNA primers for amplification of mitochondrial cytochrome c oxidase subunit I from diverse metazoan invertebrates. In *Molecular Marine Biology and Biotechnology* (Vol. 3, Issue 5).

Francis, R. M. (2017). pophelper: an R package and web app to analyse and visualize population structure. *Molecular Ecology Resources*, *17*(1), 27–32. https://doi.org/10.1111/1755-0998.12509

Fujisawa, T., & Barraclough, T. G. (2013). Delimiting Species Using Single-Locus Data and the Generalized Mixed Yule Coalescent Approach: A Revised Method and Evaluation on Simulated Data Sets. *Systematic Biology*, *62*(5), 707–724. https://doi.org/10.1093/SYSBIO/SYT033

Fukuda, M. V., & Barroso, R. (2019). First report of brooding of eggs in the deep-sea genus *Anguillosyllis* (Annelida: Syllidae). *Journal of the Marine Biological Association of the United Kingdom*, *99*(8), 1775–1777. https://doi.org/10.1017/S0025315419000754

Gage, J. D., & Tyler, P. A. (1991). *Deep-sea biology: a natural history of organisms at the deep-sea floor*. Cambridge University Press.

Galaska, M. P., Sands, C. J., Santos, S. R., Mahon, A. R., & Halanych, K. M. (2017a). Geographic structure in the Southern Ocean circumpolar brittle star Ophionotus victoriae (Ophiuridae) revealed from mtDNA and single-nucleotide polymorphism data. *Ecology and Evolution*, *7*(2), 475–485. https://doi.org/10.1002/ECE3.2617

Galaska, M. P., Sands, C. J., Santos, S. R., Mahon, A. R., & Halanych, K. M. (2017b). Crossing the divide: Admixture across the antarctic polar front revealed by the brittle star astrotoma agassizii. *Biological Bulletin*, *232*(3), 198–211. https://doi.org/10.1086/693460/ASSET/IMAGES/LARGE/FGA6.JPEG

Gallego, R., Lavery, S., & Sewell, M. A. (2014). The meroplankton community of the oceanic Ross Sea during late summer. *Antarctic Science*, *26*(4), 345–360. https://doi.org/10.1017/S0954102013000795

Gambi, M. C., Castelli, A., & Guizzardi, M. (1997). Polychaete populations of the shallow soft bottoms off Terra Nova Bay (Ross Sea, Antarctica): distribution, diversity and biomass. *Polar Biology*, *17*(3), 199–210. https://doi.org/10.1007/s003000050123

Gaytán, Á., Bergsten, J., Canelo, T., Pérez-Izquierdo, C., Santoro, M., & Bonal, R. (2020). DNA Barcoding and geographical scale effect: The problems of undersampling genetic diversity hotspots. *Ecology and Evolution*, *10*(19), 10754–10772. https://doi.org/10.1002/ECE3.6733

Ge, M., Mo, J., Ip, J. C. H., Li, Y., Shi, W., Wang, Z., Zhang, X., & Xu, Q. (2022). Adaptive biomineralization in two morphotypes of Sternaspidae (Annelida) from the Northern China Seas. *Frontiers in Marine Science*, *9*, 984989. https://doi.org/10.3389/FMARS.2022.984989/BIBTEX

Georgieva, M. N., Wiklund, H., Ramos, D. A., Neal, L., Glasby, C. J., & Gunton, L. M. (2023). The Annelid Community of a Natural Deep-sea Whale Fall off Eastern Australia. *Records of the Australian Museum*, *75*(3), 167–213. https://doi.org/10.3853/J.2201-4349.75.2023.1800

Gladstone, W., Murray, B. R., & Hutchings, P. (2020). Promising yet variable performance of cross-taxon biodiversity surrogates: a test in two marine habitats at multiple times. *Biodiversity and Conservation*, *29*(9–10), 3067–3089. https://doi.org/10.1007/S10531-020-02015-4/TABLES/4

Glasby, C. J., Wilson, R. S., & Bakken, T. (2011). Redescription of the Indo-Pacific polychaete *Neanthes pachychaeta* (Fauvel, 1918) n. comb. (Annelida, Phyllodocida, Nereididae) and its synonyms. *Zoosystema*, *33*(3), 361–375. https://doi.org/10.5252/z2011n3a5

Glover, A. G., Dahlgren, T., Wiklund, H., Mohrbeck, I., & Smith, C. (2016). An End-to-End DNA Taxonomy Methodology for Benthic Biodiversity Survey in the Clarion-Clipperton Zone, Central Pacific Abyss. *Journal of Marine Science and Engineering*, *4*(1), 2. https://doi.org/10.3390/jmse4010002

Glover, A. G., Paterson, G., Bett, B., Gage, J., Myriam Sibuet, Sheader, M., & Hawkins, L. (2001). Patterns in polychaete abundance and diversity from the Madeira Abyssal Plain, northeast Atlantic. *Deep Sea Research Part I: Oceanographic Research Papers*, *48*(1), 217–236. https://doi.org/10.1016/S0967-0637(00)00053-4

Glover, A. G., & Smith, C. R. (2003). The deep-sea floor ecosystem: current status and prospects of anthropogenic change by the year 2025. *Environmental Conservation*, *30*(3), 219–241. https://doi.org/10.1017/S0376892903000225

Glover, A. G., Smith, C. R., Paterson, G. L. J., Wilson, G. D. F., Hawkins, L., & Sheader, M. (2002). Polychaete species diversity in the central Pacific abyss: local and regional patterns, and relationships with productivity. *Marine Ecology Progress Series*, *240*, 157–170. https://doi.org/10.3354/MEPS240157

Glover, A. G., Wiklund, H., Chen, C., & Dahlgren, T. G. (2018). Point of view: Managing a sustainable deep-sea 'blue economy' requires knowledge of what actually lives there. *ELife*, *7*. https://doi.org/10.7554/eLife.41319

Gogarty, B., McGee, J., Barnes, D. K. A., Sands, C. J., Bax, N., Haward, M., Downey, R., Moreau, C., Moreno, B., Held, C., & Paulsen, M. L. (2020). Protecting Antarctic blue carbon: as marine ice retreats can the law fill the gap? *Climate Policy*, *20*(2), 149–162. https://doi.org/10.1080/14693062.2019.1694482

González-Wevar, C. A., Gérard, K., Rosenfeld, S., Saucède, T., Naretto, J., Díaz, A., Morley, S. A., Brickle, P., & Poulin, E. (2019). Cryptic speciation in Southern Ocean *Aequiyoldia eightsii* (Jay, 1839): Mio-Pliocene trans-Drake Passage separation and diversification. *Progress in Oceanography*, *174*, 44–54. https://doi.org/10.1016/j.pocean.2018.09.004

González-Wevar, C. A., Hüne, M., Segovia, N. I., Nakano, T., Spencer, H. G., Chown, S. L., Saucède, T., Johnstone, G., Mansilla, A., & Poulin, E. (2017). Following the Antarctic Circumpolar Current: patterns and processes in the biogeography of the limpet Nacella (Mollusca: Patellogastropoda) across the Southern Ocean. *Journal of Biogeography*, *44*(4), 861–874. https://doi.org/10.1111/jbi.12908

González-Wevar, C. A., Nakano, T., Cañete, J. I., & Poulin, E. (2010). Molecular phylogeny and historical biogeography of *Nacella* (Patellogastropoda: Nacellidae) in the Southern Ocean. *Molecular Phylogenetics and Evolution*, *56*(1), 115–124. https://doi.org/10.1016/j.ympev.2010.02.001

Gooday, A. J., Holzmann, M., Caulle, C., Goineau, A., Kamenskaya, O., Weber, A. A. T., & Pawlowski, J. (2017). Giant protists (xenophyophores, Foraminifera) are exceptionally diverse in parts of the abyssal eastern Pacific licensed for polymetallic nodule exploration. *Biological Conservation*, *207*, 106–116. https://doi.org/10.1016/j.biocon.2017.01.006

Gostel, M. R., & Kress, W. J. (2022). The Expanding Role of DNA Barcodes: Indispensable Tools for Ecology, Evolution, and Conservation. *Diversity 2022, Vol. 14, Page 213*, *14*(3), 213. https://doi.org/10.3390/D14030213

Grant, D. M., Brodnicke, O. B., Evankow, A. M., Ferreira, A. O., Fontes, J. T., Hansen, A. K., Jensen, M. R., Kalaycı, T. E., Leeper, A., Patil, S. K., Prati, S., Reunamo, A., Roberts, A. J., Shigdel, R., Tyukosova, V., Bendiksby, M., Blaalid, R., Costa, F. O., Hollingsworth, P. M., … Ekrem, T. (2021). The Future of DNA Barcoding: Reflections from Early Career Researchers. *Diversity 2021, Vol. 13, Page 313*, *13*(7), 313. https://doi.org/10.3390/D13070313

Grant, Rachel A., Griffiths, H. J., Steinke, D., Wadley, V., & Linse, K. (2011). Antarctic DNA barcoding; a drop in the ocean? *Polar Biology*, *34*(5), 775–780. https://doi.org/10.1007/s00300-010-0932-7

Grant, Rachel Anne, & Linse, K. (2009). Barcoding Antarctic Biodiversity: current status and the CAML initiative, a case study of marine invertebrates. *Polar Biology*, *32*(11), 1629–1637. https://doi.org/10.1007/s00300-009-0662-x

Grassle, J. F., & Maciolek, N. J. (1992). Deep-Sea Species Richness: Regional and Local Diversity Estimates from Quantitative Bottom Samples. *Https://Doi.Org/10.1086/285329*, *139*(2), 313–341. https://doi.org/10.1086/285329

Griffiths, H. J. (2010). Antarctic Marine Biodiversity – What Do We Know About the Distribution of Life in the Southern Ocean? *PLoS ONE*, *5*(8), e11683. https://doi.org/10.1371/journal.pone.0011683

Griffiths, H. J., Anker, P., Linse, K., Maxwell, J., Post, A. L., Stevens, C., Tulaczyk, S., & Smith, J. A. (2021). Breaking All the Rules: The First Recorded Hard Substrate Sessile Benthic Community Far Beneath an Antarctic Ice Shelf. *Frontiers in Marine Science*, *8*, 76. https://doi.org/10.3389/fmars.2021.642040

Griffiths, H. J., Barnes, D. K. A., & Linse, K. (2009). Towards a generalized biogeography of the Southern Ocean benthos. *Journal of Biogeography*, *36*(1), 162–177. https://doi.org/10.1111/j.1365-2699.2008.01979.x

Griffiths, H. J., Danis, B., & Clarke, A. (2011). Quantifying Antarctic marine biodiversity: The SCAR-MarBIN data portal. *Deep-Sea Research Part II: Topical Studies in Oceanography*, *58*(1–2), 18–29. https://doi.org/10.1016/j.dsr2.2010.10.008

Griffiths, H. J., Van de Putte, A. P., & Danis, B. (2014). *Data distribution: Patterns and implications*.

Grygier, M. J. (1989). 3 New Species of *Myzostoma* (Myzostomida). *Proceedings of the Biological Society of Washington*, *102*(3), 793–804.

Guggolz, T., Meißner, K., Schwentner, M., Dahlgren, T. G., Wiklund, H., Bonifácio, P., & Brandt, A. (2020). High diversity and pan-oceanic distribution of deep-sea polychaetes: *Prionospio* and *Aurospio* (Annelida: Spionidae) in the Atlantic and Pacific Ocean. *Organisms Diversity and Evolution*, *20*(2), 171–187. https://doi.org/10.1007/S13127-020-00430-7/FIGURES/5

Gunton, L. M., Kupriyanova, E., & Alvestad, T. (2020). Two new deep-water species of Ampharetidae (Annelida: Polychaeta) from the eastern Australian continental margin. *Records of the Australian Museum*, *72*(4), 101–121. https://doi.org/10.3853/J.2201-4349.72.2020.1763

Gutt, J. (2008). The expedition ANTARKTIS-XXIII/8 of the research vessel" Polarstern" in 2006/2007. *Berichte Zur Polar-Und Meeresforschung (Reports on Polar and Marine Research)*, *569*.

Gutt, J., Barratt, I., Domack, E., d'Acoz, C. d'Udekem, Dimmler, W., Grémare, A., Heilmayer, O., Isla, E., Janussen, D., & Jorgensen, E. (2011). Biodiversity change after climate-induced ice-shelf collapse in the Antarctic. *Deep Sea Research Part II: Topical Studies in Oceanography*, *58*(1), 74–83.

Gutt, J., Barratt, I., Domack, E., d'Udekem d'Acoz, C., Dimmler, W., Grémare, A., Heilmayer, O., Isla, E., Janussen, D., Jorgensen, E., Kock, K.-H., Sophia Lehnert, L., López-Gonzáles, P., Langner, S., Linse, K., Eugenia Manjón-Cabeza, M., Meißner, M., Montiel, A., Raes, M., … Jorgensen, E. (2011). Biodiversity change after climate-induced ice-shelf collapse in the Antarctic. *Deep Sea Research Part II: Topical Studies in Oceanography*, *58*(1), 74–83. https://doi.org/10.1016/J.DSR2.2010.05.024

Gutt, J., Barratt, I., Domack, E. W., d'Udekem d'Acoz, C., Dimmler, W., Grémare, A., Heilmayer, O., Isla, E., Janussen, D., Jorgensen, E., Kock, K.-H., Lehnert, L. S., López-Gonzáles, P. J., Langner, S., Linse, K., Manjón-Cabeza, M. E., Meißner, M., Montiel, A., Raes, M., … Smith, C. (2010). Macro benthos in surface sediments sampled during POLARSTERN cruise ANT-XXIII/8. In *In supplement to: Gutt, J et al. (2011): Biodiversity change after climate-induced ice-shelf collapse in the Antarctic. Deep Sea Research Part II: Topical Studies in Oceanography, 58(1-2), 74-83, https://doi.org/10.1016/j.dsr2.2010.05.024*. PANGAEA. https://doi.org/10.1594/PANGAEA.718106

Gutt, J., Isla, E., Xavier, J. C., Adams, B. J., Ahn, I. Y., Cheng, C. H. C., Colesie, C., Cummings, V. J., di Prisco, G., Griffiths, H., Hawes, I., Hogg, I., McIntyre, T., Meiners, K. M., Pearce, D. A., Peck, L., Piepenburg, D., Reisinger, R. R., Saba, G. K., … Wall, D. H. (2021). Antarctic ecosystems in transition – life between stresses and opportunities. *Biological Reviews*, *96*(3), 798–821. https://doi.org/10.1111/brv.12679

Gutt, J., Sirenko, B. I., Smirnov, I. S., & Arntz, W. E. (2004). How many macrozoobenthic species might inhabit the Antarctic shelf? *Antarctic Science*, *16*(1), 11–16. https://doi.org/10.1017/S0954102004001750

Halanych, K. M., & Janosik, A. M. (2006). A review of molecular markers used for Annelid phylogenetics. *Integrative and Comparative Biology*, *46*(4), 533–543. https://doi.org/10.1093/ICB/ICJ052

Halanych, K. M., & Mahon, A. R. (2018). Challenging Dogma Concerning Biogeographic Patterns of Antarctica and the Southern Ocean. *Annual Review of Ecology, Evolution, and Systematics*, *49*(1), 355–378. https://doi.org/10.1146/annurev-ecolsys-121415-032139

Halpern, B. S., Walbridge, S., Selkoe, K. A., Kappel, C. V., Micheli, F., D'Agrosa, C., Bruno, J. F., Casey, K. S., Ebert, C., Fox, H. E., Fujita, R., Heinemann, D., Lenihan, H. S., Madin, E. M. P., Perry, M. T., Selig, E. R., Spalding, M., Steneck, R., & Watson, R. (2008). A global map of human impact on marine ecosystems. *Science*, *319*(5865), 948–952. https://doi.org/10.1126/SCIENCE.1149345/SUPPL_FILE/HALPERN_SOM.PDF

Hartman, O. (1954). Australian Nereidae including descriptions of three new species and one genus, together with summaries of previous records and keys to species. *Transactions of the Royal Society of South Australia*, *77*, 1–41.

Hartman, O. (1964). *Polychaeta errantia of Antarctica* (Vol. 3). American geophysical union.

Hartman, O. (1966). *Polychaeta Myzostomidae and Sedentaria of Antarctica* (Vol. 7). American Geophysical Union. https://doi.org/10.1029/AR007

Hartman, O. (1967). *Polychaetous annelids collected by the USNS Eltanin and Staten Island cruises, chiefly from Antarctic seas*. Allan Hancock Foundation University of Southern California. https://www.worldcat.org/title/polychaetous-annelids-collected-by-the-usns-eltanin-and-staten-island-cruises-chiefly-from-antarctic-seas/oclc/3515925

Havermans, C., Nagy, Z. T., Sonet, G., De Broyer, C., & Martin, P. (2011). DNA barcoding reveals new insights into the diversity of Antarctic species of *Orchomene* sensu lato (Crustacea: Amphipoda: Lysianassoidea). *Deep Sea Research Part II: Topical Studies in Oceanography*, *58*(1–2), 230–241. https://doi.org/10.1016/J.DSR2.2010.09.028

He, X., Wang, H., Xu, T., Zhang, Y., Chen, C., Sun, Y., Qiu, J. W., Zhou, Y., & Sun, J. (2023). Genomic Analysis of a Scale Worm Provides Insights into Its Adaptation to Deep-Sea Hydrothermal Vents. *Genome Biology and Evolution*, *15*(7). https://doi.org/10.1093/GBE/EVAD125

Hebert, P. D. N., Cywinska, A., Ball, S. L., & Dewaard, J. R. (2003). Biological identifications through DNA barcodes. *Proceedings of the Royal Society B*, *270*(1512), 313–321. https://doi.org/10.1098/rspb.2002.2218

Hebert, P. D. N., Ratnasingham, S., & DeWaard, J. R. (2003). Barcoding animal life: Cytochrome c oxidase subunit 1 divergences among closely related species. *Proceedings of the Royal Society B: Biological Sciences*, *270*(SUPPL. 1). https://doi.org/10.1098/RSBL.2003.0025

Hebert, P. D. N., Stoeckle, M. Y., Zemlak, T. S., & Francis, C. M. (2004). Identification of Birds through DNA Barcodes. *PLOS Biology*, *2*(10), e312. https://doi.org/10.1371/journal.pbio.0020312

Heimeier, D., Lavery, S., & Sewell, M. A. (2010). Using DNA barcoding and phylogenetics to identify Antarctic invertebrate larvae: Lessons from a large scale study. *Marine Genomics*, *3*(3–4), 165–177. https://doi.org/10.1016/J.MARGEN.2010.09.004

Hein, J. R., Mizell, K., Koschinsky, A., & Conrad, T. A. (2013). Deep-ocean mineral deposits as a source of critical metals for high- and green-technology applications: Comparison with land-based resources. In *Ore Geology Reviews* (Vol. 51, pp. 1–14). Elsevier. https://doi.org/10.1016/j.oregeorev.2012.12.001

Held, C. (2000). Phylogeny and biogeography of serolid isopods (Crustacea, Isopoda, Serolidae) and the use of ribosomal expansion segments in molecular systematics. *Molecular Phylogenetics and Evolution*, *15*(2), 165–178. https://doi.org/10.1006/mpev.1999.0739

Held, C. (2003). Molecular evidence for cryptic speciation within the widespread Antarctic crustacean Ceratoserolis trilobitoides (Crustacea, Isopoda). In *Antarctic biology in a global context* (pp. 135–139).

Held, C., & Wägele, J. W. (2005). Cryptic speciation in the giant Antarctic isopod *Glyptonotus antarcticus* (Isopoda, Valvifera, Chaetiliidae). *Scientia Marina*, *69*(S2), 175–181. https://doi.org/10.3989/scimar.2005.69s2175

Helm, K. P., Bindoff, N. L., & Church, J. A. (2011). Observed decreases in oxygen content of the global ocean. *Geophysical Research Letters*, *38*(23), 23602. https://doi.org/10.1029/2011GL049513

Hemery, L. G., Eléaume, M., Roussel, V., Améziane, N., Gallut, C., Steinke, D., Cruaud, C., Couloux, A., & Wilson, N. G. (2012). Comprehensive sampling reveals circumpolarity and sympatry in seven mitochondrial lineages of the Southern Ocean crinoid species *Promachocrinus kerguelensis* (Echinodermata). *Molecular Ecology*, *21*(10), 2502–2518. https://doi.org/10.1111/j.1365-294X.2012.05512.x

Hessler, R., & Sanders, H. (1967). Faunal diversity in the deep-sea. *Deep Sea Research and Oceanographic Abstracts*, *14*(1), 65–78. https://doi.org/10.1016/0011-7471(67)90029-0

Hickerson, M. J., Carstens, B. C., Cavender-Bares, J., Crandall, K. A., Graham, C. H., Johnson, J. B., Rissler, L., Victoriano, P. F., & Yoder, A. D. (2010). Phylogeography's past, present, and future: 10 years after. *Molecular Phylogenetics and Evolution*, *54*(1), 291–301. https://doi.org/10.1016/J.YMPEV.2009.09.016

Hilbig, B. (2004). Polychaetes of the deep Weddell and Scotia Seas—composition and zoogeographical links. *Deep Sea Research Part II: Topical Studies in Oceanography*, *51*(14–16), 1817–1825. https://doi.org/10.1016/J.DSR2.2004.07.015

Hilbig, B., Gerdes, D., & Montiel, A. (2006). Distribution patterns and biodiversity in polychaete communities of the Weddell Sea and Antarctic Peninsula area (Southern Ocean). *Marine Biological Association of the United Kingdom. Journal of the Marine Biological Association of the United Kingdom*, *86*(4), 711. https://doi.org/10.1017/S0025315406013610

Hsueh, P.-W. (2019). *Neanthes* (Annelida: Nereididae) from Taiwanese waters, with description of seven new species and one new species record. *Zootaxa*, *4554*(1), 173–198. https://doi.org/10.11646/zootaxa.4554.1.5

Huang, D., Meier, R., Todd, P. A., & Chou, L. M. (2008). Slow Mitochondrial COI Sequence Evolution at the Base of the Metazoan Tree and Its Implications for DNA Barcoding. *Journal of Molecular Evolution*, *66*(2), 167–174. https://doi.org/10.1007/s00239-008-9069-5

Hunter, R. L., & Halanych, K. M. (2010). Phylogeography of the Antarctic planktotrophic brittle star *Ophionotus victoriae* reveals genetic structure inconsistent with early life history. *Marine Biology*, *157*(8), 1693–1704. https://doi.org/10.1007/s00227-010-1443-3

Hutchings, P. (1998). Biodiversity and functioning of polychaetes in benthic sediments. *Biodiversity and Conservation*, *7*(9), 1133–1145. https://doi.org/10.1023/A:1008871430178/METRICS

Hutchings, P., & Kupriyanova, E. (2018). Cosmopolitan polychaetes - Fact or fiction? Personal and historical perspectives. *Invertebrate Systematics*, *32*(1), 1–9. https://doi.org/10.1071/IS17035

Huybrechts, P. (2002). Sea-level changes at the LGM from ice-dynamic reconstructions of the Greenland and Antarctic ice sheets during the glacial cycles. *Quaternary Science Reviews*, *21*(1–3), 203–231. https://doi.org/10.1016/S0277-3791(01)00082-8

Ibrahim, N. F., Ibrahim, Y. S., & Sato, M. (2019). New record of an estuarine polychaete, *Neanthes glandicincta* (annelida, nereididae) on the eastern coast of peninsular Malaysia. *ZooKeys*, *2019*(831), 81–94. https://doi.org/10.3897/zookeys.831.28588

Imbrie, J. (1984). The orbital theory of Pleistocene climate: Support from a revised chronology of the marine δ18O record. *Milankovitch and Climate, Understanding the Response to Orbital Forcing, Part 1*, 269–305.

Ingels, J., Aronson, R. B., & Smith, C. R. (2018). The scientific response to Antarctic ice-shelf loss. In *Nature Climate Change* (Vol. 8, Issue 10, pp. 848–851). Nature Publishing Group. https://doi.org/10.1038/s41558-018-0290-y

IPBES. (2019). *Global assessment report on biodiversity and ecosystem services of the Intergovernmental Science-Policy Platform on Biodiversity and Ecosystem Services.* (E. Brondizio, J. Settele, S. Díaz, & H. Ngo (Eds.)). IPBES secretariat. https://doi.org/https://doi.org/10.5281/zenodo.3831673

ISA. (2018). *International Seabed Authority – Exploration Areas*. https://www.isa.org.jm/contractors/exploration-areas

Jamieson, A. J., & Onda, D. F. L. (2022). Lebensspuren and müllspuren: Drifting plastic bags alter microtopography of seafloor at full ocean depth (10,000 m, Philippine Trench). *Continental Shelf Research*, *250*, 104867. https://doi.org/10.1016/J.CSR.2022.104867

Janosik, A. M., & Halanych, K. M. (2010). Unrecognized Antarctic Biodiversity: A Case Study of the Genus *Odontaster* (Odontasteridae; Asteroidea). *Integrative and Comparative Biology*, *50*(6), 981–992. https://doi.org/10.1093/icb/icq119

Jenkins, T. L., Castilho, R., & Stevens, J. R. (2018). Meta-analysis of northeast Atlantic marine taxa shows contrasting phylogeographic patterns following post-LGM expansions. *PeerJ*, *6*, e5684. https://doi.org/10.7717/peerj.5684

Johnson, J. S., Bentley, M. J., Roberts, S. J., Binnie, S. A., & Freeman, S. P. H. T. (2011). Holocene deglacial history of the northeast Antarctic Peninsula - A review and new chronological constraints. *Quaternary Science Reviews*, *30*(27–28), 3791–3802. https://doi.org/10.1016/j.quascirev.2011.10.011

Johnson, M., Zaretskaya, I., Raytselis, Y., Merezhuk, Y., McGinnis, S., & Madden, T. L. (2008). NCBI BLAST: a better web interface. *Nucleic Acids Research*, *36*(suppl_2), W5–W9. https://doi.org/10.1093/NAR/GKN201

Jombart, T., & Ahmed, I. (2011). adegenet 1.3-1: new tools for the analysis of genome-wide SNP data. *Bioinformatics*, *27*(21), 3070–3071. https://doi.org/10.1093/BIOINFORMATICS/BTR521

Jombart, T., & Bateman, A. (2008). adegenet: a R package for the multivariate analysis of genetic markers. *Bioinformatics*, *24*(11), 1403–1405. https://doi.org/10.1093/BIOINFORMATICS/BTN129

Jombart, T., Devillard, S., & Balloux, F. (2010). Discriminant analysis of principal components: A new method for the analysis of genetically structured populations. *BMC Genetics*, *11*(1), 1–15. https://doi.org/10.1186/1471-2156-11-94/FIGURES/9

Jones, K. R., Klein, C. J., Halpern, B. S., Venter, O., Grantham, H., Kuempel, C. D., Shumway, N., Friedlander, A. M., Possingham, H. P., & Watson, J. E. M. (2018). The Location and Protection Status of Earth's Diminishing Marine Wilderness. *Current Biology*, *28*(15), 2506-2512.e3. https://doi.org/10.1016/J.CUB.2018.06.010

Jumars, P. A. (1981). Limits in predicting and detecting benthic community responses to manganese nodule mining. *Mar. Min.*, *3*(1), 213–229.

Jumars, P. A., Dorgan, K. M., & Lindsay, S. M. (2015). Diet of Worms Emended: An Update of Polychaete Feeding Guilds. *Annual Review of Marine Science*, *7*(1), 497–520. https://doi.org/10.1146/annurev-marine-010814-020007

Kaiser, S., Barnes, D. K. A., Sands, C. J., & Brandt, A. (2009). Biodiversity of an unknown Antarctic Sea: assessing isopod richness and abundance in the first benthic survey of the Amundsen continental shelf. *Marine Biodiversity*, *39*(1), 27–43. https://doi.org/10.1007/s12526-009-0004-9

Kaiser, S., Brandão, S. N., Brix, S., Barnes, D. K. A., Bowden, D. A., Ingels, J., Leese, F., Schiaparelli, S., Arango, C. P., Badhe, R., Bax, N., Blazewicz-Paszkowycz, M., Brandt, A., Brenke, N., Catarino, A. I., David, B., De Ridder, C., Dubois, P., Ellingsen, K. E., … Yasuhara, M. (2013). Patterns, processes and vulnerability of Southern Ocean benthos: a decadal leap in knowledge and understanding. *Marine Biology*, *160*(9), 2295–2317. https://doi.org/10.1007/s00227-013-2232-6

Katoh, K. (2002). MAFFT: a novel method for rapid multiple sequence alignment based on fast Fourier transform. *Nucleic Acids Research*, *30*(14), 3059–3066. https://doi.org/10.1093/nar/gkf436

Katoh, Kazutaka, & Standley, D. M. (2013). MAFFT Multiple Sequence Alignment Software Version 7: Improvements in Performance and Usability. *Molecular Biology and Evolution*, *30*(4), 772–780. https://doi.org/10.1093/MOLBEV/MST010

Kearse, M., Moir, R., Wilson, A., Stones-Havas, S., Cheung, M., Sturrock, S., Buxton, S., Cooper, A., Markowitz, S., Duran, C., Thierer, T., Ashton, B., Meintjes, P., & Drummond, A. (2012). Geneious Basic: An integrated and extendable desktop software platform for the organization and analysis of sequence data. *Bioinformatics*, *28*(12), 1647–1649. https://doi.org/10.1093/BIOINFORMATICS/BTS199

Keeling, R. F., Körtzinger, A., & Gruber, N. (2009). Ocean Deoxygenation in a Warming World. *Https://Doi.Org/10.1146/Annurev.Marine.010908.163855*, *2*(1), 199–229. https://doi.org/10.1146/ANNUREV.MARINE.010908.163855

Kersken, D., Janussen, D., & Arbizu, P. M. (2019). Deep-sea glass sponges (Hexactinellida) from polymetallic nodule fields in the Clarion-Clipperton Fracture Zone (CCFZ), northeastern Pacific: Part II—Hexasterophora. *Marine Biodiversity*, *49*(2), 947–987. https://doi.org/10.1007/s12526-018-0880-y

Khlebovich, V. V. (1996). Fauna of Russia and neighbouring countries. Polychaetous Annelids Volume III. Polychaetes of the family Nereididae of the Russian Seas and the adjacent waters. *Russ. Acad. Sci., Zool. Inst., New Ser*, *140*, 1–221.

Kim, S. (2019). Complex life under the McMurdo Ice Shelf, and some speculations on food webs. *Antarctic Science*, *31*(2), 80–88. https://doi.org/10.1017/S0954102018000561

Kim, B. M., Amores, A., Kang, S., Ahn, D. H., Kim, J. H., Kim, I. C., Lee, J. H., Lee, S. G., Lee, H., Lee, J., Kim, H. W., Desvignes, T., Batzel, P., Sydes, J., Titus, T., Wilson, C. A., Catchen, J. M., Warren, W. C., Schartl, M., … Park, H. (2019). Antarctic blackfin icefish genome reveals adaptations to extreme environments. *Nature Ecology & Evolution 2019 3:3*, *3*(3), 469–478. https://doi.org/10.1038/s41559-019-0812-7

Kim, S. L., Choi, H., Eyun, S. Il, Kim, D., & Yu, O. H. (2022). A New *Branchipolynoe* (Aphroditiformia: Polynoidae) Scale Worm from the Onnuri Deep-sea Hydrothermal Vent Field, Northern Central Indian Ridge. *Zoological Studies*, *61*. https://doi.org/10.6620/ZS.2022.61-21

Knowlton, N. (1993). Sibling species in the sea. *Annual Review of Ecology and Systematics*, *24*, 189–216. https://doi.org/10.1146/ANNUREV.ES.24.110193.001201

Knox, G. A. (2006). *Biology of the southern ocean*. CRC Press.

Knox, G. A., & Cameron, D. B. (1998). *The marine fauna of the Ross Sea: Polychaeta* (Vol. 108). National Institute of Water and Atmospheric Research.

Kobayashi, G., Goto, R., Takano, T., & Kojima, S. (2018). Molecular phylogeny of Maldanidae (Annelida): Multiple losses of tube-capping plates and evolutionary shifts in habitat depth. *Molecular Phylogenetics and Evolution*, *127*, 332–344. https://doi.org/10.1016/J.YMPEV.2018.04.036

Kongsrud, J. A., Eilertsen, M. H., Alvestad, T., Kongshavn, K., & Rapp, H. T. (2017). New species of Ampharetidae (Annelida: Polychaeta) from the Arctic Loki Castle vent field. *Deep Sea Research Part II: Topical Studies in Oceanography*, *137*, 232–245. https://doi.org/10.1016/J.DSR2.2016.08.015

Kozlov, A. M., Darriba, D., Flouri, T., Morel, B., & Stamatakis, A. (2019). RAxML-NG: a fast, scalable and user-friendly tool for maximum likelihood phylogenetic inference. *Bioinformatics*, *35*(21), 4453–4455. https://doi.org/10.1093/BIOINFORMATICS/BTZ305

Krabbe, K., Leese, F., Mayer, C., Tollrian, R., & Held, C. (2010). Cryptic mitochondrial lineages in the widespread pycnogonid Colossendeis megalonyx Hoek, 1881 from Antarctic and Subantarctic waters. *Polar Biology*, *33*(3), 281–292. https://doi.org/10.1007/s00300-009-0703-5

Krell, F. T. (2004). Parataxonomy vs. taxonomy in biodiversity studies - Pitfalls and applicability of "morphospecies" sorting. *Biodiversity and Conservation*, *13*(4), 795–812. https://doi.org/10.1023/B:BIOC.0000011727.53780.63/METRICS

Kvist, S. (2014). Does a global DNA barcoding gap exist in Annelida? *Mitochondrial DNA*, 1–12. https://doi.org/10.3109/19401736.2014.984166

Lau, S. C. Y., Strugnell, J. M., Sands, C. J., Silva, C. N. S., & Wilson, N. G. (2021). Evolutionary innovations in Antarctic brittle stars linked to glacial refugia. *Ecology and Evolution*, *11*(23), 17428–17446. https://doi.org/10.1002/ECE3.8376

Lau, S. C. Y., Strugnell, J. M., Sands, C. J., Silva, C. N. S., & Wilson, N. G. (2023a). Genomic insights of evolutionary divergence and life histories innovations in Antarctic brittle stars. *Molecular Ecology*, *00*, 1–21. https://doi.org/10.1111/MEC.16951

Lau, S. C. Y., Wilson, N. G., Golledge, N. R., Naish, T. R., Watts, P. C., Silva, C. N. S., Cooke, I. R., Allcock, A. L., Mark, F. C., Linse, K., & Strugnell, J. M. (2023b). Genomic evidence for West Antarctic Ice Sheet collapse during the Last Interglacial Period. *BioRxiv*, 2023.01.29.525778. https://doi.org/10.1101/2023.01.29.525778

Lau, S. C. Y., Wilson, N. G., Silva, C. N. S., & Strugnell, J. M. (2020). Detecting glacial refugia in the Southern Ocean. *Ecography*. https://doi.org/10.1111/ecog.04951

Lee, G. H. S. M. G.-S. (2021). A New Record of Paramphicteis weberi (Polychaeta: Terebellida: Ampharetidae) in Korean Fauna. *Animal Systematics, Evolution and Diversity*, *37*(2), 165–170. https://doi.org/10.5635/ASED.2021.37.2.008

Lee, J. R., Raymond, B., Bracegirdle, T. J., Chadès, I., Fuller, R. A., Shaw, J. D., & Terauds, A. (2017). Climate change drives expansion of Antarctic ice-free habitat. *Nature*, *547*(7661), 49–54. https://doi.org/10.1038/nature22996

Leese, F., & Held, C. (2008). Identification and characterization of microsatellites from the Antarctic isopod Ceratoserolis trilobitoides: nuclear evidence for cryptic species. *Conservation Genetics*, *9*(5), 1369–1372. https://doi.org/10.1007/s10592-007-9491-z

Leigh, J. W., & Bryant, D. (2015). *POPART: full-feature software for haplotype network construction*.

Leiva, C., Riesgo, A., Avila, C., Rouse, G. W., & Taboada, S. (2018). Population structure and phylogenetic relationships of a new shallow-water Antarctic phyllodocid annelid. *Zoologica Scripta*, *47*(6), 714–726. https://doi.org/10.1111/ZSC.12313

Leiva, C., Riesgo, A., Combosch, D., Belén Arias, M., Giribet, G., Downey, R., Nathan, |, Kenny, J., & Sergi Taboada, |. (2022). Guiding marine protected area network design with comparative phylogeography and population genomics: An exemplary case from the Southern Ocean. *Diversity and Distributions*, *00*, 1–17. https://doi.org/10.1111/DDI.13590

Leiva, C., Taboada, S., Kenny, N. J., Combosch, D., Giribet, G., Jombart, T., & Riesgo, A. (2019). Population substructure and signals of divergent adaptive selection despite admixture in the sponge Dendrilla antarctica from shallow waters surrounding the Antarctic Peninsula. *Molecular Ecology*, *28*(13), 3151–3170. https://doi.org/10.1111/MEC.15135

Leray, M., Knowlton, N., Ho, S. L., Nguyen, B. N., & Machida, R. J. (2019). GenBank is a reliable resource for 21st century biodiversity research. *Proceedings of the National Academy of Sciences of the United States of America*, *116*(45), 22651–22656. https://doi.org/10.1073/PNAS.1911714116/SUPPL_FILE/PNAS.1911714116.SAPP.PDF

Levin, L., Blair, N., DeMaster, D., Plaia, G., Fornes, W., Martin, C., & Thomas, C. (1997). Rapid subduction of organic matter by maldanid polychaetes on the North Carolina slope. *Journal of Marine Research*, *55*(3), 595–611. https://doi.org/10.1357/0022240973224337

Li, Y., Tassia, M. G., Waits, D. S., Bogantes, V. E., David, K. T., & Halanych, K. M. (2019). Genomic adaptations to chemosymbiosis in the deep-sea seep-dwelling tubeworm Lamellibrachia luymesi. *BMC Biology 2019 17:1*, *17*(1), 1–14. https://doi.org/10.1186/S12915-019-0713-X

Lim, S.-C., Wiklund, H., Glover, A. G., Dahlgren, T. G., & Tan, K.-S. (2017). A new genus and species of abyssal sponge commonly encrusting polymetallic nodules in the Clarion-Clipperton Zone, East Pacific Ocean. *Systematics and Biodiversity*, *15*(6), 507–519. https://doi.org/10.1080/14772000.2017.1358218

Lindgren, J., Hatch, A. S., Hourdez, S., Seid, C. A., & Rouse, G. W. (2019). Phylogeny and Biogeography of *Branchipolynoe* (Polynoidae, Phyllodocida, Aciculata, Annelida), with Descriptions of Five New Species from Methane Seeps and Hydrothermal Vents. *Diversity 2019, Vol. 11, Page 153*, *11*(9), 153. https://doi.org/10.3390/D11090153

Linse, K., Apeland, B., Brandt, A., Clark, W., Dahlgren, T. G., Davies, C., Dreutter, S., Grant, S. M., Glover, A. G., Felding, S., Felderwisch, L., Mackenzie, M., MacSween, K., Makela, A., Polfrey, S., Quirk, S., Reid, W., Robst, J., Smith, A., … Trathan, P. (2018). *RSS James Clark Ross JR17003a Cruise Report - Larsen C Benthos*. https://www.bodc.ac.uk/resources/inventories/cruise_inventory/report/16954/

Linse, K., Cope, T., Lörz, A.-N., & Sands, C. (2007). Is the Scotia Sea a centre of Antarctic marine diversification? Some evidence of cryptic speciation in the circum-Antarctic bivalve L*issarca notorcadensis* (Arcoidea: Philobryidae). *Polar Biology*, *30*(8), 1059–1068. https://doi.org/10.1007/s00300-007-0265-3

Linse, K., Copley, J. T., Connelly, D. P., Larter, R. D., Pearce, D. A., Polunin, N. V. C., Rogers, A. D., Chen, C., Clarke, A., Glover, A. G., Graham, A. G. C., Huvenne, V. A. I., Marsh, L., Reid, W. D. K., Roterman, C. N., Sweeting, C. J., Zwirglmaier, K., & Tyler, P. A. (2019). Fauna of the Kemp Caldera and its upper bathyal hydrothermal vents (South Sandwich Arc, Antarctica). *Royal Society Open Science*, *6*(11), 191501. https://doi.org/10.1098/rsos.191501

Linse, K., Grant, S., Whittle, R., Reid, W., McKenzie, M., Federwisch, L., Polfrey, S., & Apeland, B. (2020). *Benthic seafloor images from Prince Gustav Channel and Duse Bay, Eastern Antarctic Peninsula, March 2018 (Version 1.0) [Data set]. UK Polar Data Centre, Natural Environment Research Council, UK Research & Innovation.* https://doi.org/10.5285/48DCEF16-6719-45E5-A335-3A97F099E451

Linse, K., Griffiths, H. J., Barnes, D. K. A., Brandt, A., Davey, N., David, B., De Grave, S., D'Udekem d'Acoz, C., Eléaume, M., Glover, A. G., Hemery, L. G., Mah, C., Martín-Ledo, R., Munilla, T., O'Loughlin, M., Pierrat, B., Saucède, T., Sands, C. J., Strugnell, J. M., & Enderlein, P. (2013). The macro- and megabenthic fauna on the continental shelf of the eastern Amundsen Sea, Antarctica. *Continental Shelf Research*, *68*, 80–90.

Löbl, I., Klausnitzer, B., Hartmann, M., & Krell, F.-T. (2023). The Silent Extinction of Species and Taxonomists—An Appeal to Science Policymakers and Legislators. *Diversity 2023, Vol. 15, Page 1053*, *15*(10), 1053. https://doi.org/10.3390/D15101053

Lodge, M., Johnson, D., Le Gurun, G., Wengler, M., Weaver, P., & Gunn, V. (2014). Seabed mining: International Seabed Authority environmental management plan for the Clarion–Clipperton Zone. A partnership approach. *Marine Policy*, *49*, 66–72. https://doi.org/10.1016/J.MARPOL.2014.04.006

Lohse, K. (2009). Can mtDNA Barcodes Be Used to Delimit Species? A Response to Pons et al. (2006). *Systematic Biology*, *58*(4), 439–442. https://doi.org/10.1093/SYSBIO/SYP039

Maciolek, N. J. (2020). *Anguillosyllis* (Annelida: Syllidae) from multiple deep-water locations in the northern and southern hemispheres.. *Zootaxa*, *4793*(1), 1–73–1–73. https://doi.org/10.11646/ZOOTAXA.4793.1.1

Magalhães, W. F., Hutchings, P., Oceguera-Figueroa, A., Martin, P., Schmelz, R. M., WETZEL, M. J., WIKLUND, H., Maciolek, N. J., KAWAUCHI, G. Y., & WILLIAMS, J. D. (2021). Segmented worms (Phylum Annelida): a celebration of twenty years of progress through Zootaxa and call for action on the taxonomic work that remains. *Zootaxa*, *4979*(1), 190–211–190–211. https://doi.org/10.11646/ZOOTAXA.4979.1.18

Mahcene, H. R., Villalobos-Guerrero, T. F., Kurt, G., Denis, F., & Daas, T. (2023). A new species of *Perinereis* Kinberg, 1865 (Annelida: Nereididae) from the Western Mediterranean Sea revealed by morphological and molecular approaches. *Mediterranean Marine Science*, *24*(2), 454–460. https://doi.org/10.12681/mms.33969

Mahon, A. R., Arango, C. P., & Halanych, K. M. (2008). Genetic diversity of *Nymphon* (Arthropoda: Pycnogonida: Nymphonidae) along the Antarctic Peninsula with a focus on *Nymphon australe* Hodgson 1902. *Marine Biology*, *155*(3), 315–323. https://doi.org/10.1007/s00227-008-1029-5

Malinsky, M., Trucchi, E., Lawson, D. J., & Falush, D. (2018). RADpainter and fineRADstructure: Population Inference from RADseq Data. *Molecular Biology and Evolution*, *35*(5), 1284–1290. https://doi.org/10.1093/MOLBEV/MSY023

Malmgren, A. J. (1866). *Nordiska Hafs-Annulater. [part three of three]*. fversigt af Königlich Vetenskapsakademiens förhandlingar, Stockholm.

Marchant, J. (2017). Giant iceberg's split exposes hidden ecosystem. *Nature*, *549*(7673), 443–443. https://doi.org/10.1038/549443a

Maroni, P. J., Baker, B. J., Moran, A. L., Woods, H. A., Avila, C., Johnstone, G. J., Stark, J. S., Kocot, K. M., Lockhart, S., Saucède, T., Rouse, G. W., & Wilson, N. G. (2022). One Antarctic slug to confuse them all: the underestimated diversity of *Doris kerguelensis. Invertebrate Systematics*, *36*(5), 419–435. https://doi.org/10.1071/is21073

Martin, D., Capa, M., Martínez, A., & Costa, A. C. (2022). Taxonomic implications of describing a new species of *Loimia* (Annelida, Terebellidae) with two size-dependent morphotypes. *European Journal of Taxonomy*, *833*, 60–96. https://doi.org/10.5852/EJT.2022.833.1887

McClain, C. R., Balk, M. A., Benfield, M. C., Branch, T. A., Chen, C., Cosgrove, J., Dove, A. D. M., Gaskins, L. C., Helm, R. R., Hochberg, F. G., Lee, F. B., Marshall, A., McMurray, S. E., Schanche, C., Stone, S. N., & Thaler, A. D. (2015). Sizing ocean giants: patterns of intraspecific size variation in marine megafauna. *PeerJ*, *3*(1). https://doi.org/10.7717/PEERJ.715

Medlin, L., Elwood, H. J., Stickel, S., & Sogin, M. L. (1988). The characterization of enzymatically amplified eukaryotic 16S-like rRNA-coding regions. *Gene*, *71*(2), 491–499. https://doi.org/https://doi.org/10.1016/0378-1119(88)90066-2

Meier, R., Zhang, G., & Ali, F. (2008). The Use of Mean Instead of Smallest Interspecific Distances Exaggerates the Size of the "Barcoding Gap" and Leads to Misidentification. *Systematic Biology*, *57*(5), 809–813. https://doi.org/10.1080/10635150802406343

Meierotto, S., Sharkey, M. J., Janzen, D. H., Hallwachs, W., Hebert, P. D. N., Chapman, E. G., & Smith, M. A. (2019). A revolutionary protocol to describe understudied hyperdiverse taxa and overcome the taxonomic impediment. *Deutsche Entomologische Zeitschrift 66(2): 119-145*, *66*(2), 119–145. https://doi.org/10.3897/DEZ.66.34683

Meirmans, P. G. (2020). genodive version 3.0: Easy-to-use software for the analysis of genetic data of diploids and polyploids. *Molecular Ecology Resources*, *20*(4), 1126–1131. https://doi.org/10.1111/1755-0998.13145

Meredith, M. P., & King, J. C. (2005). Rapid climate change in the ocean west of the Antarctic Peninsula during the second half of the 20th century. *Geophysical Research Letters*, *32*(19), n/a-n/a. https://doi.org/10.1029/2005GL024042

Meyer, A., Bleidorn, C., Rouse, G. W., & Hausen, H. (2008). Morphological and molecular data suggest a cosmopolitan distribution of the polychaete *Proscoloplos cygnochaetus* Day, 1954 (Annelida, Orbiniidae). *Marine Biology*, *153*(5), 879–889. https://doi.org/10.1007/s00227-007-0860-4

Moles, J., Derkarabetian, S., Schiaparelli, S., Schrödl, M., Troncoso, J. S., Wilson, N. G., & Giribet, G. (2021). An approach using ddRADseq and machine learning for understanding speciation in Antarctic Antarctophilinidae gastropods. *Scientific Reports 2021 11:1*, *11*(1), 1–14. https://doi.org/10.1038/s41598-021-87244-5

Monro, C. C. A. (1930). Polychaete worms. *Discovery Reports, Cambridge*, *2*, 1–222. http://biodiversitylibrary.org/page/15904801

Moon, K. L., Chown, S. L., & Fraser, C. I. (2017). Reconsidering connectivity in the sub-Antarctic. *Biological Reviews*, *92*(4), 2164–2181. https://doi.org/10.1111/brv.12327

Moore, J. M., Carvajal, J. I., Rouse, G. W., & Wilson, N. G. (2018). The Antarctic Circumpolar Current isolates and connects: Structured circumpolarity in the sea star Glabraster antarctica. *Ecology and Evolution*, *8*(21), 10621–10633. https://doi.org/10.1002/ece3.4551

Mora, C., Tittensor, D. P., Adl, S., Simpson, A. G. B., & Worm, B. (2011). How Many Species Are There on Earth and in the Ocean? *PLOS Biology*, *9*(8), e1001127. https://doi.org/10.1371/JOURNAL.PBIO.1001127

Morris, E. M., & Vaughan, D. G. (2003). *Spatial and Temporal Variation of Surface Temperature on the Antarctic Peninsula And The Limit of Viability of Ice Shelves* (pp. 61–68). American Geophysical Union (AGU). https://doi.org/10.1029/ar079p0061

Mou, J., Liu, K., Huang, Y., He, X., Zhang, S., Wang, J., Lin, J., Lin, H., & Liu, W. (2022). The macro-and megabenthic fauna on the continental shelf of Prydz Bay, east Antarctica. *Deep Sea Research Part II: Topical Studies in Oceanography*, *198*, 105052. https://doi.org/10.1016/J.DSR2.2022.105052

Mu, W., Liu, J., & Zhang, H. (2018). Complete mitochondrial genome of *Benthodytes marianensis* (Holothuroidea: Elasipodida: Psychropotidae): Insight into deep sea adaptation in the sea cucumber. *PLOS ONE*, *13*(11), e0208051. https://doi.org/10.1371/JOURNAL.PONE.0208051

Mugnai, F., Meglécz, E., Costantini, F., Abbiati, M., Bavestrello, G., Bertasi, F., Bo, M., Capa, M., Chenuil, A., Colangelo, M. A., De Clerck, O., Gutiérrez, J. M., Lattanzi, L., Leduc, M., Martin, D., Matterson, K. O., Mikac, B., Plaisance, L., Ponti, M., … Wangensteen, O. S. (2021). Are well-studied marine biodiversity hotspots still blackspots for animal barcoding? *Global Ecology and Conservation*, *32*, e01909. https://doi.org/10.1016/J.GECCO.2021.E01909

Mullineaux, L. S. (1987). Organisms living on manganese nodules and crusts: distribution and abundance at three North Pacific sites. *Deep Sea Research Part A, Oceanographic Research Papers*, *34*(2), 165–184. https://doi.org/10.1016/0198-0149(87)90080-X

Naciri, Y., & Linder, H. P. (2015). Species delimitation and relationships: The dance of the seven veils. *TAXON*, *64*(1), 3–16. https://doi.org/10.12705/641.24

Naish, T., Powell, R., Levy, R., Wilson, G., Scherer, R., Talarico, F., Krissek, L., Niessen, F., Pompilio, M., Wilson, T., Carter, L., DeConto, R., Huybers, P., McKay, R., Pollard, D., Ross, J., Winter, D., Barrett, P., Browne, G., … Williams, T. (2009). Obliquity-paced Pliocene West Antarctic ice sheet oscillations. *Nature*, *458*(7236), 322–328. https://doi.org/10.1038/nature07867

Naughten, K. A., Holland, P. R., & De Rydt, J. (2023). Unavoidable future increase in West Antarctic ice-shelf melting over the twenty-first century. *Nature Climate Change 2023*, 1–7. https://doi.org/10.1038/s41558-023-01818-x

Neal, L., Abrahams, E., Wiklund, H., Rabone, M., Bribiesca-Contreras, G., Stewart, E. C. D., Dahlgren, T. G., & Glover, A. G. (2023). Taxonomy, phylogeny, and biodiversity of Lumbrineridae (Annelida, Polychaeta) from the Central Pacific Clarion-Clipperton Zone. *ZooKeys*, *1172*(1172), 61. https://doi.org/10.3897/ZOOKEYS.1172.100483

Neal, L., Barnich, R., Wiklund, H., & Glover, A. G. (2012). A new genus and species of Polynoidae (Annelida, Polychaeta) from Pine Island Bay, Amundsen Sea, Southern Ocean—a region of high taxonomic novelty. *Zootaxa*, *3542*(1), 80. https://doi.org/10.11646/zootaxa.3542.1.4

Neal, L., Linse, K., Brasier, M. J., Sherlock, E., & Glover, A. G. (2018a). Comparative marine biodiversity and depth zonation in the Southern Ocean: evidence from a new large polychaete dataset from Scotia and Amundsen seas. *Marine Biodiversity*, *48*(1), 581–601. https://doi.org/10.1007/s12526-017-0735-y

Neal, L., Brasier, M. J., & Wiklund, H. (2018b). Six new species of *Macellicephala* (Annelida: Polynoidae) from the Southern Ocean and south Atlantic with re-description of type species. *Zootaxa*, *4455*(1), 1–34. https://doi.org/10.11646/zootaxa.4455.1.1

Neal, L., Mincks Hardy, S. L., Smith, C. R. C., & Glover, A. G. A. (2011). Polychaete species diversity on the West Antarctic Peninsula deep continental shelf. *Marine Ecology Progress Series*, *428*, 119–134. https://doi.org/10.3354/meps09012

Neal, L., Wiklund, H., Gunton, L. M., Rabone, M., Bribiesca-Contreras, G., Dahlgren, T. G., & Glover, A. G. (2022a). Abyssal fauna of polymetallic nodule exploration areas, eastern Clarion-Clipperton Zone, central Pacific Ocean: Amphinomidae and Euphrosinidae (Annelida, Amphinomida). *ZooKeys*, *1137*(1137), 33. https://doi.org/10.3897/ZOOKEYS.1137.86150

Neal, L., Wiklund, H., Rabone, M., Dahlgren, T. G., & Glover, A. G. (2022b). Abyssal fauna of polymetallic nodule exploration areas, eastern Clarion-Clipperton Zone, central Pacific Ocean: Annelida: Spionidae and Poecilochaetidae. *Marine Biodiversity*, *52*(5), 1–48. https://doi.org/10.1007/S12526-022-01277-1/FIGURES/22

Neal, L., Wiklund, H., Muir, A. I., Linse, K., & Glover, A. G. (2014). The identity of juvenile Polynoidae (Annelida) in the Southern Ocean revealed by DNA taxonomy, with notes on the status of Herdmanella gracilis Ehlers sensu Augener. *Memoirs of Museum Victoria*, *71*, 203–216.

Nicholls, K. W., Pudsey, C. J., & Morris, P. (2004). Summertime water masses off the northern Larsen C Ice Shelf, Antarctica. *Geophysical Research Letters*, *31*(9), n/a-n/a. https://doi.org/10.1029/2004GL019924

Nolan, E. T., Barnes, D. K. A., Brown, J., Downes, K., Enderlein, P., Gowland, E., Hogg, O. T., Laptikhovsky, V., Morley, S. A., Mrowicki, R. J., Richardson, A., Sands, C. J., Weber, N., Weber, S., & Brickle, P. (2017). Biological and physical characterization of the seabed surrounding Ascension Island from 100-1000 m. *Journal of the Marine Biological Association of the United Kingdom*, *97*(4), 647–659. https://doi.org/10.1017/S0025315417000820

Nordenskjöld, O., & Andersson, J. G. (1905). *Antarctica*. Hurst and Blackett.

Nygren, A. (2014). Cryptic polychaete diversity: a review. *Zoologica Scripta*, *43*(2), 172–183. https://doi.org/10.1111/zsc.12044

Nygren, A., Norlinder, E., Panova, M., & Pleijel, F. (2011). Colour polymorphism in the polychaete Harmothoe imbricata (Linnaeus, 1767). *Marine Biology Research*, *7*(1), 54–62. https://doi.org/10.1080/17451001003713555

Nygren, A., & Sundberg, P. (2003). Phylogeny and evolution of reproductive modes in *Autolytinae* (Syllidae, Annelida). *Molecular Phylogenetics and Evolution*, *29*(2), 235–249. https://doi.org/https://doi.org/10.1016/S1055-7903(03)00095-2

Nỳvlt, D., Košler, J., Mlcoch, B., Mixa, P., Lisá, L., Bubík, M., & Hendriks, B. W. H. (2011). The Mendel Formation: Evidence for Late Miocene climatic cyclicity at the northern tip of the Antarctic Peninsula. *Palaeogeography, Palaeoclimatology, Palaeoecology*, *299*(1–2), 363–384. https://doi.org/10.1016/j.palaeo.2010.11.017

O'Hara, T. D., Hugall, A. F., Thuy, B., Stöhr, S., & Martynov, A. V. (2017). Restructuring higher taxonomy using broad-scale phylogenomics: The living Ophiuroidea. *Molecular Phylogenetics and Evolution*, *107*, 415–430. https://doi.org/10.1016/J.YMPEV.2016.12.006

O'Hara, T. D., Hugall, A. F., Woolley, S. N. C., Bribiesca-Contreras, G., & Bax, N. J. (2019). Contrasting processes drive ophiuroid phylodiversity across shallow and deep seafloors. *Nature*, *565*(7741), 636–639. https://doi.org/10.1038/s41586-019-0886-z

Oksanen, J., Guillaume Blanchet, F., Friendly, M., Kindt, R., Legendre, P., McGlinn, D., Minchin, P. R., O'Hara, R. B., Simpson, G. L., Solymos, P., Stevens, M. H. H., Szoecs, E., & Wagner, H. (2019). *vegan: Community Ecology Package*. https://cran.r-project.org/package=vegan

Olsgard, F., Brattegard, T., & Holthe, T. (2003). Polychaetes as surrogates for marine biodiversity: Lower taxonomic resolution and indicator groups. *Biodiversity and Conservation*, *12*(5), 1033–1049. https://doi.org/10.1023/A:1022800405253/METRICS

Orsi, A. H., Nowlin, W. D., & Whitworth, T. (1993). On the circulation and stratification of the Weddell Gyre. *Deep-Sea Research Part I*, *40*(1), 169–203. https://doi.org/10.1016/0967-0637(93)90060-G

Orsi, A. H., Whitworth, T., & Nowlin, W. D. (1995). On the meridional extent and fronts of the Antarctic Circumpolar Current. *Deep Sea Research Part I: Oceanographic Research Papers*, *42*(5), 641–673. https://doi.org/10.1016/0967-0637(95)00021-W

Ortiz, D., Pekár, S., Bilat, J., & Alvarez, N. (2021). Poor performance of DNA barcoding and the impact of RAD loci filtering on the species delimitation of an Iberian ant-eating spider. *Molecular Phylogenetics and Evolution*, *154*, 106997. https://doi.org/10.1016/J.YMPEV.2020.106997

Osborn, K. J., & Rouse, G. W. (2011). Phylogenetics of Acrocirridae and Flabelligeridae (Cirratuliformia, Annelida). *Zoologica Scripta*, *40*(2), 204–219. https://doi.org/10.1111/j.1463-6409.2010.00460.x

Oschlies, A. (2021). A committed fourfold increase in ocean oxygen loss. *Nature Communications 2021 12:1*, *12*(1), 1–8. https://doi.org/10.1038/s41467-021-22584-4

Palumbi, S. R. (1996). Nucleic acids II: the polymerase chain reaction. *Molecular Systematics*, *2*(1), 205–247.

Pamungkas, J., Glasby, C. J., & Costello, M. J. (2021). Biogeography of polychaete worms (Annelida) of the world. *Marine Ecology Progress Series*, *657*, 147–159. https://doi.org/10.3354/MEPS13531

Pante, E., Schoelinck, C., & Puillandre, N. (2015). From Integrative Taxonomy to Species Description: One Step Beyond. *Systematic Biology*, *64*(1), 152–160. https://doi.org/10.1093/SYSBIO/SYU083

Pantó, G., Pasotti, F., Macheriotou, L., & Vanreusel, A. (2021). Combining Traditional Taxonomy and Metabarcoding: Assemblage Structure of Nematodes in the Shelf Sediments of the Eastern Antarctic Peninsula. *Frontiers in Marine Science*, *8*, 890. https://doi.org/10.3389/FMARS.2021.629706/BIBTEX

Parapar, J., López, E., Gambi, M. C., Núñez, J., & Ramos, A. (2011). Quantitative analysis of soft-bottom polychaetes of the Bellingshausen Sea and Gerlache Strait (Antarctica). *Polar Biology*, *34*(5), 715–730. https://doi.org/10.1007/s00300-010-0927-4

Parry, L., Tanner, A., & Vinther, J. (2014). The origin of annelids. *Palaeontology*, *57*(6), 1091–1103. https://doi.org/10.1111/PALA.12129

Paterson, G. L. J., Glover, A. G., Barrio Froján, C. R. S., Whitaker, A., Budaeva, N., Chimonides, J., & Doner, S. (2009). A census of abyssal polychaetes. *Deep Sea Research Part II: Topical Studies in Oceanography*, *56*(19–20), 1739–1746. https://doi.org/10.1016/J.DSR2.2009.05.018

Paterson, G. L. J., Neal, L., Altamira, I., Soto, E. H., Smith, C. R., Menot, L., Billett, D. S. M., Cunha, M. R., Marchais-Laguionie, C., & Glover, A. G. (2016). New *Prionospio* and *Aurospio* Species from the Deep Sea (Annelida: Polychaeta). *Zootaxa*, *4092*(1), 1–32–1–32. https://doi.org/10.11646/ZOOTAXA.4092.1.1

Paterson, G. L. J., Wilson, G. D. F., Cosson, N., & Lamont, P. A. (1998). Hessler and Jumars (1974) revisited: abyssal polychaete assemblages from the Atlantic and Pacific. *Deep Sea Research Part II: Topical Studies in Oceanography*, *45*(1–3), 225–251. https://doi.org/10.1016/S0967-0645(97)00084-2

Paxton, H., Wiklund, H., Alexander, F., & Taboada, S. (2017). Is the Antarctic *Ophryotrocha orensanzi* (Annelida: Dorvilleidae) a circumpolar non-specialized opportunist? *Systematics and Biodiversity*, *15*(2), 105–114. https://doi.org/10.1080/14772000.2016.1218371/SUPPL_FILE/TSAB_A_1218371_SM0576.DOCX

Peck, L. S. (2016). A Cold Limit to Adaptation in the Sea. In *Trends in Ecology and Evolution* (Vol. 31, Issue 1, pp. 13–26). Elsevier Ltd. https://doi.org/10.1016/j.tree.2015.09.014

Peck, L. S. (2018). *Chapter 3 Antarctic Marine Biodiversity*. https://doi.org/10.1201/9780429454455

Pérez-Portela, R., Almada, V., & Turon, X. (2013). Cryptic speciation and genetic structure of widely distributed brittle stars (Ophiuroidea) in Europe. *Zoologica Scripta*, *42*(2), 151–169. https://doi.org/10.1111/J.1463-6409.2012.00573.X

Perez, M., Aroh, O., Sun, Y., Lan, Y., Juniper, S. K., Young, C. R., Angers, B., & Qian, P. Y. (2023). Third-Generation Sequencing Reveals the Adaptive Role of the Epigenome in Three Deep-Sea Polychaetes. *Molecular Biology and Evolution*, *40*(8). https://doi.org/10.1093/MOLBEV/MSAD172

Peterson, B. K., Weber, J. N., Kay, E. H., Fisher, H. S., & Hoekstra, H. E. (2012). Double Digest RADseq: An Inexpensive Method for De Novo SNP Discovery and Genotyping in Model and Non-Model Species. *PLOS ONE*, *7*(5), e37135. https://doi.org/10.1371/JOURNAL.PONE.0037135

Pettibone, M. H. (1976). Revision of the genus *Macellicephala* McIntosh and the subfamily Macellicephalinae Hartmann-SchrAder (Polychaeta: Polynoidae). *Smithsonian Contributions to Zoology*.

Pettibone, M. H. (1997). Revision of the Scaleworm Genus *Eulagisca* Mcintosh (Polychaeta: Polynoidae) with the Erection of the Subfamily Eugaliscinae and the New Genus *Pareulagisca. Proceedings of the Biological Society of Washington*.

Pielou, E. C. (1969). *An introduction to mathematical ecology*. Wiley-Interscience.

Piepenburg, D., Schmid, M. K., & Gerdes, D. (2002). The benthos off King George Island (South Shetland Islands, Antarctica): Further evidence for a lack of a latitudinal biomass cline in the Southern Ocean. *Polar Biology*, *25*(2), 146–158. https://doi.org/10.1007/s003000100322

Pimm, S. L., Jenkins, C. N., Abell, R., Brooks, T. M., Gittleman, J. L., Joppa, L. N., Raven, P. H., Roberts, C. M., & Sexton, J. O. (2014). The biodiversity of species and their rates of extinction, distribution, and protection. *Science*, *344*(6187). https://doi.org/10.1126/SCIENCE.1246752/SUPPL_FILE/PIMM.SM.PDF

Pineda-Metz, S. E. A., Gerdes, D., & Richter, C. (2020). Benthic fauna declined on a whitening Antarctic continental shelf. *Nature Communications*, *11*(1), 1–7. https://doi.org/10.1038/s41467-020-16093-z

Pons, J., Barraclough, T. G., Gomez-Zurita, J., Cardoso, A., Duran, D. P., Hazell, S., Kamoun, S., Sumlin, W. D., & Vogler, A. P. (2006). Sequence-based species delimitation for the DNA taxonomy of undescribed insects. *Systematic Biology*, *55*(4), 595–609. https://doi.org/10.1080/10635150600852011

Posada, D. (2008). jModelTest: Phylogenetic Model Averaging. *Molecular Biology and Evolution*, *25*(7), 1253–1256. https://doi.org/10.1093/MOLBEV/MSN083

Post, A. L., Galton-Fenzi, B. K., Riddle, M. J., Herraiz-Borreguero, L., O'Brien, P. E., Hemer, M. A., McMinn, A., Rasch, D., & Craven, M. (2014). Modern sedimentation, circulation and life beneath the Amery Ice Shelf, East Antarctica. *Continental Shelf Research*, *74*, 77–87. https://doi.org/10.1016/J.CSR.2013.10.010

Post, A. L., Lavoie, C., Domack, E. W., Leventer, A., Shevenell, A., & Fraser, A. D. (2017). Environmental drivers of benthic communities and habitat heterogeneity on an East Antarctic shelf. *Antarctic Science*, *29*(1), 17–32. https://doi.org/10.1017/S0954102016000468

Pudsey, C. J., & Evans, J. (2001). First survey of Antarctic sub–ice shelf sediments reveals mid-Holocene ice shelf retreat. *Geology*, *29*(9), 787–790. https://doi.org/10.1130/0091-7613(2001)029<0787:fsoasi>2.0.co;2

Pudsey, C. J., Evans, J., Domack, E. W., Morris, P., & Del Valle, R. A. (2001). Bathymetry and acoustic facies beneath the former Larsen-A and Prince Gustav ice shelves, north-west Weddell Sea. *Antarctic Science*, *13*(3), 312–322. https://doi.org/10.1017/S095410200100044X

Pudsey, C. J., Murray, J. W., Appleby, P., & Evans, J. (2006). Ice shelf history from petrographic and foraminiferal evidence, Northeast Antarctic Peninsula. *Quaternary Science Reviews*, *25*(17–18), 2357–2379. https://doi.org/10.1016/j.quascirev.2006.01.029

Puillandre, N., Brouillet, S., & Achaz, G. (2021). ASAP: assemble species by automatic partitioning. *Molecular Ecology Resources*, *21*(2), 609–620. https://doi.org/10.1111/1755-0998.13281

Puillandre, N., Lambert, A., Brouillet, S., & Achaz, G. (2012). ABGD, Automatic Barcode Gap Discovery for primary species delimitation. *Molecular Ecology*, *21*(8), 1864–1877. https://doi.org/10.1111/j.1365-294X.2011.05239.x

Purkey, S. G., & Johnson, G. C. (2010). Warming of Global Abyssal and Deep Southern Ocean Waters between the 1990s and 2000s: Contributions to Global Heat and Sea Level Rise Budgets. *Journal of Climate*, *23*(23), 6336–6351. https://doi.org/10.1175/2010JCLI3682.1

Quartino, M. L., Klöser, H., Schloss, I. R., & Wiencke, C. (2001). Biomass and associations of benthic marine macroalgae from the inner Potter Cove (King George Island, Antarctica) related to depth and substrate. *Polar Biology*, *24*(5), 349–355. https://doi.org/10.1007/s003000000218

R Core Team. (2023). A Language and Environment for Statistical Computing. In *R Foundation for Statistical Computing* (p. https://www.R-project.org). R Foundation for Statistical Computing. http://www.r-project.org

Rabone, M., Wiethase, J. H., Simon-Lledó, E., Emery, A. M., Jones, D. O. B., Dahlgren, T. G., Bribiesca-Contreras, G., Wiklund, H., Horton, T., & Glover, A. G. (2023). How many metazoan species live in the world's largest mineral exploration region? *Current Biology*, *33*(12), 2383-2396.e5. https://doi.org/10.1016/J.CUB.2023.04.052

Rack, W., & Rott, H. (2004). Pattern of retreat and disintegration of the Larsen B ice shelf, Antarctic Peninsula. *Annals of Glaciology*, *39*, 505–510.

Radashevsky, V. I., Pankova, V. V., Neretina, T. V., Stupnikova, A. N., & Tzetlin, A. B. (2016). Molecular analysis of the *Pygospio elegans* group of species (Annelida: Spionidae). *Zootaxa*, *4083*(2), 239–250–239–250. https://doi.org/10.11646/ZOOTAXA.4083.2.4

Radulovici, A. E., Vieira, P. E., Duarte, S., Teixeira, M. A. L., Borges, L. M. S., Deagle, B. E., Majaneva, S., Redmond, N., Schultz, J. A., & Costa, F. O. (2021). Revision and annotation of DNA barcode records for marine invertebrates: report of the 8th iBOL conference hackathon. *Metabarcoding and Metagenomics 5: E67862*, *5*, e67862-. https://doi.org/10.3897/MBMG.5.67862

Rambaut, A. (2018). FigTree–Tree Figure Drawing Tool Version v. 1.4. 4. *Institute of Evolutionary Biology, University of Edinburgh: Edinburgh*.

Ramirez-Llodra, E., Brandt, A., Danovaro, R., De Mol, B., Escobar, E., German, C. R., Levin, L. A., Martinez Arbizu, P., Menot, L., Buhl-Mortensen, P., Narayanaswamy, B. E., Smith, C. R., Tittensor, D. P., Tyler, P. A., Vanreusel, A., & Vecchione, M. (2010). Deep, diverse and definitely different: Unique attributes of the world's largest ecosystem. *Biogeosciences*, *7*(9), 2851–2899. https://doi.org/10.5194/BG-7-2851-2010

Ramirez-Llodra, E., Tyler, P. A., Baker, M. C., Bergstad, O. A., Clark, M. R., Escobar, E., Levin, L. A., Menot, L., Rowden, A. A., Smith, C. R., & van Dover, C. L. (2011). Man and the Last Great Wilderness: Human Impact on the Deep Sea. *PLOS ONE*, *6*(8), e22588. https://doi.org/10.1371/JOURNAL.PONE.0022588

Ratnasingham, S., & Hebert, P. D. N. (2013). A DNA-Based Registry for All Animal Species: The Barcode Index Number (BIN) System. *PLOS ONE*, *8*(7), e66213. https://doi.org/10.1371/JOURNAL.PONE.0066213

Raupach, M. J., Thatje, S., Dambach, J., Rehm, P., Misof, B., & Leese, F. (2010). Genetic homogeneity and circum-Antarctic distribution of two benthic shrimp species of the Southern Ocean, *Chorismus antarcticus* and *Nematocarcinus lanceopes. Marine Biology*, *157*(8), 1783–1797. https://doi.org/10.1007/s00227-010-1451-3

Raupach, M. J., & Wägele, J.-W. (2006). Distinguishing cryptic species in Antarctic Asellota (Crustacea: Isopoda) - a preliminary study of mitochondrial DNA in Acanthaspidia drygalskii. *Antarctic Science*, *18*(2), 191–198. https://doi.org/10.1017/S0954102006000228

Ravara, A., Rizzo, A. E., & Lana, P. (2017). Nephtyidae Grube, 1850. In A. Schmidt-Rhaesa (Ed.), *Handbook of Zoology Online*. De Gruyter.

Ravara, A., Wiklund, H., Cunha, M. R., & Pleijel, F. (2010). Phylogenetic relationships within Nephtyidae (Polychaeta, Annelida). *Zoologica Scripta*, *39*(4), 394–405. https://doi.org/10.1111/J.1463-6409.2010.00424.X

Read, G. (2007). Taxonomy of sympatric New Zealand species of *Platynereis*, with description of three new species additional to P. australis (Schmarda)(Annelida: Polychaeta: Nereididae). *Zootaxa*, *1558*(1), 1–28.

Read, G., & Fauchald, K. (2020a). *World Polychaeta database. Neanthes Kinberg, 1865*. World Register of Marine Species. http://www.marinespecies.org/aphia.php?p=taxdetails&id=129378

Read, G., & Fauchald, K. (2020b). *World Polychaeta database. Nereididae Blainville, 1818.* World Register of Marine Species. http://www.marinespecies.org/aphia.php?p=taxdetails&id=22496 on 2020-02-05

Reid, P. A., Stammerjohn, S. E., Massom, R. A., Barreira, S., Scambos, T. A., & Lieser, J. (2020). Sea ice extent, concentration, and seasonality [in “State of the Climate in 2019”]. *Bulletin of the American Meteorological Society*, *101*(8), S304–S306.

Rex, M. A., Etter, R. J., Morris, J. S., Crouse, J., McClain, C. R., Johnson, N. A., Stuart, C. T., Deming, J. W., Thies, R., & Avery, R. (2006). Global bathymetric patterns of standing stock and body size in the deep-sea benthos. *Marine Ecology Progress Series*, *317*, 1–8. https://doi.org/10.3354/MEPS317001

Riddle, M. J., Craven, M., Goldsworthy, P. M., & Carsey, F. (2007). A diverse benthic assemblage 100 km from open water under the Amery Ice Shelf, Antarctica. *Paleoceanography*, *22*(1), n/a-n/a. https://doi.org/10.1029/2006PA001327

Riehl, T., & Kaiser, S. (2012). Conquered from the Deep Sea? A New Deep-Sea Isopod Species from the Antarctic Shelf Shows Pattern of Recent Colonization. *PlosOne. 7*(11), e49354. https://journals.plos.org/plosone/article?id=10.1371/journal.pone.0049354

Riehl, T., Wölfl, A. C., Augustin, N., Devey, C. W., & Brandt, A. (2020). Discovery of widely available abyssal rock patches reveals overlooked habitat type and prompts rethinking deep-sea biodiversity. *Proceedings of the National Academy of Sciences of the United States of America*, *117*(27), 15450–15459. https://doi.org/10.1073/PNAS.1920706117/SUPPL_FILE/PNAS.1920706117.SAPP.PDF

Riesgo, A., Taboada, S., & Avila, C. (2015). Evolutionary patterns in Antarctic marine invertebrates: An update on molecular studies. *Marine Genomics*, *23*, 1–13. https://doi.org/10.1016/J.MARGEN.2015.07.005

Rignot, E., Jacobs, S., Mouginot, J., & Scheuchl, B. (2013). Ice-shelf melting around Antarctica. *Science (New York, N.Y.)*, *341*(6143), 266–270. https://doi.org/10.1126/science.1235798

Rochette, N. C., & Catchen, J. M. (2017). Deriving genotypes from RAD-seq short-read data using Stacks. *Nature Protocols 2017 12:12*, *12*(12), 2640–2659. https://doi.org/10.1038/nprot.2017.123

Rodrigo, A. P., & Costa, P. M. (2019). The hidden biotechnological potential of marine invertebrates: The Polychaeta case study. *Environmental Research*, *173*, 270–280. https://doi.org/10.1016/J.ENVRES.2019.03.048

Rogers, A. D., Frinault, B. A. V., Barnes, D. K. A., Bindoff, N. L., Downie, R., Ducklow, H. W., Friedlaender, A. S., Hart, T., Hill, S. L., Hofmann, E. E., Linse, K., McMahon, C. R., Murphy, E. J., Pakhomov, E. A., Reygondeau, G., Staniland, I. J., Wolf-Gladrow, D. A., & Wright, R. (2020). Antarctic Futures: An Assessment of Climate-Driven Changes in Ecosystem Structure, Function, and Service Provisioning in the Southern Ocean. *Annual Review of Marine Science*, *12*(1), annurev-marine-010419-011028. https://doi.org/10.1146/annurev-marine-010419-011028

Rogers, A. D., Tyler, P. A., Connelly, D. P., Copley, J. T., James, R., Larter, R. D., Linse, K., Mills, R. A., Garabato, A. N., Pancost, R. D., Pearce, D. A., Polunin, N. V. C., German, C. R., Shank, T., Boersch-Supan, P. H., Alker, B. J., Aquilina, A., Bennett, S. A., Clarke, A., … Zwirglmaier, K. (2012). The Discovery of New Deep-Sea Hydrothermal Vent Communities in the Southern Ocean and Implications for Biogeography. *PLoS Biology*, *10*(1), e1001234. https://doi.org/10.1371/journal.pbio.1001234

Ronquist, F., Teslenko, M., Van Der Mark, P., Ayres, D. L., Darling, A., Höhna, S., Larget, B., Liu, L., Suchard, M. A., & Huelsenbeck, J. P. (2012). MrBayes 3.2: Efficient Bayesian Phylogenetic Inference and Model Choice Across a Large Model Space. *Systematic Biology*, *61*(3), 539–542. https://doi.org/10.1093/SYSBIO/SYS029

Rott, H., Abdel Jaber, W., Wuite, J., Scheiblauer, S., Floricioiu, D., Van Wessem, J. M., Nagler, T., Miranda, N., & Van Den Broeke, M. R. (2018). Changing pattern of ice flow and mass balance for glaciers discharging into the Larsen A and B embayments, Antarctic Peninsula, 2011 to 2016. In *Cryosphere* (Vol. 12, Issue 4, pp. 1273–1291). Copernicus GmbH. https://doi.org/10.5194/tc-12-1273-2018

Rott, H., Floricioiu, D., Wuite, J., Scheiblauer, S., Nagler, T., & Kern, M. (2014). Mass changes of outlet glaciers along the Nordensjköld Coast, northern Antarctic Peninsula, based on TanDEM-X satellite measurements. *Geophysical Research Letters*, *41*(22), 8123–8129. https://doi.org/10.1002/2014GL061613

Rott, H., Skvarca, P., & Nagler, T. (1996). Rapid collapse of northern Larsen Ice Shelf, Antarctica. *Science*, *271*(5250), 788–792. https://doi.org/10.1126/science.271.5250.788

Rousset, V., Pleijel, F., Rouse, G. W., Erséus, C., & Siddall, M. E. (2007). A molecular phylogeny of annelids. *Cladistics*, *23*. https://doi.org/10.1111/j.1096-0031.2006.00128.x

Ruhl, H. A., & Smith, K. L. (2004). Shifts in deep-sea community structure linked to climate and food supply. *Science*, *305*(5683), 513–515. https://doi.org/10.1126/SCIENCE.1099759/SUPPL_FILE/RUHL.SOM.PDF

Sahade, R., Lagger, C., Torre, L., Momo, F., Monien, P., Schloss, I., Barnes, D. K. A., Servetto, N., Tarantelli, S., Tatián, M., Zamboni, N., & Abele, D. (2015). Climate change and glacier retreat drive shifts in an Antarctic benthic ecosystem. *Science Advances*, *1*(10), e1500050. https://doi.org/10.1126/sciadv.1500050

Salazar-Vallejo, S. I. (2012). Revision of *Flabelligera* Sars, 1829 (Polychaeta: Flabelligeridae). *Zootaxa*, *3203*(3203), 1–64. https://doi.org/10.11646/zootaxa.3203.1.1

Sanders, H. L. (1968). Marine Benthic Diversity: A Comparative Study. *Https://Doi.Org/10.1086/282541*, *102*(925), 243–282. https://doi.org/10.1086/282541

Sands, C. J., O'Hara, T., Barnes, D. K. A., & Martín-Ledo, R. (2015). Against the flow: evidence of multiple recent invasions of warmer continental shelf waters by a Southern Ocean brittle star. *Frontiers in Ecology and Evolution*, *3*(JUN), 63. https://doi.org/10.3389/FEVO.2015.00063

Sañé, E., Isla, E., Gerdes, D., Montiel, A., & Gili, J. M. (2012). Benthic macrofauna assemblages and biochemical properties of sediments in two Antarctic regions differently affected by climate change. *Continental Shelf Research*, *35*, 53–63. https://doi.org/10.1016/j.csr.2011.12.008

Sato, M. (2013). Resurrection of the genus *Nectoneanthes* Imajima, 1972 (Nereididae: Polychaeta), with redescription of *Nectoneanthes oxypoda* (Marenzeller, 1879) and description of a new species, comparing them to *Neanthes succinea* (Leuckart, 1847). *Journal of Natural History*, *47*(1–2), 1–50. https://doi.org/10.1080/00222933.2012.743609

Scambos, T. A., Berthier, E., Haran, T., Shuman, C. A., Cook, A. J., Ligtenberg, S. R. M., & Bohlander, J. (2014). Detailed ice loss pattern in the northern Antarctic Peninsula: widespread decline driven by ice front retreats. *The Cryosphere*, *8*(6), 2135–2145. https://doi.org/10.5194/tc-8-2135-2014

SCAR Antarctic Biodiversity Portal. (2022). *SCAR Biodiversity Portal*. https://data.biodiversity.aq/occurrence/search/?taxon=2316861

Scher, H. D., & Martin, E. E. (2006). Timing and climatic consequences of the opening of drake passage. *Science*, *312*(5772), 428–430. https://doi.org/10.1126/science.1120044

Schlick-Steiner, B. C., Steiner, F. M., Seifert, B., Stauffer, C., Christian, E., & Crozier, R. H. (2010). Integrative Taxonomy: A Multisource Approach to Exploring Biodiversity. *Https://Doi.Org/10.1146/Annurev-Ento-112408-085432*, *55*, 421–438. https://doi.org/10.1146/ANNUREV-ENTO-112408-085432

Schubert, A., & Reise, K. (1986). Predatory effects of *Nephtys hombergii* on other polychaetes in tidal flat sediments. *Mar. Ecol. Prog. Ser*, *34*, 117–124.

Schüller, M. (2011). Evidence for a role of bathymetry and emergence in speciation in the genus *Glycera* (Glyceridae, Polychaeta) from the deep Eastern Weddell Sea. *Polar Biology*, *34*(4), 549–564. https://doi.org/10.1007/s00300-010-0913-x

Schüller, M., & Ebbe, B. (2014). Chapter 5.1 polychaetes. In *Biogeographic Atlas of the Southern Ocean. Scientific Committee on Antarctic Research, Cambridge* (pp. 134–137).

Schüller, M., Ebbe, B., & Wägele, J.-W. W. (2009). Community structure and diversity of polychaetes (Annelida) in the deep Weddell Sea (Southern Ocean) and adjacent basins. *Marine Biodiversity*, *39*(2), 95–108. https://doi.org/10.1007/s12526-009-0009-4

Shannon, C. E., & Weaver, W. (1949). *The mathematical theory of communication. Urbana, Illinois: University of Illinois.* University of Illinois.

Shimabukuro, M., Santos, C. S. G., Alfaro-Lucas, J. M., Fujiwara, Y., & Sumida, P. Y. G. (2017). A new eyeless species of *Neanthes* (Annelida: Nereididae) associated with a whale-fall community from the deep Southwest Atlantic Ocean. *Deep Sea Research Part II: Topical Studies in Oceanography*, *146*, 27–34. https://doi.org/10.1016/J.DSR2.2017.10.013

Simon-Lledó, E., Amon, D. J., Bribiesca-Contreras, G., Cuvelier, D., Durden, J. M., Ramalho, S. P., Uhlenkott, K., Arbizu, P. M., Benoist, N., Copley, J., Dahlgren, T. G., Glover, A. G., Fleming, B., Horton, T., Ju, S. J., Mejía-Saenz, A., McQuaid, K., Pape, E., Park, C., … Jones, D. O. B. (2023). Carbonate compensation depth drives abyssal biogeography in the northeast Pacific. *Nature Ecology & Evolution 2023 7:9*, *7*(9), 1388–1397. https://doi.org/10.1038/s41559-023-02122-9

Sjölin, E., Erséus, C., & Källersjö, M. (2005). Phylogeny of Tubificidae (Annelida, Clitellata) based on mitochondrial and nuclear sequence data. *Molecular Phylogenetics and Evolution*, *35*(2), 431–441. https://doi.org/https://doi.org/10.1016/j.ympev.2004.12.018

Smale, D. A., & Barnes, D. K. A. (2008). Likely responses of the Antarctic benthos to climate-related changes in physical disturbance during the 21st century, based primarily on evidence from the West Antarctic Peninsula region. *Ecography*, *31*(3), 289–305. https://doi.org/10.1111/j.0906-7590.2008.05456.x

Smith, C. R. (1994). Tempo and mode in deep-sea benthic ecology: punctuated equilibrium revisited. *Palaios*, *6*, 3–13. https://doi.org/10.1017/S2475262200008340

Smith, C. R., & Baco, A. R. (2003). Ecology of whale falls at the deep-sea floor. *Oceanography and Marine Biology*, *41*, 311–354.

Smith, C. R., Mincks, S., & DeMaster, D. J. (2008a). The FOODBANCS project: introduction and sinking fluxes of organic carbon, chlorophyll-a and phytodetritus on the western Antarctic Peninsula continental shelf. *Deep Sea Research Part II: Topical Studies in Oceanography*, *55*(22–23), 2404–2414. https://doi.org/10.1016/j.dsr2.2008.06.001

Smith, C. R., De Leo, F. C., Bernardino, A. F., Sweetman, A. K., & Arbizu, P. M. (2008b). Abyssal food limitation, ecosystem structure and climate change. *Trends in Ecology & Evolution*, *23*(9), 518–528. https://doi.org/10.1016/J.TREE.2008.05.002

Smith, C. R., & DeMaster, D. J. (2008). Preface and brief synthesis for the FOODBANCS volume. *Deep-Sea Research Part II: Topical Studies in Oceanography*, *55*(22–23), 2399–2403. https://doi.org/10.1016/j.dsr2.2008.08.001

Smith, C. R., & Demopoulos, A. W. J. (2003). The deep Pacific ocean floor. *Ecosystems of the World*, 179–218.

Smith, K. L., Ruhl, H. A., Kahru, M., Huffard, C. L., & Sherman, A. D. (2013). Deep ocean communities impacted by changing climate over 24 y in the abyssal northeast Pacific Ocean. *Proceedings of the National Academy of Sciences of the United States of America*, *110*(49), 19838–19841. https://doi.org/10.1073/PNAS.1315447110/SUPPL_FILE/SD01.XLSX

Snelgrove, P. V. R. (1999). Getting to the bottom of marine biodiversity: Sedimentary habitats: Ocean bottoms are the most widespread habitat on earth and support high biodiversity and key ecosystem services. *BioScience*, *49*(2), 129–130. https://doi.org/10.2307/1313538/2/BISI.1999.49.2.129-FU01.JPEG

Snelgrove, P. V. R., & Smith, C. R. (2002). A riot of species in an environmental calm: the paradox of the species-rich deep-sea floor. In *Oceanography and Marine Biology* (pp. 319–320). CRC Press.

Srivathsan, A., Lee, L., Katoh, K., Hartop, E., Kutty, S. N., Wong, J., Yeo, D., & Meier, R. (2021). ONTbarcoder and MinION barcodes aid biodiversity discovery and identification by everyone, for everyone. *BMC Biology*, *19*(1), 1–21. https://doi.org/10.1186/S12915-021-01141-X/TABLES/6

Stewart, E. C. D., Bribiesca-Contreras, G., Taboada, S., Wiklund, H., Ravara, A., Pape, E., De Smet, B., Neal, L., Cunha, M. R., Jones, D. O. B., Smith, C. R., Glover, A. G., & Dahlgren, T. G. (2023). Biodiversity, biogeography, and connectivity of polychaetes in the world's largest marine minerals exploration frontier. *Diversity and Distributions*, *29*(6), 727–747. https://doi.org/10.1111/DDI.13690

Stiller, J., Tilic, E., Rousset, V., Pleijel, F., & Rouse, G. W. (2020). Spaghetti to a Tree: A Robust Phylogeny for Terebelliformia (Annelida) Based on Transcriptomes, Molecular and Morphological Data. *Biology 2020, Vol. 9, Page 73*, *9*(4), 73. https://doi.org/10.3390/BIOLOGY9040073

Stramma, L., Schmidtko, S., Levin, L. A., & Johnson, G. C. (2010). Ocean oxygen minima expansions and their biological impacts. *Deep Sea Research Part I: Oceanographic Research Papers*, *57*(4), 587–595. https://doi.org/10.1016/J.DSR.2010.01.005

Stribling, J. B., Pavlik, K. L., Holdsworth, S. M., & Leppo, E. W. (2008). Data quality, performance, and uncertainty in taxonomic identification for biological assessments. *Https://Doi.Org/10.1899/07-175.1*, *27*(4), 906–919. https://doi.org/10.1899/07-175.1

Strugnell, J. M., Pedro, J. B., & Wilson, N. G. (2018). Dating Antarctic ice sheet collapse: Proposing a molecular genetic approach. *Quaternary Science Reviews*, *179*, 153–157. https://doi.org/10.1016/j.quascirev.2017.11.014

Strugnell, J. M., Rogers, A. D., Prodöhl, P. A., Collins, M. A., & Allcock, A. L. (2008). The thermohaline expressway: the Southern Ocean as a centre of origin for deep-sea octopuses. *Cladistics*, *24*(6), 853–860. https://doi.org/10.1111/J.1096-0031.2008.00234.X

Strugnell, J. M., Watts, P. C., Smith, P. J., & Allcock, A. L. (2012). Persistent genetic signatures of historic climatic events in an Antarctic octopus. *Molecular Ecology*, *21*(11), 2775–2787. https://doi.org/10.1111/j.1365-294X.2012.05572.x

Sulpis, O., Boudreau, B. P., Mucci, A., Jenkins, C., Trossman, D. S., Arbic, B. K., & Key, R. M. (2018). Current CaCO3 dissolution at the seafloor caused by anthropogenic CO2. *Proceedings of the National Academy of Sciences of the United States of America*, *115*(46), 11700–11705. https://doi.org/10.1073/PNAS.1804250115/SUPPL_FILE/PNAS.1804250115.SAPP.PDF

Summers, M. M., & Rouse, G. W. (2014). Phylogeny of Myzostomida (Annelida) and their relationships with echinoderm hosts. *BMC Evolutionary Biology*, *14*(1). http://bmcevolbiol.biomedcentral.com/articles/10.1186/s12862-014-0170-7

Surugiu, V. (2005). The use of polychaetes as indicators of eutrophication and organic enrichment of coastal waters: A study case–Romanian Black Sea coast. *Analele Ştiinţifice Ale Universităţii "Al. I. Cuza" Iaşi, s. Biologie Animală*, *51*, 55–62.

Sweetman, A. K., Thurber, A. R., Smith, C. R., Levin, L. A., Mora, C., Wei, C. L., Gooday, A. J., Jones, D. O. B., Rex, M., Yasuhara, M., Ingels, J., Ruhl, H. A., Frieder, C. A., Danovaro, R., Würzberg, L., Baco, A., Grupe, B. M., Pasulka, A., Meyer, K. S., … Roberts, J. M. (2017). Major impacts of climate change on deep-sea benthic ecosystems. *Elementa*, *5*. https://doi.org/10.1525/ELEMENTA.203/112418

Taboada, S., Leiva, C., Bas, M., Schult, N., & McHugh, D. (2017). Cryptic species and colonization processes in *Ophryotrocha* (Annelida, Dorvilleidae) inhabiting vertebrate remains in the shallow-water Mediterranean. *Zoologica Scripta*, *46*(5), 611–624. https://doi.org/10.1111/ZSC.12239

Taboada, S., Riesgo, A., Wiklund, H., Paterson, G. L. J., Koutsouveli, V., Santodomingo, N., Dale, A. C., Smith, C. R., Jones, D. O. B., Dahlgren, T. G., & Glover, A. G. (2018a). Implications of population connectivity studies for the design of marine protected areas in the deep sea: An example of a demosponge from the Clarion-Clipperton Zone. *Molecular Ecology*, *27*(23), 4657–4679. https://doi.org/10.1111/mec.14888

Taboada, S., Leiva, C., Junoy, J., Alexander, F., & Riesgo, A. (2018b). A new member of the genus *Antarctonemertes* (Hoplonemertea, Nemertea) from Antarctic waters. *Polar Biology*, *41*(7), 1463–1473. https://doi.org/10.1007/S00300-018-2298-1/TABLES/3

Taboada, S., Ríos, P., Mitchell, A., Cranston, A., Busch, K., Tonzo, V., Cárdenas, P., Sánchez, F., Leiva, C., Koutsouveli, V., Cristobo, J., Xavier, J. R., Hentschel, U., Rapp, H. T., Morrow, C., Drewery, J., Romero, P. E., Arias, M. B., Whiting, C., & Riesgo, A. (2022). Genetic diversity, gene flow and hybridization in fan-shaped sponges (*Phakellia* spp.) in the North-East Atlantic deep sea. *Deep Sea Research Part I: Oceanographic Research Papers*, *181*, 103685. https://doi.org/10.1016/J.DSR.2021.103685

Taboada, S., Whiting, C., Wang, S., Ríos, P., Davies, A. J., Mienis, F., Kenchington, E., Cárdenas, P., Cranston, A., Koutsouveli, V., Cristobo, J., Rapp, H. T., Drewery, J., Baldó, F., Morrow, C., Picton, B., Xavier, J. R., Arias, M. B., Leiva, C., & Riesgo, A. (2023). Long distance dispersal and oceanographic fronts shape the connectivity of the keystone sponge *Phakellia ventilabrum* in the deep northeast Atlantic. *Frontiers in Marine Science*, *10*, 1177106. https://doi.org/10.3389/FMARS.2023.1177106/BIBTEX

Tamura, K., Stecher, G., & Kumar, S. (2021). MEGA11: Molecular Evolutionary Genetics Analysis Version 11. *Molecular Biology and Evolution*, *38*(7), 3022–3027. https://doi.org/10.1093/MOLBEV/MSAB120

Thatje, S., Hillenbrand, C.-D., & Larter, R. (2005). On the origin of Antarctic marine benthic community structure. *Trends in Ecology & Evolution*, *20*(10), 534–540. https://doi.org/10.1016/J.TREE.2005.07.010

Thiel, H. (1992). Deep-sea Environmental Disturbance and Recovery Potential. *Internationale Revue Der Gesamten Hydrobiologie Und Hydrographie*, *77*(2), 331–339. https://doi.org/10.1002/IROH.19920770213

Thiel, H., Schriever, G., Bussau, C., & Borowski, C. (1993). Manganese nodule crevice fauna. *Deep-Sea Research Part I*, *40*(2), 419–423. https://doi.org/10.1016/0967-0637(93)90012-R

Thoma, M., Jenkins, A., Holland, D., & Jacobs, S. (2008). Modelling Circumpolar Deep Water intrusions on the Amundsen Sea continental shelf, Antarctica. *Geophysical Research Letters*, *35*(18). https://doi.org/10.1029/2008GL034939

Thomas-Bulle, C., Bertrand, D., Nagarajan, N., Copley, R. R., Corre, E., Hourdez, S., Bonnivard, É., Claridge-Chang, A., & Jollivet, D. (2022). Genomic patterns of divergence in the early and late steps of speciation of the deep-sea vent thermophilic worms of the genus *Alvinella*. *BMC Ecology and Evolution*, *22*(1), 1–17. https://doi.org/10.1186/S12862-022-02057-Y/FIGURES/7

Thornhill, D. J., Mahon, A. R., Norenburg, J. L., & Halanych, K. M. (2008). Open-ocean barriers to dispersal: a test case with the Antarctic Polar Front and the ribbon worm *Parborlasia corrugatus* (Nemertea: Lineidae). *Molecular Ecology*, *17*(23), 5104–5117. http://doi.wiley.com/10.1111/j.1365-294X.2008.03970.x

Thorpe, S. E., Heywood, K. J., Brandon, M. A., & Stevens, D. P. (2002). Variability of the southern Antarctic Circumpolar Current front north of South Georgia. *Journal of Marine Systems*, *37*(1–3), 87–105. https://doi.org/10.1016/S0924-7963(02)00197-5

Tiedemann, R., Sarnthein, M., & Shackleton, N. J. (1994). Astronomic timescale for the Pliocene Atlantic δ18O and dust flux records of Ocean Drilling Program Site 659. *Paleoceanography*, *9*(4), 619–638. https://doi.org/10.1029/94PA00208

Timm, L. E., Bracken-Grissom, H. D., Sosnowski, A., Breitbart, M., Vecchione, M., & Judkins, H. (2020). Population genomics of three deep-sea cephalopod species reveals connectivity between the Gulf of Mexico and northwestern Atlantic Ocean. *Deep Sea Research Part I: Oceanographic Research Papers*, *158*, 103222. https://doi.org/10.1016/J.DSR.2020.103222

Timm, L. E., Moahamed, B., Churchill, D. A., & Bracken-Grissom, H. D. (2018). *Bathynomus giganteus* (Isopoda: Cirolanidae) and the canyon: a population genetics assessment of De Soto Canyon as a glacial refugium for the giant deep-sea isopod. *Hydrobiologia*, *825*(1), 211–225. https://doi.org/10.1007/S10750-018-3563-6/TABLES/5

Toews, D. P. L., & Brelsford, A. (2012). The biogeography of mitochondrial and nuclear discordance in animals. *Molecular Ecology*, *21*(16), 3907–3930. https://doi.org/10.1111/J.1365-294X.2012.05664.X

Turner, J., Colwell, S. R., Marshall, G. J., Lachlan-Cope, T. A., Carleton, A. M., Jones, P. D., Lagun, V., Reid, P. A., & Iagovkina, S. (2005). Antarctic climate change during the last 50 years. *International Journal of Climatology*, *25*(3), 279–294. https://doi.org/10.1002/joc.1130

Uchida, H., Tanase, H., & Kubota, S. (2009). An extraordinarily large specimen of the polychaete worm *Eunice aphroditois* (Pallas) (Order Eunicea) from Shirahama, Wakayama, central Japan. *Kuroshio Biosphere*, *5*, 9–15. https://repository.kulib.kyoto-u.ac.jp/dspace/handle/2433/179218

UN Ocean Conference. (2018). *Marine Protected Area in the Weddell-Sea, Antarctica*. https://oceanconference.un.org/commitments/?id=16038

van der Loos, L. M., & Nijland, R. (2021). Biases in bulk: DNA metabarcoding of marine communities and the methodology involved. *Molecular Ecology*, *30*(13), 3270–3288. https://doi.org/10.1111/MEC.15592

van der Reis, A. L., Norrie, C. R., Jeffs, A. G., Lavery, S. D., & Carroll, E. L. (2022). Genetic and particle modelling approaches to assessing population connectivity in a deep sea lobster. *Scientific Reports 2022 12:1*, *12*(1), 1–16. https://doi.org/10.1038/s41598-022-19790-5

Van Dover, C. L. (2000). *The ecology of deep-sea hydrothermal vents*. Princeton University Press.

Vaughan, D. G., Marshall, G. J., Connolley, W. M., Parkinson, C., Mulvaney, R., Hodgson, D. A., King, J. C., Pudsey, C. J., & Turner, J. (2003). Recent rapid regional climate warming on the Antarctic Peninsula. *Climatic Change*, *60*(3), 243–274. https://doi.org/10.1023/A:1026021217991

Vences, M., Thomas, M., Bonett, R. M., & Vieites, D. R. (2005a). Deciphering amphibian diversity through DNA barcoding: chances and challenges. *Philosophical Transactions of the Royal Society B: Biological Sciences*, *360*(1462), 1859–1868. https://doi.org/10.1098/RSTB.2005.1717

Vences, M., Thomas, M., Van Der Meijden, A., Chiari, Y., & Vieites, D. R. (2005b). Comparative performance of the 16S rRNA gene in DNA barcoding of amphibians. *Frontiers in Zoology*, *2*(1), 1–12. https://doi.org/10.1186/1742-9994-2-5/FIGURES/5

Verkaik, K., Hamel, J. F., & Mercier, A. (2017). Impact of ocean acidification on reproductive output in the deep-sea annelid *Ophryotrocha* sp. (Polychaeta: Dorvilleidae). *Deep Sea Research Part II: Topical Studies in Oceanography*, *137*, 368–376. https://doi.org/10.1016/J.DSR2.2016.05.022

Vernet, M., Geibert, W., Hoppema, M., Brown, P. J., Haas, C., Hellmer, H. H., Jokat, W., Jullion, L., Mazloff, M., Bakker, D. C. E., Brearley, J. A., Croot, P., Hattermann, T., Hauck, J., Hillenbrand, C. D., Hoppe, C. J. M., Huhn, O., Koch, B. P., Lechtenfeld, O. J., … Verdy, A. (2019). The Weddell Gyre, Southern Ocean: Present Knowledge and Future Challenges. *Reviews of Geophysics*, *57*(3), 623–708. https://doi.org/10.1029/2018RG000604

Vetter, E. W., & Dayton, P. K. (1998). Macrofaunal communities within and adjacent to a detritus-rich submarine canyon system. *Deep Sea Research Part II: Topical Studies in Oceanography*, *45*(1–3), 25–54. https://doi.org/10.1016/S0967-0645(97)00048-9

Villalobos-Guerrero, T. F. (2019). Redescription of two overlooked species of the *Perinereis nuntia* complex and morphological delimitation of *P. nuntia* (Savigny in Lamarck, 1818) from the Red Sea (Annelida, Nereididae). *Zoosystema*, *41*(1), 465. https://doi.org/10.5252/zoosystema2019v41a24

Villalobos-Guerrero, T. F., & Bakken, T. (2018). Revision of the *Alitta virens* species complex (Annelida: Nereididae) from the North Pacific Ocean. In *Zootaxa* (Vol. 4483, Issue 2, pp. 201–257). Magnolia Press. https://doi.org/10.11646/zootaxa.4483.2.1

Villalobos-Guerrero, T. F., Kara, J., Simon, C., & Idris, I. (2022). Systematic review of *Neanthes* Kinberg, 1865 (Annelida: Errantia: Nereididae) from southern Africa, including a preliminary molecular phylogeny of the genus. *Marine Biodiversity 2022 52:2*, *52*(2), 1–30. https://doi.org/10.1007/S12526-021-01244-2

Vinogradova, N. G. (1997). Zoogeography of the Abyssal and Hadal Zones. *Advances in Marine Biology*, *32*(32), 325–387. https://doi.org/10.1016/S0065-2881(08)60019-X

Wang, Y., & Li, X. (2016). A new *Maldane* species and a new Maldaninae genus and species (Maldanidae, Annelida) from coastal waters of China. *ZooKeys*, *2016*(603), 1–16. https://doi.org/10.3897/zookeys.603.9125

Washburn, T. W., Menot, L., Bonifácio, P., Pape, E., Błażewicz, M., Bribiesca-Contreras, G., Dahlgren, T. G., Fukushima, T., Glover, A. G., Ju, S. J., Kaiser, S., Yu, O. H., & Smith, C. R. (2021). Patterns of Macrofaunal Biodiversity Across the Clarion-Clipperton Zone: An Area Targeted for Seabed Mining. *Frontiers in Marine Science*, *8*, 626571. https://doi.org/10.3389/FMARS.2021.626571/BIBTEX

Washburn, T. W., Turner, P. J., Durden, J. M., Jones, D. O. B., Weaver, P., & Van Dover, C. L. (2019). Ecological risk assessment for deep-sea mining. *Ocean & Coastal Management*, *176*, 24–39. https://doi.org/10.1016/J.OCECOAMAN.2019.04.014

Weaver, P. P. E., & Billett, D. (2019). Environmental Impacts of Nodule, Crust and Sulphide Mining: An Overview. *Environmental Issues of Deep-Sea Mining*, 27–62. https://doi.org/10.1007/978-3-030-12696-4_3

Weigert, A., & Bleidorn, C. (2016). Current status of annelid phylogeny. *Organisms Diversity & Evolution*, *16*(2), 345–362. https://doi.org/10.1007/s13127-016-0265-7

Weston, J. N. J., Jensen, E. L., Hasoon, M. S. R., Kitson, J. J. N., Stewart, H. A., & Jamieson, A. J. (2022). Barriers to gene flow in the deepest ocean ecosystems: Evidence from global population genomics of a cosmopolitan amphipod. *Science Advances*, *8*(43), 6672. https://doi.org/10.1126/SCIADV.ABO6672/SUPPL_FILE/SCIADV.ABO6672_DATA_FILE_S1.ZIP

Wieczorek, J., Bloom, D., Guralnick, R., Blum, S., Döring, M., Giovanni, R., Robertson, T., & Vieglais, D. (2012). Darwin core: An evolving community-developed biodiversity data standard. *PLoS ONE*, *7*(1). https://doi.org/10.1371/journal.pone.0029715

Wiklund, H., Neal, L., Glover, A. G., Drennan, R., Rabone, M., & Dahlgren, T. G. (2019). Abyssal fauna of polymetallic nodule exploration areas, eastern Clarion-Clipperton Zone, central Pacific Ocean: Annelida: Capitellidae, Opheliidae, Scalibregmatidae, and Travisiidae. *ZooKeys*, *2019*(883), 1–82. https://doi.org/10.3897/zookeys.883.36193

Wiklund, H., Rabone, M., Glover, A. G., Bribiesca-Contreras, G., Drennan, R., Stewart, E. C. D., Boolukos, C. M., King, L. D., Sherlock, E., Smith, C. R., Dahlgren, T. G., & Neal, L. (2023). Checklist of newly-vouchered annelid taxa from the Clarion-Clipperton Zone, central Pacific Ocean, based on morphology and genetic delimitation. *Biodiversity Data Journal 11: E86921*, *11*, e86921-. https://doi.org/10.3897/BDJ.11.E86921

Wilson, N. G., Hunter, R. L., Lockhart, S. J., & Halanych, K. M. (2007). Multiple lineages and absence of panmixia in the “circumpolar” crinoid *Promachocrinus kerguelensis* from the Atlantic sector of Antarctica. *Marine Biology*, *152*(4), 895–904. https://doi.org/10.1007/s00227-007-0742-9

Wilson, N. G., Schrödl, M., & Halanych, K. M. (2009). Ocean barriers and glaciation: evidence for explosive radiation of mitochondrial lineages in the Antarctic sea slug *Doris kerguelenensis* (Mollusca, Nudibranchia). *Molecular Ecology*, *18*(5), 965–984. https://doi.org/10.1111/j.1365-294X.2008.04071.x

Wilson, R. S. (1984). *Neanthes* (Polychaeta: Nereididae) from Victoria with descriptions of two new species. *Proceedings of the Royal Society of Victoria*, *96*(4), 209–226.

Wilson, R. S. (1988). Synonymy of the genus *Nectoneanthes* Imajima, 1972, with *Neanthes K*inberg, 1866 (Polychaeta: Nereididae). *Proceedings of the Biological Society of Washington*, *101*(1), 4–10.

Woodall, L. C., Sanchez-Vidal, A., Canals, M., Paterson, G. L. J., Coppock, R., Sleight, V., Calafat, A., Rogers, A. D., Narayanaswamy, B. E., & Thompson, R. C. (2014). The deep sea is a major sink for microplastic debris. *Royal Society Open Science*, *1*(4). https://doi.org/10.1098/RSOS.140317

Worsaae, K., Kerbl, A., Di Domenico, M., Gonzalez, B. C., Bekkouche, N., & Martínez, A. (2021). Interstitial Annelida. *Diversity 2021, Vol. 13, Page 77*, *13*(2), 77. https://doi.org/10.3390/D13020077

Wu, P., Sun, J., & Yang, T. (1985). *Nereidae (Polychaetous annelids) of the Chinese coast*. Springer-Verlag.

Yool, A., Martin, A. P., Fernández, C., & Clark, D. R. (2007). The significance of nitrification for oceanic new production. *Nature 2007 447:7147*, *447*(7147), 999–1002. https://doi.org/10.1038/nature05885

Zachos, J., Pagani, M., Sloan, L., Thomas, E., & Billups, K. (2001). Trends, Rhythms, and Aberrations in Global Climate 65 Ma to Present. *Science*, *292*(5517), 686–693. https://doi.org/10.1126/SCIENCE.1059412

Zamani, A., Dal Pos, D., Fric, Z. F., Orfinger, A. B., Scherz, M. D., Bartoňová, A. S., & Gante, H. F. (2022a). The future of zoological taxonomy is integrative, not minimalist. *Systematics and Biodiversity*, *20*(1), 1–14. https://doi.org/10.1080/14772000.2022.2063964

Zamani, A., Zdenek, Fric, F., Hugo, Gante, F., Hopkins, T., Orfinger, A. B., Scherz, M. D., Sucháčková Bartoňová, A., Davide, & Pos, D. (2022b). DNA barcodes on their own are not enough to describe a species. *Systematic Entomology, 47*(3), 385–389. https://doi.org/10.1111/SYEN.12538

Zamani, A., Vahtera, V., Sääksjärvi, I. E., & Scherz, M. D. (2021). The omission of critical data in the pursuit of 'revolutionary' methods to accelerate the description of species. *Systematic Entomology*, *46*(1), 1–4. https://doi.org/10.1111/SYEN.12444

Zhang, J., Kapli, P., Pavlidis, P., & Stamatakis, A. (2013). A general species delimitation method with applications to phylogenetic placements. *Bioinformatics*, *29*(22), 2869–2876. https://doi.org/10.1093/BIOINFORMATICS/BTT499

Zhang, K., Sun, J., Xu, T., Qiu, J. W., & Qian, P. Y. (2021). Phylogenetic Relationships and Adaptation in Deep-Sea Mussels: Insights from Mitochondrial Genomes. *International Journal of Molecular Sciences 2021, Vol. 22, Page 1900*, *22*(4), 1900. https://doi.org/10.3390/IJMS22041900

Zhang, Y. Y., Sun, J., Chen, C., Watanabe, H. K., Feng, D., Zhang, Y. Y., Chiu, J. M. Y., Qian, P. Y., & Qiu, J. W. (2017). Adaptation and evolution of deep-sea scale worms (Annelida: Polynoidae): insights from transcriptome comparison with a shallow-water species. *Scientific Reports. 7*(1), 1–14. https://doi.org/10.1038/srep46205